Cell models for the study of the association of *EIF2AK3*/PERK with progressive supranuclear palsy and neurodegeneration

Thesis submitted as partial fulfilment of the degree of
Doctor of Philosophy

Reta Lila Weston Institute
and Department of Clinical and Movement Neurosciences
Queen Square Institute of Neurology
University College London

February 2020

Bimali Hapuarachchi

Declaration

I, Bimali Hapuarachchi confirm that the work presented in this thesis is my own. Where information has been derived from other sources, I confirm that this has been indicated in the thesis.

ABSTRACT

A genome-wide association study (GWAS) identified *EIF2AK3* as a risk factor for progressive supranuclear palsy (PSP). *EIF2AK3* encodes protein kinase R-like endoplasmic reticulum kinase (PERK), which senses unfolded protein accumulation within the endoplasmic reticulum (ER) lumen. PERK kinase activity has been genetically associated with increased PSP risk. The associated single nuclear polymorphism (SNP), rs7571971, is in linkage disequilibrium with coding SNPs of *EIF2AK3*: rs867529($Ser_{136}Cys$), rs13045($Gln_{166}Arg$) and rs1805165($Ala_{704}Ser$), forming coding haplotypes of three highly conserved residues; Haplotype A (conserved): S_{136}-R_{166}-S_{704} and Haplotype B (divergent): Cys_{136}-Gln_{166}-Ala_{704}. A previous study showed that the divergent risk Haplotype *B* (HapB) has increased PERK activity suggesting that this forms the basis of the genetic risk. The polymorphisms could therefore affect either functional domain (or both).

Our aim was to investigate if the two major coding haplotypes of PERK impart differences in the activation of PERK either by impaired homodimerization and/or kinase activity.

We generated isogenic HEK293 cell lines for Tet-inducible expression of PERK coding haplotypes with a C-terminal myc-tag to discern from endogenous PERK. With Western blot analyses, we demonstrated robust, inducible expression of myc-tagged PERK. Interestingly, with subsequent passages, the freeze-thawed HapB PERK variants alone underwent C-terminal cleavage as evidenced by loss of the myc-tag which resulted not only in increased PERK protein but also reduced levels of activated p-PERK and p-eIF2α. Myc cleaved HapB cells also showed a significant delayed and impaired kinase activity, alongside increased cell death following induction of the UPR. However, we failed to obtain any evidence for a connection between impaired HapB PERK activity and tau aggregation, even with the more aggregation-prone 2N4R-tau (P301L) and additional seeding with brain lysates from the rTg4510 mouse and with inhibition of ubiquitin proteasome system (UPS) with MG132.

In summary, we established stable isogenic cell lines for Tet-inducible expression of PERK functional haplotypes. Although the C-terminus myc tag cleavage of the passage 2 HapB cells resulted in reduced PERK activation leading to an impaired UPR, a necessary further control to validate these conclusions would be to include untagged passage 2 HapB cells. This is essential to clarify as to whether the underlying reduced HapB PERK activity following cell passaging is due to an artefact following myc cleavage or due to posttranslational modifications inherent to HapB PERK.

Impact Statement

To date nineteen debilitating neurodegenerative disorders have been identified that are united by a common pathology – tau protein. The tauopathies affect nearly eight million people globally. No cure has yet been found. The ER stress sensor PERK is heavily implicated in the pathogenesis and progression of tauopathy. However, the underlying mechanism by which the PERK pathway impairs neuronal function remains unknown. A recent GWAS identified the *EIF2AK3* gene, encoding PERK, as a genetic risk factor for PSP – one of the 19 tauopathies – and evidence directly correlates increased PERK activity with tau progression. PERK senses when the cell is under stress from an onslaught of defective protein into the ER and initiates the protective unfolded protein response (UPR).

This work in this thesis has advanced the understanding of PERK in PSP by developing a simple biological model consisting of cells that contain different forms of the PERK protein, as coded for by different variants of the PERK gene. This has provided an extremely useful platform for further investigation. Along the way we discovered that the form of PERK produced by the risk-associated version of its gene displayed significantly reduced activity following its C-terminal cleavage. This could have a significant bearing on tau accumulation and could potentially suggest a possible basis of how PERK gene variation contributes to disease risk.

The literature abounds with evidence for PERK activation and the UPR response in neurodegenerative proteopathies; our work demonstrates that the increased risk of PSP conferred by HapB could contribute to tauopathic progression. PERK Hap B is widespread, found in almost a third of Northern European populations. Our findings interrogate this haplotype more: How does HapB increase tauopathy risk in carriers of the allele? More crucially is the epigenetic question: are those with reduced PERK activity more susceptible to (possibly modifiable) environmental risk factors for tauopathies?

The cell models now provide opportunities for further investigation into how PERK variants contribute to PSP and, crucially, how the deleterious aspects can be reduced or reversed. Specifically, we want to explore outcomes following the generation of high levels of normal and aberrant tau and how the different PERK haplotypes influence the cellular response and subsequent tau accumulation.

Our work contributes to the global long-term aim: better to understand the mechanism(s) by which tau and Hap B collaborate to induce neuronal dysfunction. The wider benefits of this work can be seen locally in identifying reliable and reproducible laboratory methods of using cell models for

neurodegenerative disease, and for the wider community in identifying potential cellular pathway targets for therapeutics which could identify pharmacologic and genetic approaches to inhibit PERK *in vivo*, and in *in vitro* models of tauopathy.

The identification of a pathogenic PERK-tau cycle departs from the classic model by identifying an effector of disease (PERK) that can cause neuronal dysfunction (downstream) while also potentiating tau aberrancies (upstream). Therefore, the PERK pathway offers a unique focus for novel therapeutic targets to modulate disease multifactorially. Ongoing discovery of the mechanisms by which PERK damages neurons will identify the problem, and then pharmaco-therapeutic research will better arrive at potential solutions.

Dr John Steele with the author

ACKNOWLEDGMENTS

To my supervisor, Dr Rohan de Silva: thank you for your scientific wisdom and Swiss/Sri Lankan ;-)-precision during these past few years. Your guidance and advice have elevated this thesis beyond my highest expectations. Even though at times it seemed like I would be submitting it to you as a retirement present. To my secondary supervisor, Prof Tom Warner: thank you for your tireless support, good humour and tolerance.

To my hunky backing singers: Maz Ehteheramyan and Joe Hamilton: thank you both for your hard work, experimental planning sessions and for not exposing the fact that I hadn't a clue what I was doing half the time.

To Dr Abi Li: thank you for your intelligent and rigorous critiques of my project. You were always there when anything went wrong, or right, and never scolded me for sending my supply requests too late.

To my co-workers and friends Nayomi Hondhamuni, Nanet Willumsen, Ioanna Sevastou and Nuria Setó-Salvia: your love and support made coming into the lab a pleasure (almost) and made it so much more fun. To Luke Hill: thank you for your camaraderie and allowing me to vent all my frustrations over a plate of substitute meat. To everyone in the first floor of WS: thank you for the food, and always being there to lend a hand. You've been so supportive.

To the Reta Lila Weston Trust and PSPA: I'm so grateful for your funding of this work. I must also thank the staff at the Queen Square Brain Bank for providing tissue from PSP samples for DNA and protein extraction. But more importantly, the patients and their families for whom PSP was not an academic thesis, but a daily companion and a mountain to climb. I do hope the work we have done here, with your invaluable contributions, makes it an easier mountain for generations to come.

To Prof John Steele: for agreeing to the selfie (and for his part in first describing Steele-Richardson-Olszewski syndrome, aka PSP).

Finally, to the three very special men in my life: Pete, Adam & Len. To paraphrase PG Wodehouse: if it hadn't been for your constant discussions and presence, all this would have been finished in half the time. You kept me nearly sane through the difficult days and ensured that while I was standing on the shoulders of giants at work I was also standing on bricks of Lego at home. Love you x.

Table of Contents

List of Figures and List of Tables

List of Tables

List of abbreviations

3R-tau	Three microtubule binding repeat isoform of tau
4R-tau	Four microtubule binding repeat isoform of tau
ΔN296	Homozygous deletion of codon 296
Aβ	Amyloid Beta
ACE	A/C rich enhancer
AD	Alzheimer's disease
ALS	Amyotrophic lateral sclerosis
ATF4	Activating transcription factor 4
ATF6	Activating transcription factor 6
ATP	Adenosine triphosphate
bZIP	Basic leucine zipper domain
BACE1	beta-site amyloid precursor protein cleaving enzyme 1
BCL2	B-cell lymphoma 2
Bim	BCL-2-interacting mediator of cell death
BiP	Binding immunoglobulin protein
BSA	Bovine serum albumin
CAT	Chloramphenicol acetyl transferase
CD	Circular dichroism
CDK5	Cyclin dependent kinase 5
CB	Coiled bodies
CBD	Corticobasal degeneration
cDNA	complementary DNA
CHO	Chinese hamster ovary
CHOP	C/EBP homologous protein
C-lobe	C terminal lobe
C-Src	Src-tyrosine kinase
C-Term	Carboxy terminal
CoQ10	Co-enzyme Q10
CRHR1	Corticotrophin releasing hormone receptor 1
DAPI	4′,6-diamidino-2-phenylindole
DEPC	Diethylpyrocarbonate
DMEM	Dulbecco's Modified Eagle Medium
DMSO	Dimethyl sulphoxide
DNA	Deoxyribonucleic acid
dNTP	Deoxynucleoside triphosphate

dT	deoxythymine
Dox	Doxycycline
DR5	Death receptor 5 protein
DTT	Dithiothreitol
ECL	Enhanced chemiluminescence
E. coli	*Escherichia coli*
EDTA	Ethylenediaminetetraacetic acid
EGTA	ethylene glycol-bis (β-aminoethyl ether)-N, N, N′, N′-tetra acetic acid
eIF2*α*	Eukaryotic initiation factor 2 subunit alpha
EIF2AK3	Eukaryotic translation initiation factor 2- alpha kinase 3
EM	Electron microscopy
ER	Endoplasmic reticulum
ERAD	Endoplasmic reticulum associated protein degradation pathway
ERSE	ER stress response element
ESE	Exon splicing enhancer
ESS	Exon splicing silencer
FamPSP	Familial PSP study
FBS	Fetal Bovine Serum
FITR	Fourier transform infrared spectroscopy
FOX13	Forkhead Box 13 protein
FRT	Flippase recognition target
FTD	Frontotemporal dementia
Fyn	Non-receptor tyrosine-protein kinase
gDNA	genomic DNA
GAD34	Growth arrest and DNA damage inducible 34
GCF	GC-rich sequence DNA binding factor
GCN2	General control nonderepressible 2
GWAS	Genome wide association study
GST	Glutathione S-transferase
GSK3β	Glycogen synthase kinase-3 beta
GFP	Green fluorescent protein
GLS	Golgi localization region 1
GDP	Guanosine-5'-diphosphate
GTP	Guanosine-5'-triphosphate
HapB	PERK haplotype B
HBSS	Hanks buffered saline solution
HCL	Hydrochloric acid
HD	Huntington disease

HRI	Heme-regulated eIF2α kinase
HRP	Horseradish peroxidase
Hsp70	Heat shock protein 70
IκB	Inhibitor of Nuclear Factor Kappa B Kinase B
IP	Immunoprecipitation
IRE1	Inositol requiring enzyme 1
ISE	Intron splicing enhancer
ISM	Intron splicing modulator
ISS	Intron splicing silencer
JNK	Jun amino-terminal kinases
Kb	Kilobase
KEAP1	Kelch-like ECH associated protein
LB	Lewy bodies
LB	Luria-Bertani
LOD	Logarithm of the odds
LD	Linkage disequilibrium
mRNA	Messenger RNA
MAM	Mitochondria associated ER membranes
MAPs	Microtubule-associated proteins
MAPK	Mitogen activated protein kinase
MAPT	Microtubule-associated protein tau
MG132	Carbo-benzoxy-leucyl-leucyl-leucinal
MT	Microtubule
MTBR	Microtubule-binding repeat domain
MDS	Movement disorder society
MOBP	Myelin associated oligodendrocyte basic protein
MOPS	3-(N-morpholino) propanesulfonic acid
mRNA	Messenger ribonucleic acid
NEAA	Non-essential amino acid
NFκB	Nuclear Factor kappa-light-chain-enhancer of activated B cells
NFT	Neurofibrillary tangle
NT	Neuropil threads
NRF2	Nuclear factor erythroid 2–related factor 2
NINDS	National Institute of Neurological Disorders and Stroke
N-lobe	N-terminal lobe
NSF	N-ethylmaleimide-sensitive factor
ORF	Open reading frame
PBS	Phosphate buffered saline

PBST	Phosphate buffered saline tween
pFRT/TO	FLP Recombination Target/Tet Operator
PCR	Polymerase chain reaction
PD	Parkinson's disease
P1,2 etc	Passage 1, 2 etc
PERK	Protein kinase R-like endoplasmic reticulum kinase
PHF	Paired helical filaments
PHF-Tau	Paired helical filamentous Tau
PKA	cAMP activated protein kinase A
PKR	Double-stranded RNA dependent protein kinase
PMD	Protein misfolding disorder
PPE	Polypurine enhancer
PP1	Protein phosphatase 1
PSP	Progressive supranuclear palsy
PSP-CBS	PSP-Corticobasal syndrome
PSP-SL	PSP-speech/language disorders
PVDF	Polyvinylidene fluoride
rER	Rough endoplasmic reticulum
RIPA	Radioimmunoprecipiation assay
RNA	Ribonucleic acid
ROI	Region of interest
RPIA	Ribose-5-phosphate isomerase A protein
RS	Richardson Syndrome
RT	Reverse Transcription
RT-PCR	Reverse transcription polymerase chain reaction
SAPK	Stress-activated Protein Kinase
sER	Smooth endoplasmic reticulum
SERCA	Sarcoplasmic/ER calcium ATPase
S1P	Site-1 protease
S2P	Site-2 protease
SDS-PAGE	Sodium dodecyl sulphate-polyacrylamide gel electrophoresis
SF	Straight filaments
SNP	Single nuclear polymorphism
SiRNA	Small interfering RNA
SnRNA	Small nuclear RNA
SnRNP	Small nuclear ribonucleoprotein particles
SOS1	Son of sevenless-1
sPSP	Society for PSP

SRP	Signal recognition particle
STX6	Syntaxin 6
TAE	Tris-acetate-EDTA
TBS	Tris-buffered saline
TBST	Tris-buffered saline with Tween-20
TE	Tris-EDTA
Ths	Thioflavin S
T-Rex	Tet-inducible expression system
TRIzol	Total RNA isolation
Tg	Thapsigargin
Tm	Tunicamycin
TNF α	Tumour necrosis factor-α
TRAF2	Tumour necrosis factor-α (TNFα)-receptor-associated factor 2
TIQ	Tetrahydroisoquinoline
UPR	Unfolded protein response
UPS	Ubiquitin proteasome system
UV	Ultraviolet
VCP	Valosin-containing protein
WGA	Wheatgerm Agglutinin
XBP1	X-Box binding protein 1

Chapter 1

Introduction

1.1 Progressive Supranuclear Palsy

Progressive supranuclear palsy (PSP) is a neurodegenerative disease characterised by mature age at onset and rapid progression, occurring predominantly sporadically in the population. Currently no definitive symptomatic or curative treatment exists (Brusa et al., 2004; Pastor and Tolosa, 2002; Steele et al., 1964). It is considered among the parkinsonian conditions, the second most common after Parkinson's disease (PD) and thus is the most common type of atypical parkinsonism (Litvan et al., 1996). The precise pathophysiology of PSP has evaded a significant (and ongoing) body of research. At the time of writing there is still no pathonognomic biological marker for diagnosis. However, it is important to note that research has revealed some significant clues: at a molecular level we know PSP to be one of the tauopathies (Flament et al., 1991). This cluster of neurodegenerative disorders (of which Alzheimer's disease (AD) is the most common) demonstrates abnormalities in the microtubule-associated protein, tau (MAPT). This manifests in the degeneration of discrete and disease-specific neural regions within the brain and in the case of PSP these are: corpus striatum, globus pallidum, subthalamic nucleus, substantia nigra, oculomotor complex, periaqueductal grey matter, dentate nucleus of the cerebellum, as well as some cortical regions such as the superior frontal gyrus and pericalcarine (Tolnay and Probst., 2003; Irwin., 2007).

1.2 Historical Context

The features of PSP were first reported by Posey in 1904 and then again just a year later by Spiller in 1905 illustrating typical features of as yet unnamed PSP (Goetz., 1996). Sixty years later in a landmark paper it was described as a unique disease by Steele, Richardson and Olszewski and accordingly the syndrome took on the awkward name: Steele-Richardson-Olszewski syndrome (Steele et al., 1964). The background to this major development in the wider knowledge of the disease can be seen in 1963, at the American Neurological Association annual meeting. Dr John Clifford Richardson presented eight patients from Toronto, all distinguished by the now classic symptoms: gaze paresis, axial rigidity, gait disturbance, dysarthria, dysphagia and developing dementia. Olszewski and Steele demonstrated the consistent underlying pathology in these cases. They reported the widespread loss of neurons and brought attention to the characteristic neurofibrillary tangles (NFTs), mainly in the diencephalon, brainstem and cerebellum. More

significantly, even at this early point they established the presence of filamentous inclusions in both neurons and glia (Steele et al., 1964). In the initial paper in 1963, they had adopted the term first used by Veerhaart when describing a case, he had observed in 1958: 'heterogeneous system degeneration' (Veerhart., 1958). Richardson wisely proposed it be called progressive supranuclear palsy: this intuitive description breaks away from the eponymous (and descriptively useless) traditions of Parkinson and Alzheimer: the gradual and inexorable deterioration gives *Progressive*; the pathological regions affected are principally the portion of midbrain in which *supranuclear* ocular movement is controlled and lastly *palsy* meaning paralysis, specifically of movement of the eye.

Prior to 1964, cases presenting in this way had been considered a variant of the more established PD: as *forms frustes* of the *paralysis agitans* (Richardson et al., 1963). Clearly the condition did not arise *de novo* in the 1960s and retrospective analysis reveals such evidence as typical PSP posturing in clinical photographs and the Denny-Brown film archives (reviewed by Goetz., 1996). Notwithstanding the earlier reference to Posey, one of Charcot's pupils – Dutil – may lay claim to having described the first documented PSP case in 1889 (Goetz., 1996). Retrospective clinico-detective work has even thrown up the suggestion by Larner (Larner., 2002) that Dickens may have alluded to a case of PSP in 1857 in one of his lesser known pieces: '*The lazy tour of two idle apprentices*', though there can develop an element of esoteric one-upmanship with these discoveries. It has been suggested that the cases of 'arteriosclerotic pseudo-parkinsonism', described in the 1920s by Queen Square doyen MacDonald Critchley was also PSP masquerading as a Parkinson variant (Critchley., 1929). It was a reasonable and justifiable assessment to make without contemporary imaging or the knowledge of opportunity to observe a levodopa response. Even neuropathological assessment post-mortem typically misdiagnosed PSP as postencephalitic parkinsonism or a form of AD (Golbe., 2014).

Given the clinically distinct and overt presentation of PSP, it is perhaps surprising that no formal description existed prior to the mid-twentieth century. However, given its target demographic being the late-middle aged it would inevitably become more apparent as life-expectancy increased with each generation. The great achievement of Steele, Richardson and Olszewski was to identify and thereby allow categorization of the disease and by 1972 Steele had reported a case series of 73 PSP patients. They humbly acknowledged they were only midwives to the formal birth and that "further observations may broaden the clinical spectrum of the disease." (Steele et al., 1964).

1.3 Role of tau in AD and PSP over the last 50 years

The development of our understanding of the neuropathology of PSP also dates back to that epoch-making presentation in Atlantic City and the contribution of Professor Olszewski in particular. These pathological markers observed in PSP were further validated when Pollock and colleagues reported that the filamentous aggregates found in brains from patients with PSP shared antigenic denominators with tau protein (Pollock et al., 1986). The mid-eighties proved a fertile time for tau research and NFTs isolated from AD brains had already demonstrated abnormally phosphorylated tau (Brion et al., 1985; Grundke-Iqbal et al., 1986; Kosik et al., 1986; Wood et al., 1986). Tau, which had initially risen to prominence in 1975 from the work of Weingarten and colleagues was known to be a species of phosphoprotein promoting the auto-assembly of tubulin into microtubules, thereby stabilizing them (Weingarten et al., 1975). There followed a flurry of discovery studies which demonstrated that the hyperphosphorylation of tau inhibited its ability to assemble microtubules (Cleveland et al., 1977; Jameson et al.,1980; Linwall and Cole.,1984), which in turn informed the work of multiple groups identifying abnormal, hyperphosphorylated tau as a major constituent of the injurious NFTs of AD (Brion et al., 1985a; Ksiezak et al., 1992; Kopke et al., 1993; Kenessey et al., 1993). Around the same time endogenous tau within the human brain was shown naturally to exist in equal ratio containing either three microtubule-binding repeat domains (3R) or four microtubule-binding repeat domains (4R) in the carboxy terminal (C-term) of the tau protein (Goedert et al., 1989; Andreadis et al., 1992). Now we know that altered 3R:4R-tau ratios lead to either elevations of tau inclusions predominantly composed of 3R tau (i.e. 3R-tauopathies), those with predominantly 4R tau (i.e. 4R-tauopathies) and that changes to the equal ratio of either the 3R or 4R tau isoforms in the healthy adult brain is key to tau regulated neurodegeneration (D'Souza and Schellenberg., 2005; Sergeant et al., 2005; Goedert and Jakes., 2005).

Specifically, the tauopathic element discovered by Flament and colleagues (1991) in PSP relates to the formation of 4R tau. It is this distortion of the ratio of 4R- to 3R-tau which has been repeatedly shown to correlate with tau hyperphosphorylation and neurotoxicity; on the current received hypothesis this is the primary neuropathological aetiology of PSP (Mailiot et al., 1998; Schoch et al., 2016). Subcortical distribution of NFTs were initially reported in the basal ganglia, brain stem, and cerebellum (Steele et al., 1964). It was these NFTs consisting of 4R-tau which were noted by Hauw and colleagues (1994) to be severely associated with diffuse loss of the neuronal cells of the brainstem and basal ganglia while the cerebellar cortex remained unaffected. Further papers in the nineties elaborated and developed this to describe neurodegeneration in the perirhinal, inferior temporal and prefrontal cortex, with identical features to their subcortical NFTs (Figure 1) (Bergeron et al., 1997; Hauw et al., 1990; Hof et al., 1992). Microscopically, the tangles were first described by Montpetit and colleagues (1985) and Roy and colleagues (1974)

as being possessed of a globular appearance with entwined filaments sitting in parallel, reminiscent to a ball of string. Around this time tau pathology in glia was another frequently observed phenomenon in many tauopathies and in the case of PSP, phosphorylated tau was detected within the coiled bodies (CB) in oligodendroglia as being typically fine and branching (Dickson et al., 1992) as well as in astrocytes appearing as tufts of abnormal fibres which have the distinctive morphology referred to as tufted astrocytes (Yamada et al., 1992) (Figure 2).

In the late 1990s much comparative work in the laboratory was with AD brains, in which all six tau isoforms were shown to be phosphorylated and here the tau aggregations, on immunoblotting, presented as a major tau triplet (tau 55, 64 and 69 kDa) (Goedert et al., 1994). Whereas it was noted that in PSP, only the 4R isoforms are phosphorylated and so appear as a major tau doublet (tau 68 and 64 kDa) (Flament et al., 1991). From these findings of widespread tau aggregates, the hypothesis of PSP as a tauopathy from the same stable as corticobasal degeneration (CBD), frontotemporal dementia (FTD) and AD followed in short order (Dickson., 2001). Tau has been found to be the primary protein aggregating in the brains of PSP patients, making it one of the few primary tauopathies (Buee et al., 1999), whereas AD – globally the leading cause of dementia – is considered a secondary tauopathy. This is due to the latter having a famous partner in crime in the classic neuropathological double-act of tau tangles and amyloid-beta (Aβ) plaques (Kang et al., 1987). On the other hand, PSP as a primary tauopathy has solely accumulations of neurofibrillary tau protein in the basal ganglia as well as in the brainstem nuclei which corresponds to severe neuronal loss, astrogliosis and neurofibrillary degeneration in PSP.

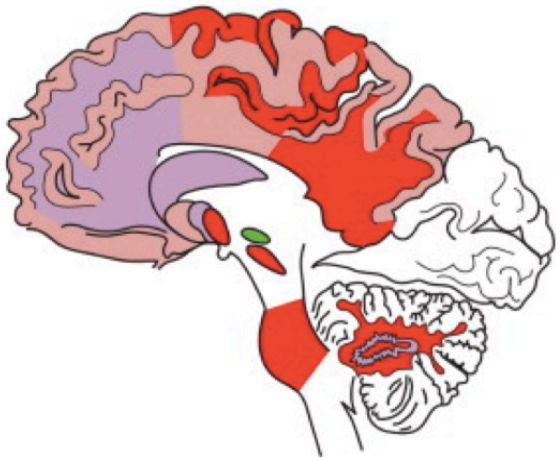

Figure 1. **Areas affected by tau pathology in PSP**. The most severely affected region is shaded in green: subthalamic nucleus; Red includes regions which are severely affected: substantia nigra, Griseum pontis, Dentate nucleus, cerebellar white matter, Globus pallidus and the parietal lobe; Purple includes regions of moderate severity: caudate and frontal cortex. Finally, the unaffected regions are in brown: cerebellar cortex (modified from Williams et al and Lees., 2009).

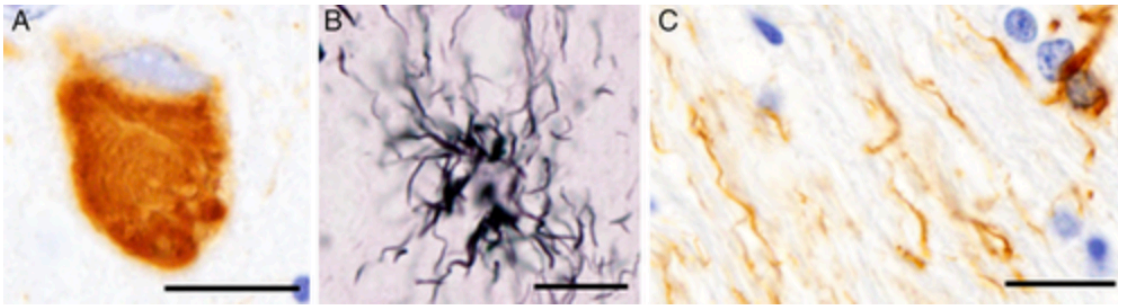

Figure 2. **Tau pathology outline in PSP**. Representative photographs showing ccharacteristic cellular pathology of PSP, including globose-type neurofibrillary tangles visualized by immunohistochemistry with anti-phosphorylated tau antibody (AT8) (A), tufted astrocytes identified by Gallyas-Graak impregnation (B), and oligodendroglial coiled bodies and threads positively stained by AT8 (C). Scale bars: 10 μm (A-C) (adapted from Mimuro and Yoshida., 2019).

1.4 Sixty years on...

As with the natural history of most clinical discoveries, the field has extended considerably since its arrival in the mid-20th century. Moreover, as additional cases began to be admitted under the PSP banner and more brains scrutinised, the initial pathological picture described by Steele and colleagues (1964) has been expanded to admit a variety of clinical phenotypes (Williams et al., 2005).

The goldrush of neurogenetic research provided the next significant developments in the study of PSP: an extended haplotype due to an inverted segment of chromosome 17 including *MAPT* was shown to be overrepresented in PSP subjects (Baker et al., 1999). *MAPT* comprises two conserved haplotypes: H1 which is associated with an increased risk of developing 4R tauopathies (Skipper et al., 2004) and H2 haplotype which is associated with decreased risk and is almost exclusively Caucasian in origin (Evans et al., 2004). Given the evidence that tau is a central player in the pathogenesis of PSP it is hardly surprising that the *MAPT* H1 haplotype has been consistently associated with increased PSP risk (Baker et al., 1999; Conrad et al., 1997; Ezquerra et al., 1999). The H1 haplotype has also been implicated in the other sporadic tauopathies: FTD, CBD and also PD. Specifically, it is the sub-haplotype, H1c, which has been shown to underpin this association with PSP (Pittman et al., 2005). Moreover, H1c is associated *in vivo* with increases in total *MAPT* transcripts in addition to 4R-tau messenger RNA (mRNA) expression which has been shown to increase the relative levels of total 4R-tau protein (Myers et al., 2005). Despite a consistent showing in the literature that PSP is associated with genetic variants in *MAPT*, its

pathogenesis is still unclear, as are – crucially – its origins (Baker et al., 1999; Pittman et al., 2005; Rademakers et al., 2005).

The prevailing orthodoxy that the H1 haplotype of *MAPT* presented the chief genetic risk factor for PSP has now been subjected to challenge. Following a PSP GWAS, three additional loci were identified: syntaxin 6 (*STX6)*, eukaryotic translation Initiation factor 2-Alpha Kinase 3 (*EIF2AK3)* and myelin-associated oligodendrocyte basic protein (*MOBP)* (Hoglinger et al., 2011). These genes are instrumental in the assembly of the cellular microstructure: *STX6* – encoding proteins for vesicle-membrane fusion at the Golgi-endosomal interface; *EIF2AK3* – instrumental in the endoplasmic reticulum unfolded protein response (UPR); and *MOBP* – for a structural component of myelin. Of these, the *EIF2AK3* association formed the basis for the original research presented in this thesis.

At cellular level, mitochondrial energy deficits have also been observed in PSP patients (Albers et al., 2000) and a growing body of evidence also suggests that microglial activation could drive tau pathology (Asai et al., 2015) with strategies now underway for developing agents targeting mitochondrial dysfunction and microglial-specific receptors. One major component of the mitochondrial respiratory chain – Coenzyme Q10 (CoQ10) – did reduce toxicity in complex I inhibition models (Abdin et al., 2008; Beal et al., 1998; Moon et al., 2005) when trialled in a preliminary six-week placebo-controlled trial of 21 patients with PSP. However, a subsequent larger one-year placebo-controlled trial of 61 subjects with PSP using clinical scales as primary outcomes failed to demonstrate any disease-modifying effect of high-dose CoQ10 (Apetauerova et al., 2016).

The anti-tau antibody trials are the latest developments in utilizing the laboratory findings in a clinical setting. Though an important caveat here is that these agents are not targeting the fundamental trigger that drives the production and aggregation of pathological tau. This remains the magic bullet. Very recently, in 2016, the PSP Genetics Consortium was formed by CurePSP, in conjunction with the Tau Consortium to elaborate upon the earlier GWAS to definitively identify protein-encoding risk genes in a PSP cohort against a control population. In this way a large proportion of individuals who have the risk alleles but do not get disease will be identified. This will enable subtle changes in protein function that can in - combination with other factors which contribute to disease pathogenesis - to be highlighted and direct future investigation. Consistent accurate diagnosis is still being refined but improvements in classification and knowledge of the disease at a genetic and molecular level are leading that charge. Once we know better what we are dealing with, then the targeted efforts can be developed to treat, cure and eradicate PSP.

1.5 Clinical Diagnosis of PSP

Accurate classification of a disease is useful both clinically in allowing patients and their doctors to 'name the beast' and manage appropriately and academically in targeting research. The diagnosis of PSP was largely based on this clinical presentation and comprised (i) possible (ii) probable and (iii) definite PSP. The latter necessitates pathological confirmation revolving around the hallmark filamentous tau inclusions in neurons and glia (Litvan et al., 1996). The National Institute of Neurological Disorders and Stroke/ Society for PSP (NINDS/SPSP) criteria were established to aid in correct clinical diagnosis.

A presentation to clinic that might earn itself a 'possible' or a 'probable' would classically be a patient over 40 with a gradually progressive history of falls and axial postural instability and saccadic abnormalities or supranuclear gaze palsy alone would meet the NINDS-SPSP criteria for "possible PSP" (NINDS-SPSP criteria). If vertical supranuclear gaze palsy and slowing of vertical saccades are also present, then a clinical diagnosis of "probable PSP" is reached (Litvan et al., 1996). Despite the use of NINDS-SPSP criteria in clinical practice, because of its increasingly recognized heterogeneity of presentation, the diagnosis of PSP remains a complex matter. One of the principal diagnostic criteria is slowness of vertical saccades but this typically develops up to three years after onset of other symptoms. This delay means that in the early stages, the disease is often misdiagnosed, frequently as PD, multiple system atrophy, dementia with Lewy bodies and other sporadic primary tauopathies (Zampieri and Fabio., 2006). In 1998, Santacruz and colleagues reported that the NINDS/SPSP criteria detected only between half and three quarters of patients within 3 years of onset largely because of absent down-gaze palsy (Santacruz et al., 1998). Other papers have the level of PSP misdiagnosis as high as 60% of pathologically confirmed cases (Collins et al., 1995; Birdi et al., 2002; Daniel et al., 1995). In the majority, early signs of PSP manifest as clinical PD: motor impairments leading to instability and falls, dysarthria and bradykinesia (Litvan and Hutton., 1998). The neurological 'B symptoms' of cognitive decline, aberrant mood and personality disorders with disordered sleep, seldom appear at onset (Golbe,1994; Grafman et al., 1995; Litvan et al., 1996).

The poor sensitivity of the existing diagnostic indicators called for refinement and improvement. In 2017, the new improved movement disorder society (MDS) criteria published by Hoglinger introduced the term "suggestive of PSP" to mop up those lost in early recognition of the disease (Hoglinger et al., 2017). In research terms this will be crucial for accurate recruitment to longitudinal studies There is flexibility to the new criteria that may also admit atypical manifestations which can only augment the totality of knowledge of PSP. The purpose of diagnostic criteria is to encompass the disease at its broadest and do so earlier in its course. They developed four categories of symptoms. They retained 'the big two': ocular-motor dysfunction and

postural instability. In a novel move they added akinesia (loss or impairment of voluntary control) and cognitive decline. The severity of each symptom dictated the level of diagnostic certainty 1-3; one being most indicative of PSP.

The MDS – Clinical Diagnosis of PSP, now comprise patients with possible PSP-SL (oculomotor dysfunction + nonfluent/agrammatic variant of primary progressive aphasia) or PSP-CBS (oculomotor dysfunction + corticobasal syndrome). These criteria permit the synthesis of research findings and clinical presentation, providing insight to the underlying pathology at a molecular level allied to the outward appearance. The diagnostic category of "probable 4 repeat tauopathy" symbolizes a new move in clinical and neuropathological diagnosis.

Thus, the putative natural history of PSP was defined to begin with a pre-symptomatic phase, during which the neuropathological hallmarks are insidiously accumulating with no overt clinical features. As this increase, the subject enters the suggestive-of-PSP phase, developing mild or isolated symptoms. At this stage they are not on the radar of the full MDS research criteria for a possible or probable PSP syndrome which will eventually be manifested. Ultimately and irreversibly they enter a fully symptomatic stage that, in the majority, would meet the research criteria for Classical/Richardson-Steele (PSP-RS) or a clinical variant of PSP (Boxer et al., 2017). Patients arrested in a limbo at the pre-PSP-RS stage may remain there until death, clinging to a variant of PSP phenotype presentation defying formal full diagnosis until post-mortem pathological assessment (Respondek et al., 2013). It is promising to see that most recently, Takigawa and colleagues (2016) addressed the increasing prevalence of PSP in Yonago City, Japan and concluded it to be due in part to an aging population, since prevalence is age related (Daniel *et al*., 1995) but it must also be seen as a success for the expansion of the criteria of inclusion to atypical PSP-phenotypes as well as increased knowledge and recognition of the condition in the earlier phase. The Japanese study is an excellent exemplar of how the increasing depth and breadth of knowledge of PSP from research is informing better results on the ground. As more cases are detected this in turn informs the global knowledge and will, it is hoped, improve matters for the patients in time.

Where the line may be drawn in terms of establishing and labelling new clinical syndromes against acknowledging overlap and points on a continuum is an ongoing discussion. Moreover, there is an element of making arbitrary and artificial distinctions if the subtypes of PSP share comparable clinical and biochemical outcomes in real terms. What difference does it make? Williams and Lees suggested in 2009 that the unique process of tau accumulation topographically and chronologically leads to different clinical phenomena in each subject at early PSP stages but then ultimately demonstrates convergence to a more homogenous clinical picture when the brain becomes more saturated with tau. Early detection of PSP is not just of academic interest for

longitudinal study, it will help enrol patients in clinical trials and offer extended support to them and their families. The uncommon presentation of common diseases remains common, so atypical appearances of PSP continue to confound universal operational criteria for clinical diagnosis (Respondek et al., 2014). The significance of an accurate diagnosis will inevitably increase, and the need for a sensitive diagnosis become vital as the field moves from academic classification and embraces treatment with bespoke disease-modifying therapies. The case for accurate clinico-pathological correlation pre-mortem has never been stronger.

1.6 Familial PSP

Whilst PSP is predominantly a sporadic disease, there have been familial forms recognized; with reports of families who do carry *MAPT* mutations (Ogaki et al., 2013). In many of the familial cases PSP was confirmed at autopsy (Rojo et al., 1999; Tetrud et al., 1996; Tuite et al., 2005). To date, no common genetic origin has been identified for the familial cases although, in 2005, one of the families presenting with an autosomal dominant PSP did demonstrate a significant linkage to chromosome 1 on genetic analysis which is explained below (Ros et al., 2005). Two of the case-control studies reported commonalities in a family history of dementia and parkinsonism but no significant correlations have emerged (Davis et al., 1988; Golbe et al., 1996).

Continental studies following up probands (index cases) for PSP have been running for the past two decades. A paper in 1999 reported on studies from Europe and North America in which 12 subjects and 22 secondary cases, all meeting typical clinical PSP criteria, were followed (Rojo et al., 1999). The presentation pattern in familial PSP was described as demonstrating “autosomal dominant inheritance with reduced penetrance” which was significant in suggesting PSP as a hereditary disorder. Given the late age at onset, it is one that will become more apparent in ageing populations, and easier to trace if not to treat. However, familial PSP is rare, much more so than its sporadic counterpart. Moreover, the array of confounding factors mentioned above in the presence of atypical presentations and varied phenotypes makes it a more complex matter.

Nonetheless, where familial PSP can be isolated, it offers great research potential and at the dawn of the 21st century familial clustering of PSP totalled 20 kindreds (Piccini et al., 2001). More recently Fujioka and colleagues reviewed post-mortem and medical records of 375 confirmed PSP cases and excluded those positive for the *MAPT* mutation. A positive family history of PSP was reported in 3% of the cases which increased to 15% if a history of PSP, parkinsonism or dementia was recorded (Fujioka et al., 2013). The following year Fujioka and colleagues (2014) found 59 affected PSP patients from 19 published PSP families with no known gene mutations in the literature (Fujioka et al., 2014). The retrospective study findings of Fujioka correlate with the

questionnaire- based study from 2009 of Donker Kaat and colleagues. They unearthed exactly a third of the patients with PSP reported at least one first-degree relative who had displayed signs or carried a diagnosis of dementia or parkinsonism. A considerable 7% of PSP subjects met criteria for an autosomal dominant mode of transmission offering further support to the body of work for familial PSP.

Other studies similarly reported an observed autosomal dominant inheritance in familial PSP cases (Brown et al., 1993). In the Brown study the three subjects (two generations and a cousin) initially presented with depression and personality change before progressing onto PSP. Later reports identified a family of five siblings with clinical PSP – two which were confirmed pathologically (Tuite et al., 2005). As mentioned above, it is the atypical presentations (even within family members) that may confound accurate analysis. Yebens and colleagues (1995) described siblings presenting with PSP; one presented typically while others had atypical syndromes including one who met the criteria and was treated for PD with levodopa to which he responded for some years. Clinically, the familial PSP cases did not record many instances of the definitive supranuclear ophthalmoparesis. Nor was there any linkage to the *MAPT* gene identified in any of these families.

1.6.1 Identification of familial PSP loci by linkage analysis

Whilst an autosomal dominant pattern of transmission with reduced penetrance is the consensus as most likely in PSP (Rojo et al., 1999), in other families a pattern consistent with autosomal recessive inheritance is displayed. This was partly due to the work done in 1997 by Conrad and colleagues who reported a dinucleotide repeat polymorphism in intron 9 of *MAPT*; a finding that has been reproduced, albeit in small series, in Caucasian samples. (Conrad et al., 1997; Morris et al., 1999). The alleles found at this locus carry between 11 and 15 repeats; A1 to A4 contain 12 to 15 repeats respectively. Subjects with the homozygous tau A0 allele, with 11 repeats was shown to have a frequency of over 90% in patients with PSP and about 70% in controls. It was thought that the marker was in linkage disequilibrium (LD) with an undefined mutation within *MAPT* or it was possible that *MAPT* dinucleotide polymorphism itself, perhaps through altered tau gene expression was responsible for increasing the risk of developing PSP (Stanford et al., 2000). Higgins and colleagues (1998) and Hoenicka and colleagues (1999) both suggested PSP could be recessively inherited while being linked to *MAPT*. This was due to this over-representation of *MAPT* A0 allele as well as the A0/A0 genotype in asymptomatic relatives of PSP subjects. Thus, they postulated the *MAPT* polymorphism to be in LD with the PSP locus on a recessive inheritance model but Rojo and colleagues (1999) similarly reported the inheritance of the A0 polymorphism by affected and unaffected individuals in two pedigrees with familial PSP but failed

to show linkage to chromosome 17. However, across *MAPT*, eight common SNPs were identified in complete LD with each other and the A0 allele. These polymorphisms have been shown to be inherited as part of H1 and H2, across the entire *MAPT* gene (Baker et al. 1999). The alleles A0, A1 and A2 are in H1; H2 contains A3 and A4. These are not specific to PSP because of the link previously established between A0 and H1 in CBD (Houlden et al., 2001). A possible conclusion of this is that PSP is aetiologically heterogeneous; there may be multiple genetic species of the disease.

At the turn of the century, the first genome-wide linkage study to be conducted in a large PSP family yielded a first locus for autosomal dominant PSP (Ros et al., 2005). Within this family, one member had neuropathologically confirmed PSP, three others had clinically identical symptoms and at least five ancestors were reported to have presented similarly. Studies on this family in Spain was defined not only by clinical symptoms but also by using the results of ^{18}F fluorodopa and ^{18}F-deoxyglucose positron emission tomography studies which highlighted the long arm of chromosome 1q31.1. Haplotype analysis around a chromosomal region with a maximum multipoint logarithm of the odds (LOD) score identified a 3.4 cM candidate disease locus between markers D1S238 and D1S2823 on this chromosome and in that locus at least three genes with as yet unknown relevance to PSP were identified: *DBCCR1-like*, *ENSGOOOOO1815167* and *ENSG00000162670.* The *DBCR1* gene is expressed in some cancers and largely in the brain, as is *ENSG00000162670*. Currently little else is known about these suggested genes. The locus highlighted in this familial form of PSP has not been previously associated with PSP or any other related neurodegenerative disorder.

1.6.2 *Familial MAPT mutations found in PSP*

Mutations in the *MAPT* gene are only occasionally associated with familial PSP (Table 1). Of the ten known *MAPT* mutations associated with familial PSP, nine of these were located within the tau microtubule-binding repeat domain (MTBR). The outlying mutation has been identified on exon 1 (Borroni et al., 2011) (Figure 3).

In 2000, Stanford and colleagues highlighted a new silent mutation (S305S) in *MAPT* located in exon 10, forming part of a stem loop structure from the 5′ splice donor site. This mutation had been detected in two sisters, they had presented differently and only one with confirmed PSP. This mutation does not give rise to a change in the amino acid sequence of tau but, functional exon trapping experiments did reveal that by inducing a 4.8-fold increase in exon 10 splicing, there was a resultant 4R-tau, leading to the discovery of the first molecular lesion implicated in PSP.

A further mutation in the MTBR was detected in studies of a familial atypical PSP: two siblings from a consanguineous marriage. Analysis in one sibling showed a homozygous deletion of codon 296 (delN296) in exon 10 of *MAPT*, which increased exon 10 inclusion (Pastor et al., 2001). This deletion is in the sequence that corresponds to the tubulin-binding repeat of tau. A further report identified this mutation in a 39-year-old male presenting with postural instability and falls. His pedigree represented an autosomal dominant pattern (Rossi et al., 2004). In both observed studies the homozygous state produced the worse phenotype, whereas heterozygosity produced a milder condition more akin to PD with reduced penetrance also demonstrating a response to levodopa.

A third mutation, identified in 2005 by Ros and colleagues, was from studies of one family with early-onset autosomal dominant PSP. Here the G303V mutation of *MAPT* was identified in the 4 probands confirmed with pathology and their other relations. Neuropathology revealed characteristic hyperphosphorylated tau protein and an increased 4R:3R ratio of the isoforms. Specifically, this was associated with overexpression of 4R tau and aggregated tau. At the time of the report three further members of the family were positive for the mutation but asymptomatic, however they were all younger than the average age at onset. Such penetrance produced the conclusion that the G303V mutation is associated with autosomal dominant PSP.

The fourth mutation – IVS10+3G>A – is associated with multiple system tauopathy and presenile dementia. This mutation is associated with an amino acid change: G-to-A transition in the intron after exon 10, which may lead to increased use of the 5' splice site and account for the elevated 4R tau levels. The most commonly associated presentation is behavioural variant frontotemporal dementia with parkinsonian features. However, two individuals presented with atypical PSP (Spillantini et al., 1997; Spina et al., 2008), with dizziness, pressure headaches and postural imbalance. At post-mortem all cases demonstrated 4R deposits. The same mutation was also identified in 2014 in an Italian-Polish family. The pedigree displayed 25 members over four generations with six affected individuals (Wierza-Bobrowicz et al., 2014). DNA obtained from two affected siblings, brother and sister: both were mutation carriers. The primary presentation here had been a dementia syndrome plus a movement disorder with a compounding cardiovascular disorder.

In 2002 two pathogenic variants within exon 1 were found: pArg5His (Hyayshi et al., 2002) and pArg5Leu (Poorkaj et al., 2002). It is unknown as yet whether the former is hereditary. This missense R5L mutation was shown to lead to both neuronal and glial pathology and generate a PSP-like phenotype (Poorkaj et al., 2002). Unlike its neighbouring R5H mutation which was associated with prominent glial tau deposits (Hayashi et al., 2002). The mutations all discussed

above were familial, which accounts for a very small proportion overall of PSP cases. The R5L mutation was the first *MAPT* mutation found in sporadic PSP. Neuropathology examination revealed globose NFTs, neutrophil threads and tufted astrocytes in the basal ganglia and brainstem (Poorkaj et al., 2002). Insoluble aggregates from the sub-cortex were shown to have a predominance for 4R tau, pointing to PSP. Crucially, while the p.R5L allele of *MAPT* was shown to alter tau involvement in microtubule assembly, there has been no association with the ratio of tau isoform. Moreover, it is the only pathogenetic variation reported at the amino terminal end.

Mutation	Genomic region	Major aggregated tau isoforms	References
R5H	Exon 1	1N3R, 0N4R, 1N4R	Hayashi et al., 2002
R5L	Exon 1	1N3R, 0N4R, 1N4R	Poorkaj et al., 2002; Combs et al., 2012; Chang et al., 2008
G55R	Exon 2	Unknown	Iyer et al., 2013
A152T	Exon 7	All six isoforms§	Coppola et al., 2012; Silva et al., 2016; Kara et al., 2012
K257T	Exon 9	All six isoforms or 3R isoforms	Rizzini et al., 2000; Grover et al., 2003; Pickering-Brown et al., 2000
I260V	Exon 9	4R isoforms	Grover et al., 2003
L266V	Exon 9	ON3R + 4R isoforms	Hogg et al., 2003; Koboyashi et al., 2003
G272V	Exon 9	3R isoforms	Combs and Gamblin, 2012; Barghorn et al., 2000; Bronner et al., 2005
N279K	Exon 10	0N4R, 1N4R	D'Souza et al., 1999; Barghorn et al., 2000; Hasegawa et al., 1998; Wren et al., 2015; Hong et al., 1998
Δ280K	Exon 10	0N3R, 1N3R	Van-Swieten et al., 2007; D'Souza et al., 1999; Barghorn et al., 2000; Goedert et al., 1999; Rizzu et al., 1999; Von Bergen et al., 2001
S285R	Exon 10	Unknown	Ogaki et al., 2013
Δ296N	Exon 10	Unknown	Combs and Gamblin, 2012; Yoshida et al., 2002; Grover et al., 2002
N296H	Exon 10	4R isoforms	Yoshida et al., 2002; Grover et al., 2002
K298E	Exon 10	Unknown	Iovino et al., 2014
P301L	Exon 10	4R isoforms	Hutton et al., 1998; D'Souza et al., 1999; Combs et al., 2012; Barghorn et al., 2000
P301S	Exon 10	4R isoforms	Goedert et al., 1999; Iovino et al., 2014; Elbaum-garfinkle et al., 2014; Brandt et al., 2005; Bugiani et al., 1999
P301T	Exon 10	Unknown	Lllado et al., 2007
G303V	Exon 10	4R isoforms	Combs and Gamblin, 2012; Ros et al., 2005
S305I	Exon 10	0N4R, 1N4R	Kovaks et al., 2008

S305N	Exon 10	Unknown	Hasegawa et al., 1998; Iijima et al., 1999
L315R	Exon 11	1N3R, 2N3R, 4R isoforms	Combs et al., 2012; Van Herpen et al., 2003
K317M	Exon 11	Unknown	Zarranz et al., 2005
K317N	Exon 11	4R isoforoms	Tacik et al., 2015
S320F	Exon 11	1N3R, 2N3R, 0N4R, 1N4R	Combs and Gamblin2012; Rosso et al., 2002
P332S	Exon 11	All isoforoms	Elbaum-garfinkle et al., 2014; Deramecourt et al., 2012
G335S	Exon 11	Unknown	Spina et al., 2008
G335V	Exon 11	Unknown	Spina et al., 2008; Neumann et al., 2005
Q336H	Exon 11	1N3R, 2N3R	Tacik et al., 2015
Q336R	Exon 11	Unknown	Pickering-Brown et al., 2004; Tacik et al., 2015
V337M	Exon 12	All isoforms	Combs and Gamblin 2012; Nacharaju et al., 1999; Dayanandan et al., 1999; Deture et al., 2000; Spillantini et al., 1996
E342V	Exon 12	0N3R, All 4R isoforms	Combs and Gamblin2012; Brandt et al., 2005; Lippa et al., 2000
S352L	Exon 12	Unknown	Combs and Gamblin2012; Nicholl et al., 2003
S356T	Exon 12	Unknown	Momeni et al., 2010
P364S	Exon 12	Unknown	Rossi et al., 2012; Popovic et al., 2014
G366R	Exon 12	Unknown	Rossi et al., 2012
K369I	Exon 12	All isoforms	Combs and Gamblin2012; Neumann et al., 2001
E372G	Exon 13	Unknown	Tacik et al.,2017
G389R (G-- > A)	Exon 13	0N3R, 0N4R, 1N3R, 1N4R	Combs et al., 2012; Pickering-Brown et al., 2000; Ghetti et al., 2000
G389R (G-- > C)	Exon 13	0N3R, 1N3R, 0N4R, 1N4R	Combs and Gamblin 2012; Ghetti et al., 2000; Murrell et al., 1999
R406W	Exon 13	All isoforms	Chang et al.,2008; Hong et al.,1998; Hasegawa et al., 1998; Dayanandan et al., 1999
N410H	Exon 13	Unknown	Kouri et al.,2014

Table 1. **Summary of the reported exonic MAPT mutations to date**. Mutations in *MAPT* generally alter the relative production of the tau isoforms and lead to changes in MT assembly, MT binding and/or the propensity of tau to aggregate (Adapted from Strang et al., 2019).

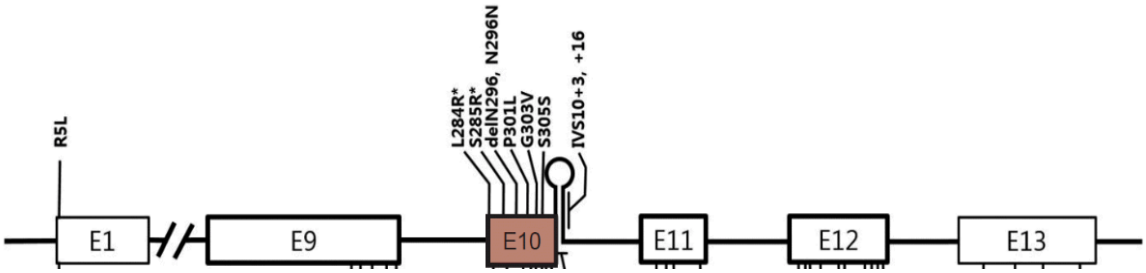

Figure 3**. A schematic diagram showing exons of *MAPT* and locations of mutations**. Mutations discovered in patients with PSP or PSP-like phenotypes are marked in the upper half of the diagram. E9 to E11 refer to number of exons within the *MAPT* gene. Note all mutations except pArg5Leu are located in exon 10 or in stem-loop structure at the boundary between exon 10 and the intron following exon 10 (Im et al., 2015).

Because prevalence is not high, where the generational penetrance of a PSP gene is low, or there is the possibility of the disease developing by combined action of multiple genes then a familial predilection could be masked (Tolosa et al., 1994). The focus of the body of PSP genetics to date has considered the common mutations in large populations or rarer ones with high penetrance in smaller family cohorts. The field is currently expanding to encompass those rarer variants without high penetrance which might offer greater insight into PSP. The Familial PSP Study ("FamPSP") has begun enrolling PSP subjects with a first-degree blood relative with a neurological or psychiatric disorder as well as PSP patients with first degree healthy blood relatives (Jabbari et al., 2019). This study aims to identify rare variants associated with PSP and also CBD. It is hoped that by tracking and delving deeper into the gene(s) implicated in familial PSP the pathophysiology and neurodegenerative mechanisms can be more explicitly characterized and by extension assist research into the genetic mutations responsible for sporadic disease.

Having provided some of the historical and clinical context for PSP, it is important to explore deeper into its aetiology by discussing *MAPT*, the gene which has been identified as the primary risk factor.

1.7 Tau protein: the molecular structure

The single human tau gene *MAPT* is located over 100 kb on the long arm of chromosome 17 at band position 17q21.1, which contains 16 exons (Neve et al., 1986; Andreadis et al., 1995). It produces three transcripts of 2, 6 and 9 kb which are differentially expressed, depending upon stage of neuronal type and maturation (Goedert et al., 1989; Nunez and Fischer., 1997; Wang et

al., 1993). The use of two alternative polyadenylation sites gives rise to axonal tau which is encoded by the 6 kb mRNA while the 2 kb *MAPT* mRNA produces nuclear tau (Wang et al., 1993) and the 9kb transcript is very specific to the retina and peripheral nervous system (Nunez and Fischer., 1997).

MAPT spans more than 130 kb. Exons 2, 3, 4A, 6, 8, and 10 can be alternatively spliced while exons 1, 4, 5, 7, 9, 11, 12, and 13 are constitutive exons (Goedert et al., 1989; Figure 4). Analysis of the human genome has revealed that almost all human genes undergo alternative splicing (Pan et al.,2008) and this is the primary contributor to proteomic complexity, as well as playing a vital role in controlling cell differentiation and development (Stamm et al.,2005). 'Vital' is not an overstatement: the mis-regulation of alternative splicing has been shown to be the cause of many life-threatening diseases (Tazi et al., 2009).

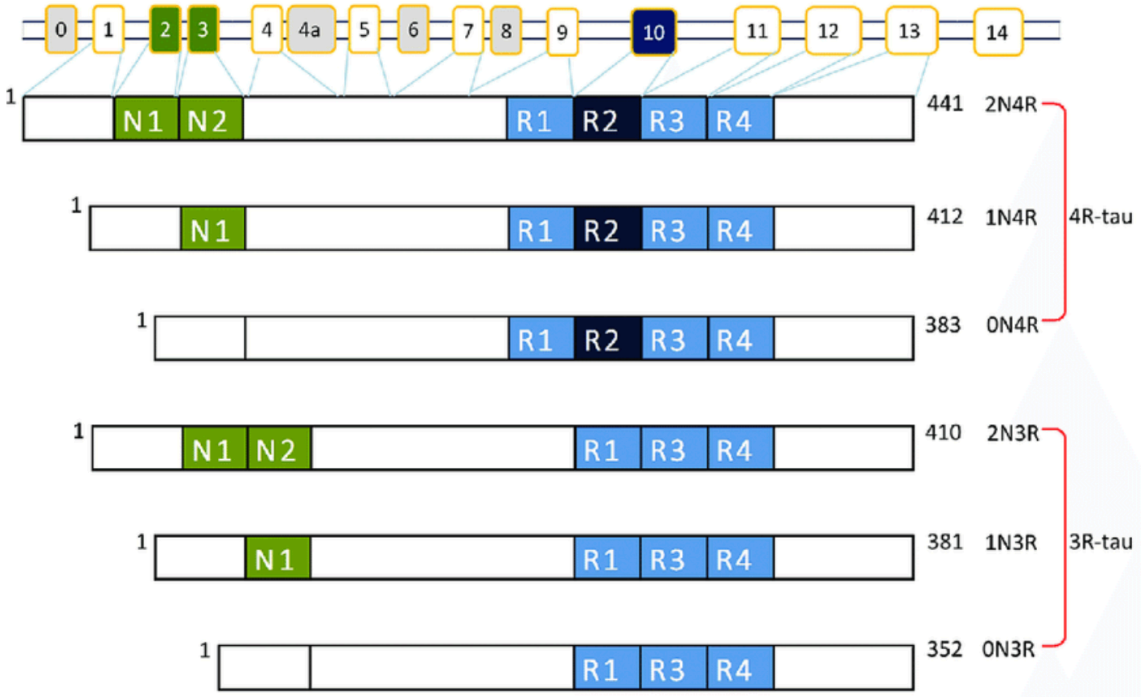

Figure 4. ***The alternative splicing processes of the MAPT gene and the resulting tau isoforms***. Alternative mRNA splicing of exon 2 (green), exon 3 (green), and exon 10 (navy) gives rise to six tau isoforms (352-441 amino acids). The constitutively spliced exons (1,4, 5, 7, 9, 11, 12, 13) are indicated in white. Exon 0 is part of the promoter, and exon 14 is noncoding. Exons 6 and 8 (grey) are not transcribed in human brain. Exon 4a (grey) is only expressed in the peripheral nervous system. The repeats of tau (R1-R4) are shown, with three isoforms having four repeats each (4R) and three isoforms having three repeats each (3R). Each repeat is 31 or 32 amino acids in length (Adapted from Wu et al., 2017).

MAPT has a GC-rich 5' untranslated region at its start encoded by a single transcribed but untranslated exon -1 while the start codon is located in exon 1 (Andreadis et sl., 1992). Exon -1 and the adjacent intron is responsible for promoter activity, with consensus binding sites for adaptor protein 2, synaptic protein 11, GC rich sequence DNA binding factor (GCF) (Andreadis et al., 1996; Sadot et al., 1996) and many other transcription factors. This promoter region is thought to be responsible for specific expression of tau in neurons since the promoter activity increases with differentiation, specifically during neurite initiation and outgrowth (Drubin et al., 1985; Ferreira et al., 1989; Brion et al.,1994; Smith et al.,1995; Heicklen-Klein et al.,2000). *MAPT* mRNA contains exon 14 but is not translated since it is part of the 3'untranslated region of tau mRNA (Andreadis et al., 1992; Goedert et al., 1989; Sawa et al., 1994). Meanwhile three other exons: exons 4A, 6, and 8 have been shown to be present in the *MAPT* mRNA of peripheral tissues (with inclusion of exon 4A resulting in the expression of 'big tau' in the peripheral nervous system) but are not transcribed in the human brain. Exon 8 is alternatively spliced and found in striated muscle, spinal cord and pituitary gland (Castle et al., 2008). Cryptic splicing sites are described in exon 6 that generate *MAPT* mRNA lacking the remaining 3' exon cassettes (Wei and Adreadis., 1998). These are found in muscle and spinal cord, but the presence of the protein remains to be determined. In the adult brain, six isoforms of tau are produced due to alternative splicing of exons: exons 2,3, and 10.

Both exons 2 and 3 undergo coupled splicing and it has been shown that exon 3 never appears independent from exon 2 and is entirely dependent upon exon 2 inclusion and is regulated by a weak branch point and a combination of exonic enhancers and silencers (Arikan et al. 2002). Splicing within the exon 2 and 3 gives rise to three isoforms: 0N (neither included), 1N (exon 2 included), or 2N (both exons 2 and 3 included). Alternative splicing of exon 10 results in tau with three or four microtubule binding repeats in the microtubule binding domain. While 0N3R tau is the predominant isoform in the foetal brain (Kosik et al., 1989) the overall ratio of 3R and 4R tau isoforms is roughly equal in the adult brain (Arendt et al., 2016; Goedert et al., 1989), although this ratio can differ in given brain regions (Majounie et al., 2013). 0N and 1N tau isoforms comprise 37% and 54% of total human brain tau, respectively, while 2N tau makes up only 9% of total tau isoforms (Goedert et al., 1990). These isoforms are thought to adopt different secondary structures, with each isoform possessing distinct regions of influence over microtubule binding. Physiologically, the tau protein is natively unfolded and intrinsically disordered with a low content of secondary structures (Avila et al., 2016). "It means that, as probed by different techniques including circular dichroism (CD), Fourier transform infrared spectroscopy (FTIR), X ray diffraction, fluorescence, and some other methods, this protein behaves as a kind of random coil, lacking a well-defined secondary structure" (Avila et al., 2016). The secondary structures that do exist include two types of helical structures: the α-helices (formed by residues 114–123 and 428–437) and the poly-proline II helices (formed by residues 175–184, 216–223, and 232–239).

Furthermore, tau has also been shown to fold with a high propensity into beta-strands. These hints of secondary structure are largely transient. The assembly of tau into microtubules is dependent on both the accessibility of specific peptide sequences in the beta sheet structures and an electrostatic charge compensation of the basic residues of tau (Sapir et al., 2012).

1.8 *Domains of Tau protein*

Overall, tau is basic, although the N-terminal is acidic up to residue 120. This acidic N-terminal projection domain features two inserts of 29 residues each encoded by exons 2 and 3 of the *MAPT* that interact with the plasma membrane, dynactin and tyrosine kinase fyn (Lee., 2005; Lebouvier et al., 2009; Pooler and Hanger., 2010). Tau regulates the motility of dynein and kinesin motor proteins through an isoform-dependant mechanism (Dixit et al., 2008). Dixit and colleagues were able to show that the shorter tau isoforms (such as 0N3R) more effectively impede the motility of both kinesin and dynein whereas the longer isoforms do not seem to have as much an effect on motor protein motility. Thus, the axonal transport of vesicles may be finely tuned by the ratio of tau isoforms expressed. The N-terminal projection domain also interacts with specific membrane proteins such as apolipoprotein A1 (preferentially binding tau which include exons 2 and 3) and also synaptophysin (preferentially binding tau in the absence of the exons 2 and 3) (Liu C. et al., 2016). Transcription factors have also been shown to interact with tau whereby the nuclear factor erythroid 2–related factor 2 (NRF2), a transcription factor involved in antioxidant response has been shown to bind to the first intron of *MAPT* enabling the inclusion of exon 3 (Wang et al.,2016).

The proline residue-rich mid region (150–240), contains serine-proline or threonine-proline motifs, which present targets for proline-directed kinases (Figure 4). Furthermore, this mid-region holds seven proline-X-X-proline motifs, these form binding sites for proteins with SH3 domains such as the phospholipase C-gamma 1 or the p85 alpha subunit of the phosphatidylinositol 3-kinase suggesting that tau can function as a scaffold protein in signalling pathways (Zabik et al., 2017; Reynolds et al., 2008). As this proline-rich tau domain harbours multiple phosphorylation sites, it has been suggested that phosphorylation might play a role in signalling by modulating its binding to the target proteins.

The N-terminal region plus the proline-rich domain is referred to jointly as the projection domain; under electron microscopy a filamentous ‘arm’ is seen projecting from the microtubular wall since the projection domain angles out to the acidic microtubule surface. This is an unstructured and acidic region which detaches from the microtubule surfaces (Hirokawa et al., 1988) to interact with the membranes or cytoskeletal proteins of adjacent cells (Brandt et al., 1995). The projection

domain can bind neurofilaments, plasma membranes or other microtubules. This array of potential binding partners suggests tau functions to integrate microtubules with other structures within the cytoplasm.

The four microtubule-binding repeat domains (MTBRs) in the C-terminal half of tau are encoded by exons 9-12. This binding domain subdivides into a basic tubulin-binding region at one end and an acidic C-terminal region at the other (Gustke et al., 1994). The overall basic C-terminal half, modulated by exon 10, has either three or four microtubule binding motifs (which alter tau affinity for microtubules) hence its basic and proline-rich flanking domains to facilitate for tight binding. Furthermore, the 3R isoforms depend on a C-terminal sequence to complement its binding, whereas the 4R isoforms depend solely on the repeat domains (Goode et al., 2000). Recorded differences between 3R and 4R isoforms, as well as altering microtubule stability, include 3R species decreasing taxol affinity for microtubules either by competition or alteration of microtubule structure (Park et al., 2008); the ability of 3R tau to reduce heparin-induced 4R tau polymerisation, potentially signifying a role for 3R tau in the prevention of aggregation (Adams et al., 2010); and differences in the shapes of fibrils of these isoforms, with 4R tau forming longer, less twisted fibrils, potentially more apt for tangle formation (Furukawa et al., 2011). Each of these differences was found to be independent of the presence or absence of N-terminal inserts.

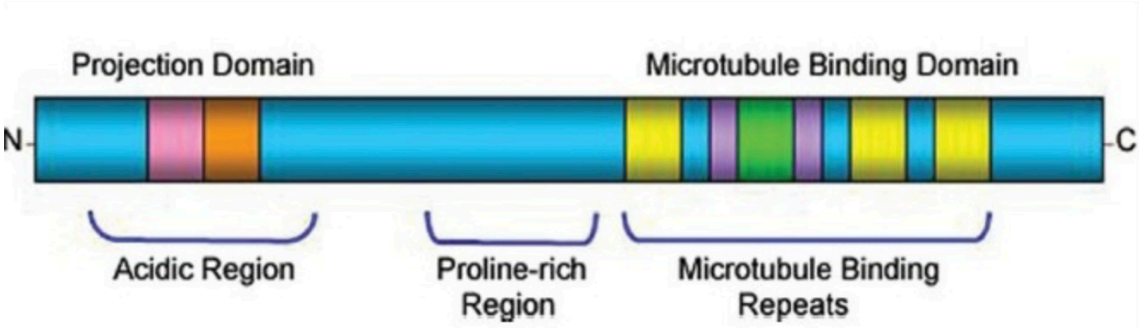

Figure 4. ***Schematic representation of the various domains of tau.*** The highly acidic N-terminal projection domain is followed by the proline-rich region and subsequently the C-term microtubule binding domain which polymerises and stabilises the microtubules (Aswathy et al., 2010).

In vitro, it has further been shown that tau with 4 microtubule-binding repeats more effectively binds to and better stabilizes microtubules compared to 3R-tau (Gustke et al., 1994; Tint et al., 1998). The rationale for better interaction from the 4R-isoforms can be discerned from both the pro-aggregation motifs outlined below (Panda et al., 2003). For tau aggregation, the two hexapeptides at the beginning of the second and third repeats: the PHF6*and PHF6 are crucial; of these PHF6* is located in the second repeat that discriminates 3R-tau from 4R-tau (von Bergen

et a., 2001). Thus, the inter-repeat region of R1 and R2 in the microtubule binding domain represents a unique microtubule-binding site which possesses double the binding affinity of any one individual repeat (Goode and Feinstein., 1994).Four-repeat tau (4R-tau) has been shown not only to bind microtubules with a greater affinity, but also act as a preferential antagonist, displacing 3R-tau from microtubules *in situ* (Lu and Kosik., 2001). Furthermore 4R-tau has also been shown to suppress the rate and extent of MT shortening while 3R-tau demonstrated little or no detectable effect. (Panda et al., 2003). Moreover, the C-terminal sequences around the core binding unit in 3R-tau strongly enhance its microtubule binding affinity (Goode et al., 2000). From the differences observed between the interplay of 3R- and 4R-tau isoforms it is possible to see the significance of alterations in the 4R:3R tau ratio resulting from the above-mentioned mutations.

Furthermore, the secondary structure of tau has been shown to crucially depend on the C-terminus folding over two regions: the proline rich microtubule binding domain and the N-terminal projection domain thereby forming a paperclip conformation. This conformation depends upon the number of microtubules binding to the MTBR of tau and also the phosphorylation of specific sites within tau (Jeganathan.,2006). Pseudo phosphorylation at the Ser_{202} makes the N-terminal region away from the C-terminal. On the other hand, pseudo phosphorylation at the $Ser_{396\text{-}404}$ site decreases the interaction of C-terminal region with the MTBR (Jeganathan et al., 2008). Thus, phosphorylation at different sites of the tau molecule could have different consequences for tau conformations and function. Notably, this association between the N-terminus and the C-terminus of tau is reduced upon tau binding to microtubules (Rapoport et al., 2002) and the conformation is readily disrupted by proline-directed tau phosphorylation which variably results in loosening and tightening of the paperclip structure (Leory et al., 2002).

Tau also interacts with tyrosine kinase c-Abl via the polyproline clusters located on the proline-rich mid region of tau (Lebouvier et al., 2009). Recent studies have also suggested a role for c-Abl in NFT formation by direct phosphorylation of tau (Derkinderen et al., 2005). Moreover, c-Abl may also induce tau phosphorylation indirectly through activation of its downstream targets, cyclin dependant kinase 5 (cdk5) and glycogen synthase kinase 3 beta (GSK-3β), which have been shown to phosphorylate tau (Hanger et al., 1992; Ishiguro et al., 1992; Lovestone et al., 1994; Michel et al., 1998; Patrick et al., 1999; Imahori and Uchida, 1997).

In tau, these C-terminal repeat sequences are highly conserved and demonstrate strong similarity to microtubule binding repeats seen in other microtubule associated proteins (Goedert et al., 1989; Friedhoff and Mandelkow., 1998). Within each of the three or four repeats are 18 very highly conserved amino acids, the other 13-14 amino acids being considered merely spacers (Butner and Kirschner 1991). However, as only 3R tau is observed in the human foetal brain a number of

factors must be involved in regulating the shift from 0N3R in foetal brain to a 1:1 ratio of 3R/4R in adult brain. Moreover, the mutations discussed so far in PSP have had the primary effect either of disrupting tau microtubule interactions or of affecting exon 10 splicing and therefore the ratio of 3R:4R tau protein. It is important to thereby to identify and understand these tau protein isoforms and/or the factors that regulate the splicing of exon 10 which may hold clues to unravelling the dysregulation of tau splicing seen in PSP.

1.9 Exon 10 splicing

Alternative splicing increases the diversity of the proteome as multiple isoforms and functionalities of a protein are expressed from a single gene. As with tau, fine regulation of alternative splicing is very important as seen with the shift from 0N3R in fetal brain to a 1:1 ratio of 3R/4R in adult brain. Then, we also have the alternative splicing of non-CNS exons for example, exon 4A in peripheral neurons that results in big tau which is needed in the higher caliber axons of PNS neurons.

Splicing is catalyzed by the spliceosome, a macromolecular machine consisting of five small nuclear RNA (snRNA) molecules (U1, U2, U4, U5 and U6 snRNA) and as much as 150 proteins (Hartmuth et al., 2002; Jurica et al., 2003). Each of the five snRNAs assembles with proteins to form small nuclear ribonucleoprotein particles (snRNP). A coordinated binding of the five snRNP to pre-mRNA results in the removal of each intron and the ligation of the flanking exons (Will et al., 2011). Alternative splicing is controlled by multiple exonic and intronic cis-elements and trans-acting splicing factors. The element in an exon that increases inclusion of the alternatively spliced exon is called exonic splicing enhancer (ESE), and that decreases inclusion is called exonic splicing silencer (ESS). The element with similar function located in an intron is called intronic splicing enhancer (ISE) or intronic splicing silencer (ISS).

Exon 10 in particular is flanked by an abnormally large intron 9 and has a weak 5’ and 3’ splice site, which can be acted upon by these *cis*-elements and *trans*-acting factors (D’Souza and Schellenberg., 2000). The 5' end of *MAPT* exon 10 contains three ESEs: a SC35-like enhancer, a polypurine enhancer (PPE), and an A/C-rich enhancer (ACE) (Kondo et al., 2004). Following the ESE region, there is an ESS (Figure 5). In addition, the 3' end of exon 10 contains another ESE sequence between the ESS and the 5' splice site. Sequences located at the end of exon 10 and at the beginning of the intron following exon 10 inhibit the splicing of exon 10, probably because of the presence of a stem-loop structure that limits access of the splicing machinery to the 5’-splice sites (Hutton et al., 1998; Spillantini et al., 1998). These include bipartite elements composed of the ISS and the intronic splicing modulator (ISM). Deletion assays revealed opposite effects of the ISS and ISM on exon 10 splicing (D’Souza and Schellenberg., 2000). The ISM is

not an enhancer by itself, but functions only in the presence of the ISS and counteracts ISS-mediated inhibition of the 5' splice site. Disruption of the stem loop leads to increased binding by the snRNP and higher levels of exon 10 inclusion and thereby increased 4R-tau expression (D'Souza and Schellenberg., 2000). Thus, mutations within specific *cis*-elements can promote or suppress inclusion of this exon, while mutations specifically within the stem loop tend to promote exon 10 inclusion.

1.10 Primary functions of Tau

Tau protein is known to be expressed in adult central and peripheral nervous systems. To a lesser extent it is expressed in the kidney, lung, and testis (Gu et al., 1996). It is most abundant in neuronal axons (Lee et al., 2001; Trojanowski et al., 1989) but has been isolated in neuronal somatodendritic compartments (Tashiro et al., 1997) as well as in oligodendrocytes and astrocytes (Klein et al., 2002).

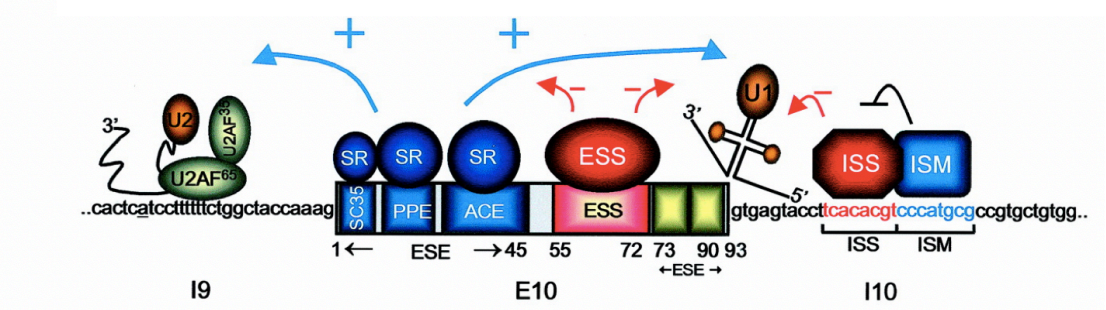

Figure 5. **Model for *MAPT* exon 10 splicing regulation.** Three ESE elements are found in exon 10 of which one includes the SC35-like, PPE, and ACE elements. An 18-nucleotide ESS sequence is located between the 5′ end of E10 and the second and third ESE elements at the 3′ end of E10. The bipartite regulatory ISS and ISM element are located in intron 10 (Souza and Schellenberg., 2002).

Natively, healthy tau is involved in microtubule stabilization and the growth of neurons (Weingarten et al., 1975). Tau accounts for more than two-thirds of the overall MAPs in the vertebrate nervous system (Nunez., 1988). It is essential for the initiation and elongation stages of microtubule assembly as well as their stabilization (Witman et al., 1976). Most synapses are distant from the cell body- the major site of protein synthesis- and therefore rely on an efficient transport system. In neurons, the traffic system consists of microtubules and microfilaments along which cargos can be moved (Hollenbeck and Saxton., 2005; Baas et al., 2006). The nucleation of tubulin is the starting point for microtubule initiation; tau is the promoter of this stage. Then, once tau binds tubulin, the elongation and stabilization take place. The most popularly reported putative method of binding is extra-protofilamental i.e. longitudinally (Al-Bassam et al., 2002).

Longitudinal binding is considered to perform a 'molecular glue'-like function averting disintegration by cross-stabilizing the lateral bonds within tubulin dimers, further stiffening the protofilament. There is an alternative proposition of lateral intra-microtubular binding from the work of Kar and colleagues in which kinesin binding was the stabilizing force (Kar et al., 2003). This is not without its detractors.

Microtubules are able to generate conformational changes of tau through binding (Woody et al., 1983; Kadavath et al., 2015). As tau binds microtubules, its negatively charged N-terminal projection domain, branches away from the microtubule-surface possibly, due to electrostatic repulsion (Hirokawa et al., 1988; Mukhopadhyay and Hoh., 2001; Kar et al., 2003; Amos., 2004). Apparently, it acts as a spacer to keep microtubules apart (Chen et al., 1992) and provides a linker to membrane components such as annexin 2 (Brandt et al., 1995; Weissmann et al., 2009; Gauthier-Kemper et al., 2011). Through small groups of protein residues, tau binds at the interface between alpha-tubulin–beta-tubulin heterodimers. These include residues 224–237, 245–253, 275–284 and 300–317. The inter-microtubule-binding site residues are less rigid (Kadavath et al., 2015). It is suspected that the repeat sequences bind directly to microtubules electrostatically through the interaction between the positive and negatively charged residues of tubulin monomers (Jho et al., 2010).

Tau is not a mono-purpose protein. In addition to the regulation of microtubule dynamics, it may also regulate axonal transport by influencing the motor proteins dynein and kinesin, which work to transport cellular material towards the cell body (minus ends) and towards the axonal terminus (plus ends), respectively (Stamer et al, 2002). Tau disrupts the binding of the motor proteins to microtubules (Dixit et al., 2008; Ebneth et al., 1998), chiefly at the synaptic end as the highest levels of tau are found at that end of the gradient (Mandell and Banker., 1996). Likely, this distribution facilitates motor proteins jettisoning their cargo close to the presynaptic terminal which increases axonal transport efficiency (Dixit et a., 2008). Tau has also been shown to bind spectrin and actin filaments, (Yu and Rasenick., 2006; He et al., 2009) which potentially allows tau-stabilized microtubules to form connections with neurofilaments which serve to make the microtubule lattices more rigid. A pool of tau remains in the axon, which is produced by (a) relatively low levels of tau phosphorylation in axons, so its binding to axonal microtubules is increased, and (b) a functional axon initial segment operating as a one-way valve, allowing tau entry to the axon but preventing retrograde travel towards the soma and dendrites (Li et al., 2011).

Tau is a major MAP and recent work has also demonstrated an involvement in the regulation of cell viability. Tau is known to be a competitive substrate of GSK-3β and, when phosphorylated it can preserve survival factors such as beta-catenin. This can serve to protect cells from acute apoptotic death (Li et al., 2007). A further function, crucial to the neuronal ultra-structure is as a postsynaptic scaffolding protein where it modulates the enzyme activity of Src tyrosine kinases –

c-Src and Fyn – as well as facilitating c-Src-mediated actin rearrangements (Sharma et al., 2007). It has been suggested that tau tethers Fyn to post synaptic density-95/N-methyl-D-aspartate receptor signalling complex (Ittner et al., 2010), so without tau, Fyn is unable to traffic into postsynaptic sites in dendrites. Tau is normally present in small quantities in dendrites, though this is probably sufficient to ensure proper distribution of postsynaptic components (Itnner et al., 2010). This role as a scaffold protein has also been explored in oligodendrocytes, where it potentially connects Fyn and microtubules to enable extension of the processes (Klein et al., 2002).

Where tau appears, as it frequently does, in other subcellular compartments new questions arise as to extra aspects to its function. Its localisation to growth cone microtubules (Di Tella et al., 1994; Black et al., 1996) and mitotic spindles (Preuss et al., 1995) produced the enquiry whether it demonstrates non-microtubule polymerizing function, as there is a significant distinction between the microtubules in these locations and axonal microtubules (Lee et al., 2005). Within growth cones are actin-binding proteins (similar to ezrin) that co-localize with actin filaments also inside (Goslin et al., 1989). During *in vitro* experiments where tau expression is reduced in growth cones, the actin-binding protein function is lost from the cones and aggregates in the axon (Di Tella et al., 1994). This finding supports the theory that localization of the ezrin-like protein to actin filaments is tau-dependent. It is hypothesised that tau may therefore be implicated in roles such as a signal transduction (Buee et al., 2000; Lee et al., 2005).

Although predominantly expressed axonally, tau is found elsewhere in the cell, including the nucleus. Prior to transport into the nucleus, it becomes phosphorylated in the cytoplasm (Greenwood et al., 1997). One theory of its nuclear role is of conferring a protective role against DNA damage for nuclear tau (Sultan et al., 2011). Tau was recently found to induce chromatin relaxation, which in turn produces DNA damage and global changes in transcription (Frost et al., 2014). The interaction of tau with mitochondria, plasma membrane and nucleic acids (Hua et al., 2003) suggests that tau may act as a mediator between microtubules and these organelles. Certainly, it has been recently demonstrated that tau associates with the endoplasmic reticulum (ER) and Golgi apparatus in interactions also modulated by phosphorylation (Perreault et al., 2009). More recently, tau has been reported to be released into the extracellular space in the absence of cell death and this may also have significant implications in the propagation of tau pathology (Medina and Avila., 2014).

Where *MAPT* is knocked out in mice the resultant phenotype is largely benign in the short-term (Harada et al., 1994), although some of the knockout lines have exhibited alterations to synaptic function and neuronal hyperexcitability (Denk and Wade Martins., 2009). The differences highlighted with respect to the wild-type mice were restricted to a decreased number of microtubules in small calibre axons (Harada et al., 1994), myotonic weakness and some

behavioural deficits (Ikegami et al., 2000). Some collateral compensation by other proteins was seen, especially in the expression of cerebellar *MAP1A* (Harada et al., 1994). *In vitro* it was observed that there is a redundancy between *MAPT* and *MAP1B* with respect to contribution to axonal growth (DiTella et al., 1996; Gonzalez-Billault et al., 2002). This finding is supported by evidence in mice knocked out for both *MAP1B* and *MAPT* presenting with defects in axonal elongation (Takei et al., 2000).

1.11 Pathogenesis through tau hyperphosphorylation

The phosphorylation of tau regulates binding to microtubules, but additionally is associated with the aggregation of aberrant tau in disease. Phosphorylation occurs in and around the MTBR, which may neutralize its positive basic charge (Jho et al., 2010) and thereby conformationally altering the MTBR (Fischer et al., 2009). This may detach tau from microtubules whereby it then accumulates in neuronal cell bodies where it forms insoluble filaments and, ultimately, produces NFTs (Lee et al., 2001; von Bergen et al., 2005). Hyperphosphorylated tau-protein molecules undergo structural changes, which transform the C-terminal part of a protein molecule into the molten globule-like state. This may cause association of the tau-protein molecules and formation of the paired helical filaments (Uversky et al., 1998). Residues 269–284 and 300–310 found in exon 10 containing the two hexapeptide motifs PHF6*($_{275}$VQIINK$_{280}$) and PHF6 ($_{306}$VQIVYK$_{311}$) are essential for tau aggregation and can form a local hairpin conformation (Kadavath et al., 20105). It is postulated that both these sequences enable the seeding of beta sheet structures seen in the formation of pathological inclusions and tau aggregation (Von Bergen et al., 2001; Von Bergen et al., 2005). Removal of one or both of these motifs reduces or abolishes tau's aggregation competence (Bergen et al., 2000; Li and Lee, 2006). Data from solid state NMR experiments have shown that the PHF6 motif is an essential site for the initial monomer-monomer contacts leading to tau aggregation (Xiang et al., 2017), suggesting that this motif regulates tau aggregation. It is therefore unsurprising that this structural peptide is capable of forming tau aggregates independently of the surrounding tau sequences (Stöhr et al., 2017), and that tau protein lacking this structural peptide is unable to aggregate (Li and Lee, 2006).

Hyperphosphorylation of paired-helical tau (PHF-tau) has been observed in the inclusions of brains from patients with AD and other neurodegenerative disorders including SF from PSP using phosphorylation dependent antibodies (e.g. AP422 (Hasegawa et al., 1996), AT100 (Matuso et al., 1994), PHF27 (Hiffmann et al., 1997), and 988 (Bussiere et al., 1999)). The longest tau-isoform 2N4R has 80 serine residues and threonine sites that may be phosphorylated by kinases present in the cytoplasm (Buee et al., 2000). Aberrant phosphorylation of human tau is likely to affect tau function by causing conformational changes, or by influencing its microtubule (MT)

binding affinity. The physiological importance of regulated tau phosphorylation/dephosphorylation is underlined by the fact that, for example, foetal tau, which consists only of the smallest isoform (ON3R) is highly phosphorylated (Lee et al., 1993). It has also been demonstrated that tau is phosphorylated during mitosis (Pope et al., 1994; Delobel et al., 2002). The precise role of tau phosphorylation during neuronal differentiation is unclear.

The degree of tau phosphorylation may be important in modulating the plasticity of MTs during neuritogenesis by regulating the binding and release of tau from MTs, and/or dictating the sub-cellular localisation. According to the needs of the cell, tau phosphorylation may be involved in the growth or retraction of neuritic processes, or in creating a mitotic spindle, by regulating the stability of the MTs that forms part of the cytoskeletal backbone of the structures. If tau may become phosphorylated at the many sites observed in AD and other tauopathies, then the resulting disassociated tau might indeed build up into insoluble inclusions, leading to pathogenesis. Alternatively, excess soluble tau may be phosphorylated following aberrant pathogenic release from the MT, perhaps to facilitate degradation.

Hyperphosphorylation may occur either by increased kinase or decreased phosphatase activity. One kinase that has received much attention is glycogen synthase kinase 3-bets (GSK3β), which, when coupled with protein kinase A, has been shown to phosphorylate tau *in vitro* to form the phospho-epitopes that are recognised by AT100, a common antibody used to detect tau pathology in AD (Zheng-Fischhofer et al., 1998). Chinese hamster ovary (CHO) and 3T3 cells transfected with tau show increased tau phosphorylation and decreased MT bundling when co-transfected with GSK3β (Wagner et al., 1996). Lithium chloride is commonly used as a non-specific GSK3β inhibitor by increasing phosphorylation levels of GSK-3β. However, the means by which this phosphorylation occurs is not yet fully delineated, but it is believed that multiple pathways play a role (Klein and Melton., 1996). Rat neurons treated with lithium chloride demonstrate a dose-dependent decrease in tau phosphorylation (Munoz-Montano et al., 1997). Furthermore, muscarinic agonists increase the inhibitory effect of protein kinase C on GSK3β, and have been shown to reversibly decrease tau phosphorylation and increase MT binding in cultured cells (Forlkenza et al., 2000).

Eight phosphorylation sites on intact, insoluble tau extracted from PSP brain were discovered by Wray et al., (2008), seven of which previously had been reported for PHF-tau in Alzheimer brain. These included Ser_{46}, Thr_{181}, Ser_{202}, Thr_{217}, Thr_{231}, Ser_{235}, Ser_{396}/Ser_{400} and Thr_{403}/Ser_{404}. Substantially more phosphorylated residues have been identified in AD PHF-tau compared to that from PSP (Morishima-Kawashima *et al.,* 1995; Hanger *et al.,* 1998; Hanger *et al.,* 2007). Moreover, although most phosphorylation sites of misfolded tau in PSP have also been identified in other tauopathies, there are some differences in spatial distribution and aggregation of tau in

each disease, which likely influences the functional phenotype (Delacourte et al., 1998; Arai et al., 2003). The kinases suspected to be responsible for tau hyperphosphorylation in PSP are: phospho-p38 MAPK, and the stress kinases (SAPK)/ Jun amino-terminal kinases (JNK-P). These are upregulated in the neurons, astrocytes and oligodendroglia exhibiting tau aggregates (Ferrer et al. 2001).

1.12 Tau pathogenesis in PSP

In vitro tau aggregation is thought to follow a nucleation–elongation mechanism (Congdon et al., 2008; Friedhoff et al., 1998) where monomers dissociated from MTs due to hyperphosphorylation are aggregation-incompetent due to their unfolded conformation. Monomer-monomer interactions, involving either disulphide bonding or the hexapeptide motifs, lead to a conformational change from an unfolded, disordered structure for monomers to a beta-sheet-rich element that begins to adopt an aggregation-competent, structured conformation. This conformational change appears to be triggered by the formation of dimers, the minimal forms of aggregated tau (Congdon et al., 2008; Friedhoff et al., 1998). Dimer formation, thermodynamically disfavoured at physiological conditions, promotes further aggregation to form a critical nucleus of aggregated tau sufficient to overcome the rate-limiting step. Subsequent steps involve the addition of assembly-competent monomers and dimers to form larger oligomers, protomers, paired helical or straight filaments (PHFs or SFs respectively) and neurofibrillary tangles (NFTs).

Whilst the NFTs are common to both PSP and AD it is their distribution which offers the point of differentiation; in PSP they are primarily localized to the sub-cortex and found in both neurons and glia. By contrast, in AD, they are more diffuse, helicoidal and primarily cortical and neuronal in distribution (Pittman et al., 2008; Houghton and Litvan., 2007). The NFTs seen in PSP comprise 15-18nm straight (SF), unpaired tau filaments (although filaments with a longer periodicity have been described) comprising at least 6 protofilaments 2-5nm in diameter as identified by immunoelectron microscopy (Tellez-Nagel., 1973; Dickson., 1985). In AD, the paired helical filaments (PHFs) and straight filaments vary in width between 10-20 nm and a half-periodicity of 80 nm (Wischik et al., 1985; Crowther et al. 1985; Pollanen et al., 1984).

These SFs have also been noted within the glial cells of PSP patient brains (Nishimura., 1992; Arima., 1997). Tufted astrocytic 22-nm filaments were observed to be straight but irregular with jagged contours whereas the 14-nm SFs observed in coiled bodies contain a relatively smooth surface (Takahasi et al., 2008). With electron microscopy (EM), the SFs are seen to be comprised primarily of abnormally hyperphosphorylated tau proteins and thus are said to represent an earlier stage in the development of the PHF (Goedert et al., 1988; Kosik, 1997; Kondo et al., 1988;

Wischik et al., 1988; Crowther et al., 1991; Lee et al., 1991). In the early 1980s, Dickson and colleagues showed that SFs share an antigenic determinant with the NFTs of AD. Moreover, this antigenic determinant could be localised in the PSP pathological inclusions and not in normal brain cells. Morris and colleagues (1999) did suggest that there may be regions, such as the substantia nigra where the *MAPT* expression may be preferentially weighted to 4R tau mRNA (Morris et al., 1999). Overexpression in the brainstem regions, which is where the greatest burden of gliosis and NFT deposition is located, has to be seen to play an important role in the pathogenesis of PSP (Chambers et al., 1999). Moreover, the NFTs of PSP are different from those seen in AD, in the latter the tangles stain with ubiquitin antibodies (He et al., 1993; Perry et al., 1987); PSP-associated tangles do not (Fergusson et al., 2000). Moreover, PSP tangles stain less well with thioflavin S: a benzothiazole dye which increases its fluorescence upon the binding of tau aggregates (Irwin et al., 2013).

The ultrastructural differences of SF and PHF were examined in detail by Fitzpatrick and colleagues (2018) who observed that the differences between the two stemmed from the way they lined up with each other (Figure 6). In PHFs, the C-shaped subunits paired up symmetrically, tethered at the base of each core protofibril subunit by anti-parallel interactions between the $_{332}$PGGGQ$_{336}$ motif in β-sheet 3 with hydrogen bonds stitching the core subunits together. In SFs, the two core subunits joined asymmetrically and interacted weakly. Although the two subunits came close to touching via their R3 domains—at $_{321}$KCGS$_{324}$ on one C domain, and $_{313}$VDLSK$_{317}$ on the other—they were not held together via hydrogen bonds, salt bridges, or hydrophobic interactions. Instead, a region appearing as a fuzzy density on the cryo-EM appeared to span the two which was speculated to be the N-terminus of tau looping back around to stabilize the SF core. Perhaps filaments in 4-repeat tauopathies, weave the R2 domain into their core, which would exclude 3-repeat tau. Such differences in the fibril core could form the basis of different “strains” of tau.

Holmes and colleagues (2014) reported that tau strains, extracted from people and animals with different tauopathies and mutations, retain their distinctive physical attributes and pathogenic characteristics when passed between animals or in cell culture. In a recent study Narasimhan and colleagues took samples from the frontal cortices of post-mortem brains with AD, PSP, or CBD, and purified the resulting lysate to enrich for insoluble tau deposits (Narasimhan et al., 2017). They, then injected these samples into the hippocampi of wild type mice and analysed the results three months later. All the lysates seeded mouse tau pathology, but with strikingly different results. The AD tau produced the fewest deposits, while CBD tau was more potent, spreading farther through the brain. However, PSP tau spread the fastest. In fact, this lysate extracted from two PSP patients who had extensive frontal cortical tau pathology was 300 times more potent than AD-tau or CBD-tau in seeding neuronal tau aggregates *in vitro* (Narasimhan et al., 2017). In

particular, AD tau seeded aggregation only in neurons. CBD tau and PSP tau affected additional neuronal subtypes and also triggered tau deposition in oligodendrocytes and astrocytes. In the latter, CBD tau deposits resembled the astrocytic plaques seen in the human disease, while PSP tau frequently caused “tufted” astrocytes like those in human PSP. This showed that different seeding properties exist within tau inclusions, thereby confirming the existence of phenotypic diversity among pathogenic tau strains.

1.13 Genetic risk factors associated with PSP

Currently the chief culprit in terms of genetic risk factors for PSP is *MAPT*. The *MAPT* H1/H2 haplotypes are defined by a large number of common polymorphisms that are in complete LD due to the ancient inversion which prevented recombination between the haplotypes (Cruts et al., 2005). The common *MAPT* H1 haplotype has been associated with a substantially increased risk of PSP by numerous groups (Conrad et al., 1997; Baker et al., 1999; Pator et al., 2004; Rademakers et al., 2005; Pittman et al., 2005; Melquist et al., 2007). This association was further supported by findings of the 2011 GWAS of PSP, in which the *MAPT* H1 haplotype was by far the strongest susceptibility locus (Hoglinger et al.,2011). Despite the fact that association between *MAPT* H1 haplotype and PSP has been previously described, the mechanism leading to disease still needs elucidation as the H1 haplotype is relatively common among populations (Dickson et al., 2007).

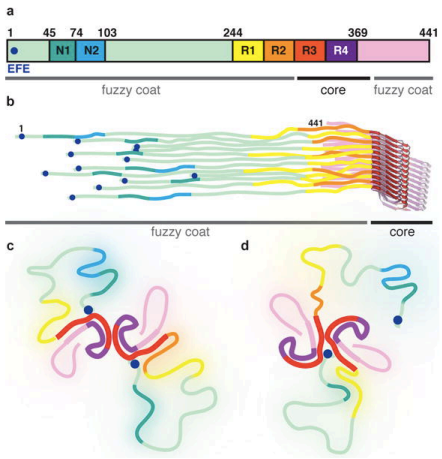

Figure 6. **Schematic representation of full-length tau filaments from the AD brain.** 2N4R tau, the longest tau isoform in human brain is indicated(a). The six different isoforms pack randomly along the helical axis (b). Comparison between PHFs (c) and SFs (d) are indicated with the amino-terminal in PHFs, folding back to form an additional, less ordered β-sheet against β1–β2 of the ordered core, which then becomes disordered, and folds back to form an interaction with the core. However, in SFs, only a single additional β-

sheet can form, and the amino-terminus of one of the protofilaments forms part of the protofilament interface (Fitzpatrick et al., 2018).

Some *in vitro* studies have suggested higher transcription levels of *MAPT* off the H1 allele compared to H2 (Kwok et al., 2004; Rademakers et al., 2005) suggesting that, possibly, the lifelong higher expression of 4R-tau could be associated with the onset of PSP. *In vitro,* and in brain, the H1 allele, compared to its counterpart H2 haplotype, is associated with increased splicing of exon 10 and decreased inclusion of exon 3 (Caffrey et al., 2006; Caffrey et al., 2008; Majounie et al., 2013). Regional association studies have determined the SNP rs8070723 to have the highest association for H1/H2 haplotype clade (Hoglinger et al., 2011). By controlling for rs8070723, the same association studies determined the highest correlated SNP for risk of PSP is the rs242557/A allele, which defines the H1c sub-haplotype (Ezquerra et al., 2011). H1c is over-represented in PSP patients as compared to controls (Pittman et al., 2005). This association was valid for both RS and PSP-P compared to controls. The rs242557 SNP that defines H1c resides in a highly conserved repressor domain in the *MAPT* promoter (Rademakers et al., 2014). Using a cellular assay, Myers and colleagues (Myers et al., 2007) showed that the risk allele (A) was associated with significantly higher transcription levels off the *MAPT* core promoter. However, this has not been replicated in vivo—single-cell quantitation may be necessary to resolve cell-type specific vulnerability. Furthermore, a second common variant, H1b was shown to be not associated with PSP and H2 was negatively associated as a protective allele (Pittman et al., 2005; Rademakers et al., 2005). Due to the extended region of LD (Pittman et al., 2004) that resulted due to a large chromosomal inversion of the region on chromosome 17q containing *MAPT* (Hardy et al., 2005; Stefansson et al., 2005), several other genes, including N-ethylmaleimide-sensitive factor (*NSF*) and corticotropin releasing hormone receptor 1 (*CRHR1*) are also defined by the H1/H2 dichotomy and are thus likely associated with PSP (Vandrovcova et al., 2009).

More recently Heckman and colleagues (Heckman et al., 2019) identified that the increased risk of PSP associated with the H1 haplotype being driven primarily by 3 H1 subhaplotypes: H1d, H1g and H1o. This was done by comparing the genotypes of 802 autopsy-confirmed PSP cases from the Mayo Clinic Brain Bank and 1,312 living, clinically normal controls. By weight of their data, the rs242557 SNP that tags the H1c haplotype in particular continued to be central player. The commonest of the risk sub-haplotypes H1c, H1d, H1g, and H1o, all conferred odds ratios between 1.86 and 3.64, carrying the risk allele (A) of rs242557. It has been suggested that H1 is not only a risk factor for PSP but may also influence age at symptom onset (Baba et al., 2006), but this is disputed as other papers have not found any effect on onset age or severity (Litvan et al., 2001). Currently it is unknown whether there is a rarer mutation on the H1 haplotype which is the key to PSP, or whether the answer is contained within the haplotype itself. Calculations of population-attributable risk suggest that only ~68% of the risk of PSP can be accounted for by

the H1 haplotype, suggesting there may be additional risk genes involved in PSP (Im et al., 2015).

In 2011, an international consortium published a GWAS that included a large majority of pathologically proven and clinical PSP cases available in Western Europe and the United States. Their aim was to identify further gene variants associated with increased risk of PSP other than the *MAPT* H1 haplotype (Hoglinger et al., 2011). This two-stage analysis involved more than 1,100 pathology confirmed cases against a comparable cohort of clinically diagnosed cases against more than 6,500 controls in the initial discovery stage followed by a replication stage including 1051 clinically and pathologically diagnosed cases. This uncovered three novel risk loci (Figure 7) with associations fulfilling a genome-wide significance threshold of $p<5 \times 10^{-8}$. This included rs1411478 at the syntaxin-6 (*STX6*) gene on chromosome 1 ($p= 1.8 \times 10^{-9}$; OR=1.2700). The second association, rs1768208 ($p=1.0 \times 10^{-9}$; OR=1.3700), implicated the myelin-associated oligodendrocyte protein (*MOBP*) gene. As expected, SNPs in the *MAPT* region showed the strongest association ($p=< 5 \times 10^{-8}$; OR=5.11). A total of 58 SNPs defining the 17q21.31 region of LD and H1/H2 haplotypes were associated with p-values varying from 1.5×10^{-116} for rs8070723 to 9.5×10^{-18} for rs242557. Furthermore, conditional analysis for SNPs within the H1/H2 clade for those associations independent of the H1/H2 division revealed only one SNP, rs242557 in the large promoter region of *MAPT* that retained association with genome-wide significance ($p= 4.2 \times 10^{-70}$). This corroborated earlier findings of the specific association with PSP of the H1c sub-haplotype that is defined by rs242557 (Pittman et al., 2005) and further supports the importance of rs242557 and the conserved promoter regulatory sequence that it resides in.

In addition to confirming the above associations, the second stage and pooled analyses uncovered association of the rs7571971 ($p=3.2 \times 10^{-13}$; OR=1.33) in the *EIF2AK3* gene (Hoglinger et al, 2011) (Figure 8). *EIF2AK3* encodes Protein kinase R-like endoplasmic reticulum kinase (PERK), an integral membrane protein of the ER and one of three sensors for unfolded protein that initiate the unfolded protein response (UPR). No functional links have yet been established between these three genes and disease pathophysiology. However, an epigenetic association has been established between the level of methylation at the 17q21.31 region and the H1 haplotype, indicating that epigenetic mediators have a contribution to disease risk (Li et al., 2014).

Another GWAS was completed in 152 cases and 3311 controls of CBD in a discovery phase and 67 cases and 439 controls in a replication phase (Kouri et al., 2015). Associations were found at the 17q21 locus of *MAPT, Inc-KIFI13B-1,* a long noncoding RNA, and Son of sevenless-1 (*SOS1)*, a potential tau phosphatase. Tests also revealed associations at known PSP SNP sites for *MOBP* and *MAPT H1c.* This confirmed that CBD and PSP share genetic risk factors for both *MAPT* and *MOBP*. This strengthened the known association between variants in *MAPT* and tau pathology

evident in both diseases. Importantly it also revealed a novel pathogenic linkage common to both diseases between *MOBP* and white matter oligodendrocyte pathology.

Although these GWAS have yielded very exciting results, these common variants alone do not account fully for what is known of the heritability of PSP. In fact, SNPs that show positive associations in genetic studies are not necessarily those that alter susceptibility to disease. Instead, disease associated SNPS are often co-inherited with true causative genetic variations, which may even lie in adjacent genes. In the case of the *STX6* and *EIF2AK3*, however, nearby variants were found in each gene that alter the coding region and are tightly linked to the risk SNPs, suggesting the coding changes may be pathogenic. In the case of *MOBP,* studies in the near future have an opportunity to understand how failure of MOBP's normal role in myelin sheath stabilization may contribute to a common disease mechanism, and what relationships may exist for transsynaptic spread of misfolded tau. As with all genetic association studies, the next challenge for us was to determine the functional underpinnings of the *EIF2AK3* associations and determine how their allelic differences influence risk.

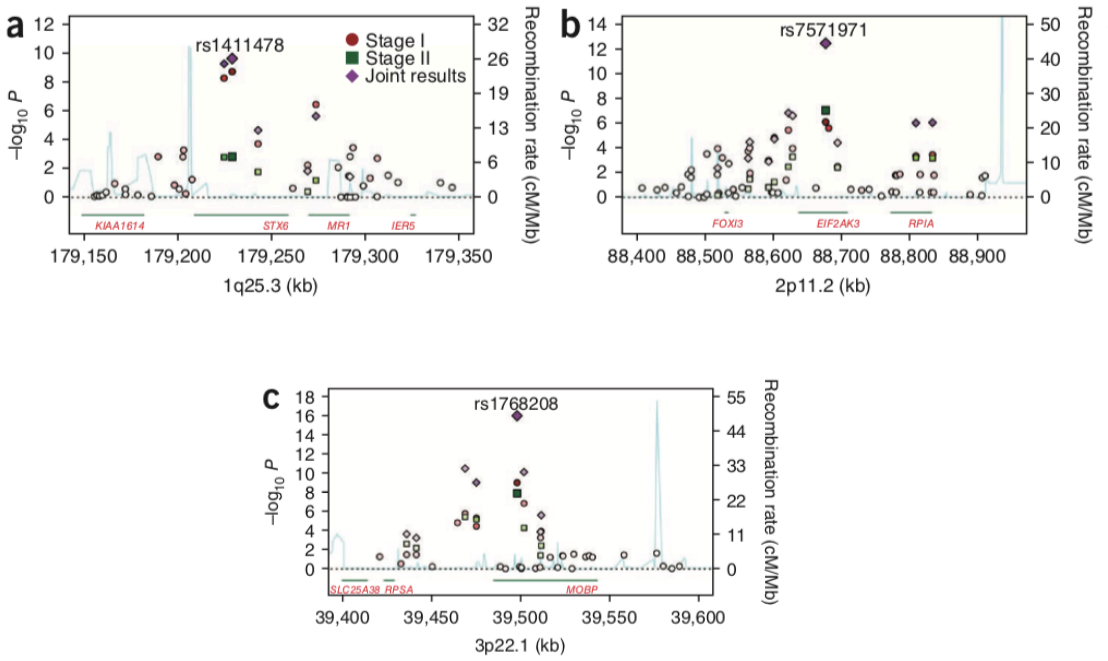

Figure 7. **GWAS of PSP to identify genes that modify risk**. Regional association plots are shown for the association results for 1q25.3 *STX6* (a); 2p11.2 *EIF2AK3* (b) and 3p22.1 *MOBP* regions (c) (Hoglinger et al., 2011).

1.14 Protein production and role of ER in membrane and secretory proteins

The endoplasmic reticulum (ER) is an intracellular membrane system of enclosed sacs and tubules. It provides the cellular workshop that is the primary site for the maturation of secretory proteins. Structurally, ER comprises specific functional domains: the nuclear envelope, rough and smooth ER (rER and sER), and communicatory elements in contact with other organelles (Rozpedek et al., 2015). A common luminal space is shared between the nuclear envelope and throughout the reticular formations of the ER, as demonstrated in cerebellar Purkinje neurons (Terasaki et al., 1994; Dayel et al., 1999). Its origin is postulated to be from selective invagination of the plasma membrane (Braakman and Bulleid., 2011). According to its sub-cellular position, function and cell type, it may form flattened sacs, cisternal sheets, linear tubules, polygonal reticula and three-way junctions (Lee and Chen, 1988; Dreier and Rapoport, 2000). Present in all eukaryotic cell types except for mature erythrocytes, ova, embryonic and prokaryotic cells, it is especially prominent in neurons, hepatocytes, adreno-cortical cells, retinal cells, myocytes, interstitial cells and steroid-synthesising cells. Its function is crucial, providing the site of translation, folding and transport of newly synthesized proteins to the cell membrane; these are integral membrane proteins and transmembrane receptors or else they may also be proteins secreted by exocytosis. The final element prior to secretion of the finished protein is a quality control process to ensuring correct folding and packaging of the product.

The rER accommodates around 1/3 of the cellular protein synthesis (Zhang and Kauffman., 2006). During the initial translation, most proteins on the secretory pathway present a hydrophobic N-terminal signal sequence (Schechter., 1975; Nyathi et al., 2013). This signal sequence is detected by a cytosolic ribonucleoprotein, the signal-recognition particle (SRP). This binds the protein and slows the synthetic process through ‘elongation arrest’ and directs polypeptides to the translocon within the ER which is composed of the Sec61αβγ complex; once here, this permits the translocation of the developing polypeptide chain across and into the ER membrane (Johnson and Van Wes., 1999; Saraogi and Shan., 2011). At this point, as protein synthesis resumes, the short hydrophobic tag is detached and nascent chains are co-translationally injected into the lumen of the ER where the folding of the polypeptide chain occurs (Gilmore et al., 1982; Meyer and Dobberstein., 1980; Walter and Blobel., 1981; Braakman and Bulleid., 2011). Chronologically, once the newly synthesized protein monomers have folded, they also could assemble within the ER into higher order structures (Hurtley and Helenius., 1985). Combining the translation and translocation processes permits sequential folding to enhance folding efficiency, which is particularly significant for multi-domain proteins (Netzer and Hartl., 1997). Moreover, to ensure high fidelity, ER resident chaperone proteins occupy various sites of nascent proteins to ensure they fold correctly. Once this process is successful, a molecular tag allows the protein to exit the ER lumen. However, if a protein continually fails to achieve the correct conformation, it

will be targeted by the endoplasmic reticulum associated protein degradation pathway (ERAD) (Meusser et al., 2005).

The ER is highly sensitive to environmental changes; nutrient or energy deprivation, disrupted calcium homeostasis, oxidative stress, and chiefly, the accumulation of aberrant or excessive protein (Schroder and Kaufman., 2005; Verkhratsky et al., 2004). Any of these intrinsic or extrinsic disruptions may produce ER stress, which increases the mass of aberrant protein accumulating within the ER lumen. This in turn initiates a complex signal transduction cascade; the UPR (Wu and Kuafmann., 2006; Ron and Walter., 2007). Braakman and Hebert (2013) described the efficacy of this quality control mechanism at producing a system that effectively produces and dispatches acceptable proteins as a range from nearly total 'success' to as low as in one protein in every four making it through.

1.15 ER stress and causes of ER stress

The ER must be dynamic and adaptable to meet changing demands whether due to infection, injury, or due to physiological changes in cell cycling, nutrient status or other environmental changes. Where the system is thrown off, there develops an unwanted accumulation of unfolded proteins within the ER. This triggers the 'clean-up operation' of the UPR (Xu et al., 2005) to reduce ER stress and restore homeostasis. Along the protein-folding chain there has to be equilibrium between the protein load in the ER and the folding capacity to process this load. Else a bottleneck occurs. The backlog of misfolded proteins in the ER is damaging to cells (ER stress); consequently, in higher eukaryotes, three ER transmembrane proteins act as ER stress sensors and monitor protein folding conditions in the ER: inositol requiring enzyme 1 (IRE1), PERK and activating transcription factor (ATF) 6. These proteins have ER luminal domains that sense the ER protein-folding environment and cytoplasmic effector domains that signal downstream UPR responses, enabling the detection of these misfolded proteins. The myriad possible conditions (physiological or pathological) affecting or potentially affecting protein folding include glucose starvation, under glycosylation of glycoproteins, calcium flux, protein overproduction and secretion, and classically, failure of protein folding, transport or degradation can all contribute to ER stress (Schroder and Kaufman., 2005). The final destiny for many of the proteins synthesized will be integral to the life of the cell by mediating crucial signalling including but not limited to cell surface receptors, transporters, or even polypeptide hormones. Consequently, stringent quality control is essential (Oakes and Papa., 2015). The quality control mechanism has a fail-safe and if the UPR is unsuccessful in re-establishing ER homoeostasis, ER stress overwhelms the cell, leading to self-destruction – apoptosis (Kim et al., 2008). The ER stress response is activated following the capacity of ER-resident chaperone proteins being saturated by the influx of aberrant

proteins. The UPR is an evolutionarily conserved response and deletion of a single UPR initiator or signalling protein is often sufficient to cause embryonic or perinatal lethality (Harding et al., 2000). The UPR was first discovered when an accumulation of unfolded proteins in the ER were observed to induce the specific transcriptional upregulation of ER resident chaperone proteins (Kozutsumi et al., 1988).

The 78 kDa glucose-regulated protein, GRP78 (also known as binding immunoglobulin protein or BiP), is a HSP70 chaperone which binds to nascent proteins as they enter the ER and to sites on the luminal domains of PERK, ATF6 and IRE1. Misfolded proteins can sequester the available BiP, leading to the loss of BiP-mediated repression of the UPR sensors (Lin et al., 2008). Dissociation of BiP from transmembrane sensors on the ER lumen triggers the UPR. In acute stress, signal transduction via PERK rapidly inhibits protein translation so that more proteins do not continue to overload the ER. PERK activation is rapidly reversed upon restoration of homeostasis. If stress is prolonged, longer term adaptations are made via transcriptional upregulation of genes targeting ER resident chaperones, enzymes and ER biogenesis. These misfolded proteins will be removed from the cell by one of these two processes:

(1) ER-associated degradation (ERAD) which exports damaged proteins back into the cytoplasm for degradation and clearance by the proteasome.

(2) Aggresome formation where damaged proteins are compacted with other cellular debris into juxtanuclear complexes and presented for recycling via autophagy (Schonthal., 2012).

This process of proteostasis (Balch et al., 2008) is fundamental to maintaining cellular health and wellbeing, as it prevents abnormal protein aggregation which leads, as we have seen, to conditions such as PSP. The reason why the tauopathies as well as ALS, HD and prion diseases are all characterized by a long latent, sub-clinical phase is the stealth accumulation of abnormal proteins aggregating in the brain, which will eventually decompensate and develop altered synaptic function, neuronal loss and clinical symptoms (Selkoe., 2003). Hence why this group of diseases is now classified as protein misfolding disorders (PMDs) (Soto., 2003). The explanation for the correlation of protein misfolding and ageing, is that the intricate balance of synthesis, folding, and degradation of proteins becomes thrown off by individually negligible mutations which exert a disproportionate downstream effect, resulting in the accumulation of aberrant aggregating proteins (Finkel., 2005). It is through the assembly into protein aggregates of an amyloid type that misfolded proteins exert their cytotoxic effect through mechanisms as yet not understood (Invernizzi et al., 2012). One observed mechanism has been the exposed hydrophobic patch observed on misfolded proteins which permits a means of interaction and aggregation with other proteins. In the main, the native monomeric protein is an alpha helix, whereas the misfolded oligomers exhibit aberrant beta sheet conformation (Soto and Estrada., 2008). Protein folding, and aberrant permutations thereof, can be considered the index event endorsing

neurodegeneration. The number of targets whose misfolding and aggregation is shown to be associated with pathology is increasing (Valastyan et al., 2014) and the misfolded proteins are largely disease specific. The synthesis of the considerable body of research into all the PMDs resoundingly suggests that derangement to ER function is a common denominator across the disease burdens. (Matus et al., 2011).

1.16 Unfolded Protein Response

Joseph Sambrook is credited with pioneering the UPR field with his 1977 studies into the response of mammalian cells infected with a misfolded form of viral protein. He and Mary-Jane Gething observed that accumulation of this aberrant ER protein resulted in two proteins, GRP78 (BiP) and GRP94 being upregulated (Kozutsumi et al., 1988). They demonstrated that overexpressing an unfolded variant of the influenza hemagglutinin protein (HA) was sufficient to induce BiP and GRP94 expression (Gething and Sambrook., 1992) and this signalling pathway was designated the *u*nfolded *p*rotein *r*esponse (UPR).

The objective of the UPR is to restore to normal the baseline function of the ER via multiple sequential and concurrent approaches, when it is in danger of becoming overwhelmed by a large number of misfolded proteins. The means of achieving this are through the increased expression of chaperone proteins to prevent protein aggregation and facilitate the correct folding of nascent proteins. Moreover, there is a mechanism, to reduce the volume of protein transmitting through the ER by relaxation and activation of protein translation inhibition. Finally, through the ERAD pathway, the cell can clear the unfolded proteins (Bravo et al., 2013). The UPR mediates all these aspects of cytoprotection, acting as an integrated intracellular signalling pathway updating the cell with protein folding status and traffic updates through ER lumen to the cytoplasm and the nucleus. In addition to this vital housekeeping role, elements of the UPR are also implicated in regulating processes such as lipid and cholesterol metabolism and also driving the response to inflammation and cell differentiation (Rutkowski and Hegde., 2010).

In yeasts, a single sensor of unfolded proteins, IRE1 controls the UPR (Cox et al., 1993; Mori et al., 1993). In metazoan cells there are two additional signalling branches, one controlled by the ER membrane-resident kinase PERK (of which more later) and the membrane-bound transcription factor ATF6 (Walter and Ron., 2011) (Figure 8). Both UPR sensors bind to the ER lumenal chaperone BiP, then, as misfolded proteins accumulate in the lumen, they bind and sequester BiP, thereby initiating the UPR (Bertolotti et al., 2000; Ma et al., 2002; Shen et al., 2002). The activated UPR co-ordinates downstream effectors to launch an adaptive response during which it tries to re-establish folding homeostasis by inducing the expression of chaperones.

Two distinct cellular events to mitigate protein misfolding are triggered: first is whereby the translation is globally attenuated to reduce protein synthesis and enhance degradation of the aberrant proteins. The second event involves a transcriptional upregulation of proteostatic target genes (Hetz and Papa., 2017). If the UPR remains induced for too long then it kicks into its role as an apoptotic executor killing off these cells (Chakrabarti et al., 2011). Cell fate regulation by the UPR has recently been shown to be key in the pathogenesis of ER stress-related disorders (Oslowski and Urano., 2011).

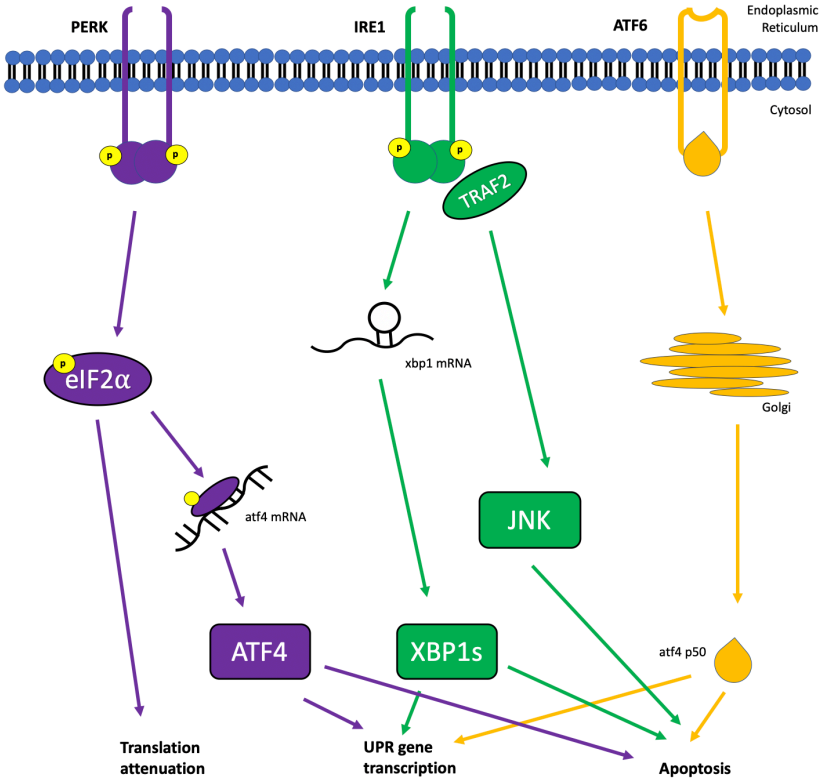

Figure 8. **Signalling pathways of the unfolded protein response**. Unfolded proteins accumulate in the ER lumen, which leads to activation of the ER stress sensors ATF6, PERK, and IRE1, which induce a signalling cascade termed the UPR. The UPR involves the downregulation of translation and the activation of transcription factors that regulate genes promoting ER homeostasis and cell survival. During prolonged or severe ER stress, however, genes that induce apoptosis are upregulated.

1.16.1 IRE1

IRE1 is a type I transmembrane serine/threonine receptor protein kinase. It is a major component of the UPR and is the most established and most conserved arm (Cox et al. 1993). IRE1 is composed of an ER lumenal stress-sensing domain and an RNase domain facing the cytoplasm.

The lumenal domain will sense the presence of unfolded proteins and will also organize the high-order oligomerization of IRE1. When unfolded proteins competitively bind to BiP, the activation of IRE1 is mediated. In the absence of unfolded protein, BiP associates with the lumenal domain of IRE1 to render it and maintain it in the 'off' position. As levels of unfolded protein increase, BiP then dissociates from IRE1 to associate preferentially with the unfolded proteins. IRE1 is therefore free to dimerize/oligomerize which leads to its activation (Bertolotti et al., 2000; Zhou et al., 2006; Kimata et al., 2007). It remains frustratingly unclear how IRE1 is activated by ER stress in mammals, since it was shown in yeast that deletion of the kA2 binding domain, the BiP/HRP78 equivalent, did not alter the activation ability.

Activation can also take place when unfolded proteins interact directly with the IRE1 lumenal domain to induce oligomerization and activation without the BiP intermediary. The studies in yeast demonstrated that formation of active IRE1 oligomers is promoted through formation of a central groove, akin to peptide binding pocket of major histocompatibility complexes (MHCs (Adams et al., 2019). It is thought unfolded proteins bind these grooves. In the sensory domain of IRE1 lumenal region, peptide fragments or unfolded proteins are detected through the groove. The crystal structure of yeast IRE1 similarly revealed that when two monomers of IRE1 joined together they created the deep groove from the lumenal domain with abundant β-strands constituting β-sheet platforms and short α-helices (Umebyashi et al., 1999). Given that MHC binds various peptides, this structural quirk strongly supports the concept that that IRE1's lumenal domain directly binds misfolded proteins (Credle et al., 2005). Thus, as misfolded protein accumulates in the lumen, the lumenal domains multimerize, juxtaposing IRE1α's kinase domains, which results in *trans*-autophosphorylation; this conformationally activates IRE1α's RNase domain (Korennykh et al., 2012). Downstream, cytosolic kinase domains are trans-phosphorylated, which subsequently activates RNase. Although oligomerization driven *trans*-autophosphorylation is a common cell signalling mechanism, IRE1 does not signal downstream via phosphorylation. It is the conformational change (not yet clear if phosphorylation causes this conformational change, or not) that follows from nucleotide binding which activates IRE1's RNase domain (Pap et al., 2003; Aragon et al., 2009; Korennykh et al., 2009). This conformational change induced in its cytosolic domain allows binding to the adaptor protein tumour necrosis factor-α (TNFα)-receptor-associated factor 2, known as TRAF2. This leads to activation of the Jun N-terminal kinase (JNK) pathway and the nuclear translocation of Nuclear Factor kappa-light-chain-enhancer of activated B cells (NFκB) via Inhibitor of Nuclear Factor Kappa B Kinase B (IκB) kinase, and subsequent production of TNFα (Urano et al., 2000). Upregulation of inflammatory cytokines, and activation of pro-apoptotic B cell lymphoma 2 (Bcl2) family members via JNK, shift cell fate towards apoptosis (Li et al., 2018).

Under normal conditions *XBP1* (X-box-binding protein 1) mRNA is translated into its protein that associates with membranes via its two hydrophobic regions (HR) HR1 and HR2. Upon *XBP1* mRNA translation, HR1 and HR2 on the nascent polypeptide associate with the ER membrane and bring the *XBP1* mRNA ribosome nascent chain complex to the vicinity of the IRE1, facilitating IRE1 mediated splicing of *XBP1* mRNA. Oligomerization of IRE1 activates the RNase domain, which cleaves *XBP1* mRNA (which encodes XBP-1 protein, a transcription factor of the basic leucine zipper (bZIP) family at two discrete stem-loop structures through an unconventional cytoplasmic splicing reaction (Cox and Walter., 1996; Yoshida et al., 2001). Both unspliced and spliced XBP1 share the N-terminal region containing the bZIP domain, but it is in their C-terminal regions where they differ. As it is the C-terminal region of spliced XBP1 which contains a transcriptional activation domain, spliced XBP1 therefore functions as a potent transcription factor (Yoshida et al., 2001). Spliced XBP1 translocates to the nucleus, where it induces transcription a substantial number of genes (Yamamoto et al., 2007). The transcriptional targets of XBP1 are highly enriched for ERAD factors, ER chaperones, and enzymes required for lipid biosynthesis and protein glycosylation across diverse mammalian cell types (Lee et al., 2003; Shoulders et al., 2013; Yamamoto et al., 2004). Up-regulation of these molecules by IRE1-to-XBP1 induction therefore enhances the ER's capacity to better fold new proteins (Cornejo et al., 2013).

1.16.2 ATF6

In mammalian cells, ER-resident ATF6 is present as two isoforms, α and β, both of which are ubiquitously expressed (Haze et al., 2001; Yoshida et al., 1998). The C-terminal section of these isoforms protrude into the ER lumen, leaving the N-terminus to face the cytosol. This N-terminal domain encompasses DNA binding and transcriptional activation domains. The N- and C-termini are separated by a 20-amino acid transmembrane domain. Although isoforms α and β possess significant sequence homology, they exhibit divergent transcriptional activation domains. ATF6α is a potent transcriptional activator, whereas ATF6β is a poor transcriptional activator and may inhibit activation by ATF6α (Thuerauf et al., 2007). ATF6α is thought to be chiefly responsible for transcriptional regulation of pro-survival genes following the UPR and ER stress, however, ATF6β may also be involved (Haze et al., 2001; Therauf et al., 2007; Yamamoto et al., 2007).

ATF6 signalling is believed to be controlled by the ER chaperone BiP. Under normal growth conditions, ATF6 is an ER membrane protein associated with BiP (Shen et al., 2002). ATF6 is retained in the ER through BiP binding the ATF6 lumenal domain. When BiP dissociates from ATF6 it reveals the Golgi localization sequences (GLS; Shen et al., 2002) which enables ATF6 to be translocated to the Golgi to undergo proteolytic cleavage by site-specific cleavage by S1P (Site-1 protease) and S2P (Site-2 protease). This enables the release of the transcriptionally

active cytoplasmic transcription factor which moves to the nucleus where it upregulates genes involved in ER protein folding, secretion, and degradation.

The ER stress-induced activation of ATF6 requires its dissociation from the inhibitory regulation of BiP, though how it effects this release is debated and two competing models have been proposed (Bertolotti et al., 2000). First, the competition model, assumes that BiP-ATF6 complex to be highly dynamic; ER stress generates a surplus of misfolded substrates that compete with ATF6 for BiP binding. This diverts BiP away from ATF6 toward misfolded proteins (Morimoto., 2002). The second, active triggering model, hypothesizes a BiP-ATF6 complex actively dissociated by a signal generated from misfolded proteins. One speculation in the literature is that parts of the lumenal tails of ATF6, IRE1 and PERK can present as “surrogate” substrates, behaving as ‘decoy’ unfolded protein recognized by BiP. In support of both these models, Dissociation of BiP from ATF6 in ER-stressed cells depends on conformational changes of BiP (Shen et al., 2002). These conformational changes were also necessary for the release of folding substrates, indicating that BiP may bind to ATF6 and unfolded proteins in a similar manner. If the BiP/UPR sensor complexes are highly dynamic, increasing amounts of unfolded proteins in the ER should efficiently compete with the sensors for BiP binding and reduce the amount of these complexes rapidly. On the other hand, a low off-rate of BiP from the sensor proteins would indicate a different mode of association and suggest that dissociation may be triggered by yet unknown modifications of either BiP or the UPR sensors.

1.16.3 PERK

Like IRE1, PERK is a type-1 ER membrane serine/threonine protein kinase. It belongs to the eukaryotic initiation factor 2 subunit alpha (eIF2*α*) kinase subfamily (Harding et al., 1999). eIF2α is a translational factor responsible for control of the initiation step of protein synthesis, this has been implicated in long-term synaptic plasticity and memory formation. PERK was originally discovered whilst screening for kinases capable of phosphorylating eIF2α and, a year later, Harding et al., (2000) identified PERK as being the kinase responsible for instigating the attenuation of protein synthesis during ER stress (Harding et al., 1999, Shi et al., 1998, Hayes et al., 1999). Prior to the work of these groups, three protein kinases; general control non-depressible 2 (GCN2) (Ramirez et al., 1991) double- stranded RNA-dependent protein kinase (PKR) (Srivastava et al., 1995) and heme- regulated eIF2α kinase (HRI) (Chen and London, 1995) had previously been identified as eIF2α kinases. PERK was found to phosphorylate eIF2α on serine 51 and was also found to undergo autophosphorylation indicating that PERK is an ER membrane spanning protein that initiates translational arrest during ER stress by first phosphorylating itself and then eIF2α (Harding et al., 1999, Shi et al., 1998). The PERK arm of

the UPR acts primarily on translation. However, PERK is also known for its function in insulin processing; indeed, failure of activation of PERK is known to result in diabetes. Wolcott-Rallison syndrome, characterized by infantile diabetes due to pancreatic hypoplasia, is caused by mutations in *EIF2AK3* (Delepine et al., 2000). Similarly, *EIF2AK3* knockout mice were normal at birth but were shown to develop diabetes with maturation due to loss of beta cell mass (Harding et al., 2011). Hence, PERK function is also necessary for normal exocrine and endocrine pancreatic development. PERK-mediated signalling pathways are complex and vary between tissue and cell type but exert a significant and clear role in cell fate and tumorigenesis.

1.17 Domains of PERK

PERK is constituted of a lumenal domain and a kinase domain. The lumen is the inner space of the ER, which does not have any contact with the cytoplasm. The lumenal domain detects unfolded/misfolded proteins that accumulate in the ER lumen. The dimerization domain of PERK faces the lumen i.e. It is within the luminal domain. The protein then spans the ER membrane and the C-terminal domain is in contact with the cytoplasm, thus aptly named the cytoplasmic domain. This cytoplasmic domain has serine/threonine protein kinase activity. The lumenal dimerization domain is structurally and functionally similar to that of IRE1 and cytoplasmic eIF2α kinase domain homologues: HRI, GCN2, and PKR (Harding et al., 1999; Llu et al., 2000; Shi et al., 1998).

1.17.1 Lumenal domain of PERK

Recent work by Carrara et al., (2016) demonstrated how the human PERK lumenal domain structure forms ringed tetramer architecture. The tetramer consists of individual monomers predominantly composed of β-strands arranged into β-pleated sheets with dual helices. The lumenal domain sub-divides into three functional structural motifs: dimerization, β-sandwich and tetramer domains (Figure 10). The dimerization sub-domain comprises a series of anti-parallel β-strands forming the dimerization interface between the PERK monomers. The β-sheet is the central feature of this subdomain, consisting of three long anti-parallel β-strands with β8 forming direct interactions to β8 from the opposing monomer. The “β-sandwich” subdomain consists of β-strands arrayed in a bi-layer β-sandwich fold that likely stabilizes the other subdomains. The tetramer subdomain consists mainly of β-strands and one α-helix that come together to create a cleft, which interacts with the opposite PERK monomer in a helix swap that most likely acts to stabilize the transient tetramer interface. The two dimers of the PERK lumenal domain dock onto each other to form a tetramer via the tetramerization domain.

The tetramer interface is transient but may exert a regulatory role in UPR activation. This is supported by findings that tetramer interface mutants reduce levels of PERK and eIF2α phosphorylation. The tetramer has been shown to increase the efficiency of PERK auto-phosphorylation in cells (Liu et al., 2002). This is an emerging concept as it is well-established that a dimer is sufficient for auto-phosphorylation to occur in both PERK (Ma et al., 2002). The tetramer is thought to provide a robust platform for phosphorylation and thereby increase phosphorylation efficiency (Carrara et al., 2016). As the lumenal domain dictates oligomerization status for both IRE1 and PERK; could the dimer and tetramer be seen to represent lower and higher states of autoactivation? Shifting between these states may provide a key part of the PERK sensor's ability to activate and respond to accumulation of misfolded proteins within the ER.

The lumenal domain remains a target of interest. In 2016, Wang and colleagues showed that lumenal domain of PERK interacts directly with misfolded proteins to suppress aggregation and its peptide-binding site flexibly adopts multiple conformations. It was suggested that the structural flexibility allowed the domain to bind various different types of misfolded proteins. In follow up work Wang et al., (2018), showed that, of the three lumenal sub-domains, the β-sandwich domain was able to adopt multiple conformations to enable the peptide-binding site to interact with a variety of misfolded proteins with side chains of different sizes and different hydrophobicity. In the tetrameric structure of the lumenal domain, the docked tetramerization domains are flanked by the β-sandwich domains from two dimers. Simultaneous binding of the β-sandwich domains to one chain of misfolded polypeptide may greatly enhance the possibility of docking and interaction between the two tetramerization domains of the lumenal domain. Overall, the β-sandwich domain is ideally positioned for interactions with misfolded proteins to induce oligomerization of PERK for ER stress activation.

In terms of binding within this sub-domain, it was observed that the PERK lumenal domain binds misfolded proteins via hydrophobic interactions (like most molecular chaperones). A large hydrophobic patch was noted on the N-terminal surface of the β-sandwich domain (Wang et al., 2018). The residues within the PERK lumenal domain constituting this hydrophobic patch are highly conserved (Figure 10). Mutations within the β-sandwich domain which included Δ298 and Δ344,in which residues 298–309 and residues 344–355 were replaced by the flexible linker were seen to diminish the binding capability of the PERK lumenal domain to the peptide substrate (Wang et al., 2018)

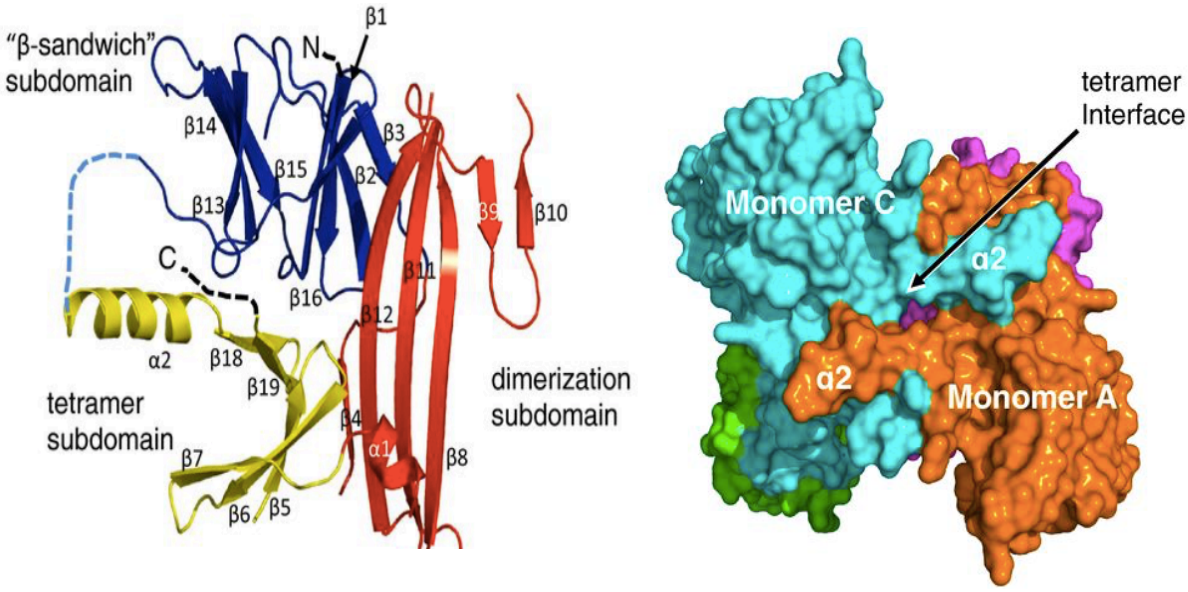

Figure 9. **3D-model of PERK tetramer formation**. The left-hand image indicates an Individual PERK lumenal domain monomer which is divided into subdomains with the red ribbon representing dimerization subdomain, blue ribbon representing the beta-sandwich subdomain and the yellow ribbon representing the tetramer subdomain. On the right sand, a 3D model of a PERK tetramer is indicated with the construction of four PERK monomers (monomer A in orange, monomer B in magenta, monomer C in cyan, and monomer D in green) (Carrara et al., 2015).

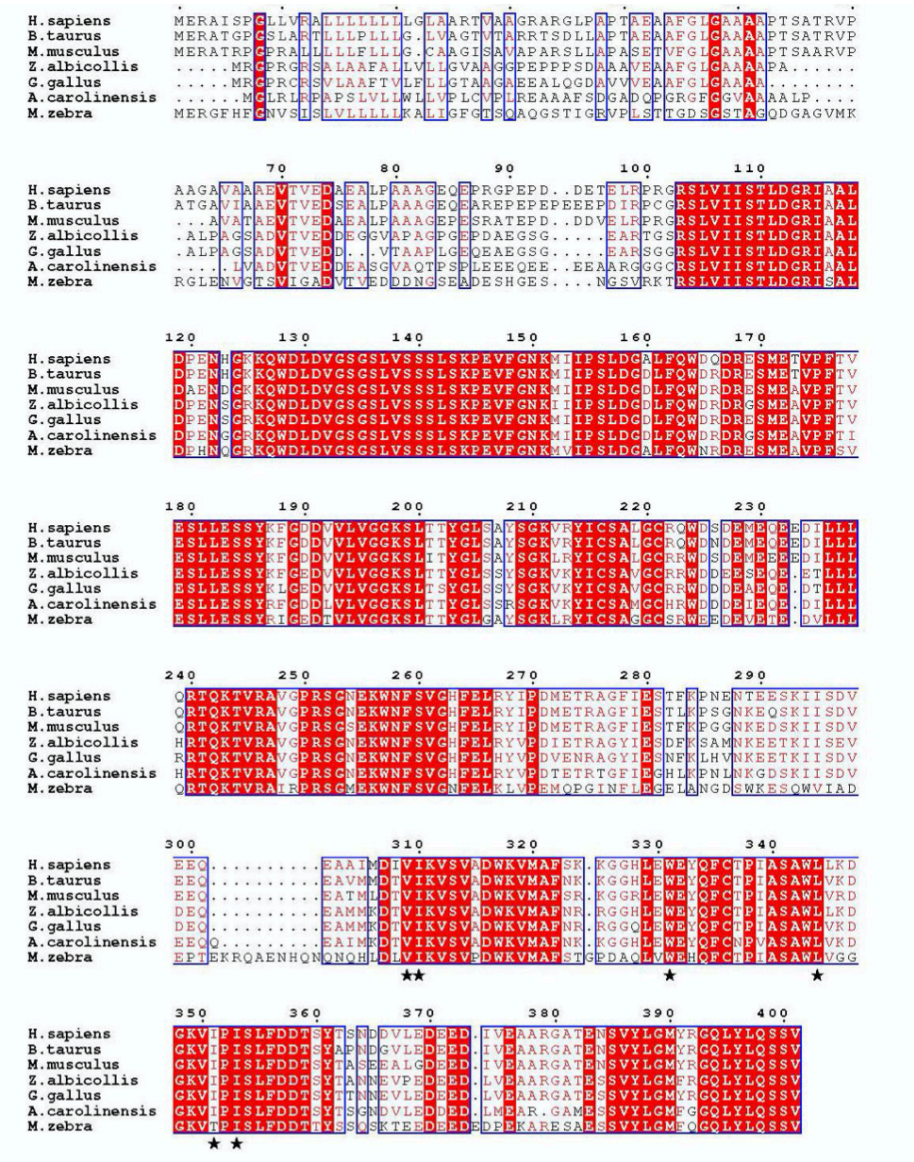

Figure 10. **The sequence alignment of PERK lumenal domain from various species**. It is likely that the PERK lumenal domain (residues 1-420) binds misfolded proteins via hydrophobic interactions. Highlighted in red indicates the residues within the PERK lumenal domain which are highly conserved amongst the different species. The PERK lumenal domain contains a hydrophobic peptide-binding groove that can accommodate a stretch of peptide of about 10 residues. The misfolded proteins have been shown to be inserted into the hydrophobic pocket of the peptide-binding groove within the PERK lumenal domain via the PERK residues at position 165, 316, 318, 388, 389, and 391. These residues are very well conserved in sequence alignment among multiple species. It is highly likely that the PERK lumenal domain could utilize this peptide-binding groove to interact with the misfolded proteins to suppress protein aggregations. Further residues that are currently being investigated for the possibility of being involved in forming the peptide-binding groove for the misfolded proteins are marked by asterisks (Wang et al., 2016).

1.17.2 Kinase domain of PERK

The kinase domain of PERK contains a larger C-terminal lobe (C-lobe) with two short *β*-strands, seven *α*-helices and a long activation loop and a smaller N-terminal lobe (N-lobe) comprising three *α*-helices and five *β*-strands with a short hinge loop linking the two lobes (Cui et al., 2011). (Figure 11). The N-lobe was shown to provide the interfaces for kinase domain dimerization and is constituted by two back-to back PERK monomers where it forms a homodimer. This provides the suggestion that one PERK homodimer inserts its flexible activation loop into the catalytic site of the adjacent homodimer in a manner similar to the transphosphorylation mechanism proposed for IRE1 (Korennykh et al., 2009). This same folding has also been reported in PKR (Padyana *et al.*, 2005).

The PERK kinase domain structure supports the theory that phosphorylation of the Thr_{980} also contributes to the stability of the activation loop and of the substrate-binding helix αG in PERK. The phosphate moiety of Thr_{980} was shown to form a charge–charge interaction with the side chains of Lys_{631} and Arg_{634} from helix α-C and the side chain of Arg_{934} from the C-lobe (Cui et al., 2011). These interactions partially stabilized the activation loop which then secured the position and orientation of helix α-G – the docking site for eIF2α – through interactions which include charge–charge interactions between Arg_{1025} from helix α-G and Tyr_{988} from the activation loop, hydrogen bonds between Arg^{1033} in helix α-G and the backbone carbonyl groups of Leu_{987} and Met_{989} from the activation loop, and hydrophobic interactions among Leu_{987}, Tyr_{988} and Ile_{1028} (Cui et al., 2011).

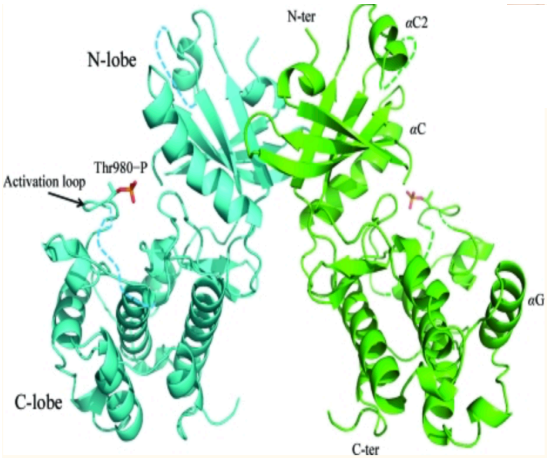

Figure 11. **Structure of the PERK dimer formed following kinase domain dimerization**. Two PERK kinase domains from two individual PERK monomers are coloured in cyan and green, respectively. Dimerization of the kinase domain occurs through its N-terminal lobe whereby the Thr980 residues are phosphorylated in (Cui et al., 2011).

1.18 How is PERK activated upon ER stress?

In normal, unstressed conditions, PERK rests in the form of an inactive monomer. Studies in yeast have showed how the mammalian PERK lumenal domain functionally substitutes for the yeast IRE1 lumenal domain although the yeast genome does not have a PERK equivalent. This supports that IRE1 and PERK share functionally homologous and interchangeable region that sense unfolded proteins that are conserved between yeast and humans (Harding et al., 1999; Liu et al., 2000; Yoshida et al., 1998). As previously described, removal of BiP/GRP78 from the PERK lumenal domain triggers oligomerization and thus, autophosphorylation (Ma et al., 2002). This knowledge has produced the speculation that PERK activation by ER stress may be similar to the activation of IRE1 itself (Bertolotti et al., 2000; Liu et al., 2000). Lumenal domain centres on three prevailing models for how PERK senses accumulating unfolded proteins within the ER.

(1) In response to ER stress, the large N-terminal domains of both IRE1 and PERK reside in the ER lumen and dimerize, in a ligand-independent manner (Liu et al., 2000). The binding of BiP to PERK involves the folded lumenal domain of PERK and the ATPase domain of BiP (Carrara et al., 2015). Other studies, however, suggested a canonical interaction with the substrate-binding domain of BiP and an unstructured region of the PERK lumenal domain adjacent to the transmembrane part of the protein (Ma et al., 2002). It has been shown that the lumenal domains of IRE1 and PERK interact with BiP in the resting state (Bertolotti et al., 2000; Liu et al., 2000; Okamura et al., 2000), so it has been proposed that excess unfolded proteins under ER stress compete with BiP to occupy the lumenal domains of IRE1 and PERK. Thus, it can be noted how ER stress promotes the reversible dissociation of BiP from the PERK and IRE1 lumenal domains, leading to their homodimerization and trans autophosphorylation. As expected, displacement of BiP from IRE1 and PERK was shown to correlate with formation of activated PERK and IRE1; similarly, overexpression of BiP attenuates their activation (Berolotti et al., 2000). Such results are consistent with a model in which BiP represses signalling through PERK and IRE1 while protein misfolding relieves this repression in its release of BiP from the PERK and IRE1 lumenal domains.

(2) It has been suggested that BiP is not the sole chaperone initiating the UPR for all the ER transmembrane sensors (Kimata et al., 2004). In this model of UPR activation the unfolded proteins directly bind IRE1α or PERK without an intermediary. This direct interaction of unfolded proteins with lumenal domains induces sufficient conformational changes and oligomerization to initiate the UPR. It was previously held that, given that the ER lumenal structure of yeast IRE1 suggests direct binding with unfolded proteins

triggered the UPR, it is plausible (with the structural similarities between IRE1 and PERK) that PERK binds to accumulating unfolded protein within the ER, which induces the conformational changes that produce PERK phosphorylation of eIF2α (Gardner et al., 2011; Korennykh et al., 2012). It has been shown that the lumenal domain utilizes a conserved hydrophobic groove at the C-terminal domain for recognition and interaction with misfolded proteins. Multiple binding sites for the PERK lumenal domain, along with direct binding of PERK to the misfolded protein can cause PERK to oligomerize. It has also been suggested that peptide binding to the PERK lumenal domain produces a stabilized complex structure conformation, more disposed to form oligomers via a stacking format. These combined mechanisms allow PERK to stack along the misfolded proteins of ER stress. It is therefore likely that direct binding of unfolded/misfolded proteins to IRE1/PERK is determined by the individual nature of the protein: IRE1 is intolerant of acidic residues and, similar to PERK, favours hydrophobic residues (Gardner et al., 2011).

(3) Synthesises the two preceding models suggests that both BiP dissociation and the direct binding of peptides may cause the UPR activation (Ron and Walter., 2009). This could present a more reliable and efficient method of handling unfolded/misfolded proteins, allowing the detection of a broader range of unfolded proteins via BiP or direct binding.

1.19 Downstream effectors activated via PERK

Translation is initiated when the ternary complex of the eIF2 GTPase, GTP and initiator methionyl-tRNA binds the 40S ribosomal subunit to generate a 43S preinitiation complex (Hershey., 1991). When the 60S ribosomal subunit joins, there is a concomitant hydrolysis of Guanosine-5'-triphosphate (GTP) to Guanosine-5'-diiphosphate (GDP). When GDP bound to eIF is exchanged for GTP, another round of initiation begins. This exchange reaction requires the guanine nucleotide exchange factor eIF2B. Phosphorylated eIF2α stabilizes the eIF2-GDP-eIF2b exchange complex which in turn prevents the GDP-GTP exchange reaction. The resulting reduction in eIF2-GTP levels leads to the inhibition of the overall rate of protein synthesis (Hershey., 1991).

Not all translation ceases after PERK/phospho-eIF2α activation. A few mRNA transcripts are induced through the presence of upstream open reading frames (ORF) in their 5′UTRs which leads to their preferential translation in periods of low ternary complex (Harding *et al*. 2000; Lu *et al*. 2004). Activating transcription factor 4 (ATF4) is one of these proteins which induces the expression of several proteins involved in cellular metabolism, redox homeostasis and apoptosis

(Blais *et al*. 2004; Vattem and Wek 2004). These ORFs enable the escape of ATF4 from massive gene translation suspension, whereas ATF4 translation often ceases under normal conditions (no ER stress) (Chen et al., 2013; Su et al., 2008). ATF4, like other members of cAMP-responsive element-binding protein family, targets a broad range of molecules, and has been shown to act as a pro-apoptotic factor under ER stress (Cao et al., 2012). Approximately half of all PERK-dependent UPR target genes are ATF4- dependent, including genes that aid amino acid metabolism, redox regulation and protein secretion (Harding et al., 2003). During pronounced or prolonged ER stress, the transcription factor C/EBP homologous protein (CHOP) is induced. CHOP is a member of the bZip family of transcription factors, which contains an ER stress response element (ESRE) in its promoter (Wang et al., 1997; Zinszner et al., 1998; Ma et al., 2002). It forms heterodimers with members of the C/EBP and Fos-Jun families (Ubeda et al., 1996; Ubeda et al. 1999) and induces apoptosis (Zinszner et al., 1998; Matsumoto et al., 1996). CHOP suppresses B-cell lymphoma 2 (Bcl2), induces BCL-2-interacting mediator of cell death (Bim) and Death receptor 5 protein (DR5), promotes caspase activation and is proapoptotic in many cell types (Mccullough et al., 2001; Silva et al., 2005; Song et al., 2008; Li et al., 2009; Y.-H. Zhang et al., 2011; Carlisle et al., 2014), though another of its targets, Growth arrest and DNA damage inducible 34 (GADD34), may more strongly correlate to ER stress-induced cell death (Rutkowski et al., 2006). GADD34 has been found to function as a cofactor for protein phosphatase 1 by binding the phosphatase catalytic subunit and directing it to dephosphorylate eIF2α (Novoa et al., 2001). Under the regulation of eIF2α, GADD34/ protein phosphatase 1 (PPI) form a feedback loop to control translation: under conditions of ER stress, PERK phosphorylates eIF2α which induces the expression of GADD34, which in turn eventually mediates the dephosphorylation of eIF2α by PP1, returning protein translation to its resting state after the UPR has succeeded in correcting the ER stress.

1.20 NRF2: a second substrate of PERK

Nuclear factor erythroid 2 (NRF2) activation during the UPR was established following identification of NRF2 as a substrate of PERK (Cullinan et al., 2003). NRF2 belongs to the cap 'n' collar family of transcription factors (Chan et al., 1993; Moi et al., 1994), and is maintained inactive in a cytoplasmic complex with the microtubule associated protein KEAP1 (Kelch-like Ech-associated protein 1) (Alam et al., 1999; Itoh et al., 1997; Itoh et al., 1999). NRF2 is required for free radical scavenging, detoxication of xenobiotics and maintenance of redox potential (Osburn & Kensler, 2008). In 2013, Cullinan and colleagues showed that ER stress induces NRF2 nuclear translocation in a PERK-dependent manner, similar to oxidative stress-inducing agents. Crucially, this activation process does not require reactive oxygen species to accumulate, nor the phosphorylation of eIF2α. Identifying NRF2 as a PERK substrate lends weight to the hypothesis

that PERK signalling has pro-survival attributes. During ER stress, NRF2 phosphorylation by PERK dissociates the NRF2-KEAP1 complex which permits NRF2 to translocate to the nucleus (Cullinan et al., 2003). NRF2 helps maintain levels of the redox buffer glutathione via transcription of genes encoding proteins responsible for glutathione maintenance (Zhang and Kaufman, 2008, Cullinan and Diehl, 2006) and also activates the transcription of various antioxidant genes (Zhang, 2006). Given the role of NRF2 in combating oxidative stress, it was proposed to have a cytoprotective role in NRF2 signalling in response to ER stress. NRF2 signalling is known to be a requirement for survival during the UPR; NRF2−/− cells have been shown to be sensitive to a variety of ER stress inducers, and the overexpression of NRF2 enhances survival during the UPR (Cullinan et al., 2003; Cullinan and Diehl., 2004). As such the PERK-NRF2 signalling forms part of a protective signalling response (Cullinan et al., 2003).

In summary, PERK signalling initiates two independent pathways of gene and protein expression. By direct phosphorylation of eIF2α and NRF2, PERK is key in regulating many facets of the overall cellular response to ER stress. The attenuation of protein translation (Harding et al., 1999) and subsequent cell cycle arrest (Brewer and Diehl., 2000) provide cells with the 'breathing space' to conserve energy and, in conjunction with IRE1 and ATF6-dependent transcriptional activity, to resume normal protein folding status in the ER. Secondly, the work of Harding and colleagues (2003) implicates PERK in the activation of two different regulators of redox homeostasis, NRF2 and ATF4. Activation of both these transcriptional regulators is dependent upon PERK activation, which demonstrates an unambiguous mechanism for the significant oxidative stress experienced in $PERK^{-/-}$ cells. The lack of induction in glutathione biosynthetic enzymes in these cells, coupled with the severe sensitivity to ER stress in $NRF2^{-/-}$ as well as $ATF4^{-/-}$ cells demonstrates the requirement for both NRF2 and ATF4 signalling in the ER stress response.

1.21 PERK in neurodegeneration

The short-term reduction of protein synthesis in times of cellular stress is considered to be protective in allowing cells to conserve energy resources and simultaneously enhancing the gene-specific translation of stress-related mRNAs, which works to reconfigure gene expression better to meet the challenge of cellular stress (Paschen et al., 2007). During the severe and prolonged chronic cellular stress associated with neurodegenerative diseases, the activation of PERK protracted such that eIF2α is permanently hyperphosphorylated, leading to a sustained repression of mRNA translation. An enhanced, prolonged increase in eIF2α phosphorylation is deleterious for *de novo* protein synthesis and cellular maintenance for neuronal plasticity and memory consolidation, which produces the outward decline in cognitive function (Klann et al,

2007; Alberini., 2008). All of this highlight how a balanced UPR/PERK/eIF2α pathway is paramount for maintaining cellular homeostasis during stress.

Several groups have reported UPR activation with phospho-PERK and phospho-eIF2α in AD brain (Hamos et al., 1991; Hoozemans et al., 2009, 2005; Chang et al., 2002; Nijholt et al., 2011; O'Connor et al., 2008). Levels of phospho-eIF2α correlate with elevated beta-site amyloid precursor protein cleaving enzyme 1 (BACE1) levels in transgenic mice and this was also found in AD patient brains (O'Connor et al., 2008). BACE1 is one of the proteases responsible for cleaving amyloid precursor protein into Aβ. In the AD brains, levels of Binding immunoglobulin protein (BiP) were found to be increased in the temporal cortex and the hippocampus against controls (Hoozemans et al., 2005). Comparing expression of BiP in the different Braak stages of AD suggests that UPR activation occurs early on in AD. Exposure of cells to Aβ oligomers or fibrils in different *in vitro* models also triggered ER stress, which was shown to lead to phosphorylation of eIF2α, PERK and other indicators of UPR activation (Katayama et al., 2004).

UPR activation is associated with hyperphosphorylated tau. Phospho-PERK is observed in neurons and glia exhibiting tau pathology (Nijholt et al., 2011). IRE1 and PERK phosphorylation are recorded in AD as already mentioned above and a wide range of frontotemporal dementias (Nijholt et al., 2012). Cell models suggest that inducing ER stress by exposure to Aβ oligomers correlates with the induction of tau phosphorylation (Resende et al., 2008). The interplay of ER stress, Aβ mediated neurotoxicity and tau hyperphosphorylation is clearly significant (Resende et al., 2008). Induction of UPR signaling co-induces tau phosphorylation, possibly via activation of GSK-3β (Sakagami et al 2013), which presents a direct link between UPR activation and neurodegeneration. In AD brains, neurons with phospho-PERK co-express active GSK-3β (Hoozemans et al., 2009). Furthermore, ERAD can be blocked by tau accumulation, which induces UPR activation in the rTg4510 mouse model of tau pathology (Abisambra et al., 2013). This presents a novel mechanism of tau toxicity arising from the disruption of normal proteostasis. As there was no evident change in protein secretion in AD or the tauopathic brain, Abisambra noted ERAD damage as a possible mechanism for the ER stress. He discussed in his work how ER stress can arise due to impairment of ERAD as shown previously in *in vitro* models of synucleinopathy and a polyglutamine expansion disease (Cooper et al., 2006; Duenwald and Lindqust., 2008). Polyglutamine caused toxicity via ER stress by trapping essential components of the ERAD machinery comprised largely of the VCP heterocomplex which plays an important role in the transport of ERAD proteins from the ER membrane to the proteasome. Abisambra further discussed how tau associated with hrd1; a VCP-associated E3 ubiquitin ligase which helps target proteins with lesions in their luminal or transmembrane domains to the ERAD (Abisambra et al., 2013) which may implicate tau in specific impairment of ERAD. This would then cause accumulation of proteins that have the same type of defects, potentiating disequilibrium of

proteostasis. Alternatively, tau may even exert a general blockage of ERAD, accounting for overall accumulation of ERAD-bound proteins in the ER.

Unsurprisingly, dopaminergic neurons in PD have proved the most established location for the chronic activation of the UPR. Activated phospho-PERK and phospho-eIF2α are significantly elevated in dopaminergic neurons compared to age-matched control brains (Hoozemans et al., 2007; Hoozemans et al., 2012). However, there is no evidence of colocalization of α-synuclein with phospho-PERK and phospho-eIF2α, which suggests that α-synuclein does not play a direct role in activating the UPR although α-synuclein has been shown to be localized to the mitochondria associated ER membranes (MAM) (Le Masson et al., 2014).

In PSP, activation of the PERK pathway has been shown in human PSP tissue samples and elevated phospho-PERK levels correlate with increasing levels of tau (Stutzbach et al., 2015). However, in this same study, some elderly controls also exhibited moderate pPERK staining in the hippocampus (Stutzbach et al., 2015). A correlation analysis demonstrated that PERK activation increased with both age and tau pathology. Furthermore, pPERK positive brain cells were also positive for diffuse tau suggesting that PERK activation precedes the formation of NFTs and thus may be an early event in disease pathogenesis. Therefore, it is likely that soluble tau conformers rather than NFTs lead to PERK-induced ER stress. This is important because evidence suggests that soluble oligomeric tau, but not insoluble tau, is most likely responsible for tau-induced neurotoxicity (O'Leary et al., 2010; de Calignon et al., 2012). Therefore, the formation of soluble/diffuse tau intermediates may activate a cell damage pathway that is only visible pathologically using ER stress markers for the PERK pathway. This could help to explain why the number of neurons lost in tauopathic patient brains far exceeds the number of tau tangles. It is likely that multiple mechanisms of cell death are activated when tau begins to accumulate, and PERK activation appears to be one of the major routes.

Whether PERK and tau directly influence one another remains an unanswered question. Evidence by Hoozemans et al., (2009) also indicated that PERK activation may temporally precede overt tau aggregation and could be triggered by undetectable levels of abnormal tau. PERK may therefore affect tau pathology in one or more ways as the genetic data implicating both PERK and tau in PSP supports a plausible temporal relationship between PERK activation and tau aggregation. PERK could influence whether a cell forms aggregates, either at the point of protein delivery to the cytoplasm or at the point of aggregation. Moreover, PERK could also influence downstream effects of tau aggregation as the UPR and tau intersect in several protein degradation pathways, including the proteasome system (Yen, 2011), which is the target of the ERAD pathway (Travers et al., 2000), and the endosome to lysosome pathway (Guo & Lee, 2011). Another finding that could account for the connection between PERK variation and tauopathy is the association of tau with the rough endoplasmic reticulum (Iqbal et al., 2009).

Recent work demonstrated that abnormally phosphorylated tau partially colocalized with several subcellular compartments, including the ER (Tang et al., 2015). This colocalization would bring tau aggregates and the UPR machinery in close proximity, providing an opportunity for these two processes to interact more directly with one another.

While the UPR is activated by misfolded proteins within the ER, and aggregated misfolded tau occurs in PSP, AD, and other tauopathies, tau is a cytosolic protein and does not necessarily appear to traffic through the ER as part of a secretory pathway. In normal neurons, most tau protein is intracellular and attached to microtubules. In tauopathies, tau aggregates in the cytoplasm of cells, in cellular processes, and at nerve terminals. Recent work in mouse models of α-synucleinopathies and studies on PD autopsy material (Colla et al., 2012) suggest that small amounts of α-synuclein can be found in the ER, and that in the disease state, these levels are elevated, thereby activating the ER stress response. Still, since there is no direct evidence that tau traffics through the ER, or evidence of tau aggregates in the ER, it is unlikely that misfolded tau directly activates the canonical UPR. This view is supported by the fact that in PSP, pPERK and pEIF2α are activated in cells with no observable tau pathology, but we cannot exclude the possibility that very low or undetectable levels of aggregated tau are present. Rather, a more likely explanation is that tau-induced cytoplasmic events act to trigger the UPR by an unknown mechanism, which in turn influences the degradation of tau.

1.22 Background to this thesis

In the largest GWAS for PSP one of the genome wide significant association involved the SNP rs7571971 that is resident in a non-coding region in intron 2 of *EIF2AK3* (Hoglinger et al., 2011). This SNP is in linkage disequilibrium (LD) (r2>0.8) with a series of coding SNPs which alter conserved residues within PERK (Ferrari et al., 2014; Stutzbach et al., 2013; Liu et al., 2012). It has been suggested that the associated alleles are linked to changes in PERK activity, further suggesting that PERK modulation could hold therapeutic possibility. Considering that inheritance of this SNP increases risk for a wide spectrum of PSP, AD, and lower bone mineral density (Liu et al., 2011; Stutzbach et al., 2015; Hoozemans et al., 2011) the advantages of successful therapy would be considerable. However, another less likely but still plausible explanation is that PSP risk in this region comes from a regulatory element that is intronic, within *EIF2AK3*, or in a close by intergenic region and that this element controls expression of another gene. Also, the true PSP association could be from nearby genes (e.g. *FOXI3* or *RPIA*) though this is less likely since the signal from SNPs in highlighting these genes are not as significant as SNPs within *EIF2AK3.* However, the strength of the genetic evidence indicates that *EIF2AK3* and not an adjacent locus is the gene that confers risk for PSP.

The SNP rs7571971 incorporates the coding SNPs rs867529; $Ser_{136}Cys$, rs13045; $Gln_{166}Arg$ and rs1805165; $Ala_{704}Ser$ as well as the intronic, rs4972221, producing the functional coding haplotypes: A: Ser_{136}-Arg_{166}-Ser_{704}; B: Cys_{136}-Gln_{166}-Ala_{704}, and D: Ser_{136}-Gln_{166}-Ser_{704} (Liu et al.,2012). Haplotype A and Haplotype B are two common haplotypes with predicted frequencies of 0.64 and 0.29, respectively; Haplotype D has a frequency of 0.06; and 4 rare PERK haplotypes of frequency close to 1/1000 were also reported (Liu et al., 2012 and Ferrari et al., 2014). It was observed that the haplotypes A and D completely correlated with rs7571971 allele C of the PSP non-risk allele whereas haplotype B completely correlated with allele T, the PSP risk allele. This suggested that the basis of risk in PSP is borne by functional differences of Haplotype B. Moreover, Haplotype B has been noted to have an association with lower bone mineral density (Liu et al., 20120). In Liu's work, human β-lymphocytes homozygous for Haplotype B demonstrated significantly more eIF2α phosphorylation compared to Haplotype A in response to treatment with the ER stress-inducing drug Thapsigargin (Liu et al., 2012). The haplotype that confers high risk for PSP produces the more active form of PERK, suggesting that activation of the UPR is pathogenic in PSP and not a protective response. This is consistent with observations in prion protein induced neurodegeneration. Moreno et al., (2012) showed that during prion replication, synaptic failure and neuronal loss is temporally associated with UPR activation and inhibition of translation. When translation is restored using over-expression of GADD34 to dephosphorylate eIF2α, survival of infected animals is prolonged. In contrast, when the UPR is activated using salubrinal, survival is decreased (Moreno et al., 2012). Both observations are consistent with activation of the PERK/eIF2α arm of the UPR enhancing neurodegeneration, as proposed here for PSP. Similarly, when a PERK inhibitor was administered to P301L tau transgenic mice it was shown to restore protein synthesis rates, protect against further neuronal loss and lowered levels of phospho-tau (Radford et al., 2015). However, one must bear in mind that PERK inhibition may lead to the same symptoms as Wolcott–Rallison syndrome. The absence of PERK protein and abrogation of kinase function by the Wolcott–Rallison PERK mutations cause clinical phenotypes that closely align with those seen in the *Perk*$^{-/-}$ mouse which include pancreatic insufficiency. The *Perk*$^{-/-}$ mice and Wolcott–Rallison patients typically do not survive to an advanced age when PSP symptoms emerge (Yuan et al., 2018).

Meanwhile, pharmacologic PERK activation as recently demonstrated by Bruch et al., (2017) showed not only reduced tau phosphorylation but also reduced tau conformational changes and 4-repeat tau isoforms, significantly improved memory and locomotor function, reduced tau pathology, and prevented dendritic spine and motoneuron loss in P301S tau mice treated with the pharmacological PERK activator CCT020312 thereby indicating that at the functional and cellular level, PERK activation mitigates the detrimental effects of tauopathy (Bruch et al., 2017). This interpretation is consistent with several previous reports of increased UPR activity to protect

cells from various forms of protein aggregation (Boyce et al., 2005; Loewen and Feany., 2010; Vaccaro et al., 2013).

Thus, these coding changes of *EIF2AK3* described above are potentially functional variants of PERK which may affect its role in the UPR. At least one of the three changes, S136C (rs867529), is predicted consistently to be a deleterious substitution for PERK (Burke et al., 2007). It is notable that the three coding SNPs affect the three highly conserved residues, two in the lumenal domain of PERK, responsible for homodimerization/auto activation of PERK and one at the active site kinase domain of the protein (Figure 12). This strongly suggests that the three residues of haplotype A (Ser136-Arg166-Ser704) are crucial for the proper functioning of the protein. HapA and HapD differ only at the middle amino acid at position166— and thus it is plausible that this amino acid alone does not account for the difference in PERK activation. As the non-risk (A and D) and risk haplotypes (B) differ at both positions 166 and 704, it is not clear which one or maybe even if both substitutions are crucial for the allelic difference. The tauopathy-associated *PERK* alleles are not conserved in other species, and moreover, are distinct from previously identified human PERK variants associated with Wolcott–Rallison syndrome (reviewed in Yuan et al., 2018).

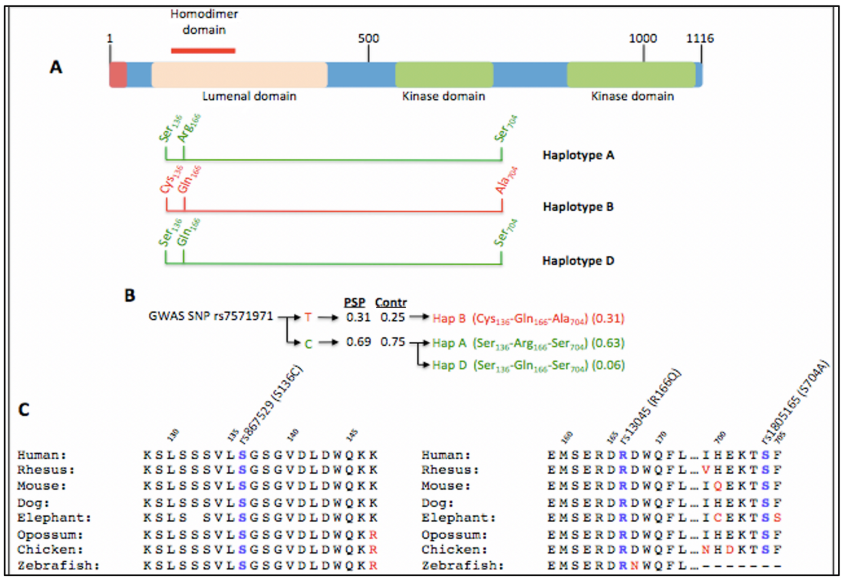

Figure 12. **Scheme of PERK protein.** The different PERK domains with relative positions of residues defining coding haplotypes are indicated in (A). The relationship of LD amongst SNP alleles in PSP subjects and control subjects (Contr) is reported in (B). Haplotype B segregates with the risk allele (T) of the GWAS associated SNP rs7571971 whereas the haplotyoes A and D segregates with the non-risk allele (C) as indicated in (B). The T allele frequencies between PSP and control population was 0.31 and 0.25 respectively, whereas the non-risk c allele frequencies between the PSP and control population was 0.69 and 0.75 respectively. Residues defining common haplotype A and their flanking domains are highly conserved across species (C) (modified from Liu et al., 2012).

Hypothesis and Aims

The primary purpose of this project was to develop cell models for the study of the functional basis of coding variation of the *EIF2AK3* gene, encoding PERK, that is associated with risk of PSP. PERK is an important sensor of cell stress, particularly ER stress due to unfolded proteins that are generally associated with the pathophysiology of neurodegenerative proteinopathies, including the tauopathies. The association with PSP is linked to one of three coding haplotypes that has higher PERK activity and contributes to and co-localises with tau pathology in AD and PSP. The three coding single-nucleotide polymorphisms (SNPs) affect three highly conserved residues, two in the lumenal domain of PERK, responsible for homodimerization/auto-activation of PERK and one at the active site kinase domain of the protein. In order to address the hypothesis that the three polymorphisms of PERK could affect either functional domain (or both) and alter PERK kinase activity we aimed to assess the functional importance of these coding haplotypes by

(1) Creating stable isogenic cell lines for Tet-inducible expression of PERK functional haplotypes HapA and HapB: We utilised the Flp-In T-Rex system (Life Technologies) to create isogenic cell lines with Tet-inducible expression of the PERK variants. Owing to the cytotoxicity of PERK overexpression and activation, gene expression was tightly regulated using the Tet-inducible expression system (T-Rex). Furthermore, in order to selectively eliminate the contributions of endogenous *EIF2AK3*, all exogenous expression constructs harbour silent mutations that will make them siRNA resistant.

(2) Characterising UPR activity: We utilised the above stable cell lines for regulated expression of the PERK coding haplotypes and mutants and qualitative and quantitative comparison of UPR as a result of ER stress, with focus on downstream markers of the PERK branch, including p-eIF2α, as well as the IRE1α and ATF6 branches of UPR.

(3) Comparing tau pathological markers: As PERK and UPR activation are associated with tau pathological progression, we also used markers for tau pathology, including sarkosyl-insoluble tau and presence of PHF1 immunoreactivity for pathological tau phospho-epitopes and MC1 for pathological conformation epitopes. The HEK293 cells, which have very low basal tau expression levels, formed the basis of the study of exogenous overexpression of tau isoforms and mutants that cause familial FTLD and we investigated the effect of excess wild-type and mutant tau over-expression on PERK activation.

2 Methods and Materials

2.1 *Methods*

2.1.1 *Molecular Biology*

2.1.1.1 *DNA restriction digests*

Typical restriction digests were carried out in a total volume of 50 μL, containing 5 μL 10 x buffer as supplied with the endonuclease by the manufacturer (ThermoFisher), 2.5 μL of each restriction endonuclease, 5 μL bovine serum albumin solution (0.1 mg/mL) and approximately 5 μg DNA. The reaction mixture was made up to 50 μL with nuclease free water. Uncut experimental DNA and a no-enzyme 'mock' digestion were used as controls. Digestions were incubated at 37°C for 1 hour.

2.1.1.2 Polymerase *chain reaction*

Polymerase chain reactions (PCRs) was performed using the FastStart PCR Master (Roche) kit, the Master Mix of which contains all the buffers, deoxynucleoside triphosphate (dNTPs) and polymerase required. Primers were diluted to 3 μM, using 5 μL per reaction of each forward and reverse primer. As the template deoxyribonucleic acid (DNA) was a plasmid preparation it was routinely diluted 1000-fold and 5 μL used per reaction (approximately 10 ng of plasmid DNA). This mixture was increased in volume to 25 μL with nuclease free water and then mixed with 25 μL High Fidelity Master Mix. To detect possible DNA contamination, a negative control was included in each run. This control was prepared by replacing template DNA with nuclease free water.

Temperature cycling was achieved by using a Techne Mastercycler. Usually the cycles were preceded by a 4 min initial denaturation at 95°C. This both activates the previously inactive FastStart Taq DNA Polymerase and denatures template DNA. This step is then followed by 30 cycles of denaturation at 95°C for 15 s, the annealing temperature (variable, depending on the ideal conditions for the primers) for 30 s and elongation at 72°C for 45 s. Thirty cycles were enough to produce an adequate amount of PCR product. For low concentrations of target DNA, the number of cycles was increased to 40. The final step was performed at 72°C for 7 min. The PCR products were refrigerated at 4°C until the samples were needed.

2.1.1.3 Agarose gel electrophoresis

Routine gels, used for checking restriction fragment lengths and PCR products, were made by melting 1% (w/v) agarose (Sigma-Aldrich) in 1 x Tris-acetate (TAE) buffer, heated in a microwave oven for approximately 2 min. Gels were cast, with the addition of 1 μL GelRed™ (Biotium), using combs to create wells into which DNA samples could be loaded. The size of the wells made was appropriate for the volume of the sample. Once fully set, the gels were submerged in 1 x TAE buffer in a suitable electrophoresis tank. Samples were mixed with 6 x DNA gel loading dye (ThermoFisher) and loaded into the wells alongside a 1 kilobase (kb) DNA ladder (Hyperladder I; ThermoFisher). Electrophoresis was routinely carried out at 100 V for approximately 90 min, or until the dye fronts had migrated approximately 3/4 down the gel. DNA was visualised with an ultraviolet (UV) transilluminator, and records were made using the 600 nm channel on the Odyssey FC imager (LiCor).

2.1.1.4 DNA *fragment purification and extraction*

Restriction or PCR products were separated by electrophoresis as described above, using a gel made with 2 % (w/v) low melting point agarose (Sigma-Aldrich) in 1 x TAE buffer. QIAquick Gel Extraction Kit (Qiagen) was used to extract and purify DNA. This involved cutting out the bands of interest from the gel using a sterile scalpel blade and weighing each excised slice. Three volumes of solubilization buffer QG (Qiagen) were added (100 mg gel = 100 μL) and the excised gel bands melted at 50°C for 10 min until the gel slice had completely dissolved. After solubilizing the gel slice, isopropanol and binding buffer QG (Qiagen) were added and the solution added to the QIAquick column. This results in binding of DNA fragments to the silica matrix. The columns were spun at 9,409 g for 1 min and the flow through discarded. After washing away impurities and residual salts with buffer PE (Qiagen), the DNA fragments were eluted from the column using 25 μL nuclease free water. The columns were left to stand for 4 min to increase the yield and then centrifuged at 9,409 g for 1 min. The purified DNA was analyzed on a 1 % (w/v) agarose gel.

2.1.1.5 DNA ligation into plasmid vectors

2.1.1.5.1 Sub-cloning

Purified fragments of plasmid vector and insert DNA were combined so that there was a 10:1 molar excess of insert to vector DNA, using 50 ng vector DNA. This was mixed with 1 μL 10 x T4 DNA ligase buffer and 0.5 units of DNA ligase (Promega). The ligation mixture was supplemented

with 1 μL of 10 mM adenosine triphosphate (ATP) (New England BioLabs). The volume was increased to 10 μL with nuclease free water and the mixture was incubated overnight at 4°C.

2.1.1.5.2 Ligation of PCR products into pGEM-T

High fidelity PCR reactions generate 5' adenosine overhangs. The pGEM-T vector (Promega) contains linearized vector DNA with compatible 3' thymidine overhangs, T4 DNA ligase and 2 x ligase buffer. Usually a 5 μL volume of agarose gel purified PCR product was used in overnight ligation at 4°C in a total volume of 10 μL.

2.1.1.6 E. coli *transformation and routine preparation of plasmid DNA*

Escherichia coli (*E. coli*) strain JM109 was transformed with plasmids using a heat shock method. High efficiency competent cells (Promega) were thawed on ice and 50 μL aliquots were mixed with 5 μL ligated DNA mixture, or 1 μL of a 1:10,000 dilution of plasmid DNA preparation in nuclease free water. Following 20 min incubation on ice, the cells/DNA mixture was incubated for a carefully timed 60 s at 42°C, using a dry heat block. After a further 2 min on ice, 950 μL Luria-Bertani (LB; Sigma-Aldrich) was added, and the cells were allowed to recover for 1 h at 37°C with gentle agitation. The cells were then gently pelleted in a microcentrifuge at 600 g for 10 min and resuspended in 100 μL LB medium. Cell suspensions were spread onto LB agar plates using a sterile glass rod and grown under selection with appropriate antibiotics (100 μg/mL ampicillin for pFRT/TO vector). The plates were wrapped in cling film to prevent dehydration, and incubated overnight at 37°C.

Single colonies were picked from the plates with a sterile pipette tip and used to inoculate 3 mL LB supplemented with selection antibiotics as with the agar plates. After overnight incubation at 37°C with vigorous shaking, 2 mL was centrifuged at 12,000 g. The pelleted cells were then used to make plasmid preparations using the Plasmid Miniprep Kit (Qiagen). Briefly this involved the alkali lysis of the cells and binding of the DNA to a spin column, before eluting the washed DNA in 50 μL nuclease free water. Occasionally, larger scale plasmid preparations were made using the Plasmid Midi Kit (Qiagen) according to the manufacturer's instructions. The procedure for this was similar to the minipreparation, apart from increased volumes. For example, 25 mL bacterial culture was used, and the DNA binding column operated under gravity flow. To reduce the volume of eluted DNA, there was a precipitation step using isopropanol, before pelleting by centrifugation and dissolving in 150 μL of nuclease free water.

2.1.1.7 Endonuclease free preparation of plasmid DNA

A 2 mL LB culture was inoculated using a single colony from an agar plate of *E. coli* transformed with the plasmid for preparation. After overnight incubation at 37˚C with shaking, 200 μL was used to inoculate 100 mL of LB (supplemented with antibiotic) in a conical flask. After a second overnight incubation at 37˚C with shaking, endotoxin-free (Endofree) plasmid preparations were made using the Endofree preparation kit (Qiagen) according to the manufacturer's instructions. Briefly, this involved pelleting of the cells by centrifugation of 6000 g for 20 min, alkali lysis of the cells (P2 buffer), and removal of lipid and protein using a syringe filter (P1 and P3 buffer), endotoxin removal by incubating with a kit component (Buffer QC), elution with buffer QN and precipitation with isopropanol, before pelleting of DNA in 70 % ethanol (v/v) by centrifugation and dissolving in 250 μL of nuclease free water. Endofree preparations of plasmid DNA were checked for purity and quantified spectrophotometrically using the Nanodrop ND1000 (ThermoFisher). The absorbance at 260 nm and 280 nm was measured. An OD_{260}/OD_{280} value of 1.8 indicated pure DNA.

2.1.1.8 Characterisation *of constructs via sequencing*

The DNA samples to be sequenced were diluted in nuclease free water to 100 ng/mL. 10 μL of sample and 3.2 pmol/μL of the purchased sequencing primers were submitted to Source Bioscience (Cambridge) for sequencing. All primers are detailed in the Appendix.

2.1.2 Cell *culture*

2.1.2.1 *Flp-In T-REx 293*

The Flp-In T-REx™ cell line (passage 1) was purchased from Invitrogen. The cells were routinely cultured in Dulbecco's Modified Eagle Medium (DMEM) supplemented with 10 % Foetal Bovine Serum (FBS) (v/v) and 1% penicillin/streptomycin solution (v/v) and maintained at 37˚C in 100 % relative humidity and 5 % carbon dioxide. The medium was changed every three days.

Cells were sub-cultured by diluting (splitting) at a ratio between 1:5 and 1:100 (routinely 1:100 for untransfected cells and 1:5 for transfected cells under antibiotic selection) after reaching 80 % confluency, approximately 7 days after sub-culture. This involved discarding the culture medium, washing the cells with 1 x Phosphate Buffered Saline (PBS) (Sigma-Aldrich) and rinsing the adherent cells with 1 x trypsin solution (Invitrogen) at 37˚C for approximately 5 min. Fresh media

was added to the detached cells and spun at 1000 x g for 10 min. The cell pellet was resuspended in complete DMEM for the untransfected cells and DMEM supplemented with selection antibiotics for the PERK stable cell lines and used to further seed T75 tissue culture flasks. This was done by accomplishing an initial seeding density of 1.0 x 10^6 cells in a total surface area of 7,500 mm^2 of a T75 tissue culture flask supplemented with 15 ml of complete DMEM medium to obtain approximately a confluent cellular T75 flask of 8.5 x 10^6 cells following seven days in culture.

Long term storage of cell cultures was achieved by harvesting: by trypsinisation of cells from a 25 cm^2 flask, pelleting by centrifugation at 1000 x g for 5 min, and suspending the cells in 1 mL freezing medium. Suspensions were then transferred to cryotubes and slowly frozen in a bath of isopropanol in a -80°C freezer. Following at least 24 h freezing time, the cryotubes were transferred to a sub-liquid nitrogen freezer.

To thaw cells that are stored in liquid nitrogen, a cryotube containing the cells was placed for 2 min in a water bath (37°C). Because dimethyl sulphoxide (DMSO) is toxic to the cells, the thawed cell suspension was immediately diluted in 10 mL of pre-warmed cell culture medium. The cell suspension was centrifuged at 1000 x g for 5 min at room temperature. The supernatant was discarded, and the cell pellet was carefully resuspended with 5 mL of pre-warmed cell culture medium. The cell suspension was transferred into a T25 cell culture flask. After one day of culturing, the cell culture medium was changed. To do so, the old medium was aspirated, and 5 mL of fresh pre-warmed cell culture medium was carefully pipetted to the cells. As soon as the cells reached up to 80 % confluence, they were transferred into a T75 cell culture flask.

For plating the exact number of cells for chapters 3, 4, 5, and 6 the cell count was determined using the Neubauer chamber. The medium from a cell culture flask was removed and 3.5 mL of trypsin was added, and the flask was incubated for 5 min in the CO_2 incubator. The reaction was stopped by adding 10 mL of Dulbecco's Modified Eagle Medium (DMEM) and the cell suspension was transferred to a 15 mL centrifugation tube, which was centrifuged at 1000 x g for 5 min at room temperature. The supernatant was discarded, and the cell pellet was resuspended in 12 mL medium. For cell counting, 20 µL of cell suspension was mixed with 40 µL of 0.4 % trypan blue solution and 20 µL DMEM medium in a 1.5 mL reaction tube and 10 µL of this suspension was applied on a Neubauer chamber. After counting the cells in four big squares, the cell concentration was determined as follows:

$$\text{Number of cells/mL} = \frac{\text{total number of cells counted} \times \text{dilution factor} \times \text{chamber factor}}{4}$$

The chamber factor for the Neubauer chamber used was 104 (each square has an area of 0.01 cm^2 and a depth of 0.1 mm, which results in a volume per square of 0.1 µL). The dilution factor for the procedure described above was 4.

2.1.2.2 Transfection *with Lipofectamine® 3000*

Stable transfection of T-REx™ 293 cells was achieved through targeted chromosomal integration of the PERK expression plasmid pcDNA5 Flp Recognition Target/Tet operator (FRT/TO). For this purpose, the Flp/FRT recombination site specific system was used and Lipofectamine® 3000 (Promega) was used as the transfection agent.

The genetically modified T-REx™ 293 cells carry a Flp recognition target (FRT) site in their genome. The FRT site is also present in the expression vector pcDNA5 FRT/TO. These artificially introduced FRT sites are the target sequences for the Flp recombinase, which is encoded by the helper plasmid pOG44. The Flp recombinase mediates the DNA recombination and therefore leads to the integration of pcDNA5 FRT/TO-PERK into the genome of T-REx™ 293 cells.

All transfections of mammalian cell cultures were carried out using Lipofectamine® 3000 (ThermoFisher) according to the manufacturer's instructions. The lipofectamine® 3000 is a specially designed cationic lipid which facilitates DNA and small interfering RNA (siRNA) delivery into cells (Chesnoy and Huang, 2000; Hirko et al., 2005).

Splitting of the cells was done three times over the course of twenty-one days to ensure the cells were fully recovered from thawing. Twenty-four hours before transfection the cells were seeded at 0.5 x 10^6 cells/mL so that they would be at the desired concentration of 1 x 10^6 cells/mL at time of transfection. On the day of transfection, the concentration of plasmid pcDNA5/FRT/TO-PERK and pOG44 was assessed via NanoDrop at 260 nm. The pcDNA5/FRT-PERK constructs were used to transfect the cell line, using lipofectamine® 3000 as a transfection agent and the pOG44 Flp-Recombinase Expression Vector (ThermoFisher) in a 1:9 ratio (3 µg of plasmid DNA added to 27 µg of pOG44). As per protocol, the ratio of plasmid DNA to pOG44 were added along with 125 µL Opti-MEM™ medium (Invitrogen) and incubated for 5 min at room temperature. Meanwhile 7.5 µL Lipofectamine® 3000 was added to 125 µL Opti-MEM™ medium. The plasmid mix was then combined with the Lipofectamine® 3000 mix, and the whole was incubated at room

temperature for 15 min before being added to cells. Medium was replaced 12 h later with 3 mL fresh DMEM.

Transient transfections were performed similarly with only the use of a single FRT/TO-PERK plasmid transfection (5 μg/μL).

2.1.2.3 Hygromycin *B kill curve*

Before stable transfected cell lines were selected, the optimal hygromycin B concentration was determined by performing a kill curve titration. Hygromycin B acts as the selective antibiotic as successfully stable transfected T-REx^{TM} 293 cells express the hygromycin B resistance gene, which is encoded by the expression plasmid pcDNA5 FRT/TO.

Cells were plated at 3.0 x 10^5 cells/mL in a 24-well tissue culture plate. Twenty-four hours later when the cells had reached a high confluence of 80 %, increasing amounts of hygromycin B (50-1000 μg/mL; Invitrogen) was added to duplicate wells of cells plated in complete growth media. A no-antibiotic control was included. Media were replaced every three days for up to a week and each day the cultures were examined for visual signs of toxicity. The following antibiotic doses were determined: low dose (minimal visual toxicity), optimal dose (lowest antibiotic concentration in which all cells are dead after one week of selection) and high dose (visual toxicity in the first 2-3 days).

2.1.2.4 Cell *line cloning and selection*

Fourteen wells were set up in 3 x 6-well plates at 1.0 x 10^6 cells/mL seeding density and transfected according to the protocol mentioned above. Cells transfected with the vector pFRT/TO/ chloramphenicol acetyl transferase (CAT) and POG44 was used as a positive control. Transfected cultures were split and plated at 0.25 x 10^6 cells/mL seeding density 48 h later, and fresh media containing hygromycin B (100 μg/mL) was added. Cell viability and count was assessed daily for three weeks, and media was replaced by fresh hygromycin B every four days. Wells where the presence of clones was observed, were transferred to 12-well plates by trypsinising the cells and transferring with the use of cloning rings. Once the cells had reached 80 % confluency the cells were split and transferred on to 6-well plates. Cells were grown in a 6-well plate until they reached 80 % to 90 % confluence and were then transferred to a T25 cell culture flask.

Emerging clones were compared based on target product production and growth performance. PERK levels were assessed by western-blot analysis and viability performance were assessed via Cell Titer-Glo® Luminescent Cell Viability Assay (Promega).

2.1.2.5 Induction *of gene expression*

To induce expression of PERK, cells were seeded into 12-well plates at a seeding density of 0.25 x 10^6 cells/mL. The next day fresh medium containing doxycycline (Dox) (0-1000 ng/mL; Sigma-Aldrich) was added in increasing concentration to duplicate wells to the cells and incubated for 24 h at 37°C. Cells were harvested, and western blot analyses used to assay for gene expression. The optimal concentration of Dox with full activation of PERK gene expression in Tet-On Flp-In 293 cells was obtained with 100 ng/mL Dox.

2.1.2.6 Methods of cell detachment

When cells were ready to be passaged, in addition to the above-mentioned method of trypsination, cell detachment was also carried out using cell scrapers, Accutase and PBS-EDTA. For cell scraping, Corning cell scrapers were used to lift off the adherent cells by gently scraping the growth surface of the T75 tissue culture flasks. For accutase detachment, similar to trypsin, cells were washed in 1xPBS followed by an adequate volume of 5 ml of Accutase detachment solution being added to cover the growth surface of the T75 tissue culture flasks. Cells were then allowed to detach at 37 C for 5 min before being resuspended in fresh medium to continue cell culture. PBS-EDTA solution supplemented without the presence of Magnesium and Calcium Ions were similarly used to enable cell detachment. Following aspiration of cell culture media, 5 ml of PBS-EDTA was added and the flasks were then struck against the palm of the hand to help in detaching the cells.

2.1.3 Protein *Chemistry*

2.1.3.1 Total *protein extraction from cell cultures*

Cultures of Dox induced PERK cells in 6-well tissue culture plates were washed in 1 mL of ice-cold PBS-EDTA per well and lysed in 250 μL of freshly made Radioimmunoprecipitation assay buffer (RIPA; supplemented with protease and phosphatase inhibitors, both Sigma-Aldrich). The plates were placed on a high-speed shaker for 10 min at 4°C and the lysate collected

using a P1000 pipette tip. Shearing of high molecular mass DNA was achieved by two short bursts of 10 s sonication. The samples were then centrifuged at 14,000 rpm for 15 min. The clear lysate was transferred to fresh 1.5mL centrifuge tubes and samples stored at -20˚C until required.

2.1.3.2 Sarkosyl-*insoluble and PHF preparation from mammalian cells*

Cells were harvested from T25 culture flasks. Firstly, the cells were washed in 3 mL of ice-cold PBS-ethylenediaminetetraacetic acid (EDTA) followed by the addition of 1.5 mL of sarkosyl lysis buffer (supplemented with protease and phosphatase inhibitors). The flasks were placed on a high-speed shaker for 10 min at 4˚C and lysates collected using a cell scraper. The lysates were then subject to mechanical disruption with the use of a glass mortar and pestle. Samples were then spun at 20,000 x g for 20 min at 4˚C. Supernatant collected, and half retained for total homogenate analyses. The total homogenate was stored at -20˚C. The remainder of the supernatant was stored at 4˚C. The pellet was resuspended in sarkosyl lysis buffer and spun at 20,000 x g for 20 min at 4˚C. The supernatant was then combined with the previous supernatant and brought to 1 % N-lauroylsarcosinate (wt/vol) (Sigma-Aldrich) and incubated for 1 h at room temperature with slow agitation before being centrifuged at 4˚C 100,000 x g for 1 h. The supernatant (sarkosyl-soluble) was collected and stored at -20˚C. The pellets of insoluble material were resuspended in a small volume (typically 25 μL) of 1 xTris-buffered saline (TBS) (100 mM). The resuspended pellets were left at room temperature overnight and stored at 4˚C the next day.

2.1.3.3 Total *protein preparation from brain tissue*

Frozen brain tissue samples were weighed and combined with ice cold RIPA buffer (supplemented with protease and phosphatase inhibitor) to give a 5:1 ratio of buffer to tissue. The mixture was then homogenised with a TissueRuptor (Qiagen) for 60 s. The tissue debris was pelleted by centrifugation at 20,000 x g for 20 min at 4˚C. Supernatant was collected, and the pellet resuspended once more in ice cold brain homogenisation buffer. The mixture was resuspended at 20,000 x g for 20 min at 4˚C and the supernatant combined with the previous supernatant and stored at -20˚C.

2.1.3.4 Protein *concentration determination*

Total protein preparations from cell cultures and tissue homogenates had variable protein concentrations. The concentrations of protein preparations were determined using the BioRad Protein Assay based on the Braford method (Bradford., 1976). This ensured that equal amounts of protein were loaded per sample onto polyacrylamide gels for subsequent immunoblot analysis. The maximum absorbance of the acidic dye, Coomassie Blue G-250, when bound to a protein shifts from 465 nm to 595 nm. A quantitation of sample protein was made using a standard curve derived from known concentrations of Bovine serum albumin (BSA).

Using a 2.0 mg/mL stock solution of BSA, a set of 800 μL standard dilutions were made in deionized water with a range of 0 to 125 μg/mL. Samples were diluted 1:4 by mixing 5 μL with 15 μL of nuclease free water. Diluted samples and the BSA standards were added in triplicates to a 96-well clear bottom plate. A 1000 μL of Reagent A (BioRad) was mixed with 20 μL of Reagent S (BioRad) and 25 μL of this solution was added to each well. A 200 μL volume of undiluted protein assay dye Reagent B (BioRad) was then added to each sample and diluted BSA standard and incubated at room temperature for 10 min. Three empty wells without sample but with the protein assay reagents were used as a negative control. Absorbance at 600 nm (A_{600}) was measured using a Spark 10M (Tecan) microplate reader.

The absorbance values were averaged and the values from the empty wells were subtracted from the remaining values. A standard curve was plotted using the BSA standard at 600 nm values (y-axis) versus their concentration in μg/mL (x-axis). The unknown sample concentrations were determined using the standard curve. The final concentration of the unknown samples was obtained by multiplying by the dilution factor used.

2.1.3.5 Immunoblot *analysis of proteins*

Immunoblot analysis of proteins is a separation of protein according to molecular weight using sodium dodecyl sulphate-polyacrylamide gel electrophoresis (SDS-PAGE), a long-standing molecular biology procedure (Laemmli, 1970), followed by immobilisation by transfer to a membrane and detection of specific proteins by enzyme conjugated antibodies.

Equal masses of 20 μg of protein samples was prepared by mixing with 10 % vol/vol reducing agent (Invitrogen) and adding 4 x XT sample buffer (BioRad). The solution was made up to 30 μL with 1 x TBS (Sigma-Aldrich) and denatured at 100˚C for 10 min. For the SDS-PAGE step the BioRad criterion system was used, which comprises pre-made 4-12 % polyacrylamide gels.

Samples were loaded into the wells of the gel alongside SeeBlue (Invitrogen) pre-stained molecular mass markers. Electrophoresis was performed in buffer containing 3-(N-morpholino) propanesulfonic acid (MOPS, BioRad) at 200 V until the dye front reached the bottom of the gel, normally 50 min. The apparatus was then disassembled, and the separated proteins were transferred to TransBlot nitrocellulose membranes (BioRad) using the semidry blot method. Briefly, this entails a non-submerged apparatus where a 200 V electrophoresis is applied for 10 min and transfer of the protein from the gel onto the membrane occurs whilst being submerged in semi dry transfer pads. Removal of the pre-stained molecular mass markers from the gel to the membrane was used to verify complete protein transfer. Occasionally, a wet transfer method was used. For the wet transfer method four sheets of 3MM chromatography paper (Whatman®) and one nitrocellulose sheet of HybondTM-C Extra (Amersham Life Science) were cut to a size slightly larger than the gel and soaked in transfer buffer. Two flat sponges were also soaked in transfer buffer. The gel was detached from the apparatus and placed in the transfer buffer to keep wet. The sponges were placed one on each electrode plate and two pieces of filter paper were placed on the side of the black electrode. The gel was gently separated from the plates and added on top of the filter paper. Polyvinylidene Fluoride (PVDF) paper was added on top carefully to avoid bubbles between the gel and the paper. Two more filter papers were added on top and the red flat electrode put on top to sandwich the gel. This was placed in a transfer tank with transfer buffer to fill to the top. Electrodes were plugged in such that the gel was on the negative side and the H-bond membrane on the positive side. The transfer buffer was fun for 2 h at 200 mV and 200 mA at 4 °C. Afterwards, the sandwich was opened up with the positive side (red) on the bottom. The papers were removed, and the top right corner cut to mark that the membrane was face up. The gel was removed, and the membrane kept in transfer buffer to stay moist.

Excess protein binding sites of the membranes were blocked by incubation for 1 h with 5 % (w/v) fat-free milk powder (Marvel) in PBS (Sigma-Aldrich). Primary antibodies against the proteins of interest were diluted at defined ratios of PBS-Tween (PBST; Sigma-Aldrich) and incubated with the membranes for a defined period. Typically, this was overnight incubation at 4°C with gentle agitation. Membranes were then washed three times with PBST, each wash lasting 10 min. A secondary antibody (IRDye® manufactured by LiCor) against the primary antibody and conjugated to a 700 nm or an 800 nm fluorophore was then incubated with the membrane, typically at 1:20,000 dilution in PBST for 1 h at room temperature with gentle agitation. This was followed by another set of three washes in PBST followed by a final wash in PBS, each wash lasting 10 min.

Presence of fluorescence was confirmed by the Odyssey FC imager. Odyssey FC imager enables two colour detection. Therefore, all blots were double labelled, and each had one secondary antibody labelled with the IRDye® 800CW which was detected by the 800 nm channel and another labelled with the IRDye 680RD® which was detected by the 700 nm channel. In general, IRDye

800CW® was used to detect the lower-abundance protein while the IRDye 680RD® was used to detect the more abundant protein.

For resolving low molecular weight proteins, a 16.5 % polyacrylamide Tris-Tricine gel was used with Tris/Tricine running buffer (BioRad). Samples were prepared similar to above apart from the use of 4 x protein sample loading buffer (LiCor). This sample loading buffer is suitable to detect low molecular weight bands. The Spectra™ multicolour low range protein ladder (ThermoFisher) was included and the gels run at 100 V for 90 min. A wet transfer was used where the separated proteins were transferred using the XCell II™ blot Module (ThermoFisher). Briefly this entails the 30 V electrophoresis for 2 h of the protein from the gel onto the PVDF membrane whilst being submerged in Transfer Buffer (Invitrogen) containing 20 % methanol. Blocking and antibody incubation was performed as described above.

2.1.3.6 *Native gel electrophoresis*

Cell lysates were prepared by the addition of 4 x NativePage™ sample buffer (ThermoFisher) and 5 % Digitonin (ThermoFisher) and homogenised by pipetting the solution up and down several times. The lysates were treated with 2 units of Benzonase endonuclease (ThermoFisher) per μL of sample and incubated at room temperature for 60 min followed by centrifugation at 20,000 x g for 30 min at 4°C.

Samples were made up to 10 μL in preparation for electrophoresis by the addition of Nativepage™ 5% G-250 sample additive (v/v) and deionized water. The XCell™ *SureLock*™ Mini-Cell system was used (ThermoFisher). Gels consisted of NativePage™ Novex 4-16 % Bis-Tris gels and the gels were run using both the dark blue and light blue cathode running buffers (Invitrogen). NativeMark™ unstained protein standard was used as a marker and the gels were run at 150 V for 120 min. Proteins were transferred to PVDF (Invitrogen) using the wet transfer detailed above. Visualization of proteins on the membrane was carried out with the use of Ponceau Red (Invitrogen). The membranes were soaked in 1:100 Ponceau Red stain under gentle agitation for 5 min and then washed extensively in water until the proteins were well defined. The membrane was destained completely by repeated washing in water followed by re-activation of the membrane by 20 % methanol (v/v).

Blocking of excess protein binding sites and probing with primary antibody was carried out as described above. A secondary antibody against the primary antibody and conjugated to horseradish peroxidase (HRP) was then incubated with the membrane typically at 0.4 μg/mL in Tris-Buffered Saline-Tween 20 (TBST; Sigma-Aldrich) for 1 h at room temperature, followed by

three sets of washes as described above. Presence of HRP was detected by enhanced chemiluminescence (ECL) using the Super Signal West Pico kit (Perbio Science). Briefly, this detection method is based on the emission of light during the reaction of HRP with luminol in the presence of hydrogen peroxide and an azine enhancer. Blots were washed with the ECL reagents for 1 min and imaged using the chemiluminescence channel on the Odyssey FC imager. Different exposure times were used between 10 s and 1 min depending on the strength of the signal.

2.1.3.7 Immunoprecipitation *of PERK from cell culture extracts and brain homogenates*

Cell extracts were pre-cleared by diluting in RIPA buffer as mentioned above. The pre-cleared lysate was immunoprecipitated (IP) with the use of protein A/G magnetic beads (Pierce™, ThermoFisher). Pierce Protein A/G magnetic beads contain a recombinant Protein A/G (approximately 50,500 Da) that combines the immunoglobulin-G binding domains of both Protein A and Protein G.

Briefly for IP, the cell lysate was combined with either 10 μg of c-Myc (SantzCruz) or PERK (SantaCruz) antibody and the reaction incubated overnight with rotation at 4°C. Pre-washed Pierce Protein A/G magnetic beads were then added to the antigen sample/antibody mixture and incubated at room temperature for 1 h with mixing. The bound antigen was then washed twice with 500 μL wash buffer (Invitrogen) and once with 500 μL purified water before being dissociated from the beads. Dissociation was carried out by eluting with 100 μL of 1 x reducing sample buffer (Invitrogen). The supernatant was stored at -20°C until further use.

2.1.3.8 Densitometry *of immunoblots and RT-PCR gels*

Immunoblots and reverse transcription-polymerase chain reaction (RT-PCR) gels were regularly quantified by densitometry. Immunoblots were imaged using the Odyssey FC: 700 nm, 800 nm and 600 nm channels for western blots and RT-PCR gels respectively. The images were quantified using the ImageStudio Lite software (LiCor). Within this system, a region of interest (ROI) was drawn around the largest/brightest band and copied to make enough ROIs for all the bands to be quantified, all of the same size dimensions. The ROIs were then positioned so that each band was covered and had an adjacent ROI (top/bottom) to act as the local background reading. Mean intensities of each ROI were then transferred to a Microsoft Excel spreadsheet. In order to calculate net band intensity, background readings were subtracted from band intensity readings.

2.1.4 DNA *and RNA chemistry*

2.1.4.1 RNA *isolation*

For this procedure RNase free conditions were maintained throughout by, treating instruments and surfaces with RNaseZAP™, RNase decontamination solution (ThermoFisher), treating solutions with 0.1 % (v/v) diethylpyrocarbonate (DEPC) for 15 min followed by autoclaving.

Ribonucleic acid (RNA) was harvested from cell cultures by lysing the cells for 10 min in 1 mL of TRIzol (Life Technologies) per 1 x 10^6 cells/mL. Lysates were incubated for 5 min at room temperature to enable complete dissociation of the nucleoproteins complex. The lysates were incubated for a further 3 min upon the addition of 0.2 mL of chloroform per 1 mL of TRIzol™ reagent followed by a brief vortex. Samples were centrifuged for 15 min at 12,000 x g at 4˚C during which the mixture separates into a lower red phenol-chloroform, interphase and a colourless upper aqueous phase. The aqueous phase containing the RNA was transferred to a new tube and stored at -80˚C. The interphase and organic phase containing DNA and protein was also stored at -80˚C until further use.

RNA was precipitated with the use of 0.5 mL of isopropanol to the aqueous phase per 1 mL of TRIzol™ and incubated for 10 min at room temperature. The samples were centrifuged at 12,000 x g for 10 min at 4˚C and the precipitate resuspended in 75 % ethanol (v/v) per 1 mL of Total RNA isolation (TRIzol™). The RNA was washed by centrifuging the samples at 7,500 x g at 4˚C for 4 min and air drying the RNA pellet for 10 min. The RNA was solubilized by resuspending the pellet in 25 μL of RNase-free water and incubating at 60˚C for 1 min. Contaminating DNA was removed by treating the sample with 1 unit of RNA Qualified (RQ) 1 RNase-free DNase (Promega), with the addition of 1.2 μL 10 x buffer, incubated at 37˚C for 1 h. The DNase activity was stopped with 2 μL RQ1 stop solution (Promega) and the RNA was re-precipitated by adding 180 μL diethyl pyrocarbonate (DEPC) treated deionized water, 10 μL 3M sodium chloride and 500 μL 100% ethanol, mixing and freezing in liquid nitrogen, thawing at room temperature and centrifugation at 11,000 x g for 10 min at 4˚C. Pelleted RNA was washed once more with 70 % (v/v) ethanol followed by centrifugation at 11,000 x g for 10 min and air dried for 10 min. The RNA was resuspended in 50 μL nuclease free water and stored at -80˚C.

RNA yield was determined by measuring the absorbance at 260 nm and 280 nm using the Nanodrop™ spectrophotometer. The RNA concentration was calculated using the formula: A260 × dilution × 40 = μg RNA/mL. The A260/280 ratio was calculated and a ratio of 2 was considered pure.

2.1.4.2 DNA *isolation*

The interphase and lower phenol-chloroform phase was incubated at room temperature for 3 min with 0.3 mL of 100 % ethanol before being centrifuged at 2000 x g for 5 min at 4˚C to pellet the DNA. The pellet was resuspended in 1 mL of 0.1 M sodium citrate in 10 % ethanol (v/v) per 1 mL of TRIzol™ reagent and incubated for 30 min at room temperature. The DNA was then centrifuged twice at 2000 x g for 5 min at 4˚C and the supernatant discarded. The pellet was then washed in 2 mL of 75 % ethanol (v/v) per 1 mL of TRIzol™ and incubated at room temperature for 20 min before being centrifuged at 2000 x g for 5 min at 4˚C. The DNA pellet was air dried for 10 min and solubilized by resuspending in 0.6 mL of 8 mM sodium hydroxide (Sigma-Aldrich) and centrifuging at 12,000 x g for 10 min at 4˚C. DNA yield was determined as explained above. The DNA was stored at -20˚C.

2.1.4.3 Reverse *transcription of RNA*

Production of single stranded complementary DNA (cDNA) from RNA templates was achieved using the Superscript® III First-Strand Synthesis System (Thermo Fisher). Five μg of RNA was combined with 50 μM oligo deoxythymine (dT) primers and 10 mM dNTP mix and made up to 10 μL with DEPC-treated water. The tubes were incubated at 65˚C for 5 min and then placed on ice for 2 min. The cDNA synthesis mix consisting of 10 x RT buffer, 25 mM $MgCl_2$, 0.1M dithiothreitol (DTT), 40 U/μL RNaseOUT™ and 200 U/μL of Superscript™ III RT was combined with the RNA/primer mixture and incubated at 50˚C for 50 min. The reaction was terminated by incubating at 85˚C for 5 min. The cDNA was then treated with 1 μL of RNase H (Sigma-Aldrich) for 20 min at 37˚C to remove the RNA template. Preparations of cDNA were stored at -20˚C, before being used as template for PCR reactions.

2.1.4.4 Semi-*quantitative RT-PCR*

This method was used to measure comparative levels of mRNA transcripts of genes of interest from samples of similar ells under defined test conditions. Primers were designed for specific amplification of cDNA fragments from genes of interest, with actin being used as a house keeping control, to equalise total RNA concentrations.

Firstly, RNA was prepared as mentioned above. Then single-stranded cDNA templates were prepared by reverse transcription. The PCR method used was as described above. Amplified products were separated by agarose gel electrophoresis and densitometrically analysed. In the case of genomic DNA, the PCR was carried out the same as above using 100 ng of starting product.

2.1.5 Enzyme *assays of cell extracts*

2.1.5.1 Cell viability-CellTiter-Glo® Luminescent Cell Viability Assay

Cell viability was quantified by a colorimetric assay based on quantitation of the ATP present, an indicator of metabolically active cells. The homogeneous "add-mix-measure" format results in cell lysis and generation of a luminescent signal proportional to the amount of ATP present. The amount of ATP is directly proportional to the number of cells present in culture.

Cells were grown in 96-well plates (60 usable wells per plate) until they were around 50-60 % confluent. Test compounds were added to the wells and incubated accordingly. The plate and its contents were equilibrated at room temperature for 30 min. An equal volume of CellTiter-Glo ® reagent equal to the volume of cell culture media was added and incubated for 2 min in an orbital shaker to induce cell lysis. Media only wells were used as controls. The plates were incubated at room temperature for 10 min to stabilize the luminescent signal. Luminescence was recorded using a Spark10M (Tecan) microplate reader.

Luminescence measurements were plotted on the y-axis and treatments on the x-axis. A direct relationship was observed between luminescence and the number of cells in culture.

2.1.5.2 Generation *of an ATP standard curve*

One μM ATP (Sigma-Aldrich) was prepared and using this as the stock solution serial tenfold dilutions of ATP in culture medium were prepared (1 μM to 10 nM). One hundred μL volumes of ATP concentrations were added in triplicate to the 96-well tissue culture test plate. An equal volume of CellTiter-Glo ® reagent was added and the above protocol followed to obtain luminescence measurements.

2.1.6 *Microscopy*

2.1.6.1 Light *and fluorescence microscopy*

Cell cultures were analysed by phase contrast and bright-field light microscopy. For the analysis of cells expressing green fluorescent protein (GFP), the stage was illuminated with 450 nm to 490 nm light filtered from an Argon UV bulb. For the analysis of cells expressing red fluorophore, the stage was illuminated with 510 nm to 560 nm light.

2.1.6.2 Electron *microscopy*

Sarkosyl-insoluble fractions (1 μL) were placed on the center of a Formvar/carbon coated 400 nickel mesh grids. Non-specific binding was prevented by incubating the grid on a drop of incubation buffer for 5 min. The grid was incubated overnight at 4°C in a glass humidified chamber using a drop of primary antibody. The grid was washed three times with incubation buffer (10 min each), before being incubated with the use of secondary antibody at room temperature for 1.5 h. The grid received two washes, prior to incubation with 2 % glutaraldehyde (v/v) in PBS for 5 min. The grid was then washed in PBS and water (30 s). Two per cent uranyl acetate was added to the grid and left for 30 s followed by the samples being dried before imaging on a JEOL JEM-1010 transmission electron microscope with digital image capture. Representative images (total=15) were taken per sample and one was randomly selected for presentation. Images were collected by Dr Ioanna Sevastou.

2.1.6.3 Immunocytochemistry

2.1.6.3.1 Sample *preparation and primary antibody incubation*

Cells were grown on glass cover slips in 6-well tissue culture plates for immunostaining. Cells were washed once with PBS. Coverslips were fixed by using 4 % paraformaldehyde solution in PBS (Life Technologies) for 10 min at room temperature. The coverslips were washed three times with ice-cold PBS. The cells were permeabilised with ice cold 80 % methanol (v/v) for 5 min at -20˚C. The coverslips were washed three times in PBS, with each wash lasting 5 min. Samples were then blocked for 30 min with 1 % BSA, 22.52 mg/mL glycine in PBST to block unspecific binding of the antibodies. The cells were incubated in diluted antibody in 1 % BSA in PBST overnight at 4˚C. To examine the co-distribution of two or more different antigens in the same sample, a double immunofluorescence procedure was performed where two primary antibodies from different host species was used.

2.1.6.3.2 *Antibody detection*

Primary antibody treated samples were washed three times in PBS, with each wash lasting 5 min. The cells were then incubated with secondary antibody in 1 % BSA for 1 h at room temperature in the dark. Normally a 1:1000 dilution of secondary antibody was used. The samples were washed three times with PBS for 5 min each in the dark. Samples without secondary antibodies were used as negative controls.

2.1.6.3.3 Counterstaining

For nucleic counterstaining, the coverslips were incubated with 4′,6-diamidino-2-phenylindole (DAPI; DNA/nuclear stain; Biotium) at a concentration of 1µg/mL dissolved in PBS for 5 min. This was performed after the third wash following secondary antibody incubation. The DAPI was then washed off the cells by rinsing the coverslips twice in PBS.

2.1.6.3.4 Mounting

Coverslips were mounted with a drop of mounting medium onto glass cover slides and sealed with nail polish to prevent drying and movement under microscope. The slides were stored in the dark at 4˚C for 24 h before imaging.

2.1.6.4 High-*content screening*

The Opera Phenix high-content screening system was used to image cells in 96-well glass bottom tissue culture plates. This screening system enables simultaneous multicolour confocal image acquisition at record speed and captures fine subcellular detail with very high-resolution images.

Cells were plated in 96-well glass-bottom, black, tissue culture plates (Perkin-Elmer) and immunocytochemistry carried out as described above. The plates were imaged at both 40 x and 60 x using the water immersive objective lens. Confocal images were obtained by imaging z-stacks of nine planes with 0.5 µm distance and was acquired from ten fields per well. Images were acquired using the 488 nm, 543 nm, 633 nm and the 405 nm laser. Images were analysed using the Harmony software. As a first step in the image analysis sequence, a maximum intensity projection image was generated including all the images of the confocal image stack. The nuclei were detected on the 405 nm channel image using the *Find Nuclei* building block. Subsequently, the cell membrane was detected on the 594 nm channel with *Find cells.* Once the borders of each cell had been established, using the 488 nm and 543 nm channels, the *Calculate Image* building block was included which created a combined image of the two channels for object detection and *Find Image Region* building block created the regions of interest in the whole image using the pixels with intensity higher than the threshold of non-treated cells. Further building blocks were added to calculate intensity, morphology and texture properties. Briefly, the *intensity* building block calculated the mean intensity for a specific region of interest, the *morphology* building block calculated both the area as well as the roundness for each channel. Finally, bright and dark regions within each cellular region for each individual channel was identified by the *texture* building block. Readouts were generated and 500 single cell results used per treatment. All non-expressing cells and cells with saturated pixels were excluded from the analysis using the *Select Population* building block.

2.1.6.5 ER *staining*

ER-Tracker™ Green dye (BODIPY) was used to stain the endoplasmic reticulum (ER). One mM stock solution of the dye was made up with DMSO. The media were removed from the cells and rinsed with Hank's Balanced Saline Solution (HBSS; Life Technologies) before a 1:1000 dilution of the ER-Tracker™ stock solution was added and the cells incubated for 30 min at 37°C. The staining solution was replaced with fresh probe-free medium and the cells viewed using the 488 nm laser on the Opera Phenix screening system.

2.1.6.6 Cell *membrane staining*

Wheatgerm Agglutinin (WGA) conjugated to Fluor® 633 nm (far-red fluorescence) was used a plasma membrane marker (ThermoFisher). WGA binds to sialic and N-acetylglucosaminyl residues found exclusively on the cell membrane.

One mg/mL stock solution was prepared by dissolving WGA conjugate in 5 mL of PBS. The cells were fixed as described above and rinsed once in HBSS. A dilution of 1:200 dilution of WGA in HBSS was used to label the cells. The cells were incubated at 37˚C for 10 min and cells washed twice in PBS before proceeding to with additional counterstains.

2.1.6.7 Thioflavin *S staining*

The formation of tau amyloid aggregates can be monitored by the fluorescence resulting from amyloid binding by thioflavin S (ThS). Upon binding to tau aggregates, ThS exhibits a red shift in fluorescence (excitation: 450 nm; peak emission: 510 nm). ThS has weak emission at 510 nm before amyloid binding, but this fluorescence increases significantly in the presence of an amyloid protein such as the aggregated tau.

Cells were fixed and permeabilized as described above. Cells were stained in 0.01 % (w/v) ThS (Sigma-Aldrich) solution for 5 min before washing the coverslips three times in 70 % ethanol (v/v), with each wash lasting 5 min. A final wash was done by rinsing the coverslips in distilled water. Cells were DAPI stained and mounted as described above and fluorescence measured using the 488 nm channel of the Phenix imaging system.

2.1.7 Genotyping

2.1.7.1 TaqMan *Assay for analysing genetic variation*

TaqMan Assay was used to amplify and detect specific variants in target brain genomic DNA (gDNA). DNA was isolated using the protocol described above and the concentration was standardised to 5 ng/µL and a total of 10 ng of DNA was used in each reaction. Ninety-six well PCR plates were used. A master mix comprising 40 x TaqMan Genotyping Assay (TaqMan forward and reverse oligonucleotides and their respective labelled probe pairs) and 2 x TaqMan Genotyping master mix was combined with nuclease free water. 25 µL aliquots were added to each well. Plates were sealed with a clear plastic film (ABgene, UK) to prevent excess evaporation

and then centrifuged at 1,000 rpm for 1 min. Each plate underwent the following PCR program on an Agilent Mx3000P Thermal Cycler PCR System (ThermoFisher): Enzyme activation at 95˚C for 10 min, followed by 40 cycles of denaturation at 95˚C for 15 s and annealing and extension at 62˚C for 60 s. A no template control was included as well as positive controls for each homozygous allele and a known sample containing heterozygous alleles.

2.1.7.1.1 Sample *analysis*

The sequence detection machine read all plates and three different genotypes were identified. Output was both an allelic discrimination plot and in a text output file. Each well of the 96-well reaction plate was represented as an individual point on the plot and variation in clustering due to the genotype of the target allele was represented as a scatter plot.

2.1.7.2 *Restriction fragment length polymorphism*

By performing a digestion on a genomic sample and determining fragment lengths through a gel assay it is possible to ascertain whether or not the enzymes cut the expected restriction sites. A failure to cut the genomic sample results in an identifiably larger than expected fragment implying that there is a mutation at the point of the restriction site which is rendering it protection from nuclease activity.

DNA was isolated from the patient brains as described above. Restriction digests for the GWAS snp (C/T) and (G/A) was carried out typically in 10 μL volume using the Hin PI and Bsa I restriction enzymes, respectively and products analysed on a 1 % (w/v) agarose gels. Three samples positive for each homozygous non-risk (CC) and risk allele (TT) along with three heterozygous samples (CT) were chosen at random and sent for Sanger sequencing (Source Bioscience) for quality control.

2.1.8 Transfection of rTg4510 mouse brain lysate into PERK cells

HapA, HapB PERK cell lines and Flp-In 293 cells were plated at an initial cell density of 0.3 x 10^6 cells per well in a 6-well tissue culture plate, with each well comprising a surface area of 9.6 cm^2. 24 h later, at 60% cell confluency, cells were transfected with 2.5μg of either 2N4R tau or 2N4R (P301L) tau using Lipofectamine 3000 as detailed above. The next day, rTg4510 tauopathic mouse brain homogenate (obtained from Dr Ioanna Sevastou; Eisai Pharmaceuticals) was

transfected into the cells using Lipofectamine 3000 (Invitrogen). Transfection complexes were made by combining 125 µL Opti-MEM (Gibco) +7.5 µL Lipofectamine 3000 (Invitrogen) along with Opti-MEM + 8 µg/mL rTg4510 mouse brain homogenate in a total volume of 250 µL per well. Transfected preparations were incubated at room temperature for 15 min before transfecting into either 2N4R or 2N4R (P301L) transfected HapA, HapB cells or Flp-In 293 cells. Dox induction was carried out on the HapA and HapB cells 24 hours later and cells cultured for a further six days. Sarkosyl soluble and insoluble fractions were obtained using the methods detailed above.

2.1.9 Statistical Analyses

Statistical analysis was carried out using Prism statistical analysis software (GraphPad Software Inc.). Three technical repeats were carried out per experiment using three different HapA and HapB clones obtained from the same round of transfection and three biological repeats were next carried out per experiment, using triplicate HapA and HapB clones obtained from three fresh rounds of independent stable cell transfections. As the data was not normally distributed due to the low number of technical repeats, the outcome differences between Haplotype A and Haplotype B cell lines are expressed using nonparametric statistical analyses. Where cell death is reported, the analyses has been indicated as a percentage of control where the data was normalised so that the largest mean in each data set was defined at 100% and the values plotted as a percentage difference against the control. Where appropriate, the statistical comparisons included either the Mann-Whitney test (two independent groups with one continuous dependant variable), Kruskal Wallis test (two or more independent groups and independent variable) or a Friedman's Test (three or more matched groups of data defined by one factor i.e., non-parametric repeated measure ANOVA). Further, to the above assumptions, the following assumptions also had to be met before embarking on either the Man Whitney U test or the Kruskal Wallis nonparametric analyses test:

Assumption 1: Data are unpaired (i.e. Data are not matched)

Assumption 2: Independence of observations (We have two different cell haplotypes (HapA, HapB) with neither cell type being in more than one group).

Assumption 3: Data are sampled from non-Gaussian populations: - As our number of repeats were very low (n of 3) our data did not follow a normal distribution and hence a non-parametric test was utilised

Assumption 4: The two groups follow data distribution with the same shape enabling the difference between the medians and its confidence interval to be reported if the p value is significant.

2.2 Materials

2.2.1 Molecular *biology reagents*

TAE Buffer	40 mM Tris-HCl pH 8.0 (Sigma-Aldrich) 20 mM Acetic acid (Merck) 1 mM ethylenediamine tetra acetic acid (EDTA; Merck)
6 x Agarose gel loading dye	10% wt/vol Glycerol (Merck) 0.4% wt/vol Orange G (Merck)
TE buffer	10 mM Tris.HCL pH 8.0 (Sigma-Aldrich) 1 mM EDTA (Merck)
LB broth	20 g/L LB broth (Life Technologies) Deionized water Autoclaved at 121^0C for 15 mins
LB agar	32 g/L LB agar (Life Technologies) mixed in deionized water and autoclaved at 121^0C for 15 mins

2.2.2 Cell *culture reagents*

All components supplied by Sigma-Aldrich unless stated otherwise.

Flp-In HEK 293 medium	DMEM
	10% FBS
	1% vol/vol Non-Essential Amino Acid (NEAA) solution
	20 units/mL Penicillin
	20 mg/mL Streptomycin
	100 μg/mL Zeocin™ (Invitrogen)
	15 μg/mL Blasticidin
Freezing Medium	90% vol/vol Flp-In HEK 293 medium
	10% vol/vol DMSO
Stable Flp-In culture medium	DMEM
	10% FBS
	1% NEAA
	20 units/mL Penicillin 20 mg/mL Streptomycin
	100 μg/mL Hygromycin b
	15 μg/mL Blasticidin

Dox induction media	Stable Flp-In culture media
	10 ng/mL Dox
Trypsin solution	10% vol/vol 10 x Trypsin-EDTA solution
	90% vol/vol 1 x PBS

2.2.3 Protein *chemistry reagents*

RIPA buffer	10 mM Tris-HCL pH 7.4 (Sigma-Aldrich)
	0.8 M sodium chloride (Merck)
	1mM ethylene-glycol-bis (2-aminoethylether)-N, N, N', N'-
	Tetra acetic acid (EGTA; Merck)
	0.1% wt/vol sodium dodecyl sulphate (SDS; Merck)
	1% vol/vol protease inhibitor cocktail (Sigma-Aldrich)
	1% vol/vol phosphatase inhibitor cocktail (Roche)
	10% wt/vol sucrose (Merck)
Sarkosyl lysis buffer	10 μM Tris-HCl (pH 7.5) (Sigma-Aldrich)
	10 μM EDTA (Sigma-Aldrich)
	10 μm Sodium Chloride (Sigma-Aldrich)
	1 % Sarkosyl (Sigma-Aldrich)

	1 % vol/vol protease inhibitor cocktail (Sigma-Aldrich)
	1% vol/vol phosphatase inhibitor cocktail (Roche)
PBST/TBST	PBS/TBS supplemented with 0.1% vol/vol Tween 20

2.2.4 ER *stress inducers*

Thapsigargin	0.5 mg Thapsigargin (Sigma-Aldrich) dissolved in 1 mL DMSO, 0.2 μm filtered
Tunicamycin	5 mg Tunicamycin (Sigma-Aldrich) dissolved in 1 ml DMSO, 0.2 μm filtered
Brefeldin A	5 mg Brefeldin A (Sigma-Aldrich) dissolved in 1 ml DMSO, 0.2 μm filtered
Glucose-free culture media	DMEM, no glucose (Sigma-Aldrich)
	10% FBS
	1% vol/vol Non-Essential Amino Acids (NEAA) solution
	20 units/mL Penicillin
	20 mg/mL Streptomycin
	100 μg/mL Hygromycin B
	15 μg/mL Blasticidin

2.2.5 *Antibodies*

2.2.5.1 Primary *antibodies*

Protein detected	Antibody name	Source	Species	Dilution
PERK	B5	Santa Cruz	Mouse	1:2000
PERK	C33E10	Cell Signalling	Rabbit	1:1000
PERK C-Term	P0074	Sigma-Aldrich	Rabbit	1:2000
Phospho-PERK	192591	Abcam	Rabbit	1:2000
eIF2α	D3	Santa Cruz	Mouse	1:2000
p-eIF2α	E90	Abcam	Rabbit	1:2000
Ire1	B12	Santa Cruz	Mouse	1:200
p-Ire1	5253	Abcam	Rabbit	1:500
ATF6	F7	Santa Cruz	Mouse	1:200
ATF4	D4B8	Cell Signalling	Rabbit	1:500
XBP-1	F4	Santa Cruz	Mouse	1:50
PDI	H-160	Santa Cruz	Rabbit	1:100
c-Myc	Sc-40	Santa Cruz	Mouse	1:1000
CHOP	11419	Abcam	Mouse	1:1000
BiP	21685	Abcam	Rabbit	1:100
BiP	ET-21.	Sigma-Aldrich	Rabbit	1:250
Actin	13E5	Cell Signalling	Rabbit	1:1000
Actin	A2228	Sigma-Aldrich	Mouse	1:1000
Total Tau	K9JA	DAKO	Rabbit	1:10,000
Total Tau	Tau-5	ThermoFisher	Mouse	1:250
Tau (conformational)	MC1	Peter Davies[1]	Mouse	1:500
Tau (Conformational)	ALZ50	Peter Davies[1]	Mouse	1:500
Phospho-tau	PHF1	Peter Davies[1]	Mouse	1:500
Phospho-tau	AT8	ThermoFisher	Mouse	1:500

1. P. Davies, Litwin Zucker Centre for Alzheimer's Research, Long Island, Manhasset, U.S.A

2.2.5.2 Secondary *antibodies*

Protein detected	**Conjugate**	**Source**	**Species**	**Dilution**
Mouse IgG	IRDye 800CW	Li-Cor	Donkey	1:20,000
Rabbit IgG	IRDye 800 CW	Li-Cor	Donkey	1:20,000
Mouse IgG	IRDye 680RD	Li-Cor	Donkey	1:20,000
Rabbit IgG	IRDye 680RD	Li-Cor	Donkey	1:20,000
Mouse IgG	Alexa Fluor 488	ThermoFisher	Goat	1:1000
Rabbit IgG	Alexa Fluor 488	ThermoFisher	Goat	1:1000
Mouse IgG	Alexa Fluor 568	ThermoFisher	Goat	1:1000
Rabbit IgG	Alexa Fluor 568	ThermoFisher	Goat	1:1000
Mouse IgG	HRP	Santa Cruz	Goat	0.4 μg/mL
Mouse IgG	10 nm Gold	Abcam	Goat	1:50

3 Inducible isogenic PERK expression in Flp-In™ TREx 293 cells

3.1 Overview

Stable isogenic cell lines for Tet-inducible expression of PERK functional haplotypes A, B, C, and D were created by utilising the Flp-In™ T-REx system (Life Technologies) to create isogenic cell lines with Tet-inducible expression of the PERK variants. Synthetic haplotypes B1, B2, and B3 were designed by individually swapping each coding SNP of haplotype B to that of haplotype A in order to assess which of the three SNP alleles singly, or in combination, are crucial for the functional differences. Using the Flp-In™ T-REx system to generate the PERK isogenic cell lines ensured that the integration sites for all *EIF2AK3* variants were identical and thus eliminated differences due to positional effects. Owing to the cytotoxicity of PERK overexpression and activation, gene expression was tightly regulated using the Tet-inducible expression system (T-Rex). Inducible expression in the cells was characterised by western blot and immunocytochemistry.

3.2 Background

Overexpression of PERK promotes its autoactivation in the absence of ER stress through enforced oligomerization and insufficient levels of BiP for inhibition, leading to phosphorylation and activation of eIF2α, which in turn, leads to induction of UPR and attenuated protein synthesis (Harding et al., 2000). Previous work showed that PERK overexpression could thus affect cell growth and induce cell death (Brewer and Diehl, 2000). However, these previous studies were conducted with constitutive overexpression, resulting in the neurotoxicity due to the sustained over-activation of PERK in animal models. On the other hand, endogenous PERK, and phospho-PERK are at extremely low levels and barely detectable by cognate antibodies. As a consequence, for detection of the endogenous PERK, we have to resort to enrichment by immunoprecipitation (IP) of the cell and tissue lysates. This is a laborious and expensive process due to the large quantities of antibody required. Furthermore, the alterations of PERK activation due to each of the SNPs that confer coding changes are likely to show subtle differences which could not be as easily apparent if expression levels of PERK are low to begin with. Therefore, in order to overcome these obstacles, particularly as constitutive overexpression of PERK could cause significant cell death, we selected a Tet-inducible system together with approved antibiotic-free serum, to minimise leakiness in transgene expression. When required, PERK expression was induced by adding doxycycline (Dox), a more potent tetracycline derivative, to the medium.

For the work in this thesis, we cloned the coding haplotype variants of PERK into the human Flp-In™ T-REx HEK-293 cell line, derived from the widely used human embryonic kidney cell line, HEK-293. One vial of passage 1 (P1) 1 x 10^7 Flp-In T-Rex cells was supplied frozen in 1 ml of 90 % complete medium and 10% DMSO from ThermoFisher Scientific. We selected to purchase this HEK-293 cell line as it was the only cell line at the time which had the benefit of already containing a single integrated FRT site as introduced by transfection of the pFRT/lacZeo plasmid as well as stably expressing the Tet repressor as introduced by transfection of the pcDNA6/TR plasmid. This commercial cell line had also been shown to be successful in generating robust tetracycline-inducible expression of various different genes of interest as reported by different groups (Ward et al., 2011; Chruscicka et al., 2015). Further, the purchase of this commercially available Tet-inducible cell line enabled the ease and rapid generation of a single transfection of each of the PERK plasmids to generate the required seven stable cell lines. The Flp-In T-Rex cell lines were tested for both zeocin resistance (confirms integration of the pFRT/LacZeo plasmid) and Blasticidin resistance (confirms integration of the pcDNA6/TR plasmid) as quality control mechanisms.

Due to recombination occurring between the specific FRT sites on the interacting DNA molecules, there is minimal opportunity for introduction of mutations at the recombination site. This allows for the generation of isogenic stable cell lines with PERK protein expression being constant across the population of cells. Further, all recombination events are in principle identical and allow for bulk selection of positive clones that will be isogenic. In our cell model the Flp-In™ T-Rex™ inducible expression vector system controls expression of PERK by using Tet-repressor promoters. Dox binds the Tet-repressor, causing a conformational change and release of transcriptional repression of PERK, thereby enabling transcription and subsequent translation of the PERK protein (Figure 13).

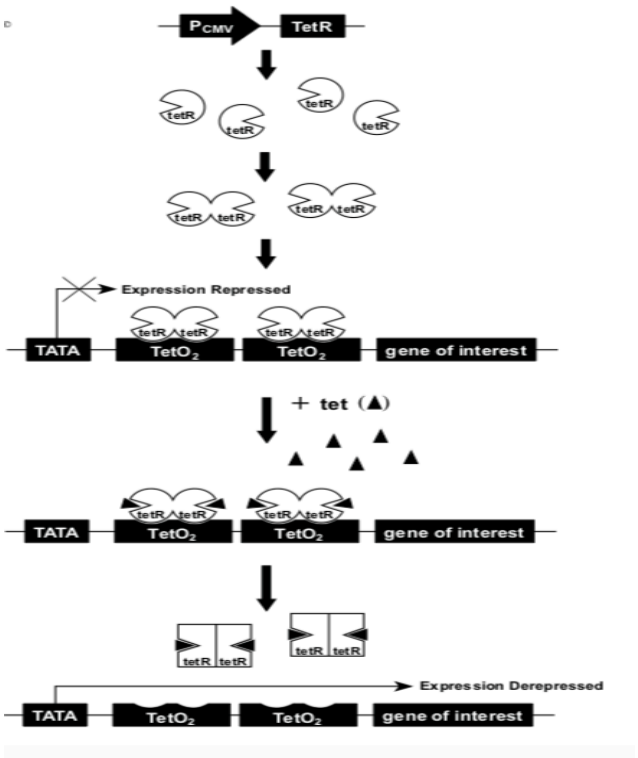

Figure 13. **Induction of PERK expression by addition of Dox**. In the absence of Dox, the Tet repressor (expressed from the pcDNA6/TR plasmid) forms a homodimer that binds with extremely high affinity to each TetO2 sequence in the promoter of the pcDNA5/FRT/TO vector and thereby represses transcription of PERK (Hillen and Berens, 1994). The 2 TetO2 sites in the promoter of pcDNA5/FRT/TO serve as binding sites for 4 molecules (or 2 homodimers) of the Tet repressor. Upon addition, dox penetrates the cell membrane and binds with high affinity to the constitutively expressed Tet-repressor thereby causing a conformational change in the repressor that renders it unable to bind to the Tet operator. The Tet repressor: Dox complex then dissociates from the Tet operator and enables induction of transcription from PERK (Adapted from Invitrogen, Flp-In TREx 293 manual).

3.3 PERK *mammalian expression plasmid construction*

The final destination plasmid expression vector for the *EIF2AK3* cDNA to express PERK haplotypes in the Flp-In 293 system is pcDNA 5/FRT/TO. This vector has multiple cloning sites to enable insertion of cDNA sequence downstream to the CMV promoter which is fused to the 2 x TetO2 sequences.

The inserted EIF2AK3 cDNA was inserted with the following modifications (Figure 14):

1. Carboxy terminal myc tag for distinguishing exogenous from endogenous PERK
2. 7 silent nucleotide changes in an siRNA target sequence between 2540-2560 bp to enable selective siRNA silencing of the endogenous gene

3. Coding sequence changes to represent the PERK haplotypes A, B, C, and D and synthetic haplotypes B1, B2 and B3.

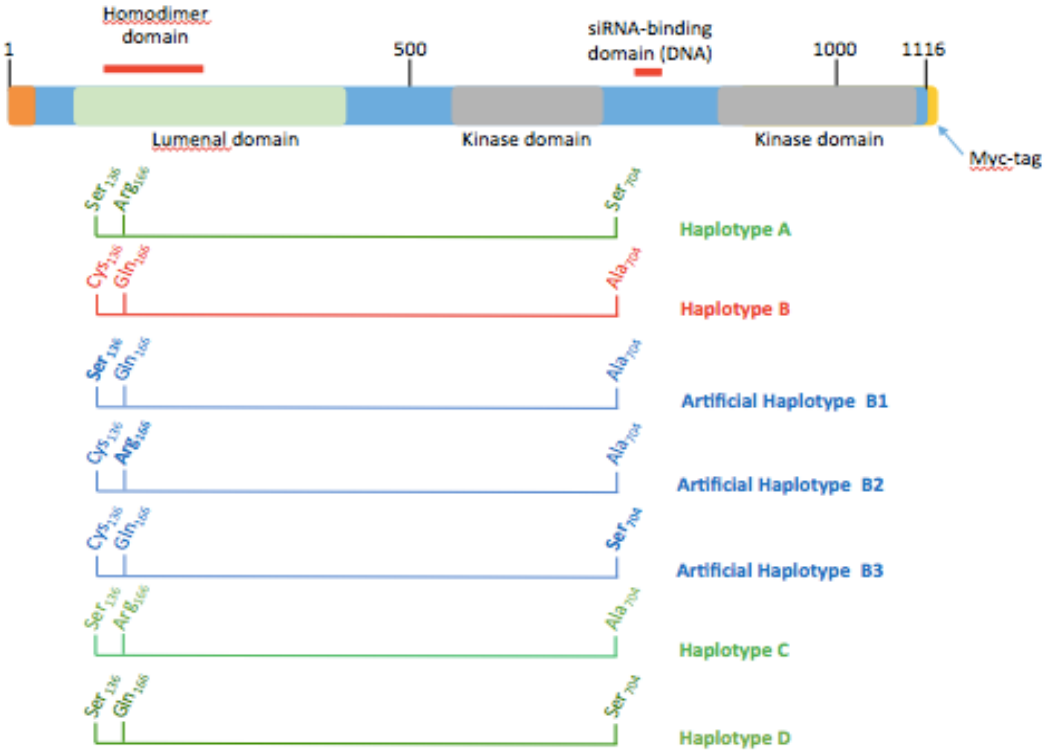

Figure 14. **Scheme of PERK protein domains with relative positions of residues defining coding haplotypes.** Individual coding alleles of haplotype A were swapped to create the three artificial haplotypes B1, B2, and B3. The target sequence for the siRNA that effectively knocks down endogenous *EIF2AK3* expression was incorporated. This renders the exogenous *EIF2AK3* variant resistant to this siRNA, enabling knockdown of the endogenous gene and rescue by induction of transgene expression. A carboxy-terminal myc-tag was also incorporated in order to discern between exo- and endogenous PERK.

The PERK cDNA was opted to be sequentially cloned in two parts as (Figure 15):
(1) The 1168 bp 3' coding sequence (PERK 3') contained the modified siRNA- binding sequence and the carboxy terminal myc-tag. This common fragment is shared by all haplotypes and
(2) The larger 2250 bp 5' coding region contained the three coding SNP variants that define the coding haplotypes.

We designed and obtained synthetic sequences of 1168 bp of the *EIF2AK3* cDNA incorporating a sequence coding a myc tag (GAGCAGAAACTCATCTCTGAAGAGGATCTGTAG) at the 3' end, followed by a stop codon. The sequences at 2540-2560 bp (TGGACCATGAGGACATCAG) were changed in order not to affect coding but to create a unique sequence on the exogenous gene to enable selective siRNA silencing of the endogenous gene as previously demonstrated by Harding and colleagues in 2000. The synthetic sequence was also designed with flanking *Xho* and *EcoRI* sites for subsequent sub cloning into the 2250 bp PERK constructs.

EIF2AK3 haplotypes: The GWAS-associated SNP rs7571971 belongs to a region of LD spanning most of the *EIF2AK3* gene. This includes the coding SNPs; rs867529 ($S_{136}C$), rs13045 ($Q_{166}R$) and rs1805165 ($A_{704}S$), forming the functional coding haplotypes: ***A***: S_{136}-R_{166}-S_{704}; ***B***: C_{136}-Q_{166}-A_{704},; **C:** S_{136}-R_{166} -A_{704} and ***D***: S_{136}-Q_{166}-S_{704}. Haplotype B segregates with the GWAS SNP-associated minor T-allele and increased PERK activation (Liu et al., 2011), suggesting that it bears the risk for PSP due to increased activity of PERK. These findings support our hypothesis that the association with *EIF2AK3* could manifest via allelic differences in *EIF2AK3*/PERK function and the increased activity of the PSP associated haplotype B contributes to pathways that lead to tau pathology. Interestingly, the S_{136} and Q_{166} residues are in the lumenal domain of PERK (Figure 12) with possible influence on homodimerization, essential for PERK activation whereas, the S_{704} residue, due to its vicinity to the kinase domain may affect PERK kinase activity. Therefore to determine which of the three amino acid coding changes is responsible for the difference in PERK activity between haplotype A and haplotype B, each of the three SNPs of haplotype A were swapped with that of haplotype B creating the artificial haplotypes **B1**:S_{136}- Q_{166}-A_{704}; **B2:** C_{136}- R_{166}- A_{704} and **B3:** C_{136}-Q_{166}- S_{704}. The seven PERK variants were represented in each of the seven 2250 bp inserts of the synthetic pUC57 plasmids. Two restriction endonucleases were incorporated at either end of the construct for final insertion into the pcDNA5/FRT/TO via the *Kpn1* and *Apa1* restriction sites.

Due to the aforementioned modifications, we opted for gene synthesis by design (Genewiz). Recently, as costs for commercial gene synthesis have dropped dramatically, this is by far the more efficient and cost-effective way of obtaining the coding constructs with multiple modifications, obviating the need for the very involved procedures of site-directed mutagenesis and PCR-based methods for these modifications. Hence the 1168 bp and 2250 bp PERK plasmids were cloned into and supplied in pUC57 plasmids by Genewiz, USA.

The full-length PERK plasmids were derived by ligating the 1168 bp *Xho* and *EcoRI* fragment into the multiple cloning site of the pUC57 2250 bp PERK plasmids cut with *Xho* and *EcoR1*. The final PERK expression plasmids were then derived by ligating the 3400 bp *Kpn1/Apa1* full length PERK fragments into the multiple cloning site of pcDNA5/pFRT/TO expression plasmid cut with *Kpn1*

and *Apa1*. Correct construction of plasmids was confirmed by Sanger sequencing of the insert using flanking primers for the 5' and 3' end and internal primers. Each of the seven expression plasmids were then purified using the Endo-free Plasmid purification kit (Qiagen) for endotoxin-free plasmid suitable for transfection into the Flp-In 293 cells.

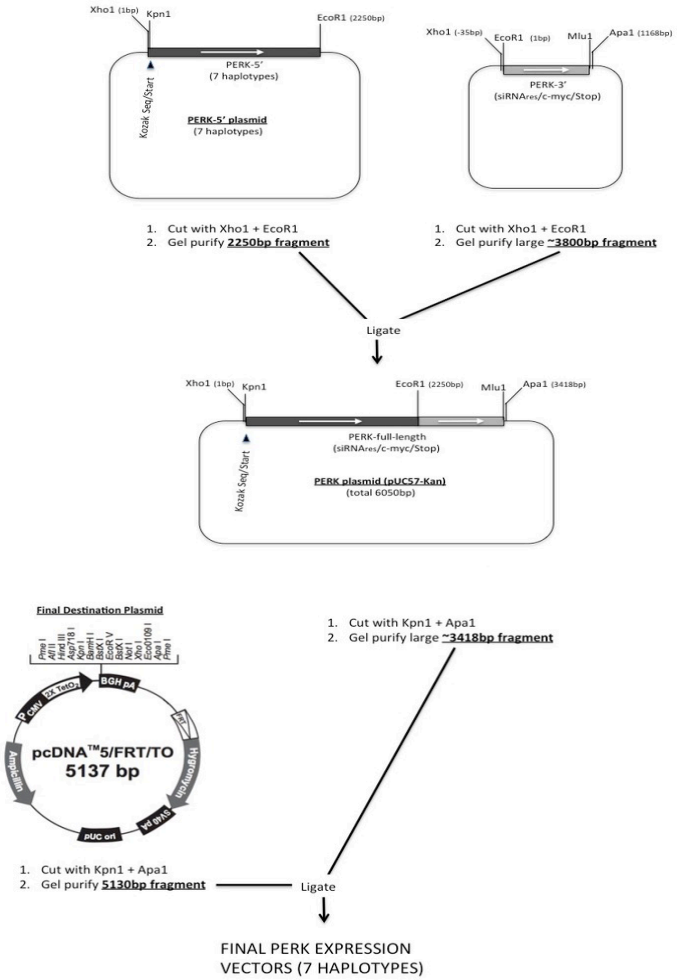

Figure 15. **Representative plasmid constructs for PERK overexpression.** The three main plasmids used to make the synthetic PERK constructs are shown. Fuller description of plasmid expression products is explained above.

3.4 Determination *of Hygromycin sensitivity*

To successfully generate stable cell lines expressing PERK, the minimum concentration of hygromycin B required to kill the untransfected Flp-In™ host cell line was determined using the CellTiter-Glo luminescent cell viability assay. All cells were killed in seven days at 200 µg/mL, 400 µg/mL, and 600 µg/mL of hygromycin B with most cells killed at 100 µg/mL (Figure 16). As a result, we chose hygromycin B concentration of 100 µg/mL for selection of cells transfected with the PERK plasmids.

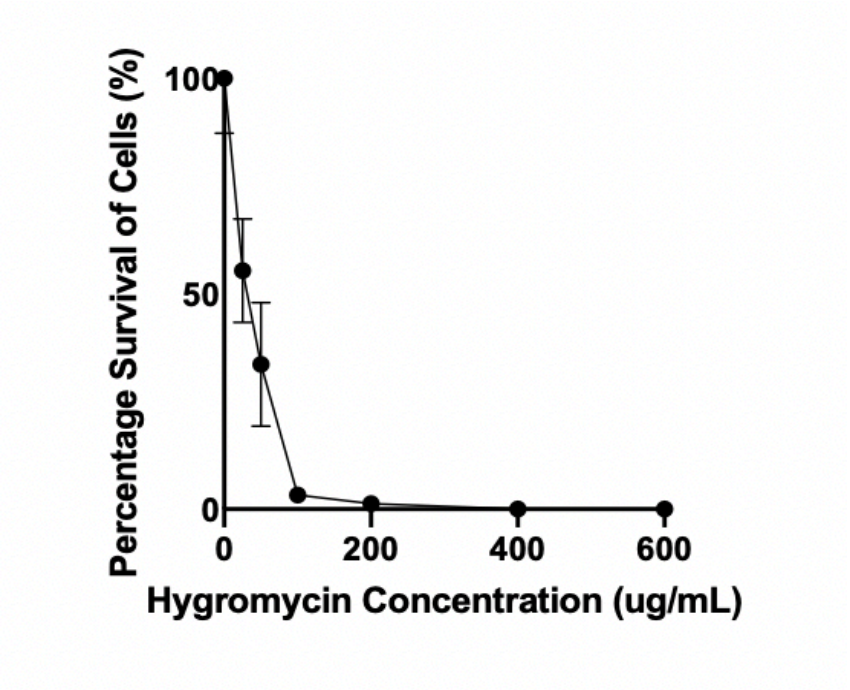

Figure 16. **Hygromycin B sensitivity curve for Flp-In™ TREx 293 cells**. Passage 2 cells were seeded at a density of 0.5 x 10^6 cells/well and incubated with a range of concentrations of hygromycin B. Each concentration was treated in triplicate wells and three biological replicates derived from three independent rounds of this experiment were included. After one week, cell viability was measured using the CellTiter Glo assay. The cell viability data was normalised so that the smallest mean in each data set was defined as 0% and the largest mean in each data set was defined at 100%. The minimal hygromycin B concentration to kill the majority of cells within 7 days was determined to be 100 µg/mL. Data points are expressed as mean of 3 experiments ± SEM.

3.5 Tet-On PERK founder cell lines

3.5.1 Transfection and selection of PERK cell lines

Flp-In™ TREx 293 cells were transfected with a 9:1 ratio of pOG44:pcDNA™5-FRT-TO-PERK plasmid DNA using the Lipofectamine 3000 transfection reagent (Thermo Fisher) as above. Forty-eight h after transfection, the cells were split into fresh medium containing 100 μg/mL hygromycin B. The cells were fed selection media every 4 days until cell colonies were visible. Five hygromycin-resistant foci were picked for each haplotype and expanded into 6-well plates. These continued to grow under selective conditions for 21 days, with expansion into T25 tissue culture flasks.

3.5.2 Characterisation *of PERK cell lines*

For induction of PERK expression 0, 0.01, 0.1, and 1 μg/mL of Dox were included in the medium of each of the plates for the seven haplotypes. Following 24 h incubation with Dox, total protein extractions were made and immunoblots probed with c-Myc mouse monoclonal antibody (SC4, Santa Cruz Biotechnologies), N-terminus rabbit PERK antibody (H-300, Santa Cruz Biotechnologies) and rabbit monoclonal actin antibody (13E5, Cell Signalling Technology). PERK protein was detected with each haplotype at very low concentrations of Dox (10 ng/mL) as a clean band at 125 kDa (Figure 17a). In the absence of Dox, exogenous PERK indicated by myc-positive band was absent, while a faint band indicative of endogenous PERK was observed in the blot probed by the PERK antibody. There was no overt difference in levels of expression of the different PERK haplotypes as concentrations of Dox were increased. To test if PERK induction occurred with lower concentrations of Dox, the A and B PERK cells were induced for 24 h with Dox concentrations of 0-15 ng/mL (Figure 17b). Induction was initially observed in both haplotypes at a concentration of 10 ng/mL Dox with concentrations below 10 ng/mL failing to induce the exogenous PERK expression. 10 ng/mL of Dox concentration was therefore chosen to induce expression of PERK.

3.5.3 Time-dependent induction of PERK

To examine the time-dependent Dox induction of the PERK gene, a time-course experiment was set up using 10 ng/mL Dox induction with protein lysates being obtained at 18 h, 24 h and then again at 48 h post-induction, from haplotype A and B cell lines. Immunoblot analysis of cell extracts were carried out from 6-well plates, with 30 ug of protein concentration used per sample and immunoblotting was carried out as described above. In the absence of Dox, a very faint

PERK-positive band could be detected (Figure 18a). Robust PERK expression is seen at 18 h after induction with signal intensity observed even after 48 h following induction (Figure 18a). We chose to carry out induction with 10 ng/mL Dox for 18 h for all subsequent experiments as this time point would be the most favourable for our experimental working conditions as anything of a shorter duration would be impossible to work around due to time constraints. We then extended the analysis to all haplotypes using the repeated measure analysis of Friedman's test which indicated no significant differences and hence, showed comparable levels of PERK expression at 18 h post Dox induction (Figure 18b and Figure 18c).

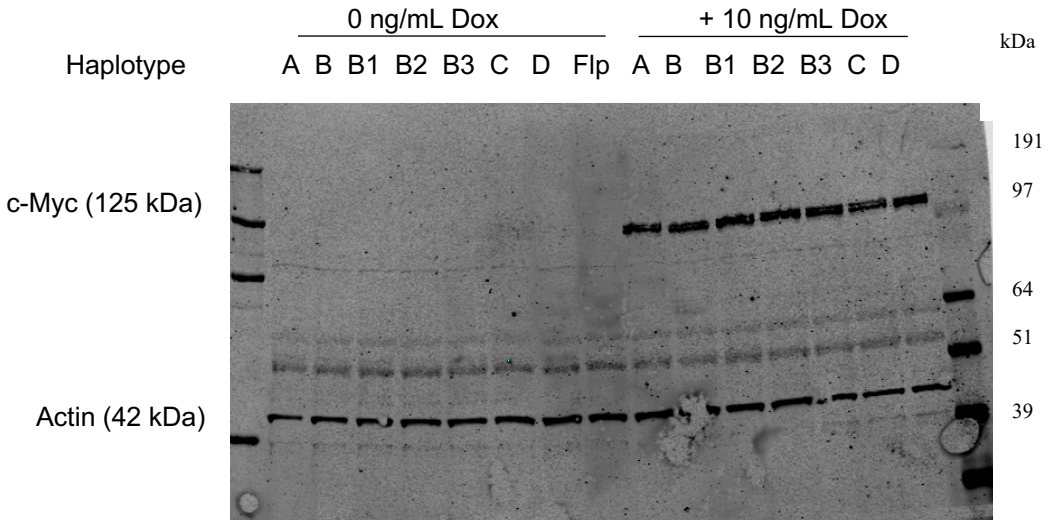

Figure 17a.i. **Representative Western blots showing expression of c-Myc and β-actin proteins in Dox induced and uninduced stable PERK cell lysates**. Cell lysates were collected following Dox induction for 24 h at concentrations of 0, and 10 ng/mL of Dox. The protein concentration in each cell lysate was adjusted to 20 μg of protein per well. SeeBlue^{Tm} Plus2 Pre-stained protein standard ladder was included. There is a clear absence of a c-Myc signal in the uninduced samples.

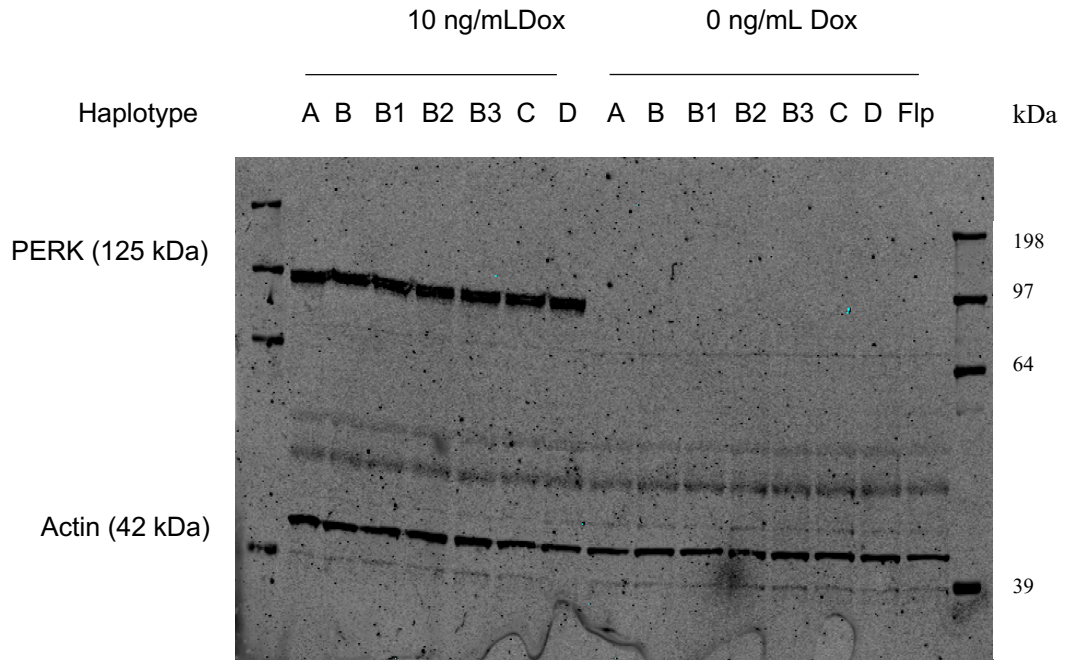

Figure 17a.ii. **Representative Western blots showing expression of PERK and β-actin proteins in Dox induced and uninduced stable PERK cell lysates**. Cell lysates were collected following Dox induction for 24 h at concentrations of 0, and 10 ng/mL of Dox. The protein concentration in each cell lysate was adjusted to 20 μg of protein per well. .SeeBlue^{Tm} Plus2 Pre-stained protein standard ladder was included. A very strong signal can be observed in the induced samples probed with PERK antibody, indicative of exogenous PERK.

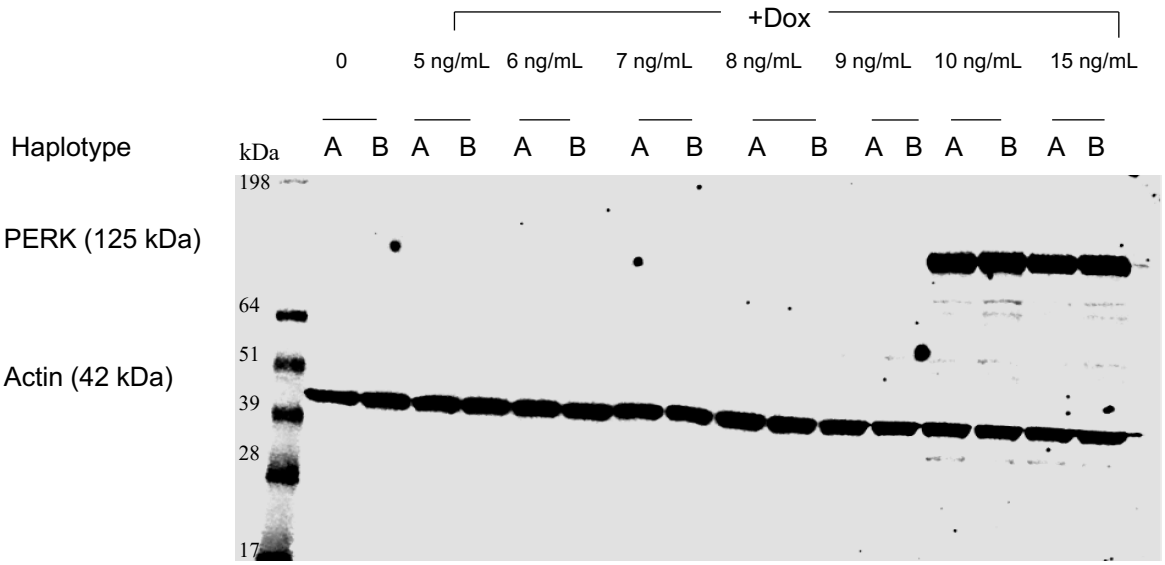

Figure 17b. **Representative Western blot showing expression of PERK upon 24h Dox induction in haplotypes A and B**. No detectable expression at Dox concentrations between 5-9 ng/mL is observed with a band being observed at concentrations of 10 and 15 ng/mL of Dox; lacking any dose response.

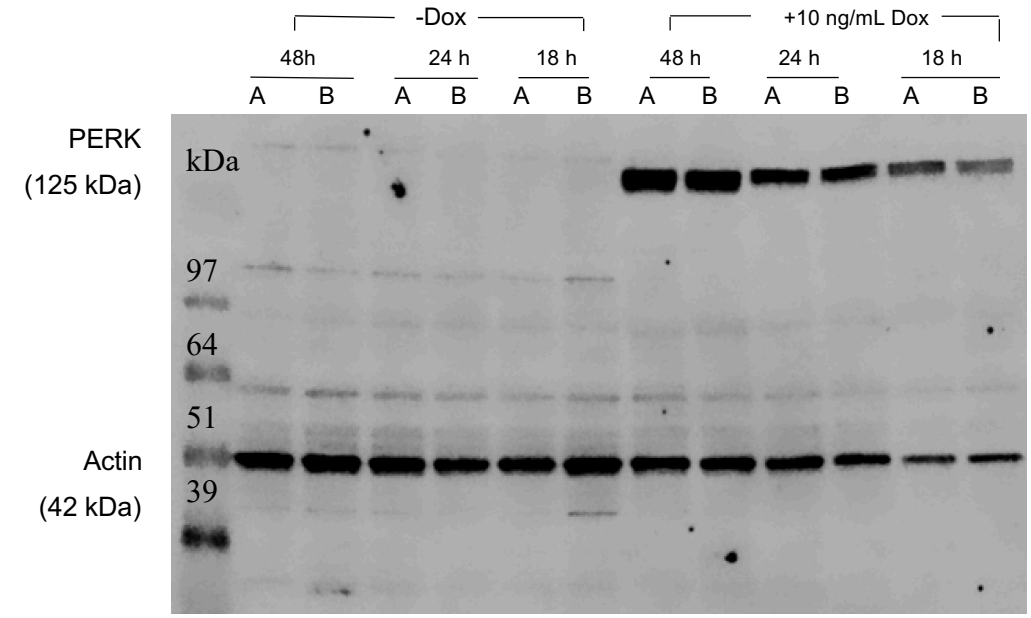

Figure 18a. Time dependent expression of Dox induced PERK expression. A representative western blot for induced haplotype A and B cells which were cultured in the presence of 10 ng/mL of Dox for 18, 24, and 48 h is shown. Each treatment duration was carried out in triplicate wells for each cell line and three independent experiments carried out. Immunoblots were probed with PERK antibody and actin was used as loading control. A band for PERK is observed following Dox induction in both HapA and HapB cells for 18 hours.

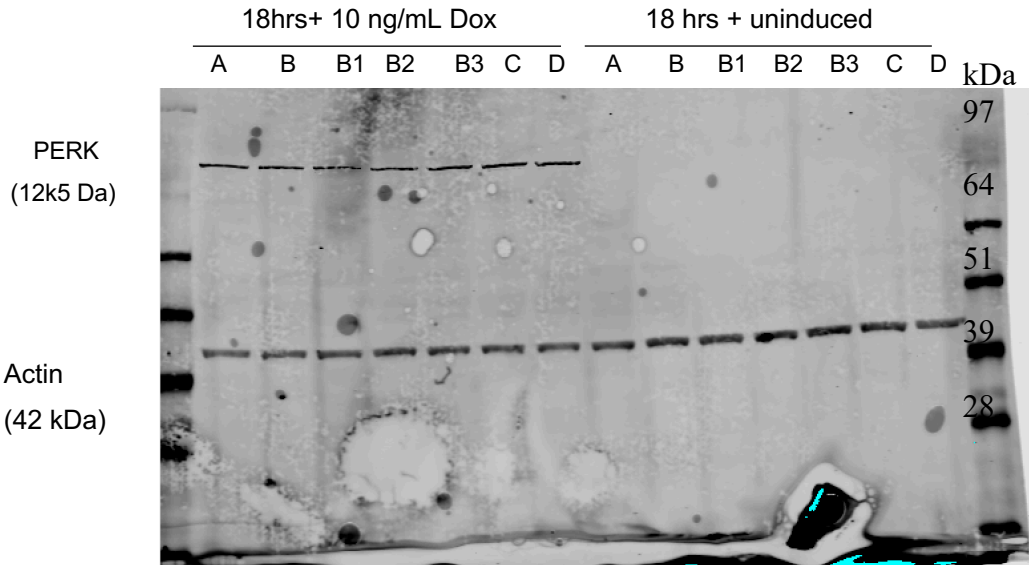

Figure 18b. 18 h, 10 ng/mL Dox induction in all PERK haplotypes. A representative western blot for all seven PERK haplotypes cultured in the presence or absence of 10 ng/mL of Dox for 18, h is shown. Immunoblots were probed with PERK antibody and actin was used as loading control. A band for PERK is observed following Dox induction in both HapA and HapB cells for 18 hours.

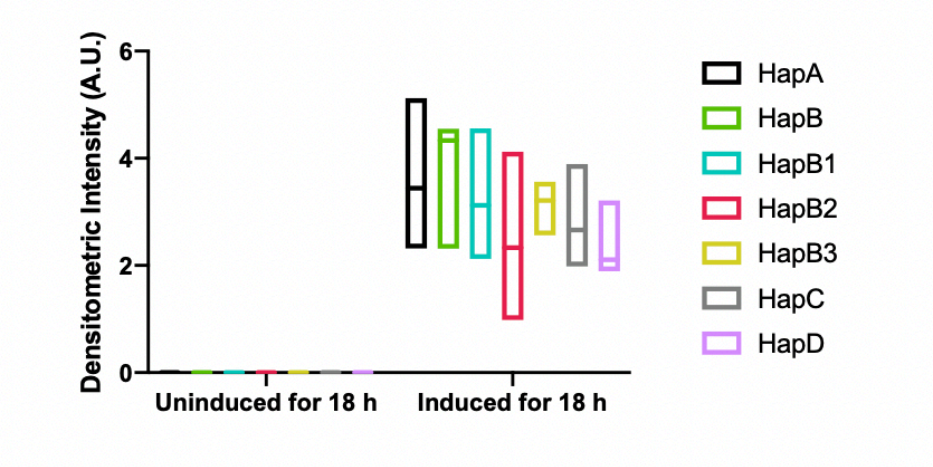

Figure 18c. Comparable levels of PERK in all 7 PERK haplotypes following 18 h of 10 ng/mL Dox induction. The data from Figure 18b is analysed and depicted as a box and violin plot with the median indicated by the line in the middle. Three clones per haplotype were tested for each condition and the experiment repeated independently three times using new clones obtained from fresh stable transfections. A repeated measure analysis using the Friedman's Test was carried out and no significant changes were depicted at induction following 18 hours between any of the 7 haplotypes (F_r=6, df=6 p>0.9999, n=3).

3.5.4 PERK activation and cell viability

The viability of the cells following PERK activation (induction by 10 ng/mL Dox) was monitored every 6 h by the CellTiter-Glo luminescent cell viability assay (Figure 19). Addition of Dox on naïve Flp-In cells for prolonged durations was previously observed to have no significance on cell death. Increased cell death following induction in the PERK cell lines was observed when Dox induced cell viability values were expressed as a percentage change against the uninduced HapB control cells (normalised to 100% as the uninduced HapB data set contained the largest mean). Cell death is observed following Dox induction which is possibly due to PERK overexpression and activation. 10 ng/mL Dox induction for 18 h was chosen as the standard dose for future experiments since cell death at this time point was not shown to be significantly reduced when compared with cell death following six hours post PERK activation.

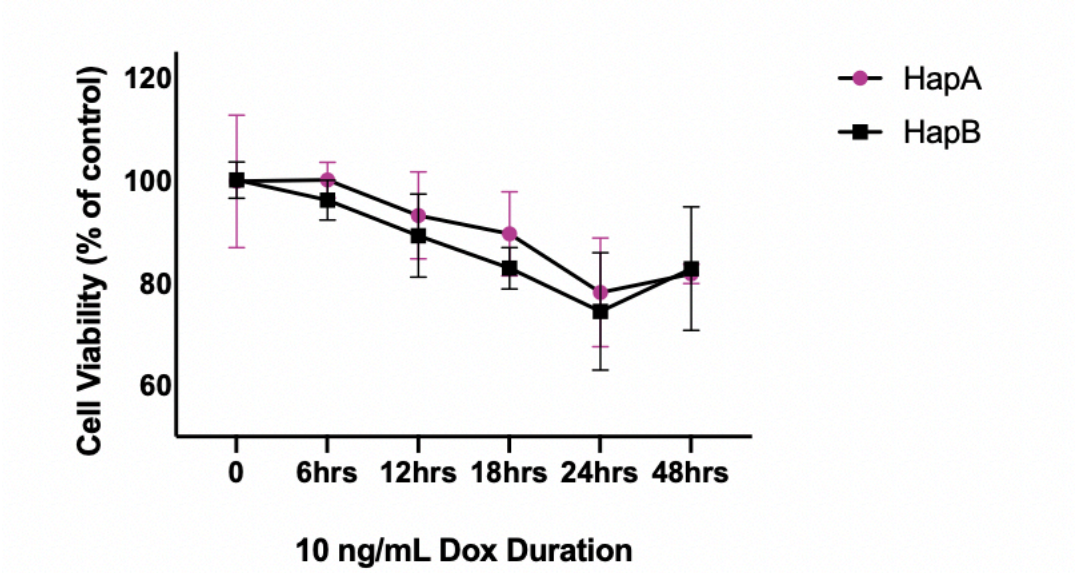

Figure 19. Viability of PERK A and B cells during duration of induction with 10ng/ml Dox. The number of dead cells were assessed at 6 hourly time points from both HapA and HapB cells after Dox induction. Each time point consisted of triplicate wells of each cell line and three biological replicates were carried out. Data was plotted as percentage of control whereby the uninduced HapB cells (largest mean in the data set) were normalised to 100% cell viability. As the data did not follow a Gaussian distribution, the non-parametric Wilcoxon matched paired test was used to compare the Dox induction time points between HapA and HapB. The Wilcoxon test pairing was deemed to effective (rs(Spearman) 0.9429, p=0.0083 (**))) and hence the Wilcoxon matched pairs signed rank test was carried out. This did not identify any significant differences in cell death between either of the two cell lines at any of the time points (W=-15, p=0.1562 (2-tailed), n=3).

3.5.5 *Knockdown of endogenous PERK*

Small interfering RNA (siRNA) is a highly specific and efficient tool to selectively silence target genes. In our study, we introduced silent mutations into the exogenous PERK sequence that made it resistant to the siRNA targeting the same region in the endogenous gene, enabling selective knockdown of the endogenous PERK and induced expression of only the exogenous PERK. We opted for this so as to study the effects of the latter in the absence of endogenous PERK expression. However, in the Flp-In 293 cell line, as it with brain tissue, endogenous PERK levels are extremely low. With Western blot analysis, trace levels of endogenous PERK were difficult to detect and thus, we were unable to test the siRNA knockdown. Using the western blot probed with the PERK antibody in Figure 17a and Figure 17b, a fold-difference of approximately 150 was estimated between the exogenous PERK over endogenous PERK by comparing the intensity levels of induced and uninduced samples. For this reason, we surmised that the very

high expression levels of induced exogenous PERK would overcome any effect of the endogenous PERK.

3.5.6 *Dox withdrawal on PERK expression*

To observe if induction could be switched off following Dox withdrawal, PERK expression was induced in the haplotype A and B cells by addition of 10 ng/mL Dox for 18 h, and then cell culture medium replaced with Tet-free medium and PERK protein levels detected by Western blot for 1-6 days. Even after 6 days, PERK signal intensity did not show any significant decreases, with both haplotype variants following removal of Dox, and at 6 days was not restored to basal levels (Figure 20).

3.5.7 Immunocytochemistry

PERK haplotype A and B cell lines were grown for 18 h on coverslips in the presence or absence of 10 ng/mL Dox. Cells were then fixed with 4% paraformaldehyde and stained using standard immunocytochemistry procedures. Nuclei were visualized with DAPI. Only the induced PERK cells had strong green straining around the majority of nuclei indicating specific PERK immunoreactivity (Figure 21). Due to the very low endogenous expression levels of PERK in HEK-293 cells as evidenced in our immunoblots, we failed to observe endogenous PERK in the uninduced cell lines using the anti-PERK B5 antibody. PERK was observed to be mainly surrounding the nuclei in Dox induced cells with the staining pattern being consistent between the different induced haplotypes. A cytoplasmic counterstain should have been used in conjunction with the ER stain to better highlight the ER organelle within the cell body. To confirm the specificity of this antibody staining to the ER, an ER-tracker™ BODIPY® was utilised. However, although this stain works well with live cells, we did not see ER staining in the formaldehyde-fixed cells.

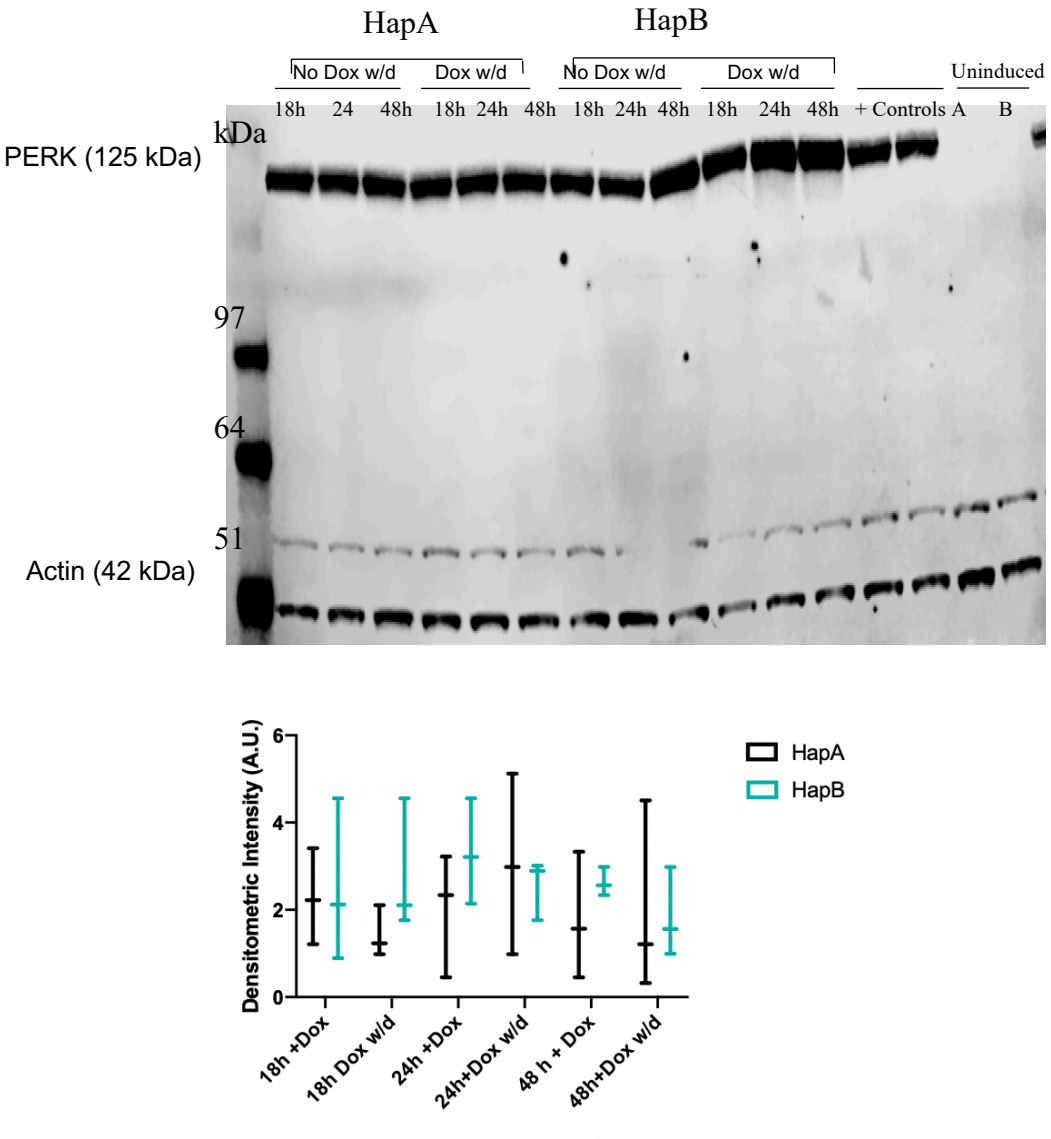

Figure 20. Immunoblots of PERK expression following Dox withdrawal. A representative western blot is shown for HapA and HapB cells treated with 10 ng/mL Dox for 18, 24, 48 h with and without Dox withdrawal after which cells were lysed and immunoblotting carried out. Each treatment was done in triplicate wells for each cell line and the experiment was repeated three times using new PERK cell clones from new transfections. Endogenous levels of PERK are indicated in the uninduced samples (last two lanes). Densitometric quantification of PERK induction was carried out by following equalisation against the corresponding actin band. An interleaved box and whiskers plot depicting all three experimental points per treatment are indicated. A Wilcoxon matched pairs signed rank test was carried out with no significant differences being observed between HapA and HapB following Dox withdrawal (W=13, p=0.2188 (2 tailed)), n=3).

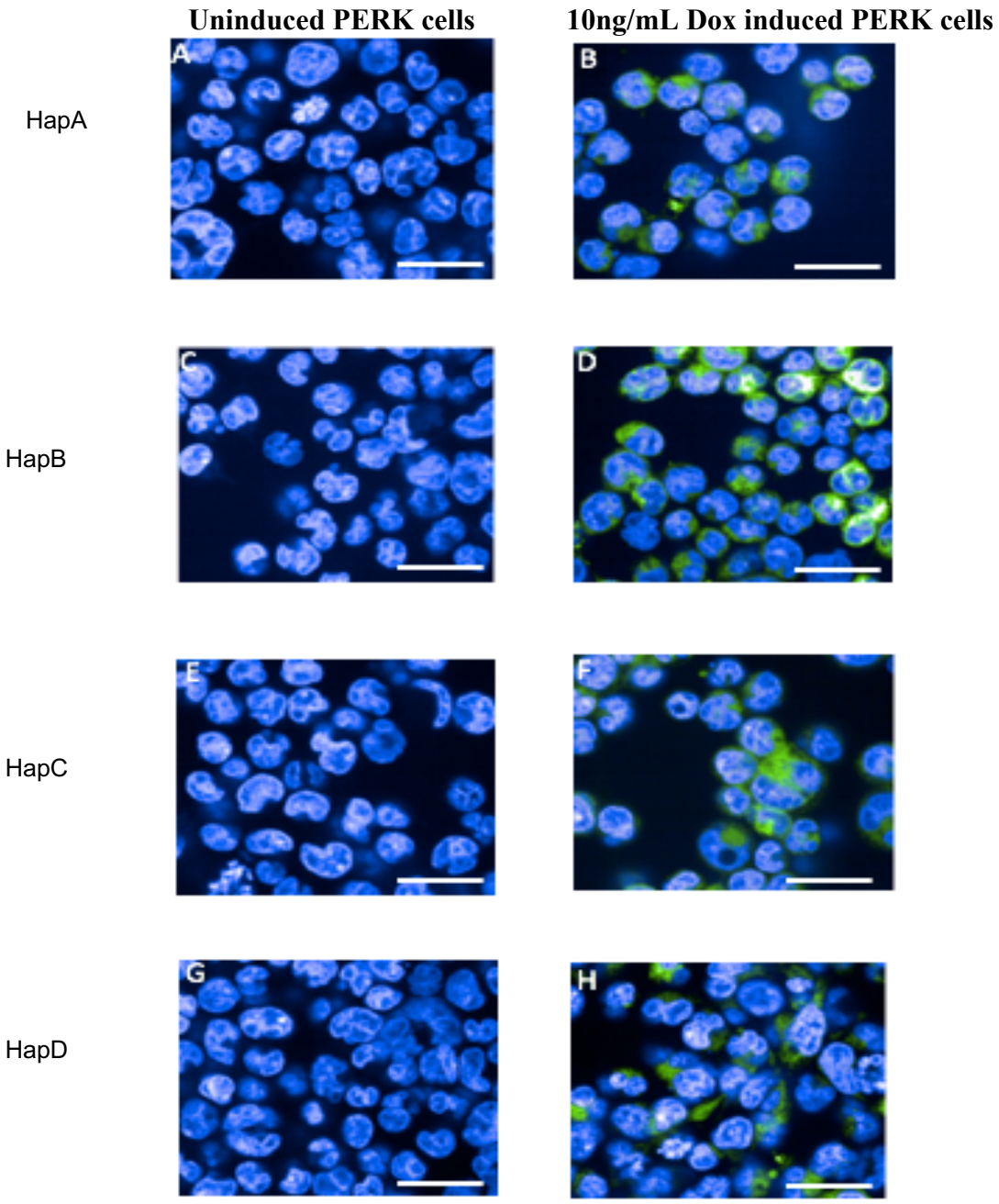

Figure21. Immunocytochemical confirmation of PERK expression. Stable uninduced PERK cell lines Hap A (panel A) , HapB (panel C) , HapC (panel E) and HapD (panel G) are indicated in the left-hand column. 10 ng/mL Dox induced PERK cells lines HapA (panel B), HapB (panel D), HapC (panel F) and HapD (panel H) are indicated in the right-hand columns. Each uninduced and induced cell line was fixed and immunostained for PERK using the B5 anti-PERK primary antibody and the anti-mouse secondary fluorescent antibody conjugated to Alexa Fluor 488 dye. PERK is stained strongly in the presence of Dox induction and the nuclear staining (blue) is observed with DAPI. Endogenous levels of PERK are observed to be barely visible as seen in each of the uninduced cell lines. Each row represents a separate clonal cell line. All panels are at the same magnification. Bars = 50 μm.

3.6 Discussion

We successfully created stable isogenic cell lines for inducible expression of the PERK risk and non-risk coding haplotype together with artificial variants. These cells form the basis of subsequent investigations of differences in the role of the different haplotypes in the biochemistry of the ER unfolded protein response and response to stress conditions that could be linked to a role in tau-based neurodegenerative pathways in the tauopathies.

The important advantages of this expression system are that the transgene is integrated into the same chromosomal site, thus enabling isogenic expression and studies without the possible confounds of positional effects, including disruption of other genes, or differences in gene expression levels. Furthermore, with tight regulation of gene expression, potential toxic effects of the overexpressed transgene can be avoided during work up and development of the cell lines.

However, a significant drawback of the Tet-On system that emerged from our work was the lack of any fine-tuning of expression levels by varying levels of Dox. As described above, gene expression is completely suppressed at Dox concentrations up to 9ng/ml after which, maximal expression levels ensue at 10ng/ml without any discernible dose response. Noting the extremely low levels of endogenous PERK, expressed transgene levels are clearly at massively higher levels (and not dosable), and could therefore result in a system where we may not be able to detect subtle differences between the risk and non-risk haplotypes. It is widely recognised that excess levels of PERK lead to its constant autoactivation due to the overwhelming of inhibitory BiP levels. In subsequent work described in this thesis, this disadvantage became evident though we were nevertheless able to observe some striking differences in with the risk Haplotype B (and its artificial variants), compared to all the other non-risk haplotypes.

An ability to fine-tune the expression levels of the PERK haplotypes to better reflect levels in the brain would have provided significant advantages in being able to model ‘true’ haplotype specific effects. A suitable alternative would be the utilisation of CRISPR/Cas-9 based genome editing to successively knock-in each of the coding SNP variants within the endogenous *EIF2AK3* gene in a neuronal cell line, preferably the SH-SY5Y line, or in iPSC-derived neurons. This would provide a more appropriate model to study the role of the PERK haplotypes in a neuronal milieu, and in relation to tau-related neurodegeneration without the confounding effects of excess levels of PERK that are constitutively activated.

However, as has emerged from our subsequent work, tissue expression of PERK is very sparse and through our study of PERK in autopsy brain tissue from the Queen Square Brain Bank, PERK, activated phospho-PERK and downstream UPR markers of the PERK pathway are barely detectable with conventional Western blot and immunocytochemistry techniques. In work with our

collaborators at the University of California, San Diego, it is clear that we would require initial enrichment procedures such as immunoprecipitation in order to detect the low levels of brain PERK (Jonathan Lin & Shauna Yuan; personal communication).

In summary, we successfully developed the Tet-inducible Flp-In^{TM} cell system for inducible expression of the haplotypic expression of PERK expression, with tight repression in the absence of Dox. On Dox induction, we observed rapid overexpression of the exogenous PERK and, despite autoactivation, within the timeframe of our experiments, observed only modest cytotoxicity. In subsequent chapters in this thesis, we describe the characterisation of this model and investigation into possible roles in tau pathogenesis.

4 Carboxy-terminal cleavage and reduced PERK haplotype B activity

4.1 *Overview*

The Tet-On conditional expression system was used for inducible overexpression of Myc-tagged PERK non-risk haplotypes A, C, and D and risk haplotype B, and synthetic sub-haplotypes B1, B2 and B3 in Flp-In™ - 293 cells with the aim of assessing any functional differences of PERK haplotypes in activation of the UPR. To ensure that each stably transfected cell clone expresses the transgene in all cells and at constant levels, for prolonged periods of time, each cell line was passaged up to five times and cell lysates probed by Western blot with the Myc-antibody.

After first passage of the stable clones, we observed loss of the Myc-tag exclusively in the cells expressing the PERK haplotype B (HapB) and the artificial HapB sub-haplotypes. However, we confirmed the significantly increased overexpression of the PERK HapBs with an antibody against the N-terminus and C-terminus of PERK, confirming that only the C-terminal Myc-tag was missing. We determined loss of Myc was not due to deletion of the transgene as, with genomic amplification of the PERK HapB cells from passage 2 (P2), we confirmed correct integration and presence of the full-length PERK HapB transgene into the predetermined chromosome locus in the Flp-In™ 293 cells. Using a primer pair, including one targeting the Myc-tag for specific detection of transgene expression, RT-PCR was carried out and we confirmed correct Tet-induced transcription of the PERK HapB transgenes in the P2 cells at similar levels as the other non-risk haplotypes. These data suggest that the exogenous PERK HapB proteins are specifically susceptible to C-terminal cleavage or misfolding following translation with general instability of the PERK HapB resulting in reduced PERK activity.

4.2 *Background*

Tagging of exogenously expressed proteins, usually with small peptides, is an established method to aid in distinguishing them from the endogenous protein. In this work, the synthetic transgene was engineered to include a C-terminal Myc tag, a decapeptide sequence EQKLISEEDL, which corresponds to the C-terminal amino acids (410-419) of human c-Myc protein. The small size of the Myc-tag compared to other commonly used tags (e.g. glutathione S-transferase (GST); 211 amino acid, green fluorescent protein (GFP); 238 amino acids) makes it less likely to disrupt the target protein's properties (conformation, function and localisation). In the case of PERK, previous work by David Ron's group (Yan et al., 2002) showed that the C-terminal Myc-tag does not affect PERK function. We therefore also decided utilised the myc tag

in our cell model to investigate differences in exogenous PERK function between HapA and HapB cell lines.

4.3 *Loss of Myc tag HapB stable clones after passaging*

Passage 1 (P1) stable cells were maintained in culture for 7 days in complete HEK medium lacking Dox in order not to activate the exogenous PERK expression. Furthermore, certified Tet-free FBS was used during cell growth and maintenance so as to avoid possible toxicity from leaky induction of the transgene expression due to traces of tetracycline and antibiotics in standard FBS. Once the cells reached a confluency of approximately 90%, the cells at P1 were split and induced with 10 ng/mL Dox and transgene expression analysed by western blot. Data were collected from twelve independent experiments, i.e. repeat generation of stable clones, over four passages.

With Western blots (Fig 22), all stable cell clones at P1 had robust overexpression of the induced PERK transgene as evidenced by positive labelling with the Myc antibody. However, we were struck by the consistent absence of Myc-positive band at P2 and beyond (P3 and P4) limited to those cells with induced expression of the risk haplotype, HapB and the artificial sub-haplotypes, HapB1, B2 and B3 whereas, transgenic PERK from cells expressing HapA, C, and D retained the Myc-tag (Fig 22). In order to ascertain if this was an artefact inherent to the first batch of stable cells, we repeated production of stable cells from multiple independent transfections and consistently observed this phenomenon of the loss of the Myc tag with just the risk haplotypes (HapB, B1, B2 and B3) (Figure 23).

4.4 Expression of recombinant HapB PERK despite the loss of Myc

In order to examine if there was complete loss of HapB PERK alongside the loss of the Myc signal, Western blots of HapA and HapB cells at P1, P2, P3 and P4 were probed with a mouse monoclonal PERK antibody targeting the N-terminal region of PERK (Santa Cruz) (Figure 24) to ascertain if the exogenous, overexpressed PERK is indeed present and if there is evidence of

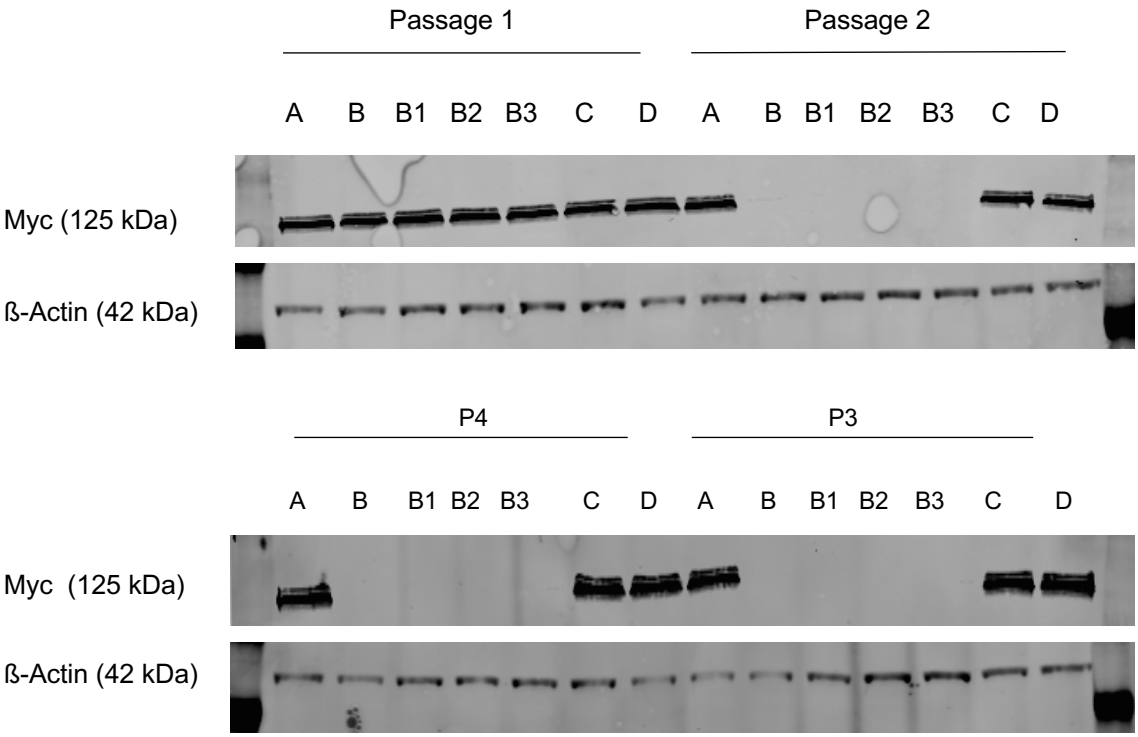

Figure 22. Immunoblot screening of Myc-tagged PERK expression in P1, P2, P3 and P4 PERK cells. Note the clear presence of the Myc-positive band with HapA,C, and D cells at all passages and absence of this band in P2 and subsequent passages in cells expressing the risk haplotypes, HapB, B1, B2,and B3. Beta-Actin was included as a normalisation control. Two clones were tested for each passage per cell line and twelve rounds of fresh stable transfections were conducted (n=2).

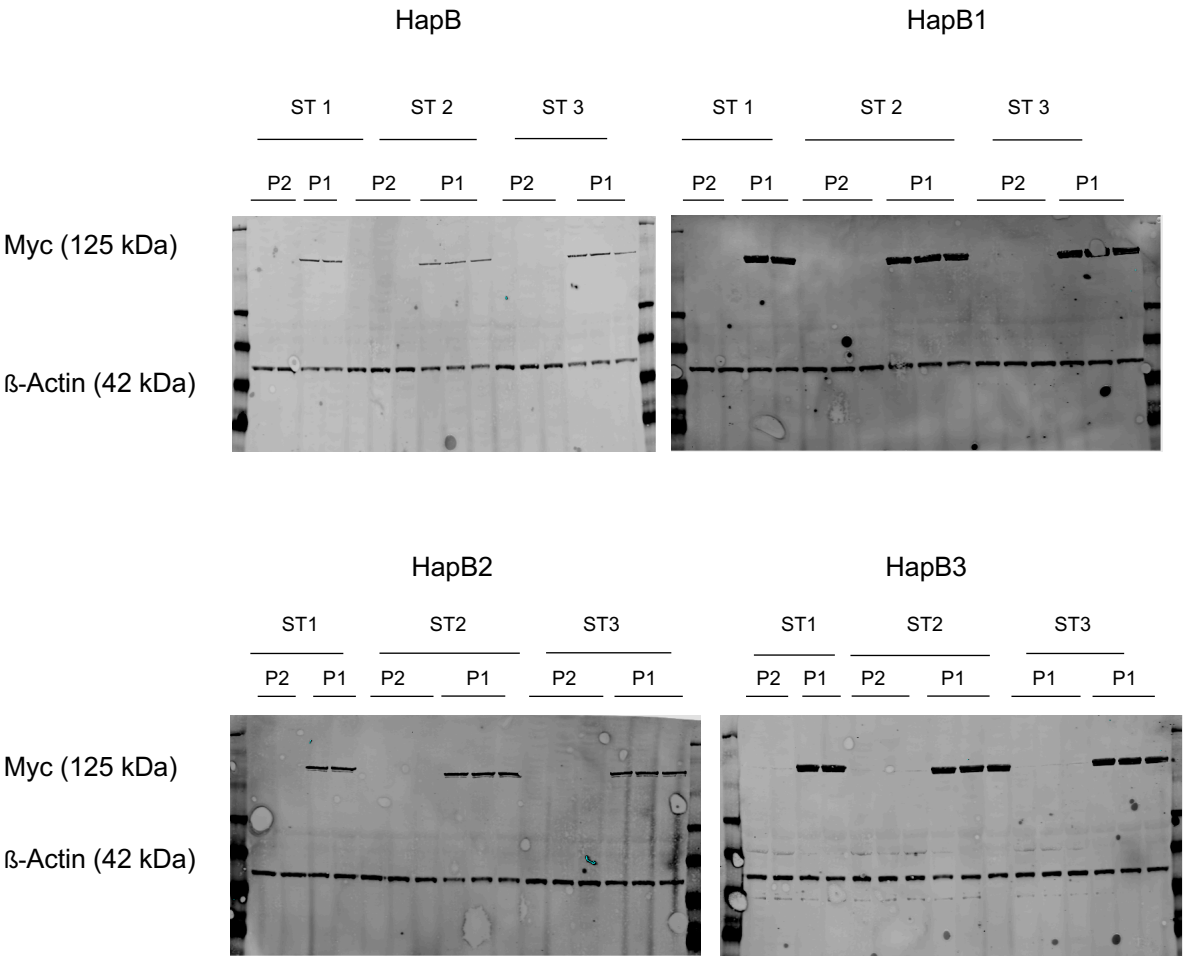

Figure 23. Immunoblot screening of Myc-tagged PERK expression in P1 and P2 HapB clones obtained from three independent stable transfections. Triplicate clones of induced P1 and P2 cells of HapB, B1, B2, and B3 were probed with Myc (Sc-40) antibody and ß-actin used as a normalisation control. The loss of the Myc band was evident in P2 cells expressing HapB and the sub hapB variants across independent stable transfections with only a trace band visible following passaging. Passage is indicated as (P), three individual clones are represented for both P1 and P2 in stable transfections 2 and 3, and two individual clones are represented for P1 and P2 in stable transfection 1 .Stable transfections are indicated as (ST).

proteolytic cleavage or degradation resulting in loss of the C-terminal Myc tag. The median and the 95% confidence level of the expression levels of PERK for each haplotype for passages 1-4 were plotted by normalising within each sample through its own ß-actin band. Immunoblotting was carried out three times using three independent clones obtained from three separate stable transfections.

HapB PERK was found to be present and at slightly increased levels in P2 and subsequent passages (P3, P4) although not significant. No difference in PERK intensity levels was found in either of the passages for HapA, HapC or HapD. Further, there was no discernible difference in the molecular weight of HapA and P2 HapB PERK, with no bands being visible at lower molecular weights for P2 HapB. No significant difference between levels of PERK expression was observed between the HapB sub-haplotypes. Our results show that although the Myc tag is missing from the HapB cells, a substantial amount of the exogenous PERK is overexpressed in HapB. This indicates that the Myc tag is lost due to cleavage very close to the C-terminus of PERK.

4.5 *Confirming PERK HapB transgene integration transcription*

Genomic integration of the full-length PERK plasmids in cells from P1, P2 and P3 was confirmed by isolating DNA from each of the induced PERK lines. The genomic DNA was used as a template in the PCR reactions, with a gene-specific primer combination that spanned the exon-exon boundary junction 8 and 9 of the PERK plasmid, enabling only the inserted cDNA to be amplified. A 255 bp amplicon was present in each of the seven PERK variants in all passages (Figure 25) confirming the stable integration of the PERK transgene into the Flp-In^{TM} -293 cell genome. The absence of an amplicon in the Flp-In^{TM} -293 cells used as a negative control was noted.

We used RT-PCR (Figure 26) in PERK induced clones at P1, P2, P3, P4 and P5 obtained from two independent experiments, to test if the PERK transgenes were being transcribed. Single-stranded cDNA was derived from RNA from PERK induced cells. This cDNA was used as a template for PCR, optimized so as to specifically amplify only the Myc-tagged transcripts. The presence of an amplicon at 431 bp confirmed that the transgene was transcribed by P1 through to P5 expressing all haplotype variants, including HapB.

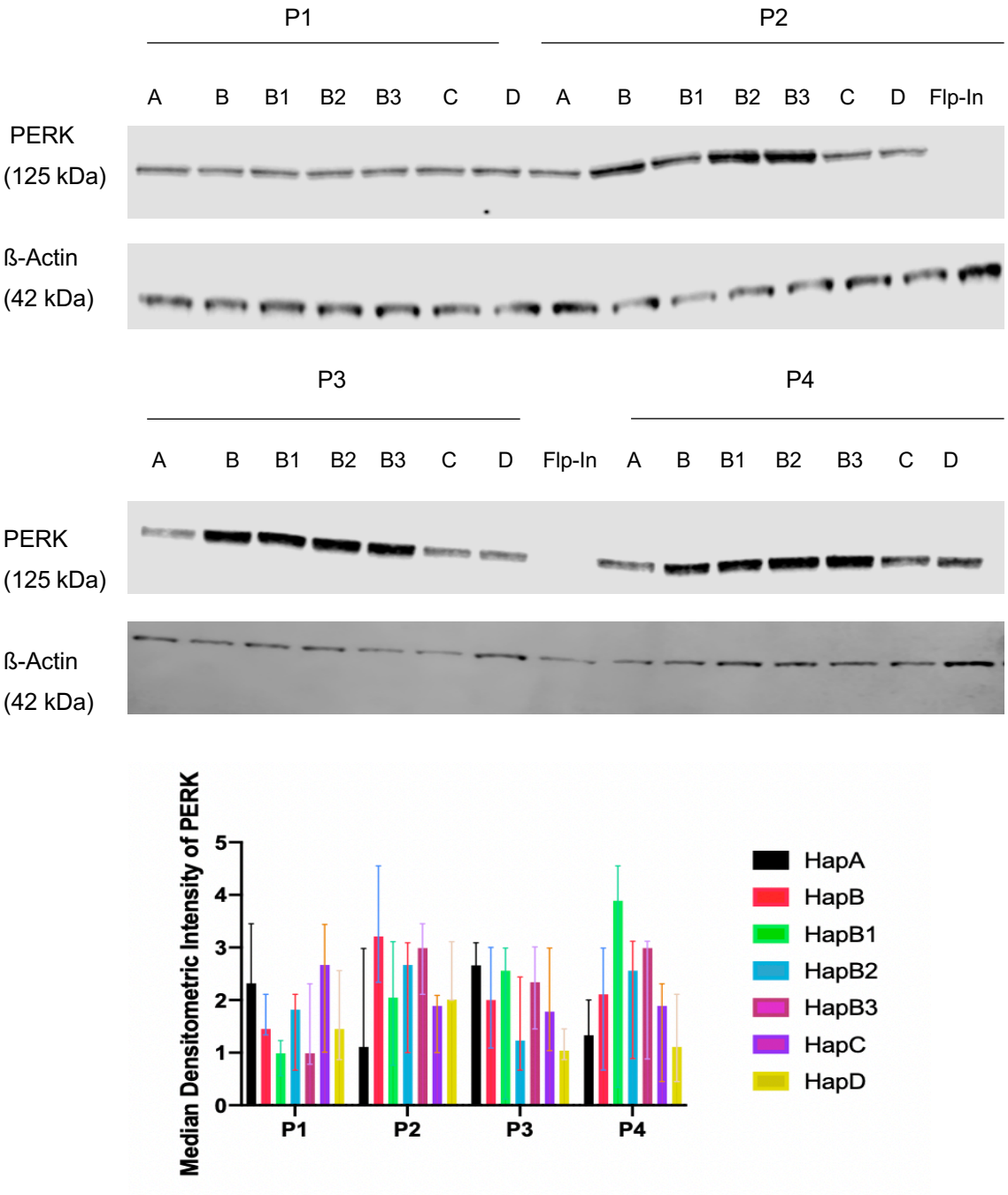

Figure 24. Immunoblot screening of total PERK expression in PERK P1, P2, P3 and P4 clones. All seven PERK haplotypes obtained from passages P1-P4 were probed with PERK (B-5) antibody targeting the N-terminal region and ß-actin used as a normalisation control. The Flp-In^{TM}-293 (Flp-In) cells were included as a negative control. The 95% confidence interval of the median densitometric PERK intensities of each cell line has been plotted. Passage is indicated as (P). Although there is a general trend of increased levels of PERK following passaging in the HapB and sub HapB cell lines, the non-parametric Friedman's test indicated no significant differences between the passages in either of the seven PERK cell lines (n=3, (F_r=4.224, df=6 p=0.6464, n=3).

.

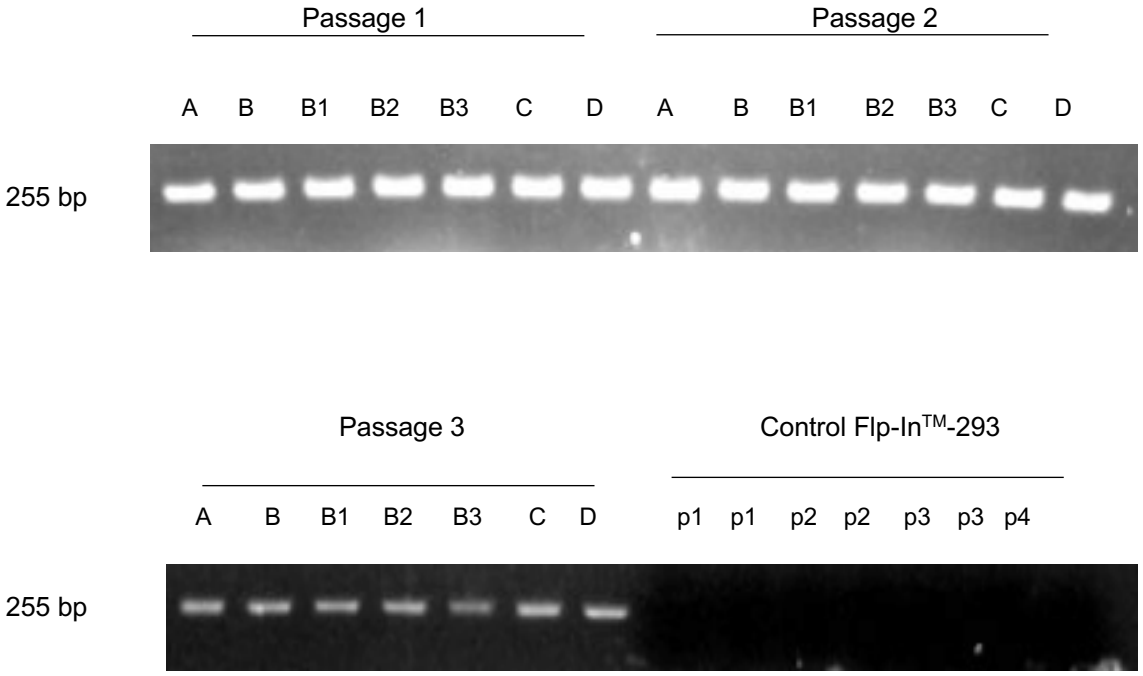

Figure 25. Confirmation of PERK transgene integration and retention in the Flp-In™-293 recipient genome. Each lane shows a different induced PERK haplotype at P1, P2 and P3. Naïve Flp-In™- 293 cells were used as negative controls. The presence of a 255 bp band is observed across all haplotypes and passages which is absent in the control Flp-In™-293 line confirming the incorporation and retention of the transgene into the genome of the Flp-In™-293 cells over multiple passages (n=2).

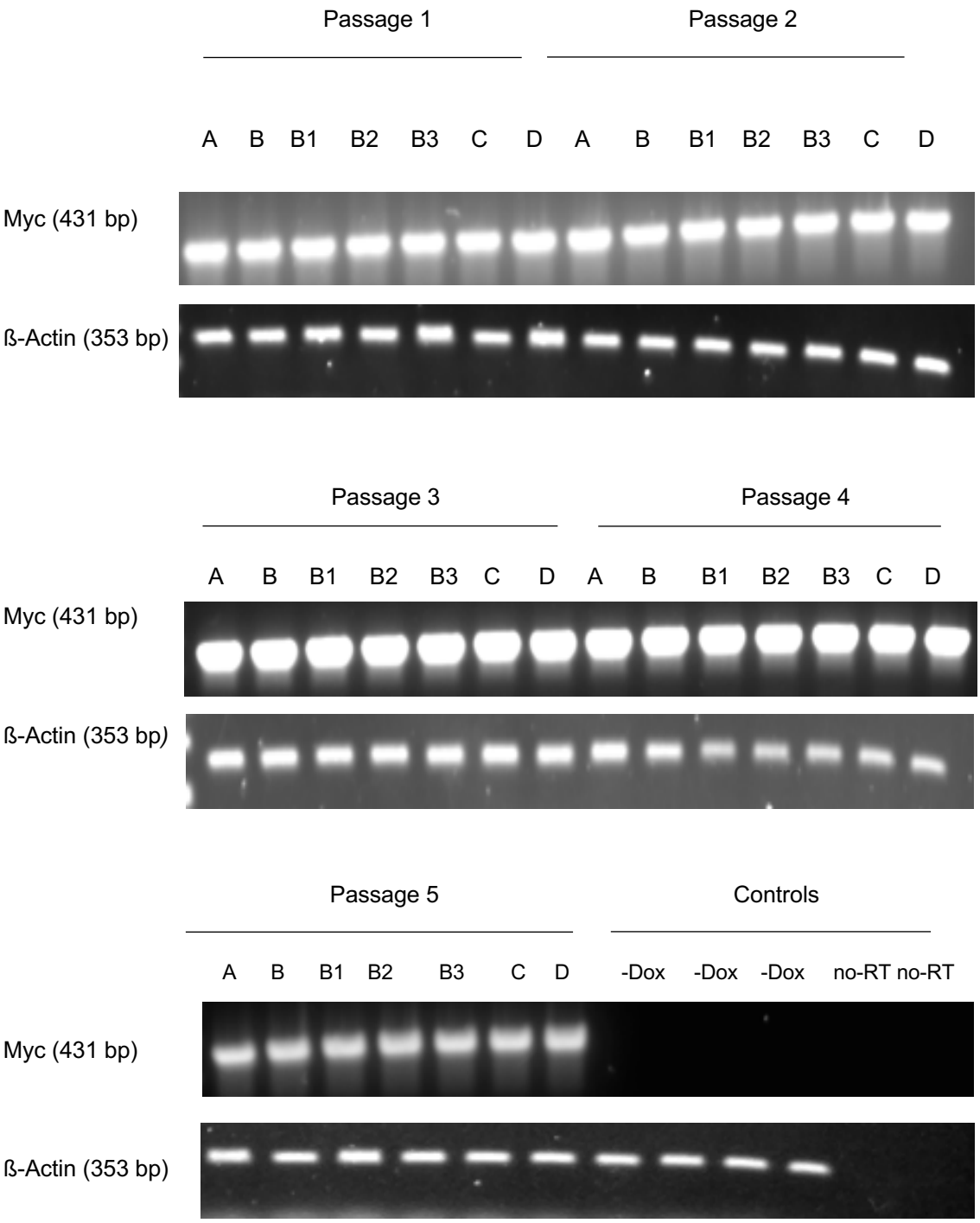

Figure 26: RT-PCR confirmation of transcription of Myc tagged PERK in induced PERK P1, P2, P3, P4 and P5 cells. Following passaging, induction of PERK was carried out by 10 ng/mL Dox for 18 hours followed by RT-PCR of the RNA samples. A house keeping gene, ß-Actin was used as a control. Uninduced samples are indicated as (-Dox) and two no reverse transcriptase controls (no-RT) were used as negative controls to rule out genomic contamination. A clear band for myc tagged PERK is visible in all haplotypes and in all tested passages, indicating that there is no loss of myc tag following transcription (n=2).

4.6 *Fluorescent immunocytochemistry*

With the selective loss of the Myc-tag in the passaged HapB cells, we optimised fluorescent immunocytochemical staining of the transgenic PERK with the Myc antibody as described in Section 3. DAPI was used to stain nuclear DNA (blue). With the induced P1 cells, there was strong perinuclear Myc staining consistent with ER localisation. Similar staining was also observed at P2 with HapA, C, and D cells (Figure 27a), confirming retention of the Myc tag. In contrast, consistent with the Western blot results, lack of Myc staining confirms that the Myc is absent in Dox induced HapB variant P2 cells (Figure 27b). The complete loss of the Myc tag occurred in P2 clones of all HapB and sub-HapB variants was observed from three independent stable clones derived from three multiple rounds of transfections. It is interesting to note that DAPI staining shows some blebbing and nuclear fragmentation specifically in passage 2 induced HapB cells. This would be an interesting idea to follow up using a TUNNELL assay/caspase activity to determine if apoptosis and general cell health of HapB is compromised following myc cleavage.

4.7 *Immunoblot analysis of PERK pathway*

With the loss of the Myc tag of the induced PERK HapB and HapB sub-variants at P2, we carried out western blot analysis to compare PERK activation using an anti phospho-PERK (p-PERK) antibody. Activation of eIF2α, ATF4 and CHOP was assessed to observe if the loss of the Myc signal at P2 affects downstream activation of the HapB PERK pathway. Typical examples of immunoblots are shown in Figure 28a. PERK and eIF2α activation was calculated by first normalising the total protein and phospho-protein levels against their ß-actin. The ratio between the phospho-protein and the total protein was then calculated and the mean densitometric intensity plotted as PERK activation and eIF2α activation, respectively. The data were collected from 3 independent experiments using three new stable clones for each repeat.

Total PERK expression was increased in each HapB variant at P2 as observed by an increase in band intensity of the PERK N-terminus targeted antibody which however, failed to show a significant increase following normalisation against ß- actin. Meanwhile total PERK levels remained unchanged upon passaging in the HapA, C, and D cell lines. At P1, overexpression of exogenous PERK after Dox induction led to the expected activation of PERK as shown by increased phospho-PERK. However, after passaging, although the immunoblots indicated a trend of increased levels of total PERK and decreased levels of phospho-PERK, this was not observed following statistical analysis (Figure 28a). Intriguingly, we did not note any changes with the other downstream markers of the PERK pathway. However, there was a trend of reduced phospho-eIF2α levels in HapB and HapB1 cells which failed to reach significance (Figure 28b, Figure 28c). Further work should look into including the uninduced cell lines as an appropriate negative control.

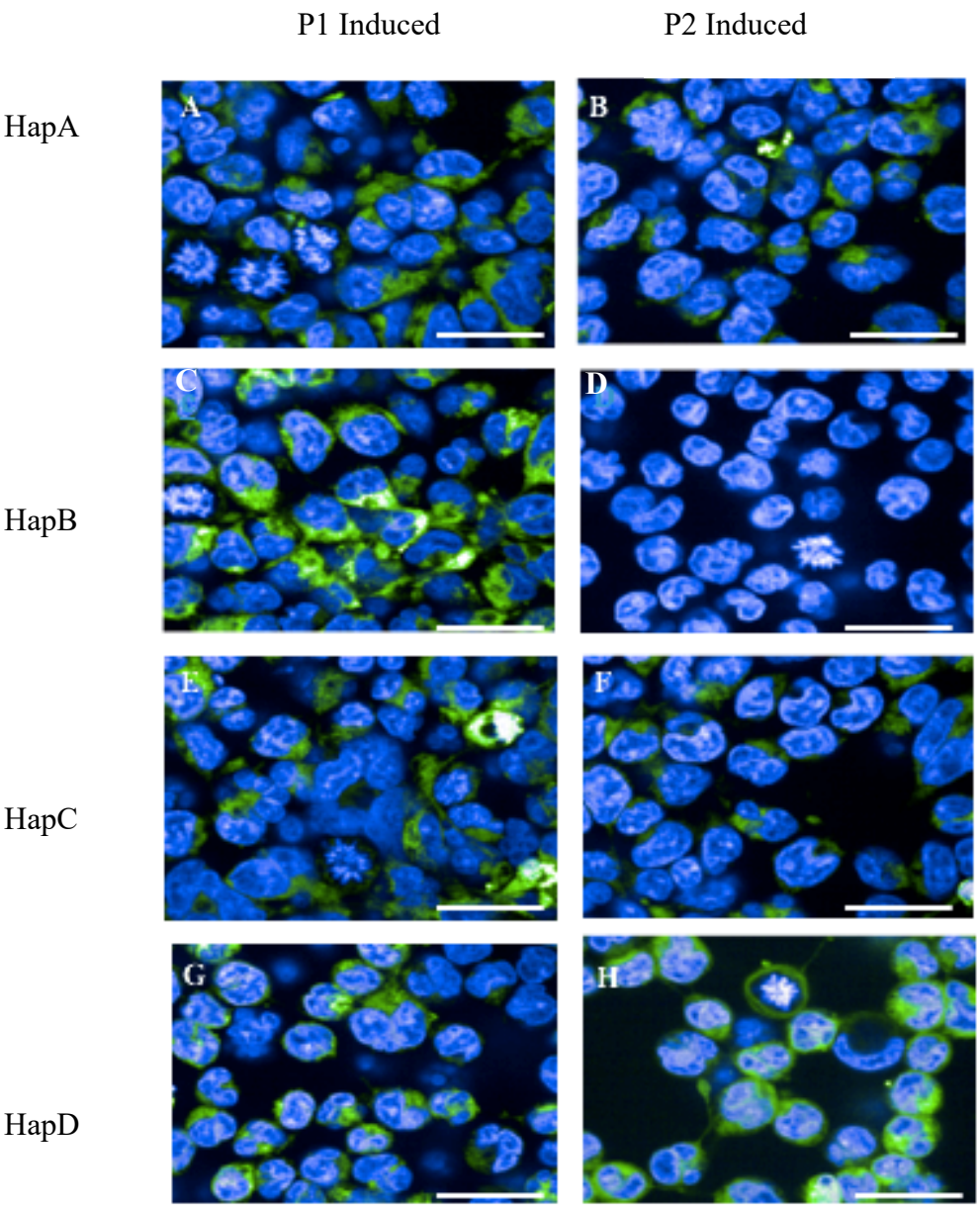

Figure 27a. Myc tagged PERK expression in P1 and P2 cell lines. Fluorescent micrographs of Dox induced P1 HapA (panel A), B (panel C) , C (panel E), and D cells (panel G) and P2 induced HapA (panel B) , B (Panel D), C (Panel F), and D cells (Panel H) were fixed in 4% PFA and immunostained for myc using the 9E10 myc mouse-primary antibody and the goat anti-mouse secondary fluorescent antibody conjugated to Alexa Fluor 488 dye. Immunoreactivity of nuclei was visualized with DAPI (blue). Strong green fluorescent staining around the nuclei in the induced P1 and P2 Hap A, C, and D (Panel A, B, C, E, F,G, H), confirm presence of Myc-tagged PERK. However, the Myc staining is absent in the HapB P2 cells (Panel F). Bars = 50 μm.

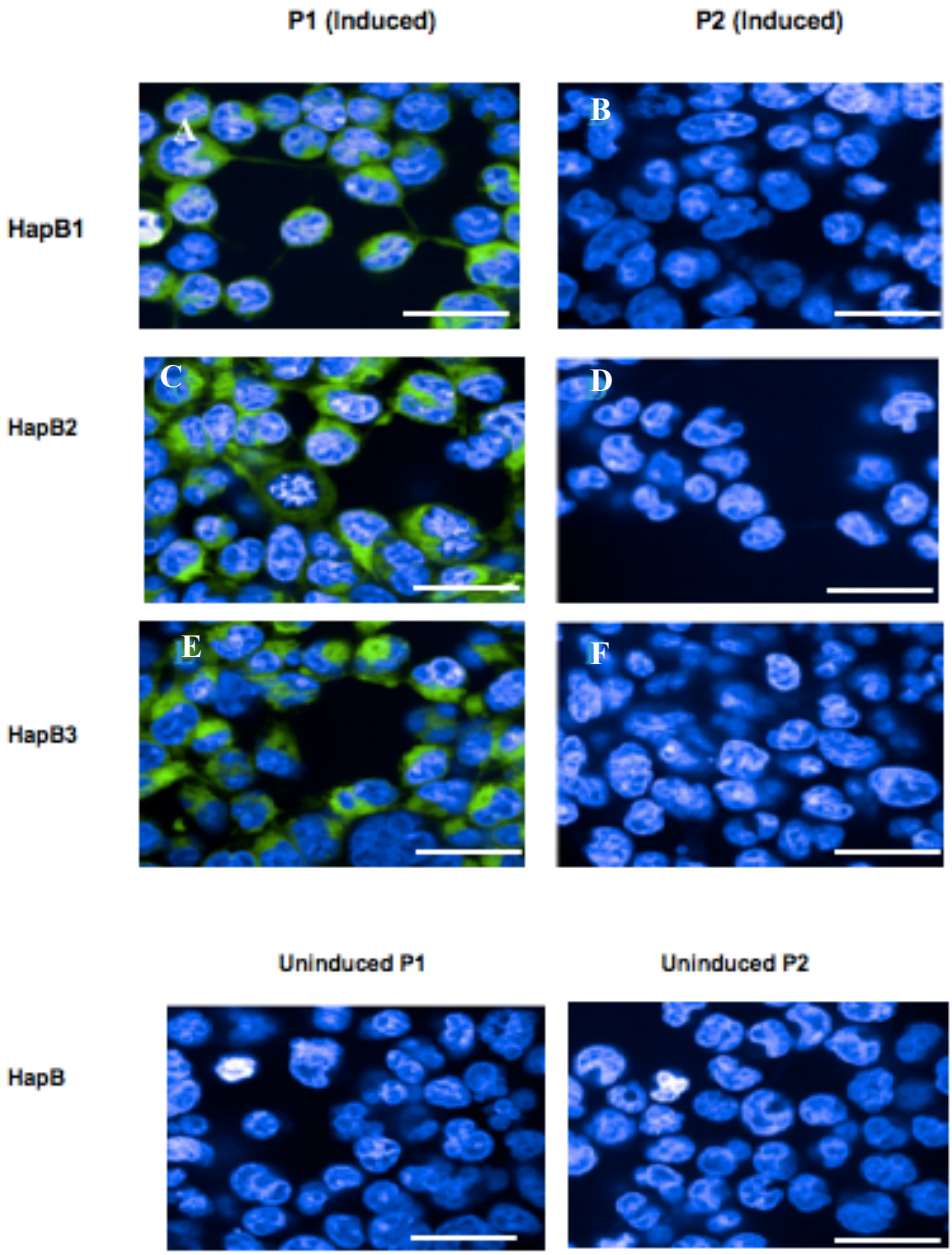

Figure 27b. Myc tagged PERK expression in sub HapB P1 and P2 cell lines. Fluorescent micrographs of Dox induced HapB1, B2, B3, cells at P1 (Panel A,C,E) and HapB1, B2, B3 cells at P2 (Panel B,D,F) and uninduced HapB cells at P1 and P2 were used as negative controls, along with a secondary antibody-only control. Immunoreactivity of nuclei was visualized with DAPI and Myc-tagged PERK staining was visualised by using a goat anti-mouse secondary fluorescent antibody conjugated to Alexa Fluor 488 dye. Strong green staining around the nuclei in the P1 sub HapB cells (Panel A,C,E), confirm presence of Myc-tagged PERK. However, the Myc staining is absent in the sub Hap B1, B2, and B3 P2 cells (Panels B,D,E). Bars = 50 μm

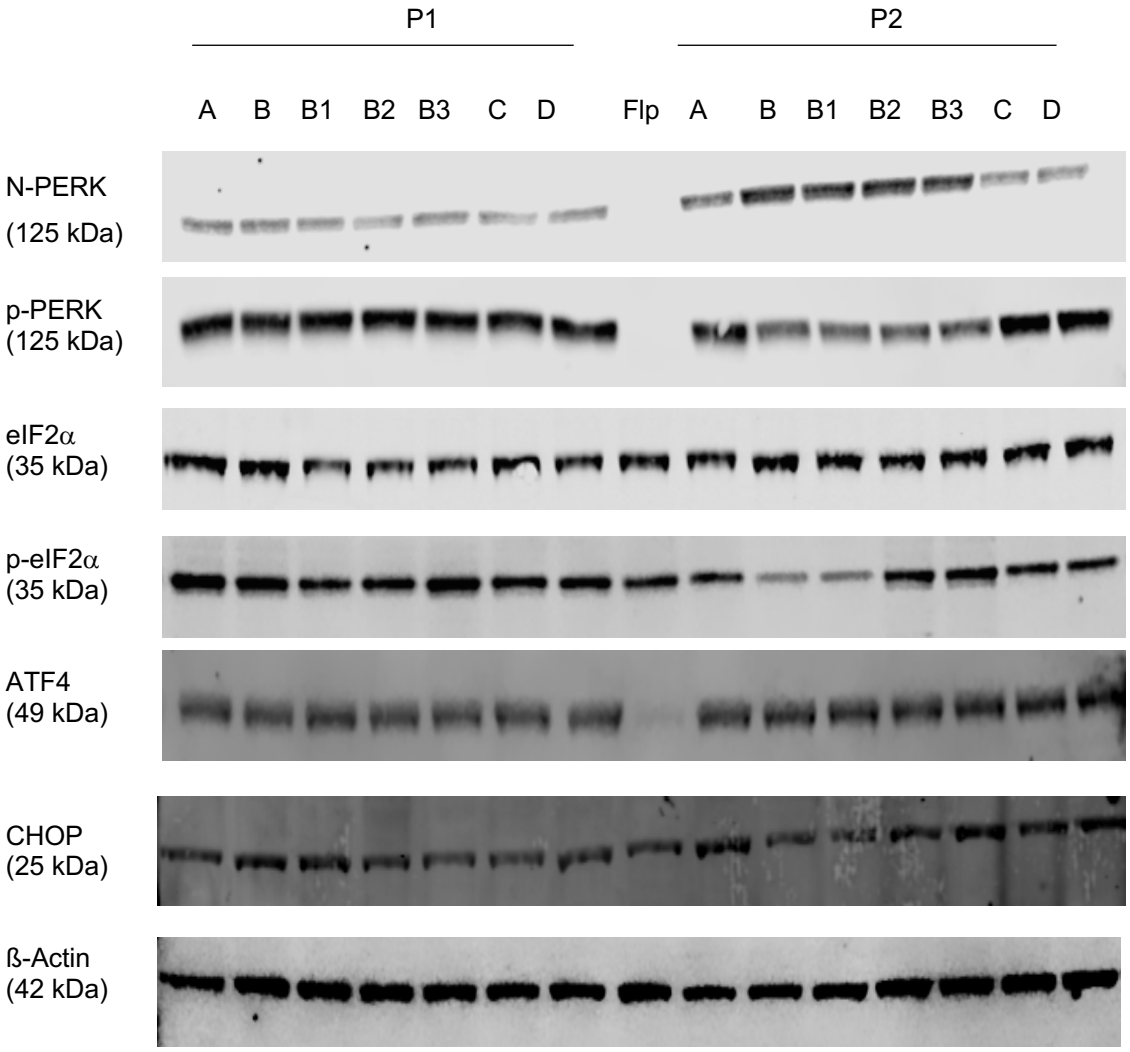

Figure 28a. PERK pathway immunoblots of P1 and P2 PERK cell lines. Typical immunoblot analysis of PERK and PERK pathway markers. Cells for the different haplotypes of PERK at P1 and P2 were treated with 10 ng/mL Dox for 18 hours with untreated cells (Flp-In^{TM}-293) used as controls. Total protein extract, 30 μg, was loaded in each well. PERK amino-terminus (N-PERK) and p-PERK antibodies were used to detect PERK levels and activation. EIF2α, p-eIF2α, ATF4 and CHOP antibodies were used to assess activation of the downstream markers of the PERK pathway. ß-Actin was used a normalisation control. Note the increased band intensity for N terminus-PERK and corresponding decreased band intensity of p-PERK and p-eIF2α in the HapB P2 lines (B, B1 for p-eIF2α). Flp-In^{TM}-293 cells (Flp) fail to show a clear band for PERK, p-PERK and ATF4 due to low endogenous level expression.

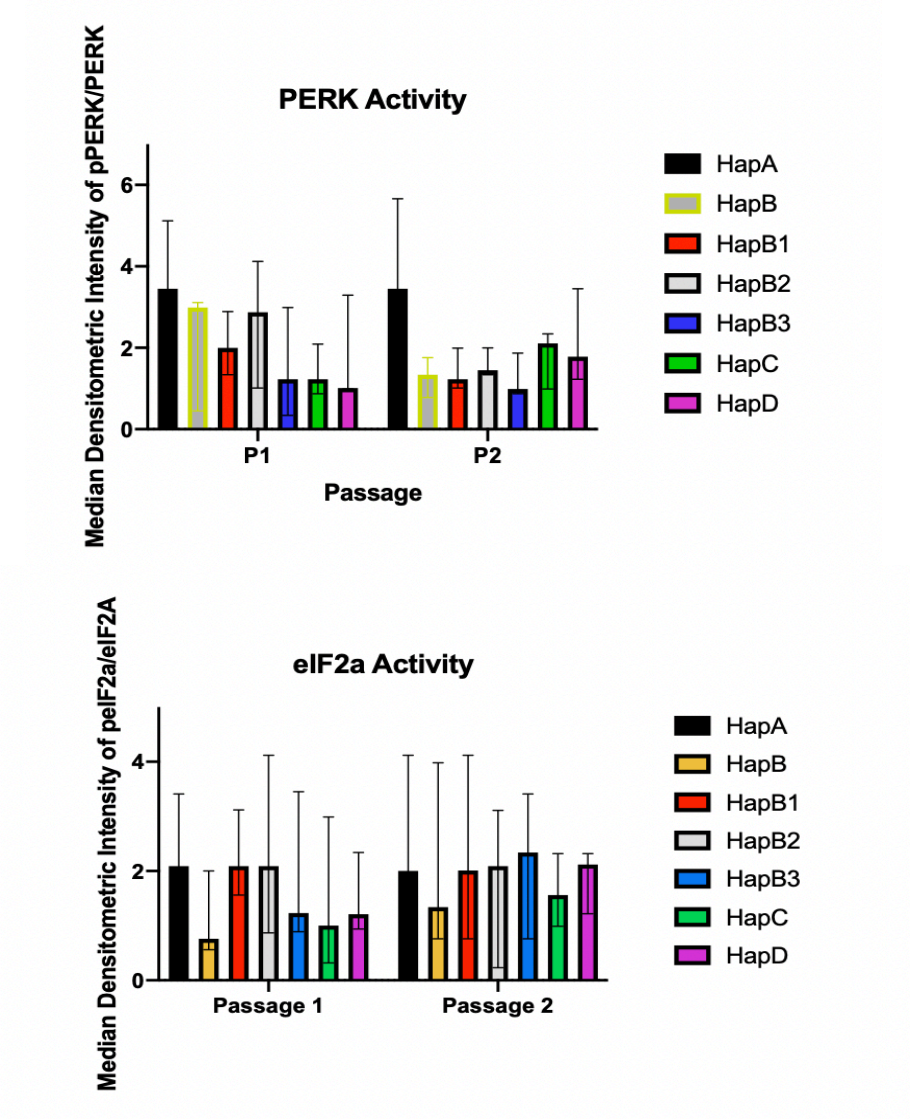

Figure 28b. Densitometric quantification of P1 and P2 PERK and eIF2α activation immunoblots. Blots were described in the legend to Figure 28a. PERK activity levels and eIF2α activity levels are expressed as a ratio of phospho protein: total protein following normalisation against each corresponding ß-actin band. The 95% confidence interval of the median densitometric PERK intensities of each cell line has been plotted using triplicate cell clones per passage and each experiment repeated independently three times. Although induction of PERK after second passage (P2) of each HapB cell line demonstrated an increased intensity of the total PERK signal and a decreased signal intensity of p-PERK signal in the immunoblots, a statistical significance for PERK activity was not observed between the 7 haplotypes following passaging using the Friedman's test ((F_r=7.714, df=6 p=0.2780, n=3). Similarly. eIF2α activity also did not yield a significant difference between the P1 and P2 cell lines ((F_r=9, df=6 p=0.1.333, n=3).

.

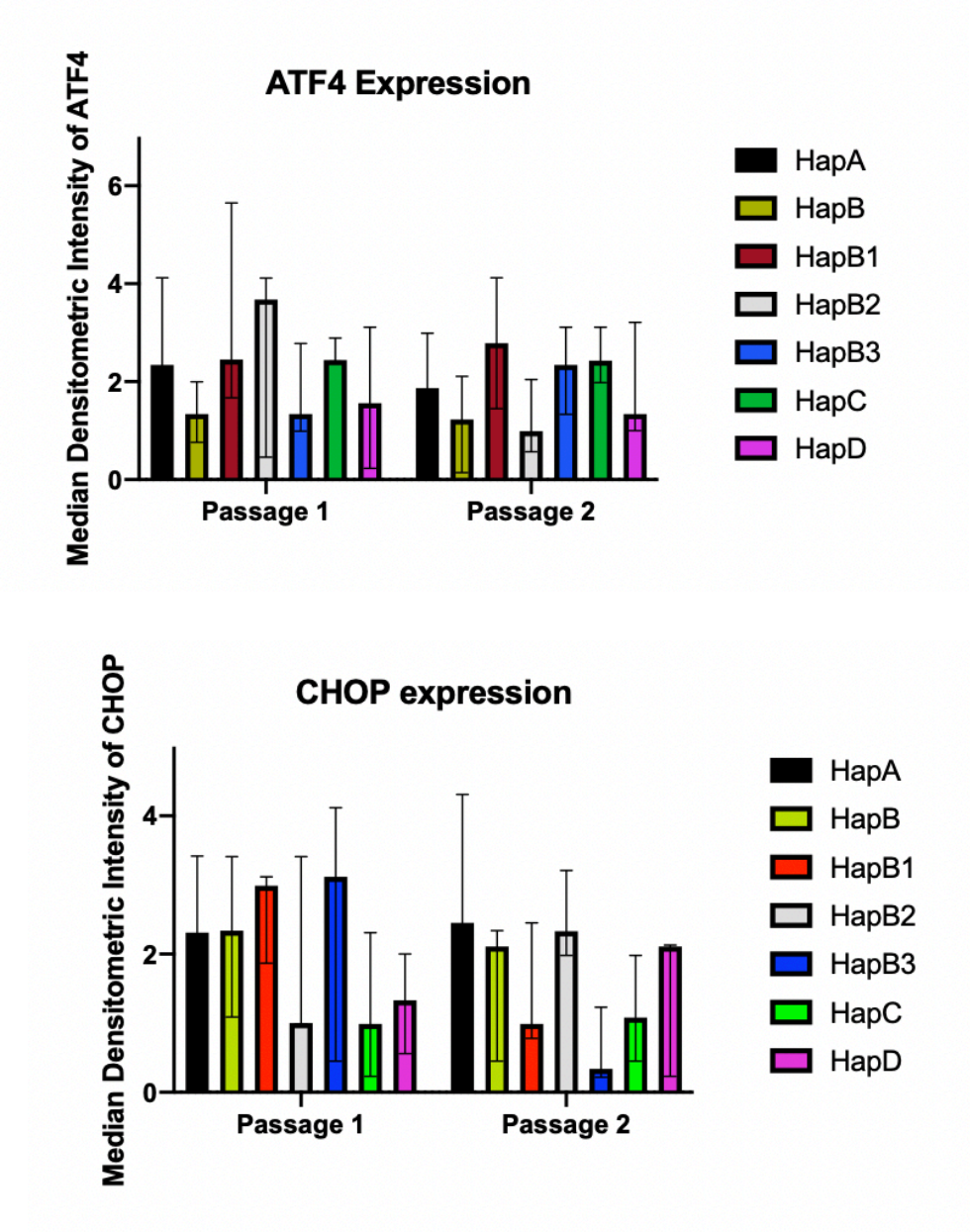

Figure 28c. Densitometric quantification of ATF4 and CHOP immunoblots. Blots were described in the legend to Figure 6a. The 95% confidence interval of the median densitometric ATF4 and CHOP intensities of each cell line following normalisation against the corresponding beta-actin has been plotted by using triplicate cell clones per passage and each experiment repeated independently three times. Induction of PERK did not result in a change in significance in band intensity of either ATF4 (F_r=9.214, df=6 p=0.1.179, n=3). or CHOP expression levels (F_r=6.857, df=6 p=0.3913, n=3) following passaging in either of the seven PERK haplotypes as tested by the Friedman's test.

To observe if reduced PERK activity is brought about by cleavage of the C-terminus, a PERK C-terminal targeted antibody P0074 (MilliPore) was used. A typical immunoblot of induced P1 and P2 HapB cells is shown in Figure 29. Three independent experiments using triplicate HapB and sub HapB clones for each were carried out and the 95% confidence interval levels of the median PERK C-term expression levels were plotted. Following passaging, we again show a trend of higher levels of overexpressed PERK in all of the HapB cell lines which failed to reach significance (Figure 29). However,, this work would have greatly benefited by comparing both the expression levels of non-risk and risk haplotypes of PERK together in the same blot using this C-terminus targeted antibody. The inclusion of the non-risk haplotypes would then enable us to determine if the previously observed increased expression of total PERK following passaging was specific to the myc cleaved HapB cells. Inclusion of both the non-risk haplotypes together with the risk haplotypes is therefore warranted before any definitive conclusion can be made. There was complete absence of a signal in the uninduced line confirming tight repression of the PERK transgene in the absence of Dox. PERK protein has 1117 amino acids – the C-terminal antibody recognises amino acids 1072-1098. Positivity with HapB variants confirm that loss of Myc tag is due to endoproteolytic cleavage in the last 19 amino acid stretch at the C-terminus of PERK and/or degradation of the Myc-tag. It would be crucial to identify the exact nature of this cleavage as its occurrence is specific to the Hap B and could point towards the functional basis of the increased risk.

4.8 Effect of cell viability in P2 HapB cells

Overexpression of HapA and HapB PERK did not show any perceivable effect on cell health. To determine cell viability of the induced P2 Myc cleaved HapB clones, we used the CellTiter-Glo luminescent cell viability assay as detailed in Chapter 2. This enabled us to determine if Myc-cleavage of HapB PERK observed at passage 2 (P2) could be affecting cell health (Fig 30). Dox induced P2 HapA and myc cleaved B cell death values were plotted as a box and whisker plot indicating the three luminescence data points obtained from each of the two cell lines following the cell death assay. Each experiment was carried out using triplicate wells of each cell line and three independent experiments carried out using clones from three new stable transfections. P2 HapB cells did not reveal a difference in cell viability when compared to HapA cells indicating that cell health was not directly compromised in the Myc cleaved P2 HapB variants following passaging (Figure 30).

4.9 Is cleavage responsible for HapB PERK instability

Noting the consistent loss of the C-terminal Myc tag at P2 with the HapB and sub HapB haplotypes, we next sought to identify the nature of the cleavage. Clearly, the cleavage occurs very close to the C-terminal end as it had no discernible effect on the size of the overexpressed PERK and expressed exogenous HapB PERK was recognised by a PERK antibody close to the C-terminus of PERK. In order to identify the cleaved C-terminus carrying the Myc-tag we carried out immunoblotting following electrophoresis on a 16% Tris-Tricine Gel for resolving low molecular weight proteins, less than 20 kDa. As the myc tag has only 10 amino acids and thereby a molecular weight of just 1.2 kDa, we expected our cleaved product to be around 1.2-2kDa.

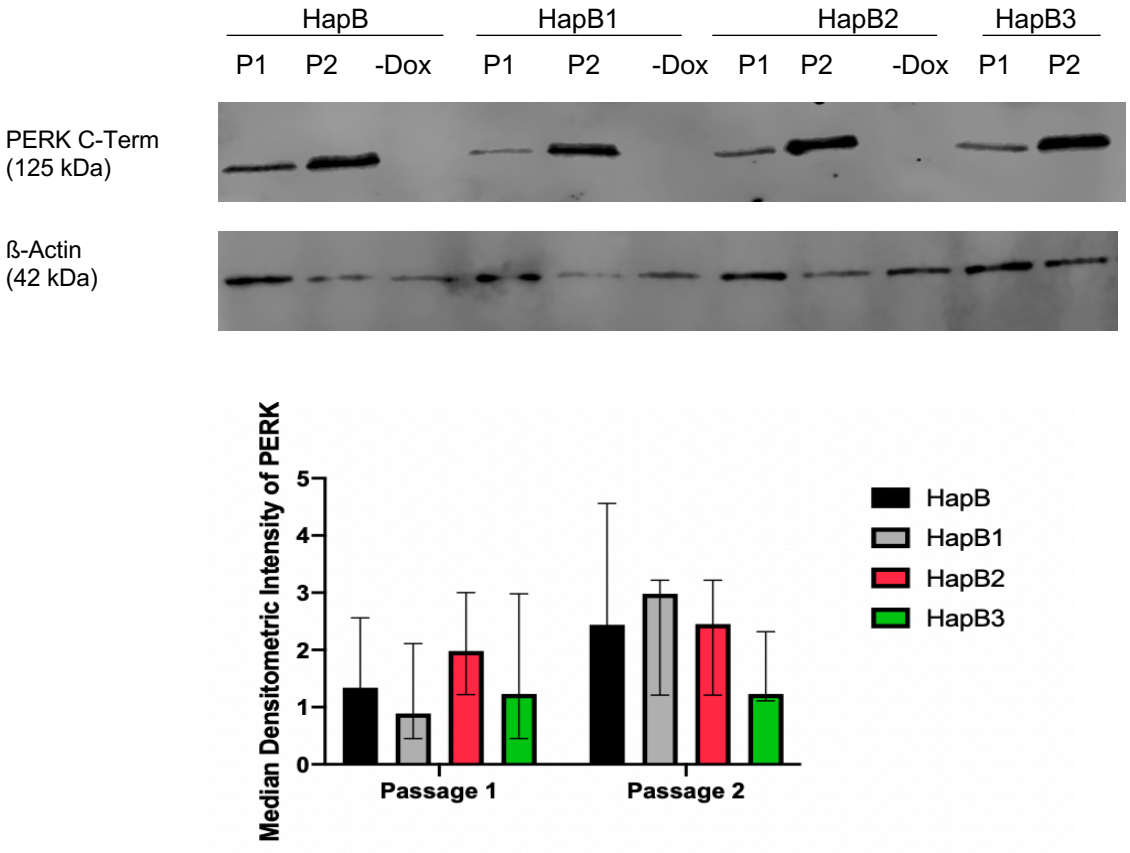

Figure 29. PERK C-terminus immunoblots from P1 and P2 HapB cells. Blots were probed with a PERK C-terminal targeted antibody and normalised against ß-actin. Uninduced lysates from each sub haplotype B were included as negative control confirming tight repression upon the absence of Dox. Expression levels of PERK was normalised against each corresponding actin band and the 95% confidence interval levels were included in the median densitometric plot. Although no significant changes in PERK C-terminus was indicated by the Friedman's test between either of the four HapB haplotypes following passaging ((F_r=1.2, df=3 p=0.8333, n=3), a trend of increased PERK expression using the PERK C-terminus targeted antibody was observed in HapB and sub HapB cells lines.

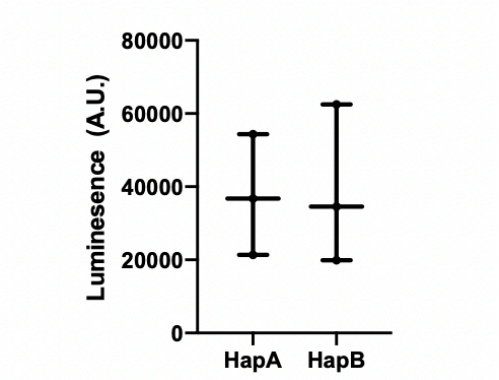

Figure 30. Cell viability of P1 and P2 PERK cells. The number of dead cells present in P2 induced HapA and HapB cells were assessed by the ATP-dependant CellTiter-Glo Luminescent Assay. Induction of PERK in P2 HapB cells did not result in a significant difference in cell death when compared to the P2 HapA cells as tested with the Mann Whitney u-test (median latencies in HapA and HapB were 39789, 30078; U = 4, p>0.999, n=3).

Equal quantities (10 μg/lane) of protein were resolved by electrophoresis followed by blotting onto PVDF membranes. Immunoblots probed with Myc and PERK antibody (Figure 31) did not reveal any bands of low molecular weight. Although further modified immunoblotting protocols were used, no Myc-positive small molecular weight bands were detected. This could have been due to degradation of the cleaved peptide or exopeptidase cleavage of the Myc tag.

4.10 Is HapB PERK instability due to protein degradation

In order to observe if the Myc of the overexpressed PERK in the HapB cells at P2 was present earlier during expression but underwent subsequent degradation, we analysed Myc-labelled PERK at earlier time points, hourly after induction for up to 12 h. Immunoblots were performed and probed with Myc antibody and normalised against ß-Actin. Myc tagged PERK is first observed as early as 3 h (Figure 32) post-induction in the HapA and HapC cells at P2, but only a faintly visible band was seen in the HapB cells 9 hours post Dox induction. Both HapA and C variants showed similar levels of Myc-tagged PERK at all time points. The time-course experiment was repeated twice more using new stable clones for each repeat.

4.11 Cell detachment during passaging does not affect the expression of Myc in HapB P2 cells

With the loss of Myc taking place during passaging we aimed to determine if mode of detachment of HapB cells from the tissue culture flask was causing the loss of the Myc tag due to trypsin treatment or through effects on the cytoskeleton. To test this, we created new PERK stable clones which were expanded using different cellular detachment methods, in addition to trypsin. Five isolated PERK clones for each haplotype were detached by using either a cell scraper, PBS-EDTA, Accutase or trypsin and then expanded into 24-well plates and subsequently T25 tissue culture flasks. The clones were then frozen, and the same method of detachment was kept constant for each clone following freeze/thawing. The freeze/thawed P0 cells were split twice and the P2 cells were Dox induced for 18 h and protein lysates obtained. Immunoblots were carried out for Myc (Figure 33). The results showed that loss of the Myc tag in the P2 HapB and sub HapB variants occurred with all modes of cell detachment, confirming that inherent cellular responses to the process of passaging (detachment, PBS wash, centrifugation, re-plating) result in the cleavage or degradation of the C-terminal Myc-tag of the HapB PERK.

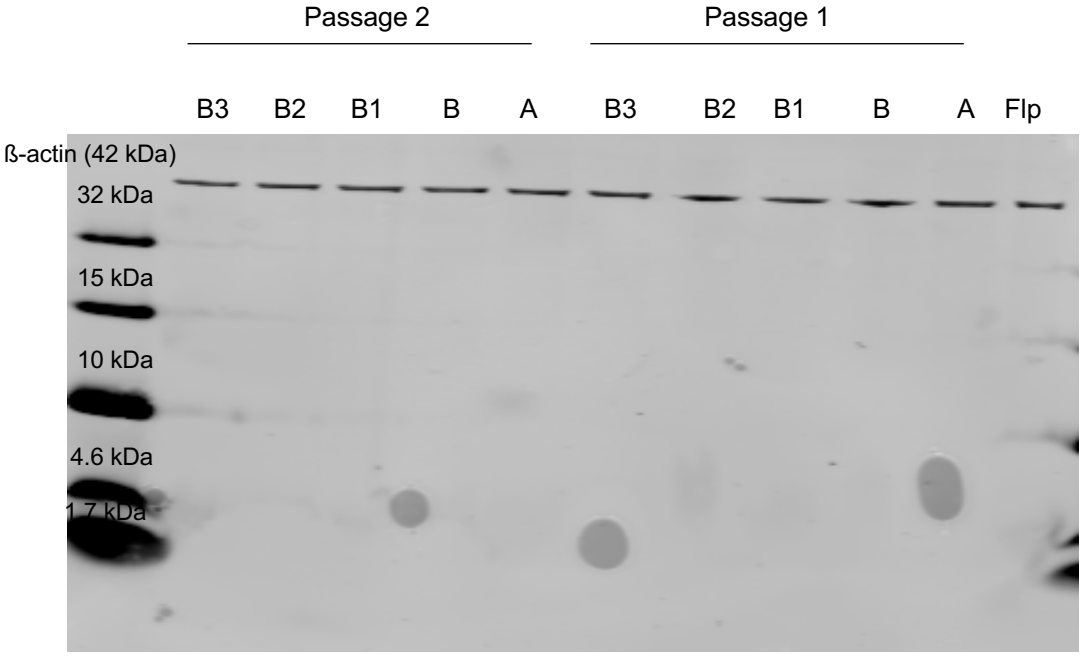

Figure 31. Low molecular weight immunoblots of P1 and P2 induced PERK cells. Immunoblot analysis of Myc tagged P1 and P2 PERK with Myc and PERK antibodies in induced HapA, HapB and sub-HapB cell lines were performed using a 16 % tris-tricine SDS gel followed by wet transfer. Flp-In^{TM}-293 (Flp) cells were used as a control. Total protein extract, 10 μg was loaded into each well. Note the absence of a low molecular weight band in the bottom of the gel in the P2 HapB and sub HapB lines similar to the P2 HapA line.

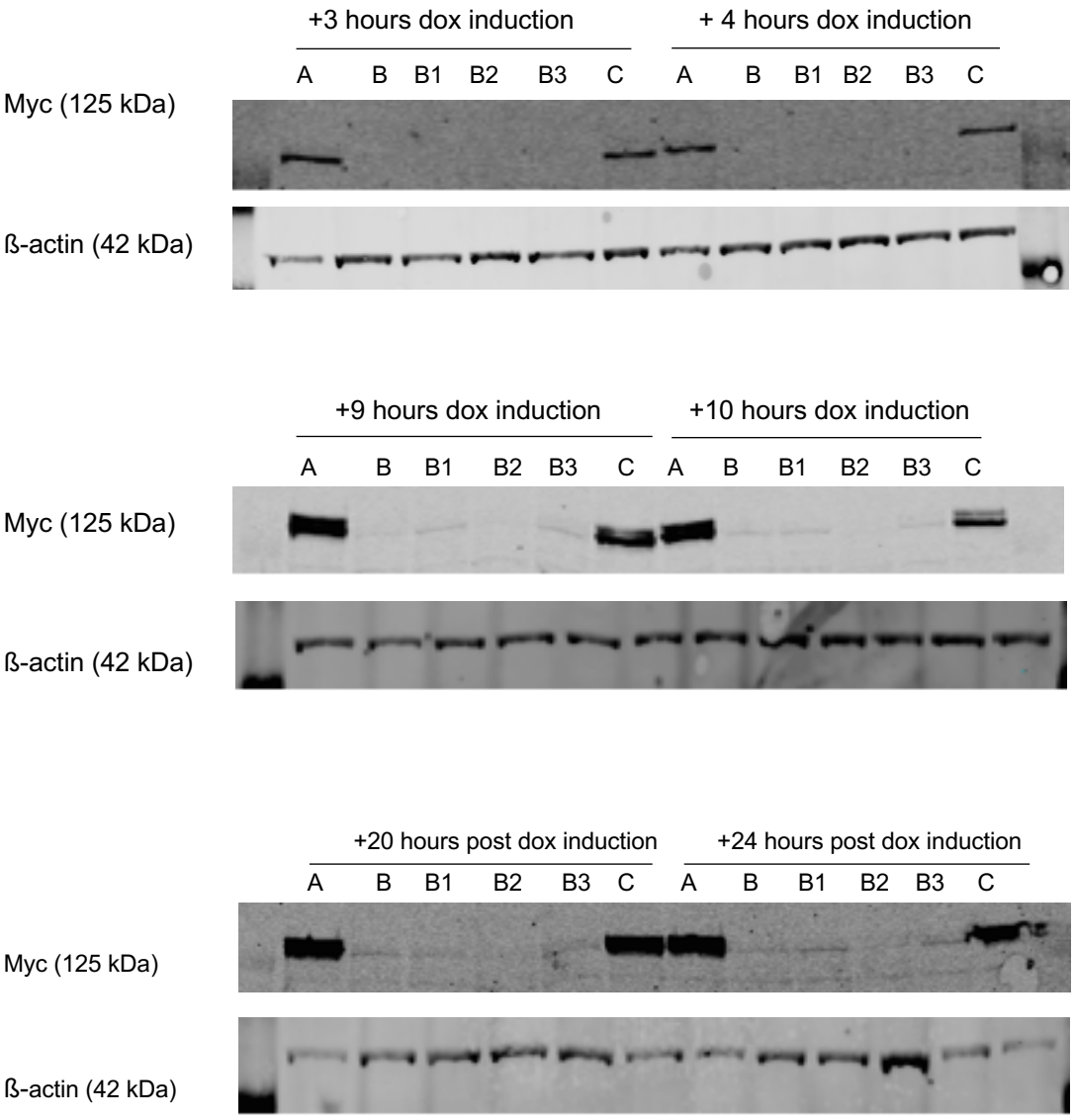

Figure 32. Immunoblot analysis of Myc tagged PERK expression in P2 cells at early time points post Dox induction. The Myc band first appears in only the HapA, and C cell lines three hours post induction with the Myc band present in the HapA and C lines at 9 hours post induction. There is only a very weak signal in the HapB variants at early time points of 9 hours and 10 hours post Dox induction and after prolonged induction. ß-Actin was included as a normalisation control.

4.12 Passaging of P1 causes reduction of Myc tagged PERK in HapA and HapB transiently transfected HEK-293 cells

In order to see if the HapB-specific loss of the Myc-tag also occurs with transient transfection, we transiently transfected HapA and HapB PERK expression plasmids for constitutive expression in HEK-293 cells. Following transfection, the cells were kept in culture for 48 hours after which the cells were split and plated onto 6-well tissue culture plates. This split was indicated as P1. Once the P1 cells were fully confluent, the cells were passaged once more and the P2 cells were kept in culture for a further 48 hours until fully confluent. The P0, P1, and P2 HapA and HapB protein lysates were collected and immunoblotted for Myc and PERK and normalised against ß-Actin (Figure 34). Analysis of the immunoblots indicated that there was no loss of Myc signal intensity in HapB transiently transfected cells at either P0 or P1. However, there was a reduced Myc signal at P2 for both HapA and HapB cells with similar levels of reductions observed between the two haplotypes although this failed to reach significance. This is an intriguing observation as, with the stably transfected cells, loss of the Myc-tag is exclusively with the HapB PERK whereas with transient transfection, both HapA and HapB see this cleavage. However, it's important to note that we did not freeze-thaw the transiently transfected cells after P1 and yet observed a decrease in Myc tagged PERK signal intensity following passaging. With our stable PERK line, the HapB Myc cleavage was only observed following freeze-thawing. Another crucial difference is the effective repression of the transgene expression during cell manipulation and splitting in the stably transfected cells whereas in the transiently transfected cells the exogenous PERK overexpression persists throughout. However, these results cannot be over interpreted until the cell lysates have been probed for total PERK. This will establish if the reduced signal we observed for Myc in P2 cells is due to loss of the PERK transgene through cell division; a feature quite commonly observed during transient gene expression. These observations give us tantalising but clear-cut difference between the HapA and HapB cells that could explain the variation in risk and warrant further investigation.

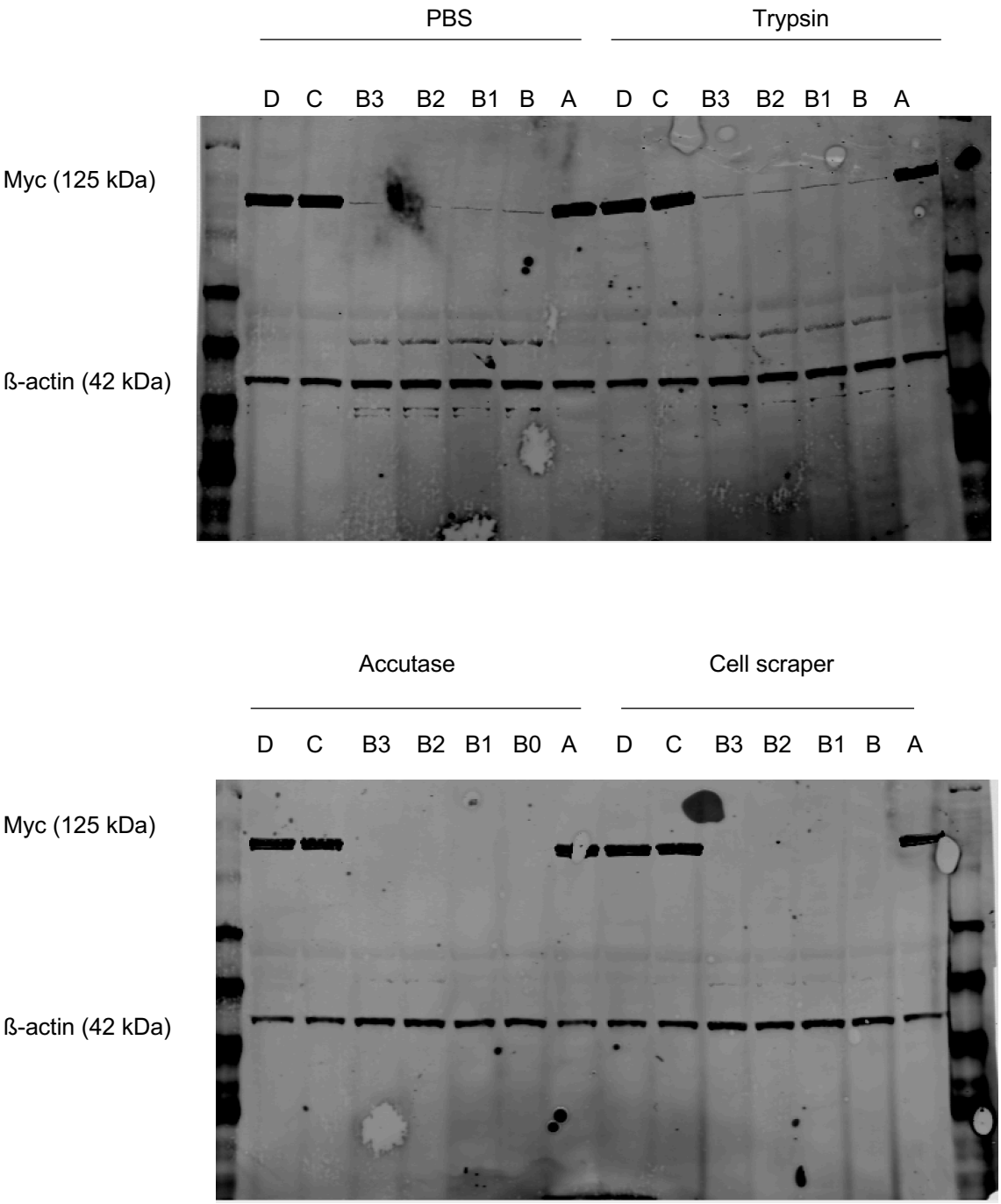

Figure 33. Immunoblot of different methods of cell detachment of P2 PERK cell lines. Each P1 line was detached from the culture plate either using trypsin, ice cold PBS-EDTA, accutase or manually scraping the cells with a cell scraper before being plated onto 6-well plates and being induced with 10 ng/mL Dox for

18 hours. Lysates were probed with Myc and normalised against ß-Actin. The loss of the Myc band occurs irrespective of the method of detachment of the P1 HapB cells.

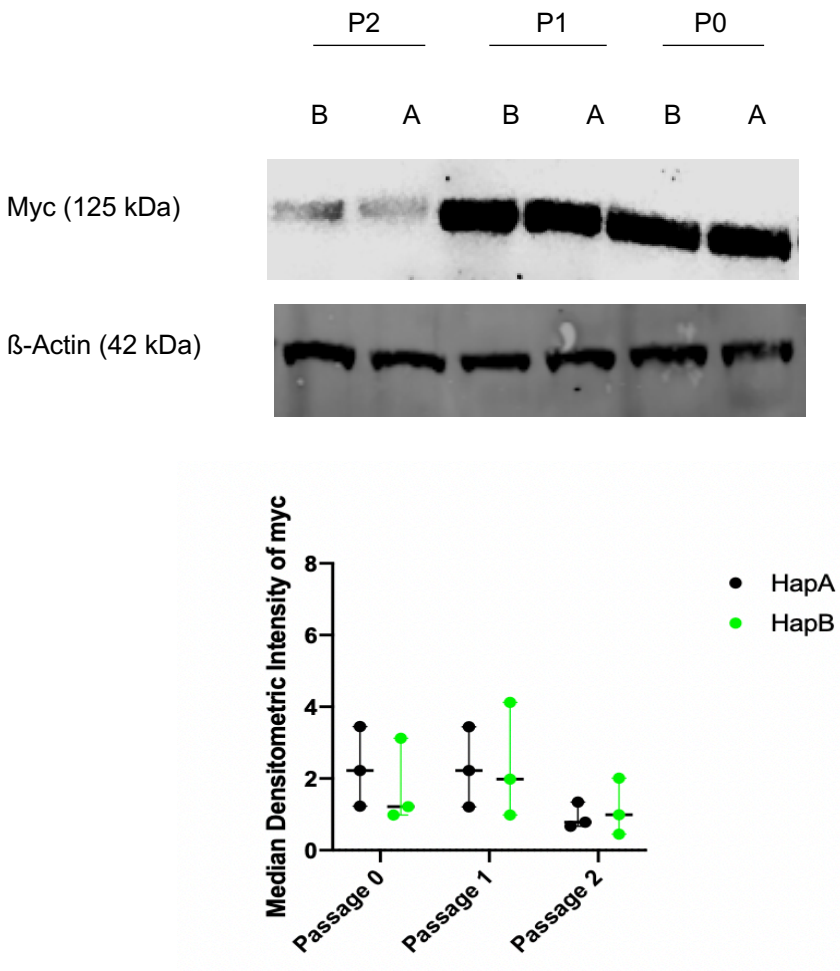

Figure 34. Effect of passaging on transiently transfected PERK HapA and HapB cells. PERK A and B full length constructs cloned into 5/FRT/TO vector were transfected into HEK-293 cells. 48 hours post transfection, the cells were split and plated onto 6-well tissue culture plates (P1). Following 90 % cell confluency, cells were split once more (P2) and plated and lysates were obtained when the cells had proliferated and showed 90% cell confluency. The protein lysates were probed for Myc and ß-Actin was included as the normalisation control. Densitometry of transiently transfected PERK A and B immunoblots is indicated as the median densitometric intensity of Myc tagged PERK protein expression for all three data points per passage per cell line. HapA and HapB PERK cells did not show a significant difference in Myc intensity in either of the three passages (P0, P1, P2) when tested with a Wilcoxon matched pairs signed rank test ((W=8, p>0.999 (2 tailed)), n=3).

4.13 *Freeze/thawing of frozen HapB PERK cell cultures could contribute to loss of Myc tag*

In order to gain insight into the possible causes of the cleavage at P2 of the Myc-tag limited to the HapB stable cell lines, we assessed freeze/thawing. If freeze thawing did have an effect on myc cleave in the HapB cells, then this would confirm an effect of the cryoprotectant DMSO in the freezing medium. New PERK stable clones were created and passaged five times without the freeze-thawing. Lysates for all seven haplotypes were collected at P1 and P5 following Dox induction for 18 hours and probed by Western blot for Myc and normalised against the ß-actin antibody. Three independent immunoblots were carried out using new PERK clones for each replicate. The clear absence of a band in the uninduced lane indicates tight repression of the transgene in the absence of Dox induction. Interestingly, HapB clones retained the Myc tag even at P5 (Figure 35) indicating that the process of freeze-thawing including the presence of DMSO was a likely contributing factor for the loss of the HapB Myc tag. Freeze/thawing of the transiently transfected PERK P0 cells was carried with the aim of replicating the conditions of the stable PERK cells. However, HapA and HapB cells failed to proliferate following freeze/thawing.

4.14 *Prolonged culture of freeze/thawed P1 HapB does not result in loss of Myc tag*

It is intriguing that passaging the P0 clones when first picked, which included freeze/thawing did not result in loss of the Myc-tag in the HapB cells at P1. Instead, loss of the Myc-tag occurred in the P2 cells on passaging the HapB P1 cells. It is to be noted that all maintenance and passaging of cells was in the absence of Dox-induction i.e. without transgene overexpression. It is plausible, however, that low levels of leaky expression could have initiated the HapB-specific loss of the Myc-tag. To test the possibility that the degradation of the Myc-tag could occur over time due to the low levels of transgene expression, we cultured the cells over 7 days. Frozen PERK P0 vials were expanded into T75 flasks before undergoing the first passage. The cells were then plated either at high cell density for 24 hours or low cell density for 7 days after which they were induced with 10 ng/mL Dox for 18 hours and protein lysates obtained. Immunoblots were probed with Myc antibody and normalised against ß-Actin (Fig 36). The experiment was repeated three times on frozen PERK lines obtained from independent transfections. Uninduced lysates (No Dox) were used as a negative control. The data were normalised to 1 using the Myc signal obtained from 24 h cultured HapA P1 cells. Our results indicate that even after 7-day culture, followed by induction, P1 HapB cells retained the Myc-tag.

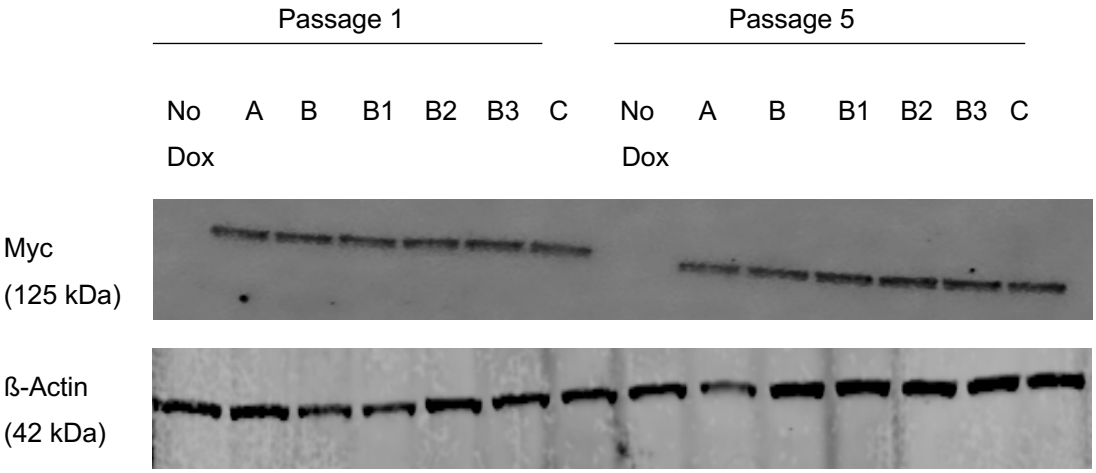

Figure 35. HapB clones kept in culture up to P5 without undergoing freeze-thaw. Newly created PERK clones underwent five passages before Dox induction and protein lysate collection. Immunoblots were performed to compare if Myc tagged PERK signal intensity persisted between P1 and P5 HapB cells when not undergoing freeze-thaw. An uninduced HapB sample from each passage was included as the negative control (No Dox). ß-Actin was included as the normalisation control. In the absence of freeze thaw, myc tagged PERK persists in HapB and sub HapB cell lines.

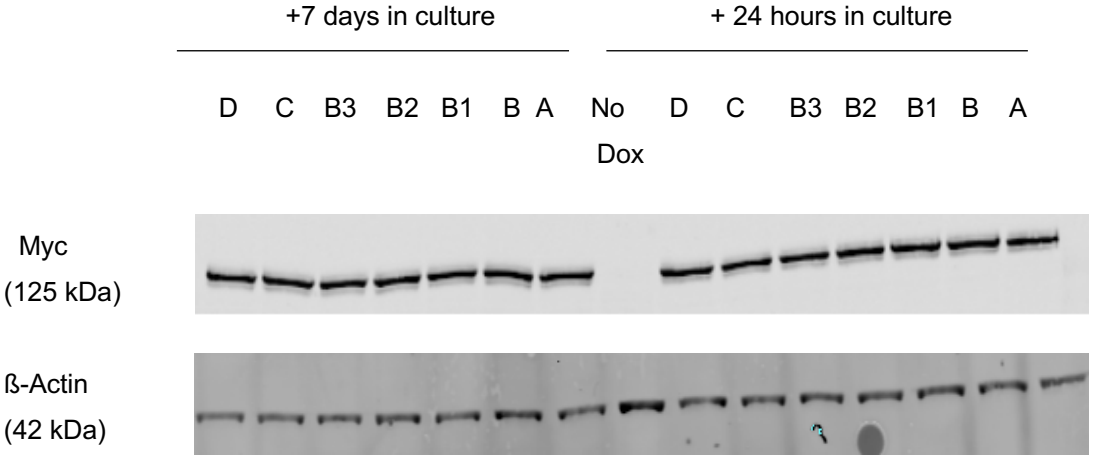

Figure 36. Effect of duration of uninduced P1 cells in culture. P1 uninduced PERK lines were left in culture for either 24 hours or 7 days before being induced with 10 ng/mL Dox. Protein lysates were collected and immunoblots were probed with Myc antibody and normalised with ß-Actin. Passage 1 Myc tagged HapB and P1 myc-tagged sub HapB PERK was shown to persist in culture conditions that were 7 days old indicating that a combination of either/or cell detachment and/or freeze thawing plays a vital role in myc cleavage of the HapB cell lines.

4.15 Presence of antibiotics in HapB culture media does not contribute to loss of Myc tag

We next examined if the two selection antibiotics present in the culture medium, Hygromycin B and Blasticidin, could be causing the loss of the Myc tag in the HapB cells, possibly due to effects during translation in the ribosome. Withdrawal of the two selection antibiotics were carried out after expansion of newly selected HapA and HapB clones. The P1 and P2 cells were cultured either in the presence or absence of selection antibiotics. P2 Dox induced HapA and HapB lysates were obtained and immunoblot analyses with Myc antibody was carried out. ß-Actin was used as the normalisation control (Figure 37). Our results show that despite the absence of the selection antibiotics the Myc tag is lost in the P2 HapB and sub HapB variants. This confirmed that Blasticidin and Hygromycin B do not play a part in the loss of the Myc-tag.

4.16 *Comparison of PERK activity in genotyped PSP brains*

We obtained frontal cortex, putamen and cerebellum sections from 6 PSP patient brains homozygous for the major *EIF2AK3* allele (C) of the GWAS associated SNP rs7571971 and 6 PSP patient brains homozygous for the minor allele (T) in order to determine the allele-specific differences in PERK and phospho-PERK and UPR markers of the PERK pathway. These brains were obtained from the Queen Square Brain Bank. All cases had confirmed PSP clinical diagnoses and were pathologically confirmed by post-mortem macro brain examination and immunohistology using antibodies against epitopes and conformations that distinguish between physiological and pathological tau. The diversity in pathological tau forms entails a diversity in tau lesion distribution, morphology, and composition with post-translational modifications of tau protein – whether phosphorylation, ubiquitination, glycation, glycosylation, conformation changes or nitration, all creating novel epitopes on tau.

Immunoblot analysis was employed to assess the levels of total PERK in the frontal cortex, cerebellum and putamen of each of these cases. Control Dox induced HapA cells included as a positive control have a clear PERK (anti-mouse B5 N-term PERK antibody) and phospho-PERK band (anti-rabbit phosphor-perk T982, Abcam) corresponding to 125 kDa. We failed to observe consistent differences in expression levels of PERK and was unsuccessful in detecting bands for phospho-PERK in the patient brain homogenates (Figure 38). Furthermore, results for total PERK expression using the PERK N-term targeted B5 antibody was highly variable with only one of three immunoblots yielding a signal. However, within that immunoblot we detected that the PERK levels for the T-homozygotes in FC and putamen (but not cerebellum) are higher. However, the

beta-actin is shown to be highly inconsistent amongst the different brain samples indicating improper protein lysate loading. The absence of detectable phospho-PERK signal was noted from all three brain regions. Enrichment by PERK and phospho-PERK immunoprecipitation of the patient brain homogenates was unsuccessful. PERK levels in the human brain are at extremely low levels, possibly below detection threshold of the antibodies. However, we are currently collaborating with the group of Dr Jonathan Lin (University of California, San Diego), who have established a method to enrich brain PERK to detectable levels (Yuan et al., 2018).

4.17 *Native gel electrophoresis to assess structural differences in PERK variants*

Noting that the coding polymorphisms that define the PERK haplotypes affect highly conserved residues within highly conserved protein domains, it is possible that the three risk variants in HapB cause structural changes and instability of the protein and impairment of dimerization necessary for autophosphorylation and activation of PERK. Native PAGE, where non-denatured protein migrates based on native structure and charge distribution and, differences in migration would therefore reflect conformational differences, or intactness of dimers or protein complexes. Protein lysates obtained from P2 PERK cells were prepared for Native Page followed by immunoblotting with PERK antibody. Unfortunately, we failed to obtain consistent results in each technical repeat. We were unable to resolve this with optimisation of different protein lysis solutions nor with the use of different durations of running buffer compositions. We believe we have begun to see emerging differences between the conformation of HapA and HapB PERK (Figure 39) with the presence of higher molecular weight oligomers being observed in P2 HapB and sub HapB variants. However, these results would need to be replicated in order to confirm this finding.

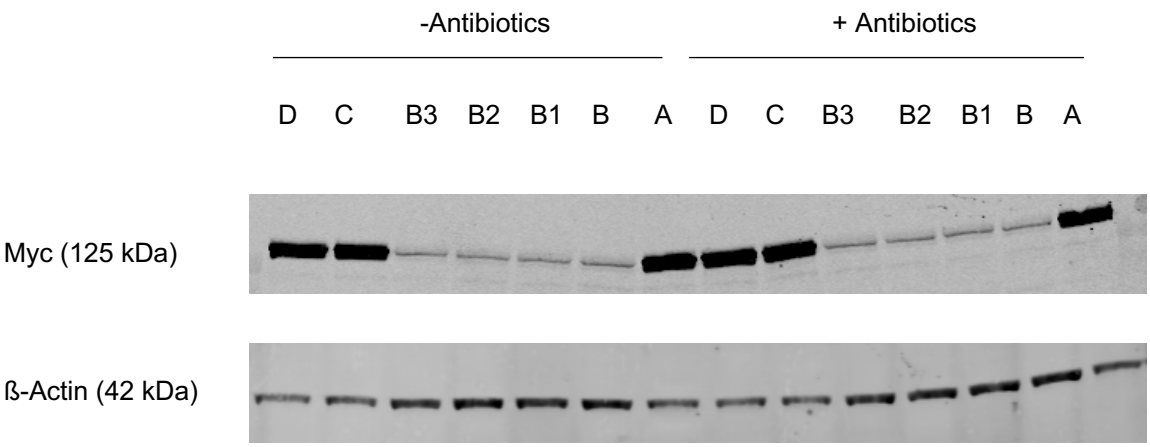

Figure 37. PERK cells cultured in the presence and absence of selection antibiotics. Fresh PERK clones were isolated following transfection and expanded into T25 tissue culture flasks. Selection antibiotics were then either withdrawn (-Antibiotics) or sustained (+ Antibiotics). Dox induced P2 lysates were immunoblotted for Myc and normalised against ß-Actin. PERK HapB Myc-tag is lost also in the absence of antibiotics. The experiment was repeated once more, using new PERK clones. The second replicate similarly showed the continued loss of the Myc tag in HapB P2 clones upon antibiotic withdrawal.

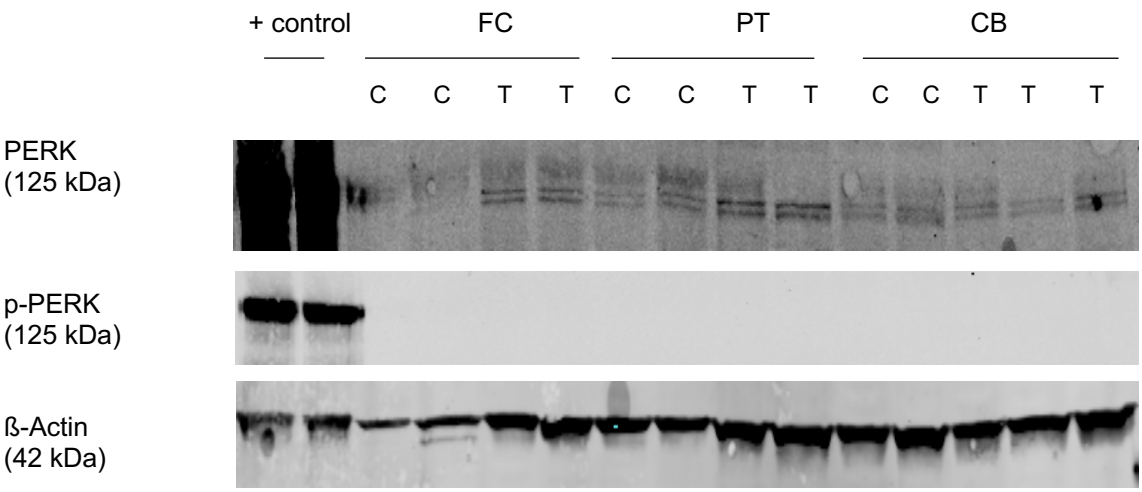

Figure 38. Comparison of PERK activity in PSP patient brains homozygous for rs7571971 C or T alleles. Immunoblot analysis of total PERK and p-PERK from frontal cortex (FC), putamen (PT) and cerebellum (CB) homogenates obtained from four PSP patient brains homozygous for either C or T allele are shown here. The PERK levels for the T-homozygotes in FC and putamen (but not cerebellum) are higher, whereas complete absence of a band is noted for p-PERK. We were unsuccessful in replicating these results with consequent blots failing to yield a detectable signal for PERK. Two Dox induced HapA cell lysates were included as positive controls. ß-Actin was included as a normalisation control.

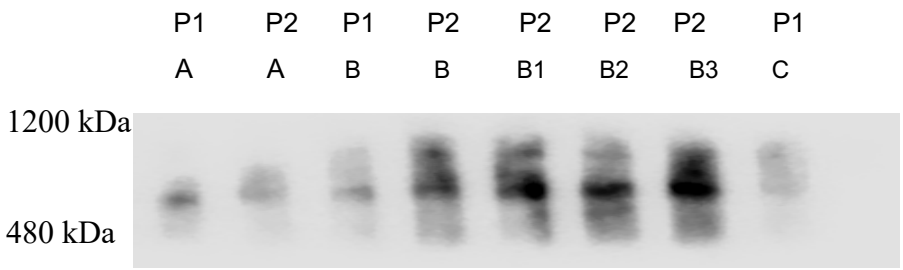

Figure 39. Native-PAGE of Dox induced P2 cells. P1 and P2 HapA and P1 HapC (lanes 1,2, and 8), P1 and P2 HapB (lane 3 and 4) and sub HapB cell lines (lanes 5-7) were probed with PERK antibody following Native-PAGE electrophoresis. Passage is indicated as P. A high molecular weight band is not observed in P1 and P2 HapA cells. P2 HapB and sub HapB lanes indicate the presence of a higher molecular weight complex which also seems to be visible in the HapC lane. Sadly, the nativepage molecular weight marker did not transfer onto the PVDF membrane. Therefore, an estimate of the expected dimers and/or PERK oligomers were obtained from previous papers which have been shown to extend as a smear from 480 kDa-1200 kDa (Sundaram et al., 2017). However, we were unable to replicate this result in subsequent blots.

4.18 Discussion

The consistent outcome of work with the stable Flp-In^{TM} 293 cell lines with inducible overexpression of the PERK haplotypes is that on second passage, with cell maintenance and passaging carried out without the induced transgene expression, was the loss of the Myc-tag of the induced expression of the HapB variant and the artificial HapB sub-variants. This also resulted in increased PERK levels but reduced PERK activity. We have now consistently shown that passaging, accompanied by freeze-thawing of the HapB cells alone results in the loss of the C-terminus Myc tag; and this is the case with the primary B haplotype and all the artificial sub-haplotypes with one each of the three risk amino acids swapped back to the non-risk (HapA) residue. We also showed that the cleaved P2 HapB PERK variants have reduced PERK auto activity. The loss of the Myc-tag is most probably due to cleavage within the extreme C-terminal sequence of the HapB PERK variants as there was no discernible reduction in protein size on Western blots. However, with low-molecular weight protein gels, we were unable to identify a cleaved peptide containing the Myc-tag. It is therefore possible that the HapB variants, through structural changes, could be susceptible to exopeptidase pruning of the C-terminal end. Steric masking of the Myc tag is less plausible as the protein would have been unravelled during denaturation and boiling prior to Western blot. The very clear reproducible Myc tag loss in the primary HapB and all three B sub-haplotypes indicates that the alteration of one out of the three highly conserved residues found in the lumenal and/or kinase domain of the protein is sufficient to cause specific loss of the Myc tag in HapB. No protease consensus sequences within the extreme end of the C-terminal region of PERK were identified with the PROSPER tool which is an integrated feature-based server for identification of protease substrates and their cleavage sites for twenty-four different proteases. Crucially, our study identified that the rarer HapC – which has the amino acid substitution only at position 704 (serine to alanine) – does *not* cause loss of Myc tag; revealing that the presence of the mutation in the kinase domain alone is not sufficient to result in reduced HapB PERK auto activity. Similarly, the rare HapD, which has the amino acid substitution in the lumenal domain at position 166 (arginine to glutamine), is also not a cause of reduced auto activity by itself. However, further work is clearly warranted to assess the effect of a sole amino acid substitution at position 136 (serine to cysteine) to determine the functional consequence of this polymorphism. Working from these data we can conclude that the presence of just two of the three highly conserved single nucleotide polymorphisms affecting the residues within the lumenal and kinase domain is capable of reducing basal HapB PERK activity possibly due to destabilisation of the protein with the ensuing cleavage at the C-terminus. Although no structural work has yet been published on HapA and HapB PERK protein folding, this would be an interesting avenue to explore to observe if HapB PERK is folded differently due to the presence

of the three snps, two which are located in the luminal domain and one of which is crucially located within the kinase domain.

With several studies confirming the association of the *EIF2AK3* SNP rs7571971 and its associated risk haplotype, HapB and risk of PSP, our work failed to demonstrate that the basis of this increased risk could be due to significant changes in PERK activity, however there is a a strong trend of increased total PERK with corresponding decreased levels of phospho PERK observed in myc cleaved HapB cells. Although our results failed to reach significance, this observed trend could point towards a protein structure destabilisation due to the C-terminal cleavage. A previous study did not show any differences in PERK levels between HapA and HapB cell lines (Stutzbach et al.,2015). However, in line with our data, they did observe reduced PERK auto activity (phospho-PERK, which also failed to reach significance), specifically in HapB homozygous human beta lymphocytes but not with haplotypes with single changes in the three amino acids (Stutzbach et al., unpublished). Aggregating these results, our study points towards the fact that changes in two out of the three amino acids to the variants seen in HapB are required for C-terminal cleavage which results in reduced basal HapB PERK activity. However, we need to be very cautious in interpreting these results as several crucial controls are lacking within this body of work which are discussed in greater detail below.

Structurally, PERK comprises two distinct sub-domains, a smaller N-terminal lobe (N-lobe) located within the lumenal domain and a larger C-terminal lobe (C-lobe) within the kinase domain, linked by a short hinge loop (Carrara et al., 2015; Wang et al., 2016; Wang et al., 2018; Figure 40). The crystal structure of the PERK kinase domain has been revealed to be highly disordered (Carrara et al., 2015). The C-lobe structure is formed by one long activation loop (residues 953–990), two short β-strands (β6–β7) and seven α-helices (αD–αJ) (Wang et al., 2016). In the inactive conformation, the activation loop and helix αG of PERK are disordered. It has been proposed that two PERK homodimers may approach each other and interdimer transphosphorylation takes place when one PERK homodimer inserts its flexible activation loop into the catalytic site of the adjacent homodimer (Line up mode) resulting in the transphosphorylation of Thr980 (Wang et al., 2018). This results in the partial stabilisation of the activation loop as well as the helix αG of PERK. This stability enables binding of eIF2α which further stabilises the activation loop (Wang et al., 2018). From our passaging work we conclude it is likely that, two of the three polymorphisms of HapB could impede luminal PERK dimerization, resulting in a proportion of PERK being unable to obtain the structural composition of the required line up model thus reducing autophosphorylation of the kinase domain. This in turn might explain the reduced HapB PERK auto activity as shown by reduced phospho-PERK expression levels. However, it is remains unclear as to why Myc cleaved HapB cells show increased levels of total PERK.

Our data as such suggest that reduced HapB PERK auto phosphorylation may also lead to reduced phosphorylation of eIF2α, its direct downstream substrate in the passaged HapB cells. Crucially sub HapB1 cells showed a trend of reduced activated eIF2α (p-eIF2α) but this failed to reach significance. However, Stutzbach and co-workers did not observe differences in p-eIF2α levels between PERK haplotypes (Stutzbach unpublished). A more recent work using transfected full length HapB PERK constructs into mouse embryonic fibroblasts, negative for the *EIF2AK3/*PERK gene showed significantly diminished basal phospho-eIF2α levels. With our cells, we observed only the passaged sub HapB1 bearing Gln_{166} and Ala_{704} polymorphisms showing a trend of reduced eIF2α phosphorylation. This contrasts with Yuan and colleagues (2018) who observed that HapC, bearing only the Ala_{704} change, showed decreased auto activity and decreased eIF2α phosphorylation. They concluded that the non-risk Ser_{704} in the kinase domain could be important for transphosphorylation, which could be the reason why HapB displays reduced phosphorylation. However, the HapB1 cells, which also show reduced eIF2α phosphorylation include this mutation in addition to the substitution at 166 ($Arg_{166}Gln$).

As the activation loop is in close proximity to Thr-980, changes within the kinase lobe which includes the presence of the Ser_{704} snp may hinder the appropriate binding of PERK monomers, thereby diminishing the levels of phospho-PERK as PERK dimerization may be impaired.

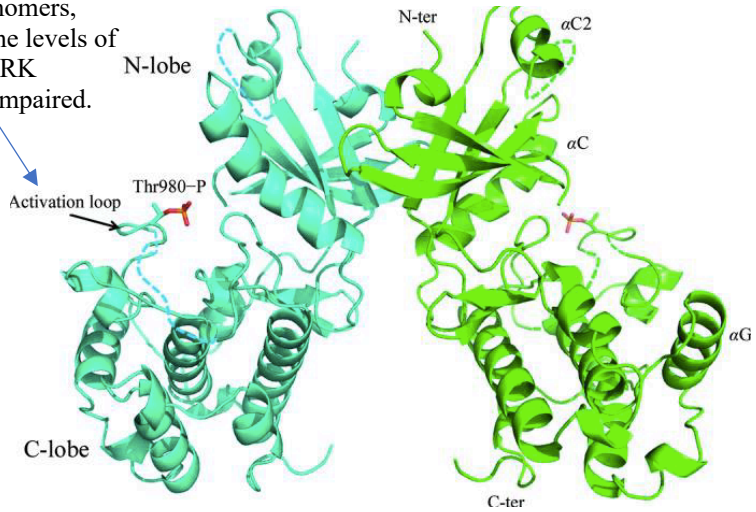

Figure 40. Overall structure of PERK dimers: The N-lobe of PERK is constituted by three α-helices (α0, αC and αC2) and five β-strands (β1–β5) and provides the interfaces for PERK dimerization. The C-lobe of PERK kinase domain is located in the cytoplasm. The N-lobe promotes PERK trans-autophosphorylation of

the C-terminal cytoplasmic kinase domain at multiple residues including Thr980 on the kinase activation loop (Sha et al., 2011).

Taken together, this indicates the need to test the 3D structure of the sub HapB haplotypes using 3D modelling to understand if the HapB Gln_{166} substitution within the PERK lumenal domain alone is capable of affecting kinase activity by influencing the stacking model required for the efficient phosphorylation activity within the cytoplasmic activation loop. Similarly, structural studies looking at the folding and dimerization of all three HapB PERK substitutions both singly and in conjunction will reveal important information as to the capability of these snps to destabilise the docking site for eIF2α which could inevitably lead to reduced eIF2α activity.

A further aim of our work was to utilize the cell model to profile downstream PERK signaling in HapA and HapB PERK and to determine whether impaired HapB PERK causes changes in ATF4 and CHOP activity. Although reduced PERK and eIF2α activity were observed with HapB after passaging this did not affect the PERK downstream components in our study. Stutzbach and colleagues similarly failed to observe changes in ATF4 expression levels in unstressed HapA and B cell lines. It is possible that absence of increase in ATF4 and initiation of the apoptotic cascade via CHOP was due to the absence of an ER-stress induction. It would be of interest to further investigate this in follow up experiments.

In order to investigate the loss of the HapB Myc tag on passaging, we showed firstly by RT-PCR that the full-length HapB Myc-tagged PERK was transcribed. Second, our immunoblot detection with antibodies targeting the PERK N- and C-termini showed that exogenous HapB PERK protein was indeed being overexpressed. As the protein displayed similar size to the other haplotypes and was recognised by the C-terminal antibody which binds to residues 1072-1098, just 18 amino acids away from the C-terminus, it is clear that the Myc-tag was lost due to cleavage beyond the antibody binding site or due to carboxypeptidase cleavage of the Myc tag. We were not able to investigate the exact nature or site of this cleavage – in the first place, this could be investigated by mass spectrometry analysis of the exogenous HapB protein following immunoprecipitation.

It's now clear that two critical processes are at play in HapB cells when loss of Myc occurs: freeze-thawing and passaging. With the observation of consistent loss of the Myc-tag after freeze-thawing and second round of passaging, we sought to assess if trypsinisation of the cells for detachment played any role and therefore tested other modes of detachment, including physical detachment of cells with a cell scraper. However, with all modes of detachment, the loss of the Myc-tag in the HapB cells after P2 persisted. It is therefore possible that cytoskeletal or cell signalling changes due to transition from the flatness of the attached cells to the rounded, detached cells could have contributed to the loss of the Myc-tag. However, continuous

maintenance of P0 HapB cells with splitting and re-plating up to P5 enabled us to identify that passaging alone does not cause loss of the Myc tag but it seems to be a concerted effect incorporating the step of freeze thaw as well (Table 2). Our results therefore implicate two other factors namely, freeze/thawing and, possibly, the presence of DMSO in the freezing medium along with cell passaging. Further work is warranted on using different freezing reagents on HapA and HapB clones following expansion to observe if Myc cleavage from HapB cells is DMSO specific. It is yet puzzling that the PERK HapB Myc cleavage did not occur at first passage, which also included a freeze/thaw step. It is crucial to note that the effects observed on HapB can be shown to be independent of presence of the exogenous PERK protein, as all procedures (including passaging, freeze/thawing, cell culture) were done without any Tet-induction of PERK expression. There is, however, the possibility that leaky expression, i.e. incomplete repression and the presence of trace levels of the exogenous PERK could have caused the observed effects. In fact, it is notable that basal, endogenous PERK levels are barely detectable, but nevertheless these trace levels are sufficient for the surveillance function of PERK.

We also showed that the Myc-tag is absent early after induction of exogenous HapB PERK at passage 2 (P2), confirming that this occurred due to changes during the second cycle of passaging and freeze/thawing. Unfortunately, due to the time constraint of the research project, we were unable to unravel this mystery by determining the exact nature of the selective removal of the Myc-tag. It is however perceivable that structural changes due to substitution of two of the three conserved amino acids rendered the C-terminus and Myc-tag of HapB PERK more vulnerable to degradation. The suggestion of larger P2 HapB and sub HapB complexes seen in our native gel electrophoresis seem to provide preliminary evidence for altered HapB conformation. Further study, including optimising NativePage, would yield important information regarding the degree of HapB stability following the formation of dimers and tetramers when compared to HapA. This will enable us to identify fundamental structural changes of HapB PERK. If this is true however it raises the puzzling aspect of why P1 HapB cells were resistant to C-terminus loss.

However,, we need to bear in mind that most of the experiments conducted in this chapter compared HapA and myc cleaved HapB cells alone. Crucially, to understand if changes to the myc cleaved HapB cells were a direct result of the exogenous over expression of HapB PERK following passaging and/or freeze thaw, we need to include both P1 and P2 induced and uninduced HapA and HapB cell lines for a more thorough and direct comparison. Further work would include repeating each of the above experiments while including these crucial negative controls. We also need to note that the reduced PERK activity observed may merely be a consequence of the myc tag. Hence, it is vital that that untagged, full length PERK constructs are created and tested in each of the above experiments to observe if a decrease in PERK activity

occurs despite the lack of a c-termini tag. Furthermore, myc cleavage may also be a consequence of the over-expression cell system utilising the Tet inducible HEK 293 cells. Therefore, for quality control it would be better suited to test the untagged PERK constructs in a non-inducible stable cell line (creating constitutively active PERK stable SHSY5Y cells). This will enable us to identify if the myc cleavage is purely an effect observed within this particular TREx inducible cell system.

With the consistent loss of the Myc-tag of HapB PERK at second passage, we also carried out transient transfection of naïve HEK293, which allowed constitutive expression and, in this case, both HapA and HapB PERK showed evidence of reduced Myc-labelled band at P2. However, we cannot conclude that this is loss of Myc-tag since we have not yet carried out immunoblotting with the PERK antibody to see if there was an overall loss of PERK after P2 . Thus, it is not clear if loss of Myc-signal was due to loss of the Myc-tag such as with HapB PERK in the stable clones or, if it is due to overall reductions in exogenous PERK due to loss or dilution of cells with expression plasmid during passaging and expansion. In order to further investigate this mystery, and determine the nature and cause of the Myc-tag cleavage, we have now moved on to investigate multiple different isogenic, inducible cell lines (for example, Flp-In CHO cells) or, using different tags (for example, poly-*His*) at either C-terminus or N-terminus of the PERK transgene. As discussed later in this thesis, in designing this experiment, we mistakenly relied on the notion that Tet-inducible expression of the transgene could be tunable, down to levels reflecting physiological PERK levels. However, our work with varying concentrations of Dox showed that expression levels could not be adjusted and instead, we observed an abrupt induction to maximal levels at 10 ng/ml. Compared to the nearly undetectable levels of endogenous PERK, the extremely high levels of exogenous PERK overwhelm the inhibitory BiP levels and undergo homodimerization and autoactivation. It is perceivable that persistently high levels of activated PERK are not conducive to normal cellular function and ttherefore, our inducible cell model might not be the best suited cell system to study any subtle haplotype effects of PERK. Nevertheless, with the consistent loss of the Myc-tag, we were surprised by this very clear-cut difference between the risk HapB and its sub-haplotypes and all the non-risk haplotypes. It would be important to pursue this serendipitous finding by clarifying the nature and cause of this cleavage and if similar C-terminal pruning occurs in the brain by assessing PSP patient brains homozygous for the major non-risk (C) allele or the minor risk (T) allele of rs7571971 and comparison to mass spectrometry sequencing of the overexpressed PERK.

HapB culture conditions	Presence of HapB Myc-tagged PERK		
	P0	P1	P2
Continuous Culture (no freeze-thaw)	✓	✓	✓
Freeze-Thaw and expanded	✓	✓	x
Clones grown in the absence of selection antibiotics, freeze thawed and expanded	✓	✓	x
Clones split using different detachment reagents, freeze thawed and expanded	✓	✓	x
Freeze-thaw and culture on semi adherent TC plates and/or culture in suspension	✓	✓	x
Transiently transfected	✓	✓	Reduced

Table 4. Summary of tissue culture conditions used for culturing HapB cells. We only observed the presence of P2 Myc tagged HapB PERK when cells were cultured and passaged continuously without the process of freeze-thaw.

5 Functional consequences of HapB PERK genetic variation

5.1 Overview

The findings of the previous chapter demonstrated that increased risk of PSP from the divergent HapB could be due to C-terminal cleavage accompanied by increased PERK protein levels but reduced PERK activity. The aim of the work covered in this chapter was to determine whether Myc-cleaved HapB signaling led to an impaired UPR, resulting in increased cell vulnerability to ER-stress associated damage. To determine the effects on the activity of the HapB PERK protein, we used four different assessments. First, HapA and HapB cell viability in response to treatment with UPR-inducing drugs was investigated. Secondly, as activation of the UPR converges on all three signaling mediators, protein expression levels for PERK, ATF6 and IRE1 were compared in HapA and Myc-cleaved HapB P2 cells using immunoblotting. Third, as a consequence of UPR activation, the ER expands to meet the increased need for protein folding capacity. Therefore, to observe if UPR signalling downstream of HapB PERK was impaired following ER stress, we also measured ER expansion using a GFP-tagged ER marker and quantified expansion of the ER membrane before and after UPR induction. Fourthly, the higher-order oligomerisation of PERK, which is required for downstream activation, is influenced by two factors: binding to unfolded proteins, which shifts PERK toward an active, oligomeric state, and binding to BiP which stabilises PERK in the inactive, monomeric state. We aimed to test if the luminal domain mutations of HapB PERK hinders BiP binding in the absence of ER stress and further, impairs BiP dissociation during conditions of acute ER stress. Taken together it was shown that following UPR activation, Myc-cleaved HapB PERK was less effective at phosphorylating eIF2α resulting in compromised cell viability.

5.2 *Background*

Previously it has been shown that hhuman β-lymphocytes homozygously expressing HapB PERK have significantly more eIF2α phosphorylation in response to treatment with the ER stress-inducing drug thapsigargin (Tg) (Liu et al., 2012) compared to cells expressing HapA PERK. This presented the first potential pathogenic mechanism for PERK's involvement in PSP. Another study in 2015 confirmed these findings showing that HapB produces the more active form of PERK, which is not a protective response, but rather increases the risk for PSP (Stutzbach et al., 2013). Another work (Yuan et al., 2018) using PSP patient iPSC-derived neurons homozygous for HapB PERK showed that a physiological consequence of HapB PERK signalling is increased neuronal cell death when exposed to ER stress. Contrary to Stutzbach and co-workers (Stutzbach

et al., 2015) and Liu and co-workers' (Liu et al., 2012) findings, Yuan and colleagues (Yuan et al, 2018) observed lower expression levels of phosphorylated eIF2α in Tg treated mouse embryonic fibroblasts homozygous for HapB indicating reduced HapB PERK activity. These studies provide conflicting results in identifying the exact functional consequences of the HapB PERK polymorphisms. It was important then to assess the activity of Myc-cleaved HapB cells following UPR activation in our Tet-On conditional expression system. Using this cell model, we were able to replicate the finding from Yuan et al., (2018) that HapB cells demonstrate impaired PERK kinase activity and increased cell death following ER stress. Further work exploring these functional differences between the sub HapB variants is warranted.

5.3 *In vitro cytotoxicity assays*

Stresses may be of two general types: either acute stresses that require immediate adjustments to the cellular protein folding environment or chronic stresses that persistently tax the folding apparatus and necessitate long-term changes in gene expression to improve the folding capacity in a quasi-permanent manner. Therefore, activation of the three proximal sensors of ER stress is managed differently during chronic stress (cells recover) versus acute stress (cells adapt). Given the timeline of this project, we decided to assess if HapB cells showed compromised adaptation to acute ER stress conditions. The Cell-Titer Glo assay was utilised to determine the dose-dependence of viability reduction in PERK HapA and Myc cleaved HapB cells when treated with thapsigargin (Tg), tunicamycin (Tm), and dithiothreitol (DTT) for 60 min.

Tg inhibits activity of the sarcoplasmic/endoplasmic reticulum calcium ATPase (SERCA) pump on the ER membrane, thereby depleting the ER of calcium ions (Denmeade and Isaacs., 2005). The ER not only stores calcium but ER–resident chaperones and folding proteins are dependent upon calcium for their vital activity. Therefore, Tg treatment induces ER stress. Tm induces ER stress by inhibiting N-linked glycosylation, a modification that occurs in the ER where sugar chains are added to some proteins in order to facilitate their proper folding and also their biological activity (Surani, 1979). This results in an accumulation of misfolded proteins in the ER lumen. Tm causes a milder form of ER stress compared to Tg and therefore can be used at low dosages without extreme toxicity. We also used the reducing agent DTT to reduce the ER environment, preventing oxidative protein folding (disulphide bond formation) while working rapidly and potently (Kaufman 1999). With short exposure to DTT, UPR induction has been observed in a number of different cell models (Nadanaka et al., 2004; Oslowski and Urano 2011).

Briefly, HapA P2 cells, P1 and P2 HapB cells and Flp-In^{TM}-293 cells were seeded at 5x10^4 cells/well in 96-well tissue culture plates and allowed to attach for 24 h. Dox induction was carried

for 18 h after which time, the media was replaced with cell medium alone, which served as the control (i.e. cells not treated with drug) and in the presence of the ER stress inducers: Tg (0-2500 nM), Tm (0-5000 ng/ml) and DTT (0-2000nM). Results obtained after 60 min are depicted in Figure 41. Each condition was tested in triplicate wells per cell line per treatment condition and the experiment repeated three times using new clones from new stable transfections. Cell viability of each untreated cell line was normalized to 100% as this contained the highest values in the data set and the smallest mean in each drug treated data set was normalized to 0%. Drug treated cells for each cell line was then depicted as a percentage difference against these controls.

As shown in Figure 41, addition of Tg, Tm or DTT caused cell death in HapA, HapB and Flp-In^{TM} 293 cell lines. Under untreated conditions we observed minimal cell death with a dose dependent increase in all cell lines following drug treatment. The dosage chosen for each ER stress reagent was unable to be obtained by calculating the IC_{50} values using the GraphPad Prism software. It was identified that the data did not fit the goodness of Fit (R squared = 0.6318) as the concentrations chosen for this experiment were very wide apart. Hence, we proceeded to use the cell viability graphs to obtain an estimate concentration at which most cell lines displayed approximately 50% cell death (Tg 1500 nM; Tm 2500 ng/mL; and DTT 1500 nM).

5.4 *PERK pathway analysis following ER stress induction*

As DTT, Tg and Tm have previously been shown to activate ER stress sensors, we analysed markers of UPR activation and those of the PERK pathway in response to the UPR inducers.

First, we aimed to determine the optimal duration of treatment for these drugs in HapA cells. In a pilot study (n=2), we analysed the time-course of eIF2α phosphorylation in HapA cells. Elevated p-eIF2α levels activated PERK pathway leads to translational repression and is a critical marker of UPR activation. Cells were treated with 1.5 µM Tg, 2.5 µg/mL Tm or 1.5 µM DTT for 0, 15, 30, 45 and 60 min before harvest. Protein lysates were analysed by Western blot with p-eIF2α, total eIF2α and ß-actin antibodies and were normalised against the corresponding beta-actin band. Dot plots indicating all data points were constructed for eIF2α activity which was calculated using the ratio between p-eIF2α : total eIF2α following normalisation against ß-actin. Increased eIF2a activation can be observed beginning at 15 min duration for Tg, Tm and DTT (Figure 42) As a preliminary testing duration we therefore decided to carry out the UPR induction at both 15 min and 30 min to compare the ER stress response in HapA and Myc-cleaved HapB PERK.

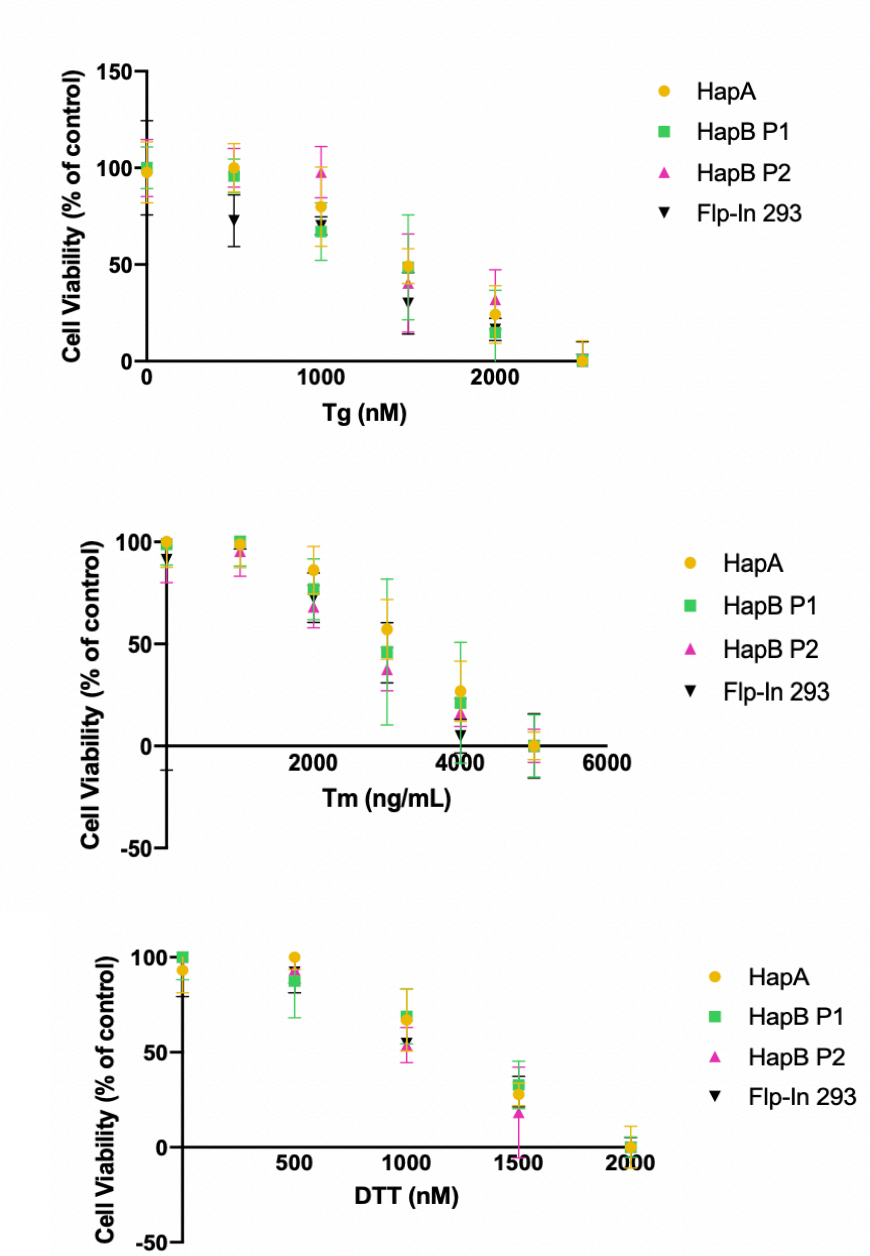

Figure 41. Cell viability assay for ER stress treatments. PERK HapA, HapB P1 and P2 and Flp-In™-293 cells were seeded at a constant density and exposed to 60 min of Tg (0-2500 nM), Tm (0--5000 ng/mL) and DTT (0-2500nM). Cell death values were plotted as a percentage difference relative to control whereby the smallest mean in each data set was defined as 0% and the largest mean in each data set was defined at 100%. Data is expressed as mean of 3 experiments ± SEM. 1500 nM Tg, 2500 ng/mL Tm and 1500 nM DTT were selected as the chosen dosages as they showed approximately 50 % cell death.

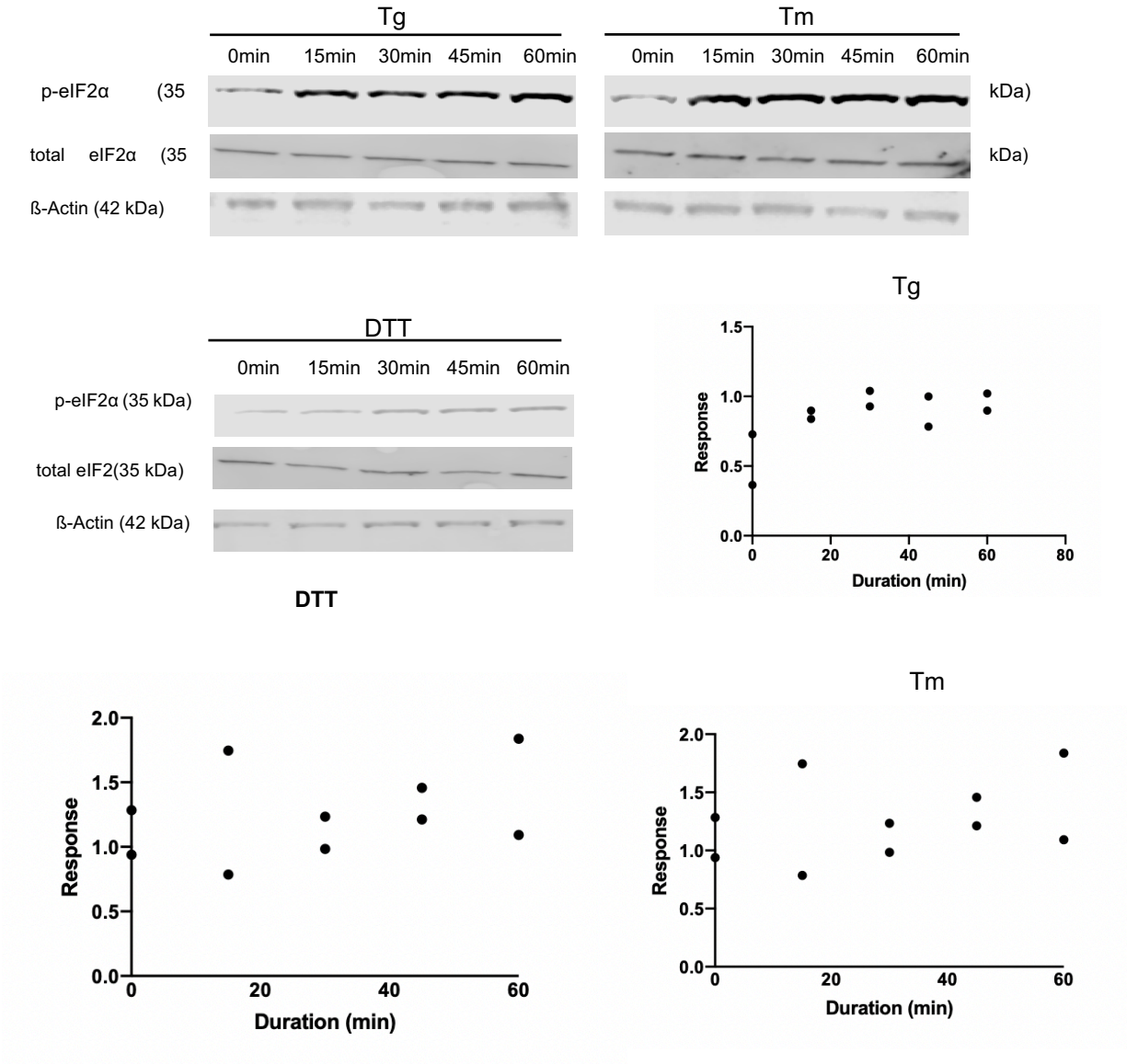

Figure 42. Tg, Tm and DTT treatment time course for eIF2α activity. Western blot bands of p-eIF2α, total eIF2α and beta-actin from HapA PERK cells following treatment with 1.5 µM Tg, 2.5 µg/mL Tm or 1.5 µM DTT for 0, 15, 30, 45 and 60 min is represented. Increased phosphorylation of eIF2α is observed at 15 min/ Tg and 15 min/Tm treatment and at 15 min/ DTT treatment. Total eIF2α remained unchanged following Tg, Tm and DTT incubation. Dot blots were represented as the ratio between p-eIF2α : total eIF2α by normalizing the p-eIF2α to the corresponding total eIF2α band following normalisation against beta-actin for each drug duration. The data is represented from two independent experiments.

In order to replicate and expand upon previous findings, we harvested cell lysates from HapA and Myc-cleaved HapB PERK cells, with and without treatment with 1.5 μM Tg (0, 15 and 30 min) (Figure 43), 2.5 μg/mL Tm (0, 15 and 30 min) (Figure 44) and 1.5 μM DTT (0, 15 and 30 min) (Figure 45). Immunoblots were used to measure PERK pathway markers by utilising antibodies for p-PERK, total PERK, p-eIF2α, total eIF2α, ATF4 and CHOP. For normalisation, protein loading levels were assessed using a rabbit polyclonal antibody to ß-actin. Data were collated from triplicate clones for each time point and the experiment repeated three times using new stable clones each time. The median densitometric intensity values for PERK and eIF2α activity and CHOP were plotted following normalisation against the corresponding ß-actin band.

With either HapA cells or myc-cleaved HapB cells treated with Tg, Tm and DTT for 15 min and 30 min, we failed to observe any statistically significant increase in PERK activation (p-PERK/total PERK) and eIF2α activation (p-eIF2α/total-eIF2α) (Figure 43 and Figure 44) although the immunoblots indicated a trend towards reduced PERK activation at 15min following Tg treatment, followed by a sharp spike in the levels of p-PERK at 30 min following Tg treatment. A similar trend is also observed for Tm treatment at both 15 min and 30 min in myc cleaved HapB cells. Although a statistically significant increase in eIF2a activity was not observed following Tg, Tm and DTT treatment, increased eIF2a activity is observed, suggesting that the ER stress cascade is initiated, albeit at very low levels. However, the large variability amongst our small data sets means that further replicates are crucial to increase the power in our study to identify if delayed myc cleaved PERK activation following 15 min Tg treatment and a stronger PERK activity response at 30 min following Tg and Tm treatment in myc cleaved HapB cells reaches statistical significance. We also assessed the CHOP and ATF4 levels, which are both downstream markers of the PERK pathway. ATF4 remained unchanged following all treatment conditions in both HapA and HapB treated cells. It was interesting to note that myc cleaved HapB cells exhibited a trend of higher levels of CHOP than the HapA cells in our immunoblots, a difference that was particularly obvious at the 30 min time point of the ER-stress response. However, this did not reach significance following statistical testing.

With DTT treatment (Figure 45), both HapA and HapB PERK cells failed to show any significant changes or interesting trends. Although HapB total PERK was barely detectable at 30 min, we failed to observe increased PERK activation (p-PERK : PERK). Interestingly in HapA cells CHOP showed a trend of increase with time whereas in HapB PERK cells CHOP levels were relatively low and did not change with time. With these data, it is not possible to discount the possibility that with DTT-induced stress, CHOP activation could occur independent of the PERK activation pathway. Within the framework of this project, it is not possible to interpret this result, though it could be possible that activation of eIF2α occurs by alternate pathways. DTT differs from the other two with the possibility of a more generalised effect on the cell by virtue of the fact that DTT is a

strong reducing agent and can reduce proteins globally. Tg and Tm have a more targeted effect that directly feeds into the PERK pathway. Hence, this could be explored further by examining a range of DTT concentrations and durations upon cell viability in DTT-treated cells compared to Tg- and Tm-treated HapA cells.

Our findings give us tantalising suggestions that carboxy-terminal-cleaved HapB PERK may undergo delayed autophosphorylation on Tg treatment, thereby lacking the activation of HapA PERK seen at 15 min, but then a strong spike in activated PERK at 30 min ensues. Intriguingly, Tm treatment does not result in delayed autophosphorylation of myc cleaved HapB. On the other hand, the trend of increased HapB PERK activation at 30 min observed with both Tg and Tm, at is also accompanied by a very small parallel increase in eIF2α activation (p-eIF2α : total-eIF2α). It is tempting to speculate that the delayed autophosphorylation of HapB could be a manifestation of the effect of the substitution of the highly conserved residues (S136C, R166Q and S704A) and impairment of dimerization that is mediated by the PERK lumenal domain and, subsequently, activation of PERK by autophosphorylation. However,, despite the elevated spike of p-PERK after 30 min, the absence of a significant increase in phosphorylation of eIF2α with Tg, Tm and DTT suggests inefficient optimisation of the drug concentrations and treatment durations required to elicit a reliable response from the UPR.

It is therefore vital that further concentrations, increased treatment durations and further technical and biological replicates are examined in detail for each treatment condition. It is only once we obtain a significantly increased phosphorylation of eIF2a following treatment with Tg, Tm and DTT that we can infer UPR changes within the two PERK haplotypes. Increasing the number of biological replicates will increase the power within our experiments enabling possibly a stronger and more robust UPR response to be detected following ER stress induction.

.

5.5 IRE1 and ATF6 pathway analysis upon UPR induction

Liu et al., (2012), Stutzbach et al., (2013) and Yuan et al., (2018) assessed only the PERK branch of the UPR to observe PERK haplotype specific changes upon ER stress treatment. For a homeostatic system that shares a common initiation mechanism and synergistic signaling cascades, it is surprising that not many investigations of the UPR have assessed all three arms in parallel. Previous studies have underlined PERK reinforcement of both the IRE1-XBP1 and ATF6 UPR arms (Teske et al., 2011; Majumder et al., 2012). It has been shown previously that XBP1-spliced accumulation is PERK dependent (Majumder et al., 2012). Furthermore, the transcription of selected ATF6 targets was augmented 6 hours after ER stress initiation in the liver, and the processing of ATF6 has been shown to be dependent on ATF4 (Teske et al., 2011).

Recent research has reported PERK-mediated IRE1 inhibition via the RPAP2 phosphatase, which has a role in diverting adaptive ER stress response towards apoptosis after 16 h of stress (Chang et al., 2018). Thus, several reinforcing positive interactions between PERK and the other UPR arms have been demonstrated. We, therefore, aimed to test if impaired HapB activity impeded IRE1 and/or ATF6 activity following UPR activation.

P2 HapA and HapB lines were treated with the same conditions as detailed above. To determine the extent to which activation of the ATF6 UPR branch occurs following Tg, Tm and DTT treatment, we performed immunoblotting using an antibody with established specificity against ATF6. ATF6 activation could only be confirmed following the aappearance of its processed 50 kDa soluble cytosolic fragment – which was not seen. Activation of IRE1 kinase activity is assayed by immunoblotting for IRE1 autophosphorylation and the active/spliced form of XBP-1. Normalization of protein loading levels were assessed using a primary goat polyclonal antibody against ß-actin. Each treatment was repeated three times using a different batch of P2 HapA and Myc cleaved HapB cells. Blots were captured and quantified with densitometry. IRE1 activity was expressed as the ratio between p-IRE1: total IRE1 following normalization against ß -actin. Typical examples of immunoblots treated for 15 min and 30 min with Tg, Tm and DTT are shown in Figure 46, Fig 47 and Fig 48 respectively.

Contrary to our expectations we failed to detect a difference in ratio between p-IRE1: total IRE1 in HapA and HapB cells following Tg, Tm and DTT treatment. Moreover, there was no difference in endogenous IRE1 and p-IRE1 in non-stressed HapA and HapB cells. As the primary target of endoribonuclease activity of IRE1 is XBP-1, we next aimed to quantify the abundance of spliced and unspliced XBP1 following UPR induction. However, with the XBP-1 antibody we used, we could not detect any bands for any XBP-1 spliced species (Figs 46, 47 and 48) and total XBP-1 levels did not vary between the haplotypes and were not observed to change following treatment. Based upon our difficulty in detecting downstream changes in IRE1 activity by immunoblotting further work is warranted whereby quantitative real-time PCR could be utilized to indicate induction of IRE1 activated target genes.

In non-stressed HapA and HapB cells, ATF6 was expressed and migrated as a single 90-kDa protein band (Figure 46, 47, and 48). Upon Tg, Tm and DTT treatment, a reduction in endogenous ATF6 was not observed at either time point, suggesting absence of proteolysis. Moreover, we did not detect a cleaved band at 50 kDa which further confirmed the absence of ATF6 activity following 30 min of Tg, Tm and DTT treatment. Thus, following acute treatment with Tg, Tm and DTT, activation of the IRE1 nor the ATF6 pathways were observed, confirming that further optimization of drug concentrations and treatment durations are warranted.

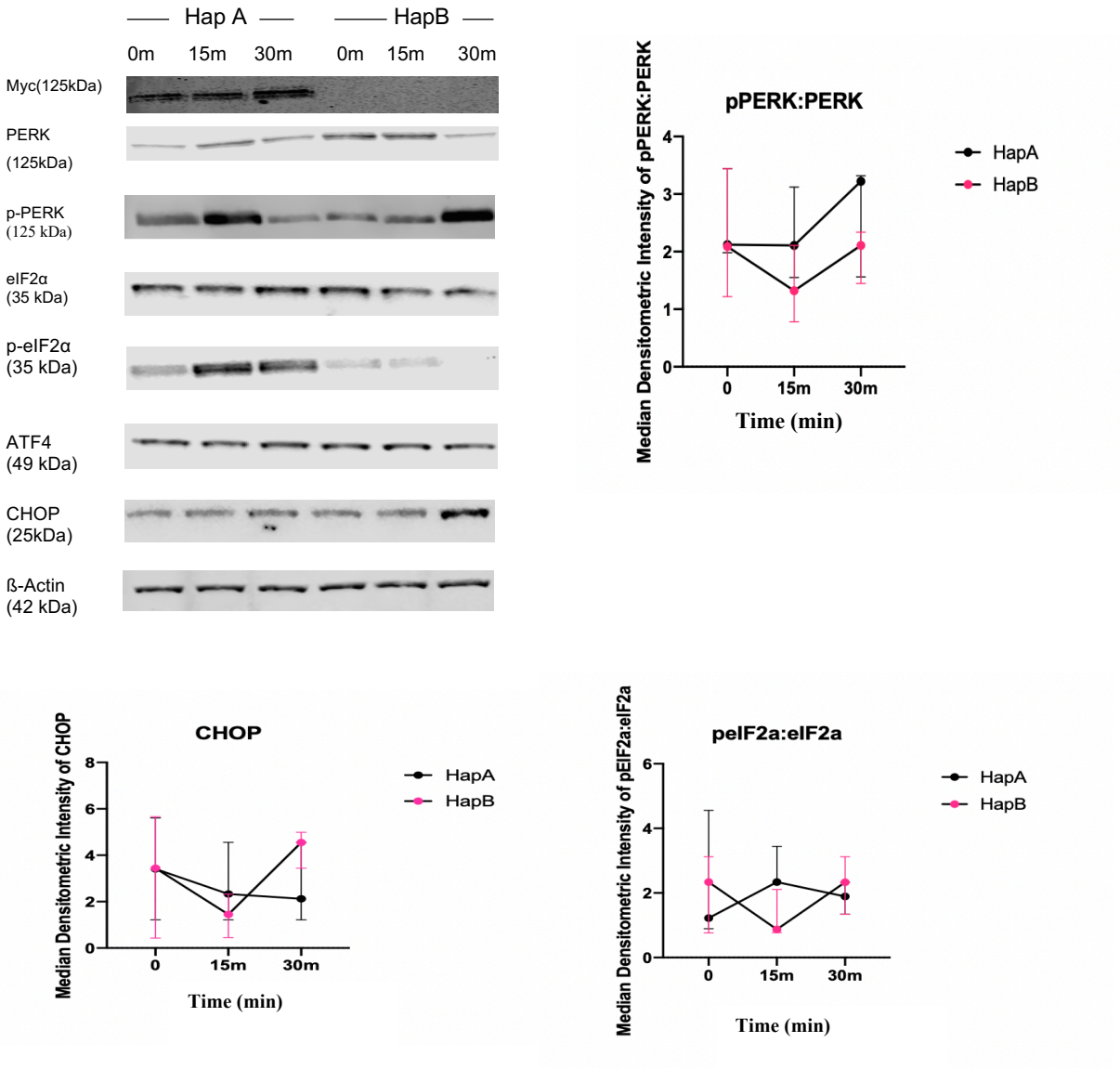

Figure 43. PERK and eIF2α activity following Tg treatment. Western blot bands comparing total PERK, p-PERK, total eIF2α, p-eIF2α, ATF4 and CHOP from PERK HapA and HapB cells following 15 and 30 m of Tg treatment is indicated in the immunoblots. Median densitometric quantification of PERK and eIF2a activity and CHOP expression levels are depicted including the 95% confidence interval for each haplotype at each treatment duration. Wilcoxon-matched pairs signed rank test was used to test for significance. No significant increase was observed following Tg treatment in either HapA or Myc cleaved HapB cells at either time point for PERK activity (rs=0.5, W=-6, p=0.25 (2 tailed)), n=3). Similarly, no significantly increased eIF2α activity (rs=-1, W=-2, p=0.75, n=3) or significant increase in CHOP expression (rs=0.5, W=0, p > 0.999, n=3) levels were observed at either time points in either cell line. This indicated that the 1.5 uM Tg concentration utilised in this study for 15 and 30 mins was insufficient to significantly activate the PERK UPR.

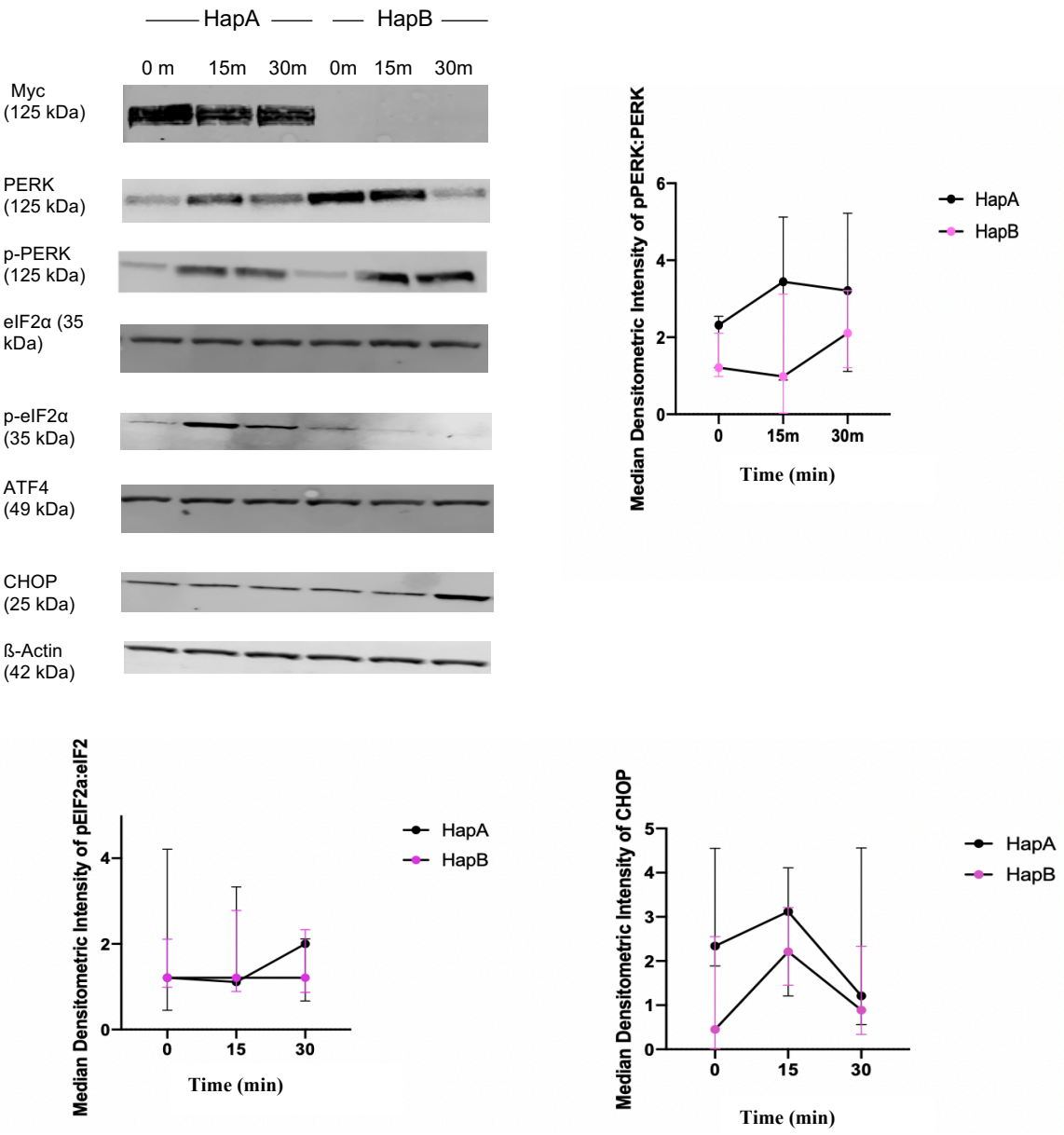

Figure 44. PERK and eIF2α activity following Tm treatment in HapA and HapB cells. Immunoblots comparing total PERK, p-PERK, total eIF2α, p-eIF2α, ATF4 and CHOP is indicated. Median densitometric quantification of PERK and eIF2a activity and CHOP expression levels are depicted including the 95% confidence interval for each haplotype at each treatment duration. Wilcoxon-matched pairs signed rank test was used to test for significance. No significant increase was observed following Tm treatment in either HapA or Myc cleaved HapB cells at either time point for PERK activity (rs=1, W=-6, p=0.25 (2 tailed)), n=3). Similarly, no significantly increased eIF2α activity (rs=-0.5, W=-6, p=0.25, n=3) and no significantly increased CHOP expression (rs=-0.5, W=-6, p 0.25, n=3) levels were observed at either time points in either cell line. This indicated that the 2.5 µg/mL Tg concentration utilised in this study for 15 and 30 min was insufficient to significantly activate the PERK UPR.

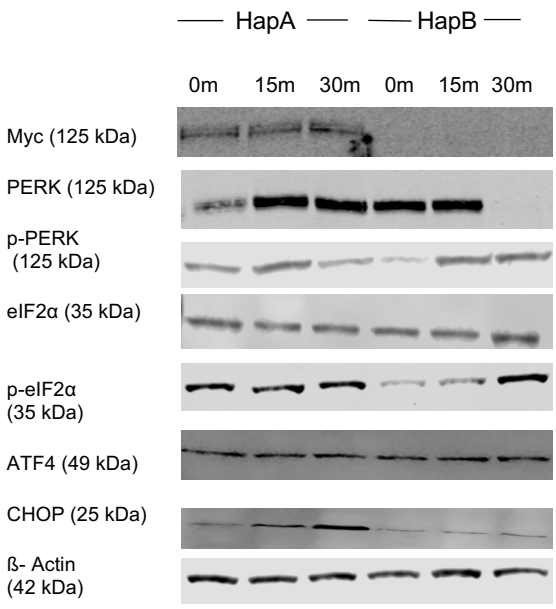

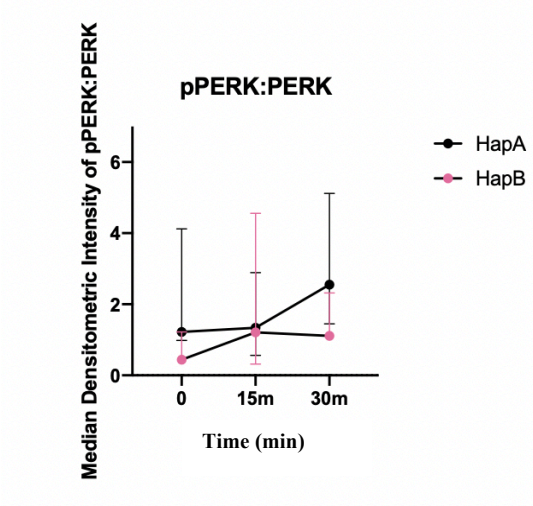

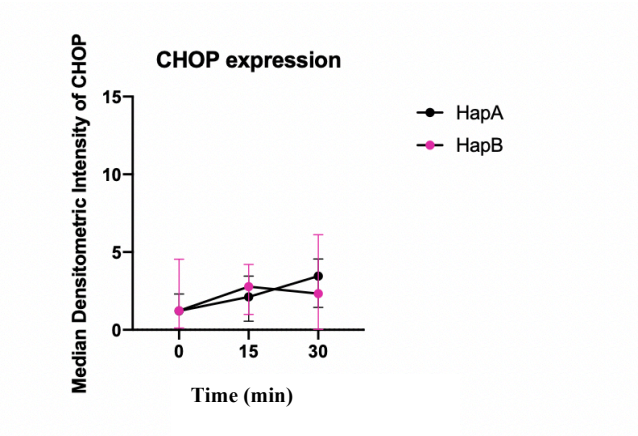

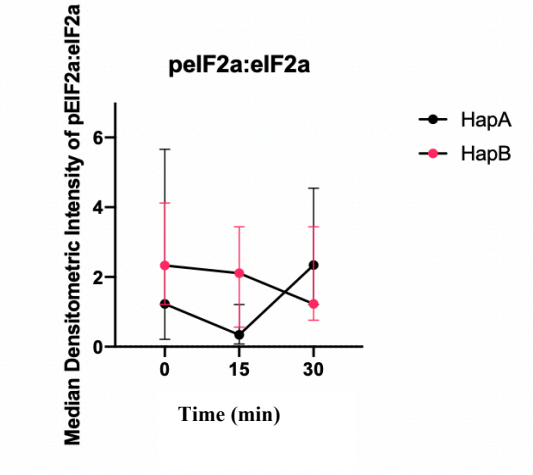

Figure 45. PERK and eIF2α activity following DTT treatment. Western blot bands comparing total PERK, p-PERK, total eIF2α, p-eIF2α, ATF4 and CHOP from HapA and HapB cell lysates are indicated in the immunoblots. Median densitometric quantification of PERK and eIF2a activity and CHOP expression levels are depicted including the 95% confidence interval for each haplotype at each treatment duration. Wilcoxon-matched pairs signed rank test was used to test for significance. No significant increase was observed following Tm treatment in either HapA or Myc cleaved HapB cells at either time point for PERK activity (rs=-0.5, W=-4, p=0.5 (2 tailed)), n=3). Similarly, no significantly increased eIF2α activity (rs=-0.5, W=-2, p=0.75, n=3) and no significantly increased CHOP expression (rs=-1, W=4, p 0.5, n=3) levels were observed at either time points in either cell line. This indicated that the 1.5 uM DTT concentration utilised in this study for 15 and 30 min was insufficient to significantly activate the PERK UPR.

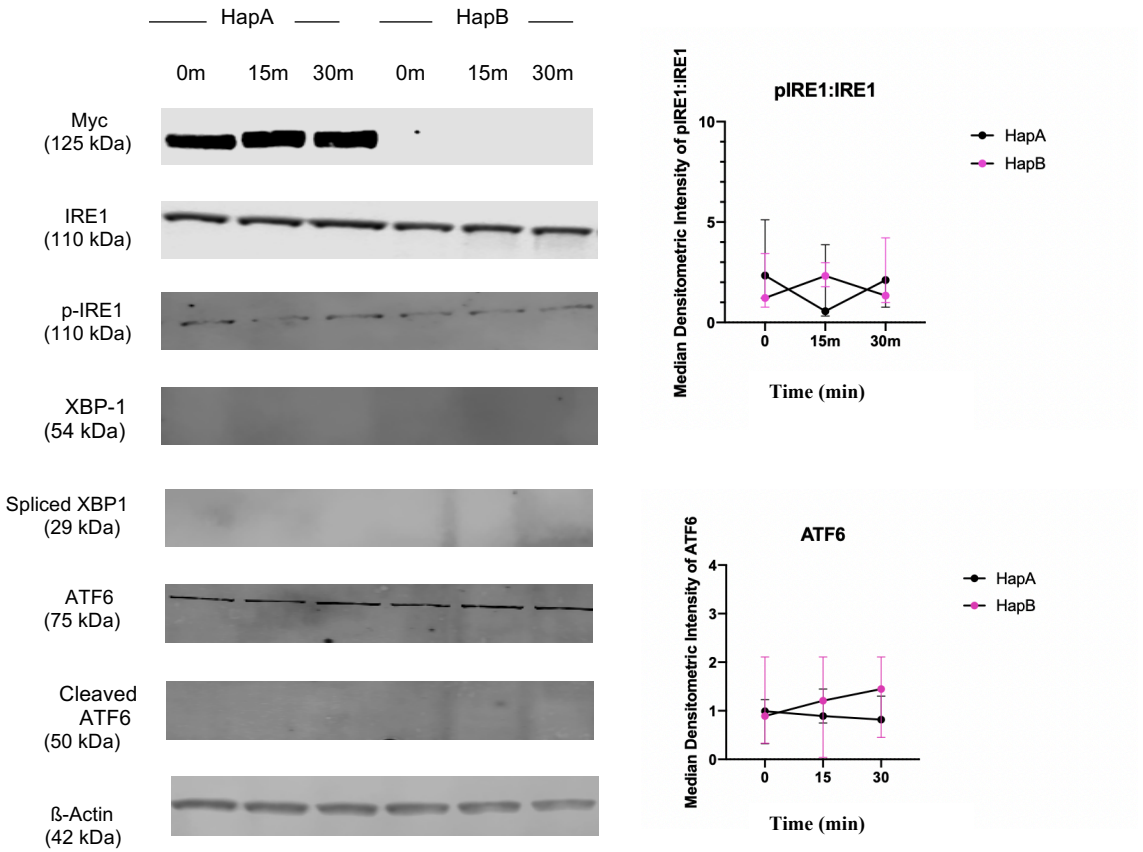

Figure 46. IRE1 and ATF6 activity following Tg treatment in HapA and HapB cells. Western blot bands for total IRE1, p-IRE1, XBP-1, spliced XBP-1 and total ATF6 (including cleaved-ATF6) from 15 min and 30 min Tg treated PERK HapA and HapB cells are indicated in the immunoblots. Mean densitometric quantification of IRE1 activity (p-IRE1 : Total IRE1) with 95% confidence interval included shows large variability in the data with no significant changes observed using a Wilcoxon-matched pairs signed rank test following Tg incubation for either IRE1 activation ((rs=0.5, W=6, p=0.25 (2 tailed)), n=3) or ATF6 expression level changes (rs=-1, W=0, p>0.999 (2 tailed), n=3). Absence of ATF6 activation (cleaved ATF6) is indicated following Tg treatment in both cell lines.

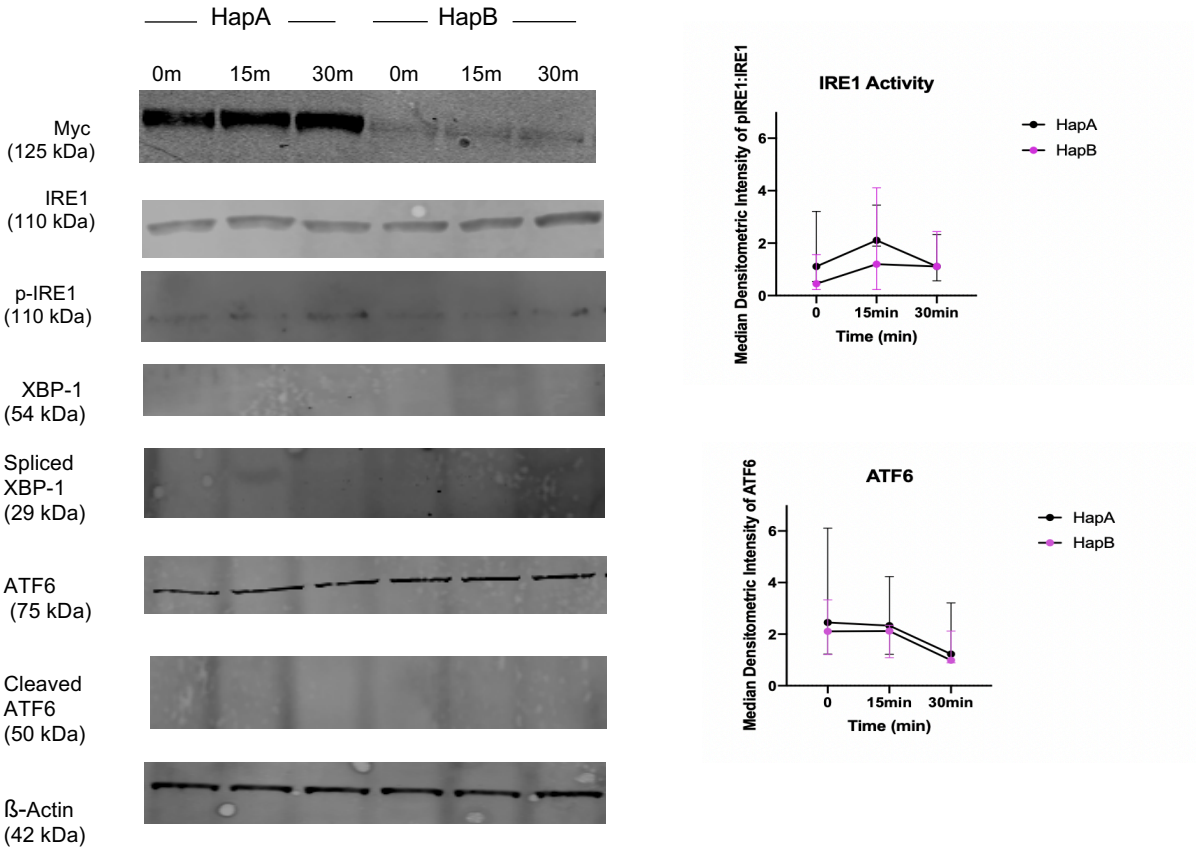

Figure 47. IRE1 and ATF6 activity following Tm treatment in HapA and HapB. Western blot bands for total IRE11, p-IRE1, XBP-1, sXBP-1 and total ATF6 (including cleaved-ATF6) from 15 min and 30 min Tm treated PERK HapA and HapB cells are indicated in the immunoblots. Mean densitometric quantification of IRE1 activity (p-IRE1 : Total IRE1) with 95% confidence interval included shows large variability in the data with no significant changes observed using a Wilcoxon-matched pairs signed rank test following Tm incubation for either IRE1 activation ((rs=0.5, W=-4, p=0.5 (2 tailed)), n=3) or ATF6 expression level changes (rs=1, W=-6, p=0.25 (2 tailed), n=3). Absence of ATF6 activation (cleaved ATF6) is indicated following Tm treatment in both cell lines.

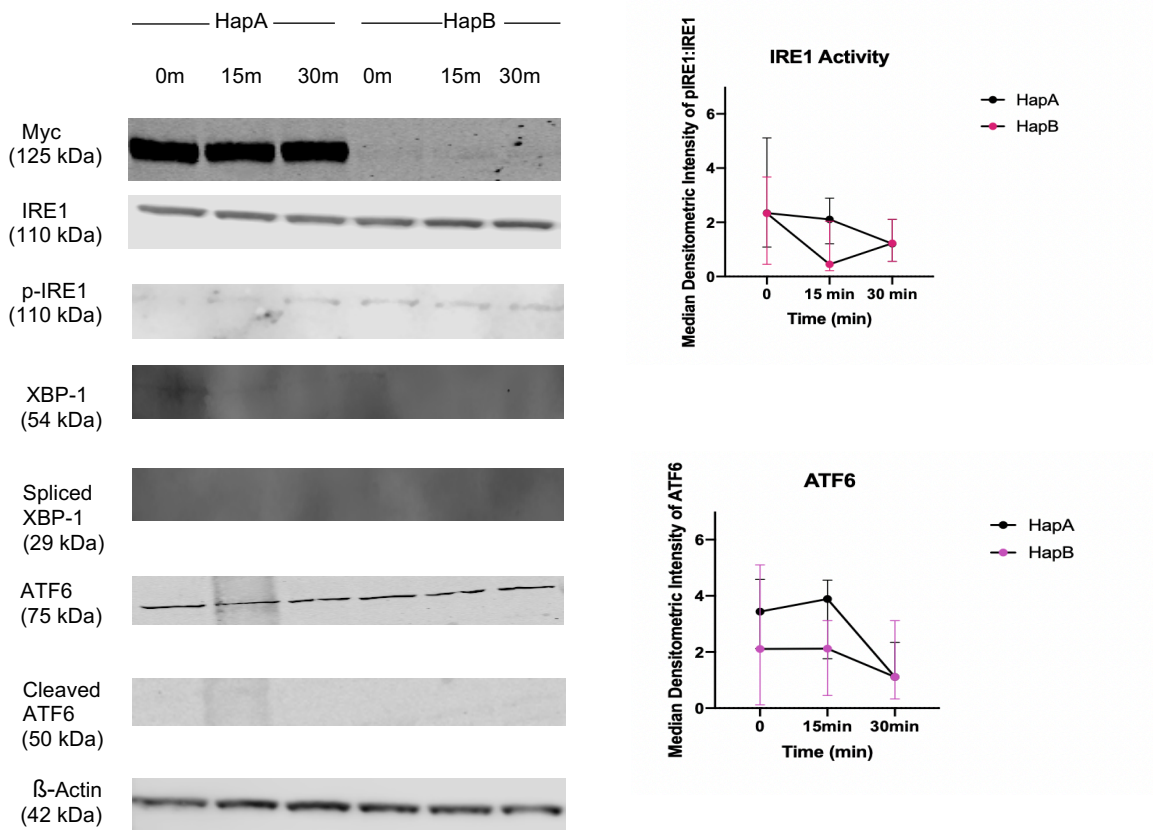

Figure 48. IRE1 and ATF6 activity following DTT treatment in HapA and HapB cells. Western blot bands for total IRE1, p-IRE1, XBP-1, sXBP-1 and total ATF6 (including cleaved-ATF6) from 15 min and 30 min DTT treated PERK HapA and HapB cells are indicated in the immunoblots. Mean densitometric quantification of IRE1 activity (p-IRE1 : Total IRE1) with 95% confidence interval included shows large variability in the data with no significant changes observed using a Wilcoxon-matched pairs signed rank test following Tm incubation for either IRE1 activation ((rs=0.5, W=-4, p=0.5 (2 tailed)), n=3) or ATF6 expression level changes (rs=0.5, W=-4 p=0.5 (2 tailed), n=3). Absence of ATF6 activation (cleaved ATF6) is indicated following Tm treatment in both cell lines.

5.6 *BiP activation in HapA and HapB cells following ER stress induction*

BiP is a highly abundant ER resident chaperone (Haas and Wabl 1983) which also plays a role in the ER stress signalling transduction process, described in Chapter 1. Carrara et al (2015) identified that when BiP is engaged in a signalling complex with IRE1 or PERK via its ATPase binding domain, its substrate binding domain remains available to interact directly with misfolded proteins. Upon the accumulation of unfolded proteins, this interaction dissociates the ATPase complex, enabling PERK and IRE1 to initiate UPR signalling. In mouse embryo fibroblasts derived from *Perk*$^{-/-}$ mice, the attenuation of protein translation following ER stress was abolished; further, BiP mRNA induction was suppressed (Harding et al., 2000). Similarly, in embryo fibroblasts derived from the Ser51Ala/Ser51Ala mutant eIF2α mice whereby eIF2α was expressed but not phosphorylated at Ser51, BiP mRNA induction by Tm was reduced (Scheuner et al., 2001). These results provided the first evidence that translational control by the PERK-eIF2α signalling pathway directly regulates BiP transcription. Therefore, we aimed to investigate if cleaved HapB dysfunction following UPR induction results in impaired activation of BiP due to reduced phosphorylation of eIF2α. We decided to examine the interaction of BiP and PERK with the use of confocal microscopy and co-Immunoprecipitation.

We used 15 and 30 min Tg, Tm and DTT treated HapA, HapB and Flp-In 293 cells to study whether these ER stress conditions may alter the levels of BiP in our PERK cells. Untreated cells were used as the negative control and the uninduced Flp-In 293 cells were used as a control against the PERK over expression. Expression of endogenous BiP and PERK were carried out using an anti- BiP and anti-PERK antibodies as described in Chapter 2. DAPI was used to stain the nuclear DNA and the PERK antibody exclusively highlighted the ER. Images were obtained from 3 independent experiments carried out in triplicates and imaged from five different regions per well. Each treatment condition was repeated three times. All three cell lines demonstrated a reticular pattern of anti-BiP staining similar to that seen with PERK. However, the BiP staining was beaded and discontinuous with some punctate spots being observed. BiP was observed to be mainly perinuclear (Figure 49). Following ER stress treatment, we observed that in both HapA and HapB cells, there was no change in the mean fluorescent intensity of BiP when compared with the untreated cells suggesting that BiP levels were not significantly increased either at rest in myc cleaved HapB cells or when our treatment conditions utilising Tg, Tm and DTT were utilised (Figures 50, 51, 52). This is hardly surprising given that we failed to see a significant increase in the PERK, IRE1 or ATF6 arms of the UPR indicating that these conditions were not optimal for ER stress induction. Negative controls (secondary antibody IgGs) showed no PERK or BiP staining.

Although PERK and BiP are known interacting partners with elevated BiP levels correlating with the induction of the UPR we were unable to see such a response using immunofluorescent techniques. Given that there were no significant differences in BiP intensity observed between the two PERK haplotypes either when untreated or following treatment with Tg, Tm or DTT it is also likely that HapB PERK activity has little effect on the activation of BiP.

As BiP is normally bound to PERK which maintains it in an inactive state upon the absence of unfolded proteins within the ER, we attempted co-IP with HapA and HapB UPR induced cells to evaluate if there were any differences in degree of binding of BiP to HapB and HapA PERK. Although we had optimised the PERK antibody conditions, we could not obtain reliable results with the BiP antibody with a high degree of non-specific binding and absence of expected band for BiP between 75 and 100kDa (Figure 53). Thus, further optimisation or use of other BiP antibodies would be required so as to confirm whether HapB interacts differently with BiP.

5.7 *ER dilation upon UPR induction does not differ between the PERK haplotypes*

With UPR activation, the ER expands to meet the increased need for protein folding capacity (Cox et al., 1997; Bernales et al., 2006; Schuck et al., 2009). The discovery that a larger ER alone alleviates ER stress argues that the role of membrane expansion during a normal UPR, when ER size and chaperone levels increase simultaneously, goes beyond merely providing space to accommodate newly synthesized folding machinery (Schuck et al., 2009). It seems reasonable that a larger ER can tolerate more misfolded proteins before essential functions break down. Moreover, a larger ER could also promote protein folding itself. Increasing ER volume could lower the concentration of folding intermediates, which may give proteins more time to fold by avoiding aggregate formation (Apetri and Horwich., 2008). Furthermore, membrane-associated processes that support protein folding or remove misfolded proteins, such as protein glycosylation or ERAD, could operate more efficiently when a larger membrane area is available (Schuck et al., 2009).

In order to assess any differences in ER membrane expansion in UPR induced HapA and HapB cells, we used live cell imaging with a green-fluorescent BODIPY® FL tagged glibenclamide. Glibenclamide (glyburide) binds to the sulphonylurea receptors of ATP-sensitive K^+ channels which are prominent on the ER. Using this GFP-tagged ER tracker, we aimed to quantify expansion of the ER before and after ER stress treatment in HapA and HapB cells. Fifteen sample images were analyzed for each treatment from triplicate wells and three independent experiments carried out. A representative image for each is shown in Figures 54, 55, 56 and 57. To quantify the expansion of the ER we used the Columbus software to first measure ER roundness using the formula: $\text{perimeter}^2/(4*pi*\text{area})$, *pi* being the mathematical constant and the results

normalised to the surface area of the ER. Unstressed cells (i.e. controls) were normalised to 1 and subsequent measurements were plotted as a percentage difference against the control.

In confocal sections through the middle of unstressed cells, the ER marked by the GFP tracker is visible as a tubular network throughout the cell with perinuclear concentration (Figure 54). Dox induction of PERK did not cause any discernible ER expansion i.e. ER morphological changes as measured by the ER roundness: ER surface area between the two haplotypes (Figure 58). Therefore, we next assessed the ER only in UPR induced HapA and HapB cells after 30 min treatments with Tg, Tm, and DTT. As shown in Figure 55 and Figure 56, exposure of the cells to either of these short-term UPR inducers did not reveal any changes in ER size or shape indicating that the acute ER stress conditions we have used herewith does not result in an expanded ER. Furthermore, there is no indication that following UPR activation, the contribution of Myc cleaved HapB PERK signalling results in an impaired ER morphology.

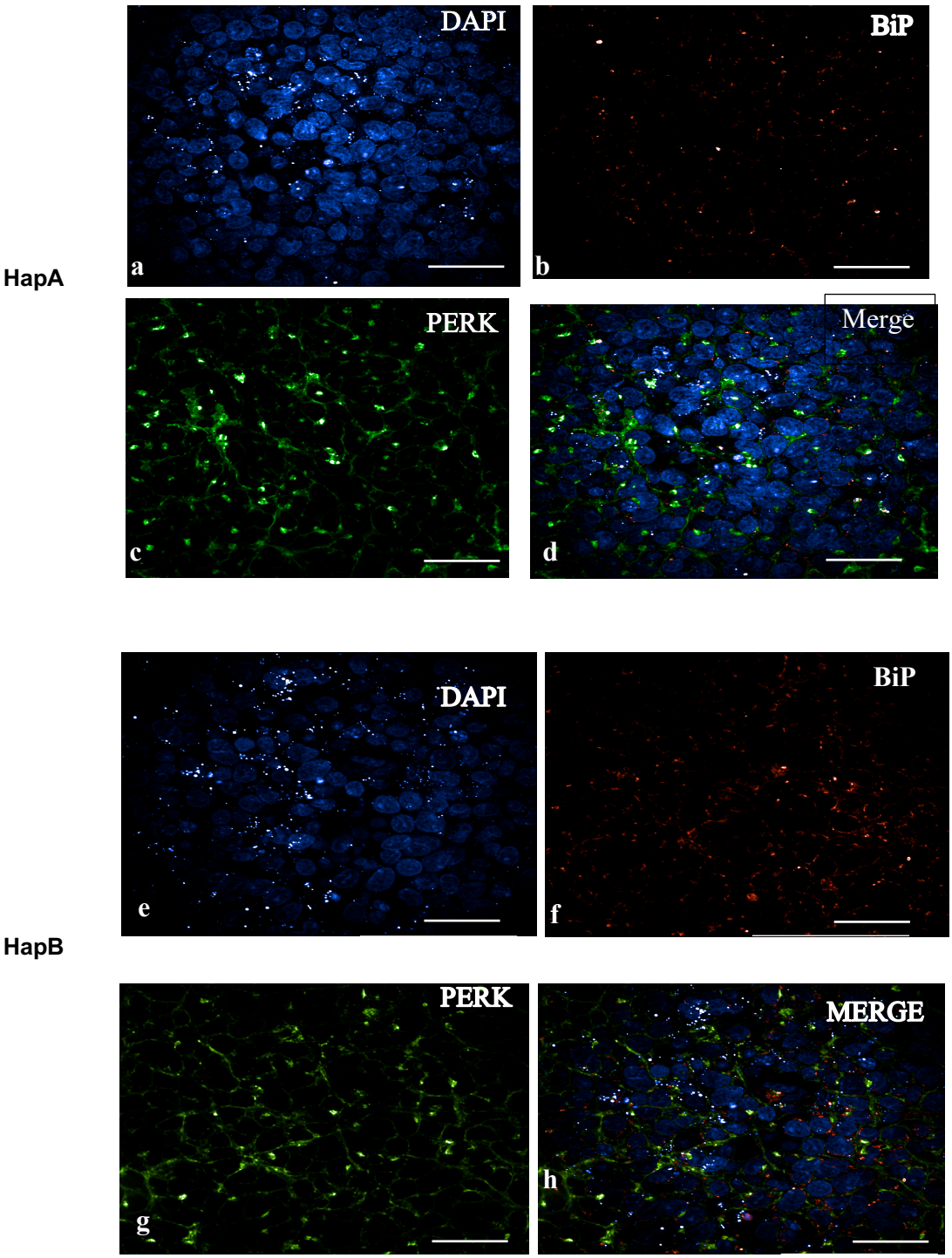

Figure 49. Staining pattern of BiP in PERK cells. HapA and myc cleaved HapB cells were grown to 80% confluence, fixed with 4% PFA and stained with anti BiP and anti-PERK antibodies and viewed under a 60× water lens using the Opera Phenix High Content Screening System. Staining for BiP (Red, panels b and f), PERK (Green panels c and g), DAPI (Blue, panels a and e) and merge of the two stains (panels, d and h) are indicated. Scale bar = 50 μm

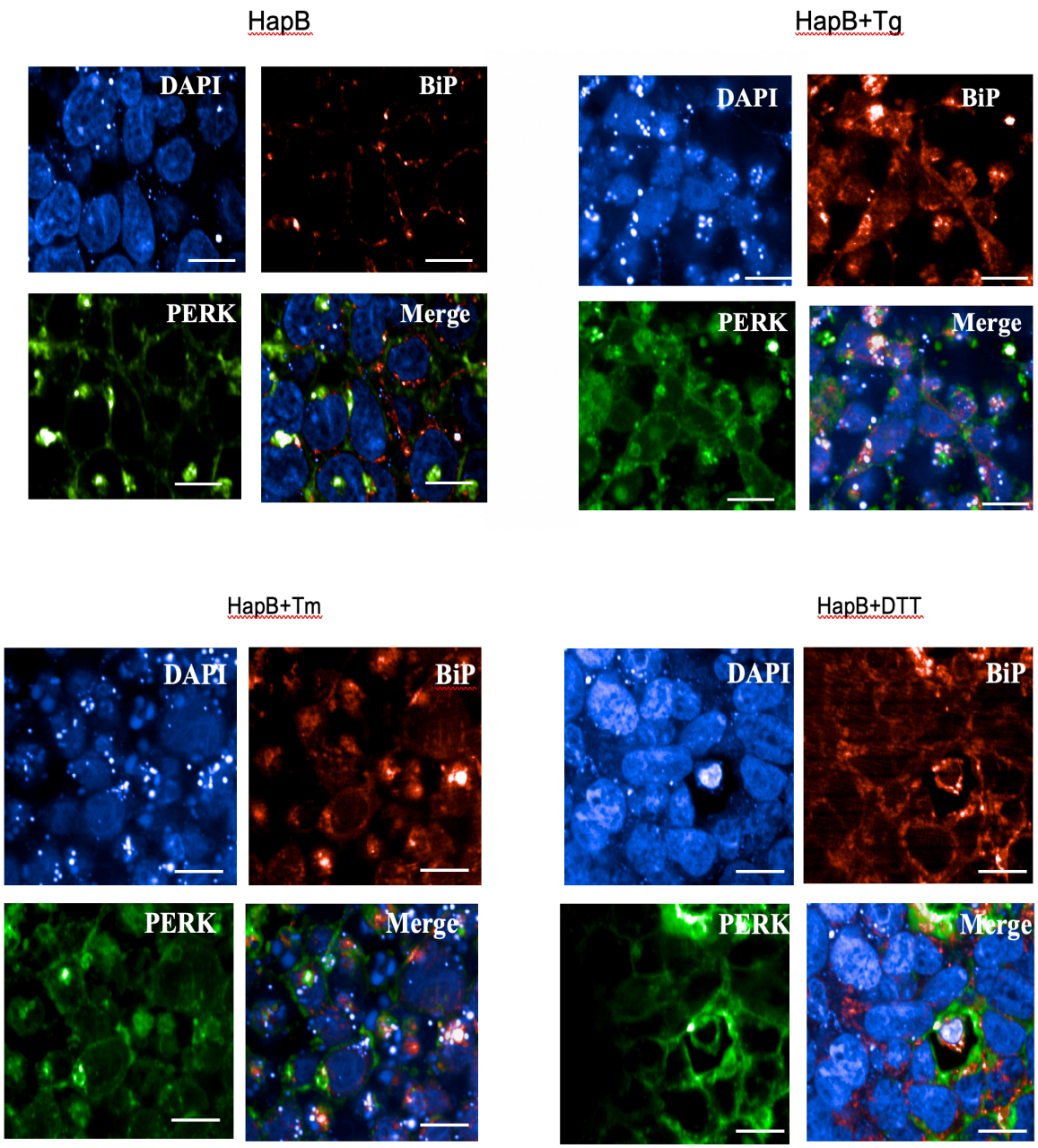

Figure 50. **ER stressed myc cleaved HapB cells stained with BiP and PERK.** HapB cells were treated with either 1.5 µM Tg, 2.5 µg/mL Tm or DTT 1.5 µM for 30 min. Cells were fixed in 4% PFA, stained with the indicated antibodies, and mounted for analyses by confocal microscopy. Pictures show labelling with PERK, BiP and DAPI colour coded as green, red and blue respectively. It is interesting to note that in our immunoblots we saw complete absence of PERK following 30 mins of DTT treatment in myc cleaved HapB cells. However, a strong PERK signal is observed at 30 mins post DTT treatment in myc cleaved HapB cells using immunocytochemistry staining techniques. Scale bar = 15 µm

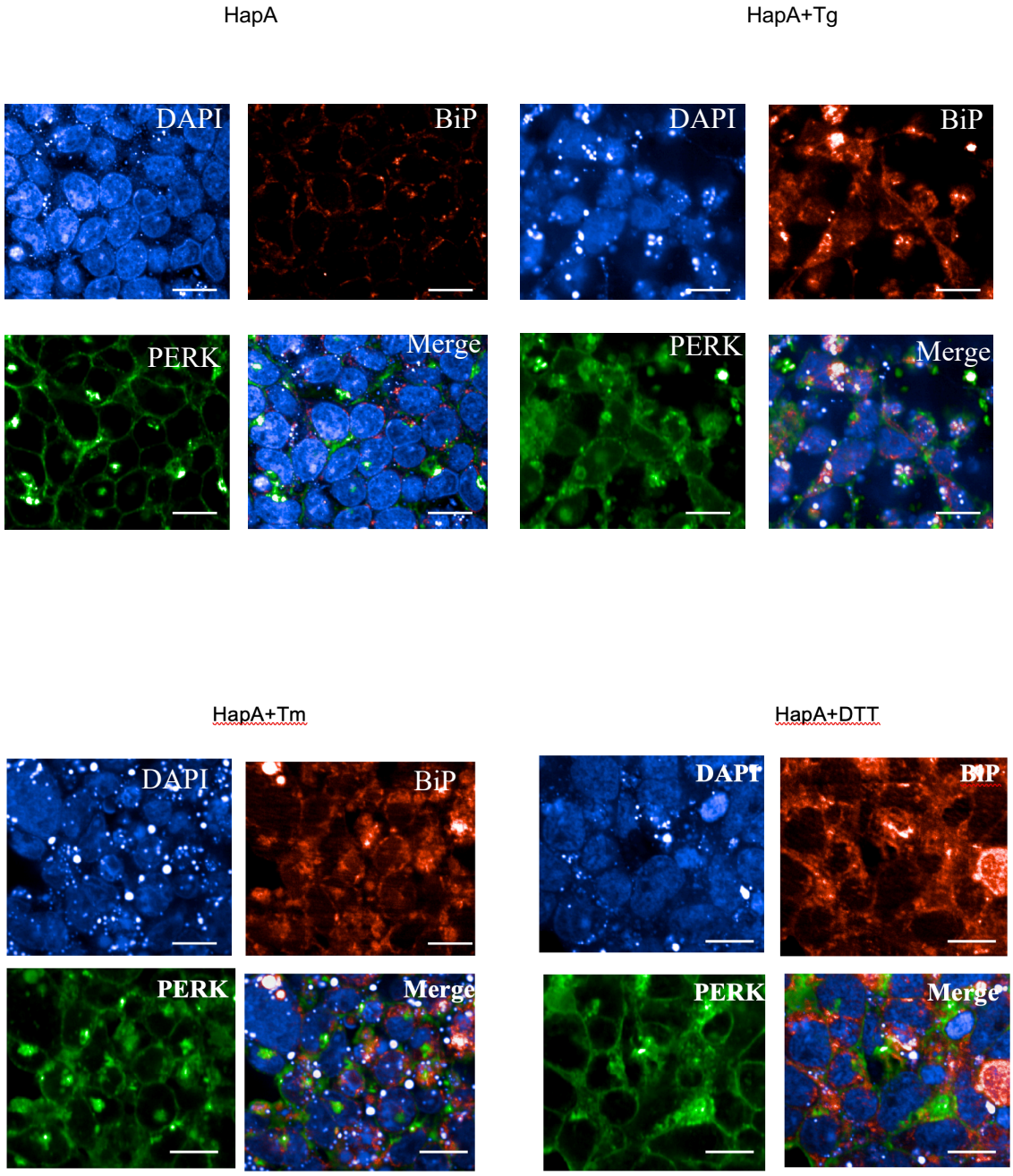

Figure 51. **ER stressed myc cleaved HapA cells stained with BiP and PERK.** HapA cells were treated with either 1.5 µM Tg, 2.5 µg/mL Tm or DTT 1.5 µM for 30 min. Cells were fixed in 4% PFA, stained with the indicated antibodies, and mounted for analyses by confocal microscopy. Pictures show labelling with PERK, BiP and DAPI colour coded as green, red and blue respectively. Fragmented nuclei are visible in both Tg and Tm treated cells and appear to be a marker of impending cell death. Scale bar = 15 µm

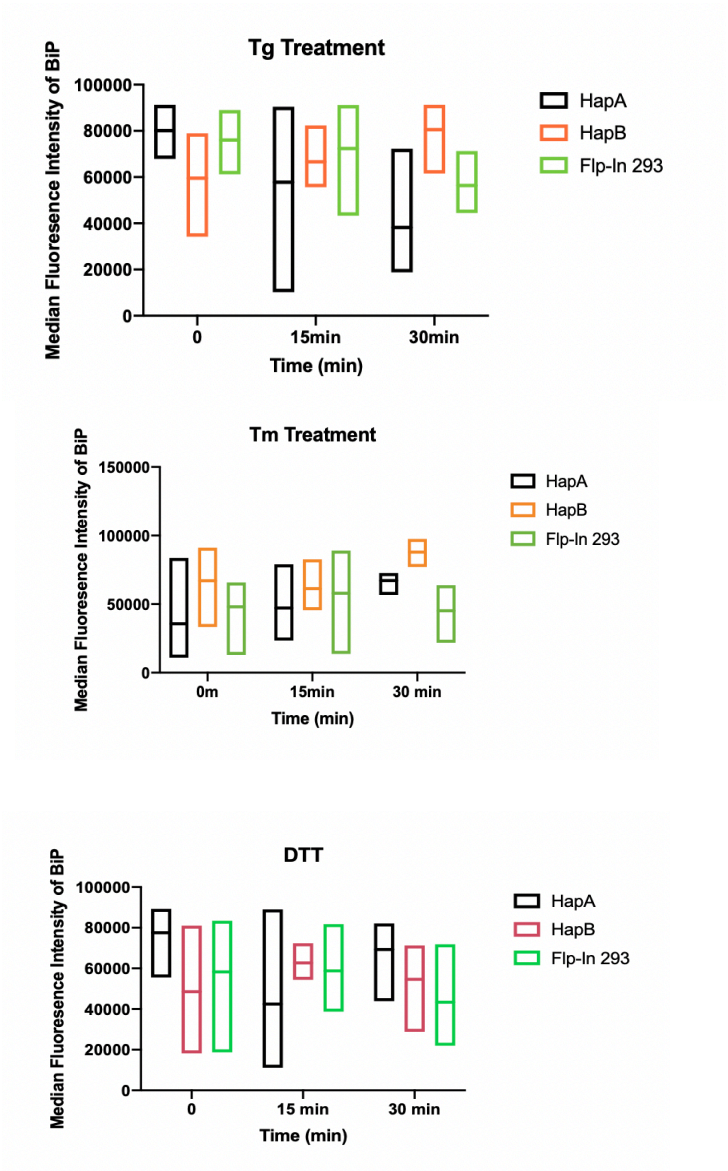

Figure 52. Median fluorescence intensity of BiP following UPR induction. 15 and 30 min Tg, Tm and DTT treated HapA, HapB cells and Flp-In 293 cells were stained for BiP and the median fluorescence intensity of BiP obtained from three independent experiments carried out using 5 wells/treatment/plate and is depicted as a box and violin plot with the median indicated. There is large variability of BiP staining and no statistical changes in BiP fluorescence intensity following Tg ((F_r=0.667, df=2 p=0.9444, n=3), Tm treatment ((F_r=4.667, df=2 p=0.1944, n=3). or DTT treatment ((F_r=0.6667, df=2 p>0.9444, n=3). was observed in either cell line when analyzed by the Friedman's test.

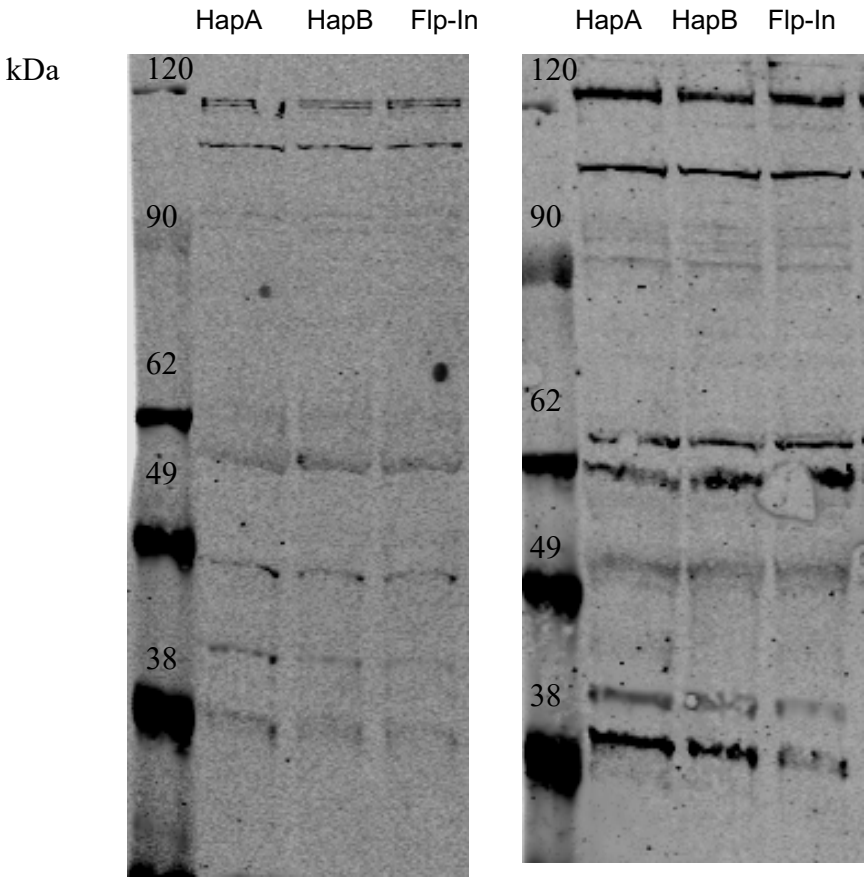

Figure 53. Immunoblots probed with BiP antibody. Optimization of two different BiP antibodies (L.H. panel- BiP targeting amino acids 600-C terminus (Abcam) and R.H. panel BiP targeting the N-terminus of BiP (Sigma-Aldrich)) are shown to produce a large number of non-specific bands, with no band visible at 78 kDa. A range of antibody dilutions, antibody incubation times, blocking reagents, wet/semi-dry transfer conditions and increased protein lysate concentrations were tested. However, specificity of the BiP antibody was not guaranteed following any of the optimization changes.

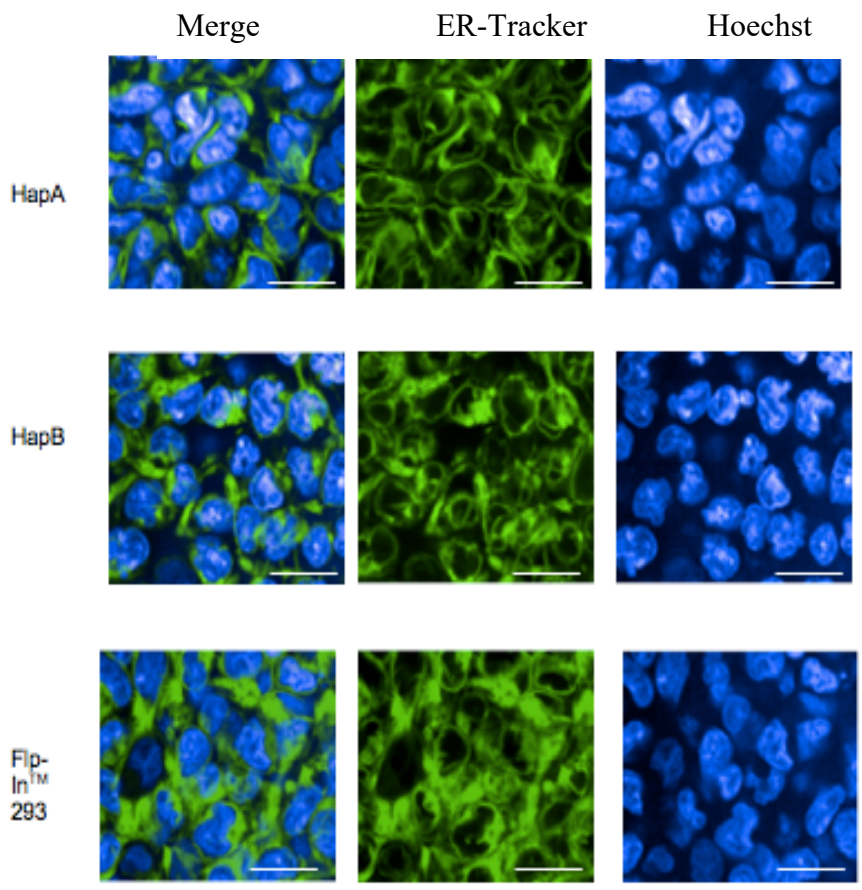

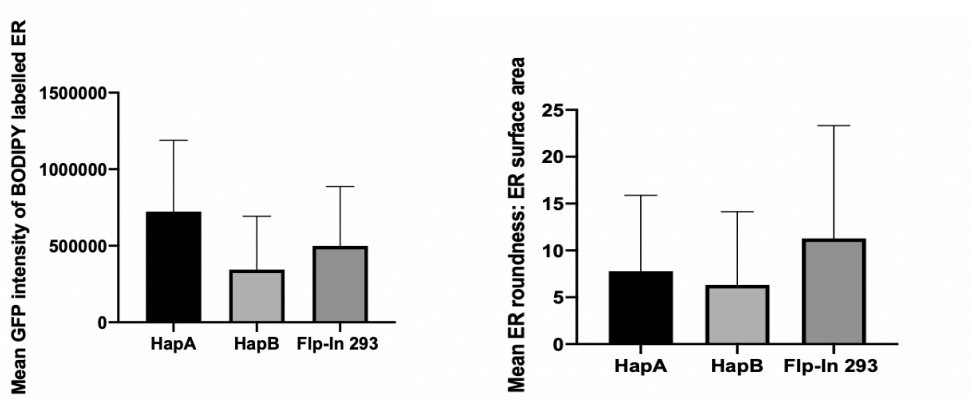

Figure 54. Confocal analysis of uninduced Flp-In™ 293 cells, PERK HapA and myc cleaved HapB cells imaged with BODIPY-ER tracker. Live-cell imaging using a 60x water immersion objective was used to obtain images of the ER stained with the BODIPY-ER tracker. The ER is observed as a large continuous perinuclear continuous membrane system surrounding the nucleus which is stained with Hoerscht. PERK over-expression following Dox induction did not result in changes in the mean fluorescence intensity of the GFP signal and morphological properties such as ER roundness: surface area was also shown to be not significantly different when tested with the Mann Whitney U test. Five different regions from triplicate wells obtained from three independent experiments were used in the analysis. Scale bars: 20μm

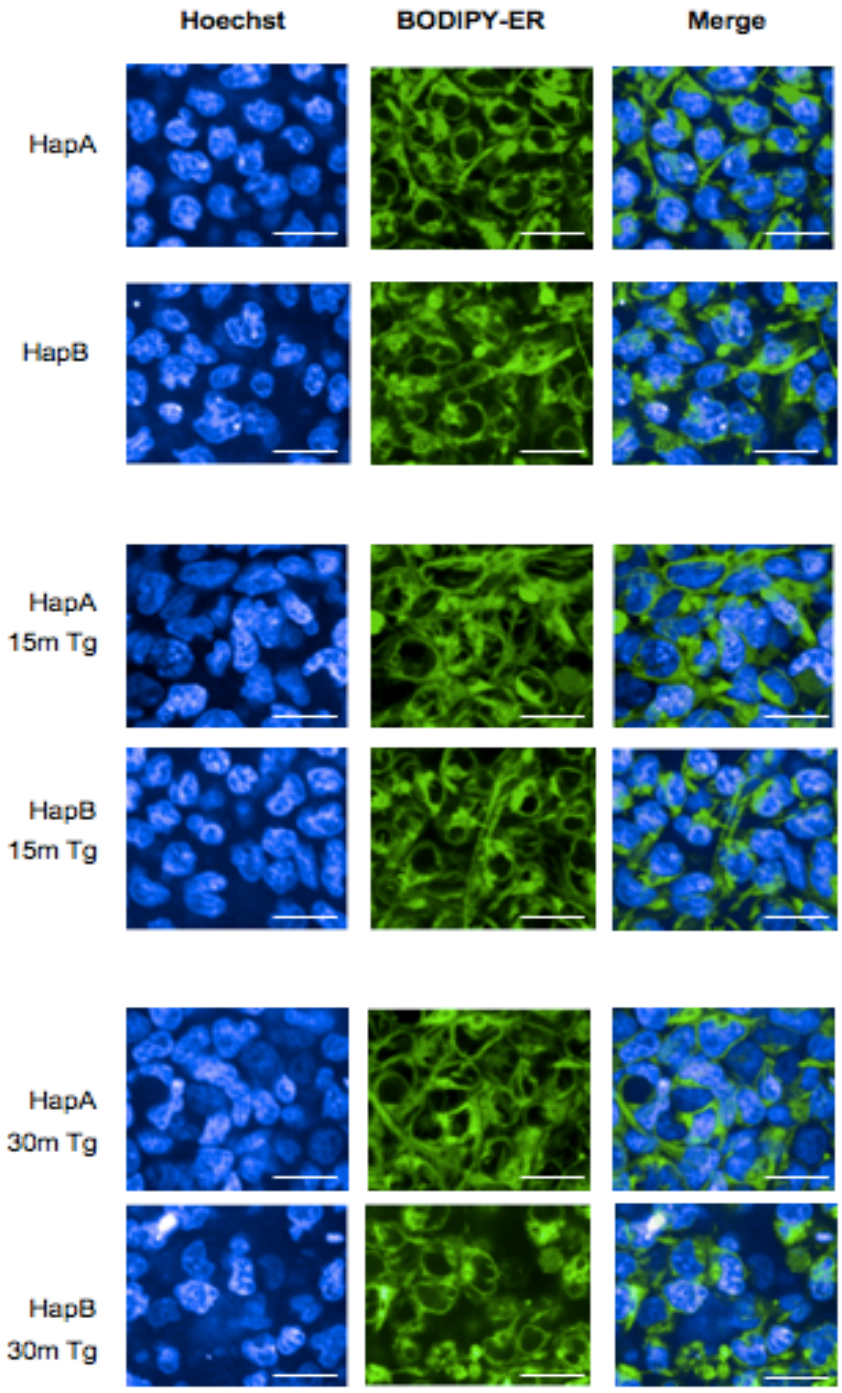

Figure 55. PERK ER membrane following pre and post treatment with 1.5 μM Tg. UPR induced HapA and HapB cells were treated for either 15 or 30 min with 1.5 uM Tg and representative images of the ER membrane obtained from five different regions per well. Each experiment was carried out in triplicate and repeated three times. Scale bar = 25 μm

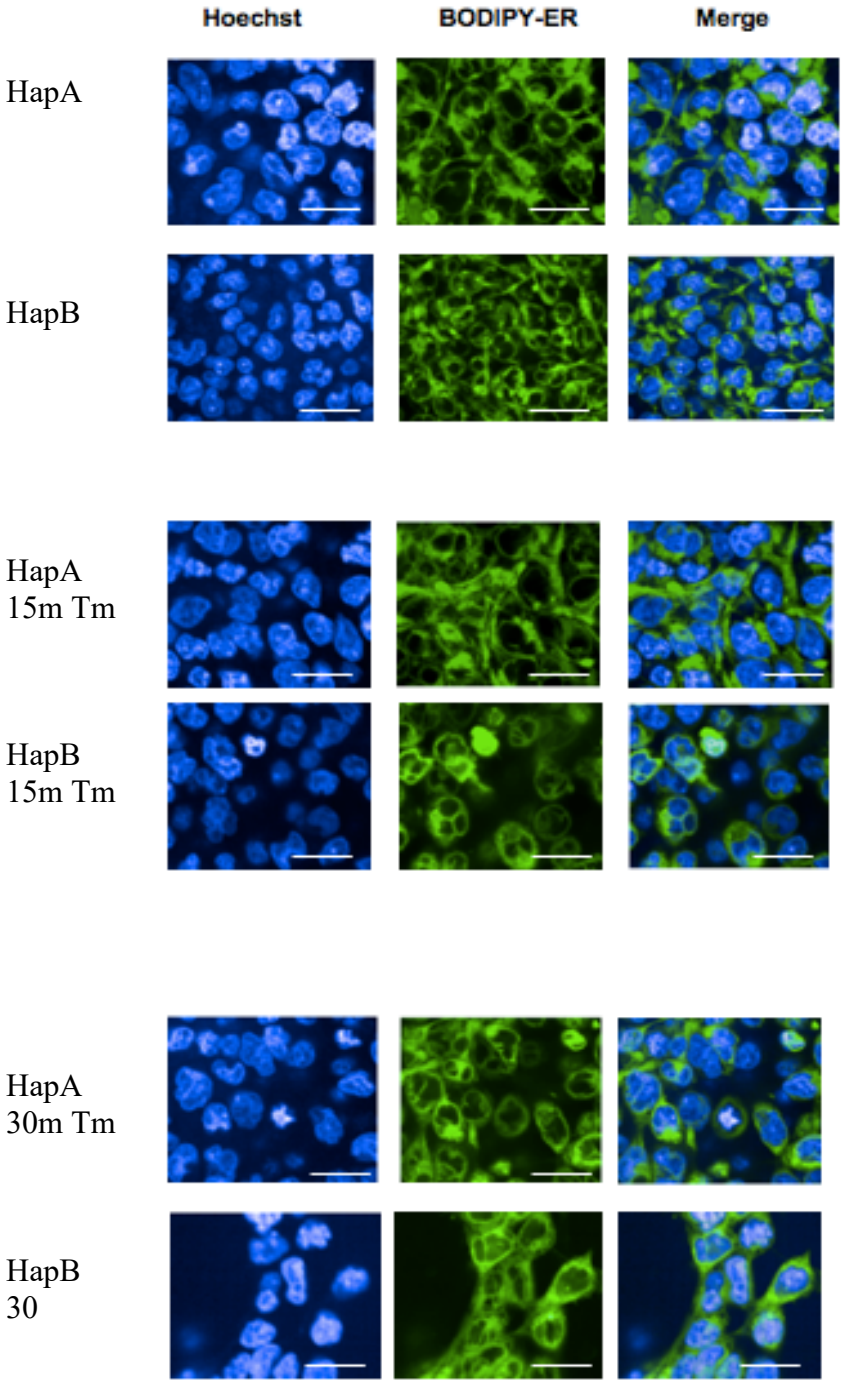

Figure 56. PERK ER membrane following pre and post treatment with 2.5 µg/mL TM. UPR induced HapA and HapB cells were treated for either 15 or 30 min with 2.5 uM Tg and representative images of the ER membrane obtained from five different regions per well. Each experiment was carried out in triplicate and repeated three times. Scale bar = 25 µm

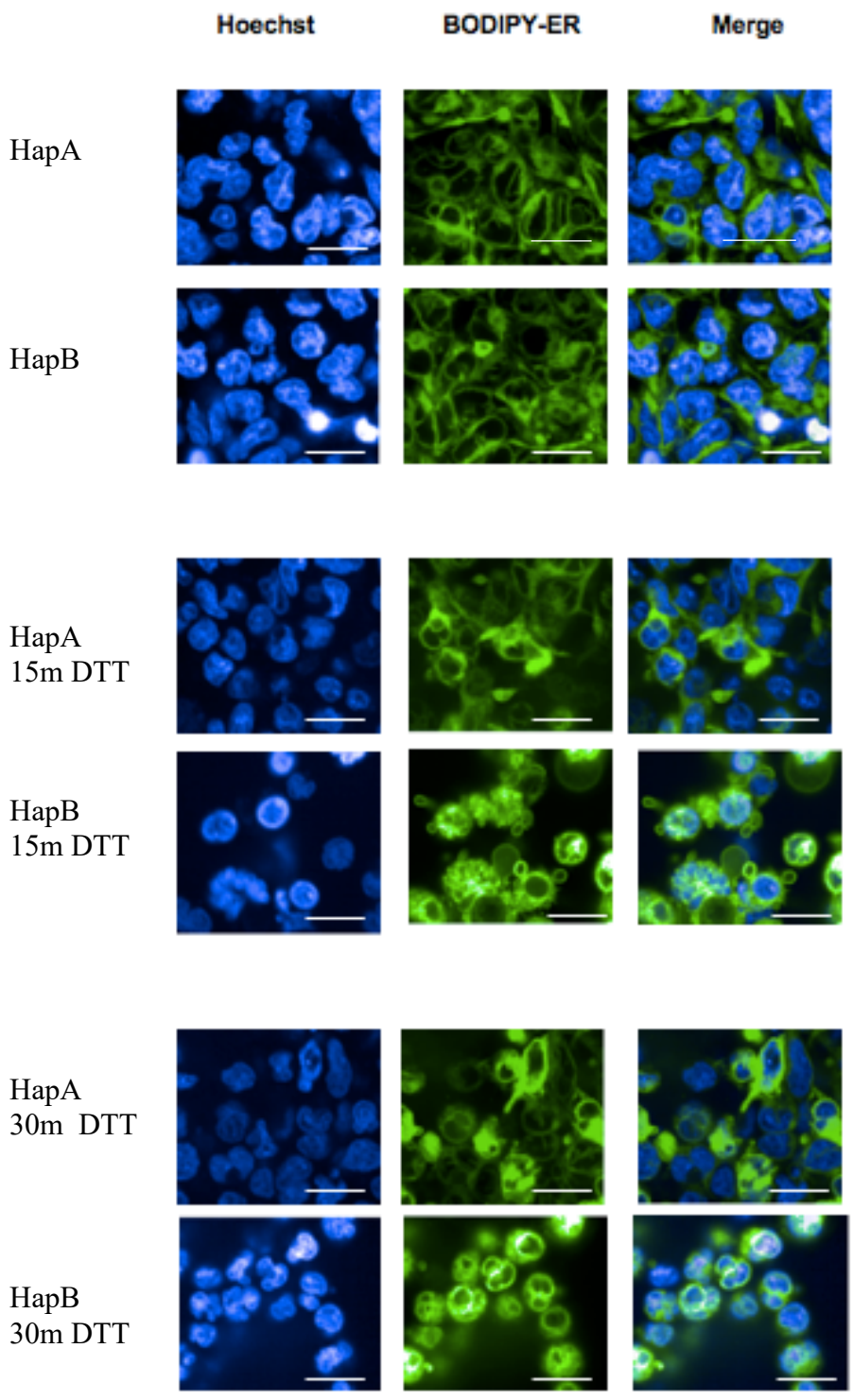

Figure 57. PERK ER membrane following pre and post treatment with 1.5 μM DTT. UPR induced HapA and HapB cells were treated for either 15 or 30 min with DTT and representative images of the ER membrane obtained from five different regions per well. It is interesting to note that following DTT treatment the nuclei of both HapA and HapB cells show blebbing and rounded nuclei which are indicative of dying cells, Each experiment was carried out in triplicate and repeated three times. Scale bar = 25 μm

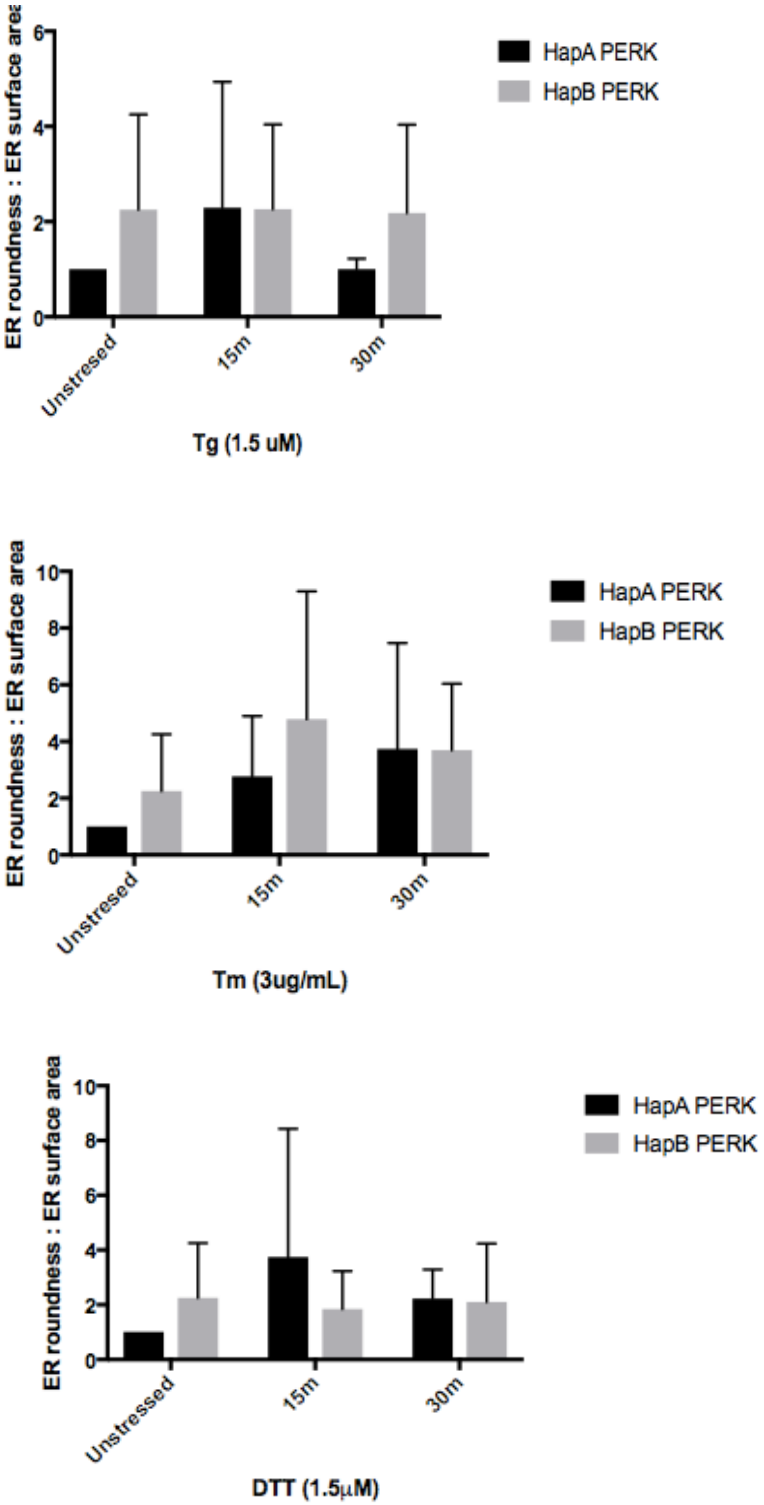

Figure 58. 30 min acute ER stress conditions do not result in ER morphological changes. Mann Whitney U test statistical analyses did not reveal any significant changes to ER roundness in either haplotype following normalization against the corresponding ER surface area due to the large variation observed within different regions of the same well. Data is expressed as a mean of 3 experiments ± SEM.

5.8 Discussion

In this study, we although we failed to replicate the previous finding that PERK HapB homozygous cells have impaired eIF2α phosphorylation compared to HapA cells we began to see emerging trends of reduced PERK activity (Yuan et al., 2018). We also observed that HapB cells showed delayed PERK phosphorylation after Tg but not with Tm treatment in two out of the three replicates. Though our results following Tg treatment largely differed from those observed by Stutzbach et al., (2013) it was intriguing to note that lower HapB phospho- PERK levels in response to Tg was a common observation, although they then demonstrated significantly higher levels of eIF2α phosphorylation following treatment. The complete loss of p-eIF2α following Tg treatment had only previously been reported in PERK $^{-/-}$ mouse embryonic fibroblasts and as a result, their ability to survive ER stress was significantly impaired (Koumenis et al., 2002). Moreover Yuan et al., (2018) observed delayed phosphorylation of eIF2α indicating slower kinetics upon the treatment of HapB cells with Tg. It should be noted however that both Koumenis et al., (2012) and Yuan et al., (2018) used longer Tg treatment durations which are more indicative of chronic ER stress conditions than the acute conditions used in our study. There is convincing evidence from our work that Myc cleaved HapB cells results in impaired PERK activation upon acute ER stress conditions. Thus it would be interesting to observe if HapB cells continue to show a negative impact on the ability of cells to phosphorylate eIF2α in the presence of chronic stress conditions which require quasi-permanent changes in cellular function in general and in ER function in particular; as opposed to tolerating stresses for relatively brief durations which demands a UPR that is relatively fast acting and also readily deactivated (Rutkowski and Kaufman., 2007).

PERK can phosphorylate Ser51 of the α-subunit of the eIF2α thereby decreasing the rate of cellular protein synthesis, which diminishes mRNA translation. Accordingly, the final outcome of the Tg and Tm treated cells should be attenuation of protein synthesis which should correlate with cell death. However, as we failed to optimise the treatment conditions and durations for each of the three drugs, we were unable to observe significant cell death under each treatment condition for either of the three cell lines. The HapB PERK coding variants alter amino acids in the PERK luminal domain involved in ER stress sensing (S136C, R166Q) and in regions of the cytosolic domain proposed to include a ‘disordered linker’ (S704A, D566V) that joins essential lobes of the PERK kinase within the cytosolic domain (Yuan et al., 2018). It seems likely that the phosphate moiety of Threonine 980 of the Myc cleaved HapB PERK is unable to efficiently form the required charge-charge interactions between the two PERK monomers following Tg treatment. It is yet unclear as to why dimerization following Tg is delayed while Tm and DTT treatment results in efficient HapB dimerization leading to prompt HapB phosphorylation. Resolving the structure of PERK kinase domains to 2.8 A Carrara et al., (2015) revealed that PERK phosphorylation

stabilises both the activation loop and the alpha helix G on the C-terminal lobe. One potentially appealing mechanism to account for reduced phosphorylation of eIF2α in HapB cells that we observed in two of the three replicates could account for the presence of the three SNPs which may result in the formation of an unstable activation loop, which is thereby unable to fix its position and orientation, thus preventing the binding of eIF2α. Further work should include similar structural studies as performed by Carrara et al., (2015) which will help identify if the protein folding of HapB is different to that of HapA.

In addition to observing a trend of decreased eIF2α phosphorylation, the HapB cells did also show a trend of increased CHOP levels which, through its pro-apoptotic activity could contribute to its decreased cell viability following prolonged UPR induction. As PERK is essential for cells to survive ER stress, reduced PERK signalling, arising in Haplotype B is likely to increase damage upon exposure to Tg and Tm, resulting in increased cell death. The transcription factor CHOP has an especially interesting role in linking eIF2α phosphorylation and ER stress. The *CHOP* gene is strongly induced by ER stress, as part of the PERK→p-eIF2α→ATF4-dependent gene expression program (Nishitoh., 2012). CHOP constitutes a relatively downstream component of the UPR that contributes to *GADD34* activation, which, in turn, counteracts the effects of PERK in the UPR and serves as a negative feed- back loop that maintains protein synthesis (Araki et al., 2003). Although the inhibition of global protein synthesis following eIF2α phosphorylation is considered a cytoprotective mechanism to let cells recover from the stress; prolonged eIF2α phosphorylation is toxic and proapoptotic. As such, cells developed protective measures to diminish the levels of eIF2α phosphorylation through the induction of GADD34 expression which assists the phosphatase PP1 to dephosphorylate eIF2α and re-initiate protein synthesis (Novoa et al., 2001). Against this background, it would be key to measure levels of *GADD34* in UPR induced HapA and HapB cells which if increased in HapB could provide an explanation for the decreased levels of p-eIF2α. It is thus possible that the failure to resolve ER-stress due to impaired PERK kinase activity, leads to an adaptive switch from homeostatic restoration to an apoptotic profile which through a mechanism that remains unclear results in the accumulation of CHOP in HapB cells. Therefore, assessment of pro-apoptotic mRNAs under the regulation of CHOP should be examined. For example, CHOP has been shown to up-regulate PUMA and BIM expression while suppressing Bcl- 2 mRNA in response to ER dysfunction (McCullough et al., 2001; Cazanave et al., 2010; Puthalakath et al., 2007). Collectively these results will help inform the molecular mechanisms that underpin HapB cell death following UPR induction.

It is clear that the Myc cleaved HapB version of the protein significantly differs from HapA in either structure (perhaps a difference in disulphide bonding conferred by the 136S>C variation) or in post-translational modifications (notably potential phosphorylation sites S136 and S704, which are ablated by HapB). These modifications are seen to account for the differences in activity

between HapA and HapB as noted in our results. HapA contains two serines (S136 and S704) not present in HapB. Phosphorylation at either of these sites could potentially affect kinase activity. As shown by Yuan et al., (2018) the S704A coding variant of HapB PERK which lies within the cytosolic serine/threonine kinase domain was less efficient at phosphorylating eIF2α following Tg treatment when compared to PERK with an intact serine at residue 704. This identified that impaired kinase activity by the S704A amino acid conversion was a cause for decreased HapB signalling compared to HapA. Furthermore, the lumenal domain of the PERK HapA protein has four cysteines that can generate two intramolecular disulfide bridges in the oxidative environment within the ER lumen. In contrast, the S136C coding variant introduced a 5^{th} luminal cysteine into the luminal domain of the HapB PERK molecule. This odd number of luminal cysteines in HapB PERK protein can cause abnormal intra and/or inter-molecular disulfide bridges compared to HapA resulting in impaired dimerization. With this in mind, it would be useful to utilize the sub HapB lines, HapC and HapD and carry out UPR induction in order to observe their differences in PERK activity.

Furthermore Carrara et al., (2015) identified that lumenal domain mutations shift the equilibrium towards a PERK monomeric population rather than a dimeric assembly, thus highly compromising the interaction between PERK monomers required for efficient dimerization. The lumenal domain of PERK spans residues Ala41 to Ile510. Based on crystallization and biochemical characterization of the lumenal domain of human PERK it has been shown that two PERK monomers are stabilized by hydrogen bonding between two interacting monomers positioned between Gly196-Leu200 and via a salt bridge utilizing Glu184 and Lys 198. Although S136 and Gln 166 has not been shown to be associated within the stabilization domain, structural analysis utilizing the HapB protein will be key in determining the positional effect of the two HapB lumenal domain mutations on dimer formation.

Furthermore, tetramer structures of PERK were shown to increase the efficiency of PERK auto-phosphorylation in comparison with dimers since it was observed to provide a sturdier platform for the phosphorylation reaction to take place (Carrara et al., 2015). Two PERK dimers come together to form closely packed tetramers via interaction of the hydrophobic core of helix α2 which includes several amino acids. In addition, these organization states were shown to impact PERK auto-transphosphorylation and signalling under ER stress conditions suggesting that the transition between dimers and tetramers might have a regulatory role in PERK signalling. Therefore, it is likely that as PERK kinase domain functions as a back-to-back dimer, perhaps tetramerization is important for enabling one PERK dimer to phosphorylate another PERK dimer during the autophosphorylation reaction. Further, a series of point mutations were generated based on the structural analysis of the tetramer subdomain. W165A was observed to partially abolish the formation of tetramers. Intriguingly this correlated with less activation of PERK

evaluated by phospho-PERK and phospho-eIF2α under ER stress conditions. This is an important finding as the W165A mutation is located adjacent to the Gln_{166} substitution within the lumenal domain of HapB with the phenotype described being identical to that observed of Myc cleaved HapB cells undergoing Tg and Tm treatment (Carrara et al., 2015). It is therefore likely that Gln_{166} also affects tetramerization and thereby affects PERK kinase domain activation resulting in reduced eIF2α phosphorylation.

PERK operates in parallel with IRE1 and ATF6 signaling effectors of the UPR. IRE1 and ATF6 initiate distinct signaling pathways and transcriptional programs to help prevent ER stress and protein misfolding. The levels of IRE1 and ATF6 in acute ER conditions in HapB cells were not different to that observed in HapA cells. However, the use of immunoblotting to identify changes within the IRE1 and ATF6 pathways were not always straightforward. Antibodies used to characterize XBP-1 and IRE1 are notoriously difficult to detect due to low endogenous levels of these proteins leading to the unavailability of good commercial antibodies for detection. The use of real-time PCR to detect the induction of mRNA of UPR target genes including XBP-1 splicing (IRE1 activation indicator) and ER-degradation-enhancing alpha-mannosidase-like protein-1 (EDEM1) and ERAD-associated E3 ubiquitin-protein ligase HRD1 (activation of ATF6) may provide an alternative approach. This is something that should be included in our further work as this would be especially useful in determining if impaired PERK kinase activity impeded the cross talk between IRE1, ATF6 and PERK. It has recently been shown that PERK drives IRE1's attenuation by promoting its dephosphorylation via the phosphatase: RPAP2 (Chang et al., 2018). RPAP2 inhibits IRE1 activity in the face of chronic ER stress, aborting cytoprotective adaptation and promoting a pro apoptotic gene: death receptor (DR) 5-mediated apoptosis. Thus, IRE1 activation as well as levels of DR5 would be crucial in identifying if HapB impedes this cross talk resulting in increased cell death following chronic ER stress conditions.

Analysis of BiP activity and ER morphology following UPR activation did not yield any haplotype specific differences following treatment. This is not surprising given that we failed to optimize the conditions for the three drugs used and hence, did not observe a significant increase in eIF2alpha phosphorylation in our immunoblots indicative of the absence of activation of the UPR. Furthermore, BiP dissociation from PERK should also not be taken as confirmation of UPR activation. Thus, it is vital that ER stress conditions are first optimized and confirmed before embarking on examining levels of total BiP via immunoblot. Optimization of the BiP antibodies for immunoblot therefore is vital, along with obtaining and testing primers for the specificity of BiP. However, levels of ER stress comparable to those induced by the pharmacological agents utilized in our study are highly unlikely to be encountered by cells in natural situations. On the other hand, cells of long-lived organisms such as those in some non-renewing tissues of mammalian species must ensure the consequences of accumulation of misfolded proteins in the ER over relatively

long periods of time. Hence, we speculate that the divergent role of HapB presented herein using potent acute pharmacological agents, might be a gross over-representation of PERK haplotype specific effects observed in the general population. PERK HapB is widespread with 30% frequency in populations of Northern-European descent and hence it is unlikely that HapB homozygous individuals face such severe consequences of reduced cell viability following ER stress (Liu et al., 2012).

Although we were unable to show a significant effect on Myc-cleaved HapB PERK reducing PERK activity and thereby diminishing phosphorylating eIF2α resulting in compromised cell viability, we did observe a strong trend towards this finding. As we have only tested the myc cleaved HapB cells, it is now crucial we bring in the passage 1 induced HapB cells to compare the UPR response following ER stress induction in both myc cleaved and uncleaved cell lines. This will shed great light on indicating if the reduced PERK activity trend that we observed is in fact due to myc cleavage or as a result of the three snps inherent to HapB PERK. Furthermore, considerable time needs to be spent optimising both acute and chronic conditions to ensure that the dosages chosen for each drug is able to elicit a clear significant increase in eIF2alpha phosphorylation. The concentrations and durations of the three drugs that were used in this study were not effective in eliciting a significantly strong UPR response and hence results can only be validated following confirmation of UPR induction. Apart from testing acute dosages, it will also be beneficial to test chronic drug dosages which would activate the long-term/apoptotic ER stress response pathway. Utilising lower concentrations for longer durations of time compared with the shorter acute stress conditions will enable us to directly compare how the PERK pathway activation differs following both chronic and acute ER stress conditions. This will also then enable us to identify if HapB cells react differently following different ER stress conditions. However, with chronic UPR induction, experiments need to be planned carefully to allow for the fact that IRE1 and/or ATF6 pathways may be activated if PERK phosphorylation is impaired and cell health is impaired. Finally, careful consideration must be made in choosing the appropriate controls. First, for each experimental condition tested we should include the untagged full length HapA and HapB PERK, passage 1 myc tagged HapA and HapB PERK as well as the passage 2 myc cleaved HapA and HapB PERK for direct comparison. Second, we need to include the Flp-In 293 cells (uninduced cell line) as a control for Doxycycline in each experimental condition, to observe the effect of Dox on the UPR response. As the use of Dox in our Tet inducible system may impede the UPR response pathway, we should also think of creating PERK stable cell lines in a non-inducible cell model system to test the true effects of PERK HapA and HapB following ER stress induction.

6 The role of *EIF2AK3* coding haplotypes on tau proteostasis

6.1 *Overview*

Two tau isoform cDNAs which were cloned into plasmid mammalian expression vectors were transiently transfected to enable the expression of full length 2N4R-tau (wild-type) and mutant 2N4R-tau (P301L) in passage 2 (P2) HapA, myc cleaved HapB and Flp-In™ 293 cells. We chose to express P301L mutated tau, among the dominantly inherited *MAPT* mutations, because of its high propensity to aggregate (Clavaguera et al. 2009, Allen et al. 2002, Bellucci et al. 2004, Scattoni et al. 2010). Also, the transgene of the rTg4510 mouse from which we derived brain homogenate for seeding carries the P301L mutation. Following overexpression of the 2N4R-tau (wild-type) and 2N4R-tau (P301L) mutant and with Dox induction of PERK, we examined whether perturbing PERK activity -as seen in myc cleaved HapB cells- affects tau aggregation. First, we carried out preliminary assessments of PERK haplotype specific differences for changes in tau protein as well as markers for pathological conformation (MC1 and ALZ-50) and phospho epitopes (AT8 and PHF1) of tau following over-expression of 2N4R-tau (wild-type) and 2N4R-tau (P301L) for seven days. Furthermore, differences of P2 PERK HapA and myc-cleaved HapB on tau aggregation relied on assessment of thioflavin S (ThS) fluorescence resulting from tau aggregates and quantification of fibrillar tau in sarkosyl insoluble fractions on western blots. We observed no detectable differences in the sarkosyl-insoluble pathological tau between P2 HapA and myc-cleaved HapB cells transfected with 2N4R-tau (wild-type) or 2N4R-tau (P301L) tau. We also did not observe differences in ThS fluorescence with 2N4R-tau (P301L) versus 2N4R-tau (wild-type) overexpressed for 7 days. This indicated that prolonged overexpression of 2N4R-tau (P301L) alone was insufficient to induce aggregation in HEK-293 cells expressing PERK. We then investigated the potential of inhibition of proteasome activity (with the use of MG132) and seeding of tau propagation mechanisms (using pooled brains from rTg4510 mice) to promote the aggregation of 2N4R-tau (P301L) tau. We failed to induce tau aggregation using MG132 but successful in identifying a greater amount of sarkosyl-insoluble tau in 2N4R-tau (P301L) transfected P2 HapA, myc-cleaved HapB and Flp-In 293 cells which were transfected with the brains from rTg4510 mice. However, a connection between PERK haplotype variation and tau aggregation could not be established using immunoblot but electron microscopy identified a higher number of tau filaments exclusively in 2N4R-tau (P301L) overexpressing Myc cleaved HapB cells transfected with rTg4510 mouse brain homogenate. Using this cell culture model of tau aggregation, we next examined if PERK is activated during the tau aggregation process but found no indication of phosphorylation of PERK or phosphorylation of eIF2α in P2 PERK impaired HapB cells or HapA cells transfected with rTg4510 mouse brain homogenate.

6.2 *Background*

The possible significance of PERK in tauopathies was first highlighted when increased PERK activation was shown in AD, FTD and PSP patient brains as well as in tau transgenic mice. This finding supported recent evidence that PERK kinase-associated pathways could play an important role in neurodegenerative disease (Hoglinger et al., 2011; Hoozemans et al., 2005; Nijholt et al., 2013). In these brains, the UPR was shown to be activated in neurons containing diffusely distributed phospho-tau, but not in neurons with densely aggregated tau (Hoozemans et al., 2005; Hoozemans et al., 2012). The mechanisms contributing to ER stress and PERK activation in neurodegeneration are not entirely clear, but several recent studies suggest it is likely that soluble tau conformers lead to tau-induced ER stress (Abisambra et al., 2013). This is important because recent evidence suggests that soluble oligomeric tau, but not insoluble tau, is most likely to be responsible for tau-induced neurotoxicity (O'Leary et al., 2010; de Calignon et al., 2012). Therefore, the formation of soluble tau intermediates may activate a cell damage pathway that is only visible pathologically using ER stress markers. However, in our work, although MG132 and transfection of tauopathic mouse brain lysate was used to induce tau aggregation we failed to observe an increase in either sarkosyl soluble or the insoluble fractions in tau over-expressing PERK cell lines. It is also interesting to note that PERK activates GSK3ß, a kinase that directly phosphorylates tau at epitopes commonly identified in tau aggregates (Nijholt et al., 2013). Moreover, tau phosphorylation has been observed following UPR activation in primary neuronal cultures from rats (Ho et al., 2012). This supports the possibility that the UPR may initiate two key features of tau pathology by generating abnormally phosphorylated tau species and promoting tau aggregation. As such, pharmacological inhibition of PERK has emerged as a potential strategy to ameliorate neurodegeneration (Hughes and Mallucci., 2018).

One study to date has compared the effect of coding haplotypes of PERK on tau function and dysfunction (Yuan et al., 2018). They observed that tunicamycin (Tm)-induced ER stress led to an increase in total tau and hyperphosphorylated tau in iPSC-derived neurons carrying the HapB PERK mutations compared to iPSC-derived neurons carrying the PERK HapA alleles. These findings suggest that due to the inability of HapB PERK to attenuate translation, synthesis of tau protein could contribute to accumulation of tau tangles. Consistent with this, pharmacological PERK activation has been shown to attenuate aggregation and toxicity of PSP-related tau mutants in mouse models (Bruch et al., 2017). Thus, while significant focus has been directed to the pathological importance of overactive or chronic PERK signalling in disease, it is clear that impaired PERK activity also promotes tau pathogenesis. We therefore aimed to test if impaired PERK activity observed in our P2 myc-cleaved HapB PERK cells, promotes the presence of misfolded tau and determine the mechanism by which this leads to cellular dysfunction.

6.3 *No increase in tau-mediated toxicity in PERK cells caused by the 2N4R-tau (P301L) mutation when expressed for 7 days*

To explore the toxic effect of 2N4R-tau (wild-type) and 2N4R-tau (P301L) overexpression on cell viability, we used the CellTiter-Glo Luminescent Cell Viability assay. We investigated whether PERK overexpression and, in particular, impaired Myc-tag cleaved PERK HapB cells could increase tau toxicity in our targeted expression system. We expressed both the 2N4R-tau (wild-type) and mutant 2N4R-tau (P301L) in the P2 cell lines of PERK HapA, Myc cleaved HapB and Flp-In^{TM} 293 cells. Dox induction was carried out 24 hours post tau transfection and cell viability measured for 1- 7 days. Triplicate wells containing cells transfected with either 2N4R-tau (wild-type) or 2N4R-tau (P301L) were included in each replicate and three biological replicates were carried out. Viability of untransfected Flp-In 293 cells was normalised to 100 % as this contained the largest values in our data set. Viability of transfected cells were then plotted as a percentage change against the untransfected Flp-In 293 cells. Data were analysed using a Friedman's test. Cell death, although not statistically significant, was observed in all three cell lines following 24 h of 2N4R-tau (wild-type) and 2N4R- tau (P301L) over-expression (Figure 59). A further decrease in cell viability was not observed between 48 h to 7 days post transfection in either the 2N4R-tau (wild-type) tau or mutant 2N4R-tau (P301L) over-expressing PERK cell lines when compared to the untransfected Flp-In 293 cells. As the empty expression vector (pCMV3.1 mammalian vector) was unavailable and hence not included in the cell viability assay, we are unable to conclude if increased cell death, 24 h post-transfection, is a consequence of tau overexpression or resulting from toxicity of the vector. Nevertheless, these results suggest that prolonged overexpression of either 2N4R-tau (wild-type) or 2N4R-tau (P301L) in Myc cleaved PERK HapB cells did not cause any loss of cell viability compared to HapA and naïve Flp-In 293 cells. Considering these data and the intention to examine long-term modifications of tau, 7 days was designated as the optimal period for tau overexpression, whilst considering the time limitations of the project.

6.4 2N4R-tau (P301L) overexpression alone for 7 days is insufficient to induce tau aggregation in PERK cells

Our transiently transfected cells express 2N4R-tau (wild-type) and 2N4R-tau (P301L) without genomic integration of the expression plasmids. Thus, the plasmids are not replicated and will only be expressed for a finite period of time. We examined tau levels at 24 h and 7 days post-transfection of 2N4R-tau (wild-type) and 2N4R-tau (P301L) in P2 HapA, Myc-cleaved HapB and Flp-In 293 cells (Figure 60). Dox induction in PERK cells was carried out 24 h post tau transfection. A well-characterised rabbit polyclonal antibody raised against the C-terminal 243-441 residues of tau (DAKO) was used to confirm the presence of total tau and mouse monoclonal

beta-actin was included as the loading control. Untransfected cells were included as a negative control. As shown in Figure 60, the total tau antibody detected both overexpressed tau variants as a band at approximately 55 kDa band both at 24 h and 7 days post-transfection. The multiple bands and smear observed around the 55 kDa mark are due to mobility shifts from extensive phosphorylation of tau at serines and threonines as well as tyrosines. However,, a serious limitation in this experiment are the saturation of the tau bands. Accurate estimation of differences in tau protein abundance between day 1 and day 7 therefore could not be made as normalisation with actin performed under these circumstances will not account for true differences in tau protein abundance between day 1 and day 7 as band intensity will not increase proportionately to indicate protein abundance and will thereby lead to either over-or-under estimation of the magnitude of tau protein abundance. Therefore, normalised data obtained using actin was not conducted under these circumstances as it cannot be relied upon and needs to be interpreted with extreme caution. However, for the purpose of this study, we selected day 7 as the duration for which PERK and Flp-In 293 cells are able to tolerate the tau overexpression as both cell viability and tau protein over expression was not overtly decreased at this chosen date.

Thioflavin S is a fluorescent dye which preferentially binds β-sheets of pathological tau aggregates and is commonly used to detect aggregated amyloidogenic proteins (Khlistunova et al., 2006). It non-selectively binds beta sheet contents of proteins, such as those in tau oligomers. Upon binding, ThS undergoes a characteristic blue shift of its emission spectrum. Conversely ThS binding to the monomeric forms will not elicit a blue shift and therefore cannot be detected with florescent microscope. Thus, ThS staining provides a quick alternative to screen for tau aggregate staining as the intensity of fluorescence allows good visualization of small amounts of amyloid deposits. However, one drawback about ThS staining is the lack of specificity. Many other tissue components including containing extensive beta sheets, such as fibrinoids, hyaline, keratin, etc, have a rather affinity for this dye.

In order to determine if induction of PERK caused ThS fluorescence and if the number of ThS positive cells differed between the PERK haplotypes, P2 HapA and myc-cleaved HapB cells were transfected with expression plasmids for 2N4R-tau (wild-type) and 2N4R-tau (P301L), Dox induced 24 h post tau transfection and cultured for 7 days. Fluorescent microscopy to detect ThS foci was carried out and co-localization with tau was detected with a fluorescently tagged secondary antibody (Alexa Fluor 596) against total tau. Although we observed some ThS positive spots in those cells overexpressing tau, there was no evidence of tau aggregation as the ThS positive spots did not co-localize with any tau accumulations (Figure 61). Thus, we conclude that in our cell model PERK induction did not result in tau aggregation as no difference in the number of ThS spots was observed between HapA, myc cleaved HapB cells or Flp-In 293 cells.

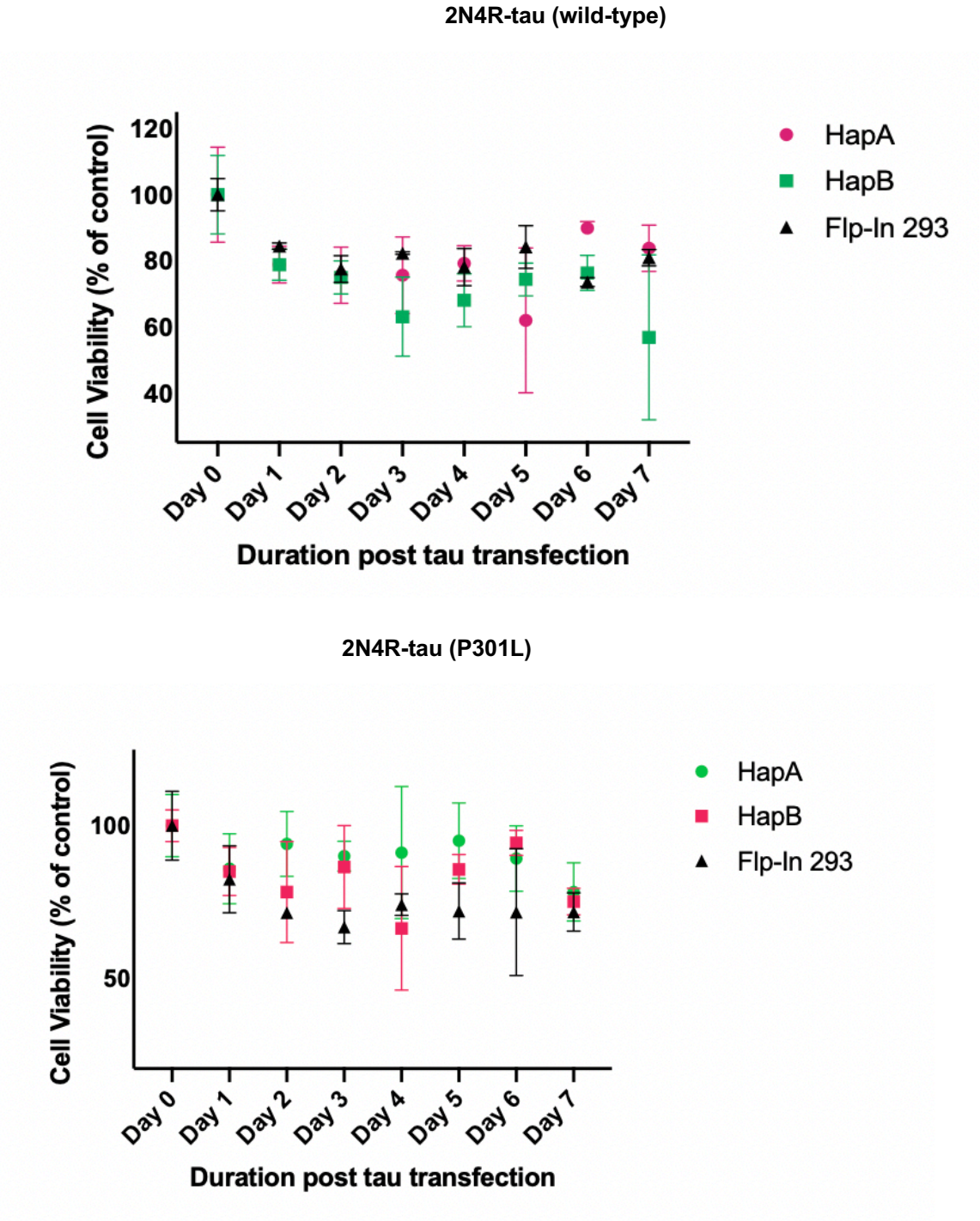

Figure 59. Cell viability assay following overexpression of 2N4R-tau (wild-type) and 2N4R-tau (P301L) in PERK and Flp-In 293 cells. Cell viability was comparable in all three cell lines in the first 24 h following tau transfection with only a modest decrease being observed thereafter. A Friedman analysis of variance was applied and indicated that cell death was not significantly altered between days 1-7 in either of the two tau isoforms 2N4R or 2N4R (P301L) transfected into the three cell lines of HapA, HapB or Flp-In 293 (F_r = 7.750, p = 0.9519). Data is expressed as mean of 3 experiments ± SEM.

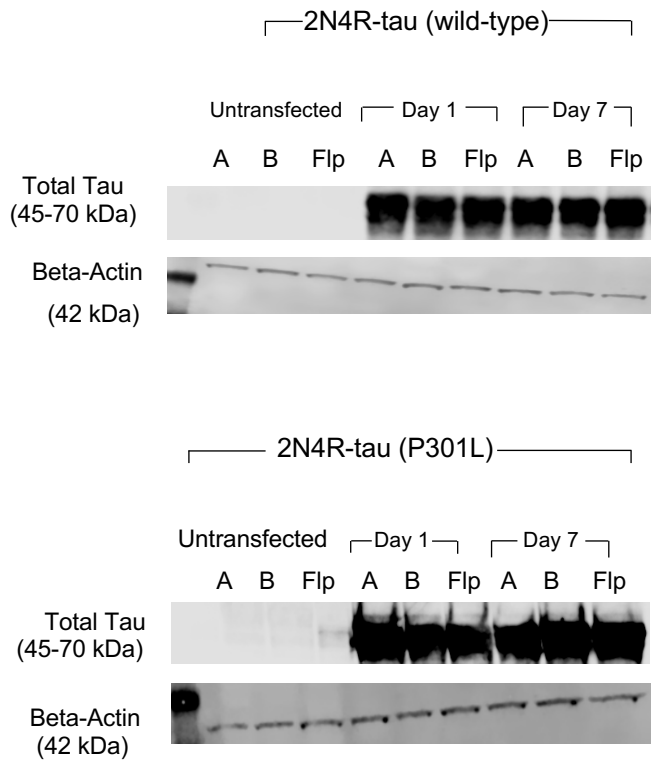

Figure 60. Consistent overexpression of tau over 7 days irrespective of PERK haplotype. P2 PERK HapA, myc-cleaved HapB and control Flp-In 293 cells were transfected transiently with expression plasmids for wild-type and 2N4R-tau (P301L). 24 h later, dox induction was carried out and cells kept in culture for either 24 h or 7 days. Cells were then lysed, and tau was detected using western blot. A rabbit polyclonal anti-tau antibody (DAKO) which recognises the amino acids 243-441 of tau was used for total tau detection and mouse beta-actin included as a loading control. Total tau levels at both 24 h post transfection and 7-days post transfection both produced a strong band indicating that tau over-expression remained strong after one week in culture. However, the strong total tau bands have become saturated and thereby underestimate protein abundance and therefore they fall outside the linear range of detection. Band intensity will therefore no longer increase proportionately to indicate protein abundance. As a result, the signal intensity of the saturated total bands at both day 1 and day 7 appears similar in both 2N4R and 2N4R (P301L). Therefore, each of the high-intensity data points were not used and normalisation not carried out.

Untransfected

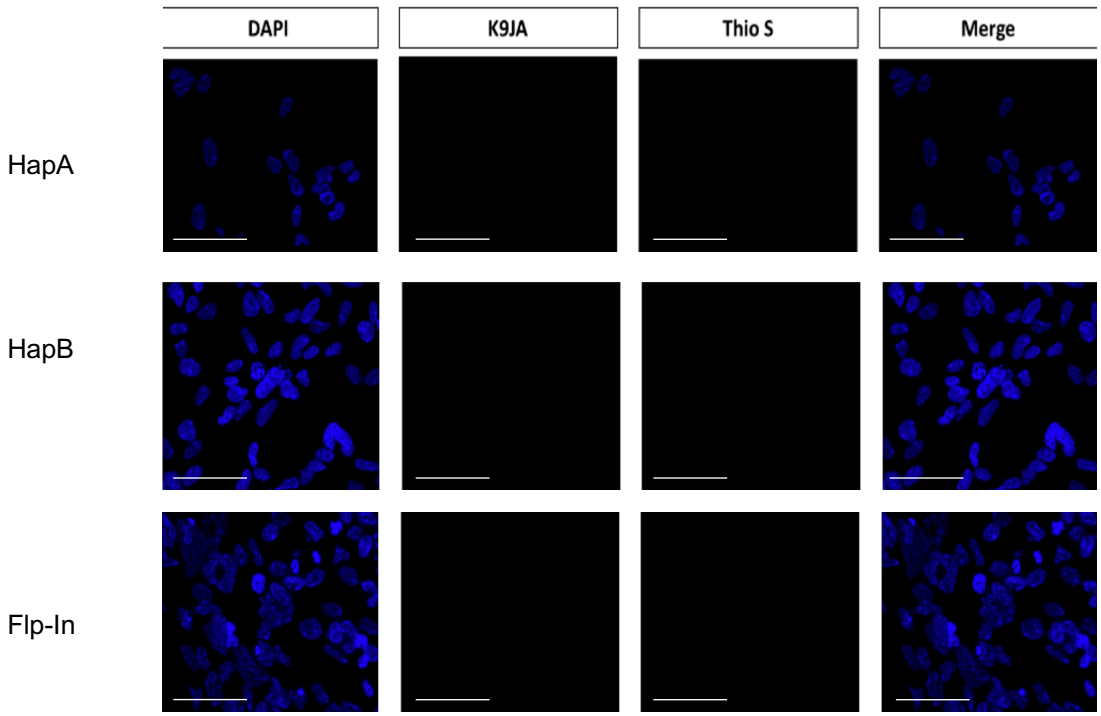

2N4R tau

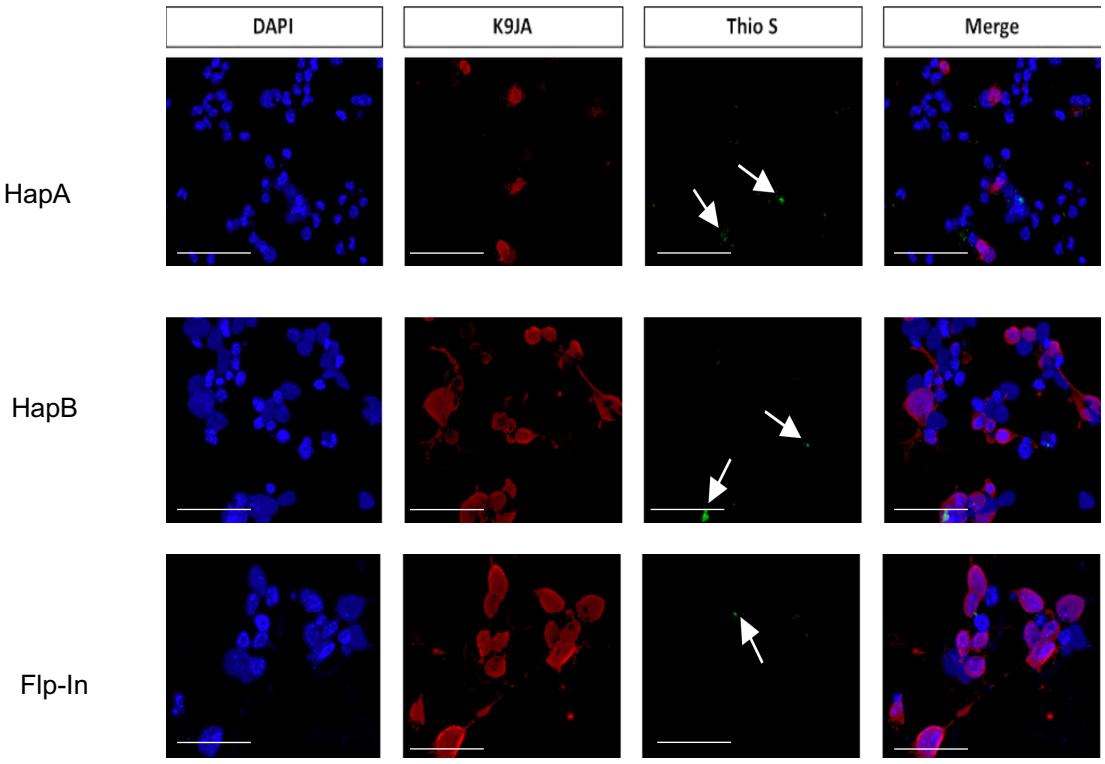

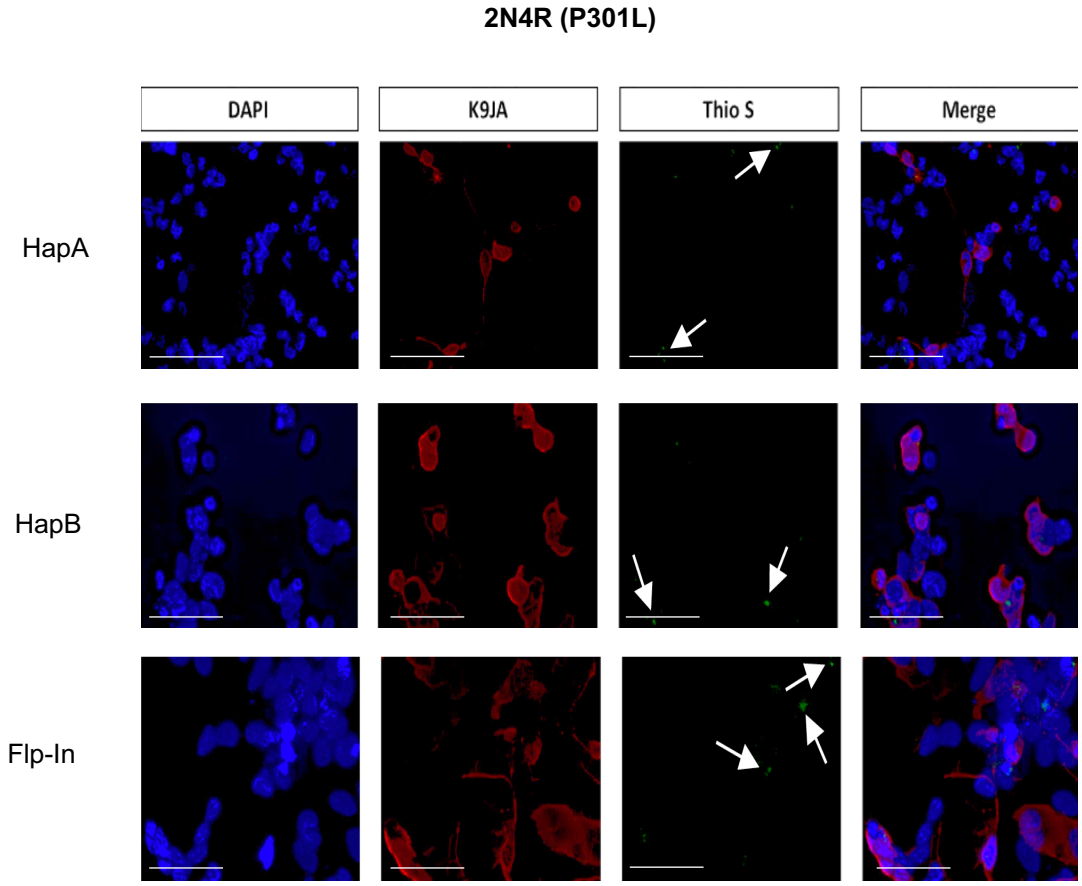

Figure 61. Induction of PERK does not result in tau aggregation: P2 PERK HapA and myc-cleaved HapB cells and control Flp-In 293 cells were transfected with expression plasmids for wild-type and 2N4R-tau (P301L). 24 h later Dox induction was carried out and cells cultured for 7 days. Cells were then fixed in 4% PFA and incubated with ThS using the conditions mentioned in Chapter 2. Overexpressed tau was immunolabelled with rabbit anti-tau antibody (K9JA) and was observed to be present within the nuclei. This is hardly surprising given that although tau is mainly known as an axonal MT-associated protein, a nuclear form of non-phosphorylated tau has been characterised in several cell lines including neurons and is mostly seen in the nucleus (Violet et al., 2014). To visualise cells with tau inclusions fluorescence resulting from aggregates binding to ThS was monitored. Untransfected cells were used as a negative control and nuclei stained with DAPI (blue). Although ThS fluorescent spots (green) were observed in the tau transfected cells, they did not co-localise with any tau accumulations (red). All scale bars at 50 μm.

6.5 *Tau phosphorylation in cells overexpressing 2N4R-tau (wild-type) and 2N4R-tau (P301L)*

We next sought to determine if cleaved HapB PERK contributed to tau aggregation and to do this we compared the levels of tau phosphorylation in the P2 PERK HapA and myc-cleaved HapB cells. Hyperphosphorylation of tau is thought to be one of the key mechanisms responsible for the normal loss of function of tau which is to promote microtubule assembly and maintain microtubule structure. This biological activity of tau is regulated by its degree of phosphorylation. In tauopathic brain, tau is abnormally hyperphosphorylated. The hyperphosphorylation inhibits the activity of tau to promote microtubule assembly and unlike normal tau, the hyperphosphorylated and oligomeric tau has been shown to sequester/capture normal tau and template it into filaments *in vitro* (Alonso et al., 1994).

Hyperphosphorylation of soluble tau is known to precede the formation of sarkosyl-insoluble, phosphorylated tau filaments (Delobel et al., 2008). Thus, P2 HapA, myc cleaved HapB and Flp-In 293 (control) cells were transiently transfected with expression plasmids for 2N4R-tau (wild-type) and 2N4R-tau (P301L). 24 h later, PERK cells were Dox induced and cells cultured for 7 days. Insoluble, fibrillar tau was isolated by high-speed (100,00 x g) centrifugation following incubation in presence of 1% sarkosyl resulting in the insoluble pellet ('sarkosyl-insoluble fraction') and the supernatant ('sarkosyl-soluble fraction'). Total lysates recovered in fractionation buffer, sarkosyl-soluble and sarkosyl-insoluble fractions were resolved by SDS-PAGE. Untransfected cells were included as a negative control. Western blot analyses with the primary antibodies anti-tau polyclonal (K9JA, Dako), PHF-1, ALZ50, and beta-actin were carried out. PHF-1 antibody recognises the phosphorylated epitopes at Ser 396 and/or Ser 404. Similarly, ALZ50 raised to paired helical filaments, recognizes early abnormal conformations of tau by targeting amino acids 2-10 and 312-342 of the tau protein.

Following normalisation against beta actin, both 2N4R-tau (wild-type) and 2N4R-tau (P301L) exhibited similar levels of tau in HapA, HapB and Flp-In 293 cells 7 days post-transfection. With comparable levels of tau, we next sought to assess the phosphorylation status of the exogenous tau. Antibodies PHF1 and ALZ50 labelled two immunoreactive bands at around 50 kDa for both tau variants in P2 HapA and myc-cleaved HapB cells as well as Flp-In 293 cells (Figure 62), indicating that exogenous tau isoforms were phosphorylated. However, there were no differences in phospho-tau levels between the wild-type and mutant exogenous tau suggesting that this is due to normal phosphorylation of the overexpressed tau. We also assessed levels of sarkosyl-insoluble tau (Figure 63). As with lysates sarkosyl-soluble tau levels (total and phospho-tau) were similar between cell types and tau variants (Figure 64). Trace amounts of tau were observed in the sarkosyl-insoluble fractions but without any discernible difference between cells and tau

variants (Figure 64). However, this insoluble, fibrillar tau did not stain for the pathological ALZ50 or PHF1 epitopes. We could not ascertain if tau staining could have been due to contamination with soluble tau.

6.6 Tau aggregation is not observed in P2 HapA or myc-cleaved HapB cells following inhibition of the ubiquitin-proteasome pathway

We next sought to determine if we could induce tau aggregation by inhibition of the proteasome. Two major proteolytic systems contribute to protein degradation inside cells, the ubiquitin–proteasome system (UPS) and the autophagy–lysosomal system (Wang et al., 2009). The identification of ubiquitin in PHFs in AD brain has led to the speculation that the ubiquitin–proteasome system may have an important role in tau degradation (Mori et al., 1987). Furthermore, it has recently been shown that phosphorylated tau is more resistant than its non-phosphorylated counterpart to proteolytic degradation (Johnson, 2006). Since then, a number of studies have investigated the effect of proteasome inhibition on tau metabolism. Some groups reported that proteasome inhibition caused elevation of tau (David et al., 2002; Zhang et al., 2005), whereas other studies suggested that tau is not a proteasome substrate (Feuilette et al., 2005; Delobel et al.,2005; Brown et al., 2005). We aimed to determine if proteasome inhibition could cause accumulation of aggregated tau in our cell model and test if tau is preferentially aggregated in myc cleaved HapB cells following inhibition of the proteasome. The pproteasome which is a large multi-subunit protease complexes, is present in both the cytoplasm and nucleus of all eukaryotic cells. The 26S proteasome is composed of two functional components: a 20S catalytic and two 19S regulatory subunits. The protease activity resides in a channel at the center of the 20S subunit and exhibits 3 distinguishable enzymatic activities: chymotrypsin-like, trypsin-like and caspase-like activities (Orlowski et al., 2000). MG132 effectively blocks this proteolytic activity of the 26S proteasome complex by being a potent inhibitor of the chymotryptic-like activity (Lee and Goldberg., 1998).

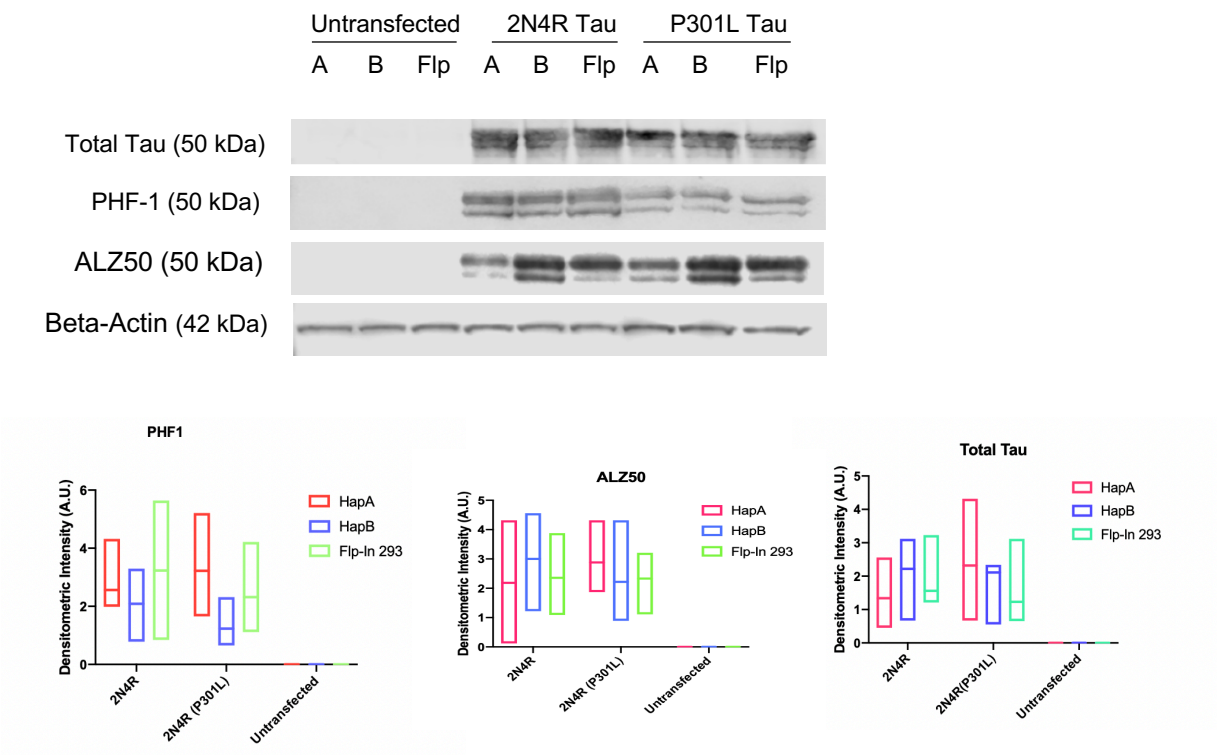

Figure 62. Total tau and pathological tau are observed in total PERK cell lysates following 7-days post-transfection. P2 HapA, myc-cleaved HapB and Flp-In 293 cells were transfected with expression plasmids for 2N4R-tau (wild-type) and 2N4R-tau (P301L). Dox induction was carried out 24 hours later and cells cultured for a further seven days. Cell lysates were immunoblotted and were probed for total tau (anti-tau antibody K9JA), phosphorylated tau (PHF1) and pathologically misfolded tau (ALZ50). Beta-actin was used as loading control. Total tau, PHF1 and ALZ50 levels in 2N4R-tau (wild-type) and 2N4R (P301L) were plotted as a box plot of the median of 3 independent experiments run in triplicate, enabling the median observation of each densitometric analysis (line in the middle of the box) and the 25th and 75th percentiles (bottom and top limits of the plot) following normalisation against the corresponding beta-actin to be visualised. No significant differences in total tau ($H(2)= 0.07353$, $p=>0.999$) or PHF1 ($H(2)=3.7814$, $p=0.2$), and ALZ50-positive tau ($H(2)= 0.28517$, $p=0.9333$) were observed in 2N4R or 2N4R (P301L) transfected HapA, HapB or Flp-In 293 cells following PERK induction using the non-parametric Kruskal Wallis test.

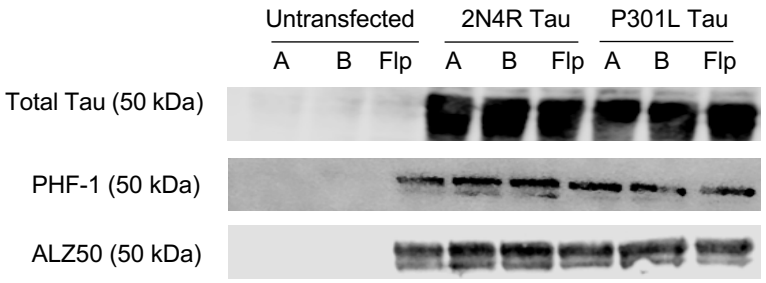

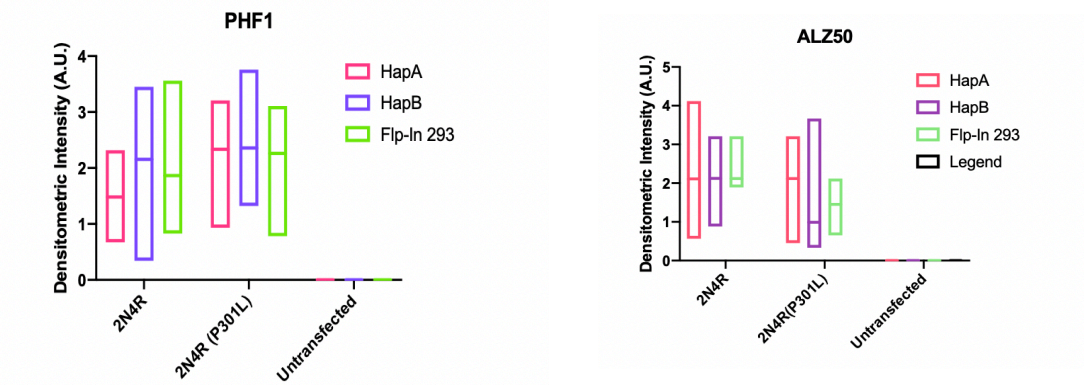

Figure 63. Pathological tau in sarkosyl-soluble fractions of HapA, HapB and Flp-in 293 cells 7-days post-transfection. P2 HapA, myc-cleaved HapB and Flp-In 293 cells were transfected with expression plasmids for 2N4R-tau (wild-type) and 2N4R-tau (P301L). 24 hours later dox induction was carried out and cells cultured for a further seven days. Cell lysates were subject to sarkosyl extraction and the supernatants (sarkosyl-soluble fraction) were immunoblotted and probed for total tau (anti-tau antibody K9JA), phosphorylated tau (PHF1) and pathologically misfolded tau (ALZ50). PHF1 and ALZ50 levels in 2N4R-tau (wild-type) and 2N4R (P301L) were plotted as a box plot of the median of 3 independent experiments run in triplicate, enabling the median observation of each densitometric analysis (line in the middle of the box) and the 25th and 75th percentiles (bottom and top limits of the plot) following normalisation against the corresponding beta-actin to be visualised. No significant differences in PHF1 ($H(2)=0.8571$, $p=0.8$), and ALZ50-positive tau ($H(2)= 0.2857$, $p=0.9333$) were observed in 2N4R or 2N4R (P301L) transfected HapA, HapB or Flp-In 293 cells following PERK induction using the non-parametric Kruskal Wallis test.

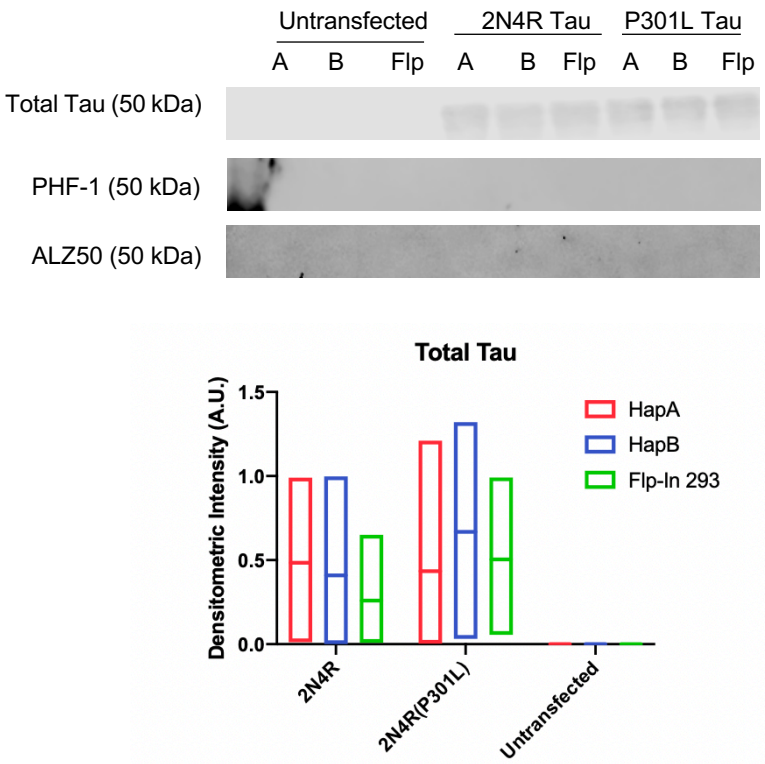

Figure 64. Sarkosyl-insoluble tau is detected in cells 7-days post tau-transfection. P2 HapA, myc-cleaved HapB and Flp-In 293 cells were transfected with expression plasmids for 2N4R-tau (wild-type) and 2N4R-tau (P301L). Dox induction was carried out 24 hours later on PERK cells and cells cultured for seven days. Cell lysates were subject to sarkosyl extraction and the pellets (sarkosyl-insoluble fraction) were immunoblotted and probed for total tau (anti-tau antibody K9JA), phosphorylated tau (PHF1) and pathologically misfolded tau (ALZ50). Total tau levels in 2N4R-tau (wild-type) and 2N4R (P301L) were plotted as a box plot of the median of 3 independent experiments run in triplicate, enabling the median observation of each densitometric analysis (line in the middle of the box) and the 25th and 75th percentiles (bottom and top limits of the plot) following normalisation against the corresponding beta-actin to be visualised. No significant differences in total tau ($H(2)= 0.857$, $p=0.9333$) were observed in 2N4R or 2N4R (P301L) transfected HapA, HapB or Flp-In 293 cells following PERK induction using the non-parametric Kruskal Wallis test.

We first compared the cytotoxicity of 0-1 μM MG132 for 24 h in P2 myc-cleaved HapB and HapA cell lines as well as Flp-In 293 cells using the CellTiter-Glo Luminescent Cell Viability Assay. Untreated cells were used as a negative control and untreated Flp-In 293 cell viability was normalized to 100 % as this contained the largest values in our data set. Subsequent measurements were plotted as a percentage change against the untreated Flp-In 293 cells. Treatment with 0-1 μM MG-132 resulted in a dose-dependent decrease in cell viability of all three cell lines tested, with myc-cleaved HapB cells not showing increased sensitivity to MG132 than HapA or Flp-In 293 cells (Figure 65). At all doses, complete cell death was observed beyond 24 h (Figure 66) whereas, within 24 h, 750 nM of MG132 caused more than 50 % cell death in all three cell lines with 1000 nM causing almost complete cell loss. Based on this, we opted for 24 h treatment with 750 nM MG132. Although this concentration caused significant cell death, we hoped that such a pronounced effect on inhibition of the proteasome as observed by increased cell death, will enable us to capture the smaller aggregated tau oligomers which may otherwise be cleared via the proteasomal pathway at lower MG132 concentrations.

To explore if proteasome inhibition could lead to accumulation of insoluble tau, 2N4R-tau (wild-type) and 2N4R-tau (P301L) tau transfected P2 HapA, myc-cleaved HapB and Flp-In 293 cells were cultured for 24 h in the presence of 0.75μM MG132. Dox induction was carried out the next day and the cells left in culture for a further 6 days in the absence of MG132 as prolonged exposure to MG132 was shown to be toxic to the cells. Sarkosyl soluble and insoluble fractions were obtained and probed for total tau, PHF1 and ALZ50. Densitometric analysis was performed by plotting a box plot for the median values for PHF1 and ALZ50 in the soluble fraction which had been normalised against the corresponding band for total tau. The median densitometric intensities were then plotted for PHF1 and AZL50 obtained from 2N4R or 2N4R (P301L) transfected MG132 treated and untreated HapA, HapB and Flp-In 293 cells.

On this occasion, we did observe a trend of increased sarkosyl-insoluble tau in cells overexpressing 2N4R-tau (P301L) as compared to 2N4R-tau (wild-type) and also in MG132 treated cells. However, these differences were not significant (Figure 67). As before, we also could not detect PHF1 or ALZ50-positive tau in the insoluble fraction. Levels of soluble tau remained unchanged following MG132 treatment, without any differences in the PHF1 and ALZ50-positive tau (Figure 68). Under the experimental conditions we selected with proteasomal inhibition, we did not observe increased accumulation of fibrillar tau. It may be necessary to optimise this experiment considering the possibility that the long period of culture (6 days) after MG132 withdrawal could have resulted in clearance of any tau aggregates.

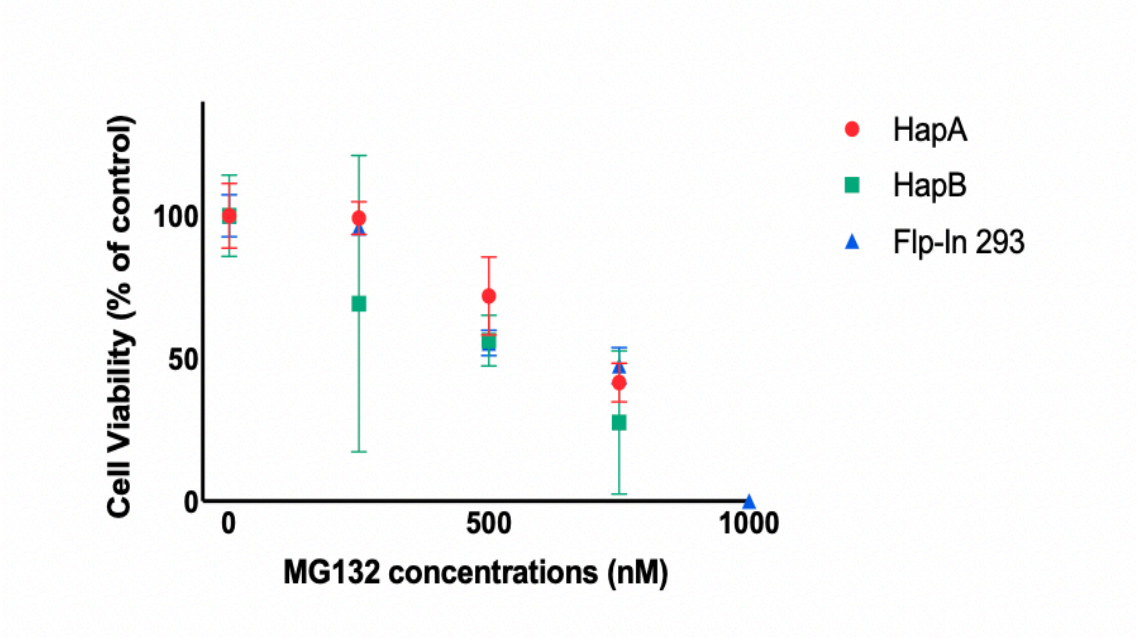

Figure 65. Cytotoxicity of MG132 on P2 PERK HapA, myc-cleaved HapB and Flp-In 293 cells. Passage 2 HapA, myc-cleaved HapB and Flp-In 293 were treated with 250, 500 750 or 1000 nM MG-132 for 24 h after which cell viability was measured using the CellTiter-Glo Luminescent assay. Three independent experiments were carried out in triplicate for each condition. Cell viability of untreated Flp-In 293 cells were normalized to 100 % and subsequent measurements plotted as a percentage change against the untransfected Flp-In 293 cells. Amongst the four concentrations tested, 750 nM MG-132 was chosen as a preliminary test concentration to induce inhibition of the UPR, although it showed more than 50 % cell death. Results represent the mean of 3 independent experiments ± SEM.

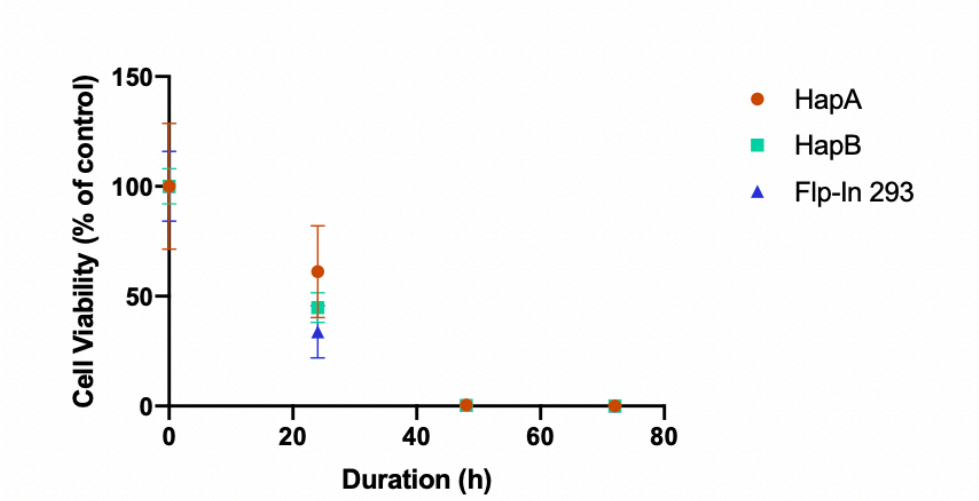

Figure 66. Cytotoxicity of treatment durations of 0.75 µM MG-132. P2 HapA, myc-cleaved HapB and Flp-In 293 cells were treated with 0.75 µM MG-132 for 24, 48 and 72 h before cell viability was measured. Three independent experiments were carried out in triplicate for each condition. Untreated Flp-In 293 cells were used as the negative control and cell viability of untreated Flp-In 293 cells normalised to 100 %. Subsequent results were plotted as a proportional change against the untreated Flp-In 293 cells. Treatment durations exceeding 24 h showed complete loss of cell viability in all three cell lines. Thus, 24 h of 0.75 µM MG132 treatment was chosen as the optimal dosage to induce inhibition of the proteasome. Although this test concentration significantly reduced cell viability, complete cell death was not observed in either of the three cell lines at this duration and was therefore chosen as a preliminary concentration to test for tau aggregation following impaired UPS inhibition. Results represent the mean of 3 experiments ± SEM

6.7 Seeded aggregation of 2N4R-tau (P301L) with rTg4510 MAPT transgenic mouse brain lysate

Tau pathology does not appear randomly throughout the brain, but rather progresses along distinct neural networks. This progression takes place by transcellular spread of pathological tau seeds via neural connections (Frost et al., 2009; Guo and Lee 2011., Kfoury et al., 2012). It has previously been shown that tau aggregates—or seeds—serve as this agent of spread, transmitting the aggregation prone state from cell to cell via prion-like mechanisms (Frost et al., 2009). As we were unable to induce tau aggregation using MG132, we next tested if we could encourage seeded aggregation of the overexpressed tau by incubation with brain lysates of the rTg4510 transgenic mouse that overexpresses the P301L mutant tau. Since its initial description in 2005 (Ramsden et al., 2005; Santacruz et al., 2005), this mouse has become a popular model, as it phenocopies the tau pathology and pronounced neurodegeneration observed in human tauopathies. rTg4510 mice express high levels of mutant tau, and they develop progressive age-related neurofibrillary tangles, neuronal loss, and behavioural impairments (Ramsden et al., 2005). Other users in our lab have used biosensor cells and demonstrated very high seeding activity of the brain lysates of this mouse.

Passage 2 HapA, myc-cleaved HapB and Flp-In 293 cell lines expressing 2N4R-tau (wild-type) and 2N4R-tau (P301L) were transfected with the rTg4510 (P301L) mouse brain lysate in the presence of Lipofectamine 3000 after which time culture medium was replaced to enable PERK activation with the use of Dox and cells cultured for a further six days. Conditions enabling the seeding of tau using the rTg4510 mouse brain lysate had previously been characterized in Flp-In 293 cells over-expressing 2N4R-tau (P301L) (Hamilton et al., 2018 unpublished; Figure 69). Cellular toxicity and levels of sarkosyl-insoluble tau was measured each day up to 7 days post transfection of rTg4510 brain lysate. It was shown that a robust signal of aggregated hyperphosphorylated tau was observed 7 days post transfection with rTg4510 mouse brain lysate. Therefore, we compared sarkosyl-insoluble and sarkosyl soluble fractions in our P2 PERK cells 6 days post rTg4510 mouse brain lysate transfection. Flp-In 293 cells transfected with only the rTg4510 mouse brain lysate was used as a negative control. Total tau from the sarkosyl-insoluble and soluble fractions of mouse brain transfected 2N4R-tau (wild-type) transfected Flp-In 293 cells were plotted as a box plot and the median tau levels of mouse brain lysate transfected P2 myc-cleaved HapB and HapA cells were plotted.

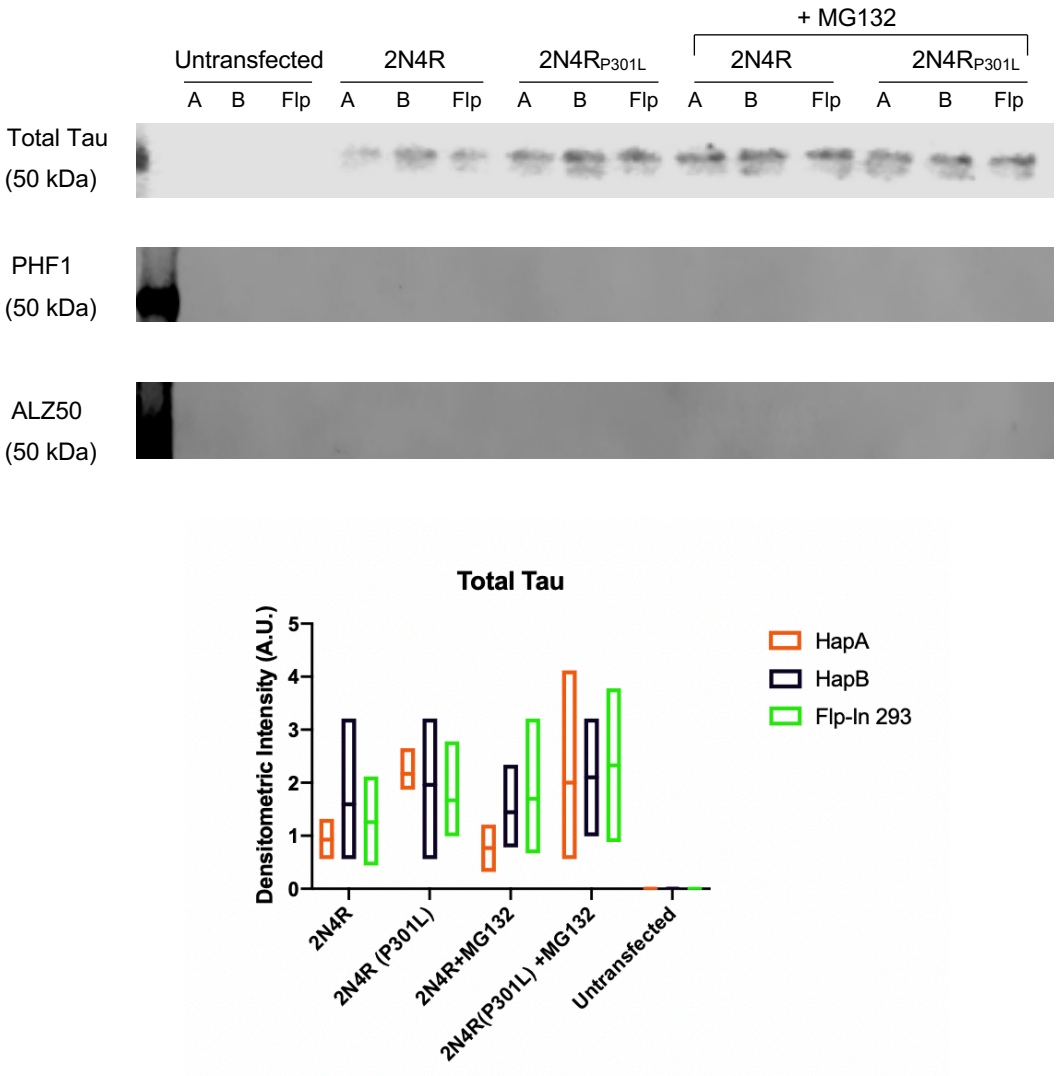

Figure 67. Treatment with 0.75 µM MG132 does not result in accumulation of aggregated tau. 2N4R-tau (wild-type) and 2N4R-tau (P301L) transfected P2 HapA, myc-cleaved HapB and Flp-In 293 cells were treated for 24 h with 0.75 µM MG132. Dox induction took place 24 h later and cells incubated for a further duration of 6 days in the absence of MG132. Protein lysates were fractionated according to sarkosyl solubility and the sarkosyl insoluble fraction probed for total tau, PHF1 and ALZ50. Addition of 0.75 µM MG132 did not result in the aggregation of hyperphosphorylated tau nor pathological tau as confirmed by the absence of a band for both sarkosyl-insoluble PHF1 and ALZ50. Total tau levels in MG132 untreated and treated 2N4R-tau (wild-type) and 2N4R (P301L) HapA, HapB and Flp-In 293 cells were plotted as a box plot of the median of 3 independent experiments run in triplicate, enabling the median observation of each densitometric analysis (line in the middle of the box) and the 25th and 75th percentiles (bottom and top limits of the plot) following normalisation against the corresponding beta-actin to be visualised. No significant differences in total tau ($H(2)= 0.1410$, $p=0.9529$) were observed in either MG132 treated or untreated 2N4R or 2N4R (P301L) transfected HapA, HapB or Flp-In 293 cells following PERK induction using the non-parametric Kruskal Wallis test.

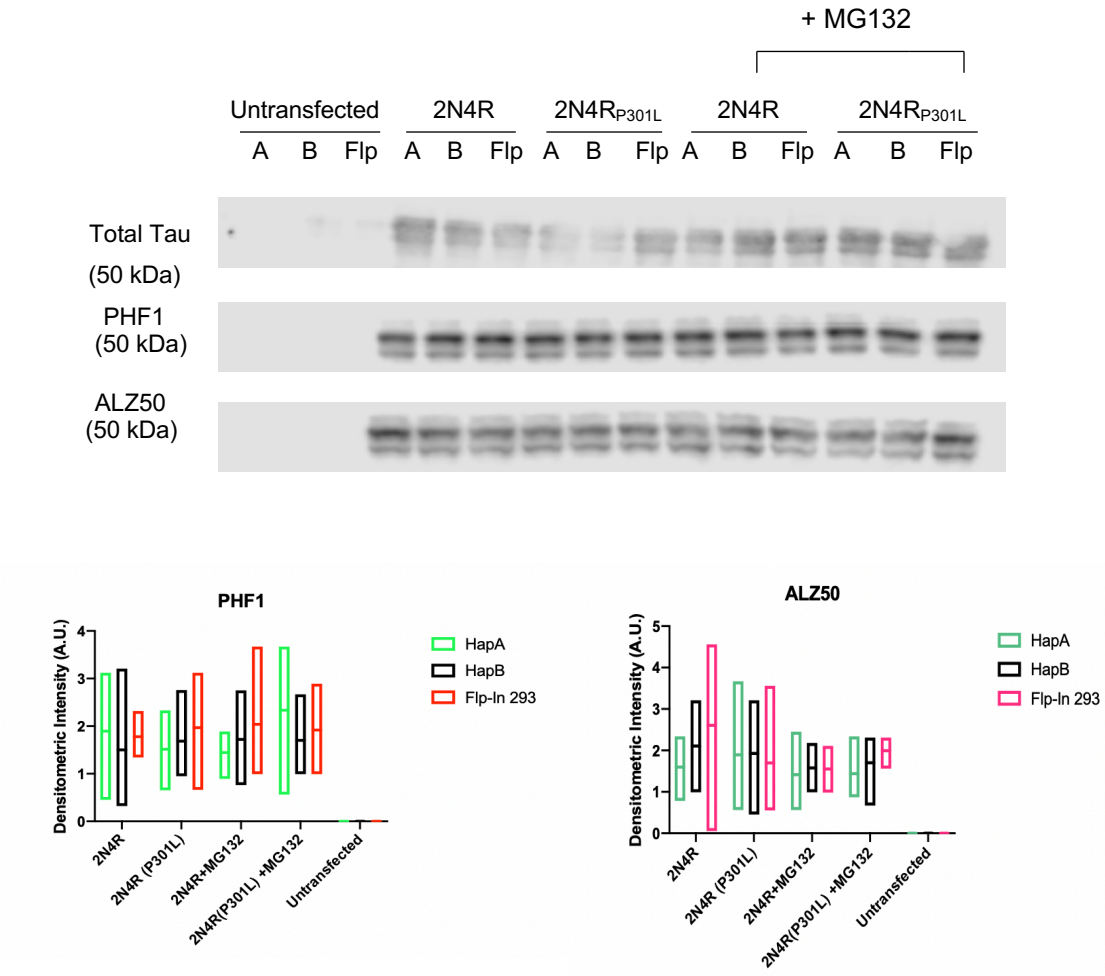

Figure 68. Levels of sarkosyl-soluble PHF1 and ALZ50 remain unchanged following treatment with MG132. P2 HapA, myc-cleaved HapB and Flp-In 293 cells transfected with 2N4R-tau (wild-type) and 2N4R-tau (P301L) tau were treated for 24 h with 0.75 μM MG132. PERK cells were induced with Dox the next day and cells incubated for a further duration of 6 days in the absence of MG132. Protein lysates were fractionated according to sarkosyl solubility and the sarkosyl soluble fraction probed for total tau, PHF1 and ALZ50. Sarkosyl soluble PHF1 and ALZ50 levels in MG132 untreated and treated 2N4R-tau (wild-type) and 2N4R (P301L) HapA, HapB and Flp-In 293 cells were plotted as a box plot of the median of 3 independent experiments run in triplicate, enabling the median observation of each densitometric analysis (line in the middle of the box) and the 25th and 75th percentiles (bottom and top limits of the plot) following normalisation against the corresponding total tau to be visualised. No significant differences in PHF1 ($H(2)= 2.075$, $p=0.3803$) or ALZ50 ($H(2) = 1.511$, $p=0.5020$) were observed in either MG132 treated or untreated 2N4R or 2N4R (P301L) transfected HapA, HapB or Flp-In 293 cells following PERK induction using the non-parametric Kruskal Wallis test.

Naïve Flp-In 293 cells transfected with only the rTg4510 mouse brain lysate did not show detectable accumulation of sarkosyl-insoluble tau. Seeded aggregation of the overexpressed tau by rTg4510 mouse brain lysate was indicated by the increased levels of sarkosyl-insoluble tau in both 2N4R-tau (P301L) and 2N4R-tau (wild-type) tau over-expressing P2 HapA, myc-cleaved HapB and Flp-In 293 cells (Figure 70). However, there were no significant differences in insoluble tau between myc-cleaved HapB and HapA cells indicating that under these conditions PERK haplotypes do not influence aggregate formation. It is important to note that the sarkosyl-insoluble tau observed in the tau overexpressing cells could be from the original rTg4510 homogenate that could have persisted during the subsequent culture period. However, it is notable that the naïve Flp-In 293 cells without tau overexpression that were also treated with the rTg4510 homogenate did not display any sarkosyl-insoluble tau (Figure 70). This gives us confidence that the sarkosyl-insoluble tau resulting from rTg4510 homogenate treatment of the tau overexpressing cells originated from the overexpressed tau. It is notable that of the sarkosyl-insoluble tau, fractions from the mutant 2N4R-tau (P301L) cells showed higher levels of PHF1 positivity compared to the 2N4R-tau (wild-type) cells (Figure 70). However, we did not reliably detect PHF1 and ALZ50 positivity in any of the other sarkosyl-insoluble fractions (Figure 70). Notably, with all treatments, we did not see any differences due to the P2 PERK HapA and myc-cleaved HapB expression showing, yet again that Myc-cleaved HapB PERK behaves the same as HapA (Figure 70 and 71). In summary, we show that treatment with rTg4510 brain homogenates does indeed cause accumulation of sarkosyl insoluble and PHF1-positive tau but there was no difference between the HapA and myc-cleaved HapB PERK cells.

As an additional test to confirm presence of fibrillar tau following treatment with seeding rTg4510 lysate, we carried out immunogold-EM of the sarkosyl-insoluble fractions of both P2 HapA and myc-cleaved HapB PERK cells overexpressing 2N4R-tau (P301L) that were treated with rTg4510 mouse brain. We carried out immunogold labelling with the anti-tau antibody Tau5 and imaged with an electron microscope (Dr Ioanna Sevastou) (Figure 72). We observed Tau5-positive straight filaments in both HapA and myc-cleaved HapB cells. The morphology of these filaments resembled those extracted from brains with PSP pathology (Taniguchi-Watanabe et al., 2016). Overall, we noted more fibrils in the PERK HapB cell extracts compared to HapA. However, this is a preliminary finding from a single experiment. Furthermore, we still cannot exclude the possibility that the fibrils could have been carried over from the initial rTg4510 lysate, However, as described above, these fibrils did not persist in the naïve Flp-In 293 cells that were similarly treated with the rTg4510 lysate which gives us confidence that the fibrils originate from the overexpressed P301L tau.

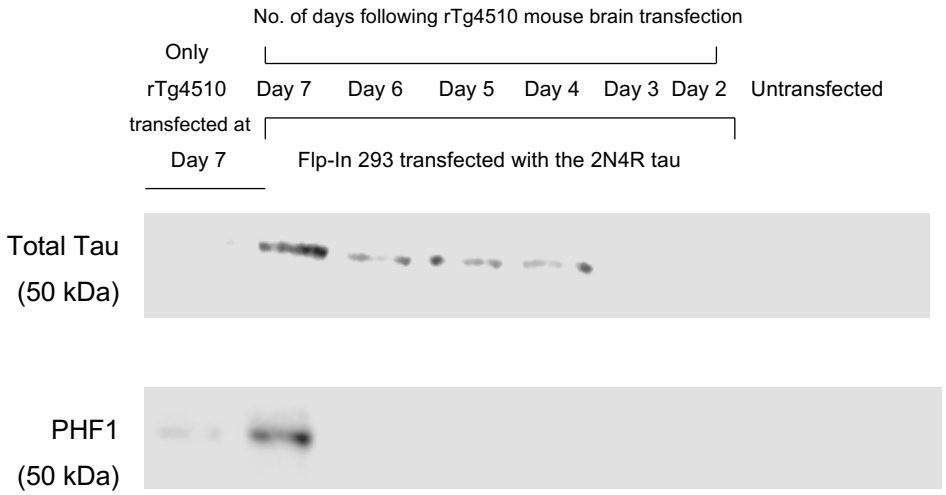

Figure 69. Prolonged Seeding with rTg4510 mouse brain lysate results in accumulation of aggregated tau (Sarkosyl insoluble tau). Flp-In 293 cells were first transfected with 2N4R-tau. 24 hours later transfection with rTg4510 mouse brain homogenate was carried out and sarkosyl insoluble fractions were obtained at 2, 3, 4, 5, 6, and 7 days post transfection. The sarkosyl insoluble fraction was probed for total tau and PHF1. Untransfected cells (last two lanes) were included as a negative control and show complete absence of tau and PHF1. The presence of a band for PHF1 is slightly visible in Flp-In 293 cells transfected with only the rTg4510 mouse brain homogenate (first lane) indicating the presence of hyperphosphorylated tau within the mouse brain lysate. Flp-In 293 cells transfected with 2N4R tau followed by transfection with the rTg4510 mouse brain homogenate showed negligible levels of total tau until day 3 post transfection. Thereafter a subtle increase in tau levels are observed at day 4, 5 and 6. Quite a prominent total tau band and PHF1 band is observed at day 7 following rTg4510 mouse brain homogenate incubation. This provides a very preliminary observation that tau aggregation could be occurring, whereby the rTg4510 tauopathic mouse brain homogenate tau seeds are utilising the 2N4R tau to propagate its aggregation in the Flp-In 293 cells. However, crucial controls are needed, including the inclusion of WT mice homogenate as a negative control and AD or PSP patient brain homogenate as a positive control to confirm if it is indeed the tau seeds from the tauopathic mice brain that is causing this increase in sarkosyl insoluble tau (adapted from Hamilton et al., unpublished).

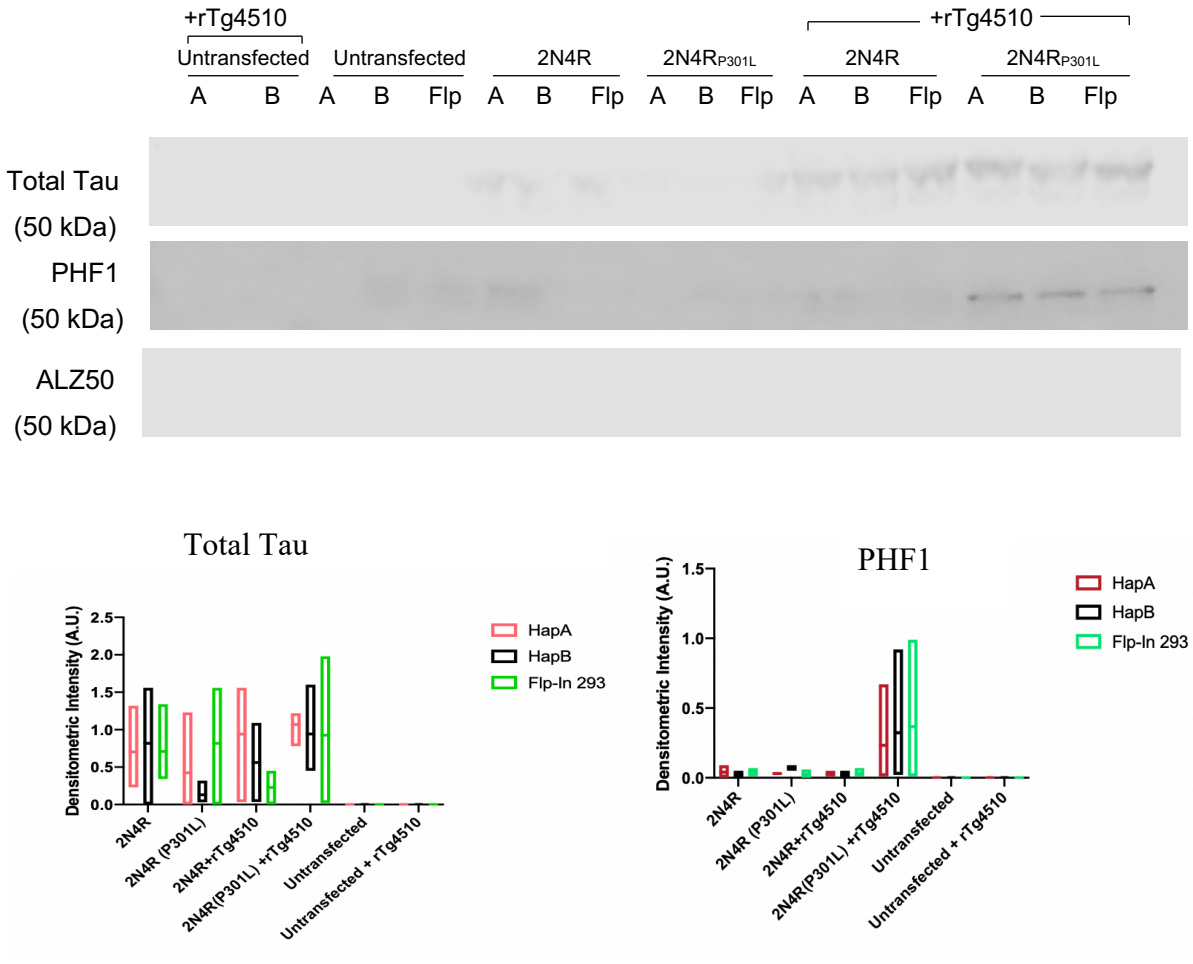

Figure 70. Seeding with rTg4510 mouse brain lysate results in accumulation of aggregated tau. 2N4R-tau (wild-type) and 2N4R-tau (P301L) transfected P2 HapA, myc-cleaved HapB and Flp-In 293 cells were transfected for 24 h by addition of 8µg/ml mouse brain lysate in the presence of Lipofectamine 3000. Dox induction was carried out on the PERK cells 24 h later and cells cultured for a further 6 days. Sarkosyl soluble and insoluble fractions of the lysates were then probed for total tau, PHF1 and ALZ50. Addition of tauopathic brain lysate resulted in the aggregation of tau in both 2N4R-tau (wild-type) and 2N4R-tau (P301L) transfected cells. Unlike the soluble fractions, none of the sarkosyl-insoluble fractions were ALZ50 positive. Sarkosyl insoluble PHF1 and total tau levels in rTg4510 transfected and untransfected 2N4R-tau (wild-type) and 2N4R (P301L) HapA, HapB and Flp-In 293 cells were plotted as a box plot of the median of 3 independent experiments run in triplicate, enabling the median observation of each densitometric analysis (line in the middle of the box) and the 25th and 75th percentiles (bottom and top limits of the plot) following normalisation against the corresponding beta-actin to be visualised. No significant differences in PHF1 ($H(2)= 0.1307$, $p=0.9441$) or total tau ($H(2) = 0.1488$, $p=0.9368$) were observed in either rTg4510 transfected or untransfected 2N4R or 2N4R (P301L) transfected HapA, HapB or Flp-In 293 cells following PERK induction using the non-parametric Kruskal Wallis test.

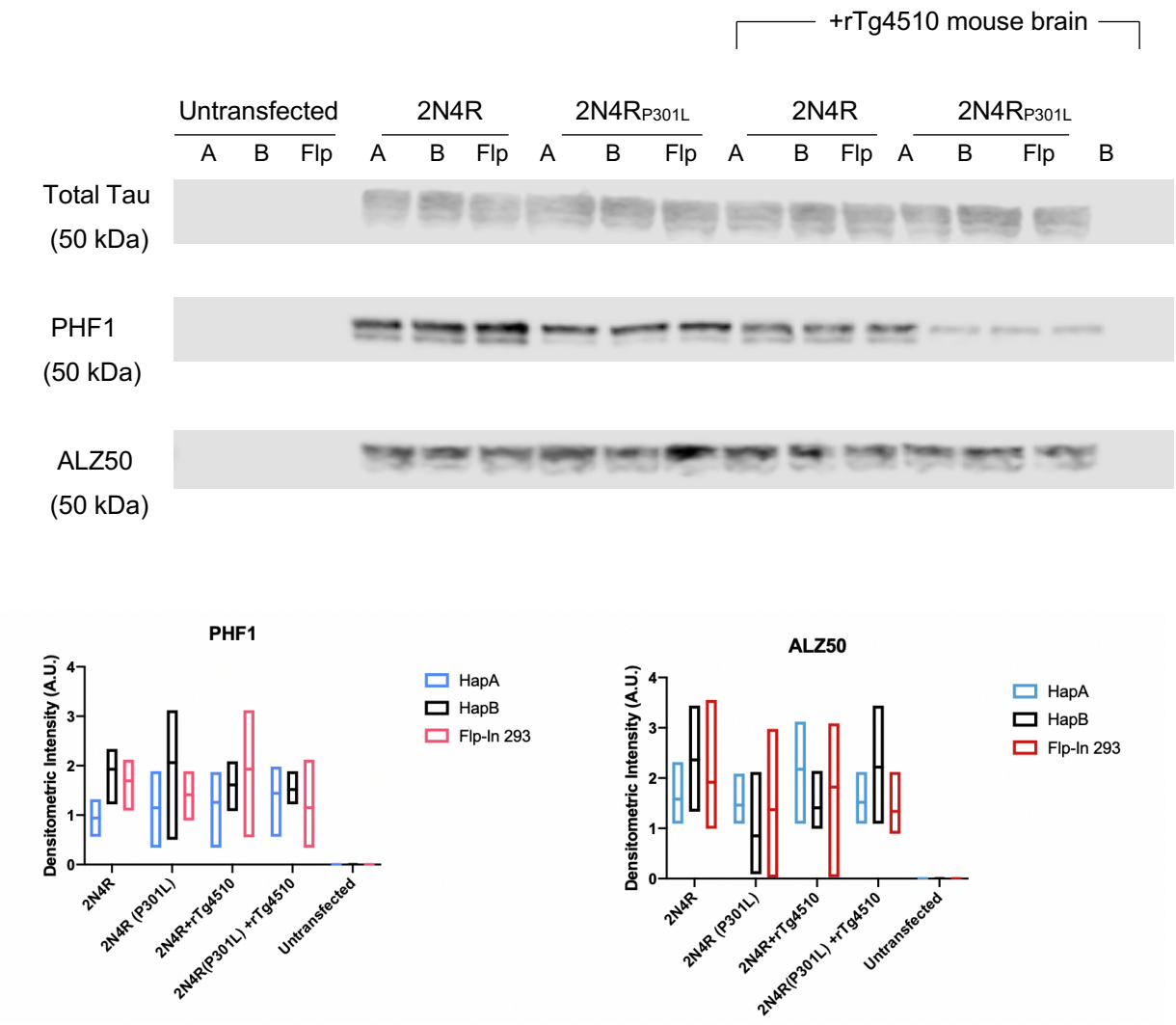

Figure 71. Reduced sarkosyl soluble PHF1-positive tau levels in cells overexpressing P301L tau. The sarkosyl-soluble fraction was probed for total tau, PHF1 and ALZ50. Soluble tau levels and ALZ50-positive tau did not change after rTg4510 seeding. Although soluble PHF1 was shown to decrease in 2N4R-tau (P301L) transfected with rTg4510 mouse brain lysate in this immunoblot, following densitometric analysis no notable decrease was observed. However, it is noteworthy that the classic tau doublet band was absent and only the higher MW band was present in the 2N4R-tau (P301L) PHF1 -positive tau cells transfected with the rTg4510 homogenate. Sarkosyl soluble PHF1 and ALZ50 levels in rTg4510 transfected and untransfected 2N4R-tau (wild-type) and 2N4R (P301L) HapA, HapB and Flp-In 293 cells were plotted as a box plot of the median of 3 independent experiments run in triplicate, enabling the median observation of each densitometric analysis (line in the middle of the box) and the 25th and 75th percentiles (bottom and top limits of the plot) following normalisation against the corresponding total-tau to be visualised. No significant differences in PHF1 ($H(2)= 2.961$, $p=0.2483$) or ALZ50 ($H(2) = 0.2417$, $p=0.9108$) were observed in either rTg4510 transfected or untransfected 2N4R or 2N4R (P301L) transfected HapA, HapB or Flp-In 293 cells following PERK induction using the non-parametric Kruskal Wallis test. Taken together, our results show that myc-cleaved HapB cells did not show any changes in the soluble tau fraction following mouse brain treatment

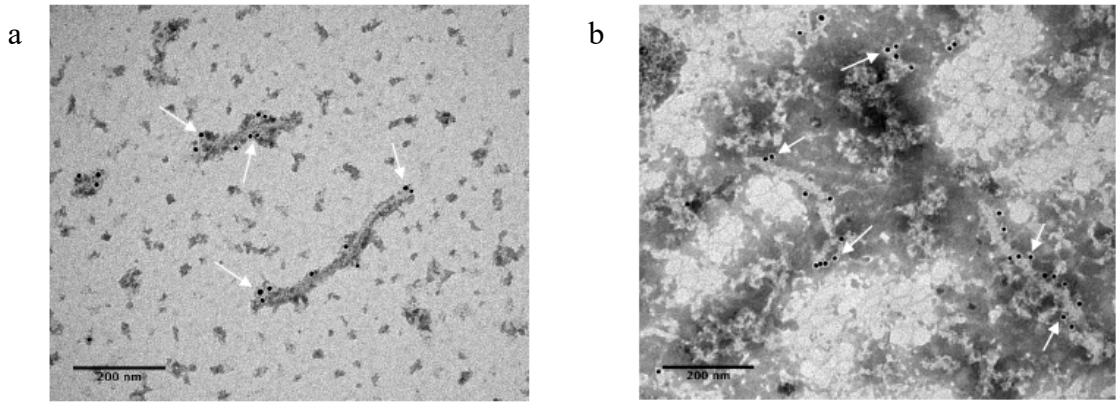

Figure 72. rTg4510 mouse brain lysate induced tau aggregates consist of filaments. Tau aggregates were isolated from P2 PERK HapA (a) and myc-cleaved HapB cells (b) that were treated with rTg4510 mouse brain homogenate. Fibrils were labelled with monoclonal antibody Tau5 and gold particle-labelled secondary antibody. Aggregates from the myc-cleaved HapB cells were not quantified as only one experiment was carried out. However, in this experiment, it looks as if more labelled tau filaments are present in the HapB panel (b). Therefore, this should be replicated, and the tau filaments quantified from subsequent experiments. The aggregates observed in HapB seem to be more amorphous assemblies when compared to HapA cells. This work would further benefit by comparing the tau filaments obtained from our PERK induced cell lines with those from PSP patient brains. As the tau seeds utilised in this work are incorporated from rTg4510 mice which carry the human tau containing the P301L mutation linked to familial frontotemporal dementia it would be of great interest to observe similarities and/or differences (straight or paired helical filaments/ diameter/ filament bundling or separation etc) between those tau filaments obtained from PSP patient brains and that observed from our work. Scale bar is 200 nm for both panels. (Work done by Dr Ioanna Sevastou).

6.8 PERK is not activated following tau aggregation

With tau aggregation induced by seeding with rTg4510 mouse brain homogenates, we next assessed if the PERK branch of the UPR is differentially activated following tau aggregation in P2 HapA and myc-cleaved HapB cells in response to this seeding. Previous work showed that tau aggregates in PSP brains are associated with UPR activation (Radford et al., 2015; Halliday et al., 2017). As yet, it is not clear how cytosolic aggregates of tau protein, which do not enter the ER lumen, can induce a response designed to counteract protein misfolding within the ER lumen. As UPR activation has been demonstrated previously in the rTg4510 model of tauopathy (Radford et al., 2015; Halliday et al., 2017; Abisambra et al., 2013) we assessed protein lysates described above of cells overexpressing P301L mutant tau that were treated with Tg4510 mouse brain lysates for PERK, p-PERK, eIF2α and p-eIF2α. Beta-actin was used as a loading control. PERK activation was estimated by normalising the p-PERK band against the corresponding total PERK and the p-eIF2α band against the corresponding total protein for eIF2α. An interleaved box and whisker plot indicating all three data points for PERK and eIF2α activity were included in the analysis.

As expected, we could not detect PERK and p-PERK in the naive Flp-In 293 cells. As shown previously, the P2 PERK myc-cleaved HapB cells consistently showed lower PERK activation (p-PERK/PERK) irrespective of 2N4R-tau (wild-type) or 2N4R-tau (P301L) overexpression or seeding by incubation with rTg4510 brain lysate. Furthermore, no significant changes in the levels of p-PERK : total PERK or p-eIF2α : total eIF2α were detected in PERK HapA cells following seeding by incubation with rTg4510 brain lysate (Figure 72). This indicated that in our model, the PERK branch of the UPR is not further activated with tau aggregation and that over-expression of either myc-cleaved HapB or HapA PERK within our cell model system does not influence levels of aggregated tau.

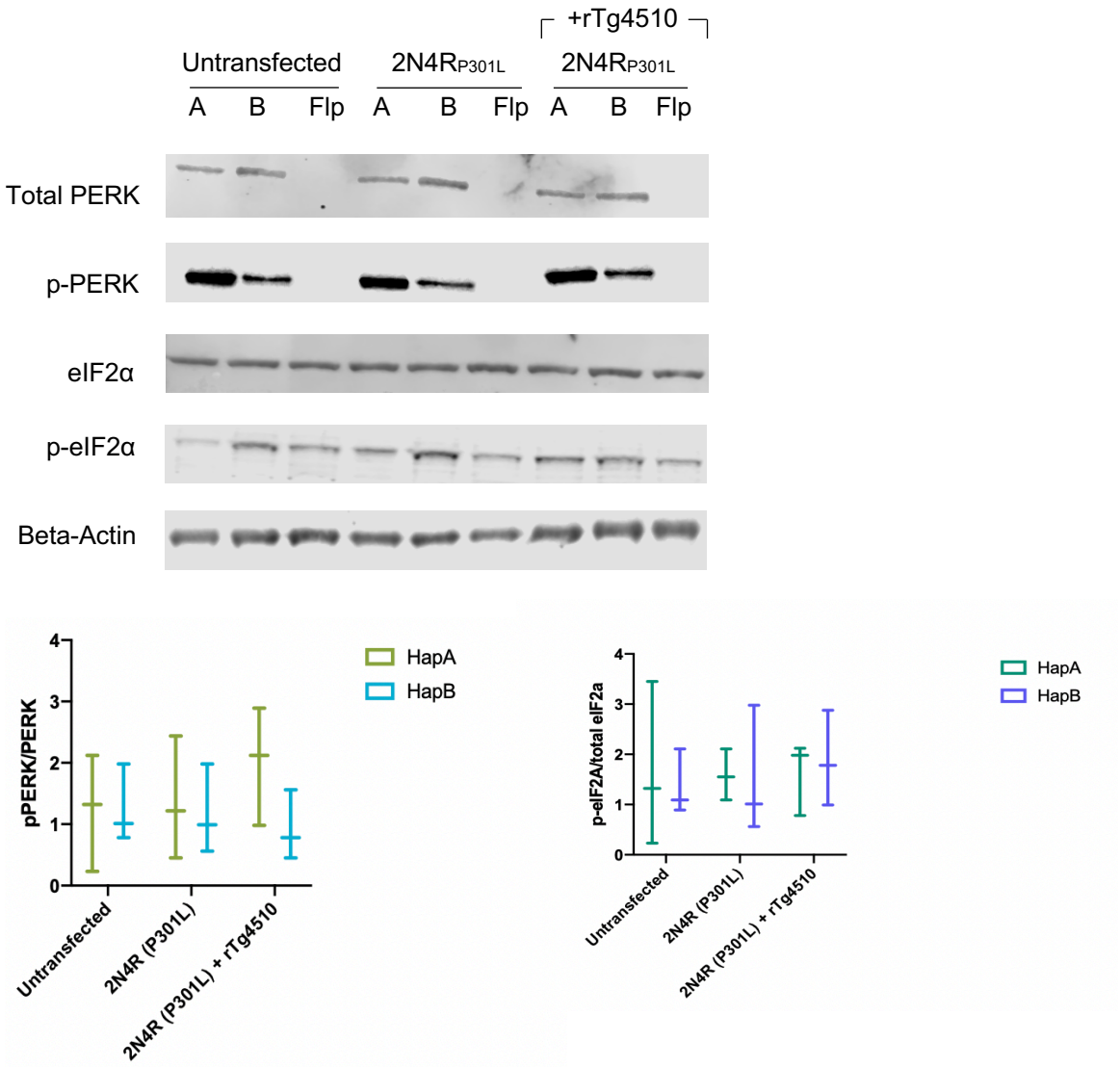

Figure 73. No increase in PERK activation following tau aggregation. P2 HapA and myc-cleaved HapB cells overexpressing 2N4R-tau (P301) were transfected with rTg4510 mouse brain lysate as described previously. Protein lysates were obtained and immunoblots conducted for PERK, p-PERK, eIF2α and p-eIF2α. Beta-actin was used as a loading control. Densitometric analysis was carried out by calculating the ratio between p-PERK : total PERK and p-eIF2α : total eIF2α following normalisation against beta-actin. Densitometric analysis was plotted as an interleaved box and whisker plot with all 3 data points being indicated per treatment. The experiment was independently replicated 3 times with each haplotype run in triplicate for each measured variable. The Mann Whitney U test indicated no difference in PERK activity between HapA and HapB cells following rTg4510 transfection (Median of HapA= 1.370; Median of HapB= 1.177; the mean ranks of HapA and HapB were 14 and 7 respectively; U=1; 2-tailed p value=0.2) and also no difference in eIF2a activity between HapA and HapB cells was noted following rTg4510 transfection (Median of HapA= 1.627; Median of HapB= 1.517 the mean ranks of HapA and HapB were 12 and 9 respectively; U=3; 2-tailed p value=0.7).

6.9 Discussion

Previous studies showed that the UPR was activated in tauopathies with tau and PERK engaging in a pathological cycle (Hoozemans et al., 2005; Nijholt et al., 2013; Unterberger et al., 2006; Hoozeman et al.,2009). This concept was supported by preclinical studies showing that targeting the PERK arm of the UPR with inhibitors or activators has therapeutic potential (Radford et al., 2015; Moreno et al., 2012; Halliday et al., 2017). It is as yet unclear if these can be translated to humans. In this chapter we investigated whether C-terminal cleaved HapB PERK in passage 2 (P2) cells, that is less effective at phosphorylating eIF2α – contribute to increased production of insoluble, fibrillar tau.

As the platform cells, HEK293, do not express tau, we transiently transfected the P2 PERK HapA and myc-cleaved HapB cells with plasmids for overexpression of the longest isoform of tau (2N4R) and the 2N4R tau incorporating the P301L pro-aggregation mutation. Using this cell-based assay we first investigated if prolonged incubation of the 2N4R-tau (P301L) in PERK impaired HapB cells induces tau misfolding and aggregation.

The tau from 2N4R-tau (wild-type) and 2N4R-tau (P301L) cells resolved as a doublet, which appears to be due to transient interactions with tubulin (Hamm et al., 2015). When analysing the tau from HapA and myc-cleaved HapB with phosphorylation and conformation sensitive antibodies, the phospho sites (PHF1) and conformationally altered sites (ALZ50) common with AD-tau also appeared in all of the 2N4R-tau (wild-type) treated cell lines. As it has been previously shown that the aggregation of tau occurred soon after abnormal phosphorylation (Perez et al., 2002) we tested the sarkosyl-insoluble fraction of these cells which revealed a small amount of tau inclusions in both 2N4R-tau (wild-type) and 2N4R-tau (P301L) tau transfected PERK and Flp-In 293 cells. However, this insoluble faction was not enriched for PHF-1 or ALZ50 even in 2N4R-tau (P301L) treated myc-cleaved HapB cells, demonstrating that these tau inclusions did not undergo conformational changes or hyperphosphorylation. Moreover, these inclusions did not form filamentous tau aggregates and were not toxic as they did not interfere with cellular viability. In this situation it raises the possibility that increased concentrations of soluble tau in our cells may cause local aggregation due to macromolecular crowding within cells which may enhance aggregation rates (Munishkina et al., 2004).

The published literature indicates that NFT formation alone is insufficient for neurodegeneration and suggests that soluble tau aggregates may be the most toxic and pathologically significant tau species (Wittman et al.,2001; Berger et al., 2007; Brunden et al., 2009; Marx., 2007). The vast majority of the full length 2N4R-tau (wild-type) and mutant 2N4R-tau (P301L) transfected tau was recovered in the sarkosyl-soluble fraction which was observed to contain a higher amount of

abnormally hyperphosphorylated, conformationally altered tau. The likely origin of this increase in tau phosphorylation observed in pathological conditions in neurons could be a decrease in the nutrients supplied by the surrounding non-neuronal cells (Houck et al., 2016). However, this is unlikely to be the cause in our cell culture, as these nutrients were mainly supplied to the cells by the addition of serum to the cell medium. As soluble hyperphosphorylated tau was also obtained from full length 2N4R-tau (wild-type) transfected Flp-In 293 cells, it seems most likely that the exogenous tau isoforms expressed in these cells are hyperphosphorylated in a physiological but not in a pathological state. Hence, the results presented here confirm that even strongly hyperphosphorylated conformationally altered soluble 2N4R-tau (P301L) had very little tendency to form insoluble aggregates in PERK impaired HapB cells.

Using our cell-based assay we next compared the aggregation potential of tau in 2N4R-tau (P301L) transfected myc-cleaved HapB cells following proteasome inhibition. The proteasomal degradation of tau, possibly without the requirement of ubiquitination, has been demonstrated recently in work done by Goldbaum et al., (2003). They showed an efficient unimpaired proteolytic system removing tau aggregates within 24 hours of aggregation in their cell model system. However, when the proteasomal machinery was inhibited by carbobenzoxy-l-leucyl-l-leucyl-l-leucinal (MG132) treatment, the aggregates were stabilized indicating that although hyperphosphorylation contributes to pathological aggregation, an age-related proteasomal dysfunction might potentiate this effect. MG132, a drug belonging to a class of peptide proteasomal inhibitors, and also considered an activator of the UPR (Lee and Goldberg., 1998) was used in our study to inhibit the proteasome. A concentration of 0.75 µM of MG132 was added to tau transfected cells for 24 hours before being replaced with fresh cell culture medium. Surprisingly, unlike the UPR inducers used in Chapter 5 we did not observe a greater cytotoxic effect of MG132 on myc-cleaved HapB cells. This raises the possibility that chronic, low dosages of cellular stress which does not directly induce ER stress is well tolerated by PERK impaired HapB cells.

MG132 treatment neither caused any increased levels of soluble tau or accumulation of insoluble tau nor any changes in pathological PHF1 and ALZ50-positive tau. Within the timeframe of this work, we could not complete a more complete optimisation of this experiment, particularly controlling for effective proteasome inhibition by MG132. This could be carried out using a commercially available proteasome activity assay kit. Thus, in order to reach any conclusions about the negative outcome of our study, it will be necessary to carry out more extensive testing of the parameters of this experiment.

We next decided to test if we were able to induce more tau aggregates within myc-cleaved HapB cells when treated with rTg4510 tauopathic mouse brain lysate. Tau seeding is an emerging

concept that suggests that pathological tau can be transmitted to otherwise healthy cells to form inclusions. Here, we established a cellular assay of tau aggregation by transfecting brain lysate from rTg4510 mice to bypass the seed formation step in cells resulting from the sole overexpression of 2N4R-tau (P301L) in myc-cleaved HapB cells. Exogenously expressed rTg4510-tau appeared to be at undetectable levels six days post transfection indicating that the signals obtained from mouse brain-transfected cell lysates is converted from cellular soluble tau and not from residual brain lysate. The mouse brain transfected 2N4R-tau (P301L) transfected cells had a greater seeding activity as the sarkosyl-insoluble fraction was enriched for aggregated PHF-1 positive tau. Although using this system we observed accumulation of aggregated, hyperphosphorylated tau -indicating that the pathological tau aggregates from the mouse-derived brain lysate has a higher seeding potency when matched with the P301L soluble tau- no differences in aggregated tau levels was observed between myc-cleaved HapB and HapA cells. Moreover, we could not see a difference in the level of phosphorylated eIF2α and we were also unable to detect changes in p-PERK in rTg4510 transfected 2N4R-tau (P301L) transfected myc-cleaved HapB cells which indicated the absence of activation of the PERK branch of the UPR in response to tau pathology *in vitro.*

Similar observations concerning the lack of UPR activation by mutant tau was made by Spatara and Robinson (2010) when using HEK293 cells expressing the mutant P301L tau, whereby the tau expression was controlled by the tetracycline-regulated T-Rex expression system. Neither splicing of XBP-1 nor induction of protein markers of the UPR were observed in their system upon the overexpression of recombinant tau. They suggested that the lack of UPR activation in their tauopathy model could be explained by the cytosolic localization of tau protein, with no indication of tau entering the ER lumen. It has been questioned previously whether UPR activation occurs in neurodegenerative models. Hashimoto et al., (2018) detected no UPR induction in amyloid precursor protein knock-in mice, single APP-overexpressing mice, and a distinct model of tauopathy: P301S Tau-Tg mice. They suggested that the UPR activation observed for different transgenic models may be an artifact resulting from the expression of membrane proteins that could generate nonspecific ER stress. However, Abisambra et al., (2013) induced expression of wild-type human 0N4R tau in HEK cells and observed a parallel increase in levels of p-PERK and soluble transgenic tau, peaking ~72 hours after induction. Moreover, cessation of tau overexpression significantly reduced p-PERK levels suggesting that tau expression at least transiently activated the UPR in HEK cells. Similarly, they also reported that 9-month aged rTg4510 mice showed higher levels of p-PERK, and BiP, and when Doxycycline administration suppressed the expression of soluble tau there was a reduction in the levels of p-PERK. This provided some insight into the nature of tau aggregation by revealing that elevated levels of tau proteins were accompanied by elevated signalling of the PERK branch of the UPR observed in HEK cells, rTg4510 animals as well as in the brains of AD patients. Moreover Yuan et al., (2018)

observed disrupted tau protein homeostasis when PERK was inhibited pharmacologically in their neuronal cultures but observed an increased level of total tau and pathological phosphorylated tau (AT8 and PHF1) during ER stress in neuronal cultures carrying the HapB *PERK* alleles without any changes in *MAPT* expression. Their findings revealed that HapB PERK showed increased vulnerability to ER stress-induced damage and compromised tau protein homeostasis compared to neurons carrying the non-risk *PERK* alleles.

These results highlight the need to carefully test our PERK cell model for early differences in tau proteastasis following UPR activation with either Tg or Tm treatment which will enable us to identify if impaired PERK signalling leads to alterations in tau levels following dysregulation of the UPR as this has been discussed as a significant driver of pathology across many neurodegenerative diseases. Furthermore, an extensive early time-course related study identifying changes of tau solubility following immediate activation of the UPR is required. This is because numerous studies have reported that soluble tau oligomers are the driving force behind tau-induced ER stress (Abisambra et al., 2013) and these could impair ER-associated degradation, resulting in UPR activation (Duennwald and Lindquist., 2008; Price et al., 2010).

While the impact of PERK impaired signalling on tau proteostasis remains unresolved in our cell model, it would be interesting to observe if P301L aggregation brought about by rTg4510 mouse lysate seeding in myc-cleaved HapB cells has any effect on cell viability. Tau aggregation induced toxicity should be noted over a period of days following tau aggregation to observe if the results are consistent with the long-term toxicity associated with the tau conformational change and aggregation observed in some transgenic mouse models (Terwel et al., 2005). Second, rTg4510 transfection followed by proteasomal inhibition can also be carried out to observe if the detergent-insoluble tau aggregates formed early in the reaction pathway (which should now be stabilised as they will no longer be cleared by the proteasome) will enable early conformational and phosphorylation properties associated with tau aggregation to be noted. These early tau aggregates may then contribute to UPR activation which in turn may highlight PERK haplotype specific differences.

In conclusion, although there is good evidence for UPR activation in some neurodegenerative diseases, its causative role across neurodegeneration is less clear. Although we failed to obtain any evidence from our immunoblots for a connection between impaired PERK activity and tau aggregation, preliminary work characterising the ultrastructure of these inclusions following rTg4510 brain transfection was encouraging. Tau5 positive tau filaments were observed in both HapA and in myc-cleaved HapB cells. There also appeared to be a higher number of tau filaments in myc-cleaved HapB cells suggesting that impaired PERK activity could be driving an increase in tau fibrilization. However, these possibilities require additional investigation. Moreover, this also

raises the possibility that subtle changes in tau aggregation may not be picked up sarkosyl fractionation. As the accumulation of insoluble tau was seen to correspond to filamentous tau aggregates in our cell model system, optimisation of thioflavin S to accurately report on the amount of beta-pleated tau fibrillary tangles may prove to be a better alternative than the sarkosyl fractions.

A further limitation of the work conducted in this chapter was that we only examined the sarkosyl insoluble fractions for a limited number of tau epitopes including total tau, PHF1 and ALZ50 and used that as a key marker of confirming tau aggregation. However, there are a number of other tau epitopes which can also be used to identify tau hyperphosphorylation (PHF1) and conformational changes (MC1). For many years, the biochemical characterization of tau aggregation and PHF formation involved well-standardized protocols based on the use of sarkosyl which resulted in two distinct types of tau oligomers: sarkosyl-soluble tau and sarkosyl-insoluble tau being confirmed. Soluble tau oligomers appear to be mainly dimers/trimers, and, in the case of insoluble tau oligomers, the structures go from dimers to form tetramers and larger structures. However, as toxic soluble tau oligomers are now known to be key in propagating tau aggregation, identification of these early stages of tau aggregation is vital. The use of the novel tau oligomer specific antibody, T22 should be utilised in future work to determine the presence of soluble tau oligomers following proteasomal inhibition and/or tauopathic mouse brain seeding as an additional measure of confirming tau aggregation. Furthermore, as ThS is notoriously non-specific, the confirmation of these soluble tau oligomers immunohistochemically can be further evaluated with the T22 antibody and if present, the degree of phosphorylation and ubiquitination of these tau species can also be determined using immunoblot and immunocytochemistry. In addition, another major limitation in this work was that the presence of sarkosyl insoluble tau following tau transfection into the PERK stable cell lines could not be reliably confirmed as our experiments crucially lacked a positive control. The use of either sarkosyl insoluble fractions from Braak stage V/VI of AD and/or PSP patient brain homogenates therefore must be included in further experiments to validate our findings. Moreover, immunoblot per se should not be solely used to confirm the presence of tau aggregation as we are unable to conclude if the signal for total tau, PHF1 and/or ALZ50 in the insoluble fraction is due to inadequate washing of the sarkosyl insoluble pellet and results in a signal carried over from residual washes of the sarkosyl soluble fraction. Moreover, the conclusions of this study are primarily dependent on data from immunoblotting experiments. Although routinely used for determining relative protein levels, this technique is inherently semi-quantitative and exhibits large variability between replicates. Therefore, the reliability of these data is questionable and would be improved by the use of more quantitative methods such as ELISA (enzyme-linked immunosorbent assay). Moreover, the experiments featured a low sample size (n=2- 3), particularly for sarkosyl-insoluble fractions which were a finite resource.

In summary, our preliminary findings make it unlikely that PERK dysfunction is the sole factor involved in increasing the risk of PSP in patients carrying the HapB PERK polymorphisms as we were unable to find any mechanistic link between tau aggregation and myc cleaved HapB and/or HapA cells. However, further work is required to induce and confirm tau aggregation in our cell model system and experiments should be designed so as to crucially optimise the appropriate conditions for proteasomal inhibition and tauopathic rTg4510 mouse brain seeding as well as including the inclusion of well thought out negative and positive controls for each marker of tau aggregation.

7 Discussion

7.1 *A summary of results*

The aim of this project was to develop cell models for the study of the functional basis of coding variations of the *EIF2AK3* gene, encoding PERK, associated with a risk of PSP. PERK is an important sensor of cell stress, particularly ER stress due to the accumulation of the unfolded proteins generally associated with the pathophysiology of neurodegenerative proteinopathies, including the tauopathies (Harding et al., 2000). The association with PSP is linked to one of three coding haplotypes with higher PERK activity and contributes to, and co-localises with, tau pathology in AD and PSP (Hoglinger et al., 2011; Chen et al., 2018). The three-coding single-nucleotide polymorphisms (SNPs) affect three highly conserved residues; two in the lumenal domain of PERK, responsible for homodimerization/auto-activation of PERK, and one at the active site kinase domain of the protein (Liu et al., 2012). The polymorphisms could therefore affect either (or both) functional domains. The aim of this project was to assess the functional importance of these coding haplotypes.

We created stable isogenic cell lines for Tet-inducible expression of each of the four PERK functional haplotypes and three sub-B artificial haplotypes utilising the Flp-In™ T-Rex™ system (Life Technologies). Derivation of the isogenic cell lines utilising the Flp-In™ T-Rex™ System enabled us to use the same integration site for all variants. We altered the target sequence for an siRNA that had previously been shown effectively to knock down endogenous *EIF2AK3* expression (Ramnarayan et al., 2016). This rendered the exogenous *EIF2AK3* variant resistant to this siRNA, enabling partial knockdown of the endogenous gene and rescue by induction of transgene expression. However, due to the significant overexpression of the exogenous PERK over the barely detectable endogenous PERK, during the course of this work we were able to delineate effects of the exogenous PERK without having to knock down the endogenous gene expression. We also incorporated a carboxy-terminal myc-tag in order to discern between exo- and endogenous PERK. Early studies showed that this does not affect localization and/or function of the protein (Harding et al., 1999). The completed *EIF2AK3* coding DNA variants were incorporated into the Tet-inducible pcDNA5/FRT/TO expression vector and inserted into the Flp-In 293 cell's genome at the previously integrated FRT site. With subsequent clone selection with hygromycin, stable PERK integrants were chosen and multiple clones (5-10 per variant) expanded. With Western blot analyses, we demonstrated robust, inducible expression of myc-tagged PERK. However, a significant drawback of the Tet-On system, emerging from our work, was the lack of any fine-tuning of PERK expression levels by varying levels of Dox. We observed that PERK expression is completely suppressed at Dox concentrations up to 9 ng/mL, after which, maximal expression levels ensue at 10 ng/mL without any discernible dose response.

Intriguingly, with subsequent passages, the HapB PERK variants alone underwent C- terminal cleavage as evidenced by loss of the myc-tag. It is also notable that this was the case with the artificial HapB sub-haplotype with each of the three amino-acids reverted to the non-risk HapB – i.e. any two of the three risk variants were sufficient to cause the cleavage whereas only one risk variant, as evidenced by the other haplotypes, did not result in the cleavage. We confirmed this with multiple clones derived from 12 completely independent rounds of transfection and cloning. With antibodies against the N-terminus and C-terminus of PERK we confirmed, however, that HapB PERK was being overexpressed at levels comparable to the other haplotypes, albeit with the loss of the C-terminal Myc-tag. We determined loss of Myc was not due to deletion of the transgene as, with genomic amplification of the PERK HapB cells from passage 2, we confirmed correct integration and presence of the full-length PERK HapB transgene into the predetermined chromosome locus in the Flp-In^{TM} 293 cells. With RT-PCR using primers specific for the transgene which included the transcribed Myc-tag we also confirmed correct transcription of HapB PERK, with Myc-tag, confirming that the Myc-tag was lost post-translation. It was noted that passaging, accompanied by freeze-thawing of the HapB cells alone, results in the loss of the C-terminal Myc tag; and this was the case with the primary B haplotype and all the artificial sub-B haplotypes. This also resulted in increased PERK levels but reduced PERK activity as evidenced by decreased PERK and eIF2α phosphorylation in the Myc cleaved HapB cells. PERK levels in the human brain are at extremely low levels and barely detectable by Western blot using commercial antibodies. For this reason, we were unable to detect, let alone quantify PERK and phospho-PERK in the genotyped PSP patient brains homozygous for the major (C) and minor allele (T) of *EIF2AK3.*

To explore whether C-terminal cleavage led to an impaired unfolded protein response (UPR) with the HapB PERK, compared to the other haplotypes, resulting in increased cell vulnerability to ER-stress associated damage, we induced the UPR with thapsigargin (Tg) and tunicamycin (Tm) treatment. We observed reduced eIF2α phosphorylation in the PERK HapB–cells compared to HapA and also showed increased CHOP levels which, through its pro-apoptotic activity could be the contributor to the decreased cell viability of the HapB cells following UPR induction. As PERK is an important player in the cell's response to ER stress, impaired HapB PERK signalling due to the C-terminal cleavage clearly renders the cells more vulnerable to Tg and Tm. Although PERK operates in parallel with IRE1 and ATF6 signaling effectors of the UPR, the levels of IRE1 and ATF6 following induction of acute ER conditions in the C-terminal-cleaved HapB PERK cells were no different to those in HapA cells. Furthermore, ER morphology following UPR activation did not yield any haplotype-specific differences indicating that any impairments in HapB PERK signaling most likely affects only the PERK branch of the UPR, resulting in impaired kinase activity and reduced phosphorylation of eIF2α, thereby resulting in reduced translation attenuation.

Having noted that HapB PERK causes increased risk of PSP and, additionally, several immunohistochemistry studies have linked PERK activation to tau pathology (Stutzbach et al., 2013; Abisambra et al., 2013; Nijholt et al., 2011; Unterberger et al., 2006; Hoozemans et al., 2009), we sought to establish if HapB PERK could contribute to increases in pathological tau and tau aggregation. We did this by transient overexpression of wild-type and P301S 2N4R-tau. Unfortunately, we failed to obtain any evidence for a connection between impaired HapB PERK activity and tau aggregation, even with the more aggregation-prone 2N4R-tau (P301L) and additional seeding with brain lysates from the rTg4510 mouse and with inhibition of ubiquitin proteasome system (UPS) with MG132.

7.2 *General discussion*

7.2.1 Limitations of the cell models

7.2.1.1 HEK-293

HEK 293 cells first were generated by Russell et al., (1977) in the early 1970s by transformation of culture of normal human embryonic kidney cells with sheared human adenovirus type 5 DNA. Genomic analysis showed that approximately 4.5 kilobases from the left arm of the viral genome became incorporated into human chromosome 19, resulting in decreased senescence of these cells (Louis et al., 1997). Thus, HEK-293 cells are not a model for normal human cells; these cells have been immortalized already by a known oncogene but are pre-malignant. However, this cell line has the advantage of being rapidly dividing, doubling daily. The continuous division and the immortality of these cells is the result of the oncogenic mutations which might include aberrations in the UPR, UPS, and/or apoptosis cascade (Ooi et al., 2016). Hence, these cells are likely to be resistant to stimuli which would be lethal to brain neurons. Therefore, results indicated in this thesis should be viewed with caution, in order to avoid an overgenerous interpretation. Further, the *in vivo* neuron is subject to stimulation by glial cells, which provide trophic support. Such culture conditions are not mimicked by the routine culture conditions for HEK-293 cells, which relies on foetal bovine serum as a supply of trophins.

However, HEK-293 cells are widely used as hosts to express recombinant proteins to study their structural, biophysical, and pharmacological properties (Baldi et al., 2007; Dalton and Barton., 2014). This cell line is an attractive heterologous system for expression of membrane proteins, not least because they have post-translational modification machineries required for the proper folding and/or optimal biological activity of target proteins but because they also exhibit high

transfection efficiency, faithful translation, and processing of proteins (Wurm., 2004) that results in higher protein yields (Backliwal et al., 2008). These attributes together with the cell size, morphology, rapid division all factored in to our establishing HEK-293 cells as our host of choice for stable overexpression of the HapA and HapB PERK proteins.

Within the time frame of this work, in order to study the role of PERK in cell lines more amenable to neuronal differentiation, we also attempted to create the necessary T-Rex Flp-In host cell lines for stable isogenic integration in SH-SY5Y, BE(2)-M17, SK-N-F1 and SK-N-MC human neuroblastoma cell lines. However, despite the establishment of optimal conditions of the selection antibiotic, Zeocin, we failed to generate any host cell clones.

7.2.1.2 Stable over-expression cell model

Transiently transfected cells are commonly used as they are quickly produced but they have many disadvantages, notably large differences in expression level among the population of cells and between experiments due mainly to variations in transfection efficiencies (Kim et al., 2010). The use of the Flp-In™ T-Rex™ system in our study enabled us to create PERK cell lines which stably express our PERK proteins of interest in an isogenic and inducible manner. This removes the possible variation in expression levels or patterns due to different sites of integration into the chromosome of our gene of interest and allowed our cells to be grown without expression of the exogenous PERK until such time as this was required. The ability to induce expression by addition to the culture medium of Dox has several advantages over transient transfection, or the generation of constitutively expressing conventional stable cell lines. There was no need for repeated, highly variable and expensive transient transfections as all the Flp-In™ T-Rex™ PERK stable cells were derived from the same parental cells which were integrated at the same site and hence had the same genetic background, allowing haplotype specific comparisons to be made. The ability of our PERK stable cell lines to be grown to the required density before induction of the PERK transgene, enabled us to avoid potentially detrimental effects upon cell growth. This was particularly important as prolonged overexpression of PERK is known to be toxic to the cells; excess PERK could autoactivate if there is insufficient BiP for inhibition, leading to induction of the UPR (Harding et al., 2000). Thus, it was encouraging to note that there was no leakage of expression of myc-tagged exogenous PERK variants in the absence of Dox induction. Therefore, expression of our PERK exogenous transgene was only induced when required, as there was less likelihood of this expression being lost due to non-expressing cells outgrowing those which were still expressing the PERK transgene. Although the level of our PERK transgene expression was thought to be regulated by varying the concentration of the inducing agent Dox, we were unable to see a dose response induction of expression of our exogenous PERK variants with

increasing Dox concentrations. We observed Dox-induced PERK expression in our cell model as an all-or-none pattern with concentrations with no expression at 9 ng/mL Dox and maximum expression levels starting abruptly at 10 ng/mL of Dox without any modulations with dose. This could be a possible setback to our study as such high levels of PERK may in turn have overwhelmed our cell model system, resulting in the masking of potential subtle differences of the functional haplotypes.

7.2.1.3 Induction with Doxycycline

Recently it has been shown that the two tetracycline analogues – Col-3 and doxycycline (Dox) – affect translation in a dose-dependent manner through direct binding to the human ribosome and also behave similarly to other general inhibitors of eukaryotic translation (Mortison et al., 2018). In the Dox affinity isolation experiments Mortison and colleagues (2018) identified 189 proteins which were specifically reduced in the presence of free Dox and intriguingly nearly all of the differentially bound proteins from the Dox pull-down datasets were known components of the human 80S ribosomal complex and its closely associated factors. When identifying the precise binding sites for these tetracyclines using A375 cells, they observed significant enrichment at a number of key rRNA sites (Figure 74). These sites corresponded to the apical loop of ribosomal helix h16, the bulge loops of helix h18, the terminal loop of helix H89, and the entrance to the polypeptide exit tunnel. They noted that these regions are in close proximity to the mRNA channel which is intimately involved in regulating translation initiation and elongation. Thus, the use of Dox within our cell model system could prove to be problematic as Dox binding to these substructures could affect translation initiation or mRNA progression during elongation, thereby confounding our results.

It was further reported (Mortison et al., 2018) that when RNA-seq was used to identify which mammalian cellular pathways were affected by these two tetracyclines, genes enriched for the UPR pathway were noted which included ATF4 and CHOP, both of which are key players in the PERK pathway. It was found that, while Col-3 induced robust, dose-dependent eIF2α phosphorylation, dox did not induce these effects at physiologically relevant concentrations, with only low levels of eIF2a phosphorylation and ATF4 expression being observed in Dox-treated A375 cells. However, these findings suggest that Dox is likely to modulate ribosomal translation which in turn may result in our Tet inducible cell model system being far from ideal in identifying PERK haplotype specific changes. Activated PERK phosphorylates eIF2α and this posttranslational modification results in the reversible repression of protein translational initiation. At present if we are to take our impaired HapB PERK activity findings at face value we crucially need to identify any selective effects Dox may have on the HEK 293 translational program and

how each of the unique binding sites for Dox on the human ribosome may influence the phosphorylation of eIF2α. While we have shown that PERK and eIF2α are activated under acute ER stress, we have not specifically looked at the phosphorylation status of either PERK or eIF2α in naïve Flp-In 293 cells treated with Dox. This is one of the limitations of our study as we did not carry out experiments to observe if the UPR initiation is triggered following binding of the Dox to the ribosome and in particular if eIF2α is indeed involved in transducing that signal.

7.2.1.4 Disease modelling

The PERK plasmid vectors used to select for our PERK stable cell lines in the studies presented in this thesis were designed with the hygromycin antibiotic resistance marker. Selective growth of the stable cells with antibiotics, even with the presence of the hygromycin resistance gene, has been previously shown variably to slow down the rate of cell division (McGaha et al., 2007). Presumably, this reduction of growth rate is caused by the dedication of much of the cells' metabolism to the production of antibiotics which maintains selection (Oung et al., 2015). This further reiterates that the cell model we have established is a very artificial one. Thus, the precise modelling of the effects of HapB PERK polymorphisms within the PSP neurodegenerative disease using our cell system is far from feasible. In addition to the aforementioned limitations, it is hard to include old age, diet, and a lifetime exposure to toxins; although it is not impossible to adjust for diet (serum deprivation) (Qiu et al., 2018), accelerate ageing (Yang et al., 2016) and even do chronic exposure to low dose-toxins (Rutkowski et al., 2006) -but yet, this is not a perfect cell culture model. The genetic and environmental factors involved can be assimilated independently, and assayed accordingly, but highly complex multi-factorial mechanisms might be at work in parallel in the development of these diseases. It is key therefore to interpret the presented data as independent biochemical responses to the stimuli presented to the model and hence to be cautious with drawing conclusions that might be relevant only to the *EIF2AK3* polymorphisms.

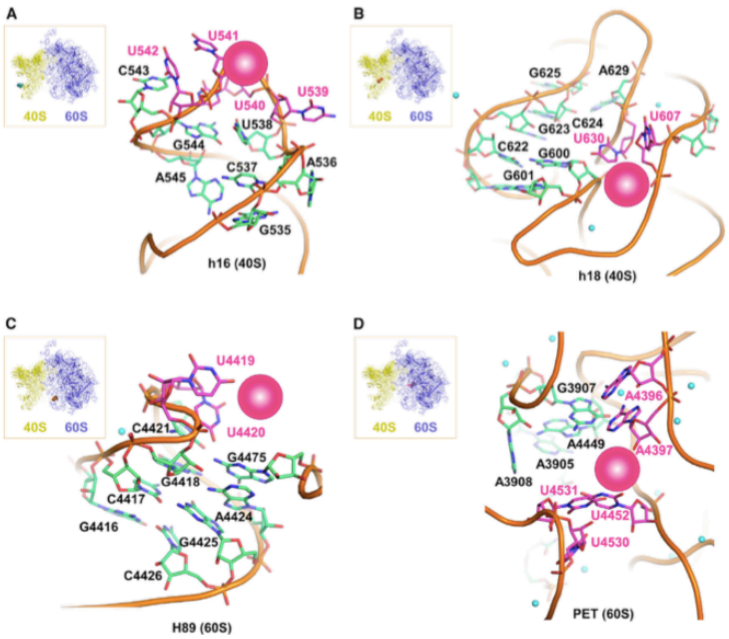

Figure 74. **Structural Representations of Putative Binding Sites for Col-3 and Dox.** Potential rRNA binding pockets for Col-3 and Dox on the small, 40S subunit h16 (A) and h18 (B) and the 60S subunit at H89 (C) and PET (D) are indicated. Crosslinked bases are highlighted in magenta and magenta spheres represent potential binding pockets for Col-3 and Dox at each site (Mortison et al., 2018).

To reduce the problems of over-simplification of an over-expression cell culture modelling of PERK variation, findings could be investigated using neuronal cultures (Yuan et al.,2018). The specialised functions of neurons and their reliance on protein translation may make them especially vulnerable to changes in PERK activity. Thus, use of the PSP patient iPSC-derived neurons carrying the HapA and HapB *EIF2AK3* polymorphisms could provide a better model of the physiological consequence of PERK HapA and HapB signalling. It was nevertheless encouraging to note that using our over-expression cell model system, we observed similar findings to Yuan et al., (2018) whereby the risk PERK HapB protein was shown to be less effective at phosphorylating eIF2α with increased cell death following exposure to ER stress inducers. Although there are limitations to using our cell model system, this model would prove useful in identifying which of the three protein coding variants making up HapB are responsible for the difference in eIF2α phosphorylation. As we have already established stable cell lines for the artificial HapB sub-haplotypes, use of our cell model will give us further insight into the role of the functional basis of each coding variation of the *EIF2AK3* gene that is associated with risk of PSP. This is especially important given the conflicting results between Stutzbach et al., (2015) and Yuan et al., (2018) – both of whose work used mouse embryonic fibroblasts negative for the PERK protein which were then transfected with the PERK HapA or HapB cDNA constructs.

Stutzbach's findings showed that HapB PERK had higher kinase activity following UPR induction with Tg as noted by the significantly increased phosphorylation of eIF2α in HapB cells (Stutbach et al., 2015). This was in line with the findings from Liu et al., (2012) using human beta-lymphocytes homozygous for PERK HapB which also demonstrated higher levels of eIF2α phosphorylation in response to Tg treatment than beta-lymphocytes homozygous for HapA PERK. However, similar to our reported findings, Stutzbach too observed lower levels of HapB PERK phosphorylation upon UPR induction. Moreover, it was greatly encouraging to note that the disease-in-a-dish model using the PSP HapA and HapB PERK patient fibroblasts used by Yuan et al., (2018) accurately recreated the pathological HapB impaired PERK activity we noted.

Bearing in mind the different cell models previously used to compare the two PERK variants it is encouraging to note that each of these studies, including the results presented in this thesis was able to replicate Stutzbach's original finding of decreased HapB PERK phosphorylation upon UPR induction. Thus, although the Tet on inducible Flp-In 293 cell culture system has its limitations, it can be argued that the ability to replicate and expand upon previous findings of PERK variation enables it to be considered a good enough model system to further explore the differences of the sub HapB PERK polymorphisms.

7.3 Further research

7.3.1 *Myc-tagged PERK*

Adding a Myc-tag to the PERK protein's C- terminus facilitated the exogenous PERK detection using the Myc-tag specific antibody. This was particularly helpful for us as we then avoided picking up detection of the endogenous PERK protein within the HEK-293 cells. It was this absence of the Myc-tag following freeze thawing and passaging of the HapB cells that enabled us to observe that HapB cells were prone to C-terminal cleavage and loss of the Myc-tag resulting in reduced PERK activity. In future work, we will attempt to identify the nature of this cleavage by targeted mass spectrometry (MS) comparing the PERK HapA cells and the passage 1 (P1) and cleaved P2 HapB cells. As the binding epitope of the C-terminal PERK antibody (P0074; Milipore) which still recognises the cleaved HapB PERK is at positions 1072-1098 of the PERK protein sequence, this strongly suggests that cleavage occurs between residues 1100 and the extreme C-terminal end of the protein. Identification of the precise nature of the cleavage would allow us to investigate if similarly, cleaved variants of PERK are present in certain cell types of HapB brains that could explain selective vulnerability. Apart from MS analysis of the HapB cleavage site, there is the distant possibility that the Myc tag in itself is vulnerable to degradation although this would not explain its retention with the other haplotypes. In order to test this, we would need to replace the

myc tag with another similar sized tag (e.g. poly-Histidine) and/or tagging each end of the N and C-termini of the protein and crucially include untagged HapB full length constructs. However, another far more superior alternative to investigate *in vitro*, the effects of the haplotypes at physiological and isogenic conditions would be the CRISPR-based conversion of the PERK haplotypes in human iPSCs differentiated to neurons. Furthermore, in order to ascertain if PERK HapB undergoes cleavage in the human brain, it would be of great interest to carry out MS studies of the genotyped PSP control brains homozygous for the major (C) and minor allele (T) of *EIF2AK3.* With a clearer knowledge of the cleavage site, it would also enable us to design antibodies to specifically recognise the cleaved protein end and determine if there is a cell-type specific propensity for cleavage that could explain selective vulnerability in PSP. It is important to note that the frequency of the risk (rs7571971) allele in the normal population is 30% whereas in PSP this is significantly increased. Investigating the regional distribution of cleaved HapB PERK could explain as to why HapB PERK increases risk of disease.

7.3.2 *HapB PERK lumenal domain polymorphisms and dimerization*

Despite the caveats regarding the model described in the work, with the consistent observation of cleaved HapB PERK in P2 cells, we succeeded with the crucial read-out that with this cleavage, UPR activation resulted in reduced HapB PERK phosphorylation compared to the other haplotypes which also results in reduced eIF2α phosphorylation. It is not clear which of the three coding polymorphisms are chiefly responsible. As mentioned above, the HapB artificial sub-haplotypes showed us that two of the three risk alleles were necessary for the HapB-specific cleavage. This could be due to destabilisation of the entire PERK protein (Carrara et al., 2015; Wang et al., 2018; Cui et al., 2011). However, as two of the three polymorphisms (S136C and R166Q) are in the lumenal domain involved in homodimer formation leading to autoactivation of PERK, we are currently investigating this region with purified recombinant protein. We have overexpressed in *E. coli* the HapA and HapB variants of just the PERK lumenal domain with a cleavable N-terminal His-tag for purification.

The monomer of PERK lumenal domain is composed of a triangular assembly of beta-sheets interspaced by two short alpha-helixes (Carrara et al., 2015) and it is when two PERK monomers come together that it forms dimers and initiates autophosphorylation (Figure 75). Carrara et al., (2015) subdivided the PERK lumenal domain into three structural motifs related by function: dimerization subdomain consisting of a series of anti-parallel beta-strands which form the dimerization interface between PERK monomers, the beta-sandwich subdomain consisting entirely of β-strands arranged into a two-layer β-sandwich fold that is likely to stabilize the other subdomains, and the tetramer subdomain which consists mainly of beta-strands and one α-helix

that come together to create a cleft, which interacts with the opposite PERK monomer in a helix swap that most likely acts to stabilise the transient tetramer interface. Furthermore, the human PERK lumenal domain protein was present exclusively as a dimer (Carrara et al., 2015). Wang and colleagues (2018) built upon this study and observed that the beta-sandwich domain of the PERK lumenal domain may represent the peptide-binding site that interacts with misfolded proteins as they observed that this domain was able to adopt multiple conformations to interact with a broad range of misfolded proteins (Wang et al., 2018). Moreover, the structural flexibility of this sandwich domain enabled the lumenal domain to recognize and bind misfolded proteins with side chains of different sizes and hydrophobicities (Wang et al., 2018). Interestingly, it was also observed that introduction of mutations at the conserved hydrophobic residues located at the bottom of the peptide-binding groove of PERK lumenal domain compromised the ability of PERK to interact with their denatured model protein. One of these mutations, W165S, is adjacent to HapB R166Q polymorphic residue (Wang et al., 2018). This PERK W165S mutant when overexpressed caused reduced PERK and eIF2α phosphorylation in response to tunicamycin treatment indicating that a sole mutation in the lumenal domain is sufficient to reduce PERK activity (Wang et al., 2018).

In order to gain insight into the effect of the polymorphisms affecting the lumenal domain (S136C and R166Q), we have overexpressed in *E.coli* the HapA and HapB variants of the lumenal domain alone (residues 32–322). We will purify the proteins using a nickel-chelating column followed by chromatography on a Superdex 200 gel-filtration column (GE Healthcare). With the latter, we will also be able to analyse size fractionation profiles to study differences in the equilibrium between the monomeric and dimerised forms to see if there is impairment of dimerization of the HapB variant compared to HapA. Further work observing the direct binding of lumenal domain of PERK to BiP will also enable us to observe if the lumenal domain of HapB accommodates efficient binding to BiP in the presence of the two snps when compared to the binding of BiP to the lumenal domain of HapA PERK.

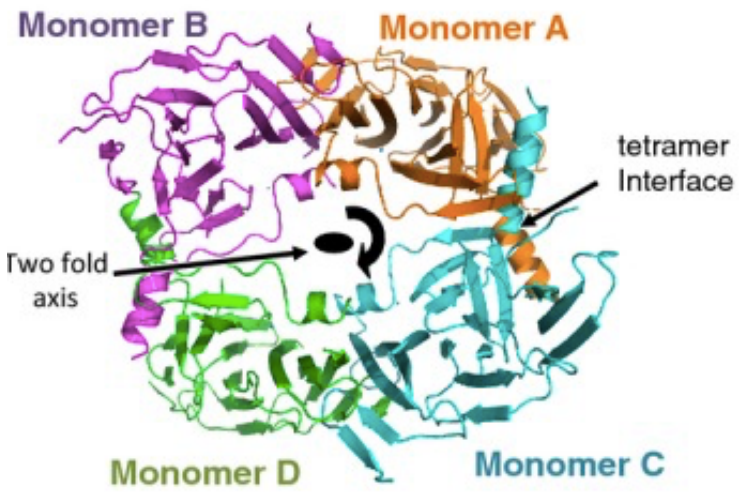

Figure 75. **The human PERK lumenal domain structure**. The individual monomers are arranged along a twofold rotation axis forming two sets of dimers A–B and C–D. Each dimer presents an inward-facing concave surface that intimately locks together at both ends to create a space in the centre of the ring tetramer. The dimerization interface involves the interaction between monomers A–B and C–D (Carrara et al.,2015).

7.3.3 Does a failure in PERK activity change the downstream effects of the UPR pathway?

Continuing our examination of the PERK pathway, a readout of cell death following ER stress indicated increased HapB PERK sensitivity to Tg and Tm dosage response curves. It would be exciting to follow this up with the sub-HapB PERK variants to observe if they too indicate increased ER stress sensitivity and compare these responses with that observed for the rarer PERK variants: HapC and HapD. Immunoblot analysis of CHOP could also be included as a readout of cell death as there was a strong shift of increased CHOP levels in the HapB PERK variants following UPR induction. This was seen systematically in response to a high concentration of Tm and Tg when treated for short durations. As HapB PERK kinase activity is observed to occur later than HapA, there would be no stress sensor present to temporality attenuate translation and this can explain the increase in cell death following acute Tg stress treatment. Although eIF2a phosphorylation levels were similarly decreased for both Tg and Tm in HapB cells, the direct downstream effector ATF4 displayed no differences between the haplotypes.

IRE1 and ATF6 pathways were explored to reveal potential crosstalk and impaired PERK's effect on the other UPR branches. ATF4, which is downstream of the PERK pathway, has been shown to upregulate IRE1 which in turn increases spliced to unspliced ratios of XBP1 (Tsuru et al., 2016). Normally with ER stress, IRE1 activation leads to the splicing of XBP1 mRNAs to form active

transcription factors that in turn transcriptionally upregulate chaperone genes (Yoshida et al., 2001). Impaired PERK should in theory therefore affect ATF4 translation and ultimately the IRE1-XBP1 signaling pathway. In our work, the UPR induction was stopped after 30 mins. Therefore, it is likely that these changes could have been more pronounced if treatment duration was increased. However, it is puzzling that although levels of eIF2α phosphorylation were observed to be severely decreased in myc-cleaved HapB cells, levels of ATF4 remained unchanged. As discussed previously, endogenous expression levels of these molecules are low and are hard to detect with available commercial antibodies. Therefore, the use of quantitative real-time PCR to measure the upregulation of the mRNA of UPR target genes may be a more reliable method to pick out subtle changes.

It is also worth noting that normally with ER stress, ATF6 translocates to the Golgi where it is cleaved to form active transcription factors (Mori et al., 2010). BiP is then transcriptionally upregulated to increase ER protein folding capacity. ATF4 has been shown to enhance the transcription of the ATF6 gene and contribute to the trafficking of ATF6 from the ER to the Golgi (Teske et al., 2011). Thus, impaired HapB PERK activity should in turn alter ATF4 levels which in turn should hinder ATF6 transcription, translocation, and ultimately BiP expression. ATF6 pathway should be therefore be investigated more thoroughly using the alternative detection methods outlined above.

HapB show emerging signs of delayed dimerization (as indicated by p-PERK) for Tg but not Tm; however, both Tg and Tm had similar results of impaired eIF2α phosphorylation. Tm prevents the posttranslational modification of N-glycosylation (Brandish et al., 1996), whereas Tg a sarcoplasmic/endoplasmic reticulum calcium ATPase inhibitor, depletes calcium in the ER (Wictome et al., 1992). Treatment with both of these ER stress inducers showed similar levels of increased p-PERK at 30 mins post treatment. It is possible that the amino acid differences between HapA and HapB (S136C and R166Q) on the lumenal domain of the protein act to promote and stabilize PERK dimerization, thereby increasing the likelihood of eIF2a kinase activity, while the change to the C-terminal cytoplasmic end of PERK (S704A) may decrease the likelihood of PERK transautophosphorylation. Therefore, it is puzzling as to why decreased calcium levels induced by Tg, but not the lack of posttranslational modifications elicited by Tm may have caused this discrepancy of HapB PERK dimerization. It will therefore help to investigate the sub HapB variants and observe if they too respond differently to Tg and Tm with opposite effects on PERK autophosphorylation observed between the two UPR inducers. While the decreased p-eIF2a in UPR induced HapB cells are a novel finding, it raises the possibility that the decrease in p-eIF2a may be independent of PERK's autophosphorylation status. It is worth noting that levels of ER stress comparable to those induced by the pharmacological agents utilized in our study are highly unlikely to be encountered by cells in natural situations. Cells of long-lived

organisms such as those in some nonrenewing tissues of mammalian species must ensure the consequences of accumulation of misfolded proteins in the ER over relatively long periods of time (Rutkowski et al., 2006; Hetz et al., 2012). Hence, we speculate that the differential role of HapB PERK presented in this thesis using potent acute pharmacological agents, might be a gross over-representation of PERK haplotype specific effects. Afterall PERK HapB is widespread with 30% frequency in populations of Northern-European descent and hence it is extremely unlikely that HapB homozygous individuals face such severe consequences of cellular dysfunction (Liu et al., 2012).

7.3.4 *Tau aggregation in PERK cells*

Although our cell model allowed for PERK genotypic profiling and characterization of UPR phenotypic manifestations this was not the sole goal of our thesis. We were also interested in observing whether impaired HapB PERK cells were more prone to tau aggregation than HapA cells thereby providing a direct link to the pathogenesis of PSP. Unfortunately, using our cell model system, we were unable to detect any differences in tau aggregation between the PERK variants. As indicated by our results, overexpression of PERK did not advocate the hyperphosphorylation of wild-type or mutant tau, conveying no relevance to sporadic PSP. However, aforementioned associations between phospho-tau deposition and UPR overactivation in tauopathies have been noted (Nijholt et al., 2011) which may result from PERK hyperactivation. In agreement, UPR induction in SK-N-SH neuroblastoma cells upregulated phosphorylation of Ser396 (PHF1 epitope) specifically, whilst total tau remained invariable (van der Harg et al., 2014). Moreover, as their work indicated, PERK activation was crucial as the selective PERK inhibitor GSK2606414 abolished this effect (van de Harg et al., 2014). Thus, despite converging evidence indicating increased tau phosphorylation, it is necessary to consider that increased PHF1 expression could also arise due to insufficient phosphatase activity. Future replications should consider sequential quantification of known tau phosphatases (e.g. PP2A - downregulated 50% in AD; Liu et al., 2005) to identify the molecular machinery responsible.

It is well known that hyperphosphorylated tau isoforms are routinely cleared by the UPS (Lee et al., 2013; Oddo et al., 2008). However, the influence of HapB PERK did not became apparent when proteasomal degradation was negated by MG132 application. Prior work has demonstrated higher endogenous PHF1 immunoreactivity in M1C cells treated with epoxomicin, a selective proteasome inhibitor (Hamano et al., 2009). Epoxomicin treatment also generated sarkosyl-insoluble, thioflavin S+ aggregates which is unsurprising as hyperphosphorylation is conducive to polymerization (Jeganathan et al., 2008). However, as thioflavin S staining was evident in all PERK cell lines, aggregates per se are unlikely to embody the risk conferred by EIF2AK3

haplotype B, congruent with the recent paradigm shift favoring soluble tau (d'Orange et al., 2018). Transient disruption of the UPS would delay tau clearance, which likely aggregates as a neuroprotective mechanism for sequestering toxic oligomers (Shiarli et al., 2006). However, as restoration of proteastasis occurred in our cell model system following the addition of Dox supplemented culture media, we would assume that resumption of tau degradation occurred, and as such any hyperphosphorylated tau by HapB PERK was lost, thereby losing the visualization of propagation of soluble oligomers and late-stage ß-sheet+ aggregates. Soluble oligomeric tau has demonstrated significant pathological capacity, including cytotoxicity in vitro (Lasagna-Reeves et al., 2010) and the ability to impair mitochondria and dysregulate synaptic transmission in vivo (Lasagna-Reeves et al., 2011). Therefore, it is important to acknowledge the reductionistic nature of this depiction as the UPS operates in conjunction with autophagy, which activates following MG132 treatment (Lagunas-Martínez et al., 2017). Markers of autophagy (e.g. LC3; Tanida et al., 2008) should also thus be assessed in future replications to investigate potential involvement.

In order to demonstrate clinical relevance, it is recommended that brains with confirmed PSP pathology are genotyped for EIF2AK3 haplotypes and immunoprecipitated tau analyzed for variation in phospho-epitopes such as PHF1.This would strengthen the suggestion that HapB PERK exhibits higher kinase activity; however, the instability of phosphorylation at post-mortem must be acknowledged (Wang et al., 2015). Immunostaining should also be performed to confirm PERK and tau co-localization as minimal evidence exists to suggest this occurs, partly due to low in vivo expression levels of endogenous PERK (Stutzbach et al., 2013; Pitera et al., 2019). Finally, involvement of downstream UPR mediators need to be assessed, particularly eIF2α, as the current study does not validate activation of the PERK pathway. Due to the interconnected nature of the UPR (Jiang et al., 2020) activation of IRE1 or ATF6 should also be determined as this could instigate compensatory mechanisms which moderate tau phosphorylation.

Although our model enabled for the accumulation of sarkosyl-insoluble tau following transfection of rTg4510 mouse brain homogenate, it took seven days before the formation of aggregated PHF-tau was detected by immunoblot. A potentially useful alternative cell culture model of tau aggregation could be the use of fluorescently tagged 2N4R (wild type) tau and 2N4R (P301L) tau which would enable us to monitor tau aggregation in real time following rTg4510 mouse brain transfection. This may bypass some of the experimental drawbacks of sarkosyl-extraction.

An increase in neuronal tau protein levels involving both total tau levels and hyperphosphorylated tau was noted following chemical inhibition of PERK signalling in iPSC-derived neurons undergoing tunicamycin-induced ER stress (Yuan et al.,2018). This is significant, as we observed that induction of the UPR resulted in impaired HapB PERK activity. Therefore, it is likely that

impaired PERK activity which may in turn be unable efficiently to attenuate translation will result in increased or sustained translation of the *MAPT* mRNA. This will increase total tau protein levels. This potential mechanism could underlie the increase in tau protein levels seen in neurons carrying HapB PERK alleles and should be tested in our cell model system as we already have established protocols of inducing the UPR with Tg and Tm with treatment durations not exceeding 30 mins. Induction of the UPR following rTg4510 mouse brain transfection into P301L transfected HapA and HapB cells may not only increase the likelihood of obtaining tau inclusions but may also enable us to observe the presence of insoluble tau inclusions much sooner than our previous time scale of seven days.

Although emerging evidence conveys that tau is secreted during physiological circumstances (Katsinelos et al., 2018), pharmacological inhibition of the ER-Golgi pathway did not alter extracellular deposition. Therefore, it is likely that cytoplasmic kinases such as GSK-3b is upregulated during UPR stress (Nijholt et al., 2013) and are directly involved in the phosphorylation process. Nonetheless, there is a growing consensus for a tau-ER interaction. For example, heightened PHF1+ tau is associated with ER membranes in JNPL3 (tauP301L) mice (Perreault et al., 2009) and 91 ER proteins have shown to co-immunoprecipitated with tau from brain tissue, with ~ 43% of proteins exclusive to AD samples (Meier et al., 2015). Furthermore, the direct role of PERK is reinforced as phospho-tau colocalizes with phospho-PERK in a murine tauopathy model (Ho et al., 2012). Interestingly, in their work phosphorylation of tau at Ser396 was elevated at 6-12 h following induction of ER stress with thapsigargin but declined by 18 h post-treatment, possibly reflecting UPS clearance of PHF1+ tau (Ho et al., 2012). Furthermore, no changes in GSKβ levels were detected throughout, excluding a role for this kinase in observed tau phosphorylation (Ho et al., 2012).

Interestingly, PERK may directly bind tau via a conserved hydrophobic motif within the lumenal domain, recently visualized by crystallography (Wang et al., 2018). The authors identified a conserved region ('WRFY') within a peptide - referred to as P16 - which mediated this interaction. A preliminary cross-reference with 0N4R tau highlights a motif within the microtubule-binding domains (275VQIV278; 306VQIV309) which exhibits a similar electrostatic sequence (i.e. hydrophobic-hydrophobic-polar-hydrophobic). Pathological mutagenesis of nearby residues (e.g. P301L) may therefore reduce binding affinity by modifying the conformation. Conversely, residue W165 within PERK facilitates binding and the adjacent R166Q mutation found in HapB could enhance this interaction. Although this remains speculative, an in vivo PERK-tau complex has recently been recognized (Fontaine et al., unpublished), supporting a primary role for PERK in tau pathology. Verifying these claims will require site-directed mutagenesis of the microtubule-binding domains which will form the basis of a subsequent kinase assay. In addition, examining

why tau mislocalises to the ER will further aid the understanding of the UPR in tauopathy pathogenesis.

7.4 Conclusion

Discovering the link between the protein PERK and the tauopathy PSP was initiated almost a decade ago by the discovery of a genetic association between the two as part of a GWAS (Hoglinger et al. 2011). Our work subsequently focused on exploring the functional biological basis of this association through establishing cellular models carrying the PERK-coding haplotypes HapA and HapB. Based on increasing evidence of the significance of PERK signalling and the UPR response in neurodegenerative proteopathies (Nijholt et al., 2013; Stutzbach et al., 2013; Bell et al., 2016) this work has shown that the increased risk of PSP conferred by Haplotype B is due to decreased PERK activation which, in turn, could contribute to tau pathology progression. The use of the sub HapB clones would be useful in identifying if impaired PERK stress-sensing arises solely from the lumenal domains or/and the slower activation kinetics of the cytosolic kinase.

PERK is crucial as a protective mechanism in cells across all organ systems (Harding et al., 2000). When it malfunctions, as in Wolcott Rallison Syndrome (WRS), the results are severe. WRS is an uncommon autosomal recessive condition which sees insulin-dependent diabetes developing in neonates and infants, associated with skeletal dysplasia and growth retardation (Wolcott and Rallison., 1972). It is caused by a lack of functional PERK (Delepine et al., 2000). It often results from deletions or mutations in the PERK gene that render the active site inactive. In WRS, *PERK* variants introduce nonsense and splice-site mutations that trigger nonsense-mediated mRNA decay with no PERK protein synthesis, or they directly mutate the kinase lobes and nullify its enzymatic activities (Feng et al., 2009). It is the absence of PERK protein and abrogation of kinase function by the WRS PERK mutations that cause the pancreatic insufficiency clinical phenotypes similar to those seen in the *Perk*$^{-/-}$ mouse (Zhang et al., 2002; Harding et al., 2001; Zhang et al., 2006). In contrast, the tauopathy-associated PERK coding variants alter amino acids in the PERK lumenal domain involved in ER stress sensing (S136C, R166Q) and in regions of the cytosolic domain proposed to include a ‘disordered linker’ (S704A, D566V) that joins essential lobes of the PERK kinase domain (Yuan et al., 2018).

Greater insights into the impact of PERK in PSP were gained through pharmacological activation and inhibition of PERK (Bruch et al. 2017; Radford et al. 2015). As reduced HapB PERK signalling promotes toxic tau aggregation (Yuan et al., 2018), pharmacologic PERK activation attenuates aggregation and toxicity of PSP-related tau mutants (Bruch et al., 2017). In mouse models, Bruch

et al. (2017) showed that PERK activation abolishes an increase in 4R tau. In addition, PERK activation also reduced many stigmata of tau pathology – both *in vitro* and *in vivo* – including tau phosphorylation, conformational change, neuronal cell viability, as well as improving memory function and motor function in the common P301S tau mouse model for PSP. Alternatively, sustained PERK signalling associated with chronic or severe ER insults is implicated in neurodegenerative diseases such as AD and in prion disease (Moreno et al., 2012; Abisambra et al., 2013; Radford et al., 2015; Devi and Ohno 2014; Moreno et al., 2013). As such, pharmacologic inhibition of PERK has emerged as a potential strategy to ameliorate neurodegeneration-associated pathologies involved in these disorders (Grande et al., 2018; Sharma et al., 2018). The compound GSK2606414 is a potent and selective PERK inhibitor recently shown to alleviate motor deficits in a rodent model of prion disease (Moreno et al., 2013). Here the compound successfully reduced the prion phenotype in both preventative and therapeutic interventions. However, treatment for more than three months caused the mice to lose 20 % of their body weight and exhibit a moderate increase in their blood glucose levels. Although these data suggest that the compound has a promising on-target effect on a pancreatic homolog of PERK, there is also the potential harm derived from the severe side effects of this PERK inhibitor.

This data can thus be extrapolated to indicate that genetic variation that either alters or regulates the level of PERK in the cell could also disrupt crucial cellular pathways and contribute to disease pathogenesis. The results presented in this thesis indicate the possibility of impaired HapB PERK heightening cellular dysfunction in response to ER stress.

Appendix One

Primers and Corresponding Sequences

Primer Name	Sequence 5'→3'	Target Sequence (bp)
Forward Primer 1	5'- AGACGATGAGACAGAGTTGCGACC -3'	288-311
Reverse Primer 1	5'- AAGGCTGGATGACACCAAGGAAC -3'	438-416
Forward Primer 2	5' – ATCCAGCCTTAGCAAACC -3'	429 – 446
Reverse Primer 2	5'- TTCTCATTGCCACTGCGAGG -3'	779 – 760
Forward Primer 3	5'- CAGATTACAGTCAGATTCCTCG -3'	1495-1516
Reverse Primer 3	5'- TGAGGATGGAAAAGCCTGC -3'	1652-1634
EcoR1-Forward Primer 4	GCCAGTTCTCACCACTGGAATTCTC	2219-2243
PERK-Eco-Reverse Primer 4	GAGAATTCCAGTGGTGAGAAC	2223-2243
Forward Primer 5	AGATGTGCAGACACACGCTC	2745-2764
Reverse Primer 6	ATGTTGGATGGCTTGAGGTC	2821-2840
CMV Forward (vector junction)	CGCAAATGGGCGGTAGGCGTG	0 – 300
BGR Reverse (vector junction)	GCCTCGACTGTGCCTTCTA	3200 – 2700

This appendix lists primers used in the study described in Chapter 3 and includes the primer sequences used for DNA amplification and sequencing.

List of References

Abdin, A.A., Hamouda, H.E., 2008. Mechanism of the neuroprotective role of coenzyme Q10 with or without L-dopa in rotenone-induced parkinsonism. Neuropharmacology 55, 1340–1346. https://doi.org/10.1016/j.neuropharm.2008.08.033

Abisambra, J.F., Jinwal, U.K., Blair, L.J., O'Leary, J.C., Li, Q., Brady, S., Wang, L., Guidi, C.E., Zhang, B., Nordhues, B.A., Cockman, M., Suntharalingham, A., Li, P., Jin, Y., Atkins, C.A., Dickey, C.A., 2013. Tau Accumulation Activates the Unfolded Protein Response by Impairing Endoplasmic Reticulum-Associated Degradation. J. Neurosci. 33, 9498–9507. https://doi.org/10.1523/JNEUROSCI.5397-12.2013

Adams, C.J., Kopp, M.C., Larburu, N., Nowak, P.R., Ali, M.M.U., 2019. Structure and Molecular Mechanism of ER Stress Signaling by the Unfolded Protein Response Signal Activator IRE1. Front. Mol. Biosci. 6, 11. https://doi.org/10.3389/fmolb.2019.00011

Adams, S.J., DeTure, M.A., McBride, M., Dickson, D.W., Petrucelli, L., 2010. Three Repeat Isoforms of Tau Inhibit Assembly of Four Repeat Tau Filaments. PLoS ONE 5, e10810. https://doi.org/10.1371/journal.pone.0010810

Allen, B., Ingram, E., Takao, M., Smith, M.J., Jakes, R., Virdee, K., Yoshida, H., Holzer, M., Craxton, M., Emson, P.C., Atzori, C., Migheli, A., Crowther, R.A., Ghetti, B., Spillantini, M.G., Goedert, M., 2002. Abundant Tau Filaments and Nonapoptotic Neurodegeneration in Transgenic Mice Expressing Human P301S Tau Protein. J. Neurosci. 22, 9340–9351. https://doi.org/10.1523/JNEUROSCI.22-21-09340.2002

Alam, J., Stewart, D., Touchard, C., Boinapally, S., Choi, A.M.K., Cook, J.L., 1999. Nrf2, a Cap'n'Collar Transcription Factor, Regulates Induction of the Heme Oxygenase-1 Gene. J. Biol. Chem. 274, 26071–26078. https://doi.org/10.1074/jbc.274.37.26071

Al-Bassam, J., Ozer, R.S., Safer, D., Halpain, S., Milligan, R.A., 2002. MAP2 and tau bind longitudinally along the outer ridges of microtubule protofilaments. J. Cell Biol. 157, 1187–1196. https://doi.org/10.1083/jcb.200201048

Alberini, C.M., 2008. The role of protein synthesis during the labile phases of memory: Revisiting the skepticism. Neurobiol. Learn. Mem. 89, 234–246. https://doi.org/10.1016/j.nlm.2007.08.007

Albers, D.S., Swerdlow, R.H., Manfredi, G., Gajewski, C., Yang, L., Parker, W.D., Beal, M.F., 2001. Further Evidence for Mitochondrial Dysfunction in Progressive Supranuclear Palsy. Exp. Neurol. 168, 196–198. https://doi.org/10.1006/exnr.2000.7607

Alonso, A.C., Zaidi, T., Grundke-Iqbal, I., Iqbal, K., 1994. Role of abnormally phosphorylated tau in the breakdown of microtubules in Alzheimer disease. Proceedings of the National Academy of Sciences 91, 5562–5566. https://doi.org/10.1073/pnas.91.12.5562

Amos, L.A., 2004. Microtubule structure and its stabilisation. Organic and Biomolecular Chemistry, 15 (2) 2153-2160. https://doi.org/10.1039/b403634d

Andreadis, A., Brown, W.M., Kosik, K.S., 1992a. Structure and novel exons of the human .tau. gene. Biochemistry 31, 10626–10633. https://doi.org/10.1021/bi00158a027

Andreadis, A., Brown, W.M., Kosik, K.S., 1992b. Structure and novel exons of the human .tau. gene. Biochemistry 31, 10626–10633. https://doi.org/10.1021/bi00158a027

Andreadis, A., Wagner, B.K., Broderick, J.A., Kosik, K.S., 2002. A τ Promoter Region Without Neuronal Specificity. J. Neurochem. 66, 2257–2263. https://doi.org/10.1046/j.1471-4159.1996.66062257.x

Apetauerova, D., Scala, S.A., Hamill, R.W., Simon, D.K., Pathak, S., Ruthazer, R., Standaert, D.G., Yacoubian, T.A., 2016. CoQ10 in progressive supranuclear palsy: A randomized, placebo-controlled, double-blind trial. Neurol. - Neuroimmunol. Neuroinflammation 3, e266. https://doi.org/10.1212/NXI.0000000000000266

Aragón, T., van Anken, E., Pincus, D., Serafimova, I.M., Korennykh, A.V., Rubio, C.A., Walter, P., 2009. Messenger RNA targeting to endoplasmic reticulum stress signalling sites. Nature 457, 736–740. https://doi.org/10.1038/nature07641

Arai, T., Ikeda, K., Akiyama, H., Tsuchiya, K., Iritani, S., Ishiguro, K., Yagishita, S., Oda, T., Odawara, T., Iseki, E., 2003. Different immunoreactivities of the microtubule-binding region of tau and its molecular basis in brains from patients with Alzheimer's disease, Pick's disease, progressive supranuclear palsy and corticobasal degeneration. Acta Neuropathol. (Berl.) 105, 489–498. https://doi.org/10.1007/s00401-003-0671-8

Araki, E., Oyadomari, S., Mori, M., 2003. Endoplasmic Reticulum Stress and Diabetes Mellitus. Intern. Med. 42, 7–14. https://doi.org/10.2169/internalmedicine.42.7

Arendt, T., Stieler, J.T., Holzer, M., 2016. Tau and tauopathies. Brain Res. Bull. 126, 238–292. https://doi.org/10.1016/j.brainresbull.2016.08.018

Arikan, M.C., Memmott, J., Broderick, J.A., Lafyatis, R., Screaton, G., Stamm, S., Andreadis, A., 2002. Modulation of the membrane-binding projection domain of tau protein: splicing regulation of exon 3. Mol. Brain Res. 101, 109–121. https://doi.org/10.1016/S0169-328X(02)00178-X

Arima, K., Nakamura, M., Sunohara, N., Ogawa, M., Anno, M., Izumiyama, Y., Hirai, S., Ikeda, K., 1997. Ultrastructural characterization of the tau-immunoreactive tubules in the oligodendroglial perikarya and their inner loop processes in progressive supranuclear palsy. Acta Neuropathol. (Berl.) 93, 558–566. https://doi.org/10.1007/s004010050652

Asai, H., Ikezu, S., Tsunoda, S., Medalla, M., Luebke, J., Haydar, T., Wolozin, B., Butovsky, O., Kügler, S., Ikezu, T., 2015. Depletion of microglia and inhibition of exosome synthesis halt tau propagation. Nat. Neurosci. 18, 1584–1593. https://doi.org/10.1038/nn.4132

Avila, J., Jiménez, J.S., Sayas, C.L., Bolós, M., Zabala, J.C., Rivas, G., Hernández, F., 2016. Tau Structures. Front. Aging Neurosci. 8, 262. https://doi.org/10.3389/fnagi.2016.00262

Baas, P.W., Brown, A., 1997. Slow axonal transport: the polymer transport model. Trends Cell Biol. 7, 380–384. https://doi.org/10.1016/S0962-8924(97)01148-3

Baba, Y., Baker, M.C., Le Ber, I., Brice, A., Maeck, L., Kohlhase, J., Yasuda, M., Stoppe, G., Bugiani, O., Sperfeld, A.D., Tsuboi, Y., Uitti, R.J., Farrer, M.J., Ghetti, B., Hutton, M.L., Wszolek, Z.K., 2007. Clinical and genetic features of families with frontotemporal dementia and parkinsonism linked to chromosome 17 with a P301S tau mutation. J. Neural Transm. 114, 947–950. https://doi.org/10.1007/s00702-007-0632-9

Backliwal, G., Hildinger, M., Hasija, V., Wurm, F.M., 2008. High-density transfection with HEK-293 cells allows doubling of transient titers and removes need for a priori DNA complex formation with PEI. Biotechnol. Bioeng. 99, 721–727. https://doi.org/10.1002/bit.21596

Baker, M., Litvan, I., Houlden, H., Adamson, J., Dickson, D., Perez-Tur, J., Hardy, J., Lynch, T., Bigio, E., Hutton, M., 1999. Association of an Extended Haplotype in the Tau Gene with Progressive Supranuclear Palsy. Hum. Mol. Genet. 8, 711–715. https://doi.org/10.1093/hmg/8.4.711

Balch, W.E., Morimoto, R.I., Dillin, A., Kelly, J.W., 2008. Adapting Proteostasis for Disease Intervention. Science 319, 916–919. https://doi.org/10.1126/science.1141448

Baldi, L., Hacker, D.L., Adam, M., Wurm, F.M., 2007. Recombinant protein production by large-scale transient gene expression in mammalian cells: state of the art and future perspectives. Biotechnol Lett 29, 677–684. https://doi.org/10.1007/s10529-006-9297-y

Barghorn, S., Zheng-Fischhöfer, Q., Ackmann, M., Biernat, J., von Bergen, M., Mandelkow, E.-M., Mandelkow, E., 2000. Structure, Microtubule Interactions, and Paired Helical Filament Aggregation by Tau Mutants of Frontotemporal Dementias †. Biochemistry 39, 11714–11721. https://doi.org/10.1021/bi000850r

Beal, M.F., Matthews, R.T., Tieleman, A., Shults, C.W., 1998. Coenzyme Q10 attenuates the 1-methyl-4-phenyl-1,2,3,6-tetrahydropyridine (MPTP) induced loss of striatal dopamine and dopaminergic axons in aged mice. Brain Res. 783, 109–114. https://doi.org/10.1016/S0006-8993(97)01192-X

Berger, Z., Roder, H., Hanna, A., Carlson, A., Rangachari, V., Yue, M., Wszolek, Z., Ashe, K., Knight, J., Dickson, D., Andorfer, C., Rosenberry, T.L., Lewis, J., Hutton, M., Janus, C., 2007. Accumulation of Pathological Tau Species and Memory Loss in a Conditional Model of Tauopathy. Journal of Neuroscience 27, 3650–3662. https://doi.org/10.1523/JNEUROSCI.0587-07.2007

Bergeron, C., Pollanen, M.S., Weyer, L., Lang, A.E., 1997. Cortical degeneration in progressive supranuclear palsy. A comparison with cortical-basal ganglionic degeneration. J. Neuropathol. Exp. Neurol. 56, 726–734.

Bernales. S., Papa. F.R., Walter. P., 2006. Intracellular signaling by the unfolded protein response. Annu Rev Cell Dev Biol. 22:487-508. doi: 10.1146/annurev.cellbio.21.122303.120200.

Bell, M.C., Meier, S.E., Ingram, A.L., Abisambra, J.F., 2016. PERK-opathies: An Endoplasmic Reticulum Stress Mechanism Underlying Neurodegeneration. Curr Alzheimer Res 13, 150–163. https://doi.org/10.2174/1567205013666151218145431

Bellucci, A., Westwood, A.J., Ingram, E., Casamenti, F., Goedert, M., Spillantini, M.G., 2004. Induction of Inflammatory Mediators and Microglial Activation in Mice Transgenic for Mutant Human P301S Tau Protein. The American Journal of Pathology 165, 1643–1652. https://doi.org/10.1016/S0002-9440(10)63421-9

Berry, R.W., Sweet, A.P., Clark, F.A., Lagalwar, S., Lapin, B.R., Wang, T., Topgi, S., Guillozet-Bongaarts, A.L., Cochran, E.J., Bigio, E.H., Binder, L.I., 2004. Tau epitope display in progressive supranuclear palsy and corticobasal degeneration. J. Neurocytol. 33, 287–295. https://doi.org/10.1023/B:NEUR.0000044190.96426.b9

Bertolotti, A., Zhang, Y., Hendershot, L.M., Harding, H.P., Ron, D., 2000. Dynamic interaction of BiP and ER stress transducers in the unfolded-protein response. Nat. Cell Biol. 2, 326–332. https://doi.org/10.1038/35014014

Birdi, S., Rajput, A.H., Fenton, M., Donat, J.R., Rozdilsky, B., Robinson, C., Macaulay, R., George, D., 2002. Progressive supranuclear palsy diagnosis and confounding features: Report on 16 autopsied cases. Mov. Disord. 17, 1255–1264. https://doi.org/10.1002/mds.10211

Black, M.M., Slaughter, T., Moshiach, S., Obrocka, M., Fischer, I., 1996. Tau is enriched on dynamic microtubules in the distal region of growing axons. J. Neurosci. Off. J. Soc. Neurosci. 16, 3601–3619.

Blais, J.D., Filipenko, V., Bi, M., Harding, H.P., Ron, D., Koumenis, C., Wouters, B.G., Bell, J.C., 2004. Activating Transcription Factor 4 Is Translationally Regulated by Hypoxic Stress. Mol. Cell. Biol. 24, 7469–7482. https://doi.org/10.1128/MCB.24.17.7469-7482.2004

Borroni, B., Archetti, S., Del Bo, R., Papetti, A., Buratti, E., Bonvicini, C., Agosti, C., Cosseddu, M., Turla, M., Di Lorenzo, D., Pietro Comi, G., Gennarelli, M., Padovani, A., 2010. *TARDBP* Mutations in Frontotemporal Lobar Degeneration: Frequency, Clinical Features, and Disease Course. Rejuvenation Res. 13, 509–517. https://doi.org/10.1089/rej.2010.1017

Boxer, A.L., Yu, J.-T., Golbe, L.I., Litvan, I., Lang, A.E., Höglinger, G.U., 2017. Advances in progressive supranuclear palsy: new diagnostic criteria, biomarkers, and therapeutic approaches. Lancet Neurol. 16, 552–563. https://doi.org/10.1016/S1474-4422(17)30157-6

Boyce, M., 2005. A Selective Inhibitor of eIF2 Dephosphorylation Protects Cells from ER Stress. Science 307, 935–939. https://doi.org/10.1126/science.1101902

Braakman, I., Bulleid, N.J., 2011. Protein Folding and Modification in the Mammalian Endoplasmic Reticulum. Annu. Rev. Biochem. 80, 71–99. https://doi.org/10.1146/annurev-biochem-062209-093836

Bradford, M.M., 1976. A rapid and sensitive method for the quantitation of microgram quantities of protein utilizing the principle of protein-dye binding. Analytical Biochemistry 72, 248–254. https://doi.org/10.1016/0003-2697(76)90527-3

Braakman, I., Hebert, D.N., 2013. Protein Folding in the Endoplasmic Reticulum. Cold Spring Harb. Perspect. Biol. 5, a013201–a013201. https://doi.org/10.1101/cshperspect.a013201

Brandish, P.E., Kimura, K.I., Inukai, M., Southgate, R., Lonsdale, J.T., Bugg, T.D., 1996. Modes of action of tunicamycin, liposidomycin B, and mureidomycin A: inhibition of phospho-N-acetylmuramyl-pentapeptide translocase from Escherichia coli. Antimicrob. Agents Chemother. 40, 1640–1644. https://doi.org/10.1128/AAC.40.7.1640

Brandt, R., Léger, J., Lee, G., 1995. Interaction of tau with the neural plasma membrane mediated by tau's amino-terminal projection domain. J. Cell Biol. 131, 1327–1340. https://doi.org/10.1083/jcb.131.5.1327

Brandt, R., Hundelt, M., Shahani, N., 2005. Tau alteration and neuronal degeneration in tauopathies: mechanisms and models. Biochimica et Biophysica Acta (BBA) - Molecular Basis of Disease 1739, 331–354. https://doi.org/10.1016/j.bbadis.2004.06.018

Bravo, R., Parra, V., Gatica, D., Rodriguez, A.E., Torrealba, N., Paredes, F., Wang, Z.V., Zorzano, A., Hill, J.A., Jaimovich, E., Quest, A.F.G., Lavandero, S., 2013. Endoplasmic Reticulum and the Unfolded Protein Response, in: International Review of Cell and Molecular Biology. Elsevier, pp. 215–290. https://doi.org/10.1016/B978-0-12-407704-1.00005-1

Brewer, J.W., Diehl, J.A., 2000. PERK mediates cell-cycle exit during the mammalian unfolded protein response. Proc. Natl. Acad. Sci. 97, 12625–12630. https://doi.org/10.1073/pnas.220247197

Brion, J.P., Couck, A.M., Passareiro, E., Flament-Durand, J., 1985a. Neurofibrillary tangles of Alzheimer's disease: an immunohistochemical study. J. Submicrosc. Cytol. 17, 89–96.

Brion, J.P., van den Bosch de Aguilar, P., Flament-Durand, J., 1985b. Senile Dementia of the Alzheimer Type: Morphological and Immunocytochemical Studies, in: Traber, J., Gispen, W.H. (Eds.), Senile Dementia of the Alzheimer Type. Springer Berlin Heidelberg, Berlin, Heidelberg, pp. 164–174. https://doi.org/10.1007/978-3-642-70644-8_13

Bronner, I.F., ter Meulen, B.C., Azmani, A., Severijnen, L.A., Willemsen, R., Kamphorst, W., Ravid, R., Heutink, P., van Swieten, J.C., 2005. Hereditary Pick's disease with the G272V tau mutation shows predominant three-repeat tau pathology. Brain 128, 2645–2653. https://doi.org/10.1093/brain/awh591

Brown, J., Lantos, P., Stratton, M., Roques, P., Rossor, M., 1993. Familial progressive supranuclear palsy. J. Neurol. Neurosurg. Psychiatry 56, 473–476. https://doi.org/10.1136/jnnp.56.5.473

Brown, M.R., Bondada, V., Keller, J.N., Thorpe, J., Geddes, J.W., 2005. Proteasome or calpain inhibition does not alter cellular tau levels in neuroblastoma cells or primary neurons. JAD 7, 15–24. https://doi.org/10.3233/JAD-2005-7103

Bruch, J., Xu, H., Rösler, T.W., De Andrade, A., Kuhn, P., Lichtenthaler, S.F., Arzberger, T., Winklhofer, K.F., Müller, U., Höglinger, G.U., 2017. PERK activation mitigates tau pathology *in vitro* and *in vivo*. EMBO Mol. Med. 9, 371–384. https://doi.org/10.15252/emmm.201606664

Brunden, K.R., Trojanowski, J.Q., Lee, V.M.-Y., 2009. Advances in tau-focused drug discovery for Alzheimer's disease and related tauopathies. Nat Rev Drug Discov 8, 783–793. https://doi.org/10.1038/nrd2959

Brusa, A., Stoehr, R., Pramstaller, P.P., 2004. Progressive supranuclear palsy: New disease or variant of postencephalitic parkinsonism? Mov. Disord. 19, 247–252. https://doi.org/10.1002/mds.10699

Buée, L., Bussière, T., Buée-Scherrer, V., Delacourte, A., Hof, P.R., 2000. Tau protein isoforms, phosphorylation and role in neurodegenerative disorders11These authors contributed equally to this work. Brain Res. Rev. 33, 95–130. https://doi.org/10.1016/S0165-0173(00)00019-9

Bugiani, O., Murrell, J.R., Giaccone, G., Hasegawa, M., Ghigo, G., Tabaton, M., Morbin, M., Primavera, A., Carella, F., Solaro, C., Grisoli, M., Savoiardo, M., Spillantini, M.G., Tagliavini, F., Goedert, M., Ghetti, B., 1999. Frontotemporal Dementia and Corticobasal Degeneration in a Family with a P301S Mutation in Tau: Journal of Neuropathology and Experimental Neurology 58, 667–677. https://doi.org/10.1097/00005072-199906000-00011

Burke, D.F., Worth, C.L., Priego, E.-M., Cheng, T., Smink, L.J., Todd, J.A., Blundell, T.L., 2007. Genome bioinformatic analysis of nonsynonymous SNPs. BMC Bioinformatics 8, 301. https://doi.org/10.1186/1471-2105-8-301

Bussière, T., Hof, P.R., Mailliot, C., Brown, C.D., Caillet-Boudin, M.L., Perl, D.P., Buée, L., Delacourte, A., 1999. Phosphorylated serine422 on tau proteins is a pathological epitope found in several diseases with neurofibrillary degeneration. Acta Neuropathol. (Berl.) 97, 221–230. https://doi.org/10.1007/s004010050978

Butner, K.A., Kirschner, M.W., 1991. Tau protein binds to microtubules through a flexible array of distributed weak sites. J. Cell Biol. 115, 717–730. https://doi.org/10.1083/jcb.115.3.717

Caffrey, T.M., Joachim, C., Paracchini, S., Esiri, M.M., Wade-Martins, R., 2006. Haplotype-specific expression of exon 10 at the human MAPT locus. Hum. Mol. Genet. 15, 3529–3537. https://doi.org/10.1093/hmg/ddl429

Caffrey, T.M., Joachim, C., Wade-Martins, R., 2008. Haplotype-specific expression of the N-terminal exons 2 and 3 at the human MAPT locus. Neurobiol. Aging 29, 1923–1929. https://doi.org/10.1016/j.neurobiolaging.2007.05.002

Cao, J., Dai, D.-L., Yao, L., Yu, H.-H., Ning, B., Zhang, Q., Chen, J., Cheng, W.-H., Shen, W., Yang, Z.-X., 2012. Saturated fatty acid induction of endoplasmic reticulum stress and apoptosis in human liver cells via the PERK/ATF4/CHOP signaling pathway. Mol. Cell. Biochem. 364, 115–129. https://doi.org/10.1007/s11010-011-1211-9

Carlisle, R.E., Brimble, E., Werner, K.E., Cruz, G.L., Ask, K., Ingram, A.J., Dickhout, J.G., 2014. 4-Phenylbutyrate Inhibits Tunicamycin-Induced Acute Kidney Injury via CHOP/GADD153 Repression. PLoS ONE 9, e84663. https://doi.org/10.1371/journal.pone.0084663

Carrara, M., Prischi, F., Nowak, P.R., Kopp, M.C., Ali, M.M., 2015. Noncanonical binding of BiP ATPase domain to Ire1 and Perk is dissociated by unfolded protein CH1 to initiate ER stress signaling. eLife 4, e03522. https://doi.org/10.7554/eLife.03522

Castle, J.C., Zhang, C., Shah, J.K., Kulkarni, A.V., Kalsotra, A., Cooper, T.A., Johnson, J.M., 2008. Expression of 24,426 human alternative splicing events and predicted cis regulation in 48 tissues and cell lines. Nat. Genet. 40, 1416–1425. https://doi.org/10.1038/ng.264

Chakrabarti, A., Chen, A.W., Varner, J.D., 2011. A review of the mammalian unfolded protein response. Biotechnol. Bioeng. 108, 2777–2793. https://doi.org/10.1002/bit.23282

Chambers, C.B., Lee, J.M., Troncoso, J.C., Reich, S., Muma, N.A., 1999. Overexpression of four-repeat tau mRNA isoforms in progressive supranuclear palsy but not in Alzheimer's disease. Ann. Neurol. 46, 325–332. https://doi.org/10.1002/1531-8249(199909)46:3<325::aid-ana8>3.0.co;2-v

Chan, J.Y., Han, X.L., Kan, Y.W., 1993. Cloning of Nrf1, an NF-E2-related transcription factor, by genetic selection in yeast. Proc. Natl. Acad. Sci. 90, 11371–11375. https://doi.org/10.1073/pnas.90.23.11371

Chang, R.C.C., Wong, A.K.Y., Ng, H.-K., Hugon, J., 2002. Phosphorylation of eukaryotic initiation factor-2α (eIF2α) is associated with neuronal degeneration in Alzheimer's disease: NeuroReport 13, 2429–2432. https://doi.org/10.1097/00001756-200212200-00011

Chang, E., Kim, S., Yin, H., Nagaraja, H.N., Kuret, J., 2008. Pathogenic missense MAPT mutations differentially modulate tau aggregation propensity at nucleation and extension steps. J Neurochem 107, 1113–1123. https://doi.org/10.1111/j.1471-4159.2008.05692.x

Chang, T.-K., Lawrence, D.A., Lu, M., Tan, J., Harnoss, J.M., Marsters, S.A., Liu, P., Sandoval, W., Martin, S.E., Ashkenazi, A., 2018. Coordination between Two Branches of the Unfolded Protein Response Determines Apoptotic Cell Fate. Molecular Cell 71, 629-636.e5. https://doi.org/10.1016/j.molcel.2018.06.038

Chen,J.,Kanai, Y., Cowan NJ, Hirokawa, N., 1992. Projection domains of MAP2 and tau determine spacings between microtubules in dendrites and axons. Nature **360**:674–677.

Chen, J.-J., London, I.M., 1995. Regulation of protein synthesis by heme-regulated eIF-2α kinase. Trends Biochem. Sci. 20, 105–108. https://doi.org/10.1016/S0968-0004(00)88975-6

Chen, Y., Wang, J.J., Li, J., Hosoya, K.I., Ratan, R., Townes, T., Zhang, S.X., 2012. Activating transcription factor 4 mediates hyperglycaemia-induced endothelial inflammation and retinal vascular leakage through activation of STAT3 in a mouse model of type 1 diabetes. Diabetologia 55, 2533–2545. https://doi.org/10.1007/s00125-012-2594-1

Chen, J.A., Chen, Z., Won, H., Huang, A.Y., Lowe, J.K., Wojta, K., Yokoyama, J.S., Bensimon, G., Leigh, P.N., Payan, C., Shatunov, A., Jones, A.R., Lewis, C.M., Deloukas, P., Amouyel, P., Tzourio, C., Dartigues, J.-F., Ludolph, A., Boxer, A.L., Bronstein, J.M., Al-Chalabi, A., Geschwind, D.H., Coppola, G., 2018. Joint genome-wide association study of progressive supranuclear palsy identifies novel susceptibility loci and genetic correlation to neurodegenerative diseases. Mol Neurodegeneration 13, 41. https://doi.org/10.1186/s13024-018-0270-8

Chruścicka, B., Burnat, G., Brański, P., Chorobik, P., Lenda, T., Marciniak, M., Pilc, A., 2015. Tetracycline-Based System for Controlled Inducible Expression of Group III Metabotropic Glutamate Receptors. J Biomol Screen 20, 350–358. https://doi.org/10.1177/1087057114559183

Clavaguera, F., Bolmont, T., Crowther, R.A., Abramowski, D., Frank, S., Probst, A., Fraser, G., Stalder, A.K., Beibel, M., Staufenbiel, M., Jucker, M., Goedert, M., Tolnay, M., 2009. Transmission and spreading of tauopathy in transgenic mouse brain. Nat Cell Biol 11, 909–913. https://doi.org/10.1038/ncb1901

Chesnoy, S., Huang, L., 2000. Structure and Function of Lipid-DNA Complexes for Gene Delivery. Annu. Rev. Biophys. Biomol. Struct. 29, 27–47. https://doi.org/10.1146/annurev.biophys.29.1.27

Cleveland, D.W., Hwo, S.-Y., Kirschner, M.W., 1977. Physical and chemical properties of purified tau factor and the role of tau in microtubule assembly. J. Mol. Biol. 116, 227–247. https://doi.org/10.1016/0022-2836(77)90214-5

Colla, E., Coune, P., Liu, Y., Pletnikova, O., Troncoso, J.C., Iwatsubo, T., Schneider, B.L., Lee, M.K., 2012a. Endoplasmic Reticulum Stress Is Important for the Manifestations of -Synucleinopathy In Vivo. J. Neurosci. 32, 3306–3320. https://doi.org/10.1523/JNEUROSCI.5367-11.2012

Colla, E., Jensen, P.H., Pletnikova, O., Troncoso, J.C., Glabe, C., Lee, M.K., 2012b. Accumulation of Toxic -Synuclein Oligomer within Endoplasmic Reticulum Occurs in -Synucleinopathy In Vivo. J. Neurosci. 32, 3301–3305. https://doi.org/10.1523/JNEUROSCI.5368-11.2012

Collins, S.J., Ahlskog, J.E., Parisi, J.E., Maraganore, D.M., 1995. Progressive supranuclear palsy: neuropathologically based diagnostic clinical criteria. J. Neurol. Neurosurg. Psychiatry 58, 167–173. https://doi.org/10.1136/jnnp.58.2.167

Combs, B., Gamblin, T.C., 2012. FTDP-17 tau mutations induce distinct effects on aggregation and microtubule interactions. Biochemistry 51, 8597–8607. https://doi.org/10.1021/bi3010818

Congdon, E.E., Kim, S., Bonchak, J., Songrug, T., Matzavinos, A., Kuret, J., 2008. Nucleation-dependent Tau Filament Formation: The importance of dimerization and an estimation of elementary rate constants. J. Biol. Chem. 283, 13806–13816. https://doi.org/10.1074/jbc.M800247200

Conrad, C., Andreadis, A., Trojanowski, J.Q., Dickson, D.W., Kang, D., Chen, X., Wiederholt, W., Hansen, L., Masliah, E., Thal, L.J., Katzman, R., Xia, Y., Saitoh, T., 1997. Genetic evidence for the involvement of ? in progressive supranuclear palsy. Ann. Neurol. 41, 277–281. https://doi.org/10.1002/ana.410410222

Cooper, A.A., 2006. -Synuclein Blocks ER-Golgi Traffic and Rab1 Rescues Neuron Loss in Parkinson's Models. Science 313, 324–328. https://doi.org/10.1126/science.1129462

Coppola, G., Chinnathambi, S., Lee, J.J., Dombroski, B.A., Baker, M.C., Soto-Ortolaza, A.I., Lee, S.E., Klein, E., Huang, A.Y., Sears, R., Lane, J.R., Karydas, A.M., Kenet, R.O., Biernat, J., Wang, L.-S., Cotman, C.W., Decarli, C.S., Levey, A.I., Ringman, J.M., Mendez, M.F., Chui, H.C., Le Ber, I., Brice, A., Lupton, M.K., Preza, E., Lovestone, S., Powell, J., Graff-Radford, N., Petersen, R.C., Boeve, B.F., Lippa, C.F., Bigio, E.H., Mackenzie, I., Finger, E., Kertesz, A., Caselli, R.J., Gearing, M., Juncos, J.L., Ghetti, B., Spina, S., Bordelon, Y.M., Tourtellotte, W.W., Frosch, M.P., Vonsattel, J.P.G., Zarow, C., Beach, T.G., Albin, R.L., Lieberman, A.P., Lee, V.M., Trojanowski, J.Q., Van Deerlin, V.M., Bird, T.D., Galasko, D.R., Masliah, E., White, C.L., Troncoso, J.C., Hannequin, D., Boxer, A.L., Geschwind, M.D., Kumar, S., Mandelkow, E.-M., Wszolek, Z.K., Uitti, R.J., Dickson, D.W., Haines, J.L., Mayeux, R., Pericak-Vance, M.A., Farrer, L.A., Alzheimer's Disease Genetics Consortium, Ross, O.A., Rademakers, R., Schellenberg, G.D., Miller, B.L., Mandelkow, E., Geschwind, D.H., 2012. Evidence for a role of the rare p.A152T variant in MAPT in increasing the risk for FTD-spectrum and Alzheimer's diseases. Hum Mol Genet 21, 3500–3512. https://doi.org/10.1093/hmg/dds161

Cornejo, V.H., Pihán, P., Vidal, R.L., Hetz, C., 2013. Role of the unfolded protein response in organ physiology: Lessons from mouse models: Physiological Function of UPR in Organs and Tissues. IUBMB Life 65, 962–975. https://doi.org/10.1002/iub.1224

Cox, J.S., Shamu, C.E., Walter, P., 1993. Transcriptional induction of genes encoding endoplasmic reticulum resident proteins requires a transmembrane protein kinase. Cell 73, 1197–1206. https://doi.org/10.1016/0092-8674(93)90648-A

Cox, J.S., Chapman, R.E., Walter. P, 1997. The unfolded protein response coordinates the production of endoplasmic reticulum protein and endoplasmic reticulum membrane. Mol Biol Cell 8(9):1805-14. doi: 10.1091/mbc.8.9.1805.

Cox, J.S., Walter, P., 1996. A Novel Mechanism for Regulating Activity of a Transcription Factor That Controls the Unfolded Protein Response. Cell 87, 391–404. https://doi.org/10.1016/S0092-8674(00)81360-4

Credle, J.J., Finer-Moore, J.S., Papa, F.R., Stroud, R.M., Walter, P., 2005. On the mechanism of sensing unfolded protein in the endoplasmic reticulum. Proc. Natl. Acad. Sci. 102, 18773–18784. https://doi.org/10.1073/pnas.0509487102

Critchley M., 1929. Arteriosclerotic parkinsonism. Brain 52, 22–83.

Crowther, R.A., 1991. Straight and paired helical filaments in Alzheimer disease have a common structural unit. Proc. Natl. Acad. Sci. 88, 2288–2292. https://doi.org/10.1073/pnas.88.6.2288

Crowther, R.A., Wischik, C.M., 1985. Image reconstruction of the Alzheimer paired helical filament. EMBO J. 4, 3661–3665.

Cruts, M., Rademakers, R., Gijselinck, I., van der Zee, J., Dermaut, B., de Pooter, T., de Rijk, P., Del-Favero, J., van Broeckhoven, C., 2005. Genomic architecture of human 17q21 linked to frontotemporal dementia uncovers a highly homologous family of low-copy repeats in the tau region. Hum. Mol. Genet. 14, 1753–1762. https://doi.org/10.1093/hmg/ddi182

Cui, W., Li, J., Ron, D., Sha, B., 2011. The structure of the PERK kinase domain suggests the mechanism for its activation. Acta Crystallogr. D Biol. Crystallogr. 67, 423–428. https://doi.org/10.1107/S0907444911006445

Cullinan, S.B., Diehl, J.A., 2006. Coordination of ER and oxidative stress signaling: The PERK/Nrf2 signaling pathway. Int. J. Biochem. Cell Biol. 38, 317–332. https://doi.org/10.1016/j.biocel.2005.09.018

Cullinan, S.B., Zhang, D., Hannink, M., Arvisais, E., Kaufman, R.J., Diehl, J.A., 2003. Nrf2 Is a Direct PERK Substrate and Effector of PERK-Dependent Cell Survival. Mol. Cell. Biol. 23, 7198–7209. https://doi.org/10.1128/MCB.23.20.7198-7209.2003

d'Orange, M., Aurégan, G., Cheramy, D., Gaudin-Guérif, M., Lieger, S., Guillermier, M., Stimmer, L., Joséphine, C., Hérard, A.-S., Gaillard, M.-C., Petit, F., Kiessling, M.C., Schmitz, C., Colin, M., Buée, L., Panayi, F., Diguet, E., Brouillet, E., Hantraye, P., Bemelmans, A.-P., Cambon, K., 2018. Potentiating tangle formation reduces acute toxicity of soluble tau species in the rat. Brain 141, 535–549. https://doi.org/10.1093/brain/awx342

Dalton, A.C., Barton, W.A., 2014. Over-expression of secreted proteins from mammalian cell lines. Protein Science 23, 517–525. https://doi.org/10.1002/pro.2439

Daniel, S.E., de Bruin, V.M.S., Lees, A.J., 1995. The clinical and pathological spectrum of Steele-Richardson-Olszewski syndrome (progressive supranuclear palsy): a reappraisal. Brain 118, 759–770. https://doi.org/10.1093/brain/118.3.759

Davis, P.H., Golbe, L.I., Duvoisin, MD, R.C., Schoenberg, B.S., 1988. Risk factors for progressive supranuclear palsy. Neurology 38, 1546–1546. https://doi.org/10.1212/WNL.38.10.1546

David, D.C., Layfield, R., Serpell, L., Narain, Y., Goedert, M., Spillantini, M.G., 2002. Proteasomal degradation of tau protein. J Neurochem 83, 176–185. https://doi.org/10.1046/j.1471-4159.2002.01137.x

Dayanandan, R., Van Slegtenhorst, M., Mack, T.G.A., Ko, L., Yen, S.-H., Leroy, K., Brion, J.-P., Anderton, B.H., Hutton, M., Lovestone, S., 1999. Mutations in tau reduce its microtubule binding properties in intact cells and affect its phosphorylation. FEBS Letters 446, 228–232. https://doi.org/10.1016/S0014-5793(99)00222-7

Dayel, M.J., Hom, E.F.Y., Verkman, A.S., 1999. Diffusion of Green Fluorescent Protein in the Aqueous-Phase Lumen of Endoplasmic Reticulum. Biophys. J. 76, 2843–2851. https://doi.org/10.1016/S0006-3495(99)77438-2

de Yébenes, J.G., Sarasa, J.L., Daniel, S.E., Lees, A.J., 1995. Familial progressive supranuclear palsy: Description of a pedigree and review of the literature. Brain 118, 1095–1103. https://doi.org/10.1093/brain/118.5.1095

de Calignon, A., Polydoro, M., Suárez-Calvet, M., William, C., Adamowicz, D.H., Kopeikina, K.J., Pitstick, R., Sahara, N., Ashe, K.H., Carlson, G.A., Spires-Jones, T.L., Hyman, B.T., 2012. Propagation of Tau Pathology in a Model of Early Alzheimer's Disease. Neuron 73, 685–697. https://doi.org/10.1016/j.neuron.2011.11.033

Delacourte, A., Sergeant, N., Wattez, A., Gauvreau, D., Robitaille, Y., 1998. Vulnerable neuronal subsets in Alzheimer's and Pick's disease are distinguished by their ? isoform distribution and phosphorylation. Ann. Neurol. 43, 193–204. https://doi.org/10.1002/ana.410430209

Delépine, M., Nicolino, M., Barrett, T., Golamaully, M., Mark Lathrop, G., Julier, C., 2000. EIF2AK3, encoding translation initiation factor 2-α kinase 3, is mutated in patients with Wolcott-Rallison syndrome. Nat. Genet. 25, 406–409. https://doi.org/10.1038/78085

Delobel, P., Flament, S., Hamdane, M., Mailliot, C., Sambo, A.-V., Bégard, S., Sergeant, N., Delacourte, A., Vilain, J.-P., Buée, L., 2002. Abnormal Tau phosphorylation of the

Alzheimer-type also occurs during mitosis: Alzheimer Tau phosphorylation in frog oocyte. J. Neurochem. 83, 412–420. https://doi.org/10.1046/j.1471-4159.2002.01143.x

Delobel, P., Leroy, O., Hamdane, M., Sambo, A.V., Delacourte, A., Buée, L., 2005. Proteasome inhibition and Tau proteolysis: an unexpected regulation. FEBS Letters 579, 1–5. https://doi.org/10.1016/j.febslet.2004.11.018

Delobel, P., Lavenir, I., Fraser, G., Ingram, E., Holzer, M., Ghetti, B., Spillantini, M.G., Crowther, R.A., Goedert, M., 2008. Analysis of Tau Phosphorylation and Truncation in a Mouse Model of Human Tauopathy. The American Journal of Pathology 172, 123–131. https://doi.org/10.2353/ajpath.2008.070627

Denk, F., Wade-Martins, R., 2009. Knock-out and transgenic mouse models of tauopathies. Neurobiol. Aging 30, 1–13. https://doi.org/10.1016/j.neurobiolaging.2007.05.010

Denmeade, S.R., Isaacs, J.T.,2005. The SERCA pump as a therapeutic target: making a "smart bomb" for prostate cancer. Cancer Biological Therapeutics 4(1):14-22. doi: 10.4161/cbt.4.1.1505.

Derkinderen, P., 2005. Tyrosine 394 Is Phosphorylated in Alzheimer's Paired Helical Filament Tau and in Fetal Tau with c-Abl as the Candidate Tyrosine Kinase. J. Neurosci. 25, 6584–6593. https://doi.org/10.1523/JNEUROSCI.1487-05.2005

Deramecourt, V., Lebert, F., Maurage, C.-A., Fernandez-Gomez, F.-J., Dujardin, S., Colin, M., Sergeant, N., Buée-Scherrer, V., Clot, F., Ber, I.L., Brice, A., Pasquier, F., Buée, L., 2012. Clinical, Neuropathological, and Biochemical Characterization of the Novel Tau Mutation P332S. JAD 31, 741–749. https://doi.org/10.3233/JAD-2012-120160

DeTure, M., Ko, L., Yen, S., Nacharaju, P., Easson, C., Lewis, J., van Slegtenhorst, M., Hutton, M., Yen, S.-H., 2000. Missense tau mutations identified in FTDP-17 have a small effect on tau–microtubule interactions. Brain Research 853, 5–14. https://doi.org/10.1016/S0006-8993(99)02124-1

Devi, L., Ohno, M., 2014. PERK mediates eIF2α phosphorylation responsible for BACE1 elevation, CREB dysfunction and neurodegeneration in a mouse model of Alzheimer's disease. Neurobiology of Aging 35, 2272–2281. https://doi.org/10.1016/j.neurobiolaging.2014.04.031

Dickson, D.W., Kress, Y., Crowe, A., Yen, S.H., 1985. Monoclonal antibodies to Alzheimer neurofibrillary tangles. 2. Demonstration of a common antigenic determinant between ANT and neurofibrillary degeneration in progressive supranuclear palsy. Am. J. Pathol. 120, 292–303.

Dickson, D.W., Rademakers, R., Hutton, M.L., 2007. Progressive Supranuclear Palsy: Pathology and Genetics. Brain Pathol. 17, 74–82. https://doi.org/10.1111/j.1750-3639.2007.00054.x

Dickson, T.C., Vickers, J.C., 2001. The morphological phenotype of β-amyloid plaques and associated neuritic changes in Alzheimer's disease. Neuroscience 105, 99–107. https://doi.org/10.1016/S0306-4522(01)00169-5

DiTella, M., Feiguin, F., Morfini, G., Cáceres, A., 1994. Microfilament-associated growth cone component depends upon Tau for its intracellular localization: Tau Protein Function in Growth Cones. Cell Motil. Cytoskeleton 29, 117–130. https://doi.org/10.1002/cm.970290204

DiTella, M.C., Feiguin, F., Carri, N., Kosik, K.S., Cáceres, A., 1996. MAP-1B/TAU functional redundancy during laminin-enhanced axonal growth. J. Cell Sci. 109 (Pt 2), 467–477.

Dixit, R., Ross, J.L., Goldman, Y.E., Holzbaur, E.L.F., 2008. Differential Regulation of Dynein and Kinesin Motor Proteins by Tau. Science 319, 1086–1089. https://doi.org/10.1126/science.1152993

Dreier, L., Rapoport, T.A., 2000. In Vitro Formation of the Endoplasmic Reticulum Occurs Independently of Microtubules by a Controlled Fusion Reaction. J. Cell Biol. 148, 883–898. https://doi.org/10.1083/jcb.148.5.883

Drubin, D.G., Feinstein, S.C., Shooter, E.M., Kirschner, M.W., 1985. Nerve growth factor-induced neurite outgrowth in PC12 cells involves the coordinate induction of microtubule assembly and assembly-promoting factors. J. Cell Biol. 101, 1799–1807. https://doi.org/10.1083/jcb.101.5.1799

D'Souza, I., Poorkaj, P., Hong, M., Nochlin, D., Lee, V.M.-Y., Bird, T.D., Schellenberg, G.D., 1999. Missense and silent tau gene mutations cause frontotemporal dementia with parkinsonism-chromosome 17 type, by affecting multiple alternative RNA splicing

regulatory elements. Proceedings of the National Academy of Sciences 96, 5598–5603. https://doi.org/10.1073/pnas.96.10.5598

D'Souza, I., Schellenberg, G.D., 2005. Regulation of tau isoform expression and dementia. Biochim. Biophys. Acta BBA - Mol. Basis Dis. 1739, 104–115. https://doi.org/10.1016/j.bbadis.2004.08.009

D'Souza, I., Schellenberg, G.D., 2002. *tau* Exon 10 Expression Involves a Bipartite Intron 10 Regulatory Sequence and Weak 5′ and 3′ Splice Sites. J. Biol. Chem. 277, 26587–26599. https://doi.org/10.1074/jbc.M203794200

D'Souza, I., Schellenberg, G.D., 2000. Determinants of 4-Repeat Tau Expression: coordination between enhancing and inhibitory splicing sequences for exon 10 inclusion. J. Biol. Chem. 275, 17700–17709. https://doi.org/10.1074/jbc.M909470199

Duennwald, M.L., Lindquist, S., 2008. Impaired ERAD and ER stress are early and specific events in polyglutamine toxicity. Genes Dev. 22, 3308–3319. https://doi.org/10.1101/gad.1673408

Ebneth, A., Godemann, R., Stamer, K., Illenberger, S., Trinczek, B., Mandelkow, E.-M., Mandelkow, E., 1998. Overexpression of Tau Protein Inhibits Kinesin-dependent Trafficking of Vesicles, Mitochondria, and Endoplasmic Reticulum: Implications for Alzheimer's Disease. J. Cell Biol. 143, 777–794. https://doi.org/10.1083/jcb.143.3.777

Elison, D., Love, S., Chimmeli, L., Harding,B., James,S.,Yong,W., Neuropathology E-Book: A Reference Text of CNS Pathology, 3rd ed. Elsevier Health Sciences, 2012.

Elbaum-Garfinkle, S., Cobb, G., Compton, J.T., Li, X.-H., Rhoades, E., 2014. Tau mutants bind tubulin heterodimers with enhanced affinity. Proceedings of the National Academy of Sciences 111, 6311–6316. https://doi.org/10.1073/pnas.1315983111

Evans, W., Fung, H.C., Steele, J., Eerola, J., Tienari, P., Pittman, A., Silva, R. de, Myers, A., Vrieze, F.W.-D., Singleton, A., Hardy, J., 2004. The tau H2 haplotype is almost exclusively Caucasian in origin. Neurosci. Lett. 369, 183–185. https://doi.org/10.1016/j.neulet.2004.05.119

Ezquerra, M., Pastor, P., Gaig, C., Vidal-Taboada, J.M., Cruchaga, C., Muñoz, E., Martí, M.-J., Valldeoriola, F., Aguilar, M., Calopa, M., Hernandez-Vara, J., Tolosa, E., 2011. Different MAPT haplotypes are associated with Parkinson's disease and progressive

supranuclear palsy. Neurobiol. Aging 32, 547.e11-547.e16. https://doi.org/10.1016/j.neurobiolaging.2009.09.011

Ezquerra, M., Pastor, P., Valldeoriola, F., Luis Molinuevo, J., Blesa, R., Tolosa, E., Oliva, R., 1999. Identification of a novel polymorphism in the promoter region of the tau gene highly associated to progressive supranuclear palsy in humans. Neurosci. Lett. 275, 183–186. https://doi.org/10.1016/S0304-3940(99)00738-7

Fergusson, J., Landon, M., Lowe, J., Ward, L., van Leeuwen, F.W., Mayer, R.J., 2000. Neurofibrillary tangles in progressive supranuclear palsy brains exhibit immunoreactivity to frameshift mutant ubiquitin-B protein. Neuroscience Letters 279, 69–72. https://doi.org/10.1016/S0304-3940(99)00917-9

Ferrari, R., Hernandez, D.G., Nalls, M.A., Rohrer, J.D., Ramasamy, A., Kwok, J.B.J., Dobson-Stone, C., Brooks, W.S., Schofield, P.R., Halliday, G.M., Hodges, J.R., Piguet, O., Bartley, L., Thompson, E., Haan, E., Hernández, I., Ruiz, A., Boada, M., Borroni, B., Padovani, A., Cruchaga, C., Cairns, N.J., Benussi, L., Binetti, G., Ghidoni, R., Forloni, G., Galimberti, D., Fenoglio, C., Serpente, M., Scarpini, E., Clarimón, J., Lleó, A., Blesa, R., Waldö, M.L., Nilsson, K., Nilsson, C., Mackenzie, I.R.A., Hsiung, G.-Y.R., Mann, D.M.A., Grafman, J., Morris, C.M., Attems, J., Griffiths, T.D., McKeith, I.G., Thomas, A.J., Pietrini, P., Huey, E.D., Wassermann, E.M., Baborie, A., Jaros, E., Tierney, M.C., Pastor, P., Razquin, C., Ortega-Cubero, S., Alonso, E., Perneczky, R., Diehl-Schmid, J., Alexopoulos, P., Kurz, A., Rainero, I., Rubino, E., Pinessi, L., Rogaeva, E., St George-Hyslop, P., Rossi, G., Tagliavini, F., Giaccone, G., Rowe, J.B., Schlachetzki, J.C.M., Uphill, J., Collinge, J., Mead, S., Danek, A., Van Deerlin, V.M., Grossman, M., Trojanowski, J.Q., van der Zee, J., Deschamps, W., Van Langenhove, T., Cruts, M., Van Broeckhoven, C., Cappa, S.F., Le Ber, I., Hannequin, D., Golfier, V., Vercelletto, M., Brice, A., Nacmias, B., Sorbi, S., Bagnoli, S., Piaceri, I., Nielsen, J.E., Hjermind, L.E., Riemenschneider, M., Mayhaus, M., Ibach, B., Gasparoni, G., Pichler, S., Gu, W., Rossor, M.N., Fox, N.C., Warren, J.D., Spillantini, M.G., Morris, H.R., Rizzu, P., Heutink, P., Snowden, J.S., Rollinson, S., Richardson, A., Gerhard, A., Bruni, A.C., Maletta, R., Frangipane, F., Cupidi, C., Bernardi, L., Anfossi, M., Gallo, M., Conidi, M.E., Smirne, N., Rademakers, R., Baker, M., Dickson, D.W., Graff-Radford, N.R., Petersen, R.C., Knopman, D., Josephs, K.A., Boeve, B.F., Parisi, J.E., Seeley, W.W., Miller, B.L., Karydas, A.M., Rosen, H., van Swieten, J.C., Dopper, E.G.P., Seelaar, H., Pijnenburg, Y.A.L., Scheltens, P., Logroscino, G., Capozzo, R., Novelli, V., Puca, A.A., Franceschi, M., Postiglione, A., Milan, G., Sorrentino, P., Kristiansen, M., Chiang, H.-H., Graff, C., Pasquier, F., Rollin, A., Deramecourt, V., Lebert, F., Kapogiannis, D., Ferrucci, L.,

Pickering-Brown, S., Singleton, A.B., Hardy, J., Momeni, P., 2014. Frontotemporal dementia and its subtypes: a genome-wide association study. Lancet Neurol. 13, 686–699. https://doi.org/10.1016/S1474-4422(14)70065-1

Ferreira, A., Busciglio, J., Cáceres, A., 1989. Microtubule formation and neurite growth in cerebellar macroneurons which develop in vitro: evidence for the involvement of the microtubule-associated proteins, MAP-1a, HMW-MAP2 and Tau. Dev. Brain Res. 49, 215–228. https://doi.org/10.1016/0165-3806(89)90023-0

Ferrer, I., Blanco, R., Carmona, M., Puig, B., 2001. Phosphorylated c-MYC expression in Alzheimer disease, Pick's disease, progressive supranuclear palsy and corticobasal degeneration. Neuropathol. Appl. Neurobiol. 27, 343–351. https://doi.org/10.1046/j.1365-2990.2001.00348.x

Feng, D., Wei, J., Gupta, S., McGrath, B.C., Cavener, D.R., 2009. Acute ablation of PERK results in ER dysfunctions followed by reduced insulin secretion and cell proliferation. BMC Cell Biol 10, 61. https://doi.org/10.1186/1471-2121-10-61

Feuillette, S., Blard, O., Lecourtois, M., Frébourg, T., Campion, D., Dumanchin, C., 2005. Tau is not normally degraded by the proteasome: Tau Not Normally Degraded by the Proteasome. J. Neurosci. Res. 80, 400–405. https://doi.org/10.1002/jnr.20414

Fischer, D., Mukrasch, M.D., Biernat, J., Bibow, S., Blackledge, M., Griesinger, C., Mandelkow, E., Zweckstetter, M., 2009. Conformational Changes Specific for Pseudophosphorylation at Serine 262 Selectively Impair Binding of Tau to Microtubules. Biochemistry 48, 10047–10055. https://doi.org/10.1021/bi901090m

Fitzpatrick, A.W.P., Falcon, B., He, S., Murzin, A.G., Murshudov, G., Garringer, H.J., Crowther, R.A., Ghetti, B., Goedert, M., Scheres, S.H.W., 2017. Cryo-EM structures of tau filaments from Alzheimer's disease. Nature 547, 185–190. https://doi.org/10.1038/nature23002

Flament, S., Delacourte, A., Verny, M., Hauw, J.-J., Javoy-Agid, F., 1991a. Abnormal Tau proteins in progressive supranuclear palsy: Similarities and differences with the neurofibrillary degeneration of the Alzheimer type. Acta Neuropathol. (Berl.) 81, 591–596. https://doi.org/10.1007/BF00296367

Flament, S., Delacourte, A., Verny, M., Hauw, J.-J., Javoy-Agid, F., 1991b. Abnormal Tau proteins in progressive supranuclear palsy: Similarities and differences with the

neurofibrillary degeneration of the Alzheimer type. Acta Neuropathol. (Berl.) 81, 591–596. https://doi.org/10.1007/BF00296367

Forlenza, O.V., Spink, J.M., Dayanandan, R., Anderton, B.H., Olesen, O.F., Lovestone, S., 2000. Muscarinic agonists reduce tau phosphorylation in non-neuronal cells via GSK-3β inhibition and in neurons. J. Neural Transm. 107, 1201–1212. https://doi.org/10.1007/s007020070034

Friedhoff, P., Schneider, A., Mandelkow, E.-M., Mandelkow, E., 1998. Rapid Assembly of Alzheimer-like Paired Helical Filaments from Microtubule-Associated Protein Tau Monitored by Fluorescence in Solution †. Biochemistry 37, 10223–10230. https://doi.org/10.1021/bi980537d

Frost, B., Ollesch, J., Wille, H., Diamond, M.I., 2009. Conformational Diversity of Wild-type Tau Fibrils Specified by Templated Conformation Change. J. Biol. Chem. 284, 3546–3551. https://doi.org/10.1074/jbc.M805627200

Frost, B., Hemberg, M., Lewis, J., Feany, M.B., 2014. Tau promotes neurodegeneration through global chromatin relaxation. Nat. Neurosci. 17, 357–366. https://doi.org/10.1038/nn.3639

Fujioka, S., Algom, A.A., Murray, M.E., Strongosky, A., Soto-Ortolaza, A.I., Rademakers, R., Ross, O.A., Wszolek, Z.K., Dickson, D.W., 2013. Similarities between familial and sporadic autopsy-proven progressive supranuclear palsy. Neurology 80, 2076–2078. https://doi.org/10.1212/WNL.0b013e318294b2eb

Fujioka, Shinsuke, Van Gerpen, J.A., Uitti, R.J., Dickson, D.W., Wszolek, Z.K., 2014. Familial Progressive Supranuclear Palsy: A Literature Review. Neurodegener. Dis. 13, 180–182. https://doi.org/10.1159/000354975

Furukawa, Y., Kaneko, K., Watanabe, S., Yamanaka, K., Nukina, N., 2011. A Seeding Reaction Recapitulates Intracellular Formation of Sarkosyl-insoluble Transactivation Response Element (TAR) DNA-binding Protein-43 Inclusions. J. Biol. Chem. 286, 18664–18672. https://doi.org/10.1074/jbc.M111.231209

Ganguly, P., Do, T.D., Larini, L., LaPointe, N.E., Sercel, A.J., Shade, M.F., Feinstein, S.C., Bowers, M.T., Shea, J.-E., 2015. Tau Assembly: The Dominant Role of PHF6 (VQIVYK) in Microtubule Binding Region Repeat R3. J. Phys. Chem. B 119, 4582–4593. https://doi.org/10.1021/acs.jpcb.5b00175

Gardner, B.M., Walter, P., 2011. Unfolded Proteins Are Ire1-Activating Ligands That Directly Induce the Unfolded Protein Response. Science 333, 1891–1894. https://doi.org/10.1126/science.1209126

Gauthier-Kemper, A., Weissmann, C., Golovyashkina, N., Sebö-Lemke, Z., Drewes, G., Gerke, V., Heinisch, J.J., Brandt, R., 2011. The frontotemporal dementia mutation R406W blocks tau's interaction with the membrane in an annexin A2–dependent manner. J. Cell Biol. 192, 647–661. https://doi.org/10.1083/jcb.201007161

Gething, M.-J., McCammon, K., Sambrook, J., 1986. Expression of wild-type and mutant forms of influenza hemagglutinin: The role of folding in intracellular transport. Cell 46, 939–950. https://doi.org/10.1016/0092-8674(86)90076-0

Ghetti, B., Oblak, A.L., Boeve, B.F., Johnson, K.A., Dickerson, B.C., Goedert, M., 2015. Invited review: Frontotemporal dementia caused by *microtubule-associated protein tau* gene (*MAPT*) mutations: a chameleon for neuropathology and neuroimaging. Neuropathol Appl Neurobiol 41, 24–46. https://doi.org/10.1111/nan.12213

Gilmore, R., Walter, P., Blobel, G., 1982. Protein translocation across the endoplasmic reticulum. II. Isolation and characterization of the signal recognition particle receptor. J. Cell Biol. 95, 470–477. https://doi.org/10.1083/jcb.95.2.470

Goedert, M., Jakes, R., 2005. Mutations causing neurodegenerative tauopathies. Biochim. Biophys. Acta BBA - Mol. Basis Dis. 1739, 240–250. https://doi.org/10.1016/j.bbadis.2004.08.007

Goedert, M., Jakes, R., 1990. Expression of separate isoforms of human tau protein: correlation with the tau pattern in brain and effects on tubulin polymerization. EMBO J. 9, 4225–4230

Goedert, M., Jakes, R., Crowther, R.A., Cohen, P., Vanmechelen, E., Vandermeeren, M., Cras, P., 1994. Epitope mapping of monoclonal antibodies to the paired helical filaments of Alzheimer's disease: identification of phosphorylation sites in tau protein. Biochem. J. 301, 871–877. https://doi.org/10.1042/bj3010871

Goedert, M., Spillantini, M.G., Jakes, R., Rutherford, D., Crowther, R.A., 1989. Multiple isoforms of human microtubule-associated protein tau: sequences and localization in

neurofibrillary tangles of Alzheimer's disease. Neuron 3, 519–526. https://doi.org/10.1016/0896-6273(89)90210-9

Goedert, M., Wischik, C.M., Crowther, R.A., Walker, J.E., Klug, A., 1988. Cloning and sequencing of the cDNA encoding a core protein of the paired helical filament of Alzheimer disease: identification as the microtubule-associated protein tau. Proc. Natl. Acad. Sci. 85, 4051–4055. https://doi.org/10.1073/pnas.85.11.4051

Goedert, M., Jakes, R., Crowther, R.A., 1999. Effects of frontotemporal dementia FTDP-17 mutations on heparin-induced assembly of tau filaments. FEBS Letters 450, 306–311. https://doi.org/10.1016/S0014-5793(99)00508-6

Goetz, C.G., 1996. An early photographic case of probable progressive supranuclear palsy. Mov. Disord. 11, 617–618. https://doi.org/10.1002/mds.870110604

Golbe, L., 2014. Progressive Supranuclear Palsy. Semin. Neurol. 34, 151–159. https://doi.org/10.1055/s-0034-1381736

Golbe, L.I., 1994. The epidemiology of PSP, in: Tolosa, E., Duvoisin, R., Cruz-Sánchez, F.F. (Eds.), Progressive Supranuclear Palsy: Diagnosis, Pathology, and Therapy. Springer Vienna, Vienna, pp. 263–273. https://doi.org/10.1007/978-3-7091-6641-3_20

Goldbaum, O., Oppermann, M., Handschuh, M., Dabir, D., Zhang, B., Forman, M.S., Trojanowski, J.Q., Lee, V.M.-Y., Richter-Landsberg, C., 2003. Proteasome Inhibition Stabilizes Tau Inclusions in Oligodendroglial Cells that Occur after Treatment with Okadaic Acid. J. Neurosci. 23, 8872–8880. https://doi.org/10.1523/JNEUROSCI.23-26-08872.2003

González-Billault, C., Engelke, M., Jiménez-Mateos, E.M., Wandosell, F., Cáceres, A., Avila, J., 2002. Participation of structural microtubule-associated proteins (MAPs) in the development of neuronal polarity: MAPs Contribution to Neuronal Polarity. J. Neurosci. Res. 67, 713–719. https://doi.org/10.1002/jnr.10161

Goode, B., Feinstein, S., 1994. Identification of a novel microtubule binding and assembly domain in the developmentally regulated inter-repeat region of tau. J. Cell Biol. 124, 769–782. https://doi.org/10.1083/jcb.124.5.769

Goode, B.L., Chau, M., Denis, P.E., Feinstein, S.C., 2000. Structural and Functional Differences between 3-Repeat and 4-Repeat Tau Isoforms: IMPLICATIONS FOR

NORMAL TAU FUNCTION AND THE ONSET OF NEURODEGENERATIVE DISEASE. J. Biol. Chem. 275, 38182–38189. https://doi.org/10.1074/jbc.M007489200

Goslin, K., Schreyer, D.J., Skene, J.H., Banker, G., 1988. Development of neuronal polarity: GAP-43 distinguishes axonal from dendritic growth cones. Nature 336, 672–674. https://doi.org/10.1038/336672a0

Grande, V., Ornaghi, F., Comerio, L., Restelli, E., Masone, A., Corbelli, A., Tolomeo, D., Capone, V., Axten, J.M., Laping, N.J., Fiordaliso, F., Sallese, M., Chiesa, R., 2018. PERK inhibition delays neurodegeneration and improves motor function in a mouse model of Marinesco-Sjögren syndrome. Human Molecular Genetics 27, 2477–2489. https://doi.org/10.1093/hmg/ddy152

Grafman, J., Litvan, I., Stark, M., 1995. Neuropsychological Features of Progressive Supranuclear Palsy. Brain Cogn. 28, 311–320. https://doi.org/10.1006/brcg.1995.1260

Greenwood, J.A., Johnson, G.V.W., 1995. Localization and in Situ Phosphorylation State of Nuclear Tau. Exp. Cell Res. 220, 332–337. https://doi.org/10.1006/excr.1995.1323

Grover, A., England, E., Baker, M., Sahara, N., Adamson, J., Granger, B., Houlden, H., Passant, U., Yen, S.-H., DeTure, M., Hutton, M., 2003. A novel tau mutation in exon 9 (1260V) causes a four-repeat tauopathy. Experimental Neurology 184, 131–140. https://doi.org/10.1016/S0014-4886(03)00393-5

Grover, A., DeTure, M., Yen, S.-H., Hutton, M., 2002. Effects on splicing and protein function of three mutations in codon N296 of tau in vitro. Neuroscience Letters 323, 33–36. https://doi.org/10.1016/S0304-3940(02)00124-6

Grundke-Iqbal, I., Iqbal, K., Tung, Y.C., Quinlan, M., Wisniewski, H.M., Binder, L.I., 1986. Abnormal phosphorylation of the microtubule-associated protein tau (tau) in Alzheimer cytoskeletal pathology. Proc. Natl. Acad. Sci. 83, 4913–4917. https://doi.org/10.1073/pnas.83.13.4913

Gu, Y., Oyama, F., Ihara, Y., 2002. τ Is Widely Expressed in Rat Tissues. J. Neurochem. 67, 1235–1244. https://doi.org/10.1046/j.1471-4159.1996.67031235.x

Guo, J.L., Lee, V.M.-Y., 2011. Seeding of Normal Tau by Pathological Tau Conformers Drives Pathogenesis of Alzheimer-like Tangles. J. Biol. Chem. 286, 15317–15331. https://doi.org/10.1074/jbc.M110.209296

Gustke, N., Trinczek, B., Biernat, J., Mandelkow, E.-M., Mandelkow, E., 1994a. Domains of tau Protein and Interactions with Microtubules. Biochemistry 33, 9511–9522. https://doi.org/10.1021/bi00198a017

Gustke, N., Trinczek, B., Biernat, J., Mandelkow, E.-M., Mandelkow, E., 1994b. Domains of tau Protein and Interactions with Microtubules. Biochemistry 33, 9511–9522. https://doi.org/10.1021/bi00198a017

Haas, I.G., Wabl, M., 1983. Immunoglobulin heavy chain binding protein. Nature 306, 387–389. https://doi.org/10.1038/306387a0

Halliday, M., Hughes, D., Mallucci, G.R., 2017. Fine-tuning PERK signaling for neuroprotection. J Neurochem 142, 812–826. https://doi.org/10.1111/jnc.14112

Hamano, T., Gendron, T.F., Ko, L.-W., Yen, S.-H., 2009. Concentration-dependent effects of proteasomal inhibition on tau processing in a cellular model of tauopathy. Int J Clin Exp Pathol 2, 561–573.

Hamm, M., Bailey, R., Shaw, G., Yen, S.-H., Lewis, J., Giasson, B.I., 2015. Physiologically relevant factors influence tau phosphorylation by leucine-rich repeat kinase 2: Modulators of Tau Phosphorylation by LRRK2. Journal of Neuroscience Research 93, 1567–1580. https://doi.org/10.1002/jnr.23614

Hamos, J.E., Oblas, B., Pulaski-Salo, D., Welch, W.J., Bole, D.G., Drachman, D.A., 1991. Expression of heat shock proteins in Alzheimer's disease. Neurology 41, 345–345. https://doi.org/10.1212/WNL.41.3.345

Hanger, D.P., Hughes, K., Woodgett, J.R., Brion, J.-P., Anderton, B.H., 1992. Glycogen synthase kinase-3 induces Alzheimer's disease-like phosphorylation of tau: Generation of paired helical filament epitopes and neuronal localisation of the kinase. Neuroscience Letters 147, 58–62. https://doi.org/10.1016/0304-3940(92)90774-2

Hanger, D.P., Betts, J.C., Loviny, T.L.F., Blackstock, W.P., Anderton, B.H., 2002. New Phosphorylation Sites Identified in Hyperphosphorylated Tau (Paired Helical Filament-Tau) from Alzheimer's Disease Brain Using Nanoelectrospray Mass Spectrometry. J. Neurochem. 71, 2465–2476. https://doi.org/10.1046/j.1471-4159.1998.71062465.

Hanger, D.P., Byers, H.L., Wray, S., Leung, K.-Y., Saxton, M.J., Seereeram, A., Reynolds, C.H., Ward, M.A., Anderton, B.H., 2007. Novel Phosphorylation Sites in Tau from Alzheimer Brain Support a Role for Casein Kinase 1 in Disease Pathogenesis. J. Biol. Chem. 282, 23645–23654. https://doi.org/10.1074/jbc.M703269200

Harada, A., Oguchi, K., Okabe, S., Kuno, J., Terada, S., Ohshima, T., Sato-Yoshitake, R., Takei, Y., Noda, T., Hirokawa, N., 1994. Altered microtubule organization in small-calibre axons of mice lacking tau protein. Nature 369, 488–491. https://doi.org/10.1038/369488a0

Harding, H.P., Zhang, Y., Bertolotti, A., Zeng, H., Ron, D., 2000. Perk Is Essential for Translational Regulation and Cell Survival during the Unfolded Protein Response. Mol. Cell 5, 897–904. https://doi.org/10.1016/S1097-2765(00)80330-5

Harding, H.P., Zeng, H., Zhang, Y., Jungries, R., Chung, P., Plesken, H., Sabatini, D.D., Ron, D., 2001. Diabetes Mellitus and Exocrine Pancreatic Dysfunction in Perk−/− Mice Reveals a Role for Translational Control in Secretory Cell Survival. Molecular Cell 7, 1153–1163. https://doi.org/10.1016/S1097-2765(01)00264-7

Harding, H.P., Zhang, Y., Ron, D., 1999. Protein translation and folding are coupled by an endoplasmic-reticulum-resident kinase. Nature 397, 271–274. https://doi.org/10.1038/16729

Harding, H.P., Zhang, Y., Zeng, H., Novoa, I., Lu, P.D., Calfon, M., Sadri, N., Yun, C., Popko, B., Paules, R., Stojdl, D.F., Bell, J.C., Hettmann, T., Leiden, J.M., Ron, D., 2003. An Integrated Stress Response Regulates Amino Acid Metabolism and Resistance to Oxidative Stress. Mol. Cell 11, 619–633. https://doi.org/10.1016/S1097-2765(03)00105-9

Hardy, J., Pittman, A., Myers, A., Fung, H.C., de Silva, R., Duckworth, J., 2006. Tangle Diseases and the Tau Haplotypes: Alzheimer Dis. Assoc. Disord. 20, 60–62. https://doi.org/10.1097/01.wad.0000201853.54493.d8

Hartmuth, K., Urlaub, H., Vornlocher, H.-P., Will, C.L., Gentzel, M., Wilm, M., Luhrmann, R., 2002. Protein composition of human prespliceosomes isolated by a tobramycin affinity-selection method. Proc. Natl. Acad. Sci. 99, 16719–16724. https://doi.org/10.1073/pnas.262483899

Hasegawa, M., Crowther, R.A., Jakes, R., Goedert, M., 1997. Alzheimer-like Changes in Microtubule-associated Protein Tau Induced by Sulfated Glycosaminoglycans: Inhibition Of Microtubule Binding, Stimulation Of Phosphorylation, And Filament Assembly Depend On The Degree Of Sulfation. J. Biol. Chem. 272, 33118–33124. https://doi.org/10.1074/jbc.272.52.33118

Hasegawa, M., Smith, M.J., Goedert, M., 1998. Tau proteins with FTDP-17 mutations have a reduced ability to promote microtubule assembly. FEBS Letters 437, 207–210. https://doi.org/10.1016/S0014-5793(98)01217-4

Hashimoto, S., Saido, T.C., 2018. Critical review: involvement of endoplasmic reticulum stress in the aetiology of Alzheimer's disease. Open Biol. 8, 180024. https://doi.org/10.1098/rsob.180024

Hauw, J.-J., Daniel, S.E., Dickson, D., Horoupian, D.S., Jellinger, K., Lantos, P.L., McKee, A., Tabaton, M., Litvan, I., 1994. Preliminary NINDS neuropathologic criteria for Steele-Richardson-Olszewski syndrome (progressive supranuclear palsy). Neurology 44, 2015–2015. https://doi.org/10.1212/WNL.44.11.2015

Hauw, J.-J., Verny, M., Delaère, P., Cervera, P., He, Y., Duyckaerts, C., 1990. Constant neurofibrillary changes in the neocortex in progressive supranuclear palsy. Basic differences with Alzheimer's disease and aging. Neurosci. Lett. 119, 182–186. https://doi.org/10.1016/0304-3940(90)90829-X

Hayashi, S., Toyoshima, Y., Hasegawa, M., Umeda, Y., Wakabayashi, K., Tokiguchi, S., Iwatsubo, T., Takahashi, H., 2002. Late-onset frontotemporal dementia with a novel exon 1 (Arg5His) tau gene mutation. Ann. Neurol. 51, 525–530. https://doi.org/10.1002/ana.10163

Hayes, J.D., Chanas, S.A., Henderson, C.J., McMahon, M., Sun, C., Moffat, G.J., Wolf, C.R., Yamamoto, M., 2000. The Nrf2 transcription factor contributes both to the basal expression of glutathione S-transferases in mouse liver and to their induction by the chemopreventive synthetic antioxidants, butylated hydroxyanisole and ethoxyquin. Biochem. Soc. Trans. 28, 33–41. https://doi.org/10.1042/bst0280033

Haze, K., Okada, T., Yoshida, H., Yanagi, H., Yura, T., Negishi, M., Mori, K., 2001. Identification of the G13 (cAMP-response-element-binding protein-related protein) gene product related to activating transcription factor 6 as a transcriptional activator of the

mammalian unfolded protein response. Biochem. J. 355, 19. https://doi.org/10.1042/0264-6021:3550019

He, Y., Duyckaerts, C., Delaère, P., Piette, F., Hauw, J.-J., 1993. Alzheimer's lesions labelled by anti-ubiquitin antibodies: comparison with other staining techniques. A study of 15 cases with graded intellectual status in ageing and Alzheimer's disease. Neuropathol Appl Neurobiol 19, 364–371. https://doi.org/10.1111/j.1365-2990.1993.tb00453.x

He, H.J., Wang, X.S., Pan, R., Wang, D.L., Liu, M.N., He, R.Q., 2009. The proline-rich domain of tau plays a role in interactions with actin. BMC Cell Biol. 10, 81. https://doi.org/10.1186/1471-2121-10-81

He, Z., Ostrowski, R.P., Sun, X., Ma, Q., Huang, B., Zhan, Y., Zhang, J.H., 2012. CHOP silencing reduces acute brain injury in the rat model of subarachnoid hemorrhage. Stroke 43, 484–490. https://doi.org/10.1161/STROKEAHA.111.626432

Heckman, M.G., Kasanuki, K., Brennan,R., Labbe,C., Vargas,E., Sotos,A., Murray,M., Koga,S., Dickson, D., Ross,O., 2019. Association of *MAPT* Subhaplotypes With Risk of Progressive Supranuclear Palsy and Severity of Tau Pathology. JAMA Neurol. 76, 710. https://doi.org/10.1001/jamaneurol.2019.0250

Heicklen-Klein, A., Ginzburg, I., 2002. Tau Promoter Confers Neuronal Specificity and Binds Sp1 and AP-2. J. Neurochem. 75, 1408–1418. https://doi.org/10.1046/j.1471-4159.2000.0751408.x

Hershey, J.W.B., 1991. Translational Control in Mammalian Cells. Annu. Rev. Biochem. 60, 717–755. https://doi.org/10.1146/annurev.bi.60.070191.003441

Hetz, C., 2012. The unfolded protein response: controlling cell fate decisions under ER stress and beyond. Nat Rev Mol Cell Biol 13, 89–102. https://doi.org/10.1038/nrm3270

Hetz, C., Papa, F.R., 2018. The Unfolded Protein Response and Cell Fate Control. Mol. Cell 69, 169–181. https://doi.org/10.1016/j.molcel.2017.06.017

Higgins, J.J., Litvan, I., Pho, L.T., Li, W., Nee, L.E., 1998. Progressive supranuclear gaze palsy is in linkage disequilibrium with the and not the -synuclein gene. Neurology 50, 270–273. https://doi.org/10.1212/WNL.50.1.270

Hirko, A., Tang, F., Hughes, J., 2003. Cationic Lipid Vectors for Plasmid DNA Delivery. CMC 10, 1185–1193. https://doi.org/10.2174/0929867033457412

Hirokawa, N., Shiomura, Y., Okabe, S., 1988. Tau proteins: the molecular structure and mode of binding on microtubules. J. Cell Biol. 107, 1449–1459. https://doi.org/10.1083/jcb.107.4.1449

Ho, Y.-S., Yang, X., Lau, J.C.-F., Hung, C.H.-L., Wuwongse, S., Zhang, Q., Wang, J., Baum, L., So, K.-F., Chang, R.C.-C., 2012. Endoplasmic Reticulum Stress Induces Tau Pathology and Forms a Vicious Cycle: Implication in Alzheimer's Disease Pathogenesis. JAD 28, 839–854. https://doi.org/10.3233/JAD-2011-111037

Hong, M., 1998. Mutation-Specific Functional Impairments in Distinct Tau Isoforms of Hereditary FTDP-17. Science 282, 1914–1917. https://doi.org/10.1126/science.282.5395.1914

Hogg, M., Grujic, Z.M., Baker, M., Demirci, S., Guillozet, A.L., Sweet, A.P., Herzog, L.L., Weintraub, S., Mesulam, M.-M., LaPointe, N.E., Gamblin, T.C., Berry, R.W., Binder, L.I., de Silva, R., Lees, A., Espinoza, M., Davies, P., Grover, A., Sahara, N., Ishizawa, T., Dickson, D., Yen, S.-H., Hutton, M., Bigio, E.H., 2003. The L266V tau mutation is associated with frontotemporal dementia and Pick-like 3R and 4R tauopathy. Acta Neuropathol 106, 323–336. https://doi.org/10.1007/s00401-003-0734-x

Hoenicka, J., Perez, M., Perez-Tur, J., Barabash, A., Godoy, M., Vidal, L., Astarloa, R., Avila, J., Nygaard, T., de Yebenes, J.G., 1999. The tau gene A0 allele and progressive supranuclear palsy. Neurology 53, 1219–1219. https://doi.org/10.1212/WNL.53.6.1219

Hof, P.R., Bouras, C., Bu□e, L., Delacourte, A., Perl, D.P., Morrison, J.H., 1992. Differential distribution of neurofibrillary tangles in the cerebral cortex of dementia pugilistica and Alzheimer's disease cases. Acta Neuropathol. (Berl.) 85, 23–30. https://doi.org/10.1007/BF00304630

Hoffmann, R., Lee, V.M., Leight, S., Varga, I., Otvos, L., 1997. Unique Alzheimer's disease paired helical filament specific epitopes involve double phosphorylation at specific sites. Biochemistry 36, 8114–8124. https://doi.org/10.1021/bi970380+

Höglinger, G.U., Respondek, G., Stamelou, M., Kurz, C., Josephs, K.A., Lang, A.E., Mollenhauer, B., Müller, U., Nilsson, C., Whitwell, J.L., Arzberger, T., Englund, E., Gelpi,

E., Giese, A., Irwin, D.J., Meissner, W.G., Pantelyat, A., Rajput, A., van Swieten, J.C., Troakes, C., Antonini, A., Bhatia, K.P., Bordelon, Y., Compta, Y., Corvol, J.-C., Colosimo, C., Dickson, D.W., Dodel, R., Ferguson, L., Grossman, M., Kassubek, J., Krismer, F., Levin, J., Lorenzl, S., Morris, H.R., Nestor, P., Oertel, W.H., Poewe, W., Rabinovici, G., Rowe, J.B., Schellenberg, G.D., Seppi, K., van Eimeren, T., Wenning, G.K., Boxer, A.L., Golbe, L.I., Litvan, I., for the Movement Disorder Society-endorsed PSP Study Group, 2017. Clinical diagnosis of progressive supranuclear palsy: The movement disorder society criteria: MDS Clinical Diagnostic Criteria for PSP. Mov. Disord. 32, 853–864. https://doi.org/10.1002/mds.26987

Holmes, B.B., Furman, J.L., Mahan, T.E., Yamasaki, T.R., Mirbaha, H., Eades, W.C., Belaygorod, L., Cairns, N.J., Holtzman, D.M., Diamond, M.I., 2014. Proteopathic tau seeding predicts tauopathy in vivo. Proceedings of the National Academy of Sciences 111, E4376–E4385. https://doi.org/10.1073/pnas.1411649111

Hollenbeck, P.J., 2005. The axonal transport of mitochondria. J. Cell Sci. 118, 5411–5419. https://doi.org/10.1242/jcs.02745

Hoozemans, J.J.M., van Haastert, E.S., Nijholt, D.A.T., Rozemuller, A.J.M., Eikelenboom, P., Scheper, W., 2009. The Unfolded Protein Response Is Activated in Pretangle Neurons in Alzheimer's Disease Hippocampus. Am. J. Pathol. 174, 1241–1251. https://doi.org/10.2353/ajpath.2009.080814

Hoozemans, J.J.M., van Haastert, E.S., Nijholt, D.A.T., Rozemuller, A.J.M., Scheper, W., 2012. Activation of the unfolded protein response is an early event in Alzheimer's and Parkinson's disease. Neurodegener. Dis. 10, 212–215. https://doi.org/10.1159/000334536

Hoozemans, J.J.M., Veerhuis, R., Van Haastert, E.S., Rozemuller, J.M., Baas, F., Eikelenboom, P., Scheper, W., 2005. The unfolded protein response is activated in Alzheimer's disease. Acta Neuropathol. (Berl.) 110, 165–172. https://doi.org/10.1007/s00401-005-1038-0

Houck, A.L., Hernández, F., Ávila, J., 2016. A Simple Model to Study Tau Pathology. J Exp Neurosci 10, JEN.S25100. https://doi.org/10.4137/JEN.S25100

Houghton, D.J., Litvan, I., 2007. Unraveling progressive supranuclear palsy: from the bedsideback to the bench. Parkinsonism Relat. Disord. 13, S341–S346. https://doi.org/10.1016/S1353-8020(08)70028-2

Houlden, H., Baker, M., Morris, H.R., MacDonald, N., Pickering-Brown, S., Adamson, J., Lees, A.J., Rossor, M.N., Quinn, N.P., Kertesz, A., Khan, M.N., Hardy, J., Lantos, P.L., St. George-Hyslop, P., Munoz, D.G., Mann, D., Lang, A.E., Bergeron, C., Bigio, E.H., Litvan, I., Bhatia, K.P., Dickson, D., Wood, N.W., Hutton, M., 2001. Corticobasal degeneration and progressive supranuclear palsy share a common tau haplotype. Neurology 56, 1702–1706. https://doi.org/10.1212/WNL.56.12.1702

Hua, Q., He, R., 2003. Tau could protect DNA double helix structure. Biochim. Biophys. Acta BBA - Proteins Proteomics 1645, 205–211. https://doi.org/10.1016/S1570-9639(02)00538-1

Hughes, D., Mallucci, G.R., 2019. The unfolded protein response in neurodegenerative disorders - therapeutic modulation of the PERK pathway. FEBS J 286, 342–355. https://doi.org/10.1111/febs.14422

Hurtley, S.M., Helenius, A., 1989. Protein Oligomerization in the Endoplasmic Reticulum. Annu. Rev. Cell Biol. 5, 277–307. https://doi.org/10.1146/annurev.cb.05.110189.001425

Hutton, M., Lendon, C.L., Rizzu, P., Baker, M., Froelich, S., Houlden, H., Pickering-Brown, S., Chakraverty, S., Isaacs, A., Grover, A., Hackett, J., Adamson, J., Lincoln, S., Dickson, D., Davies, P., Petersen, R.C., Stevens, M., de Graaff, E., Wauters, E., van Baren, J., Hillebrand, M., Joosse, M., Kwon, J.M., Nowotny, P., Che, L.K., Norton, J., Morris, J.C., Reed, L.A., Trojanowski, J., Basun, H., Lannfelt, L., Neystat, M., Fahn, S., Dark, F., Tannenberg, T., Dodd, P.R., Hayward, N., Kwok, J.B.J., Schofield, P.R., Andreadis, A., Snowden, J., Craufurd, D., Neary, D., Owen, F., Oostra, B.A., Hardy, J., Goate, A., van Swieten, J., Mann, D., Lynch, T., Heutink, P., 1998. Association of missense and 5′-splice-site mutations in tau with the inherited dementia FTDP-17. Nature 393, 702–705. https://doi.org/10.1038/31508

Ikegami, S., 2000. Muscle weakness, hyperactivity, and impairment in fear conditioning in tau-deficient mice. Neurosci. Lett. 279, 129–132. https://doi.org/10.1016/S0304-3940(99)00964-7

Im, S.Y., Kim, Y.E., Kim, Y.J., 2015. Genetics of Progressive Supranuclear Palsy. J. Mov. Disord. 8, 122–129. https://doi.org/10.14802/jmd.15033

Imahori, K., Uchida, T., 1997. Physiology and pathology of tau protein kinases in relation to Alzheimer's disease. J Biochem 121, 179–188.

Invernizzi, G., Naeem, A., Loor, J.J., 2012. Short communication: Endoplasmic reticulum stress gene network expression in bovine mammary tissue during the lactation cycle. J. Dairy Sci. 95, 2562–2566. https://doi.org/10.3168/jds.2011-4806

Iqbal, K., Liu, F., Gong, C.-X., Grundke-Iqbal, I., 2010. Tau in Alzheimer disease and related tauopathies. Curr. Alzheimer Res. 7, 656–664. https://doi.org/10.2174/156720510793611592

Irwin, D.J., Abrams, J.Y., Schonberger, L.B., Leschek, E.W., Mills, J.L., Lee, V.M.-Y., Trojanowski, J.Q., 2013. Evaluation of Potential Infectivity of Alzheimer and Parkinson Disease Proteins in Recipients of Cadaver-Derived Human Growth Hormone. JAMA Neurol 70, 462. https://doi.org/10.1001/jamaneurol.2013.1933

Irwin, D.J., Lee, V.M.-Y., Trojanowski, J.Q., 2013. Parkinson's disease dementia: convergence of α-synuclein, tau and amyloid-β pathologies. Nat Rev Neurosci 14, 626–636. https://doi.org/10.1038/nrn3549

Ishiguro, K., Omori, A., Takamatsu, M., Sato, K., Arioka, M., Uchida, T., Imahori, K., 1992. Phosphorylation sites on tau by tau protein kinase I, a bovine derived kinase generating an epitope of paired helical filaments. Neuroscience Letters 148, 202–206. https://doi.org/10.1016/0304-3940(92)90839-Y

Irwin, D.J., 2016. Tauopathies as clinicopathological entities. Parkinsonism Relat. Disord. 22, S29–S33. https://doi.org/10.1016/j.parkreldis.2015.09.020

Iovino, M., Pfisterer, U., Holton, J.L., Lashley, T., Swingler, R.J., Calo, L., Treacy, R., Revesz, T., Parmar, M., Goedert, M., Muqit, M.M.K., Spillantini, M.G., 2014. The novel MAPT mutation K298E: mechanisms of mutant tau toxicity, brain pathology and tau expression in induced fibroblast-derived neurons. Acta Neuropathol 127, 283–295. https://doi.org/10.1007/s00401-013-1219-1

Itoh, K., Chiba, T., Takahashi, S., Ishii, T., Igarashi, K., Katoh, Y., Oyake, T., Hayashi, N., Satoh, K., Hatayama, I., Yamamoto, M., Nabeshima, Y., 1997. An Nrf2/Small Maf Heterodimer Mediates the Induction of Phase II Detoxifying Enzyme Genes through Antioxidant Response Elements. Biochem. Biophys. Res. Commun. 236, 313–322. https://doi.org/10.1006/bbrc.1997.6943

Itoh, K., Wakabayashi, N., Katoh, Y., Ishii, T., Igarashi, K., Engel, J.D., Yamamoto, M., 1999. Keap1 represses nuclear activation of antioxidant responsive elements by Nrf2 through binding to the amino-terminal Neh2 domain. Genes Dev. 13, 76–86. https://doi.org/10.1101/gad.13.1.76

Ittner, L.M., Ke, Y.D., Delerue, F., Bi, M., Gladbach, A., van Eersel, J., Wölfing, H., Chieng, B.C., Christie, M.J., Napier, I.A., Eckert, A., Staufenbiel, M., Hardeman, E., Götz, J., 2010. Dendritic Function of Tau Mediates Amyloid-β Toxicity in Alzheimer's Disease Mouse Models. Cell 142, 387–397. https://doi.org/10.1016/j.cell.2010.06.036

Iyer, A., Lapointe, N.E., Zielke, K., Berdynski, M., Guzman, E., Barczak, A., Chodakowska-Żebrowska, M., Barcikowska, M., Feinstein, S., Zekanowski, C., 2013. A novel MAPT mutation, G55R, in a frontotemporal dementia patient leads to altered Tau function. PLoS One 8, e76409. https://doi.org/10.1371/journal.pone.0076409

Jabbari, E., Woodside, J., Tan, M.M.X., Pavese, N., Bandmann, O., Ghosh, B.C.P., Massey, L.A., Capps, E., Warner, T.T., Lees, A.J., Revesz, T., Holton, J.L., Williams, N.M., Grosset, D.G., Morris, H.R., 2019. The genetic and clinico-pathological profile of early-onset progressive supranuclear palsy. Movement Disorders 34, 1307–1314. https://doi.org/10.1002/mds.27786

Jameson, L., Frey, T., Zeeberg, B., Dalldorf, F., Caplow, M., 1980. Inhibition of microtubule assembly by phosphorylation of microtubule-associated proteins. Biochemistry 19, 2472–2479. https://doi.org/10.1021/bi00552a027

Jeganathan, S., Hascher, A., Chinnathambi, S., Biernat, J., Mandelkow, E.-M., 2008. Proline-directed Pseudo-phosphorylation at AT8 and PHF1 Epitopes Induces a Compaction of the Paperclip Folding of Tau and Generates a Pathological (MC-1) Conformation. J. Biol. Chem. 283, 32066–32076. https://doi.org/10.1074/jbc.M805300200

Jeganathan, S., von Bergen, M., Brutlach, H., Steinhoff, H.-J., Mandelkow, E., 2006. Global Hairpin Folding of Tau in Solution. Biochemistry 45, 2283–2293. https://doi.org/10.1021/bi0521543

Jeganathan, S., von Bergen, M., Mandelkow, E.-M., Mandelkow, E., 2008. The Natively Unfolded Character of Tau and Its Aggregation to Alzheimer-like Paired Helical Filaments. Biochemistry 47, 10526–10539. https://doi.org/10.1021/bi800783d

Jho, Y.S., Zhulina, E.B., Kim, M.W., Pincus, P.A., 2010. Monte Carlo Simulations of Tau Proteins: Effect of Phosphorylation. Biophys. J. 99, 2387–2397. https://doi.org/10.1016/j.bpj.2010.06.056

Jiang, J., Qu, Y., Liu, X., Tang, C., Wei, P., 2020. Antagonistic crosstalk fine-tunes sensitivities of IRE1 and PERK signaling during unfolded protein response (preprint). Cell Biology. https://doi.org/10.1101/2020.08.09.243527

Johnson, G.V.W., 2006. Tau phosphorylation and proteolysis: Insights and perspectives. JAD 9, 243–250. https://doi.org/10.3233/JAD-2006-9S326

Johnson, A.E., van Waes, M.A., 1999. The Translocon: A Dynamic Gateway at the ER Membrane. Annu. Rev. Cell Dev. Biol. 15, 799–842. https://doi.org/10.1146/annurev.cellbio.15.1.799

Jurica, M.S., Moore, M.J., 2003. Pre-mRNA Splicing. Mol. Cell 12, 5–14. https://doi.org/10.1016/S1097-2765(03)00270-3

Kaat, L.D., Boon, A.J.W., Azmani, A., Kamphorst, W., Breteler, M.M.B., Anar, B., Heutink, P., van Swieten, J.C., 2009. Familial aggregation of parkinsonism in progressive supranuclear palsy. Neurology 73, 98–105. https://doi.org/10.1212/WNL.0b013e3181a92bcc

Kadavath, H., Hofele, R.V., Biernat, J., Kumar, S., Tepper, K., Urlaub, H., Mandelkow, E., Zweckstetter, M., 2015. Tau stabilizes microtubules by binding at the interface between tubulin heterodimers. Proc. Natl. Acad. Sci. 112, 7501–7506. https://doi.org/10.1073/pnas.1504081112

Kang, J., Lemaire, H.-G., Unterbeck, A., Salbaum, J.M., Masters, C.L., Grzeschik, K.-H., Multhaup, G., Beyreuther, K., Müller-Hill, B., 1987. The precursor of Alzheimer's disease amyloid A4 protein resembles a cell-surface receptor. Nature 325, 733–736. https://doi.org/10.1038/325733a0

Kara, E., Ling, H., Pittman, A.M., Shaw, K., de Silva, R., Simone, R., Holton, J.L., Warren, J.D., Rohrer, J.D., Xiromerisiou, G., Lees, A., Hardy, J., Houlden, H., Revesz, T., 2012. The MAPT p.A152T variant is a risk factor associated with tauopathies with atypical clinical and neuropathological features. Neurobiology of Aging 33, 2231.e7-2231.e14. https://doi.org/10.1016/j.neurobiolaging.2012.04.006

Kar, S., 2003. Repeat motifs of tau bind to the insides of microtubules in the absence of taxol. EMBO J. 22, 70–77. https://doi.org/10.1093/emboj/cdg001

Katayama, T., Imaizumi, K., Manabe, T., Hitomi, J., Kudo, T., Tohyama, M., 2004. Induction of neuronal death by ER stress in Alzheimer's disease. J. Chem. Neuroanat. 28, 67–78. https://doi.org/10.1016/j.jchemneu.2003.12.004

Katsinelos, T., Zeitler, M., Dimou, E., Karakatsani, A., Müller, H.-M., Nachman, E., Steringer, J.P., Ruiz de Almodovar, C., Nickel, W., Jahn, T.R., 2018. Unconventional Secretion Mediates the Trans-cellular Spreading of Tau. Cell Reports 23, 2039–2055. https://doi.org/10.1016/j.celrep.2018.04.056

Kaufman, R.J., 1999. Stress signaling from the lumen of the endoplasmic reticulum: coordination of gene transcriptional and translational controls. Genes & Development 13, 1211–1233. https://doi.org/10.1101/gad.13.10.1211

Kenessey, A., Yen, S.-H.C., 1993. The extent of phosphorylation of fetal tau is comparable to that of PHF-tau from Alzheimer paired helical filaments. Brain Res. 629, 40–46. https://doi.org/10.1016/0006-8993(93)90478-6

Kfoury, N., Holmes, B.B., Jiang, H., Holtzman, D.M., Diamond, M.I., 2012. Trans-cellular Propagation of Tau Aggregation by Fibrillar Species. J. Biol. Chem. 287, 19440–19451. https://doi.org/10.1074/jbc.M112.346072

Khlistunova, I., Biernat, J., Wang, Y., Pickhardt, M., von Bergen, M., Gazova, Z., Mandelkow, E., Mandelkow, E.-M., 2006. Inducible Expression of Tau Repeat Domain in Cell Models of Tauopathy: AGGREGATION IS TOXIC TO CELLS BUT CAN BE REVERSED BY INHIBITOR DRUGS. J. Biol. Chem. 281, 1205–1214. https://doi.org/10.1074/jbc.M507753200

Kim, I., Xu, W., Reed, J.C., 2008. Cell death and endoplasmic reticulum stress: disease relevance and therapeutic opportunities. Nat. Rev. Drug Discov. 7, 1013–1030. https://doi.org/10.1038/nrd2755

Kim, T.K., Eberwine, J.H., 2010. Mammalian cell transfection: the present and the future. Anal Bioanal Chem 397, 3173–3178. https://doi.org/10.1007/s00216-010-3821-6

Kimata, Y., Ishiwata-Kimata, Y., Ito, T., Hirata, A., Suzuki, T., Oikawa, D., Takeuchi, M., Kohno, K., 2007. Two regulatory steps of ER-stress sensor Ire1 involving its cluster formation and interaction with unfolded proteins. J. Cell Biol. 179, 75–86. https://doi.org/10.1083/jcb.200704166

Kimata, Y., Oikawa, D., Shimizu, Y., Ishiwata-Kimata, Y., Kohno, K., 2004. A role for BiP as an adjustor for the endoplasmic reticulum stress-sensing protein Ire1. J. Cell Biol. 167, 445–456. https://doi.org/10.1083/jcb.200405153

Klafki, H.-W., Staufenbiel, M., Kornhuber, J., Wiltfang, J., 2006. Therapeutic approaches to Alzheimer's disease. Brain 129, 2840–2855. https://doi.org/10.1093/brain/awl280

Klann, E., Sweatt, J.D., 2008. Altered protein synthesis is a trigger for long-term memory formation. Neurobiol. Learn. Mem. 89, 247–259. https://doi.org/10.1016/j.nlm.2007.08.009

Klein, C., Kramer, E.-M., Cardine, A.-M., Schraven, B., Brandt, R., Trotter, J., 2002. Process outgrowth of oligodendrocytes is promoted by interaction of fyn kinase with the cytoskeletal protein tau. J. Neurosci. Off. J. Soc. Neurosci. 22, 698–707.

Klein, P.S., Melton, D.A., 1996. A molecular mechanism for the effect of lithium on development. Proc. Natl. Acad. Sci. 93, 8455–8459. https://doi.org/10.1073/pnas.93.16.8455

Kobayashi, T., Ota, S., Tanaka, K., Ito, Y., Hasegawa, M., Umeda, Y., Motoi, Y., Takanashi, M., Yasuhara, M., Anno, M., Mizuno, Y., Mori, H., 2003. A novel L266V mutation of the tau gene causes frontotemporal dementia with a unique tau pathology. Ann Neurol. 53, 133–137. https://doi.org/10.1002/ana.10447

Kondo, J., Honda, T., Mori, H., Hamada, Y., Miura, R., Ogawara, M., Ihara, Y., 1988. The caryl third of tau is tightly bound to paired helical filaments. Neuron 1, 827–834. https://doi.org/10.1016/0896-6273(88)90130-4

Kondo, S., Yamamoto, N., Murakami, T., Okumura, M., Mayeda, A., Imaizumi, K., 2004. Tra2β, SF2/ASF and SRp30c modulate the function of an exonic splicing enhancer in exon 10 of tau pre-mRNA: Splicing regulation of tau exon 10. Genes Cells 9, 121–130. https://doi.org/10.1111/j.1356-9597.2004.00709.x

Köpke, E., Tung, Y.C., Shaikh, S., Alonso, A.C., Iqbal, K., Grundke-Iqbal, I., 1993. Microtubule-associated protein tau. Abnormal phosphorylation of a non-paired helical filament pool in Alzheimer disease. J. Biol. Chem. 268, 24374–24384.

Korelitz, B.I., Sommers, S.C., 1975. Responses to drug therapy in ulcerative colitis. Evaluation by rectal biopsy and histopathological changes. Am. J. Gastroenterol. 64, 365–370.

Korennykh, A., Walter, P., 2012. Structural Basis of the Unfolded Protein Response. Annu. Rev. Cell Dev. Biol. 28, 251–277. https://doi.org/10.1146/annurev-cellbio-101011-155826

Korennykh, A.V., Egea, P.F., Korostelev, A.A., Finer-Moore, J., Zhang, C., Shokat, K.M., Stroud, R.M., Walter, P., 2009. The unfolded protein response signals through high-order assembly of Ire1. Nature 457, 687–693. https://doi.org/10.1038/nature07661

Kosik, K.S., Joachim, C.L., Selkoe, D.J., 1986. Microtubule-associated protein tau (tau) is a major antigenic component of paired helical filaments in Alzheimer disease. Proc. Natl. Acad. Sci. 83, 4044–4048. https://doi.org/10.1073/pnas.83.11.4044

Kosik, K.S., Orecchio, L.D., Bakalis, S., Neve, R.L., 1989. Developmentally regulated expression of specific tau sequences. Neuron 2, 1389–1397. https://doi.org/10.1016/0896-6273(89)90077-9

Kosik, K.S., Orecchio, L.D., Binder, L., Trojanowski, J.Q., Lee, V.M.-Y., Lee, G., 1988. Epitopes that span the tau molecule are shared with paired helical filaments. Neuron 1, 817–825. https://doi.org/10.1016/0896-6273(88)90129-8

Kosik K.S. (1997). Tau: structure and function. In: ed. Brain Microtubule Associated Proteins, J. Avila, R. Brandt, and K.S. Kosik, Amsterdam, Netherlands: Harwood Academic Publishers, 43-52.

Kovacs, G.G., Majtenyi, K., Spina, S., Murrell, J.R., Gelpi, E., Hoftberger, R., Fraser, G., Crowther, R.A., Goedert, M., Budka, H., Ghetti, B., 2008. White Matter Tauopathy With Globular Glial Inclusions: A Distinct Sporadic Frontotemporal Lobar Degeneration. J Neuropathol Exp Neurol 67, 963–975. https://doi.org/10.1097/NEN.0b013e318187a80f

Kouri, N., Carlomagno, Y., Baker, M., Liesinger, A.M., Caselli, R.J., Wszolek, Z.K., Petrucelli, L., Boeve, B.F., Parisi, J.E., Josephs, K.A., Uitti, R.J., Ross, O.A., Graff-Radford, N.R., DeTure, M.A., Dickson, D.W., Rademakers, R., 2014. Novel mutation in

MAPT exon 13 (p.N410H) causes corticobasal degeneration. Acta Neuropathol 127, 271–282. https://doi.org/10.1007/s00401-013-1193-7

Kouri, N., Ross, O.A., Dombroski, B., Younkin, C.S., Serie, D.J., Soto-Ortolaza, A., Baker, M., Finch, N.C.A., Yoon, H., Kim, J., Fujioka, S., McLean, C.A., Ghetti, B., Spina, S., Cantwell, L.B., Farlow, M.R., Grafman, J., Huey, E.D., Ryung Han, M., Beecher, S., Geller, E.T., Kretzschmar, H.A., Roeber, S., Gearing, M., Juncos, J.L., Vonsattel, J.P.G., Van Deerlin, V.M., Grossman, M., Hurtig, H.I., Gross, R.G., Arnold, S.E., Trojanowski, J.Q., Lee, V.M., Wenning, G.K., White, C.L., Höglinger, G.U., Müller, U., Devlin, B., Golbe, L.I., Crook, J., Parisi, J.E., Boeve, B.F., Josephs, K.A., Wszolek, Z.K., Uitti, R.J., Graff-Radford, N.R., Litvan, I., Younkin, S.G., Wang, L.-S., Ertekin-Taner, N., Rademakers, R., Hakonarsen, H., Schellenberg, G.D., Dickson, D.W., 2015. Genome-wide association study of corticobasal degeneration identifies risk variants shared with progressive supranuclear palsy. Nat. Commun. 6, 7247. https://doi.org/10.1038/ncomms8247

Koumenis, C., Naczki, C., Koritzinsky, M., Rastani, S., Diehl, A., Sonenberg, N., Koromilas, A., Wouters, B.G., 2002. Regulation of Protein Synthesis by Hypoxia via Activation of the Endoplasmic Reticulum Kinase PERK and Phosphorylation of the Translation Initiation Factor eIF2α. MCB 22, 7405–7416. https://doi.org/10.1128/MCB.22.21.7405-7416.2002

Kozutsumi, Y., Segal, M., Normington, K., Gething, M.-J., Sambrook, J., 1988. The presence of malfolded proteins in the endoplasmic reticulum signals the induction of glucose-regulated proteins. Nature 332, 462–464. https://doi.org/10.1038/332462a0

Ksiezak-Reding, H., Liu, W.-K., Yen, S.-H., 1992. Phosphate analysis and dephosphorylation of modified tau associated with paired helical filaments. Brain Res. 597, 209–219. https://doi.org/10.1016/0006-8993(92)91476-U

Kwok, J.B.J., Teber, E.T., Loy, C., Hallupp, M., Nicholson, G., Mellick, G.D., Buchanan, D.D., Silburn, P.A., Schofield, P.R., 2004. Tau haplotypes regulate transcription and are associated with Parkinson's disease. Ann. Neurol. 55, 329–334. https://doi.org/10.1002/ana.10826

Laemmli, U.K., 1970. Cleavage of Structural Proteins during the Assembly of the Head of Bacteriophage T4. Nature 227, 680–685. https://doi.org/10.1038/227680a0

Lagunas-Martínez, A., García-Villa, E., Arellano-Gaytán, M., Contreras-Ochoa, C.O., Dimas-González, J., López-Arellano, M.E., Madrid-Marina, V., Gariglio, P., 2017. MG132 plus apoptosis antigen-1 (APO-1) antibody cooperate to restore p53 activity inducing autophagy and p53-dependent apoptosis in HPV16 E6-expressing keratinocytes. Apoptosis 22, 27–40. https://doi.org/10.1007/s10495-016-1299-1

Lasagna-Reeves, C.A., Castillo-Carranza, D.L., Guerrero-Muñoz, M.J., Jackson, G.R., Kayed, R., 2010. Preparation and Characterization of Neurotoxic Tau Oligomers. Biochemistry 49, 10039–10041. https://doi.org/10.1021/bi1016233

Lasagna-Reeves, C.A., Castillo-Carranza, D.L., Sengupta, U., Clos, A.L., Jackson, G.R., Kayed, R., 2011. Tau oligomers impair memory and induce synaptic and mitochondrial dysfunction in wild-type mice. Mol Neurodegeneration 6, 39. https://doi.org/10.1186/1750-1326-6-39

Larner, A.J., 2002. Did Charles Dickens describe progressive supranuclear palsy in 1857? Mov. Disord. 17, 832–833. https://doi.org/10.1002/mds.10170

Le Masson, G., Przedborski, S., Abbott, L.F., 2014. A computational model of motor neuron degeneration. Neuron 83, 975–988. https://doi.org/10.1016/j.neuron.2014.07.001

Lebouvier, T., Scales, T.M.E., Williamson, R., Noble, W., Duyckaerts, C., Hanger, D.P., Reynolds, C.H., Anderton, B.H., Derkinderen, P., 2009. The Microtubule-Associated Protein Tau is Also Phosphorylated on Tyrosine. J. Alzheimers Dis. 18, 1–9. https://doi.org/10.3233/JAD-2009-1116

Lee, D.H., Goldberg, A.L., 1998. Proteasome inhibitors: valuable new tools for cell biologists. Trends in Cell Biology 8, 397–403. https://doi.org/10.1016/S0962-8924(98)01346-4

Lee, A.-H., Iwakoshi, N.N., Glimcher, L.H., 2003. XBP-1 Regulates a Subset of Endoplasmic Reticulum Resident Chaperone Genes in the Unfolded Protein Response. Mol. Cell. Biol. 23, 7448–7459. https://doi.org/10.1128/MCB.23.21.7448-7459.2003

Lee, C., Chen, L.B., 1988. Dynamic behavior of endoplasmic reticulum in living cells. Cell 54, 37–46. https://doi.org/10.1016/0092-8674(88)90177-8

Lee, G., 1990. Tau protein: An update on structure and function. Cell Motil. Cytoskeleton 15, 199–203. https://doi.org/10.1002/cm.970150402

Lee, V., Balin, B., Otvos, L., Trojanowski, J., 1991. A68: a major subunit of paired helical filaments and derivatized forms of normal Tau. Science 251, 675–678. https://doi.org/10.1126/science.1899488

Lee, V.M.-Y., Goedert, M., Trojanowski, J.Q., 2001. Neurodegenerative Tauopathies. Annu. Rev. Neurosci. 24, 1121–1159. https://doi.org/10.1146/annurev.neuro.24.1.1121

Lee, V.M.-Y., Kenyon, T.K., Trojanowski, J.Q., 2005. Transgenic animal models of tauopathies. Biochim. Biophys. Acta BBA - Mol. Basis Dis. 1739, 251–259. https://doi.org/10.1016/j.bbadis.2004.06.014

Lee, M.J., Lee, J.H., Rubinsztein, D.C., 2013. Tau degradation: The ubiquitin–proteasome system versus the autophagy-lysosome system. Progress in Neurobiology 105, 49–59. https://doi.org/10.1016/j.pneurobio.2013.03.001

Leroy, A., Landrieu, I., Huvent, I., Legrand, D., Codeville, B., Wieruszeski, J.-M., Lippens, G., 2010. Spectroscopic Studies of GSK3β Phosphorylation of the Neuronal Tau Protein and Its Interaction with the N-terminal Domain of Apolipoprotein E. J. Biol. Chem. 285, 33435–33444. https://doi.org/10.1074/jbc.M110.149419

Li, G., Mongillo, M., Chin, K.-T., Harding, H., Ron, D., Marks, A.R., Tabas, I., 2009. Role of ERO1-α–mediated stimulation of inositol 1,4,5-triphosphate receptor activity in endoplasmic reticulum stress–induced apoptosis. J. Cell Biol. 186, 783–792. https://doi.org/10.1083/jcb.200904060

Li, H.-L., Wang, H.-H., Liu, S.-J., Deng, Y.-Q., Zhang, Y.-J., Tian, Q., Wang, X.-C., Chen, X.-Q., Yang, Y., Zhang, J.-Y., Wang, Q., Xu, H., Liao, F.-F., Wang, J.-Z., 2007. Phosphorylation of tau antagonizes apoptosis by stabilizing beta-catenin, a mechanism involved in Alzheimer's neurodegeneration. Proc. Natl. Acad. Sci. 104, 3591–3596. https://doi.org/10.1073/pnas.0609303104

Li, W., Lee, V.M.-Y., 2006. Characterization of two VQIXXK motifs for tau fibrillization in vitro. Biochemistry 45, 15692–15701. https://doi.org/10.1021/bi061422+

Li, X., Kumar, Y., Zempel, H., Mandelkow, E.-M., Biernat, J., Mandelkow, E., 2011. Novel diffusion barrier for axonal retention of Tau in neurons and its failure in

neurodegeneration: Novel diffusion barrier for axonal retention of Tau in neurons. EMBO J. 30, 4825–4837. https://doi.org/10.1038/emboj.2011.376

Li, Y., Chen, J.A., Sears, R.L., Gao, F., Klein, E.D., Karydas, A., Geschwind, M.D., Rosen, H.J., Boxer, A.L., Guo, W., Pellegrini, M., Horvath, S., Miller, B.L., Geschwind, D.H., Coppola, G., 2014. An Epigenetic Signature in Peripheral Blood Associated with the Haplotype on 17q21.31, a Risk Factor for Neurodegenerative Tauopathy. PLoS Genet. 10, e1004211. https://doi.org/10.1371/journal.pgen.1004211

Iijima, M., Tabira, T., Poorkaj, P., Schellenberg, G.D., Trojanowski, J.Q., Lee, V.M.-Y., Schmidt, M.L., Takahashi, K., Nabika, T., Matsumoto, T., Yamashita, Y., Yoshioka, S., Ishino, H., 1999. A distinct familial presenile dementia with a novel missense mutation in the tau gene: NeuroReport 10, 497–501. https://doi.org/10.1097/00001756-199902250-00010

Lindwall, G., Cole, R.D., 1984. Phosphorylation affects the ability of tau protein to promote microtubule assembly. J. Biol. Chem. 259, 5301–5305.

Lippa, C.F., Zhukareva, V., Kawarai, T., Uryu, K., Shafiq, M., Nee, L.E., Grafman, J., Liang, Y., St George-Hyslop, P.H., Trojanowski, J.Q., Lee, V.M., 2000. Frontotemporal dementia with novel tau pathology and a Glu342Val tau mutation. Ann Neurol 48, 850–858.

Litvan, I., Agid, Y., Calne, D., Campbell, G., Dubois, B., Duvoisin, R.C., Goetz, C.G., Golbe, L.I., Grafman, J., Growdon, J.H., Hallett, M., Jankovic, J., Quinn, N.P., Tolosa, E., Zee, D.S., 1996. Clinical research criteria for the diagnosis of progressive supranuclear palsy (Steele-Richardson-Olszewski syndrome): Report of the NINDS-SPSP International Workshop. Neurology 47, 1–9. https://doi.org/10.1212/WNL.47.1.1

Litvan, I., Baker, M., Hutton, M., 2001. Tau genotype: No effect on onset, symptom severity, or survival in progressive supranuclear palsy. Neurology 57, 138–140. https://doi.org/10.1212/WNL.57.1.138

Litvan, I., Hutton, M., 1998. Clinical and Genetic Aspects of Progressive Supranuclear Palsy. J. Geriatr. Psychiatry Neurol. 11, 107–114. https://doi.org/10.1177/089198879801100208

Liu, S., Zhang, W., Zhang, M., Zhu, Q., Tian, W., 2005. Construction and identification of Fas-targeting siRNA-expressing plasmid. J. Zhejiang Univ. Sci. 6B, 673–677. https://doi.org/10.1631/jzus.2005.B0673

Liu, F., Grundke-Iqbal, I., Iqbal, K., Gong, C.-X., 2005. Contributions of protein phosphatases PP1, PP2A, PP2B and PP5 to the regulation of tau phosphorylation. European Journal of Neuroscience 22, 1942–1950. https://doi.org/10.1111/j.1460-9568.2005.04391.x

Liu, C., Song, X., Nisbet, R., Götz, J., 2016. Co-immunoprecipitation with Tau Isoform-specific Antibodies Reveals Distinct Protein Interactions and Highlights a Putative Role for 2N Tau in Disease. J. Biol. Chem. 291, 8173–8188. https://doi.org/10.1074/jbc.M115.641902

Liu, C.Y., Schröder, M., Kaufman, R.J., 2000. Ligand-independent Dimerization Activates the Stress Response Kinases IRE1 and PERK in the Lumen of the Endoplasmic Reticulum. J. Biol. Chem. 275, 24881–24885. https://doi.org/10.1074/jbc.M004454200

Liu, C.Y., Wong, H.N., Schauerte, J.A., Kaufman, R.J., 2002. The Protein Kinase/Endoribonuclease IRE1α That Signals the Unfolded Protein Response Has a Luminal N-terminal Ligand-independent Dimerization Domain. J. Biol. Chem. 277, 18346–18356. https://doi.org/10.1074/jbc.M112454200

Liu, J., Hoppman, N., O'Connell, J.R., Wang, H., Streeten, E.A., McLenithan, J.C., Mitchell, B.D., Shuldiner, A.R., 2012. A functional haplotype in *EIF2AK3* , an ER stress sensor, is associated with lower bone mineral density. J. Bone Miner. Res. 27, 331–341. https://doi.org/10.1002/jbmr.549

Lladó, A., Rodríguez-Santiago, B., Antonell, A., Sánchez-Valle, R., Molinuevo, J.L., Reñé, R., Pérez-Jurado, L.A., 2007. MAPT gene duplications are not a cause of frontotemporal lobar degeneration. Neuroscience Letters 424, 61–65. https://doi.org/10.1016/j.neulet.2007.07.008

Im, S.Y., Kim, Y.E., Kim, Y.J., 2015. Genetics of Progressive Supranuclear Palsy. JMD 8, 122–129. https://doi.org/10.14802/jmd.15033

Loewen, C.A., Feany, M.B., 2010. The Unfolded Protein Response Protects from Tau Neurotoxicity In Vivo. PLoS ONE 5, e13084. https://doi.org/10.1371/journal.pone.0013084

Louis, N., Evelegh, C., Graham, F.L., 1997. Cloning and Sequencing of the Cellular–Viral Junctions from the Human Adenovirus Type 5 Transformed 293 Cell Line. Virology 233, 423–429. https://doi.org/10.1006/viro.1997.8597

Lovestone, S., Reynolds, C.H., Latimer, D., Davis, D.R., Anderton, B.H., Gallo, J.-M., Hanger, D., Mulot, S., Marquardt, B., Stabel, S., Woodgett, J.R., Miller, C.C.J., 1994. Alzheimer's disease-like phosphorylation of the microtubule-associated protein tau by glycogen synthase kinase-3 in transfected mammalian cells. Current Biology 4, 1077–1086. https://doi.org/10.1016/S0960-9822(00)00246-3

Lu, M., Kosik, K.S., 2001. Competition for Microtubule-binding with Dual Expression of Tau Missense and Splice Isoforms. Mol. Biol. Cell 12, 171–184. https://doi.org/10.1091/mbc.12.1.171

Lu, P.D., Harding, H.P., Ron, D., 2004. Translation reinitiation at alternative open reading frames regulates gene expression in an integrated stress response. J. Cell Biol. 167, 27–33. https://doi.org/10.1083/jcb.200408003

Ma, K., Vattem, K.M., Wek, R.C., 2002. Dimerization and Release of Molecular Chaperone Inhibition Facilitate Activation of Eukaryotic Initiation Factor-2 Kinase in Response to Endoplasmic Reticulum Stress. J. Biol. Chem. 277, 18728–18735. https://doi.org/10.1074/jbc.M200903200

Marx, J., 2007. ALZHEIMER'S DISEASE: A New Take on Tau. Science 316, 1416–1417. https://doi.org/10.1126/science.316.5830.1416

Mailliot, C., Sergeant, N., Bussière, T., Caillet-Boudin, M.-L., Delacourte, A., Buée, L., 1998. Phosphorylation of specific sets of tau isoforms reflects different neurofibrillary degeneration processes. FEBS Lett. 433, 201–204. https://doi.org/10.1016/S0014-5793(98)00910-7

Majounie, E., Cross, W., Newsway, V., Dillman, A., Vandrovcova, J., Morris, C.M., Nalls, M.A., Ferrucci, L., Owen, M.J., O'Donovan, M.C., Cookson, M.R., Singleton, A.B., de Silva, R., Morris, H.R., 2013. Variation in tau isoform expression in different brain regions and disease states. Neurobiol. Aging 34, 1922.e7-1922.e12. https://doi.org/10.1016/j.neurobiolaging.2013.01.017

Majumder, M., Huang, C., Snider, M.D., Komar, A.A., Tanaka, J., Kaufman, R.J., Krokowski, D., Hatzoglou, M., 2012. A Novel Feedback Loop Regulates the Response to

Endoplasmic Reticulum Stress via the Cooperation of Cytoplasmic Splicing and mRNA Translation. Molecular and Cellular Biology 32, 992–1003. https://doi.org/10.1128/MCB.06665-11

Mandell, J.W., Banker, G.A., 1996. A spatial gradient of tau protein phosphorylation in nascent axons. J. Neurosci. Off. J. Soc. Neurosci. 16, 5727–5740.

Matsumoto, M., Minami, M., Takeda, K., Sakao, Y., Akira, S., 1996. Ectopic expression of CHOP (GADD153) induces apoptosis in M1 myeloblastic leukemia cells. FEBS Lett. 395, 143–147. https://doi.org/10.1016/0014-5793(96)01016-2

Matsuo, E.S., Shin, R.-W., Billingsley, M.L., Van deVoorde, A., O'Connor, M., Trojanowski, J.Q., Lee, V.M.Y., 1994. Biopsy-derived adult human brain tau is phosphorylated at many of the same sites as Alzheimer's disease paired helical filament tau. Neuron 13, 989–1002. https://doi.org/10.1016/0896-6273(94)90264-X

Matus, S., Glimcher, L.H., Hetz, C., 2011. Protein folding stress in neurodegenerative diseases: a glimpse into the ER. Curr. Opin. Cell Biol. 23, 239–252. https://doi.org/10.1016/j.ceb.2011.01.003

McCullough, K.D., Martindale, J.L., Klotz, L.-O., Aw, T.-Y., Holbrook, N.J., 2001. Gadd153 Sensitizes Cells to Endoplasmic Reticulum Stress by Down-Regulating Bcl2 and Perturbing the Cellular Redox State. Mol. Cell. Biol. 21, 1249–1259. https://doi.org/10.1128/MCB.21.4.1249-1259.2001

McGaha, S.M., Champney, W.S., 2007. Hygromycin B Inhibition of Protein Synthesis and Ribosome Biogenesis in Escherichia coli. AAC 51, 591–596. https://doi.org/10.1128/AAC.01116-06

Medina, M., Avila, J., 2014. The role of extracellular Tau in the spreading of neurofibrillary pathology. Front. Cell. Neurosci. 8. https://doi.org/10.3389/fncel.2014.00113

Meier, S., Bell, M., Lyons, D.N., Ingram, A., Chen, J., Gensel, J.C., Zhu, H., Nelson, P.T., Abisambra, J.F., 2015. Identification of Novel Tau Interactions with Endoplasmic Reticulum Proteins in Alzheimer's Disease Brain. J Alzheimers Dis 48, 687–702. https://doi.org/10.3233/JAD-150298

Melquist, S., Craig, D.W., Huentelman, M.J., Crook, R., Pearson, J.V., Baker, M., Zismann, V.L., Gass, J., Adamson, J., Szelinger, S., Corneveaux, J., Cannon, A., Coon, K.D., Lincoln, S., Adler, C., Tuite, P., Calne, D.B., Bigio, E.H., Uitti, R.J., Wszolek, Z.K., Golbe, L.I., Caselli, R.J., Graff-Radford, N., Litvan, I., Farrer, M.J., Dickson, D.W., Hutton, M., Stephan, D.A., 2007. Identification of a Novel Risk Locus for Progressive Supranuclear Palsy by a Pooled Genomewide Scan of 500,288 Single-Nucleotide Polymorphisms. Am. J. Hum. Genet. 80, 769–778. https://doi.org/10.1086/513320

Meusser, B., Hirsch, C., Jarosch, E., Sommer, T., 2005. ERAD: the long road to destruction. Nat. Cell Biol. 7, 766–772. https://doi.org/10.1038/ncb0805-766

Meyer, D.I., Dobberstein, B., 1980. Identification and characterization of a membrane component essential for the translocation of nascent proteins across the membrane of the endoplasmic reticulum. J. Cell Biol. 87, 503–508. https://doi.org/10.1083/jcb.87.2.503

Michel, G., 1998. Characterization of tau phosphorylation in glycogen synthase kinase-3β and cyclin dependent kinase-5 activator (p23) transfected cells. Biochimica et Biophysica Acta (BBA) - General Subjects 1380, 177–182. https://doi.org/10.1016/S0304-4165(97)00139-6

Mimuro, M. and Yoshida, M., 2020. Chameleons and mimics: Progressive supranuclear palsy and corticobasal degeneration. Neuropathology, 40(1), pp. 57–67. doi:10.1111/neup.12590

Moi, P., Chan, K., Asunis, I., Cao, A., Kan, Y.W., 1994. Isolation of NF-E2-related factor 2 (Nrf2), a NF-E2-like basic leucine zipper transcriptional activator that binds to the tandem NF-E2/AP1 repeat of the beta-globin locus control region. Proc. Natl. Acad. Sci. 91, 9926–9930. https://doi.org/10.1073/pnas.91.21.9926

Momeni, P., Wickremaratchi, M.M., Bell, J., Arnold, R., Beer, R., Hardy, J., Revesz, T., Neal, J.W., Morris, H.R., 2010. Familial early onset frontotemporal dementia caused by a novel S356T MAPT mutation, initially diagnosed as schizophrenia. Clinical Neurology and Neurosurgery 112, 917–920. https://doi.org/10.1016/j.clineuro.2010.07.015

Montpetit, V., Clapin, D.F., Guberman, A., 1985. Substructure of 20 nm filaments of progressive supranuclear palsy. Acta Neuropathol. (Berl.) 68, 311–318. https://doi.org/10.1007/BF00690834

Moon, Y., Lee, K.H., Park, J.-H., Geum, D., Kim, K., 2005. Mitochondrial membrane depolarization and the selective death of dopaminergic neurons by rotenone: protective effect of coenzyme Q10: Loss of Δψ mediates rotenone-induced apoptosis. J. Neurochem. 93, 1199–1208. https://doi.org/10.1111/j.1471-4159.2005.03112.x

Moreno, J.A., Radford, H., Peretti, D., Steinert, J.R., Verity, N., Martin, M.G., Halliday, M., Morgan, J., Dinsdale, D., Ortori, C.A., Barrett, D.A., Tsaytler, P., Bertolotti, A., Willis, A.E., Bushell, M., Mallucci, G.R., 2012. Sustained translational repression by eIF2α-P mediates prion neurodegeneration. Nature 485, 507–511. https://doi.org/10.1038/nature11058

Moreno, J.A., Halliday, M., Molloy, C., Radford, H., Verity, N., Axten, J.M., Ortori, C.A., Willis, A.E., Fischer, P.M., Barrett, D.A., Mallucci, G.R., 2013. Oral Treatment Targeting the Unfolded Protein Response Prevents Neurodegeneration and Clinical Disease in Prion-Infected Mice. Science Translational Medicine 5, 206ra138-206ra138. https://doi.org/10.1126/scitranslmed.3006767

Morimoto, R.I., 2002. Dynamic Remodeling of Transcription Complexes by Molecular Chaperones. Cell 110, 281–284. https://doi.org/10.1016/S0092-8674(02)00860-7

Morishima-Kawashima, M., Hasegawa, M., Takio, K., Suzuki, M., Yoshida, H., Titani, K., Ihara, Y., 1995. Proline-directed and Non-proline-directed Phosphorylation of PHF-tau. J. Biol. Chem. 270, 823–829. https://doi.org/10.1074/jbc.270.2.823

Mori, H., Kondo, J., Ihara, Y., 1987. Ubiquitin is a component of paired helical filaments in Alzheimer's disease. Science 235, 1641–1644. https://doi.org/10.1126/science.3029875

Morl, K., Ma, W., Gething, M.-J., Sambrook, J., 1993. A transmembrane protein with a cdc2+CDC28-related kinase activity is required for signaling from the ER to the nucleus. Cell 74, 743–756. https://doi.org/10.1016/0092-8674(93)90521-Q

Mori, K., 2010. Divest Yourself of a Preconceived Idea: Transcription Factor ATF6 Is Not a Soluble Protein! Molecular Biological of Cell 21, 1435–1438. https://doi.org/10.1091/mbc.e09-07-0600

Morris, H.R., Janssen, J.C., Bandmann, O., Daniel, S.E., Rossor, M.N., Lees, A.J., Wood, N.W., 1999. The tau gene A0 polymorphism in progressive supranuclear palsy and

related neurodegenerative diseases. J. Neurol. Neurosurg. Psychiatry 66, 665–667. https://doi.org/10.1136/jnnp.66.5.665

Mortison, J.D., Schenone, M., Myers, J.A., Zhang, Z., Chen, L., Ciarlo, C., Comer, E., Natchiar, S.K., Carr, S.A., Klaholz, B.P., Myers, A.G., 2018. Tetracyclines Modify Translation by Targeting Key Human rRNA Substructures. Cell Chemical Biology 25, 1506-1518.e13. https://doi.org/10.1016/j.chembiol.2018.09.010

Mukhopadhyay, R., Hoh, J.H., 2001. AFM force measurements on microtubule-associated proteins: the projection domain exerts a long-range repulsive force. FEBS Lett. 505, 374–378. https://doi.org/10.1016/S0014-5793(01)02844-7

Muñoz-Montaño, J.R., Moreno, F.J., Avila, J., Díaz-Nido, J., 1997. Lithium inhibits Alzheimer's disease-like tau protein phosphorylation in neurons. FEBS Lett. 411, 183–188. https://doi.org/10.1016/S0014-5793(97)00688-1

Munishkina, L.A., Cooper, E.M., Uversky, V.N., Fink, A.L., 2004. The effect of macromolecular crowding on protein aggregation and amyloid fibril formation. J. Mol. Recognit. 17, 456–464. https://doi.org/10.1002/jmr.699

Murrell, J.R., Spillantini, M.G., Zolo, P., Guazzelli, M., Smith, M.J., Hasegawa, M., Redi, F., Crowther, R.A., Pietrini, P., Ghetti, B., Goedert, M., 1999. *Tau* Gene Mutation G389R Causes a Tauopathy with Abundant Pick Body-like Inclusions and Axonal Deposits. J Neuropathol Exp Neurol 58, 1207–1226. https://doi.org/10.1097/00005072-199912000-00002

Myers, A.J., Kaleem, M., Marlowe, L., Pittman, A.M., Lees, A.J., Fung, H.C., Duckworth, J., Leung, D., Gibson, A., Morris, C.M., de Silva, R., Hardy, J., 2005. The H1c haplotype at the MAPT locus is associated with Alzheimer's disease. Hum. Mol. Genet. 14, 2399–2404. https://doi.org/10.1093/hmg/ddi241

Myers, A.J., Pittman, A.M., Zhao, A.S., Rohrer, K., Kaleem, M., Marlowe, L., Lees, A., Leung, D., McKeith, I.G., Perry, R.H., Morris, C.M., Trojanowski, J.Q., Clark, C., Karlawish, J., Arnold, S., Forman, M.S., Van Deerlin, V., de Silva, R., Hardy, J., 2007. The MAPT H1c risk haplotype is associated with increased expression of tau and especially of 4 repeat containing transcripts. Neurobiol. Dis. 25, 561–570. https://doi.org/10.1016/j.nbd.2006.10.018

Nacharaju, P., Lewis, J., Easson, C., Yen, S., Hackett, J., Hutton, M., Yen, S.-H., 1999. Accelerated filament formation from tau protein with specific FTDP-17 missense mutations. FEBS Letters 447, 195–199. https://doi.org/10.1016/S0014-5793(99)00294-X

Nadanaka, S., Yoshida, H., Kano, F., Murata, M., Mori, K., 2004. Activation of Mammalian Unfolded Protein Response Is Compatible with the Quality Control System Operating in the Endoplasmic Reticulum. MBoC 15, 2537–2548. https://doi.org/10.1091/mbc.e03-09-0693

Narasimhan, S., Guo, J.L., Changolkar, L., Stieber, A., McBride, J.D., Silva, L.V., He, Z., Zhang, B., Gathagan, R.J., Trojanowski, J.Q., Lee, V.M.Y., 2017. Pathological Tau Strains from Human Brains Recapitulate the Diversity of Tauopathies in Nontransgenic Mouse Brain. J. Neurosci. 37, 11406–11423. https://doi.org/10.1523/JNEUROSCI.1230-17.2017

Netzer, W.J., Hartl, F.U., 1997. Recombination of protein domains facilitated by co-translational folding in eukaryotes. Nature 388, 343–349. https://doi.org/10.1038/41024

Neve, R.L., Harris, P., Kosik, K.S., Kurnit, D.M., Donlon, T.A., 1986. Identification of cDNA clones for the human microtubule-associated protein tau and chromosomal localization of the genes for tau and microtubule-associated protein 2. Mol. Brain Res. 1, 271–280. https://doi.org/10.1016/0169-328X(86)90033-1

Neumann, M., Schulz-Schaeffer, W., Crowther, R.A., Smith, M.J., Spillantini, M.G., Goedert, M., Kretzschmar, H.A., 2001. Pick's disease associated with the novelTau gene mutation K369I. Ann Neurol. 50, 503–513. https://doi.org/10.1002/ana.1223

Neumann, M., Diekmann, S., Bertsch, U., Vanmassenhove, B., Bogerts, B., Kretzschmar, H.A., 2005. Novel G335V mutation in the tau gene associated with early onset familial frontotemporal dementia. Neurogenetics 6, 91–95. https://doi.org/10.1007/s10048-005-0210-y

Nicholl, D.J., Greenstone, M.A., Clarke, C.E., Rizzu, P., Crooks, D., Crowe, A., Trojanowski, J.Q., Lee, V.M.-Y., Heutink, P., 2003. An English kindred with a novel recessive tauopathy and respiratory failure. Ann Neurol. 54, 682–686. https://doi.org/10.1002/ana.10747

Nijholt, D.A.T., de Graaf, T.R., van Haastert, E.S., Oliveira, A.O., Berkers, C.R., Zwart, R., Ovaa, H., Baas, F., Hoozemans, J.J.M., Scheper, W., 2011. Endoplasmic reticulum stress

activates autophagy but not the proteasome in neuronal cells: implications for Alzheimer's disease. Cell Death Differ. 18, 1071–1081. https://doi.org/10.1038/cdd.2010.176

Nijholt, D.A.T., Nölle, A., van Haastert, E.S., Edelijn, H., Toonen, R.F., Hoozemans, J.J.M., Scheper, W., 2013. Unfolded protein response activates glycogen synthase kinase-3 via selective lysosomal degradation. Neurobiology of Aging 34, 1759–1771. https://doi.org/10.1016/j.neurobiolaging.2013.01.008

Nishimura, M., Namba, Y., Ikeda, K., Oda, M., 1992. Glial fibrillary tangles with straight tubules in the brains of patients with progressive supranuclear palsy. Neurosci. Lett. 143, 35–38. https://doi.org/10.1016/0304-3940(92)90227-X

Nishitoh, H., 2012. CHOP is a multifunctional transcription factor in the ER stress response. Journal of Biochemistry 151, 217–219. https://doi.org/10.1093/jb/mvr143

Novoa, I., Zeng, H., Harding, H.P., Ron, D., 2001. Feedback Inhibition of the Unfolded Protein Response by GADD34-Mediated Dephosphorylation of eIF2α. J. Cell Biol. 153, 1011–1022. https://doi.org/10.1083/jcb.153.5.1011

Nunez, J., 1988. Immature and mature variants of MAP2 and tau proteins and neuronal plasticity. Trends Neurosci. 11, 477–479. https://doi.org/10.1016/0166-2236(88)90004-5

Nunez, J., Fischer, I., 1997. Microtubule-associated proteins (MAPs) in the peripheral nervous system during development and regeneration. J. Mol. Neurosci. 8, 207–222. https://doi.org/10.1007/BF02736834

Nyathi, Y., Wilkinson, B.M., Pool, M.R., 2013. Co-translational targeting and translocation of proteins to the endoplasmic reticulum. Biochim. Biophys. Acta BBA - Mol. Cell Res. 1833, 2392–2402. https://doi.org/10.1016/j.bbamcr.2013.02.021

Oakes, S.A., Papa, F.R., 2015. The Role of Endoplasmic Reticulum Stress in Human Pathology. Annu. Rev. Pathol. Mech. Dis. 10, 173–194. https://doi.org/10.1146/annurev-pathol-012513-104649

O'Connor, T., Sadleir, K.R., Maus, E., et al.,Veliquette, A., Zhao, J., Cole, S., Eimer, W.,Hitt, B., Bembinster,L., Lammich, S., Lichtentathler, S., Hebert, S., De Strooper, B., Haas, C., Bennett, D., Vassar, R., 2008. Phosphorylation of the Translation Initiation

Factor eIF2α Increases BACE1 Levels and Promotes Amyloidogenesis. Neuron 60, 988–1009. https://doi.org/10.1016/j.neuron.2008.10.047

O'Leary, J.C., Li, Q., Marinec, P., Blair, L.J., Congdon, E.E., Johnson, A.G., Jinwal, U.K., Koren, J., Jones, J.R., Kraft, C., Peters, M., Abisambra, J.F., Duff, K.E., Weeber, E.J., Gestwicki, J.E., Dickey, C.A., 2010. Phenothiazine-mediated rescue of cognition in tau transgenic mice requires neuroprotection and reduced soluble tau burden. Mol Neurodegener 5, 45. https://doi.org/10.1186/1750-1326-5-45

Oddo, S., 2008. The ubiquitin-proteasome system in Alzheimer's disease. J Cellular Mol Med 12, 363–373. https://doi.org/10.1111/j.1582-4934.2008.00276.x

Ogaki, K., Li, Y., Takanashi, M., Ishikawa, K.-I., Kobayashi, T., Nonaka, T., Hasegawa, M., Kishi, M., Yoshino, H., Funayama, M., Tsukamoto, T., Shioya, K., Yokochi, M., Imai, H., Sasaki, R., Kokubo, Y., Kuzuhara, S., Motoi, Y., Tomiyama, H., Hattori, N., 2013. Analyses of the MAPT, PGRN, and C9orf72 mutations in Japanese patients with FTLD, PSP, and CBS. Parkinsonism & Related Disorders 19, 15–20. https://doi.org/10.1016/j.parkreldis.2012.06.019

Okamura, K., Kimata, Y., Higashio, H., Tsuru, A., Kohno, K., 2000. Dissociation of Kar2p/BiP from an ER Sensory Molecule, Ire1p, Triggers the Unfolded Protein Response in Yeast. Biochem. Biophys. Res. Commun. 279, 445–450. https://doi.org/10.1006/bbrc.2000.3987

O'Leary, J.C., Li, Q., Marinec, P., Blair, L.J., Congdon, E.E., Johnson, A.G., Jinwal, U.K., Koren, J., Jones, J.R., Kraft, C., Peters, M., Abisambra, J.F., Duff, K.E., Weeber, E.J., Gestwicki, J.E., Dickey, C.A., 2010. Phenothiazine-mediated rescue of cognition in tau transgenic mice requires neuroprotection and reduced soluble tau burden. Mol. Neurodegener. 5, 45. https://doi.org/10.1186/1750-1326-5-45

Ooi, A., Wong, A., Esau, L., Lemtiri-Chlieh, F., Gehring, C., 2016. A Guide to Transient Expression of Membrane Proteins in HEK-293 Cells for Functional Characterization. Front. Physiol. 7. https://doi.org/10.3389/fphys.2016.00300

Orlowski, M., Wilk, S., 2000. Catalytic Activities of the 20 S Proteasome, a Multicatalytic Proteinase Complex. Archives of Biochemistry and Biophysics 383, 1–16. https://doi.org/10.1006/abbi.2000.2036

Oung, H.-M., Lin, K.-C., Wu, T.-M., Chandrika, N.N.P., Hong, C.-Y., 2015. Hygromycin B-induced cell death is partly mediated by reactive oxygen species in rice (Oryza sativa L.). Plant Mol Biol 89, 577–588. https://doi.org/10.1007/s11103-015-0380-4

Osburn, W., Kensler, T., 2008. Nrf2 signaling: An adaptive response pathway for protection against environmental toxic insults. Mutat. Res. Mutat. Res. 659, 31–39. https://doi.org/10.1016/j.mrrev.2007.11.006

Oslowski, C.M., Urano, F., 2011. Measuring ER Stress and the Unfolded Protein Response Using Mammalian Tissue Culture System, in: Methods in Enzymology. Elsevier, pp. 71–92. https://doi.org/10.1016/B978-0-12-385114-7.00004-0

Padyana, A.K., Qiu, H., Roll-Mecak, A., Hinnebusch, A.G., Burley, S.K., 2005. Structural Basis for Autoinhibition and Mutational Activation of Eukaryotic Initiation Factor 2α Protein Kinase GCN2. J. Biol. Chem. 280, 29289–29299. https://doi.org/10.1074/jbc.M504096200

Pan, Q., Shai, O., Lee, L.J., Frey, B.J., Blencowe, B.J., 2008. Deep surveying of alternative splicing complexity in the human transcriptome by high-throughput sequencing. Nat. Genet. 40, 1413–1415. https://doi.org/10.1038/ng.259

Panda, D., Samuel, J.C., Massie, M., Feinstein, S.C., Wilson, L., 2003. Differential regulation of microtubule dynamics by three- and four-repeat tau: Implications for the onset of neurodegenerative disease. Proc. Natl. Acad. Sci. 100, 9548–9553. https://doi.org/10.1073/pnas.1633508100

Papa, F.R., 2003. Bypassing a Kinase Activity with an ATP-Competitive Drug. Science 302, 1533–1537. https://doi.org/10.1126/science.1090031

Park, I.-H., Arora, N., Huo, H., Maherali, N., Ahfeldt, T., Shimamura, A., Lensch, M.W., Cowan, C., Hochedlinger, K., Daley, G.Q., 2008. Disease-Specific Induced Pluripotent Stem Cells. Cell 134, 877–886. https://doi.org/10.1016/j.cell.2008.07.041

Pastor, P., Pastor, E., Carnero, C., Vela, R., García, T., Amer, G., Tolosa, E., Oliva, R., 2001. Familial atypical progressive supranuclear palsy associated with homozigosity for the delN296 mutation in the tau gene. Ann. Neurol. 49, 263–267. https://doi.org/10.1002/1531-8249(20010201)49:2<263::aid-ana50>3.0.co;2-k

Pastor, P., Tolosa, E., 2002. Progressive supranuclear palsy: clinical and genetic aspects: Curr. Opin. Neurol. 15, 429–437. https://doi.org/10.1097/00019052-200208000-00005

Patrick, G.N., Zukerberg, L., Nikolic, M., de la Monte, S., Dikkes, P., Tsai, L.-H., 1999. Conversion of p35 to p25 deregulates Cdk5 activity and promotes neurodegeneration. Nature 402, 615–622. https://doi.org/10.1038/45159

Perreault, S., Bousquet, O., Lauzon, M., Paiement, J., Leclerc, N., 2009. Increased Association Between Rough Endoplasmic Reticulum Membranes and Mitochondria in Transgenic Mice That Express P301L Tau. J. Neuropathol. Exp. Neurol. 68, 503–514. https://doi.org/10.1097/NEN.0b013e3181a1fc49

Pérez, M., Hernández, F., Gómez-Ramos, A., Smith, M., Perry, G., Avila, J., 2002. Formation of aberrant phosphotau fibrillar polymers in neural cultured cells: Tau aggregates in cultured cells. European Journal of Biochemistry 269, 1484–1489. https://doi.org/10.1046/j.1432-1033.2002.02794.x

Perry, G., Friedman, R., Shaw, G., Chau, V., 1987. Ubiquitin is detected in neurofibrillary tangles and senile plaque neurites of Alzheimer disease brains. Proceedings of the National Academy of Sciences 84, 3033–3036. https://doi.org/10.1073/pnas.84.9.3033

Piccini, P., 2001. Familial Progressive supranuclear Palsy: Detection of Subclinical Cases Using ^{18} F-Dopa and ^{18} Fluorodeoxyglucose Positron Emission Tomography. Arch. Neurol. 58, 1846. https://doi.org/10.1001/archneur.58.11.1846

Pickering-Brown, S., Baker, M., Yen, S.-H., Liu, W.-K., Hasegawa, M., Cairns, N., Lantos, P.L., Rossor, M., Iwatsubo, T., Davies, Y., Allsop, D., Furlong, R., Owen, F., Hardy, J., Mann, D. and Hutton, M. (2000), Pick's disease is associated with mutations in the *tau* gene. Ann Neurol., 48: 859-867. doi:10.1002/1531-8249(200012)48:6<859::AID-ANA6>3.0.CO;2-1

Pickering-Brown, S.M., Baker, M., Nonaka, T., Ikeda, K., Sharma, S., Mackenzie, J., Simpson, S.A., Moore, J.W., Snowden, J.S., de Silva, R., Revesz, T., Hasegawa, M., Hutton, M., Mann, D.M.A., 2004. Frontotemporal dementia with Pick-type histology associated with Q336R mutation in the tau gene. Brain 127, 1415–1426. https://doi.org/10.1093/brain/awh147

Pittman, A., Silva, R. de, Lees, A.J., Wood, N.W., 2008. Genetics of progressive supranuclear palsy, in: Handbook of Clinical Neurology. Elsevier, pp. 475–485. https://doi.org/10.1016/S0072-9752(07)01244-4

Pittman, A.M., 2005. Linkage disequilibrium fine mapping and haplotype association analysis of the tau gene in progressive supranuclear palsy and corticobasal degeneration. J. Med. Genet. 42, 837–846. https://doi.org/10.1136/jmg.2005.031377

Pittman, A.M., 2004. The structure of the tau haplotype in controls and in progressive supranuclear palsy. Hum. Mol. Genet. 13, 1267–1274. https://doi.org/10.1093/hmg/ddh138

Pitera, A.P., Asuni, A.A., O'Connor, V., Deinhardt, K., 2019. Pathogenic tau does not drive activation of the unfolded protein response. J. Biol. Chem. 294, 9679–9688. https://doi.org/10.1074/jbc.RA119.008263

Pollanen, M.S., Markiewicz, P., Goh, M.C., 1997. Paired Helical Filaments Are Twisted Ribbons Composed of Two Parallel and Aligned Components: Image Reconstruction and Modeling of Filament Structure Using Atomic Force Microscopy. J. Neuropathol. Exp. Neurol. 56, 79–85. https://doi.org/10.1097/00005072-199701000-00008

Pollock, NancyJ., Mirra, SuzanneS., Binder, LesterI., Hansen, LawrenceA., Wood, JohnG., 1986. Filamentous aggregates in Pick's disease, Progressive supranuclear palsy and Alzheimer's disease share antigenic determinants with microtubule-assocated tau. The Lancet 328, 1211. https://doi.org/10.1016/S0140-6736(86)92212-9

Polymeropoulos, M.H., 1997. Mutation in the -Synuclein Gene Identified in Families with Parkinson's Disease. Science 276, 2045–2047. https://doi.org/10.1126/science.276.5321.2045

Pooler, A.M., Hanger, D.P., 2010. Functional implications of the association of tau with the plasma membrane. Biochem. Soc. Trans. 38, 1012–1015. https://doi.org/10.1042/BST0381012

Poorkaj, P., Muma, N.A., Zhukareva, V., Cochran, E.J., Shannon, K.M., Hurtig, H., Koller, W.C., Bird, T.D., Trojanowski, J.Q., Lee, V.M.-Y., Schellenberg, G.D., 2002. AnR5L ? mutation in a subject with a progressive supranuclear palsy phenotype. Ann. Neurol. 52, 511–516. https://doi.org/10.1002/ana.10340

Pope, W.B., Lambert, M.P., Leypold, B., Seupaul, R., Sletten, L., Krafft, G., Klein, W.L., 1994. Microtubule-Associated Protein Tau Is Hyperphosphorylated during Mitosis in the Human Neuroblastoma Cell Line SH-SY5Y. Exp. Neurol. 126, 185–194. https://doi.org/10.1006/exnr.1994.1057

Popović, M., Fabjan, A., Mraz, J., Magdič, J., Glavač, D., Zupan, A., Novak, M.D., Bresjanac, M., 2014. Tau protein mutation P364S in two sisters: clinical course and neuropathology with emphasis on new, composite neuronal tau inclusions. Acta Neuropathol 128, 155–157. https://doi.org/10.1007/s00401-014-1293-z

Preuss, U., Döring, F., Illenberger, S., Mandelkow, E.M., 1995. Cell cycle-dependent phosphorylation and microtubule binding of tau protein stably transfected into Chinese hamster ovary cells. Mol. Biol. Cell 6, 1397–1410. https://doi.org/10.1091/mbc.6.10.1397

Price, J., Zaidi, A.K., Bohensky, J., Srinivas, V., Shapiro, I.M., Ali, H., 2009. Akt-1 mediates survival of chondrocytes from endoplasmic reticulum-induced stress. J. Cell. Physiol. n/a-n/a. https://doi.org/10.1002/jcp.22001

Progressive Supranuclear Palsy: Diagnosis, Pathology, and Therapy, 1995. . Neurology 45, 604–604. https://doi.org/10.1212/WNL.45.3.604

PSP Genetics Study Group, Höglinger, G.U., Melhem, N.M., Dickson, D.W., Sleiman, P.M.A., Wang, L.-S., Klei, L., Rademakers, R., de Silva, R., Litvan, I., Riley, D.E., van Swieten, J.C., Heutink, P., Wszolek, Z.K., Uitti, R.J., Vandrovcova, J., Hurtig, H.I., Gross, R.G., Maetzler, W., Goldwurm, S., Tolosa, E., Borroni, B., Pastor, P., Cantwell, L.B., Han, M.R., Dillman, A., van der Brug, M.P., Gibbs, J.R., Cookson, M.R., Hernandez, D.G., Singleton, A.B., Farrer, M.J., Yu, C.-E., Golbe, L.I., Revesz, T., Hardy, J., Lees, A.J., Devlin, B., Hakonarson, H., Müller, U., Schellenberg, G.D., 2011. Identification of common variants influencing risk of the tauopathy progressive supranuclear palsy. Nat. Genet. 43, 699–705. https://doi.org/10.1038/ng.859

Qiu, T., He, Y., Zhang, X., Ma, X., 2018. Novel Role of ER Stress and Mitochondria Stress in Serum-deprivation Induced Apoptosis of Rat Mesenchymal Stem Cells. CURR MED SCI 38, 229–235. https://doi.org/10.1007/s11596-018-1870-9

Rademakers, R., Melquist, S., Cruts, M., Theuns, J., Del-Favero, J., Poorkaj, P., Baker, M., Sleegers, K., Crook, R., De Pooter, T., Kacem, S.B., Adamson, J., Van den Bossche, D., Van den Broeck, M., Gass, J., Corsmit, E., De Rijk, P., Thomas, N.,

Engelborghs, S., Heckman, M., Litvan, I., Crook, J., De Deyn, P.P., Dickson, D., Schellenberg, G.D., Van Broeckhoven, C., Hutton, M.L., 2005. High-density SNP haplotyping suggests altered regulation of tau gene expression in progressive supranuclear palsy. Hum. Mol. Genet. 14, 3281–3292. https://doi.org/10.1093/hmg/ddi361

Radford, H., Moreno, J.A., Verity, N., Halliday, M., Mallucci, G.R., 2015. PERK inhibition prevents tau-mediated neurodegeneration in a mouse model of frontotemporal dementia. Acta Neuropathol. (Berl.) 130, 633–642. https://doi.org/10.1007/s00401-015-1487-z

Ramsden, M., 2005. Age-Dependent Neurofibrillary Tangle Formation, Neuron Loss, and Memory Impairment in a Mouse Model of Human Tauopathy (P301L). Journal of Neuroscience 25, 10637–10647. https://doi.org/10.1523/JNEUROSCI.3279-05.2005

Ramirez, M., Wek, R.C., Hinnebusch, A.G., 1991. Ribosome association of GCN2 protein kinase, a translational activator of the GCN4 gene of Saccharomyces cerevisiae. Mol. Cell. Biol. 11, 3027–3036. https://doi.org/10.1128/mcb.11.6.3027

Ramnarayanan, S., Kyathanahalli, C., Ingles, J., Park-York, M., Jeyasuria, P., Condon, J.C., 2016. The Unfolded Protein Response Regulates Uterine Myocyte Antioxidant Responsiveness During Pregnancy. Biology of Reproduction 95, 120–120. https://doi.org/10.1095/biolreprod.116.141804

Rapoport, M., Dawson, H.N., Binder, L.I., Vitek, M.P., Ferreira, A., 2002. Tau is essential to -amyloid-induced neurotoxicity. Proc. Natl. Acad. Sci. 99, 6364–6369. https://doi.org/10.1073/pnas.092136199

Resende, R., Ferreiro, E., Pereira, C., Oliveira, C.R., 2008. ER stress is involved in Aβ-induced GSK-3β activation and tau phosphorylation. J. Neurosci. Res. 86, 2091–2099. https://doi.org/10.1002/jnr.21648

Respondek, G., Roeber, S., Kretzschmar, H., Troakes, C., Al-Sarraj, S., Gelpi, E., Gaig, C., Chiu, W.Z., van Swieten, J.C., Oertel, W.H., Höglinger, G.U., 2013. Accuracy of the national institute for neurological disorders and stroke/society for progressive supranuclear palsy and neuroprotection and natural history in Parkinson plus syndromes criteria for the diagnosis of progressive supranuclear palsy: PSP Diagnostic Criteria. Mov. Disord. 28, 504–509. https://doi.org/10.1002/mds.25327

Respondek, G., Stamelou, M., Kurz, C., Ferguson, L.W., Rajput, A., Chiu, W.Z., van Swieten, J.C., Troakes, C., al Sarraj, S., Gelpi, E., Gaig, C., Tolosa, E., Oertel, W.H., Giese, A., Roeber, S., Arzberger, T., Wagenpfeil, S., Höglinger, G.U., for the Movement Disorder Society-endorsed PSP Study Group, 2014. The phenotypic spectrum of progressive supranuclear palsy: A retrospective multicenter study of 100 definite cases: PSP Diagnostic Criteria. Mov. Disord. 29, 1758–1766. https://doi.org/10.1002/mds.26054

Reynolds, C.H., Garwood, C.J., Wray, S., Price, C., Kellie, S., Perera, T., Zvelebil, M., Yang, A., Sheppard, P.W., Varndell, I.M., Hanger, D.P., Anderton, B.H., 2008. Phosphorylation Regulates Tau Interactions with Src Homology 3 Domains of Phosphatidylinositol 3-Kinase, Phospholipase Cγ1, Grb2, and Src Family Kinases. J. Biol. Chem. 283, 18177–18186. https://doi.org/10.1074/jbc.M709715200

Richardson, J.C., Steele, J., Olszewski, J., 1963. Supranuclear Ophthalmoplegia, Pseudobulbar Palsy, Nuchal Dystonia And Dementia. A Clinical Report On Eight Cases Of “Heterogenous System Degeneration.” Trans. Am. Neurol. Assoc. 88, 25–29.

Rizzini, C., Goedert, M., Hodges, J.R., Smith, M.J., Jakes, R., Hills, R., Xuereb, J.H., Crowther, R.A., Spillantini, M.G., 2000. *Tau* Gene Mutation K257T Causes a Tauopathy Similar to Pick’s Disease. J Neuropathol Exp Neurol 59, 990–1001. https://doi.org/10.1093/jnen/59.11.990

Rizzu, P., Van Swieten, J.C., Joosse, M., Hasegawa, M., Stevens, M., Tibben, A., Niermeijer, M.F., Hillebrand, M., Ravid, R., Oostra, B.A., Goedert, M., van Duijn, C.M., Heutink, P., 1999. High Prevalence of Mutations in the Microtubule-Associated Protein Tau in a Population Study of Frontotemporal Dementia in the Netherlands. The American Journal of Human Genetics 64, 414–421. https://doi.org/10.1086/302256

Rojo, A., Pernaute, R.S., Fontan, A., Ruiz, P.G., Honnorat, J., Lynch, T., Chin, S., Gonzalo, I., Rabano, A., Martinez, A., Daniel, S., Pramsteller, P., Morris, H., Wood, N., Lees, A., Tabernero, C., Nyggard, T., Jackson, A.C., Hanson, A., de Yebenes, J.G., 1999. Clinical genetics of familial progressive supranuclear palsy. Brain 122, 1233–1245. https://doi.org/10.1093/brain/122.7.1233

Ron, D., Walter, P., 2007. Signal integration in the endoplasmic reticulum unfolded protein response. Nat. Rev. Mol. Cell Biol. 8, 519–529. https://doi.org/10.1038/nrm2199

Ros, R., Gómez Garre, P., Hirano, M., Tai, Y.F., Ampuero, I., Vidal, L., Rojo, A., Fontan, A., Vazquez, A., Fanjul, S., Hernandez, J., Cantarero, S., Hoenicka, J., Jones, A., Ahsan, R.L., Pavese, N., Piccini, P., Brooks, D.J., Perez-Tur, J., Nyggard, T., de Yébenes, J.G., 2005a. Genetic linkage of autosomal dominant progressive supranuclear palsy to 1q31.1. Ann. Neurol. 57, 634–641. https://doi.org/10.1002/ana.20449

Ros, R., Thobois, S., Streichenberger, N., Kopp, N., Sánchez, M.P., Pérez, M., Hoenicka, J., Avila, J., Honnorat, J., de Yébenes, J.G., 2005b. A New Mutation of the τ Gene, G303V, in Early-Onset Familial Progressive Supranuclear Palsy. Arch. Neurol. 62, 1444. https://doi.org/10.1001/archneur.62.9.1444

Rossi, G., Gasparoli, E., Pasquali, C., Di Fede, G., Testa, D., Albanese, A., Bracco, F., Tagliavini, F., 2004. Progressive supranuclear palsy and Parkinson's disease in a family with a new mutation in the tau gene. Ann. Neurol. 55, 448–448. https://doi.org/10.1002/ana.20006

Rossi, G., Bastone, A., Piccoli, E., Mazzoleni, G., Morbin, M., Uggetti, A., Giaccone, G., Sperber, S., Beeg, M., Salmona, M., Tagliavini, F., 2012. New mutations in MAPT gene causing frontotemporal lobar degeneration: biochemical and structural characterization. Neurobiology of Aging 33, 834.e1-834.e6. https://doi.org/10.1016/j.neurobiolaging.2011.08.008

Rosso, S.M., Van Herpen, E., Deelen, W., Kamphorst, W., Severijnen, L.-A., Willemsen, R., Ravid, R., Niermeijer, M.F., Dooijes, D., Smith, M.J., Goedert, M., Heutink, P., Van Swieten, J.C., 2002. A noveltau mutation, S320F, causes a tauopathy with inclusions similar to those in Pick's disease. Ann Neurol. 51, 373–376. https://doi.org/10.1002/ana.10140

Roy, S., Datta, C.K., Hirano, A., Ghatak, N.R., Zimmerman, H.M., 1974. Electron microscopic study of neurofibrillary tangles in Steele-Richardson-Olszewski syndrome. Acta Neuropathol. (Berl.) 29, 175–179. https://doi.org/10.1007/BF00684775

Rozpedek, W., Markiewicz, L., Diehl, J., Pytel, D., Majsterek, I., 2015. Unfolded Protein Response and PERK Kinase as a New Therapeutic Target in the Pathogenesis of Alzheimer's Disease. Curr. Med. Chem. 22, 3169–3184. https://doi.org/10.2174/0929867322666150818104254

Russell, W.C., Graham, F.L., Smiley, J., Nairn, R., 1977. Characteristics of a Human Cell Line Transformed by DNA from Human Adenovirus Type 5. Journal of General Virology 36, 59–72. https://doi.org/10.1099/0022-1317-36-1-59

Rutkowski, D.T., Arnold, S.M., Miller, C.N., Wu, J., Li, J., Gunnison, K.M., Mori, K., Sadighi Akha, A.A., Raden, D., Kaufman, R.J., 2006. Adaptation to ER Stress Is Mediated by Differential Stabilities of Pro-Survival and Pro-Apoptotic mRNAs and Proteins. PLoS Biol. 4, e374. https://doi.org/10.1371/journal.pbio.0040374

Rutkowski, D.T., Hegde, R.S., 2010. Regulation of basal cellular physiology by the homeostatic unfolded protein response. J. Cell Biol. 189, 783–794. https://doi.org/10.1083/jcb.201003138

Sadot, E., Barg, J., Rasouly, D., Lazarovici, P., Ginzburg, I., 1995. Short- and long-term mechanisms of tau regulation in PC12 cells. J. Cell Sci. 108 (Pt 8), 2857–2864.

Sakagami, Y., Kudo, T., Tanimukai, H., Kanayama, D., Omi, T., Horiguchi, K., Okochi, M., Imaizumi, K., Takeda, M., 2013. Involvement of endoplasmic reticulum stress in tauopathy. Biochem. Biophys. Res. Commun. 430, 500–504. https://doi.org/10.1016/j.bbrc.2012.12.007

Sanders, D.W., Kaufman, S.K., DeVos, S.L., Sharma, A.M., Mirbaha, H., Li, A., Barker, S.J., Foley, A.C., Thorpe, J.R., Serpell, L.C., Miller, T.M., Grinberg, L.T., Seeley, W.W., Diamond, M.I., 2014. Distinct Tau Prion Strains Propagate in Cells and Mice and Define Different Tauopathies. Neuron 82, 1271–1288. https://doi.org/10.1016/j.neuron.2014.04.047

Santacruz, P., Uttl, B., Litvan, I., Grafman, J., 1998. Progressive supranuclear palsy: A survey of the disease course. Neurology 50, 1637–1647. https://doi.org/10.1212/WNL.50.6.1637

SantaCruz, K., 2005. Tau Suppression in a Neurodegenerative Mouse Model Improves Memory Function. Science 309, 476–481. https://doi.org/10.1126/science.1113694

Sapir, T., Frotscher, M., Levy, T., Mandelkow, E.-M., Reiner, O., 2012. Tau's role in the developing brain: implications for intellectual disability. Hum. Mol. Genet. 21, 1681–1692. https://doi.org/10.1093/hmg/ddr603

Saraogi, I., Shan, S., 2011. Molecular Mechanism of Co-translational Protein Targeting by the Signal Recognition Particle. Traffic 12, 535–542. https://doi.org/10.1111/j.1600-0854.2011.01171.x

Sawa, A., Oyama, F., Matsushita, M., Ihara, Y., 1994. Molecular diversity at the carboxyl terminus of human and rat tau. Mol. Brain Res. 27, 111–117. https://doi.org/10.1016/0169-328X(94)90191-0

Scattoni, M.L., Gasparini, L., Alleva, E., Goedert, M., Calamandrei, G., Spillantini, M.G., 2010. Early behavioural markers of disease in P301S tau transgenic mice. Behavioural Brain Research 208, 250–257. https://doi.org/10.1016/j.bbr.2009.12.002

Schechter, I., Burstein, Y., 1976. Marked hydrophobicity of the NH2-terminal extra piece of immunoglobulin light-chain precursors: possible physiological functions of the extra piece. Proc. Natl. Acad. Sci. 73, 3273–3277. https://doi.org/10.1073/pnas.73.9.3273

Schoch, K.M., DeVos, S.L., Miller, R.L., Chun, S.J., Norrbom, M., Wozniak, D.F., Dawson, H.N., Bennett, C.F., Rigo, F., Miller, T.M., 2016. Increased 4R-Tau Induces Pathological Changes in a Human-Tau Mouse Model. Neuron 90, 941–947. https://doi.org/10.1016/j.neuron.2016.04.042

Schönthal, A.H., 2012. Endoplasmic Reticulum Stress: Its Role in Disease and Novel Prospects for Therapy. Scientifica 2012, 1–26. https://doi.org/10.6064/2012/857516

Schröder, M., Kaufman, R.J., 2005. ER stress and the unfolded protein response. Mutat. Res. Mol. Mech. Mutagen. 569, 29–63. https://doi.org/10.1016/j.mrfmmm.2004.06.056

Scheuner, D., Song, B., McEwen, E., Liu, C., Laybutt, R., Gillespie, P., Saunders, T., Bonner-Weir, S., Kaufman, R.J., 2001. Translational Control Is Required for the Unfolded Protein Response and In Vivo Glucose Homeostasis. Molecular Cell 7, 1165–1176. https://doi.org/10.1016/S1097-2765(01)00265-9

Schuck, S., Prinz, W.A., Thorn, K.S., Voss, C., Walter, P., 2009. Membrane expansion alleviates endoplasmic reticulum stress independently of the unfolded protein response. Journal of Cell Biology 187, 525–536. https://doi.org/10.1083/jcb.200907074

Selkoe, D.J., 2003. Folding proteins in fatal ways. Nature 426, 900–904. https://doi.org/10.1038/nature02264

Sergeant, N., Delacourte, A., Buée, L., 2005. Tau protein as a differential biomarker of tauopathies. Biochim. Biophys. Acta BBA - Mol. Basis Dis. 1739, 179–197. https://doi.org/10.1016/j.bbadis.2004.06.020

Sharma, V.M., Litersky, J.M., Bhaskar, K., Lee, G., 2007. Tau impacts on growth-factor-stimulated actin remodeling. J. Cell Sci. 120, 748–757. https://doi.org/10.1242/jcs.03378

Sharma, V., Ounallah-Saad, H., Chakraborty, D., Hleihil, M., Sood, R., Barrera, I., Edry, E., Kolatt Chandran, S., Ben Tabou de Leon, S., Kaphzan, H., Rosenblum, K., 2018. Local Inhibition of PERK Enhances Memory and Reverses Age-Related Deterioration of Cognitive and Neuronal Properties. J Neurosci 38, 648–658. https://doi.org/10.1523/JNEUROSCI.0628-17.2017

Shen, J., Chen, X., Hendershot, L., Prywes, R., 2002. ER Stress Regulation of ATF6 Localization by Dissociation of BiP/GRP78 Binding and Unmasking of Golgi Localization Signals. Dev. Cell 3, 99–111. https://doi.org/10.1016/S1534-5807(02)00203-4

Shi, Y., Vattem, K.M., Sood, R., An, J., Liang, J., Stramm, L., Wek, R.C., 1998. Identification and Characterization of Pancreatic Eukaryotic Initiation Factor 2 α-Subunit Kinase, PEK, Involved in Translational Control. Mol. Cell. Biol. 18, 7499–7509. https://doi.org/10.1128/MCB.18.12.7499

Shiarli, A.-M., Jennings, R., Shi, J., Bailey, K., Davidson, Y., Tian, J., Bigio, E.H., Ghetti, B., Murrell, J.R., Delisle, M.B., Mirra, S., Crain, B., Zolo, P., Arima, K., Iseki, E., Murayama, S., Kretzschmar, H., Neumann, M., Lippa, C., Halliday, G., MacKenzie, J., Khan, N., Ravid, R., Dickson, D., Wszolek, Z., Iwatsubo, T., Pickering-Brown, S.M., Mann, D.M.A., 2006. Comparison of extent of tau pathology in patients with frontotemporal dementia with Parkinsonism linked to chromosome 17 (FTDP-17), frontotemporal lobar degeneration with Pick bodies and early onset Alzheimer's disease. Neuropathol Appl Neurobiol 32, 374–387. https://doi.org/10.1111/j.1365-2990.2006.00736.x

Shoulders, M.D., Ryno, L.M., Genereux, J.C., Moresco, J.J., Tu, P.G., Wu, C., Yates, J.R., Su, A.I., Kelly, J.W., Wiseman, R.L., 2013. Stress-Independent Activation of XBP1s and/or ATF6 Reveals Three Functionally Diverse ER Proteostasis Environments. Cell Rep. 3, 1279–1292. https://doi.org/10.1016/j.celrep.2013.03.024

Silva, M.C., Cheng, C., Mair, W., Almeida, S., Fong, H., Biswas, M.H.U., Zhang, Z., Huang, Y., Temple, S., Coppola, G., Geschwind, D.H., Karydas, A., Miller, B.L., Kosik,

K.S., Gao, F.-B., Steen, J.A., Haggarty, S.J., 2016. Human iPSC-Derived Neuronal Model of Tau-A152T Frontotemporal Dementia Reveals Tau-Mediated Mechanisms of Neuronal Vulnerability. Stem Cell Reports 7, 325–340. https://doi.org/10.1016/j.stemcr.2016.08.001

Silva, R.M., Ries, V., Oo, T.F., Yarygina, O., Jackson-Lewis, V., Ryu, E.J., Lu, P.D., Marciniak, S.J., Ron, D., Przedborski, S., Kholodilov, N., Greene, L.A., Burke, R.E., 2005. CHOP/GADD153 is a mediator of apoptotic death in substantia nigra dopamine neurons in an in vivo neurotoxin model of parkinsonism. J. Neurochem. 95, 974–986. https://doi.org/10.1111/j.1471-4159.2005.03428.x

Skipper, L., Wilkes, K., Toft, M., Baker, M., Lincoln, S., Hulihan, M., Ross, O.A., Hutton, M., Aasly, J., Farrer, M., 2004. Linkage Disequilibrium and Association of MAPT H1 in Parkinson Disease. Am. J. Hum. Genet. 75, 669–677. https://doi.org/10.1086/424492

Smith, C.J., Anderton, B.H., Davis, D.R., Gallo, J.-M., 1995. Tau isoform expression and phosphorylation state during differentiation of cultured neuronal cells. FEBS Lett. 375, 243–248. https://doi.org/10.1016/0014-5793(95)01221-Y

Song, B., Scheuner, D., Ron, D., Pennathur, S., Kaufman, R.J., 2008. Chop deletion reduces oxidative stress, improves β cell function, and promotes cell survival in multiple mouse models of diabetes. J. Clin. Invest. 118, 3378–3389. https://doi.org/10.1172/JCI34587

Soto, C., 2003. Unfolding the role of protein misfolding in neurodegenerative diseases. Nat Rev Neurosci 4, 49–60. https://doi.org/10.1038/nrn1007

Soto, C., 2008. Endoplasmic Reticulum Stress, PrP Trafficking, and Neurodegeneration. Dev. Cell 15, 339–341. https://doi.org/10.1016/j.devcel.2008.09.001

Soto, C., Estrada, L.D., 2008. Protein Misfolding and Neurodegeneration. Arch. Neurol. 65 (2), 184-189 https://doi.org/10.1001/archneurol.2007.56

Spatara, M.L., Robinson, A.S., 2010. Transgenic mouse and cell culture models demonstrate a lack of mechanistic connection between endoplasmic reticulum stress and tau dysfunction. J. Neurosci. Res. NA-NA. https://doi.org/10.1002/jnr.22359

Spear, E.D., Ng, D.T.W., 2003. Stress Tolerance of Misfolded Carboxypeptidase Y Requires Maintenance of Protein Trafficking and Degradative Pathways. Mol. Biol. Cell 14, 2756–2767. https://doi.org/10.1091/mbc.e02-11-0717

Spillantini, M.G., Crowther, R.A., Goedert, M., 1996. Comparison of the neurofibrillary pathology in Alzheimer's disease and familial presenile dementia with tangles. Acta Neuropathologica 92, 42–48. https://doi.org/10.1007/s004010050487

Spillantini, M.G., Crowther, R.A., Kamphorst, W., Heutink, P., van Swieten, J.C., 1998. Tau Pathology in Two Dutch Families with Mutations in the Microtubule-Binding Region of Tau. Am. J. Pathol. 153, 1359–1363. https://doi.org/10.1016/S0002-9440(10)65721-5

Spillantini, M. G., Murrell, J.R., Goedert, M., Farlow, M.R., Klug, A., Ghetti, B., 1998. Mutation in the tau gene in familial multiple system tauopathy with presenile dementia. Proc. Natl. Acad. Sci. 95, 7737–7741. https://doi.org/10.1073/pnas.95.13.7737

Spina, S., Farlow, M.R., Unverzagt, F.W., Kareken, D.A., Murrell, J.R., Fraser, G., Epperson, F., Crowther, R.A., Spillantini, M.G., Goedert, M., Ghetti, B., 2008. The tauopathy associated with mutation +3 in intron 10 of Tau: characterization of the MSTD family. Brain 131, 72–89. https://doi.org/10.1093/brain/awm280

Srivastava, S.P., Davies, M.V., Kaufman, R.J., 1995. Calcium Depletion from the Endoplasmic Reticulum Activates the Double-stranded RNA-dependent Protein Kinase (PKR) to Inhibit Protein Synthesis. J. Biol. Chem. 270, 16619–16624. https://doi.org/10.1074/jbc.270.28.16619

Stamer, K., Vogel, R., Thies, E., Mandelkow, E., Mandelkow, E.-M., 2002. Tau blocks traffic of organelles, neurofilaments, and APP vesicles in neurons and enhances oxidative stress. J. Cell Biol. 156, 1051–1063. https://doi.org/10.1083/jcb.200108057

Stamm, S., Ben-Ari, S., Rafalska, I., Tang, Y., Zhang, Z., Toiber, D., Thanaraj, T.A., Soreq, H., 2005. Function of alternative splicing. Gene 344, 1–20. https://doi.org/10.1016/j.gene.2004.10.022

Stanford, P.M., Halliday, G.M., Brooks, W.S., Kwok, J.B.J., Storey, C.E., Creasey, H., Morris, J.G.L., Fulham, M.J., Schofield, P.R., 2000. Progressive supranuclear palsy pathology caused by a novel silent mutation in exon 10 of the tau gene. Brain 123, 880–893. https://doi.org/10.1093/brain/123.5.880

Steele, J.C., 1964. Progressive Supranuclear Palsy: A Heterogeneous Degeneration Involving the Brain Stem, Basal Ganglia and Cerebellum With Vertical Gaze and

Pseudobulbar Palsy, Nuchal Dystonia and Dementia. Arch. Neurol. 10, 333. https://doi.org/10.1001/archneur.1964.00460160003001

Stefansson, H., Helgason, A., Thorleifsson, G., Steinthorsdottir, V., Masson, G., Barnard, J., Baker, A., Jonasdottir, A., Ingason, A., Gudnadottir, V., Desnica, N., Hicks, A., Gylfason, A., Jonsdottir, G., Gubjartsson, G., Sainz, J., Angarsson K., Birgisdottir, B., Ghosh, S., Olafsdottir, A., Cazier, J., Kristjansson, K., Frigge, M., Thorgeirsson, T.,Gulcher, J., Kong, A.,Stefansson, K., 2005. A common inversion under selection in Europeans. Nat. Genet. 37, 129–137. https://doi.org/10.1038/ng1508

Stern, R.A., Otvos, L., Trojanowski, J.Q., Lee, V.M., 1989. Monoclonal antibodies to a synthetic peptide homologous with the first 28 amino acids of Alzheimer's disease beta-protein recognize amyloid and diverse glial and neuronal cell types in the central nervous system. Am. J. Pathol. 134, 973–978.

Stöhr, J., Wu, H., Nick, M., Wu, Y., Bhate, M., Condello, C., Johnson, N., Rodgers, J., Lemmin, T., Acharya, S., Becker, J., Robinson, K., Kelly, M.J.S., Gai, F., Stubbs, G., Prusiner, S.B., DeGrado, W.F., 2017. A 31-residue peptide induces aggregation of tau's microtubule-binding region in cells. Nat. Chem. 9, 874–881. https://doi.org/10.1038/nchem.2754

Stutzbach, L.D., Xie, S.X., Naj, A.C., Albin, R., Gilman, S., PSP Genetics Study Group, Lee, V.M.Y., Trojanowski, J.Q., Devlin, B., Schellenberg, G.D., 2013. The unfolded protein response is activated in disease-affected brain regions in progressive supranuclear palsy and Alzheimer's disease. Acta Neuropathol. Commun. 1, 1-31. https://doi.org/10.1186/2051-5960-1-31

Stutzbach, Lauren, "Perk Genetic Variation and Function in Progressive Supranuclear Palsy" (2015). *Publicly Accessible Penn Dissertations*. 2045. https://repository.upenn.edu/edissertations/2045

Su, N., Kilberg, M.S., 2008. C/EBP Homology Protein (CHOP) Interacts with Activating Transcription Factor 4 (ATF4) and Negatively Regulates the Stress-dependent Induction of the Asparagine Synthetase Gene. J. Biol. Chem. 283, 35106–35117. https://doi.org/10.1074/jbc.M806874200

Sultan, A., Nesslany, F., Violet, M., Bégard, S., Loyens, A., Talahari, S., Mansuroglu, Z., Marzin, D., Sergeant, N., Humez, S., Colin, M., Bonnefoy, E., Buée, L., Galas, M.-C.,

2011. Nuclear Tau, a Key Player in Neuronal DNA Protection. J. Biol. Chem. 286, 4566–4575. https://doi.org/10.1074/jbc.M110.199976

Surani, M. A. H. (1979). Glycoprotein synthesis and inhibition of glycosylation by tunicamycin in preimplantation mouse embryos: compaction and trophoblast adhesion. *Cell* 18, 217-227.

Tacik, P., DeTure, M., Lin, W.-L., Sanchez Contreras, M., Wojtas, A., Hinkle, K.M., Fujioka, S., Baker, M.C., Walton, R.L., Carlomagno, Y., Brown, P.H., Strongosky, A.J., Kouri, N., Murray, M.E., Petrucelli, L., Josephs, K.A., Rademakers, R., Ross, O.A., Wszolek, Z.K., Dickson, D.W., 2015. A novel tau mutation, p.K317N, causes globular glial tauopathy. Acta Neuropathol 130, 199–214. https://doi.org/10.1007/s00401-015-1425-0
Tacik, P., Sanchez-Contreras, M., DeTure, M., Murray, M.E., Rademakers, R., Ross, O.A., Wszolek, Z.K., Parisi, J.E., Knopman, D.S., Petersen, R.C., Dickson, D.W., 2017. Clinicopathologic heterogeneity in frontotemporal dementia and parkinsonism linked to chromosome 17 (FTDP-17) due to microtubule-associated protein tau (MAPT) p.P301L mutation, including a patient with globular glial tauopathy. Neuropathol Appl Neurobiol 43, 200–214. https://doi.org/10.1111/nan.12367

Takahashi, M., Weidenheim, K.M., Dickson, D.W., Ksiezak-Reding, H., 2002. Morphological and Biochemical Correlations of Abnormal Tau Filaments in Progressive Supranuclear Palsy. J Neuropathol Exp Neurol 61, 33–45. https://doi.org/10.1093/jnen/61.1.33

Takei, Y., Teng, J., Harada, A., Hirokawa, N., 2000. Defects in Axonal Elongation and Neuronal Migration in Mice with Disrupted tau and map1b Genes. J. Cell Biol. 150, 989–1000. https://doi.org/10.1083/jcb.150.5.989

Takigawa, H., Kitayama, M., Wada-Isoe, K., Kowa, H., Nakashima, K., 2016. Prevalence of progressive supranuclear palsy in Yonago: change throughout a decade. Brain Behav. 6, e00557. https://doi.org/10.1002/brb3.557

Tang, Z., Ioja, E., Bereczki, E., Hultenby, K., Li, C., Guan, Z., Winblad, B., Pei, J.-J., 2015. mTor mediates tau localization and secretion: Implication for Alzheimer's disease. Biochim. Biophys. Acta BBA - Mol. Cell Res. 1853, 1646–1657. https://doi.org/10.1016/j.bbamcr.2015.03.003

Tanida, I., Ueno, T., Kominami, E., 2008. LC3 and Autophagy, in: Deretic, V. (Ed.), Autophagosome and Phagosome, Methods in Molecular Biology™. Humana Press, Totowa, NJ, pp. 77–88. https://doi.org/10.1007/978-1-59745-157-4_4

Taniguchi-Watanabe, S., Arai, T., Kametani, F., Nonaka, T., Masuda-Suzukake, M., Tarutani, A., Murayama, S., Saito, Y., Arima, K., Yoshida, M., Akiyama, H., Robinson, A., Mann, D.M.A., Iwatsubo, T., Hasegawa, M., 2016. Biochemical classification of tauopathies by immunoblot, protein sequence and mass spectrometric analyses of sarkosyl-insoluble and trypsin-resistant tau. Acta Neuropathol 131, 267–280. https://doi.org/10.1007/s00401-015-1503-3

Tashiro, K., Hasegawa, M., Ihara, Y., Iwatsubo, T., 1997. Somatodendritic localization of phosphorylated tau in neonatal and adult rat cerebral cortex: NeuroReport 8, 2797–2801. https://doi.org/10.1097/00001756-199708180-00029

Tazi, J., Bakkour, N., Stamm, S., 2009. Alternative splicing and disease. Biochim. Biophys. Acta BBA - Mol. Basis Dis. 1792, 14–26. https://doi.org/10.1016/j.bbadis.2008.09.017

Tellez-Nagel, I., Wisniewski, H.M., 1973. Ultrastructure of Neurofibrillary Tangles in Steele-Richardson-Olszewski Syndrome. Arch. Neurol. 29, 324–327. https://doi.org/10.1001/archneur.1973.00490290064007

Terasaki, M., Slater, N.T., Fein, A., Schmidek, A., Reese, T.S., 1994. Continuous network of endoplasmic reticulum in cerebellar Purkinje neurons. Proc. Natl. Acad. Sci. 91, 7510–7514. https://doi.org/10.1073/pnas.91.16.7510

Teske, B.F., Wek, S.A., Bunpo, P., Cundiff, J.K., McClintick, J.N., Anthony, T.G., Wek, R.C., 2011. The eIF2 kinase PERK and the integrated stress response facilitate activation of ATF6 during endoplasmic reticulum stress. MBoC 22, 4390–4405. https://doi.org/10.1091/mbc.e11-06-0510

Tetrud, J.W., Golbe, L.I., Forno, L.S., Farmer, P.M., 1996. Autopsy-proven progressive supranuclear palsy in two siblings. Neurology 46, 931–934. https://doi.org/10.1212/WNL.46.4.931

Terwel, D., Lasrado, R., Snauwaert, J., Vandeweert, E., Van Haesendonck, C., Borghgraef, P., Van Leuven, F., 2005. Changed Conformation of Mutant Tau-P301L Underlies the Moribund Tauopathy, Absent in Progressive, Nonlethal Axonopathy of Tau-

4R/2N Transgenic Mice. J. Biol. Chem. 280, 3963–3973. https://doi.org/10.1074/jbc.M409876200

Thuerauf, D.J., Marcinko, M., Belmont, P.J., Glembotski, C.C., 2007. Effects of the Isoform-specific Characteristics of ATF6α and ATF6β on Endoplasmic Reticulum Stress Response Gene Expression and Cell Viability. J. Biol. Chem. 282, 22865–22878. https://doi.org/10.1074/jbc.M701213200

Tint, I., Slaughter, T., Fischer, I., Black, M.M., 1998. Acute inactivation of tau has no effect on dynamics of microtubules in growing axons of cultured sympathetic neurons. J. Neurosci. Off. J. Soc. Neurosci. 18, 8660–8673.

Tolnay, M., Probst, A., 2003. The Neuropathological Spectrum of Neurodegenerative Tauopathies. IUBMB Life Int. Union Biochem. Mol. Biol. Life 55, 299–305. https://doi.org/10.1080/1521654032000114348

Tolosa, E., Duvoisin, R., Cruz-Sanchez, F.F. (Eds.), 1994. Progressive Supranuclear Palsy: Diagnosis, Pathology, and Therapy, Journal of Neural Transmission. Supplementa. Springer-Verlag, Wien. https://doi.org/10.1007/978-3-7091-6641-3

Travers, K.J., Patil, C.K., Wodicka, L., Lockhart, D.J., Weissman, J.S., Walter, P., 2000. Functional and Genomic Analyses Reveal an Essential Coordination between the Unfolded Protein Response and ER-Associated Degradation. Cell 101, 249–258. https://doi.org/10.1016/S0092-8674(00)80835-1

Tsuru, A., Imai, Y., Saito, M., Kohno, K., 2016. Novel mechanism of enhancing IRE1α-XBP1 signalling via the PERK-ATF4 pathway. Sci Rep 6, 24217. https://doi.org/10.1038/srep24217

Tuite, P.J., Clark, H.B., Bergeron, C., Bower, M., St George-Hyslop, P., Mateva, V., Anderson, J., Knopman, D.S., 2005. Clinical and Pathologic Evidence of Corticobasal Degeneration and Progressive Supranuclear Palsy in Familial Tauopathy. Arch. Neurol. 62, 1453. https://doi.org/10.1001/archneur.62.9.1453

Ubeda, M., Vallejo, M., Habener, J.F., 1999. CHOP Enhancement of Gene Transcription by Interactions with Jun/Fos AP-1 Complex Proteins. Mol. Cell. Biol. 19, 7589–7599. https://doi.org/10.1128/MCB.19.11.7589

Ubeda, M., Wang, X.Z., Zinszner, H., Wu, I., Habener, J.F., Ron, D., 1996. Stress-induced binding of the transcriptional factor CHOP to a novel DNA control element. Mol. Cell. Biol. 16, 1479–1489. https://doi.org/10.1128/MCB.16.4.1479

Unterberger, U., Höftberger, R., Gelpi, E., Flicker, H., Budka, H., Voigtländer, T., 2006. Endoplasmic Reticulum Stress Features Are Prominent in Alzheimer Disease but Not in Prion Diseases In Vivo: Journal of Neuropathology and Experimental Neurology 65, 348–357. https://doi.org/10.1097/01.jnen.0000218445.30535.6f

Urano, F., 2000. Coupling of Stress in the ER to Activation of JNK Protein Kinases by Transmembrane Protein Kinase IRE1. Science 287, 664–666. https://doi.org/10.1126/science.287.5453.664

Uversky, V.N., Winter, S., Galzitskaya, O.V., Kittler, L., Lober, G., 1998. Hyperphosphorylation induces structural modification of tau-protein. FEBS Lett. 439, 21–25. https://doi.org/10.1016/S0014-5793(98)01303-9

Vaccaro, A., Patten, S.A., Aggad, D., Julien, C., Maios, C., Kabashi, E., Drapeau, P., Parker, J.A., 2013. Pharmacological reduction of ER stress protects against TDP-43 neuronal toxicity in vivo. Neurobiol. Dis. 55, 64–75. https://doi.org/10.1016/j.nbd.2013.03.015

Valastyan, J.S., Lindquist, S., 2014. Mechanisms of protein-folding diseases at a glance. Dis. Model. Mech. 7, 9–14. https://doi.org/10.1242/dmm.013474

Van Herpen, E., Rosso, S.M., Serverijnen, L.-A., Yoshida, H., Breedveld, G., Van De Graaf, R., Kamphorst, W., Ravid, R., Willemsen, R., Dooijes, D., Majoor-Krakauer, D., Kros, J.M., Crowther, R.A., Goedert, M., Heutink, P., Van Swieten, J.C., 2003. Variable phenotypic expression and extensive tau pathology in two families with the noveltau mutation L315R. Ann Neurol. 54, 573–581. https://doi.org/10.1002/ana.10721

van Swieten, J., Rosso, S., Heutink, P., MAPT-Related Disorders-Retired chapter, for hisotrical refewrence only. 2000. In: Adam MP, Ardinger, HH, Pagon RA editors. GeneReviews (Internet). Seattle (WA): University of Washington, Seattle; 1993-2020.

van Swieten, J., Spillantini, M.G., 2007. Hereditary Frontotemporal Dementia Caused by Tau Gene Mutations. Brain Pathology 17, 63–73. https://doi.org/10.1111/j.1750-3639.2007.00052.x

Vandrovcova, J., Pittman, A.M., Malzer, E., Abou-Sleiman, P.M., Lees, A.J., Wood, N.W., de Silva, R., 2009. Association of MAPT haplotype-tagging SNPs with sporadic Parkinson's disease. Neurobiol. Aging 30, 1477–1482. https://doi.org/10.1016/j.neurobiolaging.2007.11.019

van der Harg, J.M., Nölle, A., Zwart, R., Boerema, A.S., van Haastert, E.S., Strijkstra, A.M., Hoozemans, J.J., Scheper, W., 2014. The unfolded protein response mediates reversible tau phosphorylation induced by metabolic stress. Cell Death Dis 5, e1393–e1393. https://doi.org/10.1038/cddis.2014.354

Vattem, K.M., Wek, R.C., 2004. Reinitiation involving upstream ORFs regulates ATF4 mRNA translation in mammalian cells. Proc. Natl. Acad. Sci. 101, 11269–11274. https://doi.org/10.1073/pnas.0400541101

Verhaart, W.J.C., 1958. Degeneration of the Brain Stem Reticular Formation, Other Parts of the Brain Stem and the Cerebellum. An Example of Heterogenous Systemic Degeneration of the Central, Nervous System. J. Neuropathol. Exp. Neurol. 17, 382–391. https://doi.org/10.1097/00005072-195804000-00021

Verkhratsky, A., 2004. Endoplasmic reticulum calcium signaling in nerve cells. Biol. Res. 37. https://doi.org/10.4067/S0716-97602004000400027

Vincenz, L., Jager, R., O'Dwyer, M., Samali, A., 2013. Endoplasmic Reticulum Stress and the Unfolded Protein Response: Targeting the Achilles Heel of Multiple Myeloma. Mol. Cancer Ther. 12, 831–843. https://doi.org/10.1158/1535-7163.MCT-12-0782

Violet, M., Delattre, L., Tardivel, M., Sultan, A., Chauderlier, A., Caillierez, R., Talahari, S., Nesslany, F., Lefebvre, B., Bonnefoy, E., BuÃ©e, L., Galas, M.-C., 2014. A major role for Tau in neuronal DNA and RNA protection in vivo under physiological and hyperthermic conditions. Front. Cell. Neurosci. 8. https://doi.org/10.3389/fncel.2014.00084

von Bergen, M., Barghorn, S., Biernat, J., Mandelkow, E.-M., Mandelkow, E., 2005. Tau aggregation is driven by a transition from random coil to beta sheet structure. Biochim. Biophys. Acta BBA - Mol. Basis Dis. 1739, 158–166. https://doi.org/10.1016/j.bbadis.2004.09.010

von Bergen, M., Barghorn, S., Li, L., Marx, A., Biernat, J., Mandelkow, E.-M., Mandelkow, E., 2001. Mutations of Tau Protein in Frontotemporal Dementia Promote Aggregation of Paired Helical Filaments by Enhancing Local β-Structure. J. Biol. Chem. 276, 48165–48174. https://doi.org/10.1074/jbc.M105196200

Wagner, P., Wang, B., Clark, E., Lee, H., Rouzier, R., Pusztai, L., 2005. Microtubule Associated Protein (MAP)-Tau: A Novel Mediator of Paclitaxel Sensitivity In Vitro and In Vivo. Cell Cycle 4, 1149–1152. https://doi.org/10.4161/cc.4.9.2038

Walter, P., Blobel, G., 1981. Translocation of proteins across the endoplasmic reticulum III. Signal recognition protein (SRP) causes signal sequence-dependent and site-specific arrest of chain elongation that is released by microsomal membranes. J. Cell Biol. 91, 557–561. https://doi.org/10.1083/jcb.91.2.557

Walter, P., Ron, D., 2011. The Unfolded Protein Response: From Stress Pathway to Homeostatic Regulation. Science 334, 1081–1086. https://doi.org/10.1126/science.1209038

Ward, R.J., Alvarez-Curto, E., Milligan, G., 2011. Using the Flp-In™ T-Rex™ System to Regulate GPCR Expression, in: Willars, G.B., Challiss, R.A.J. (Eds.), Receptor Signal Transduction Protocols, Methods in Molecular Biology. Humana Press, Totowa, NJ, pp. 21–37. https://doi.org/10.1007/978-1-61779-126-0_2

Wang, Y., Zhang, Y., Hu, W., Xie, S., Gong, C.-X., Iqbal, K., Liu, F., 2015. Rapid alteration of protein phosphorylation during postmortem: implication in the study of protein phosphorylation. Sci Rep 5, 15709. https://doi.org/10.1038/srep15709

Wang, Y., Martinez-Vicente, M., Krüger, U., Kaushik, S., Wong, E., Mandelkow, E.-M., Cuervo, A.M., Mandelkow, E., 2009. Tau fragmentation, aggregation and clearance: the dual role of lysosomal processing. Human Molecular Genetics 18, 4153–4170. https://doi.org/10.1093/hmg/ddp367

Wang, P., Li, J., Sha, B., 2016. The ER stress sensor PERK luminal domain functions as a molecular chaperone to interact with misfolded proteins. Acta Crystallogr. Sect. Struct. Biol. 72, 1290–1297. https://doi.org/10.1107/S2059798316018064

Wang, P., Li, J., Tao, J., Sha, B., 2018. The luminal domain of the ER stress sensor protein PERK binds misfolded proteins and thereby triggers PERK oligomerization. J. Biol. Chem. 293, 4110–4121. https://doi.org/10.1074/jbc.RA117.001294

Wang, X., Campbell, M.R., Lacher, S.E., Cho, H.-Y., Wan, M., Crowl, C.L., Chorley, B.N., Bond, G.L., Kleeberger, S.R., Slattery, M., Bell, D.A., 2016. A Polymorphic Antioxidant

Response Element Links NRF2/sMAF Binding to Enhanced MAPT Expression and Reduced Risk of Parkinsonian Disorders. Cell Rep. 15, 830–842. https://doi.org/10.1016/j.celrep.2016.03.068

Wang, X.-Z., 1998. Identification of novel stress-induced genes downstream of chop. EMBO J. 17, 3619–3630. https://doi.org/10.1093/emboj/17.13.3619

Wang, Y., Loomis, P.A., Zinkowski, R.P., Binder, L.I., 1993. A novel tau transcript in cultured human neuroblastoma cells expressing nuclear tau. J. Cell Biol. 121, 257–267. https://doi.org/10.1083/jcb.121.2.257

Wei, M.-L., Andreadis, A., 2002. Splicing of a Regulated Exon Reveals Additional Complexity in the Axonal Microtubule-Associated Protein Tau. J. Neurochem. 70, 1346–1356. https://doi.org/10.1046/j.1471-4159.1998.70041346.x

Weingarten, M.D., Lockwood, A.H., Hwo, S.Y., Kirschner, M.W., 1975. A protein factor essential for microtubule assembly. Proc. Natl. Acad. Sci. 72, 1858–1862. https://doi.org/10.1073/pnas.72.5.1858

Weissmann, C., Reyher, H.-J., Gauthier, A., Steinhoff, H.-J., Junge, W., Brandt, R., 2009. Microtubule Binding and Trapping at the Tip of Neurites Regulate Tau Motion in Living Neurons. Traffic 10, 1655–1668. https://doi.org/10.1111/j.1600-0854.2009.00977.x

Wierzba-Bobrowicz, T., Lewandowska, E., Zaremba, J., Berdyński, M., Żekanowski, C., Stępień, T., Felczak, P., Tarka, S., 2014. Frontotemporal lobar degeneration with MAPT mutation in an Italian-Polish family. A. Folia Neuropathol. 4, 457–466. https://doi.org/10.5114/fn.2014.47848

Will, C.L., Luhrmann, R., 2011. Spliceosome Structure and Function. Cold Spring Harb. Perspect. Biol. 3, a003707–a003707. https://doi.org/10.1101/cshperspect.a003707

Williams, D.R., de Silva, R., Paviour, D.C., Pittman, A., Watt, H.C., Kilford, L., Holton, J.L., Revesz, T., Lees, A.J., 2005. Characteristics of two distinct clinical phenotypes in pathologically proven progressive supranuclear palsy: Richardson's syndrome and PSP-parkinsonism. Brain 128, 1247–1258. https://doi.org/10.1093/brain/awh488

Williams, D.R., Lees, A.J., 2009. Progressive supranuclear palsy: clinicopathological concepts and diagnostic challenges. Lancet Neurol. 8, 270–279. https://doi.org/10.1016/S1474-4422(09)70042-0

Wischik, C.M., Novak, M., Edwards, P.C., Klug, A., Tichelaar, W., Crowther, R.A., 1988. Structural characterization of the core of the paired helical filament of Alzheimer disease. Proc. Natl. Acad. Sci. 85, 4884–4888. https://doi.org/10.1073/pnas.85.13.4884

Witman, G.B., Cleveland, D.W., Weingarten, M.D., Kirschner, M.W., 1976. Tubulin requires tau for growth onto microtubule initiating sites. Proc. Natl. Acad. Sci. 73, 4070–4074. https://doi.org/10.1073/pnas.73.11.4070

Wictome, M., Michelangeli, F., Lee, A.G., East, J.M., 1992. The inhibitors thapsigargin and 2,5-di(*tert* -butyl)-1,4-benzohydroquinone favour the E2 form of the Ca^{2+} , Mg^{2+} -ATPase. FEBS Letters 304, 109–113. https://doi.org/10.1016/0014-5793(92)80599-C

Wittmann, C.W., 2001. Tauopathy in Drosophila: Neurodegeneration Without Neurofibrillary Tangles. Science 293, 711–714. https://doi.org/10.1126/science.1062382

Wolcott, C.D., Rallison, M.L., 1972. Infancy-onset diabetes mellitus and multiple epiphyseal dysplasia. The Journal of Pediatrics 80, 292–297. https://doi.org/10.1016/S0022-3476(72)80596-1

Wood, J.G., Mirra, S.S., Pollock, N.J., Binder, L.I., 1986. Neurofibrillary tangles of Alzheimer disease share antigenic determinants with the axonal microtubule-associated protein tau (tau). Proc. Natl. Acad. Sci. 83, 4040–4043. https://doi.org/10.1073/pnas.83.11.4040

Woody, R.W., Clark, D.C., Roberts, G.C.K., Martin, S.R., Bayley, P.M., 1983. Molecular flexibility in microtubule proteins: proton nuclear magnetic resonance characterization. Biochemistry 22, 2186–2192. https://doi.org/10.1021/bi00278a020

Wren, M.C., Zhao, J., Liu, C.-C., Murray, M.E., Atagi, Y., Davis, M.D., Fu, Y., Okano, H.J., Ogaki, K., Strongosky, A.J., Tacik, P., Rademakers, R., Ross, O.A., Dickson, D.W., Wszolek, Z.K., Kanekiyo, T., Bu, G., 2015. Frontotemporal dementia-associated N279K tau mutant disrupts subcellular vesicle trafficking and induces cellular stress in iPSC-derived neural stem cells. Mol Neurodegeneration 10, 46. https://doi.org/10.1186/s13024-015-0042-7

Wu, J., Kaufman, R.J., 2006. From acute ER stress to physiological roles of the Unfolded Protein Response. Cell Death Differ. 13, 374–384. https://doi.org/10.1038/sj.cdd.4401840

Wu, X.-L., Piña-Crespo, J., Zhang, Y.-W., Chen, X.-C., Xu, H.-X., 2017. Tau-mediated Neurodegeneration and Potential Implications in Diagnosis and Treatment of Alzheimer's Disease. Chin Med J (Engl) 130, 2978–2990. https://doi.org/10.4103/0366-6999.220313

Wulf Paschen, Christopher G. Proud, Gunter Mies, 2007. Shut-Down of Translation, a Global Neuronal Stress Response:Mechanisms and Pathological Relevance. Curr. Pharm. Des. 13, 1887–1902. https://doi.org/10.2174/138161207780858401

Wurm, F.M., 2004. Production of recombinant protein therapeutics in cultivated mammalian cells. Nat Biotechnol 22, 1393–1398. https://doi.org/10.1038/nbt1026

Xiang, S., Kulminskaya, N., Habenstein, B., Biernat, J., Tepper, K., Paulat, M., Griesinger, C., Becker, S., Lange, A., Mandelkow, E., Linser, R., 2017. A Two-Component Adhesive: Tau Fibrils Arise from a Combination of a Well-Defined Motif and Conformationally Flexible Interactions. J. Am. Chem. Soc. 139, 2639–2646. https://doi.org/10.1021/jacs.6b09619

Xu, P., Raden, D., Doyle, F.J., Robinson, A.S., 2005. Analysis of unfolded protein response during single-chain antibody expression in Saccaromyces cerevisiae reveals different roles for BiP and PDI in folding. Metab. Eng. 7, 269–279. https://doi.org/10.1016/j.ymben.2005.04.002

Yamada, T., McGeer, P.L., 1990. Oligodendroglial microtubular masses: An abnormality observed in some human neurodegenerative diseases. Neurosci. Lett. 120, 163–166. https://doi.org/10.1016/0304-3940(90)90028-8

Yamada, T., McGeer, P.L., McGeer, E.G., 1992. Appearance of paired nucleated, Tau-positive glia in patients with progressive supranuclear palsy brain tissue. Neurosci. Lett. 135, 99–102. https://doi.org/10.1016/0304-3940(92)90145-W

Yamamoto, K., 2004. Differential Contributions of ATF6 and XBP1 to the Activation of Endoplasmic Reticulum Stress-Responsive cis-Acting Elements ERSE, UPRE and ERSE-II. J. Biochem. (Tokyo) 136, 343–350. https://doi.org/10.1093/jb/mvh122

Yamamoto, K., Sato, T., Matsui, T., Sato, M., Okada, T., Yoshida, H., Harada, A., Mori, K., 2007. Transcriptional Induction of Mammalian ER Quality Control Proteins Is Mediated by Single or Combined Action of ATF6α and XBP1. Dev. Cell 13, 365–376. https://doi.org/10.1016/j.devcel.2007.07.018

Yan, W., Frank, C.L., Korth, M.J., Sopher, B.L., Novoa, I., Ron, D., Katze, M.G., 2002. Control of PERK eIF2 kinase activity by the endoplasmic reticulum stress-induced molecular chaperone P58IPK. Proceedings of the National Academy of Sciences 99, 15920–15925. https://doi.org/10.1073/pnas.252341799

Yang, Y., Cheung, H.H., Tu, J., Miu, K.K., Chan, W.Y., 2016. New insights into the unfolded protein response in stem cells. Oncotarget 7, 54010–54027. https://doi.org/10.18632/oncotarget.9833

Yen, S.S., 2011. Proteasome degradation of brain cytosolic tau in Alzheimer's disease. Int. J. Clin. Exp. Pathol. 4, 385–402.

Yoshida, H., Haze, K., Yanagi, H., Yura, T., Mori, K., 1998. Identification of the *cis* -Acting Endoplasmic Reticulum Stress Response Element Responsible for Transcriptional Induction of Mammalian Glucose-regulated Proteins: Involvement of basic leucine zipper transcription factors.J. Biol. Chem. 273, 33741–33749. https://doi.org/10.1074/jbc.273.50.33741

Yoshida, H., Crowther, R.A., Goedert, M., 2002. Functional effects of tau gene mutations DeltaN296 and N296H. J Neurochem 80, 548–551. https://doi.org/10.1046/j.0022-3042.2001.00729.x

Yoshida, H., Matsui, T., Yamamoto, A., Okada, T., Mori, K., 2001. XBP1 mRNA Is Induced by ATF6 and Spliced by IRE1 in Response to ER Stress to Produce a Highly Active Transcription Factor. Cell 107, 881–891. https://doi.org/10.1016/S0092-8674(01)00611-0

Yu, J.-Z., Rasenick, M.M., 2006. Tau associates with actin in differentiating PC12 cells. FASEB J. 20, 1452–1461. https://doi.org/10.1096/fj.05-5206com

Yuan, S.H., Hiramatsu, N., Liu, Q., Sun, X.V., Lenh, D., Chan, P., Chiang, K., Koo, E.H., Kao, A.S., Litvan, I., Lin, J.H., 2018. Tauopathy-Associated PERK Alleles are Functional

Hypomorphs that Increase Neuronal Vulnerability to ER Stress. Hum. Mol. Genet. https://doi.org/10.1093/hmg/ddy297

Zabik, N.L., Imhof, M.M., Martic-Milne, S., 2017. Structural evaluations of tau protein conformation: methodologies and approaches. Biochem. Cell Biol. 95, 338–349. https://doi.org/10.1139/bcb-2016-0227

Zampieri, C., Di Fabio, R.P., 2006. Progressive Supranuclear Palsy: Disease Profile and Rehabilitation Strategies. Phys. Ther. 86, 870–880. https://doi.org/10.1093/ptj/86.6.870

Zarranz, J.J., Ferrer, I., Lezcano, E., Forcadas, M.I., Eizaguirre, B., Atares, B., Puig, B., Gomez-Esteban, J.C., Fernandez-Maiztegui, C., Rouco, I., Perez-Concha, T., Fernandez, M., Rodriguez, O., Rodriguez-Martinez, A.B., de Pancorbo, M.M., Pastor, P., Perez-Tur, J., 2005. A novel mutation (K317M) in the MAPT gene causes FTDP and motor neuron disease. Neurology 64, 1578–1585. https://doi.org/10.1212/01.WNL.0000160116.65034.12

Zhang, D.D., 2006. Mechanistic Studies of the Nrf2-Keap1 Signaling Pathway. Drug Metab. Rev. 38, 769–789. https://doi.org/10.1080/03602530600971974

Zhang, K., Kaufman, R.J., 2006. Protein Folding in the Endoplasmic Reticulum and the Unfolded Protein Response, in: Starke, K., Gaestel, M. (Eds.), Molecular Chaperones in Health and Disease. Springer-Verlag, Berlin/Heidelberg, pp. 69–91. https://doi.org/10.1007/3-540-29717-0_3

Zhang, J.Y., Liu, S.J., Li, H.L., Wang, J.-Z., 2005. Microtubule-associated protein tau is a substrate of ATP/Mg2+-dependent proteasome protease system. J Neural Transm 112, 547–555. https://doi.org/10.1007/s00702-004-0196-x

Zhang, P., McGrath, B., Li, S., Frank, A., Zambito, F., Reinert, J., Gannon, M., Ma, K., McNaughton, K., Cavener, D.R., 2002. The PERK Eukaryotic Initiation Factor 2α Kinase Is Required for the Development of the Skeletal System, Postnatal Growth, and the Function and Viability of the Pancreas. MCB 22, 3864–3874. https://doi.org/10.1128/MCB.22.11.3864-3874.2002

Zhang, W., Feng, D., Li, Y., Iida, K., McGrath, B., Cavener, D.R., 2006. PERK EIF2AK3 control of pancreatic β cell differentiation and proliferation is required for postnatal glucose homeostasis. Cell Metabolism 4, 491–497. https://doi.org/10.1016/j.cmet.2006.11.002

Zheng-Fischhofer, Q., Biernat, J., Mandelkow, E.-M., Illenberger, S., Godemann, R., Mandelkow, E., 1998. Sequential phosphorylation of Tau by glycogen synthase kinase-3beta and protein kinase A at Thr212 and Ser214 generates the Alzheimer-specific epitope of antibody AT100 and requires a paired-helical-filament-like conformation. Eur. J. Biochem. 252, 542–552. https://doi.org/10.1046/j.1432-1327.1998.2520542.x

Zhou, J., Liu, C.Y., Back, S.H., Clark, R.L., Peisach, D., Xu, Z., Kaufman, R.J., 2006. The crystal structure of human IRE1 luminal domain reveals a conserved dimerization interface required for activation of the unfolded protein response. Proc. Natl. Acad. Sci. 103, 14343–14348. https://doi.org/10.1073/pnas.0606480103

Zinszner, H., Kuroda, M., Wang, X., Batchvarova, N., Lightfoot, R.T., Remotti, H., Stevens, J.L., Ron, D., 1998. CHOP is implicated in programmed cell death in response to impaired function of the endoplasmic reticulum. Genes Dev. 12, 982–995. https://doi.org/10.1101/gad.12.7.982